Noémi Tamar do Carmo Jordão

Mestrado Integrado em Engenharia Química

Multi Stimuli-responsive Organic Salts: From preparation to functional device application

Dissertação para obtenção do Grau de Doutor em Química – Especialidade de Química-Física

Orientador: Doutor Luís C. Branco, Investigador Principal, LAQV-REQUIMTE, FCT/UNL
Co-orientador: Prof. Doutor A. Jorge Parola, Professor Associado com agregação, LAQV-REQUIMTE, FCT/UNL

Júri:

Presidente: Prof. Doutor José Paulo Barbosa Mota

Arguente(s): Prof. Doutora Ana Cristina Moreira Freire
Prof. Doutora Isabel Maria Delgado Jana Marrucho Ferreira

Vogais: Prof. Doutor José Paulo Sequeira Farinha
Prof. Doutora Paula Cristina de Sério Branco

FACULDADE DE CIÊNCIAS E TECNOLOGIA
UNIVERSIDADE NOVA DE LISBOA

Fevereiro de 2017

Multi Stimuli-responsive Organic Salts: From preparation to functional device application

“Se podes olhar, vê. Se podes ver, repara.”

José Saramago

Acknowledgments

Gostaria de agradecer, em primeiro lugar, aos meus orientadores Dr. Luís Branco e Prof. Dr. Jorge Parola pela orientação científica e conhecimentos transmitidos ao longo destes anos e acima de tudo pela oportunidade de realizar o doutoramento. Agradeço também a confiança, a paciência e a compreensão que me deram ao longo de todo este tempo.

À Fundação para a Ciência e a Tecnologia (FCT) pelo financiamento dos projectos no âmbito deste doutoramento: PTDC/QUI-QUI/104129/2008, PTDC/CTM-NAN/120658/2010 e IF/0041/2013/CP1161/CT005, PTDC/QEQ-QFI/1971/2014 and POCI-01-0145-FEDER-016387.

Ao LAQV-REQUIMTE por todo o apoio prestado e condições de trabalho (REQUIMTE/BI/006/2016) no âmbito da minha tese de doutoramento.

Ao Dr. Luís Branco por me apoiar e ser sempre tão otimista em relação a tudo! Ao Prof. Jorge Parola pelo seu incentivo ao longo destes anos. Muito obrigado!

Ao Prof. Fernando Pina pela oportunidade de desenvolver uma pequena parte do trabalho sob a sua supervisão, pelo seu entusiasmo relativamente à ciência e que nos empurra sempre para ir mais além, mas também pela paciência e disponibilidade demonstrada.

À Prof. Maria João Melo, ao Prof. João Carlos Lima e ao Dr. César Laia por toda a sua disponibilidade e/ou ajuda que prestaram ao longo desta tese.

À Prof. Madalena Dionísio e à Dr. Maria Teresa Viciosa por todo o apoio, disponibilidade e carinho com que me acolheram, mas também por todos os conhecimentos que me transmitiram e que contribuíram para o meu “crescimento”. Muito obrigado!

À Prof. Anabela Raymundo do ISA-UL pela oportunidade de realizar ensaios de reologia, o que foi uma mais valia no decorrer inicial deste trabalho.

À Ynvisible ® pela colaboração nos dispositivos electrocrómicos. Em especial, à Aida Branco pelo apoio, paciência e disponibilidade.

À Solchemar Lda pela disponibilidade de liquídos iónicos e outros reagentes utilizados no âmbito da minha tese.

Aos serviços de RMN e laboratório de análises do LAQV-REQUIMTE por todo o apoio prestado.

Ao Dr. Luís Cabrita e ao Dr. Hugo Cruz pela colaboração, paciência e disponibilidade com que efetuaram os estudos eletroquímicos. Ao Luís Cabrita por ter sempre palavras sábias e de encorajamento. Ao Hugo Cruz por tudo o que me ensinou, pela sua paciência, apoio, e incentivo. Muito obrigado!

À Raquel Gavara por tudo o que me ensinou, pelo apoio, alegria contagiante, amizade e carinho com que sempre me recebeu. Muito obrigado!

Ao Pedro Ferreira por todo o apoio, entusiasmo e contribuição para o desenvolvimento dos diariletenos. Muito obrigado!

A todas as pessoas que passaram pelo Grupo de Fotoquímica e Química Supramolecular e que conheci ao longo deste percurso e que de alguma forma deixaram um contributo na realização desta tese, aqui fica um muito obrigado! Em especial à Ana Marta por tudo o que me ensinou e pelas palavras nos momentos certos. Muito obrigado! À Rita Almendra, Neuza Gomes, Alexandra Costa e Nuno Trindade pelas horas de companheirismo passadas. Aos meus actuais colegas, alguns que me acompanharam desde o início, Artur Moro, João Avó, Tiago Moreira, Andreia Forte, Andreia Ruivo, Nuno Basílio, Karolina Zalewska, Miguel Santos. Em especial, à Sandra Gago, Márcia Pêssego e Hugo Cruz pelo apoio e paciência nestes últimos meses.

A todos os meus amigos que me acompanharam ao longo destes anos, sem vocês nada disto teria sido possível! Obrigado por todos os momentos de boa disposição e de complicidade, mas sobretudo por estarem sempre presentes nos momentos menos bons. À pequena Laura, que me faz sorrir, mesmo nos dias mais cinzentos. Foi uma enorme alegria conhecer-te! Muito obrigado a todos por tudo!

A toda a minha família. Em especial, aos meus pais por tudo o que têm feito por mim, sem eles nada disto seria possível. Muito obrigado!

Resumo

A descoberta de novos materiais que respondem eficientemente a estímulos externos, modificando as suas propriedades, de acordo com o interesse, tornou-se num tópico de investigação relevante para diversas potenciais aplicações. A integração dos materiais mais promissores em dispositivos tem sido aplicada em espelhos retrovisores de veículos, janelas "inteligentes", óculos de sol, sensores, entre outros.

Esta tese consiste no desenvolvimento e aplicação de materiais que respondem a estímulos externos, constituídos por sais fotocrómicos ou electrocrómicos. No geral, pode ser possível incorporar essas unidades na estrutura do catião ou anião, de modo a que esses materiais possam apresentar resposta ao pH, temperatura, luz ou eletricidade. Por outro lado, foram desenvolvidos polímeros iónicos contendo algumas dessas estruturas. Neste contexto, sais derivados de 4,4'-bipirídinio, diariletenos e flavílios foram, respetivamente, selecionados como unidades electrocrómicas e fotocrómicas. Para a preparação dos respetivos sais orgânicos, incluindo polímeros, foram otimizados diferentes procedimentos sintéticos e processos de purificação. Todos os sais foram caracterizados através de técnicas espectroscópicas, de modo a elucidar a sua estrutura e pureza. As propriedades térmicas, reológicas, fotoquímicas e eletroquímicas de alguns dos sais preparados foram também estudadas. A escolha adequada do contra-ião pode ser crucial para a obtenção de líquidos iónicos, bem como para modelar as suas propriedades.

Os sais electrocrómicos mais promissores baseados na unidade 4,4'-bipiridinio do tipo di- e tetra-catiónicos (simétricos e não simétricos), incluindo os polímeros iónicos mais promissores derivados de 4,4'-bipirídinio foram testados como dispositivos electrocrómicos em estado líquido, gel e sólido. Foi verificado que os substituintes e o contra-ião podem influenciar significativamente o desempenho electrocrómico do dispositivo, nomeadamente a sua reversibilidade, estabilidade, contraste de cor e tempos de transição.

Um líquido iónico à temperatura ambiente possuíndo propriedades fotocrómicas foi desenvolvido através da combinação de um derivado aniónico dos diariletenos e o catião tri-octil-metilamónio ([ALIQUAT]) e posteriormente, as suas propriedades foram estudadas.

Adicionalmente, foi desenvolvido um novo co-polímero sensível ao pH, temperatura e luz como estímulos externos. Esse co-polímero é constituído pela *N*-isopropilacrilamida e um derivado dos sais de flavílio.

A versatilidade química dos sais foto- e electrocrómicos desenvolvidos no âmbito desta tese abrem excelentes perspetivas para futuras aplicações como materiais eficientes e reversíveis a diferentes estímulos em simultâneo.

Palavras-chave:

Líquidos Iónicos, Electrocromismo, Fotocromismo, Materiais sensíveis a estímulos, Polímeros Iónicos.

Abstract

The discovery of novel and efficient stimuli-responsive materials that change their properties according to external stimuli and therefore, adjust to our demands become an interesting research topic for several potential applications. The integration of the most promissory stimuli-responsive materials in devices for antiglare car mirrors, smart windows, sunglasses, sensors, among others has been applied.

In this thesis, the development and application of stimuli-responsive materials containing ionic photochromic or electrochromic units have been explored. In general, it is possible to incorporate specific scaffolds possessing pH, temperature, and light or electron-transfer stimuli-responsive behaviour in the cation or anion structures. Also, ionic polymers based on these structures have been investigated. In this context, 4,4'-bipyridinium, diarylethenes and flavylium were selected as electrochromic and photochromic units, respectively. For the preparation of the selected organic salts including polymers, different synthetic routes and purification processes have been followed. Detailed characterization of all prepared salts by spectroscopic techniques in order to elucidate their structures and purities has been performed. Thermal, rheological, photochemical and electrochemical properties of some prepared salts were also studied. It is important to focus that the adequate selection of the counter-ions can be crucial to achieve ionic liquids as well as to tune their final properties.

The most promissory electrochromic salts based on 4,4'-bipyridinium symmetrical and non-symmetrical di and tetra-cations as well as ionic polymers were tested in liquid, gel or solid electrochromic devices. The substituents from bipyridinium scaffold as well as counter-ions can significantly influence the electrochromic performance in particular its reversibility; stability; colour contrast and transition times.

Photochromic Room Temperature Ionic Liquid based on the combination of diarylethene derivative anion with tri-octyl methylammonium ([ALIQUAT]) cation was developed and characterized.

Additionally, a new thermal, pH and photo-stimuli responsive co-polymer containing *N*-isopropylacrylamide and flavylium derivative have been prepared.

The chemical versatility of the prepared ionic photo- and electrochromic materials opens excellent perspectives for future applications as efficient and reversible multi stimuli-responsive materials.

Keywords:

Ionic Liquids, Electrochromism, Photochromism, Stimuli-responsive materials, Ionic Polymers.

Abbreviation List

[ALIQUAT]	Tri-octylmethylammonium
[AOT]	1,4-bis(2-ethylhexoxy)-1,4-dioxobutane-2-sulfonate or docusate
[BMIM]	1-butyl-3-methylimidazolium
[DCA] or [$N(CN)_2$]	Dicyanamide
[EMIM]	1-ethyl-3-methylimidazolium
[$N_{2,2,2,4}$]	Tri-ethylbutylammonium
[NTf_2]	Bis(trifluoromethanesulfonyl)imide
[OMIM]	1-octyl-3-methylimidazolium
[OTf] or [TfO]	Trifluoromethanesulfonate
[$P_{6,6,6,14}$]	Tri-hexyltetradecylphosphonium
[TBA]	Tetrabutylammonium
Abs	Absorbance
A	Quinoidal base
AH^+	Flavylium cation
AIBN	Azobisisobutyronitrile
APIs	Active pharmaceutical ingredients
ATRP	Atom transfer radical polymerization
B	Hemiketal
BASIL	Biphasic acid scavenging utilising ionic liquids
CB	Conjugated bases (A, B, Cc and Ct)
Cc	*Cis*-chalcone
CE	Colouration efficiency
CIE	"*Commission Internationale de l'éclairage*"
Ct	*Trans*-chalcone
Ct^-	Ionized *trans*-chalcone
CR	Contrast ratio
CV	Cyclic voltammetry
DMF	*N,N*-dimethylformamide
DMSO	Dimethylsulfoxide
DPV	Pulsed voltammetry (DPV)
DSC	Differential scanning calorimetry
DSSC	Dye-sensitized solar cells
E^0	Standard potential
E_c	Activation energy of cooling process
ECD	Electrochromic devices
EDOT	3,4-ethylenedioxythiophene
EGDMA	Ethylene glycol dimethacrylate
E_h	Activation energy of heating process

E_{pa}	Anodic peak potential
E_{pc}	Cathodic peak potential
ESPT	Excited state proton transfer
FTIR	Fourier transform infrared spectroscopy
GC	Glassy carbon
GLC	Gas-liquid chromatography
GPC	Gel permeation chromatography
HEMA	2-hydroxylethylmethacrylate
HPLC	High-performance liquid chromatography
I	Intensity of light
I_0	Light intensity emitted by irradiation source at a selected wavelength
ILCs	Ionic Liquid Crystals
ILs	Ionic Liquids
ITO	Indium tin oxide
IVTC	Intervalence charge-transfer
K'_a	Apparent equilibrium constant between AH^+ and CB
K_a	Equilibrium constant for the deprotonation of AH^+
k_a	Kinetic constant for the direct deprotonation reaction (formation of A)
k_{-a}	Kinetic constant for the inverse deprotonation reaction (protonation of A)
K_h	Equilibrium constant for the hydration of AH^+
k_h	Kinetic constant for the direct hydration reaction
k_{-h}	Kinetic constant for the inverse hydration reaction (dehydration of B)
K_i	Equilibrium constant for the isomerisation of Cc
k_i	Kinetic constant for the direct isomerisation reaction
k_{-i}	Kinetic constant for the inverse isomerisation reaction
K_t	Equilibrium constant for the tautomerization of the B
k_t	Kinetic constant for the direct tautomerization reaction
k_{-t}	Kinetic constant for the inverse tautomerization reaction
LCs	Liquid crystals
LCST	Lower critical solution temperature
MALDI-TOF	Matrix-assisted laser desorption/ionization time-of-flight
m.p.	Melting point
MLCT	Metal-to-ligand charge transfer
MS	Mass spectrometry
MTDSC	Modulated temperature differencial scanning calorimetry
MV	Methyl viologen di-chloride
M_n	Number average molecular weigth
M_w	Weigth average molecular weight
NIR	Near infrared
NMR	Nuclear magnetic resonance

ONB	*o*-nitrobenzyl ester
PAA	Poly(acrylic acid)
PDI	Polydispersity index
PBV	Poly(butyl viologen)
PEDOT	Poly(3,4-ethylenedioxythiophene)
PEG 400	Poly(ethylene glycol) 400
PET	Poly(ethylene terephthalate)
PEO	Poly(ethylene oxide)
PHEMA	Poly(2-hydroxyethylmethacrylate)
PILs	Poly(ionic liquids)
PMMA	Poly(methylmethacrylate)
PNIPAm	Poly(*N*-isopropylacrylamide)
PPO	Poly(propylene oxide)
PS	Poly(styrene)
Q	Charge density
RGB	Red, green, blue
RAFT	Reversible addition/fragmentation chain transfer polymerization
RTIL	Room Temperature Ionic Liquid
SCE	Saturated calomel electrode
SEC	Size exclusion chromatography
SILMs	Supported Ionic Liquid membranes
SMA	Maleic anhydride
SWV	Square-wave voltammetry
t_{90} or t_{70}	Time taken for the transmittance change by 90 or 70% of the total difference between the bleached and coloured states
T	Transmittance
T_c	Crystallization temperature
T_d	Decomposition temperature
THF	Tetrahydrofuran
TEMPO	(2,2,6,6-tetramethylpiperidin-1-yl)oxyl
TGA	Thermogravimetric analysis
T_g	Glass transition temperature
TICT	Twisted intramolecular charge-transfer
UCST	Upper critical solution temperature
UV	Ultraviolet
$\dot{\gamma}$	Shear rate
δ	Chemical shift
η	Viscosity
ε	Molar absorption coefficient
σ	Shear stress

λ	Wavelength
λ_{em}	Emission wavelength
λ_{exc}	Excitation wavelength
λ_{irr}	Irradiation wavelength
λ_{max}	Wavelength of maximum emission or absorption
$\tilde{\upsilon}$	Wavenumber
Φ_i	Quantum yield for a given process i

Content Index

Figures Index

Tables Index

1. Introduction

1. Introduction

1.1. Stimuli-responsive Materials

In the last few decades, the stimuli-responsive materials have attracted much attention due to their ability to respond to external stimuli by changing their properties such as solubility, colour, rheological and optical properties as well as permeability, among others [1,2]. Chemical, physical or biological external stimuli can be considered and the most common involves variations of pH, temperature, light, ionic strength, electron-transfer (redox) and host-guest interactions (see Figure 1.1) [2].

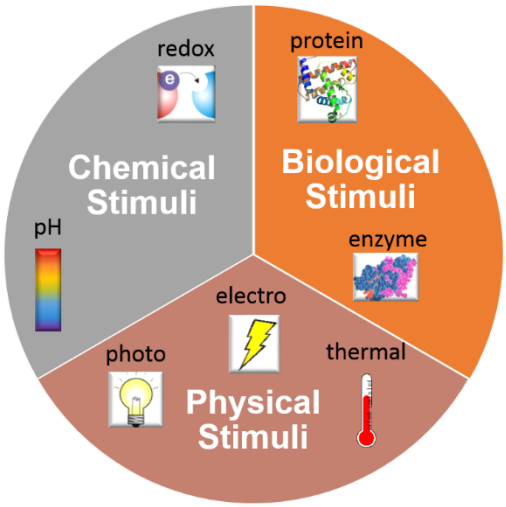

Figure 1.1 – Examples of chemical, physical and biological external stimuli.

Temperature is a very attractive external stimulus for potential application in different research areas. One example is the lower critical solution temperature (LCST), which occurs with some polymers in solution, usually in water [2]. The LCST can be defined as the critical temperature at which a polymer solution undergoes phase transition from a soluble to insoluble state [2]. The most common classes of thermo-responsive polymers, which exhibit in aqueous solution LCST behaviour include poly(acrylamides), poly(vinylethers), poly(oxazolines) and poly((oligoethylene oxide)methacrylates) [2]. The LCST behaviour becomes very exciting in water due to several proposed applications, such as tissue engineering, drug delivery, catalysis, surface engineering or information processing [2].

Light is considered as versatile stimulus, which receives much attention and it can be easily performed by irradiation of the sample in a specific wavelength [2]. Additionally, it is possible to control the exposure time and light intensity as well as the localization of the irradiated area by defining a specific area or volume [2]. Light can induce isomerisation and/or photochromism but also controllable formation of block co-polymer micelles. Some examples of photo-responsive units include azobenzene, spiropyran, spirooxaazine and fulgide derivatives [2].

Another important stimulus is related to electron-transfer process, which is obtained by incorporation of a redox-sensitive group, leading to a change on its oxidation state [2]. It is commonly used in inorganic chemistry, mainly involving oxidation or reduction processes of the

transition metals. It can be also applied to organic molecules such as dithienylethenes, ferrocene, disulfides and in paramagnetic organic molecules such as tetramethylpiperidine-1-oxyl (TEMPO) derivatives [2].

In the case of pH-responsive materials, the molecule is capable of donating or accepting protons upon an environmental change in the pH value [2].

Nowadays, these stimuli-responsive materials have found a broad range of application in materials science such as sensors, artificial muscles, molecular machines, actuators for process control, tissue engineering, self-healing surfaces, electronics and drug delivery [3].

Stimuli-responsive materials based on polymers are the most studied, due to their unique feature to respond to small environmental changes [1,4]. The reason for this interest is related to the possibility of the polymer change its properties in real time as well as reversible process and therefore, adjust to our demands [2]. The stimuli-responsive behaviour is essentially obtained by the functional groups incorporated on the polymer backbone or in appended chains. Additionally, it is possible to introduce several functional groups within one polymer in order to respond to different stimuli. The different functional groups' combinations can be integrated in parallel, serial or causal [2]. In the first case, the response of one group does not affect the response of the other and *vice-versa*. For example, Theato and co-workers reported a dual stimuli-responsive behaviour of a co-polymer containing a thermo-responsive unit, poly(*N*-isopropylacrylamide) and a fulgimide moiety as photochromic unit, which is attached to the backbone (see Figure 1.2) [5].

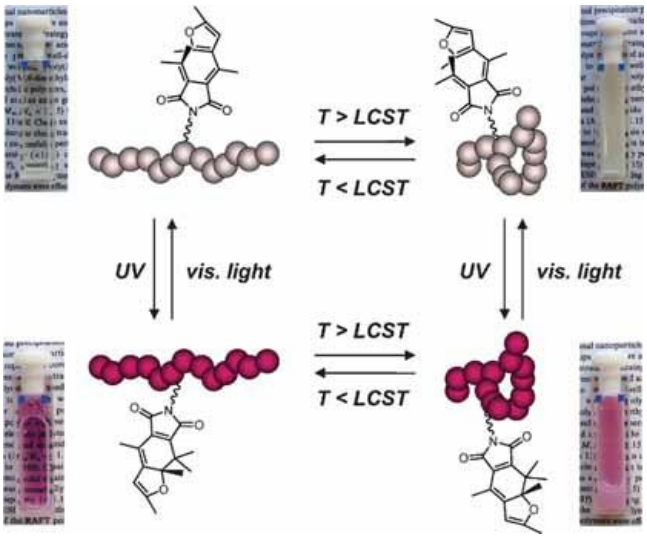

Figure 1.2 – Co-polymer containing poly(*N*-isopropylacrylamide) as thermo-responsive unit and a fulgimide moieties as photochromic unit, reported by Theato and co-workers [5]. (Source: Graphical Abstract from *Rapid Commun.*, 2010, **31**, 1456–1461).

This co-polymer shows the same lower critical solution temperature (LCST) in water before and after irradiation. So, the fulgimide photochromic transition is independent of the LCST behaviour of PNIPAm [5]. In the case of serial type, an amplified impact of the stimulated-response of one specific group by the other is observed [2]. As a consequence, an additive effect on the previous group is detected due to the other group [2]. For example, Bergbreiter and co-workers reported a

dual stimuli-responsive co-polymer, containing Poly(*N*-isopropylacrylamide) as thermo-responsive unit and 4-*N*-amino-2,2,6,6-tetramethylpiperidin-1-oxyl-4-yl (TEMPO derivative) as redox-active group (see Figure 1.3) [6].

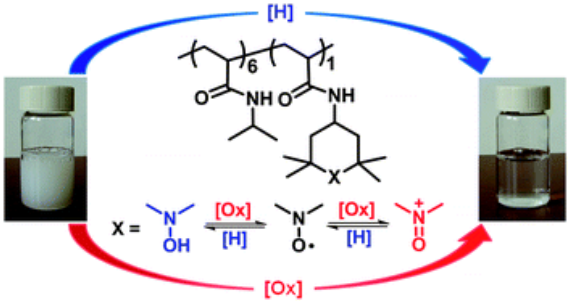

Figure 1.3 – Co-polymer formed by Poly(*N*-isopropylacrylamide) as thermo-responsive unit and 4-*N*-amino-2,2,6,6-tetramethylpiperidin-1-oxyl-4-yl (TEMPO derivative) as redox-active group, developed by Bergbreiter and co-workers [6]. (Source: Graphical Abstract from *Polym. Chem.*, 2010, 1, 631–633).

They observed that this co-polymer undergoes a reversible redox behaviour, leading to LCST changes (18 ºC to 35 – 40 ºC), when the co-polymer is oxidized ($NaOCl/H_2O$) or reduced [6].

Finally, the causal means the interplay between two or more stimuli-responsive groups [2]. When an external stimulus is applied, the corresponding group will respond and generates a new stimulus by a structural or an environmental change through the whole polymer, which then stimulates the second responsive group. As a consequence, this second group shows a response that is different from the first group [2]. However, examples of this type of functional groups combination are rare. Iwai and co-workers reported a co-polymer containing *N,N*-dimethylaminopropylacrylamide as pH-sensitive, *N*-*t*-butylacrylamide as thermo-sensitive and a benzofurazan derivative, which it was attached to the backbone via an ester linkage, as fluorophore unit (see Figure 1.4) [7].

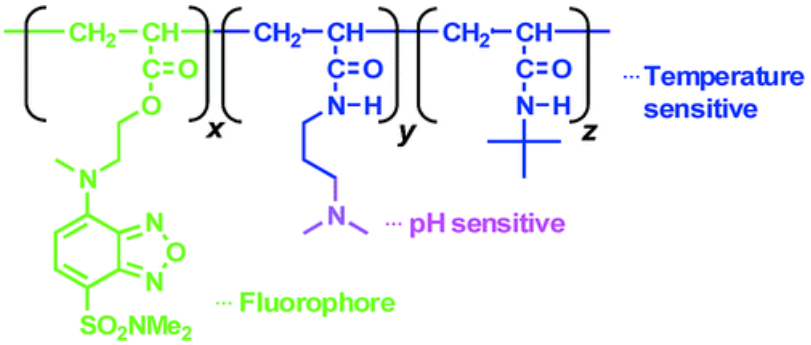

Figure 1.4 – Co-polymer prepared by Iwai and co-workers containing *N*-t-butylacrylamide as thermo-sensitive unit, *N*,*N*-dimethylaminopropylacrylamide as pH sensitive unit and a benzofurazan derivative as fluorophore unit [7]. (Source: Graphical Abstract from *J. Am. Chem. Soc.*, 2004, 126, 3032–3033).

It is established that benzofurazan groups provoke the fluorescence wavelength variation when an environmental change is induced [2]. In this context, the stimulation of the thermo-sensitive unit leads to a change on the polarity of the polymer, and it becomes more hydrophobic. As a consequence, the benzofurazan fluoresces at a different wavelength [7].

In conclusion, it is possible to prepare dual or multi stimuli-responsive materials by adequate selection of the functional groups. These materials can exhibit multifaceted behaviour by applying one or more external stimuli. The basis of the development of these stimuli-responsive materials is related with the need for a more precise control of the material properties in order to adjust to our demands. In addition, these stimuli-responsive materials require an interdisciplinary research area, with several potential applications.

1.2. Chromogenic Materials

Colour is all around us and plays an important role in our lives, once it influences our moods and emotions [8]. Bamfield and Hutchings considered that colour *"is perceptually conspicuous, a property we can discern directly using our eyes"* [9]. In general, it is possible to detect directly any change in the colour of an object by the observer, independently if it is achromatic from white to black or chromatic from colourless to coloured as well as one colour to another. Alternatively, it is also possible to measure by the use of spectrophotometric instruments [9].

Chromogenic materials are materials that display changes in the visible optical properties in response to an external stimulus, including changes in the colour or its corresponding intensity and the transition from a transparent to a scattering or reflective state [9,10]. The most commonly stimuli are temperature, electric potential, light and mechanical forces. Depending on the selected stimulus, the name of the colour change phenomena ("*chromism*") will be influenced and would start with the prefix derived from the stimulus, followed by the word "*chromism*". For example, if the stimulus is light, the colour change phenomenon is designed as photochromism. Electro- and photochromic materials will be described in detail below.

1.2.1. Electrochromic Materials

Electrochromic materials are materials that exhibit a reversible change in its optical properties that can occur when a material is electrochemically oxidised or reduced [11]. They are considered electroactive species, named as electrochrome and exhibit distinct colour switch, commonly between a transparent bleached state and a coloured state, or between two or more coloured states [11]. So, these materials are considered to be electrochromic when displaying colour changes perceptible to the human eye, i.e. in the visible region of the electromagnetic spectrum. Materials that have a multispectral energy modulation, i.e. radiation in the near infrared, thermal infrared and microwave regions, which can only be detected by sensitive equipment to those wavelengths can also be considered as electrochromic materials [12,13].

There are several inorganic and organic materials, which exhibit redox states, reduced and/or oxidised forms, with different UV-Visible absorption bands. The most important classes are transition metal oxides, Prussian blue systems (iron(II) and iron(III) hexacyanometallate complexes), viologens (1,1'-di-substituted-4,4'-bipyridinium salts), conducting polymers, transition metal and lanthanide coordination complexes, metallopolymers and metal phthalocyanines [11,14].

1. Introduction

The most widely studied transition metal oxide is tungsten trioxide (WO_3). In general, the colour results from intervalence charge-transfer (IVTC), and consists in the electron-transfer induced electrochemically between adjacent metal atoms of the same element but in different oxidation states. In the case of WO_3, the metal becomes coloured upon reduction, a univalent metal cation or proton, for example lithium (from electrolyte), is typically introduced in addition to the reducing electron [10,11].

In general, the transition metal oxides present colours in the blue or grey range to black [11]. Additionally, it is reported that metal oxides usually show higher photochemical stability comparing to the organic electrochromes, which can undergo photochemical degradation more easily [11]. It is described the application of the transition metal oxides for smart windows, thermal control of satellites and electrochromic writing paper [14].

Prussian blue is considered the earliest modern synthetic pigment, also known as iron (III) hexacyanoferrate (II) ($Fe_4[Fe(CN)_6]_3$) and it is the prototype of numerous polynuclear transition-metal hexacyanometallates, a class of insoluble mixed valence compounds [10,11,13,14]. It presented an intense blue colour, which is attributed to intervalence electron-transfer from Fe(II) to Fe(III), the former bound to the *N*-terminal of the cyanide ligand and the latter to the carbon. When the Fe(III) is electrochemically reduced to Fe(II), the intense blue colour disappears (bleaching) [10].

The general formula of these compounds is $M'_k[M''(CN)_6]_l$, where *k* and *l* are integers numbers and M′ and M″ are transition metals with different formal oxidation numbers [14]. One potential application of this metal hexacyanometallates is in displays [14].

Viologens, also known as 1,1'-di-substituted-4,4'-bipyridinium salts are electroactive species and results from mono or di-quarternization of 4,4'-bipyridine scaffold [11,15]. They may exhibit three redox states: a dication, a radical cation and a neutral compound (di-reduced species) and undergo two successive electron-transfer processes (see Scheme 1.1) [11,15].

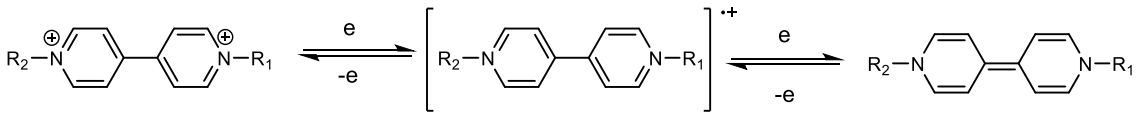

Scheme 1.1 –Three common bipyridinium cation redox states [15]. (Source: The viologens: physicochemical properties, synthesis, and applications of the salts of 4,4'-bipyridine, Wiley, 1998).

The di-cation is the most stable species and it is uncoloured while the radical cation is intensely coloured due to intense intramolecular optical charge-transfer. The colour depends, mainly, on the type and length of the substituents on the nitrogen, but also on the type of anion and on the solvent [11,15]. The use of these compounds in car rear view mirrors and its potential use in displays were reported [14].

Several resonance-stabilised aromatic molecules, such as pyrrole, thiophene, aniline, furan, indole, among others can undergo chemical or electrochemical oxidation to produce electroactive conjugated conducting polymers (see Figure 1.5) [11,16]. This polymerization process is based on monomer oxidation to give radical cation species and it is believed that involves either radical cation/radical cation coupling or reaction of radical cation with a neutral monomer [11,17]. When the

conducting polymers are in the oxidized state with positive charge carriers (p-doping), they are charge-balanced (doped) with anions and present a delocalized π-electron band structure [11].

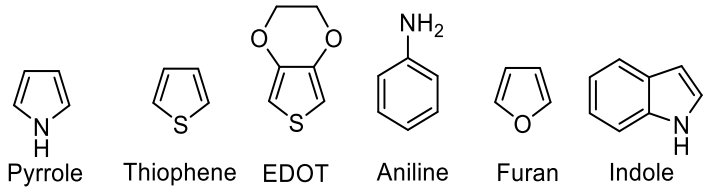

Figure 1.5 – Structure of different resonance-stabilises aromatic molecules that can undergo chemical or electrochemical oxidation to produce conducting polymers.

The reduction of p-doped conducting polymers, with simultaneous anion leaving or electrolyte cation incorporation, removes the electronic conjugation to yield the undoped electrically neutral insulating form [11,14,17]. In this way, the intrinsic optical properties of these materials are dependent on the energy gap between the valence band (highest occupied π-electron band) and conduction band (lowest unoccupied band) [11,16,17]. This characteristic becomes an advantage over the oxides because it allows fine tuning of band-gap through chemical modification. For example, polymers comprising intermediate bandgaps have different optical changes throughout the visible region and consequently they can display different colours by adequate choice of aromatic substituent groups [13,14]. Besides that, conducting polymers showed outstanding colouration efficiencies, fast switching responses, and multiple colours from the same materials [9]. For example, Reynolds and co-workers reported several polymers based on 3,4-dioxythiophene, which were used in electrochromic switches covering a large colour range (see Figure 1.6) [18]. Smart windows and displays are the most current potential applications for this class of electrochromic compounds [14].

Metal coordination complexes as electrochromic materials have great interest due to their intense colouration and redox activity [11,16]. These properties can be attributed to low-energy metal-to-ligand charge-transfer (MLCT) and, intervalence charge-transfer (IVCT) transitions, as well as intra-ligand excitation and related visible-region electronic transitions. Consequently, these chromophoric properties can be altered or eliminated upon oxidation or reduction, due to the fact that these transitions involve valence electrons [13,14]. These complexes, as well as polymers, have been also tested as type III electrochromic materials (see definition below) in all-solid-sate devices. In spite of their spectroscopic and redox properties would be enough for direct use in liquid electrochromic devices and thin-film systems [13,14]. This type of compounds are described as potential useful for switchable mirrors and near-infrared switching [14].

Phthalocyanines are tetra-azatetrabenzo derivatives of porphyrins, which are strongly coloured, possessing highly delocalised π-electron systems. Metal phathalocyanines possessing a metal ion either at the centre of a single phthalocyanine ligand, or between two rings in a sandwich-type complex, have been explored due to their electrochromic properties. Usually, the phthalocyanine complexes of transition metals comprise only a single phthalocyanine (di-anion) ring. Whereas, the phthalocyanine lanthanide complexes allow the formation of bis(phthalocyanines) structures, in which the π systems interact strongly with each other [16].

1. Introduction

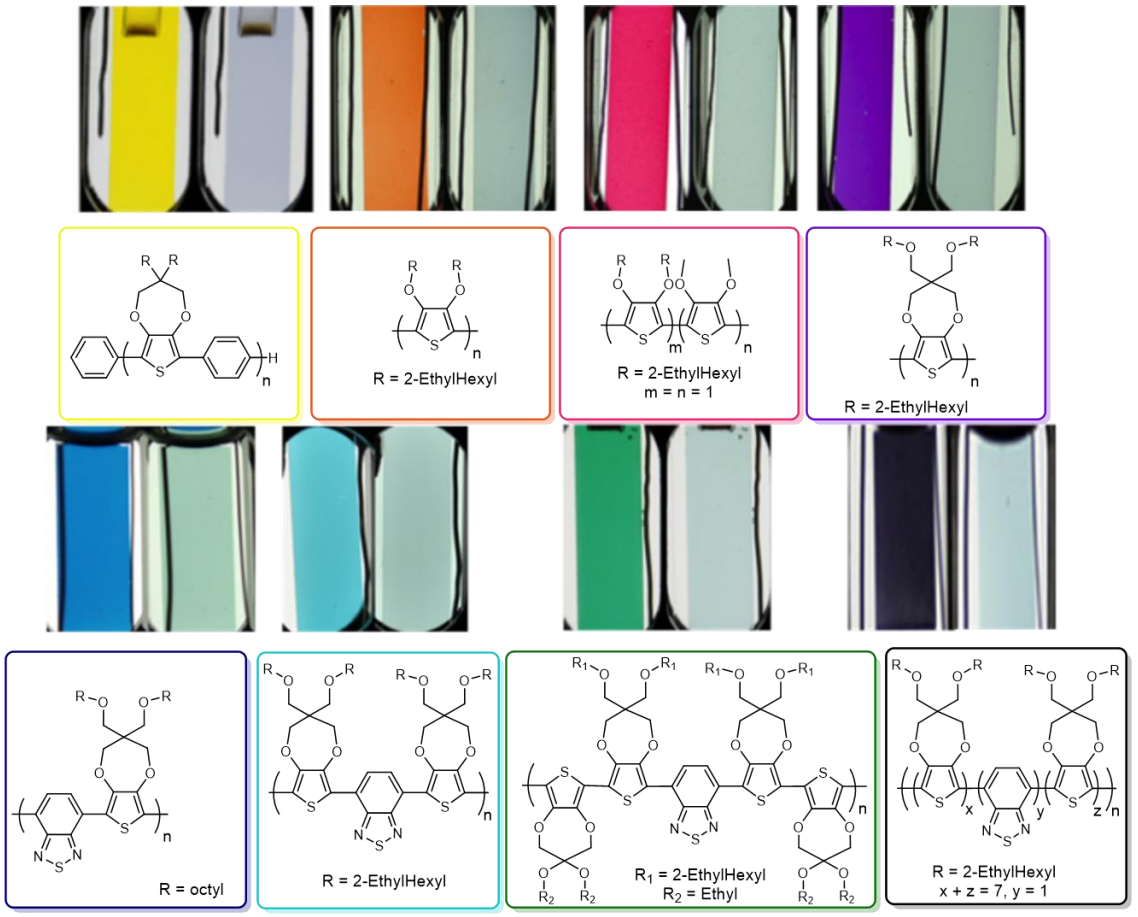

Figure 1.6 – Colour switches of different dioxythiophene derivatives [18]. (Source: Reynolds Group – https://ww2.chemistry.gatech.edu/reynolds/ECP, accessed in September of 2016).

The electrochromic materials can be classified into three types (type I, II and III) depending on the solubility of each redox state. The type I corresponds to electrochromes that are soluble in both reduced and oxidized states, i.e. the coloured species remain in solution at all time during electrochromic usage [9,11,13]. An example is the methylviologen (MV) in aqueous solution, which presents colour during a reductive electrode process [11]. Other examples include viologens that are often soluble in aqueous solution and phenothiazine such as methylene blue in non-aqueous solutions [11]. Type I electrochromes can be used in cars, as anti-dazzle and rear-view mirrors [9]. In type II, the electrochromic materials are soluble in one redox state (colourless form) but the coloured product forms a solid on the surface of the electrode followed by electron-transfer process [9,11,13]. It is described that this phase change contributes to increases the write-erase (coloured-colourless) efficiency and response time of the electrochromic bleaching [11]. Examples of type II system include aqueous cyanophenyl, heptyl or benzyl viologens systems or methoxyfluorene compounds in acetonitrile solution [11]. The solid products of electrodeposited metals such as bismuth is a common example of inorganic electrochromes type II [11]. This type of electrochromes can be used in larger mirror for commercial vehicles [9]. Finally, the type III electrochromic materials are solid in both or all redox states. The most suitable example includes metal oxides, such as tungsten oxide (WO_3). Other examples are polymeric viologens, conjugated conducting polymers such as polyanilines, polypyrroles and polythiophenes, metallopolymers,

metal hexacyanometallate such as Prussian blue and electroactive polymers based metal-*salen* complexes [9,11,13,19]. In general, these electrochromes are studied as thin films on electrode surfaces [9,11,13,19]. This type of electrochromes can be used in smart windows [9]. It is reported that the type II and III electrochromic materials showed an optical memory effect, once after electron-transfer process, no further charge injection is required in order to retain the new electrochromic state (coloured). Contrarily, the type I needs to keep current flowing until the whole solution has been electrolyzed due to the diffusion of the soluble product electrochemically generated from the electrode [13].

Nowadays, the electrochromic materials have been attracted much attention in academia and industry due to their properties and commercial applications [20]. However, the number of applications are reduced, except the amazing success of antiglare car mirrors (*Gentex)* and the adjustable-darkening windows of the *Boeing Dreamliner aircraft* [21]. Recently, the provision of large-scale electrochomic smart windows/glazing for buildings at modest costs is the ultimate goal of the investigation. Other commercial applications such as electrochromic strips as battery state-of-charge indicators, electrochromic sunglasses have been also explored. The reusable price labels, protective eyewear, controllable aircraft canopies, glare-reduction systems for offices, devices for frozen-food monitoring, camouflage materials, chameleonic fabrics, spacecraft thermal control, an optical iris for a camera lens and (non-emissive) controllable light-reflective or light-transmissive display devices for optical information and storage as potential commercial applications have been also explored [21].

1.2.2. Photochromic Materials

Photochromic materials are materials that show a reversible change of colour induced by light excitation. It is a reversible photo-induced transformation of the molecule between two states, with different geometrical and electronic structures [9,22]. These molecular structures changes may lead to significantly different physical properties such as their absorption and fluorescence spectra, refractive index, polarizability, electrical conductivity and magnetism. The photo-switching of these physical properties can be modulated by adequate design of the molecules [22]. Consequently, more sophisticated photochromic systems can be obtained [22].

For example, a thermodynamically stable form A is converted to B leading to an equilibrium designed as photo-stationary state by light excitation and B can revert to the initial state (A) by altering or removing the light source (Figure 1.7) [9,10]. If the back reaction (B to A) is photo-induced, i.e. photochemically reversible but thermally irreversible [23], it is classified as type P photochromism. On the contrary, when the back reaction occurs by removing the light source, i.e. thermally reversible, it is classified as type T photochromism [9].

Photochromism can be found in organic and inorganic materials, as well as in inorganic-organic hybrid materials, i.e. synergy of both material classes [10].

1. Introduction

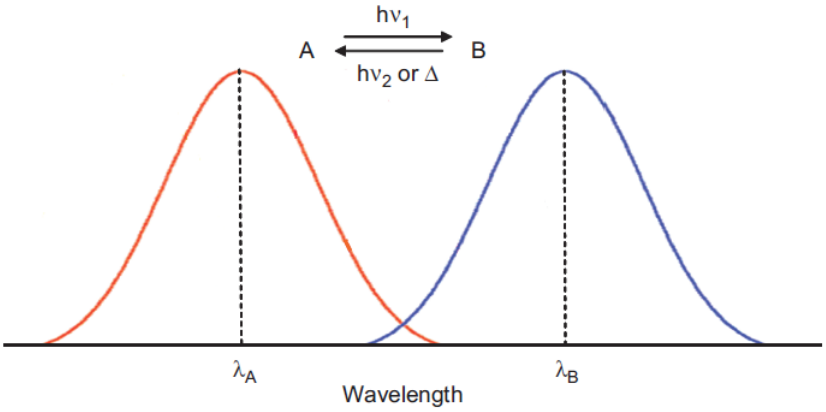

Figure 1.7 – Reversible Photochromism [9]. (Source: *Chromic Phenomena: Technological Applications of Colour Chemistry*, The Royal Society of Chemistry, 2nd ed., 2010, pp. 9–140).

The most widely inorganic photochromic materials already explored are silver halides. These are mostly transparent monocrystalline materials and when UV light is absorbed, the particles generate electron-hole pairs and react to form silver atoms (coloured), and this process repeats itself as long as the UV light is presented [10]. Simultaneously, silver is oxidized back to silver ions and a kinetic equilibrium is reached. It is also reported that the colour is dependent on the size of silver halide particles [10]. A successful application of this class of materials involves ophthalmic lenses with photochromic properties, where the silver halide crystals are trapped in a glass matrix have been described [9]. This type of material has remarkable fatigue-resistant properties comparing to other photochromic systems, which makes them ideal candidates for photonic applications. However, they have poor darkening (low colour contrast) and slow fading [9]. It is also reported that different transition-metal oxides such as tungsten oxide, molybdenum oxide, vanadium pentoxide, among others can exhibit photochromism upon band-gap excitation [9]. In the case of these oxides, it is possible to distinguish between thermochromic and photochromic effects by visible light irradiation [9,24].

The inorganic-organic hybrids result from the combination of inorganic and organic classes; this means that they combine the thermal stability as well as diverse coordination chemistry of inorganic compounds with the versatility of organic compounds [10]. The metal complexes from triphenylmethane and fluoran derivative dyes are good examples of this class of compounds. They show photochromic properties, usually tunable by the selected metal ion but they also display an irreversible photodegradation of the dyes upon exposure to light [10].

In general, organic photochromism involves the transformation between two isomers induced by light. This conversion can occur via isomerisation of a double bond or a transformation between two isomers by ring-opening or ring-closing reactions [10]. The most common classes of organic photochromic molecules are azobenzenes, spiropyrans, fulgide, diarylethenes and flavylium derivatives (Scheme 1.2) [9,25].

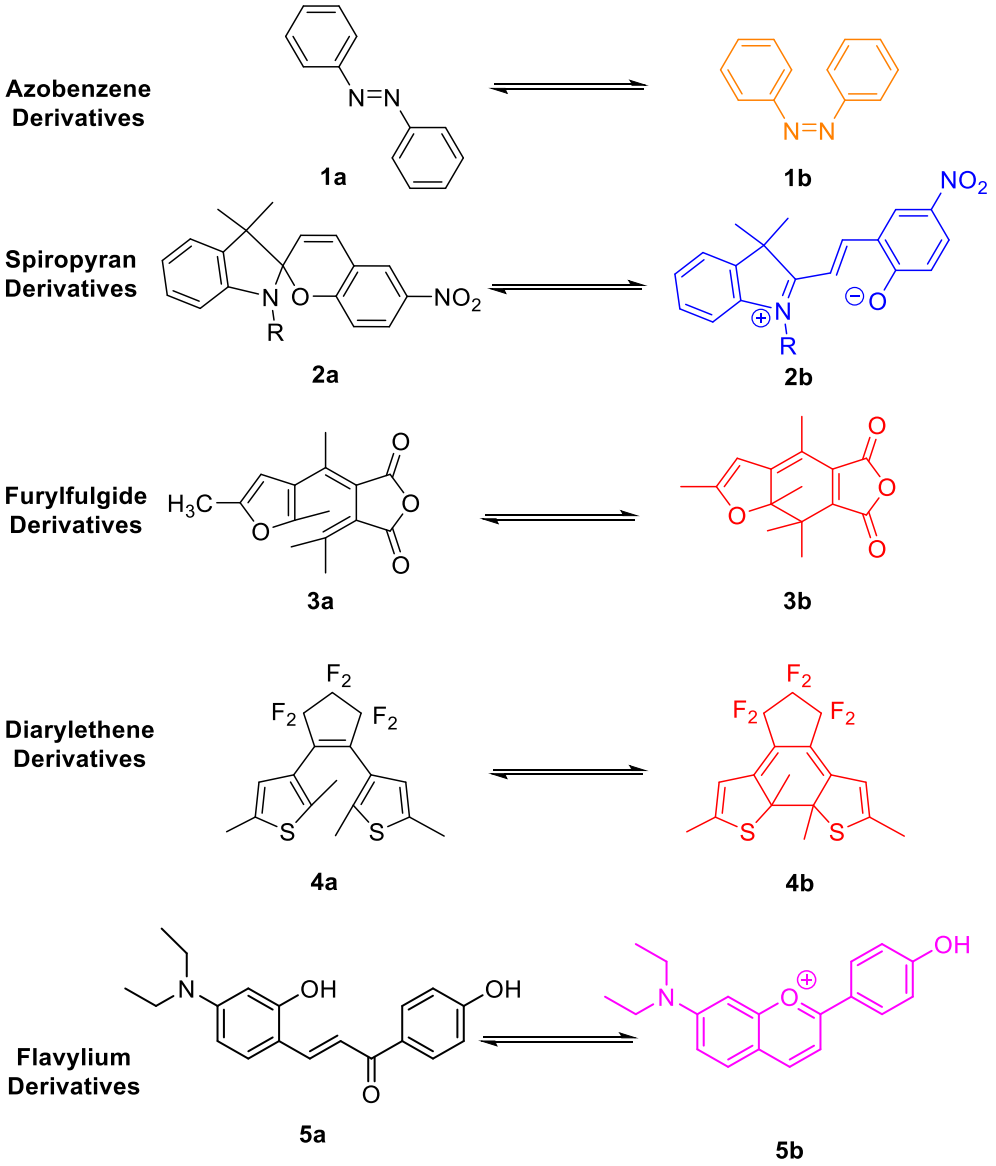

Scheme 1.2 – Typical examples of organic photochromic molecules [23,26]. (Source: *Chem. Rev.*, 2014, **114**, 12174–12277 and *J. Phys. Chem. B*, 2007, **111**, 12059–12065).

In Scheme 1.2, the azobenzene derivative (1) and spiropyran derivative (2) upon irradiation with ultraviolet (UV) light, a change in colour from yellow or colourless to orange and blue, respectively, is visible due to photo-induced transformation from left-side isomers (a) to right-side ones (b) [23]. In these cases, the colour of the photogenerated isomers (1b and 2b) disappear in the dark at room temperature, i.e. they are thermally unstable and these molecules are classified as type T photochromic molecules. On the contrary, the photo-generated isomers from furylfulgide (3) and diarylethene (4) derivatives are thermally stable and hardly turn back to the initial state (left-side isomer) in the dark at room temperature. They are classified into type P photochromic molecules and it showed a change of colour upon irradiation with UV light from colourless to red [23]. In the case of flavylium derivatives (5), the *trans*-chalcone (5a, Ct) in aqueous media at pH ~ 4.3 presents a yellow colour and it is interconverted in flavylium cation (5b, AH^+) upon irradiation with visible light. The system turns back to Ct thermally.

1. Introduction

The azobenzene family is constituted by diazene (HN=NH) derivatives, where both hydrogens are replaced by phenyl groups. These compounds, can undergo light-induced *trans-cis* isomerisation, which can be reversed by either light or thermally in the dark [9,27]. The spectroscopic properties and isomerisation mechanism can be tuned by additional substituents on the azobenzene ring [27]. There are reported several applications of this class of compounds, such as light triggered switch in a variety of polymers, surface-modified materials, protein probes and others [27].

The spiropyran derivatives constitute a class of photochromic compounds that undergo reversible photochemical cleavage of the C-O bond in the spiropyran ring, followed by the rearrangement of the molecule to give a coloured open-ring merocyanine [9,25,28].

The fulgides derivatives undergo reversibly *cis-trans* isomerisation followed by electrocyclic ring-closure and ring-opening reactions [29].

Diarylethenes are a class of photochromic molecules developed by different research groups. In particular, Irie and co-workers have been focused in the synthesis of stilbene derivatives in high to moderate yields and purity levels. This class of photochromic compounds showed a reversible transformation between the open-ring isomer, generally colourless, and the coloured ring-closed isomer induced by light. The ring-closed isomer can acquire different colours (yellow, red or blue) depending on the molecular structure [22,23]. Also, they showed thermal stability of both isomers, fatigue-resistant properties, high sensitivity, fast response and reactivity in solid state. Potential applications already described in the literature include their use in optical memories, colour switches, and actuators (or molecular machines) [23].

Flavylium salts are synthetic compounds similar to natural anthocyanins and they can readily interconvert into different species in aqueous solution, using different controlled stimuli, such as pH jumps and light [30,31]. At very acidic pH values, the flavylium cation (AH^+) is the most stable species. When pH is increased other forms are observed, in particular the photoreactive *trans*-chalcone (Ct) [30–32].

As already mentioned, photochromic molecules change their geometrical and electronic structures upon photoirradiation, leading to changes on physical properties of photogenerated isomer. These molecules can be applied in photonic devices, such as erasable optical memory media and photo-switching devices [23]. For these kind of applications, the photochromic molecules should have some relevant properties including high thermal stability of both isomers, fatigue-resistant properties (higher repeatable cycle number without significant loss of performance), high sensitivity, fast response and reactivity in solid state [23]. However, all these properties can be hardly to fulfil. For example, usually the photogenerated coloured isomer is thermally unstable and turn back to the initial state in the dark (T type of photochromic molecules). In the literature, different publications reported attempts to stabilise the photogenerated isomer by dispersing the photogenerated unstable isomers in polymeric matrices, with higher glass transition temperature (T_g). However, the achieved stability after these chemical manipulations is not enough for practical applications. Aggregate formation to stabilise the coloured isomers is another approach described

in the literature [33]. However, the results showed that the reversibility obtained for the system is poor [33]. Therefore, the development of intrinsically stable photochromic molecules in both isomers becomes desirable. In this way, furylfulgides and diarylethenes containing heterocyclic aryl groups gained much attention, due to their thermal stability; they are considered a P-type photochromic molecules. In general, the furylfulgides showed limited fatigue-resistant properties (less than 100 colouration-decolouration cycles) comparing to diarylethenes [33].
The most remarkable commercial applications of photochromic materials are centred in ophthalmic field, particularly in lenses for sunglasses. Additionally, a growing list of other potential applications such as cosmetic products, optical memories for data storage, photo-optical switches, filters, displays, among others are starting to be explored [9]. For most commercial applications, the photochromic molecules should present some requirements in particular a strong colour rapidly upon irradiation with UV light and the reaction back to colourless must be controllable and if possible must be colourless or having the minimum colour as possible. The range of colours must be on the visible spectrum and the response time must remain reproductive during several colouration-decolouration cycles [9]. There is reported that diarilethenes and spiropyrans can be excellent candidates, possessing many of these ideal requirements [9].

In general, the most studied chromogenic (photo- and electrochromic) molecules are neutral and the incorporation of permanent charges can be an advantage in order to tune their properties. In this way, the possibility to combine these structures as cations or anions with adequate counter-ions can be explored. Novel chromogenic salts or ionic liquids appears as interesting alternative for their intrinsically application as multi-stimuli chromogenic devices.
Herein, we are interested to combine those two worlds, i.e. take advantage of the peculiar properties of ionic liquids (e.g higher thermal and chemical stability; large electrochemical window; higher ionic conductivity as well as the possibility to tune the final physical-chemical properties according suitable cation-anion combinations) with the well-known properties from common chromogenic materials.

1.3. Ionic Liquids

Ionic liquids (ILs) can be defined as low-melting organic salts, conventionally lower than 100 ºC and often below room temperature, which can be classified as room temperature ionic liquids (RTILs) [34,35]. ILs are composed only by ions, usually big, bulky organic cations and smaller organic or inorganic anions (see Figure 1.8).

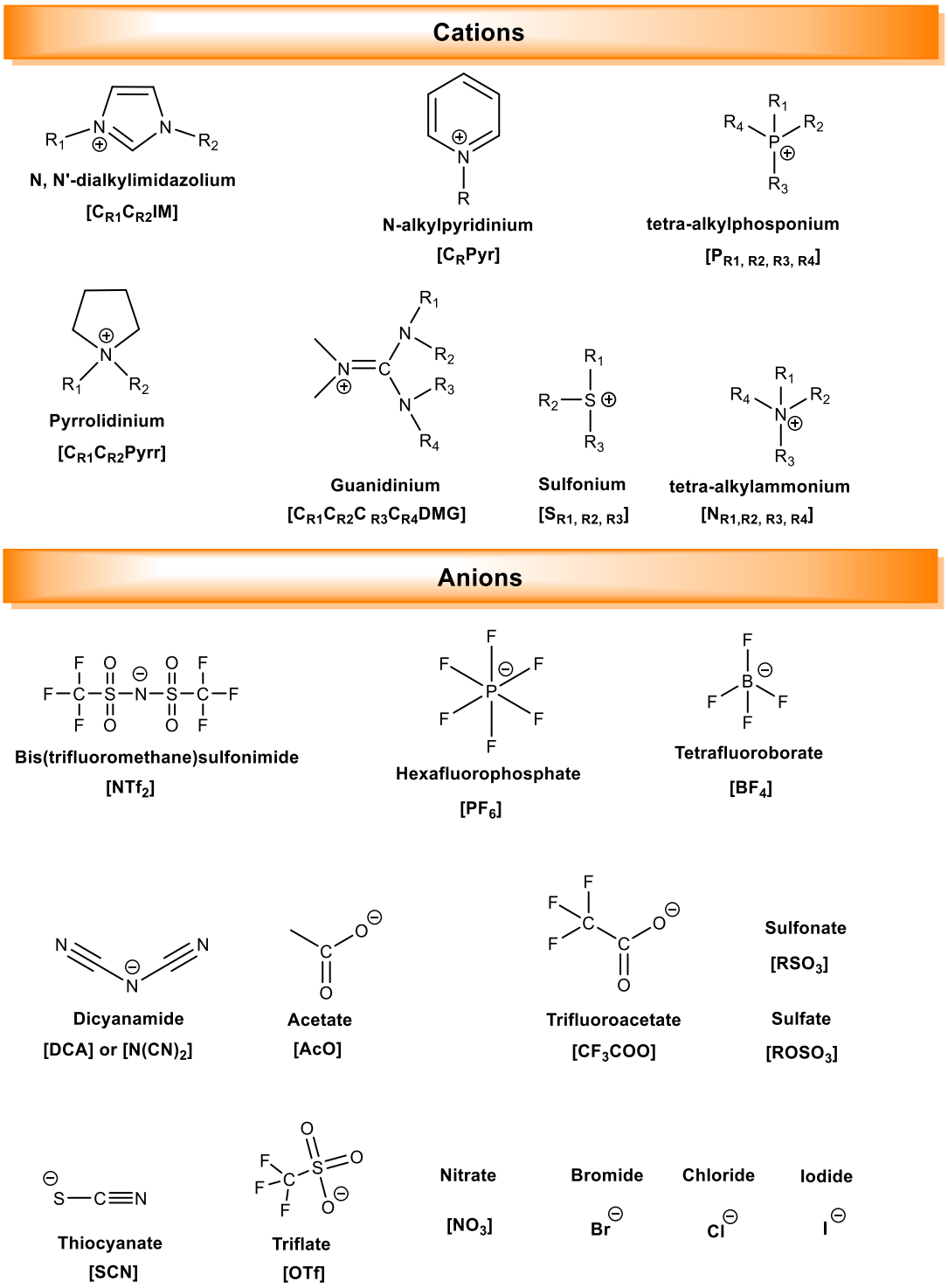

Figure 1.8 – Typical examples of cation and anion pairs used to form ionic liquids.

One of the first IL was reported by Paul Walden in 1914 [36]. He observed that the ethylammonium nitrate ([$EtNH_3$][NO_3]) is liquid at room temperature, with a melting point between 13 – 14 ºC. This salt is formed through neutralization reaction of ethylamine with concentrated nitric acid [36].

Recently, ionic liquids have received much attention, mainly due to their peculiar properties such as higher chemical and thermal stability, almost negligible vapour pressure, high ionic conductivity, large electrochemical window and excellent dissolution performance of organic, inorganic and polymeric materials, including biopolymers such as cellulose, as a result from their structures [34–36]. It should be mentioned that a few number of ILs can be distilled at low pressure without decomposition as reported by Rebelo and co-workers [37]. In particular, they demonstrated that the most commonly aprotic ILs families can be distilled at 200 – 300 ºC and low pressure [37]. The recovery of significant amounts of pure IL through re-condensation at lower temperatures, without any signs of degradation either in the distillate or the residue can be achieved [37].

As already mentioned, ILs are formed only by ions and therefore, their properties such as melting point, viscosity, density and hydrophobicity can be controlled by the suitable selection of both cation and anion [34–36]. An extremely large number of cation-anion combinations can be explored, offering opportunities to control specific properties, depending of the desired application [34–36]. For that reason, theoretical investigation became an important and interesting tool for the prediction of IL properties and anion-cation interactions studies, helping to understand the experimental determinations [38].

ILs are considered to be polar solvents and depending on the type of anion can be non-coordinating. The water miscibility of ILs can be modified from complete miscible to almost immiscible by adjusting the anion nature (see Figure 1.8). For example, if chloride is replaced for hexafluorophosphate [PF_6] anion, the salt becomes almost water immiscible [35].

In general, ILs can be prepared by two synthetic steps: the formation of the desired cation, followed by anion exchange reaction in order to form the desired product [39]. In some cases, only the preparation of the desired cation is required, for example the synthesis of ethylammonium nitrate. In this case, the preparation of the cation can be achieved by protonation with a free acid or by quaternization reaction mainly of an amine or a phosphine, usually in the presence of haloalkane [39]. When the desired cation is commercially available at reasonable cost, normally as halide form, only the anion exchange reaction is required, for example for the preparation of tetraalkylammonium salts [39]. The anion exchange reactions can be divided in different synthetic routes: direct treatment of halide salts with Lewis acids (e.g. $AlCl_3$), anion metathesis or acid-base neutralization reactions [39,40]. In the first case, it is usually a simple mixing of the Lewis acid and the halide salt resulting in the IL, and usually it is an exothermic reaction [39]. The second approach consists in metathesis reaction from halide or similar salt of the desired cation and it can be divided into two different categories depending on the water solubility of the desired IL: (1) free acids or group 1 metals/ammonium salts and (2) silver (Ag) salt metathesis [41]. The general synthetic routes as well as purification of imidazolium ILs is illustrated in Scheme 1.3.

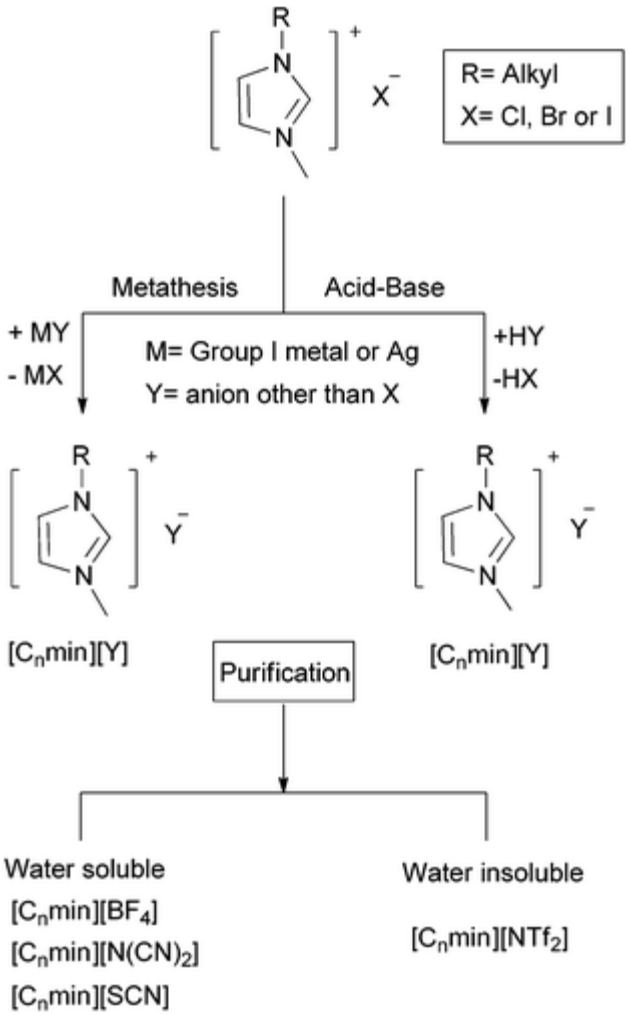

Scheme 1.3 – General procedure for the synthesis of imidazolium ILs [42]. (Source: *Green Chem*., 2013, **15**, 1341–1347).

The preparation of water soluble ILs can be a challenging process, once the separation of the desired and undesired salts can be complex [39]. The utilization of silver salts can be an appreciable alternative to prepare many water soluble salts with very high purities. However, this methodology is clearly too expensive to use in large scale processes [39]. In the case of water-immiscible ILs the purification step is more easily than correspondent water-soluble ILs [39]. Usually, when the reaction is performed in water, the desired hydrophobic ILs can be isolated through liquid-liquid phase separation.

The purification step can be a quite challenging, once the organic starting materials, volatile solvents, halide impurities and water content should be efficiently removed in order to obtain IL with higher purity levels [36,39,43]. It should be mentioned that the ILs, even that with hydrophobic character has the tendency to absorb water [36,39,43]. To remove water effectively from ILs, high temperatures and vacuum conditions are required. Similar to the water content, other impurities such as halide content have a great impact on the IL properties such as ionic conductivity, viscosity, among others and their functionality can be dramatically affected [36,39,43].

ILs appears as alternative to the conventional organic solvents possessing the possibility to tune the final properties according to the desired application. Indeed, they have been described

as "*designer solvents*" [25,44,45]. Also, ILs seem to have significant ability to dissolve organic, inorganic and polymeric materials, as previously mentioned [46,47]. Plechkova and Seddon reported a comparative property study between conventional organic solvents with ILs (Table 1.1).

Table 1.1 – Brief visual comparison of organic solvents with ILs [a], [36]. (Source: *Chem. Soc. Rev.*, 2008, **37**, 123–150).

Property	Organic solvents	Ionic liquids
Number of solvents	>1000	>1.000.000
Applicability	Single function	Multifunction
Catalytic ability	Rare	Common and tuneable
Chirality	Rare	Common and tuneable
Vapour pressure	Obeys the Clausius – Clapeyron equation	Negligible vapour pressure under normal conditions
Flammability	Usually flammable	Usually non-flammable
Solvation	Weak solvating	Strongly solvating
Polarity	Conventional polarity concepts apply	Polarity concept questionable
Tuneability	Limited range of solvents available	Virtually unlimited range means "*designer solvents*"
Cost	Normally cheap	Typically, between 2 and 100 times the cost of organic solvents
Recyclability	Green imperative	Economic imperative
Viscosity (cP)	0.2 – 100	22 – 40.000
Density (g. cm^{-3})	0.6 – 1.7	0.8 – 3.3
Refractive index	1.3 – 1.6	1.5 – 2.2

[a] The data summarised in this table are not comprehensive, nor do they represent outliers; they are meant to give a brief visual comparison of typical values.

The ILs can be divided in three generations [48]. The first generation corresponds to the earliest examples of RTILs, named as haloaluminate ILs. These ILs result from the reaction between halide salts with Lewis acids as reported by Hurley and Weir (1951). They demonstrated that aluminium chloride ($AlCl_3$) combined with 1-butylpyridinium halides in the relative molar proportions (1:2) produce a liquid at room temperature [48,49]. Later on, Wilkes and co-workers reported the dialkylimidazolium choroaluminates, which are also RTILs [48,49]. These ILs have been studied as solvent and catalyst in Friedel-Craft and other reactions. However, they react with water, as a consequence it needed to be handled in a dry-box [48]. The second generation is related with the non-haloaluminate ILs that are air- and water-stable. Wilkes and Zaworotko (1992) reported the first examples based on 1-ethyl-3-methylimidazolium cation, which it was combined with different anions such as tetrafluoroborate anion [48,50]. Posteriorly, it was observed that these ILs undergo hydrolysis under certain conditions and the toxic and corrosive hydrogen fluoride was formed as decomposition product [48,51]. Dialkylimidazolium ILs, which are combined with hydrophobic anion such as bis(trifluoromethylsulfonyl)imide ($[NTf_2]$) were reported by Bonhôte, Grätzel and co-workers (1996) [48,52]. These ILs have been investigated as reaction media in

different organic reactions. Finally, the third generation, also named as Task Specific Ionic Liquid (TSIL) or functionalized IL was introduced by Davis (2004) [53]. This generation consist on the functionalized cation or anion with a particular property to form an IL, normally for a specific application [53,54]. The functional group with particular properties or reactivities can be covalently incorporated into anion, cation or both [53,55].

Rogers and co-workers (2007) proposed that ILs can be alternatively divided also in three generations but according to their properties and applications [56]. So, the generation one corresponds to the ILs used as solvents, with unique and accessible tunable physical properties, such as melting point, thermal stability, conductivity and others [56]. In this sequence, the generation two corresponds to the ILs with targeted chemical properties such as electrochemical windows, oxygen balance, high energy balance and others combined with chosen physical properties [56]. So, these ILs provide the possibility of modified independently the properties of both cation and anion, allowing the design of new functional materials. This generation of ILs has potential application as energetic materials, lubricants, metal ion complexation and others [56]. Finally, the generation three is related with targeted biological properties, such as antibacterial, emollient, anti-inflammatory drug and others combined with chosen physical and chemical properties [56]. In this generation, biological activity is considered as the primary IL property and they can be considered as tunable active pharmaceutical ingredients (APIs) with novel performance enhancement, for example in solubility, bioavailability, elimination of polymorphism and delivery options [56]. These three generations of ILs as well as its respective examples are illustrated in Figure 1.9.

ILs have produced a great impact in chemistry, physics, and materials science due to the conceptual innovation and technological breakthroughs in the past two decades. Therefore, they have a broadest range of possible applications such as solvents or co-catalysts in different chemical reactions [40,45,54], extractive and separation media [45,57–59], functional materials [54,60,61] and active pharmaceutical ingredients (APIs) [56]. Due to the specific properties of ILs, such as high ionic conductivity, non-volatility and non-flammability, they become very attractive for use in electrochemistry field, namely in solar cells, batteries, capacitors, among others [34]. In particular, ILs have been tested as alternative electrolytes in semiconductors, batteries, fuels cells and solar cells [62]. In the Figure 1.10 is illustrated the three mainly fields of ILs as well as examples of possible applications.

In the last years, there are reported several examples of the use of ILs as alternative solvent in organic synthetic transformations and several catalytic reactions, such as Heck, Friedel-Crafts, Baylis-Hilmann, Diels-Alder, Wittig, Aldol and Michael reactions, among others [63]. In general, ILs can be an alternative to the conventional organic solvents, once it can decrease the reaction time, improve the purification steps (e.g. extraction with supercritical CO_2 or phase separation) and increase the product yields [63].

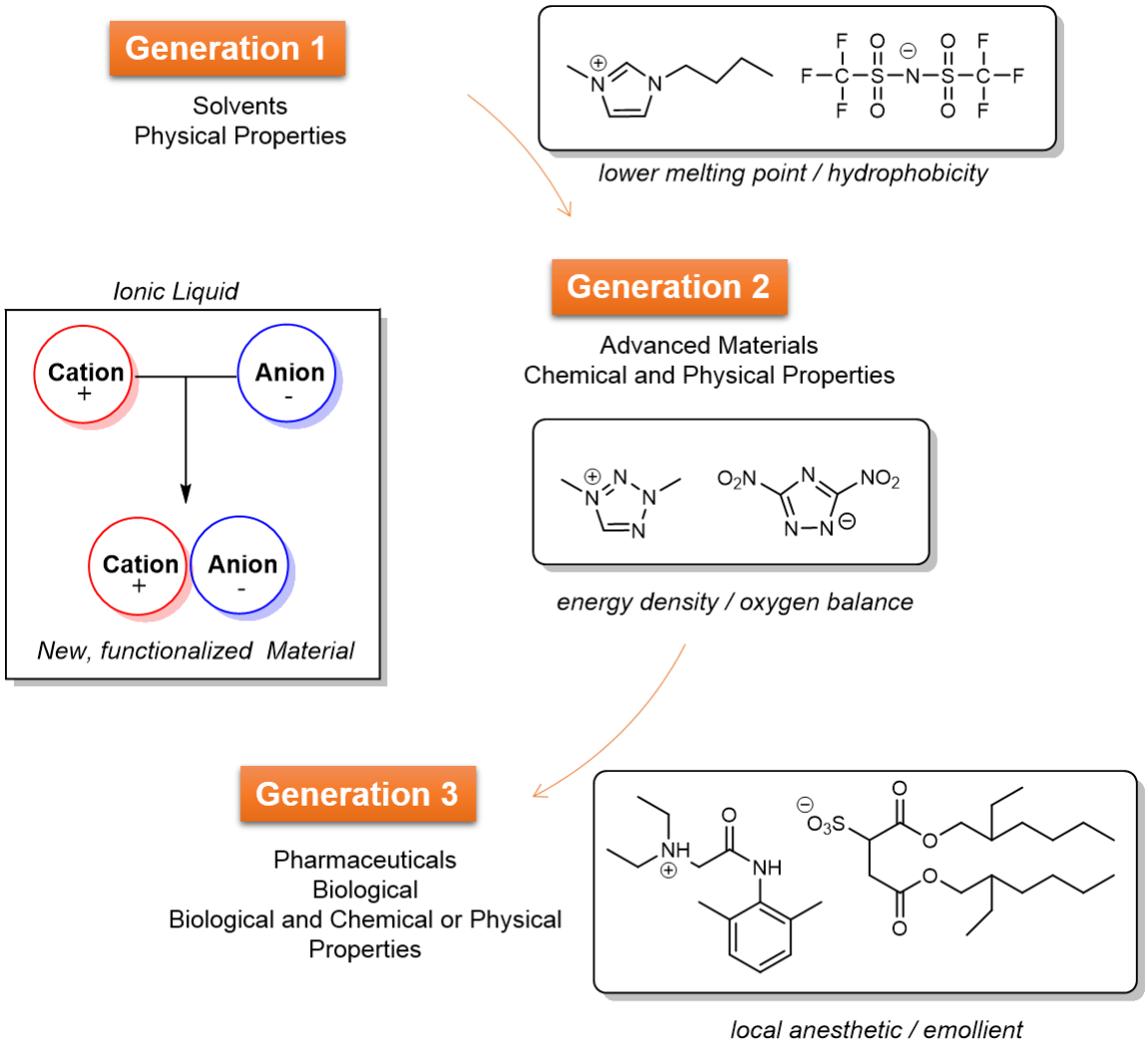

Figure 1.9 – Three generations proposed by Rogers and co-workers [56]. (Source: *New J. Chem.*, 2007, **31**, 1429–1436).

ILs have been extensively studied in homogeneous and heterogeneous catalysis taking advantage the higher stabilization and solubility of the catalysts in IL media. Additionally, the recyclability and re-use of the catalyst as well as the product purification can be significantly improved using IL approach [64–66].

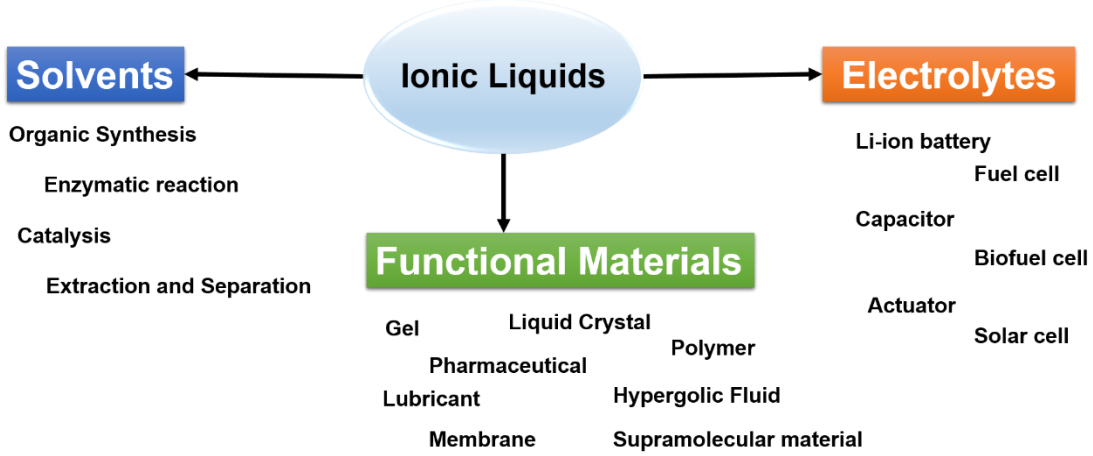

Figure 1.10 – Three mainly fields of ILs and some possible applications.

1. Introduction

In general, many transition metal complexes can be dissolved and stabilised in IL media. In this context, ILs also became an attractive alternative due to their properties such as negligible vapour pressure that allows environmental and safety manipulation of transition metal catalysts. They also can improve the catalytic activity and the possibility for efficient catalyst separation, recovery and recycling [63,67]. There are reported several attempts to improve the efficiency of the IL and catalyst recycling and it can be associated to the desired product removal by extraction processes [67]. Usually, it is described the use of organic solvents such as alkanes and ethers, which can dissolve the desired product but not the IL and catalyst. More recently, the use of supercritical CO_2 has been investigated as more sustainable and efficient extraction process, once it was found that ILs have lower solubility in supercritical CO_2, whereas the supercritical CO_2 has higher solubility in ILs [66].

Recently, the introduction of task-specific functionalities into ILs such as Brønsted acidic groups and heteroatom donors to target specific properties can open new perspectives for new and/or improved processes and strategies [68]. The development of supported ILs, where the catalysts is incorporated on the cation or anion (or both) [69] as well as chiral ILs for asymmetric synthesis [70,71] have been largely explored.

There is also reported the use of ILs in inorganic synthesis [72], polymer synthesis [73] and biocatalytic reactions [74]. For example, in biocatalysis, ILs can be used as pure solvent or co-solvent due to their capacity to stabilise different enzymatic processes [75]. The reactions can be performed in two-phase water-IL mixtures, where whole cells are suspended or a free enzyme dissolved in a water phase and the substrate in a hydrophobic IL phase [74]. Alternatively, a free enzyme dissolved in the mixture between water and a hydrophilic IL (single phase) or in pure IL, using an immobilized enzyme or dissolved free enzyme can be also performed [74].

ILs have been also investigated in pharmaceutical applications as alternative solvent in different pharmaceutical synthesis, in extraction processes for removal of drugs from aqueous solutions and in drug delivery [76]. Recently, novel active pharmaceutical ingredients based on ionic liquids (API-ILs) are reported with a significant improvement of the original drug solubility in water and biological fluids as well as their permeability, bioavailability and polymorphism effect [76].
However, the toxicity and biodegradability related to the ILs are important parameters to consider for future applications of API-ILs in medicine [77,78]. In this context, additional biological studies should be required. It is important to develop low toxic ILs by suitable combination of biocompatible cations and anions [79].

ILs have been also explored in analytical chemistry, mainly in separation and extraction processes, such as liquid-liquid extraction, additives for NMR, matrices for MALDI as well as their use in HPLC and GLC techniques [80]. Others examples of ILs applications are the quantitative and selective recovery of solutes from ILs by pervaporation using a non-porous membranes with the selective layer containing hydrophilic or hydrophobic polymers [81], supported ionic liquid membranes (SILMs), which contains the RTIL for highly selective transport of organic compounds

[58] and gas separation processes such CO_2 from N_2 and CH_4 mixtures [82], CO_2 capture [83,84], aqueous biphasic system for selective separation and extraction processes [85].

The implementation of IL technology in industrial processes in spite of the issues associated to the ILs commercialization, such as cost, have been reported [36]. One of the most successful example is Biphasic Acid Scavenging Utilising Ionic Liquids (BASIL) process developed by BASF, which produce alkoxyphenylphosphines as precursors for the synthesis of photoinitiators [36,86]. This product is obtained by the reaction of chlorophenylphosphines with alcohols and as a consequence amounts of acid are produced in the course of the reaction. For that reason, in the original process, triethylamine was typically used to scavenge the acid, leading to the production of a solid ammonium salt (triethylammonium chloride) [36]. The formation of this by-product leads to some problems during the process, such as reduction of heat transfer and reaction rates as well as reduction of yields and solid separation, once a dense insoluble past is formed [36,86]. The replace of triethylamine with 1-methylimidazolium leads to the formation of an IL (1-methylimidazolium chloride) in the course of the reaction, improving the separation step, once it is a liquid (melting point of 75 ºC) at the reaction temperature (~ 80 ºC). This by-product can be easily removed through liquid-liquid phase separation and it is possible recovery 1-methylimidazolium by deprotonation [86].
In this context, ILs contribute to improve the reaction rate, increase yields and selectivity and it is economically cost efficient process [86]. Interestingly, Merck® developed an electrolyte mixture using IL as solvent in order to dissolve the electrolyte redox system (iodine, iodides and additives) for dye-sensitized solar cells (DSSC) [87,88].

1.3.1. Task-Specific Ionic Liquids

In the last years, ILs gained much interesting in different research fields, especially due to their particular properties, involving high electrical conductivity, extended liquid-state temperature range, wide electrochemical windows (up to 5.8 V), negligible vapour pressure and others [34–36]. Besides that, the possibility to easily tune their physical and chemical properties (generation 2, according to Rogers proposal) by changing the nature of anion, cation or both, are very attractive [34–36,56]. As already mentioned, the functional group is covalently tethered to the cation, anion or both of the IL species.

It was reported several examples of the use of ILs as solvents to study photochromic molecules, but also the development of ILs intrinsically photochromic by incorporation of this functionality on the cation or anion [25]. When ILs are applied as solvent it is possible study the influence of these ILs in the performance of the photochromic molecules but also in the photo-induced step, which gives the photoproduct or in the thermal back reaction [25]. There are reported different studies where pure ILs are used as solvent to dissolve different photochromic molecules, such as *trans*-stilbene, spiropyran, diarylethenes [25].
Ozawa and Hamaguchi (2001) reported their investigation about photoisomerisation of *trans*-stilbene in a RTIL, 1-butyl-3-methylimidazolium hexafluorophosphate ([BMIM][PF_6]) [89]. They

observed through steady state irradiation, which was followed by UV absorption that the formation of the *cis-trans* isomerisation occurs in IL media, even despite being viscous [25,89]. Other example is nitrobenzospiropyran derivatives, which have been studied in different organic solvents. These studies showed that the back thermal reaction decreases with increasing of the polarity of the solvent due to the zwiterionic character of merocyanine species, which is stabilised in polar solvents, contrarily to the closed form that is stabilised in non-polar solvents [25]. Several ILs containing the same anion or cation combined with different counter-ions have been tested. In general, it was found similar behaviour relative to the organic solvents, occurring formation of merocyanine upon irradiation. It is also observed that in some cases the merocyanine is more stable and negative photochromism is observed, occurring formation of the spiropyran from the merocyanine [25]. There are also reported similar studies using other photochromic molecules. Additionally, there are examples of biphasic systems, using for example a hydrophobic IL (e.g. [BMIM][PF_6]) and water to study the photochromism of flavylium derivatives [25,30].

Different of diarylethene having *N*-heterocyclic carbenes (NHC) integrated in the diarylethene moiety have been reported by Yam and co-workers (2009) [25,90]. They developed a series of diarylethene NHC, containing an imidazolium unit, complexes with Au(I), Ag(I) and Pd(II) and a RTIL is obtained when [NTf_2] is used as anion [90]. They mentioned that this compound is photochromic but no further experimental data is available [25,90]. In the same year, Pina and Branco reported an intrinsically photochromic ILs using a well-known photochromic molecule, methyl orange that is an azobenezene derivative combined with appropriate organic cations [25,91]. When the sulfonium or phosphonium is used as cation a RTIL is obtained [25,91]. They studied the photochromism of these ILs in ethanol, matrixes of a Paraloid® B72 (an acrylic co-polymer) and as a tin films obtained by pressing the IL between two lamellae of quartz, allowing the use of pure RTILs without any additional solvent or polymeric matrix [25,91]. They observed that the thermal back reaction in ethanol depends strongly on the cation nature. In the case of ILs films, the structural organization of the ILs, specially its higher viscosity leads to slower isomerisation process [25,91]. There are also reported in the literature other examples of intrinsically photochromic ILs [25].

Previously, Hayashi and Hamaguchi (2004) reported the discovery of a magnetic IL, 1-butyl-3-methylimidazolium tetrachloroferrate, [BMIM][$FeCl_4$] [61]. They prepared this IL by simple mixing 1-butyl-3-methylimidazolium chloride [BMIM]Cl and iron (III) tetrachloride hexahydrated ($FeCl_3.6H_2O$) (see Figure 1.11).

Figure 1.11 – Response of the magnetic IL, [BMIM][$FeCl_4$] in water when a magnetic field is applied [61]. (Source: *Chem. Lett.*, 2004, 33, 1590–1591).

They observed that this IL showed a strongly response when a magnetic field is applied [61].

More recently, others magnetic ILs have been reported, where the anion, the cation or both of them contains paramagnetic properties [92,93]. The most common magnetic ILs reported is based on metal or lanthanide complexes as anion [92].

Pina and co-workers (2011) developed intrinsically electrochromic and magnetic ILs [94]. They prepared a variety of RTILs based on ethylenediaminetetraacetic metal complexes using cobalt(III), chromium (III) and iron(III) as metal, combined with 1-ethyl-3-methylimidazolium [EMIM], 1-butyl-3-methylimidazolium [BMIM], 1-octyl-3-methylimidazolium [OMIM], tri-octylmethylammonium [ALIQUAT] and tri-hexyltetradecylphosphonium [$P_{6,6,6,14}$] as cations [94].

For example, the RTIL [EMIM][CoEDTA] was studied as pure RTIL without any additional solvent and act as electrochromic materials and electrolyte simultaneously (Figure 1.12).

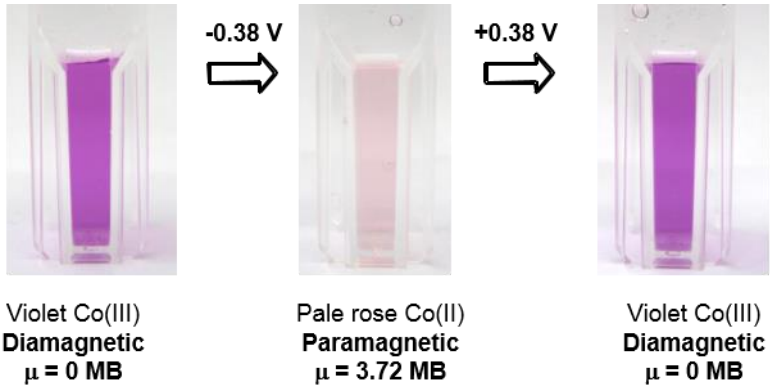

Figure 1.12 – Electrochromic and magnetic responses of [EMIM][Co(EDTA)] upon reduction/oxidation [94]. (Source: A. Branco, L. C. Branco and F. Pina, *Chem. Commun*., 2011, **47**, 2300–2302).

It presented a reversible switch of colour between violet to pale rose as well as a reversible switch from diamagnetic to paramagnetic upon reduction/oxidation [94]. They mentioned that these RTILs presented the peculiar properties of ILs together with the characteristics of electrochromic and magnetic materials used as starting materials [94]. Later on, the same group developed also an intrinsically electrochromic ILs based on vanadium oxides [95]. Herein, they demonstrated the potential application of these ILs as electrochrome material and electrolyte in liquid electrochromic cells [95]. The application of ILs as electrolyte or solvent for batteries, super-capacitors, actuators, DSSC and thermoelectrochemical cells have been also explored [96]. In the literature there are reported other examples of functionalized IL such as luminescent [97–101], photo-rheological [102], energetic [103,104], and among others.

1.4. Objectives

Nowadays, academic and industrial communities are very interested in the development and manufacture of stimuli-responsive materials that adopt or respond in real time to external changes and therefore adjust to our demands. The adequate combination of stimuli-responsive molecules with the remarkable properties of ionic liquids, especially task-specific ionic liquids is an interesting topic to explore.

In this context, this thesis is focused in the development and application of stimuli-responsive organic salts as functional and efficient devices. The external stimuli are based on the change in the pH, temperature, light and an applied electric potential. Subsequently, the innovative conversion of photo- and electrochromic salts into ionic polymers in order to improve their intrinsically chromogenic performance has been explored. Firstly, the organic electrochromic salts based on 4,4'-bipyridinium scaffold as well as ionic polymers and their possible application as electrochromic device are investigated. Then, ionic organic photochromic molecules based on diarylethene derivative and co-polymer containing flavylium scaffold have been developed. These classes of compounds can be tested as multi stimuli-responsive materials according to applied external stimuli. In particular, the diarylethene salts are simultaneously photochromic and electrochromic materials while co-polymer based flavylium responds to pH, light and temperature stimuli.

1.5. Thesis Outline

This thesis is divided in six chapters. Chapter 1 introduces the thesis, where an overview of the background about stimuli-responsive materials as well as ionic liquids is presented. In the Chapter 2, a brief state of art focusing on the development of 4,4'-bipyridinium salts have been presented. Also in this chapter, the synthesis and the chemical, physical, thermal and electrochemical properties of mono- and di-substituted-4,4'-bipyridinium salts have been described. Chapter 3 is related to the preparation of tetra-substituted-4,4'-bipyridinium salts as well as ionic electrochromic monomers and polymers. Chapter 4 reports a detailed description of the electrochromic devices application based on the most promissory di- and tetra-substituted-4,4'-bipyridinium salts as well as ionic polymers prepared in the Chapters 2 and 3 respectively. In particular, different types of devices, including liquid, gel and solid-state electrochromic devices were tested. In the Chapter 5, an overview about diarylethene derivatives, following by the preparation of symmetrical and neutral photochromic diarylethene containing two carboxylic units and its conversion in IL form is presented. Additionally, the photochromic and electrochromic properties of the diarylethene based IL were investigated. In the Chapter 6, a multi stimuli-responsive co-polymer constituted by a well-known thermo-responsive unit, *N*-isopropylacrylamide and a flavylium scaffold was prepared and characterized. This co-polymer responds to pH, light and temperature stimuli and different studies have been performed in order to elucidate its interest for potential applications.

1.6. References

1 J. Thévenot, H. Oliveira, O. Sandre and S. Lecommandoux, *Chem. Soc. Rev.*, 2013, **42**, 7099–116.

2 P. Schattling, F. D. Jochum and P. Theato, *Polym. Chem.*, 2014, **5**, 25–36.

3 H. R. Schneider, in *Chemoresponsive Materials: Stimulation by Chemical and Biological Signals*, The Royal Society of Chemistry, 2015, pp. 1–9.

4 D. Schmaljohann, *Adv. Drug Deliv. Rev.*, 2006, **58**, 1655–1670.

5 F. D. Jochum, F. R. Forst and P. Theato, *Macromol. Rapid Commun.*, 2010, **31**, 1456–1461.

6 H. Fu, D. M. Policarpio, J. D. Batteas and D. E. Bergbreiter, *Polym. Chem.*, 2010, **1**, 631–633.

7 S. Uchiyama, N. Kawai, A. P. de Silva and K. Iwai, *J. Am. Chem. Soc.*, 2004, **126**, 3032–3033.

8 R. M. Christie, Ed., in *Colour Chemistry*, The Royal Society of Chemistry, 2001, pp. 1–11.

9 P. Bamfield and M. G. Hutchings, in *Chromic Phenomena: Technological Applications of Colour Chemistry*, The Royal Society of Chemistry, 2nd edn., 2010, pp. 9–140.

10 D. Lötzsch, V. Eberhardt and C. Rabe, in *Ullmann's Encyclopedia of Industrial Chemistry*, Wiley-VCH Verlag GmbH & Co. KGaA, 2000.

11 P. M. S. Monk, R. J. Mortimer and D. R. Rosseinsky, *Electrochromism and Electrochromic Devices*, Cambridge University Press, Cambridge, 2007.

12 R. D. Rauh, *Electrochim. Acta*, 1999, **44**, 3165–3176.

13 R. J. Mortimer, *Annu. Rev. Mater. Res.*, 2011, **41**, 241–268.

14 N. M. Rowley and R. J. Mortimer, *Sci. Prog.*, 2002, **85**, 243–262.

15 P. M. S. Monk, *The viologens: physicochemical properties, synthesis, and applications of the salts of 4,4'-bipyridine*, Wiley, 1998.

16 R. J. Mortimer, *Annu. Rev. Mater. Res.*, 2011, **41**, 241–268.

17 R. J. Mortimer, A. L. Dyer and J. R. Reynolds, *Displays*, 2006, **27**, 2–18.

18 *Electrochromic Polymers from Reynolds Group (https://ww2.chemistry.gatech.edu/reynolds/ECP)*, 2016.

19 A. Branco, C. Pinheiro, J. Fonseca, J. Tedim, A. Carneiro, A. J. Parola, C. Freire and F. Pina, *Electrochem. Solid-State Lett.,* 2010, **13**, J114–J118.

20 D. R. Rosseinsky and R. J. Mortimer, *Adv. Mater.*, 2001, **13**, 783–793.

21 R. J. Mortimer, D. R. Rosseinsky and P. M. S. Monk, in *Electrochromic Materials and Devices*, Wiley-VCH Verlag GmbH & Co. KGaA, 2015, pp. I–XXVIII.

22 K. Matsuda and M. Irie, *J. Photochem. Photobiol. C Photochem. Rev.*, 2004, **5**, 169–182.

23 M. Irie, T. Fukaminato, K. Matsuda and S. Kobatake, *Chem. Rev.*, 2014, **114**, 12174–12277.

24 S. Nishio and M. Kakihana, *Chem. Mater.*, 2002, **14**, 3730–3733.

25 F. Pina and L. C. Branco, in *Ionic Liquids: Theory, Properties, New Approaches*, ed. A. Kokorin, InTech, 2011, pp. 139–166.

26 R. Gomes, A. J. Parola, C. A. T. Laia and F. Pina, *J. Phys. Chem. B*, 2007, **111**, 12059–12065.

27 H. M. D. Bandara and S. C. Burdette, *Chem. Soc. Rev.*, 2012, **41**, 1809–1825.

28 P. H. Vandewyer, J. Hoefnagels and G. Smets, *Tetrahedron*, 1969, **25**, 3251–3266.

29 H. Koshima, in *New Frontiers in Photochromism*, eds. M. Irie, Y. Yokoyama and T. Seki, Springer Japan, 2013, pp. 21–40.

30 F. Pina, M. J. Melo, C. A. T. Laia, A. J. Parola and J. C. Lima, *Chem. Soc. Rev.*, 2012, **41**, 869 – 908.

31 F. Pina, *J. Agric. Food Chem.*, 2014, **62**, 6885–6897.

32 R. Gavara, S. Gago, N. Jordão and F. Pina, *J. Phys. Chem. A*, 2014, **118**, 4723–4731.

33 M. Irie, *Chem. Rev.*, 2000, **100**, 1685–1716.

34 H. Ohno, in *Electrochemical Aspects of Ionic Liquids*, John Wiley & Sons, Inc., 2005, pp. 1–3.

35 J. L. Anthony, J. F. Brennecke, J. D. Holbrey, E. J. Maginn, R. A. Mantz, R. D. Rogers, P. C. Trulove, A. E. Visser and T. Welton, in *Ionic Liquids in Synthesis*, Wiley-VCH Verlag GmbH & Co. KGaA, 2003, pp. 41–126.

36 N. V Plechkova and K. R. Seddon, *Chem. Soc. Rev.*, 2008, **37**, 123–150.

37 M. J. Earle, J. M. S. S. Esperanca, M. A. Gilea, J. N. Canongia Lopes, L. P. N. Rebelo, J. W. Magee, K. R. Seddon and J. A. Widegren, *Nature*, 2006, **439**, 831–834.

38 E. Bodo and V. Migliorati, in *Ionic Liquids - Classes and Properties*, ed. P. S. Handy, InTech, 2011, pp. 107–126.

39 C. M. Gordon, M. J. Muldoon, M. Wagner, C. Hilgers, J. H. Davis and P. Wasserscheid, in *Ionic Liquids in Synthesis*, Wiley-VCH Verlag GmbH & Co. KGaA, 2008, pp. 7–55.

40 T. Welton, *Chem. Rev.*, 1999, **99**, 2071–2084.

41 B. Clare, A. Sirwardana and D. R. MacFarlane, in *Ionic Liquids*, ed. B. Kirchner, Springer Berlin Heidelberg, 2010, pp. 1–40.

42 H. Srour, H. Rouault, C. C. Santini and Y. Chauvin, *Green Chem.*, 2013, **15**, 1341–1347.

43 J. Yuan, D. Mecerreyes and M. Antonietti, *Prog. Polym. Sci.*, 2013, **38**, 1009–1036.

44 M. Freemantle, *Chem. Eng. News Arch.*, 1998, **76**, 32–37.

45 M. Earle, A. Forestièr, H. Olivier-Bourbigou and P. Wasserscheid, in *Ionic Liquids in Synthesis*, Wiley-VCH Verlag GmbH & Co. KGaA, 2003, pp. 174–288.

46 C. Chiappe, T. Ghilardi and C. S. Pomelli, in *Ionic Liquids (ILs) in Organometallic Catalysis*, eds. J. Dupont and L. Kollár, Springer Berlin Heidelberg, 2015, pp. 79–93.

47 B. T. Torimoto, T. Tsuda, K. Okazaki and S. Kuwabata, 2010, **871**, 1196–1221.

48 M. Freemantle, in *An Introduction to Ionic Liquids*, The Royal Society of Chemistry, 2009.

49 C. A. Angell, W. Xu, M. Yoshizawa, A. Hayashi, J.-P. Belieres, P. Lucas and M. Videa, in *Electrochemical Aspects of Ionic Liquids*, John Wiley & Sons, Inc., 2005, pp. 5–23.

50 J. S. Wilkes and M. J. Zaworotko, *J. Chem. Soc., Chem. Commun.*, 1992, 965–967.

51 R. P. Swatloski, J. D. Holbrey and R. D. Rogers, *Green Chem.*, 2003, **5**, 361–363.

52 P. Bonhôte, A.-P. Dias, N. Papageorgiou, K. Kalyanasundaram and M. Grätzel, *Inorg.*

Chem., 1996, **35**, 1168–1178.

53 J. H. Davis Jr., *Chem. Lett.*, 2004, **33**, 1072–1077.

54 R. Giernoth, *Angew. Chem., Int. Ed.*, 2010, **49**, 2834–2839.

55 A. E. Visser, R. P. Swatloski, W. M. Reichert, R. Mayton, S. Sheff, A. Wierzbicki, J. H. Davis, Jr. and R. D. Rogers, *Chem. Commun.*, 2001, 135–136.

56 W. L. Hough, M. Smiglak, H. Rodriguez, R. P. Swatloski, S. K. Spear, D. T. Daly, J. Pernak, J. E. Grisel, R. D. Carliss, M. D. Soutullo, J. H. Davis, Jr. and R. D. Rogers, *New J. Chem.*, 2007, **31**, 1429–1436.

57 A. Banet Osuna, A. Šerbanović, M. Nunes da Ponte, H. Matsubara, I. Ryu and J. Dupont, in *Green Separation Processes*, Wiley-VCH Verlag GmbH & Co. KGaA, 2006, pp. 207–249.

58 L. C. Branco, J. G. Crespo and C. A. M. Afonso, *Angew. Chem., Int. Ed.*, 2002, **41**, 2771–2773.

59 S. Werner, M. Haumann and P. Wasserscheid, *Annu. Rev. Chem. Biomol. Eng.*, 2010, **1**, 203–230.

60 Y. Zhang, H. Gao, Y.-H. Joo and J. M. Shreeve, *Angew. Chem., Int. Ed.*, 2011, **50**, 9554–9562.

61 S. Hayashi and H. Hamaguchi, *Chem. Lett.*, 2004, **33**, 1590–1591.

62 H. Ohno, in *Electrochemical Aspects of Ionic Liquids*, Wiley, 2011.

63 M. Earle, P. Wasserscheid, P. Schulz, H. Olivier-Bourbigou, F. Favre, M. Vaultier, A. Kirschning, V. Singh, A. Riisager, R. Fehrmann and S. Kuhlmann, in *Ionic Liquids in Synthesis*, Wiley-VCH Verlag GmbH & Co. KGaA, 2008, pp. 265–568.

64 J. P. Hallett and T. Welton, *Chem. Rev.*, 2011, **111**, 3508–3576.

65 C. Hardacre and V. Parvulescu, Eds., *Catalysis in Ionic Liquids*, The Royal Society of Chemistry, 2014.

66 S. Keskin, D. Kayrak-Talay, U. Akman and Ö. Hortaçsu, *J. Supercrit. Fluids*, 2007, **43**, 150–180.

67 D. J. Cole-Hamilton and R. P. Tooze, *Catalyst Separation, Recovery and Recycling*, Springer, 2006.

68 S. Doherty, in *Catalysis in Ionic Liquids: From Catalyst Synthesis to Application*, The Royal Society of Chemistry, 2014, pp. 44–308.

69 R. Fehrmann, A. Riisager and M. Haumann, *Supported Ionic Liquids: Fundamentals and Applications*, WILEY-VCH Verlag, 2014.

70 K. Zalewska and L. C. Branco, *Mini. Rev. Org. Chem.*, 2014, **11**, 141–153.

71 T. Payagala and D. W. Armstrong, *Chirality*, 2012, **24**, 17–53.

72 T. Welton, F. Endres, S. Z. El Abedin, M. Antonietti, B. Smarsly and Y. Zhou, in *Ionic Liquids in Synthesis*, Wiley-VCH Verlag GmbH & Co. KGaA, 2008, pp. 569–617.

73 D. M. Haddleton, T. Welton and A. J. Carmichael, in *Ionic Liquids in Synthesis*, Wiley-VCH Verlag GmbH & Co. KGaA, 2008, pp. 619–640.

74 S. Klembt, S. Dreyer, M. Eckstein and U. Kragl, in *Ionic Liquids in Synthesis*, Wiley-VCH

Verlag GmbH & Co. KGaA, 2008, pp. 641–661.

75 F. van Rantwijk and R. A. Sheldon, *Chem. Rev.*, 2007, **107**, 2757–2785.

76 I. M. Marrucho, L. C. Branco and L. P. N. Rebelo, *Annu. Rev. Chem. Biomol. Eng.*, 2014, **5**, 527–546.

77 K. J. Kulacki and G. A. Lamberti, *Green Chem.*, 2008, **10**, 104–110.

78 R. F. M. Frade, A. A. Rosatella, C. S. Marques, L. C. Branco, P. S. Kulkarni, N. M. M. Mateus, C. A. M. Afonso and C. M. M. Duarte, *Green Chem.*, 2009, **11**, 1660–1665.

79 H. Garcia, R. Ferreira, M. Petkovic, J. L. Ferguson, M. C. Leitao, H. Q. N. Gunaratne, K. R. Seddon, L. P. N. Rebelo and C. Silva Pereira, *Green Chem.*, 2010, **12**, 367–369.

80 R. J. Soukup-Hein, M. M. Warnke and D. W. Armstrong, *Annu. Rev. Anal. Chem.*, 2009, **2**, 145–168.

81 T. Schafer, C. M. Rodrigues, C. A. M. Afonso and J. G. Crespo, *Chem. Commun.*, 2001, 1622–1623.

82 H. Karkhanechi, S. Salmani and M. Asghari, *ChemBioEng Rev.*, 2015, **2**, 290–302.

83 E. D. Bates, R. D. Mayton, I. Ntai and J. H. Davis, *J. Am. Chem. Soc.*, 2002, **124**, 926–927.

84 G. V. S. M. Carrera, N. Jordão, M. M. Santos, M. N. da Ponte and L. C. Branco, *RSC Adv.*, 2015, **5**, 35564–35571.

85 M. G. Freire, A. F. M. Claudio, J. M. M. Araujo, J. A. P. Coutinho, I. M. Marrucho, J. N. C. Lopes and L. P. N. Rebelo, *Chem. Soc. Rev.*, 2012, **41**, 4966–4995.

86 *BASF (http://www2.basf.us/corporate/051004_ionic.htm)*, 2016.

87 *Merck (http://www.merck-performance-materials.com/en/solar_and_energy/solar_and_energy.html)*, 2016.

88 *Chemical Engineering (http://www.chemengonline.com/ionic-liquids-create-sustainable-processes/?printmode=1)*, 2016.

89 R. Ozawa and H. Hamaguchi, *Chem. Lett.*, 2001, **30**, 736–737.

90 V. W.-W. Yam, J. K.-W. Lee, C.-C. Ko and N. Zhu, *J. Am. Chem. Soc.*, 2009, **131**, 912–913.

91 L. C. Branco and F. Pina, *Chem. Commun.*, 2009, 6204–6206.

92 E. Santos, J. Albo and A. Irabien, *RSC Adv.*, 2014, **4**, 40008–40018.

93 K. D. Clark, O. Nacham, J. A. Purslow, S. A. Pierson and J. L. Anderson, *Anal. Chim. Acta*, 2016, **934**, 9–21.

94 A. Branco, L. C. Branco and F. Pina, *Chem. Commun.*, 2011, **47**, 2300–2302.

95 A. Branco, J. Belchior, L. C. Branco and F. Pina, *RSC Adv.*, 2013, **3**, 25627–25630.

96 D. R. MacFarlane, N. Tachikawa, M. Forsyth, J. M. Pringle, P. C. Howlett, G. D. Elliott, J. H. Davis, M. Watanabe, P. Simon and C. A. Angell, *Energy Environ. Sci.*, 2014, **7**, 232–250.

97 S. Gago, L. Cabrita, J. C. Lima, L. C. Branco and F. Pina, *Dalton Trans.*, 2013, **42**, 6213–6218.

98 P. S. Campbell, M. Yang, D. Pitz, J. Cybinska and A.-V. Mudring, *Chem. Eur. J.*, 2014,

20, 4704–4712.

99 S. Tang, A. Babai and A. Mudring, *Angew. Chem., Int. Ed.*, 2008, **47**, 7631–7634.

100 J. M. Delgado, A. Raymundo, M. Vilarigues, L. C. Branco and C. A. T. Laia, *Chem. Eur. J.*, 2015, **21**, 726–732.

101 S. Tang, J. Cybinska and A. Mudring, *Helv. Chim. Acta*, 2009, **92**, 2375–2386.

102 J. Avó, M. T. Cidade, V. Rodriguez, J. C. Lima and A. J. Parola, *J. Phys. Chem. B*, 2015, **119**, 6680–6685.

103 E. Sebastiao, C. Cook, A. Hu and M. Murugesu, *J. Mater. Chem. A*, 2014, **2**, 8153–8173.

104 Q. Zhang and J. M. Shreeve, *Chem. Rev.*, 2014, **114**, 10527–10574.

2. Electrochromic Organic Salts: 4,4’-Bipyridinium Derivatives

Publications associated with this chapter:

N. Jordão, L. Cabrita, F. Pina and L. C. Branco, *Chem. Eur. J.*, 2014, **20**, 3982–3988.

N. Jordão, H. Cruz, A. Branco, F. Pina and L. C. Branco, *ChemPlusChem*, 2015, **80**, 202–208.

2. Electrochromic Organic salts: 4,4’ – Bipyridinium Derivatives

2.1. Introduction

One of the most organic electrochromic molecules widely studied are viologens, also designed as 4,4’-bipyridinium salts. They are electroactive species with relevant electrochromic properties and electron-accepting nature. They can be prepared from mono- or di-quarternization, i.e. nucleophilic substitution reaction of 4,4’-bipyridine scaffold [1,2].

These type of salts have been widely applied as redox indicators in biology [2,3], herbicides [2], antibacterial agents [4,5], chemically modified electrodes [6], photocatalytic reduction of water to hydrogen [7,8], liquid crystals [9–11] and electrochromic display devices [12] (Scheme 2.1).

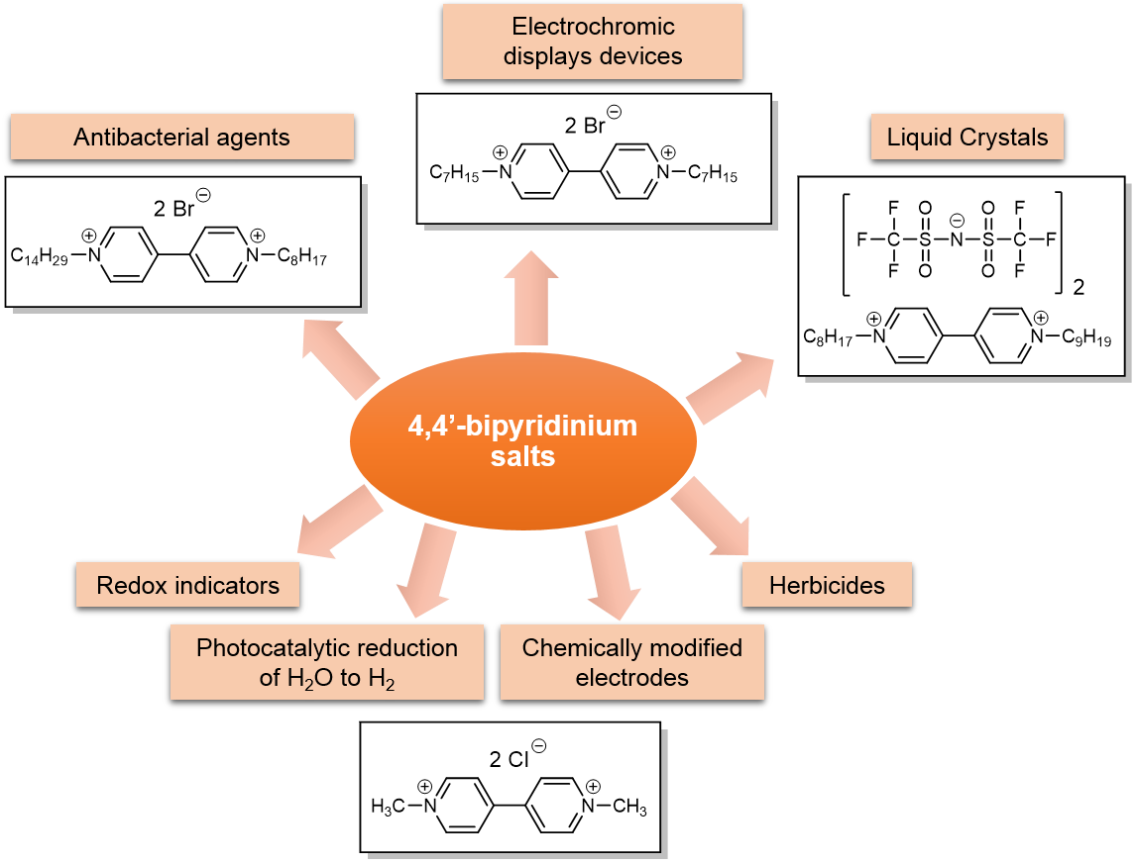

Scheme 2.1 – Common applications of 4,4’-bipyridinium salts and their reported chemical structures.

Michaelis and Hill (1933) investigated 4,4’-bipyridinium salts as redox indicators in biological studies [3]. They reported that their potential range is very negative (more cathodic) and under specific conditions can be more negative than any organic system used as indicators, accompanied with a significant degree of reversibility [3,13]. The authors also reported that these salts differ from other indicators, mainly due to the fact that its exhibit colour in the reduced form and the redox potential is independent of pH [3].

Years later, *Imperial Chemical Industries* (ICI) discovery the potential herbicidal activity of methyl viologen di-chloride (MV), which was commercial named as Paraquat® and published that in 1958 [2]. Paraquat® is the active ingredient in weed killers such as Gramoxone ®, Dextrone X®, Esgram®, or Pathclear® and is a component for others herbicides such as Toxer Total ®,

Herbaxon®, among others [2]. Paraquat is also considered a non-selective weed killer that kills all green tissue when it comes into contact with it [2]. Their herbicidal properties were attributed to their strong reductant properties, especially their ability to reduce molecular oxygen and it was found to be related to the redox potential [6,13,14]. Recently, the application of 4,4'-bipyridinium salts as potent antibacterial agents have been explored, once the antibacterial activity of these compounds remains mostly unreported, despite of their prevalence and amphiphilic nature [4,5].

Lezna and Centeno (1996) reported an example of chemically modified electrodes using methyl viologen (MV) [6]. They reported the spectroelectrochemistry of methyl viologen at a thin mercury film electrode/fluoride solution interface [6].

Other interesting example was reported by Gratzel (1981), where the MV is used as one-electron redox mediator in the reduction of water to hydrogen [7].

Recently, ionic liquid crystals (ILCs) received much attention due to the possibility to combine many applications and features of liquid crystals (LCs) together with ILs [15]. In particular, 1,1'-dialkyl-4,4'-bipyridinium salts containing long alkyl chains can exhibit liquid crystalline properties [9–11,15–18]. The anion seems to be essential to induce the liquid crystalline state, usually a smectic A phase. For example, bromide and iodide salts based on di-n-heptyl and di-n-octyl-4,4'-bipyridinium do not show any mesomorphic behaviour.
In general, 1,1'-di-alkyl-4,4'-bipyridinium di-bromide and di-iodide have stable crystal phases up to the decomposition temperature in the range 250 – 300 ºC [19]. When the halide anion is replaced by one bulkier and less symmetric such as [NTf_2] anion, a stable room temperature smectic A phase is observed [18].

Schoot and co-workers from *Philips Research Laboratories* (1973) reported the first electrochromic display using viologens [12]. Firstly, *Philips* (1970) and *Imperial Chemical Industries (ICI)* (1971) patented 1,1'-di-heptyl-4,4'-bipyridinium and cyanophenyl paraquat, respectively. At the same time, Barclay's group were also investigated other displays based on 1,1'-di-heptyl-4,4'-bipyridinium and their works was not published until after their program was discontinued [20].

Interestingly, viologens are used as electrochromic materials in anti-glare car rear-view mirrors, precisely automatic-dimming "*night vision safety*" (NVS) mirror commercialised by *Gentex Company* [20].

The 4,4'-bipyridinium salts may exhibit three redox states: a di-cation, a radical cation and a neutral compound (di-reduced species) through two successive electron-transfer processes (Scheme 2.2) [1,2].

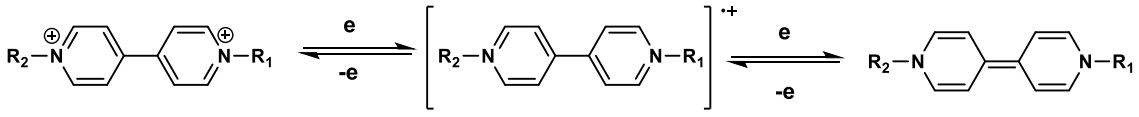

Scheme 2.2 – Three common viologen redox states [2]. (Source: *The viologens: physicochemical properties, synthesis, and applications of the salts of 4,4'-bipyridine*, Wiley, 1998).

2. Electrochromic Organic salts: 4,4’ – Bipyridinium Derivatives

The di-cation is the most stable species and colourless when pure, unless optical charge-transfer with the anion or other charge-donating species occurs [1,2]. This effect is stronger for iodide anion than bromide or chloride anions [1]. Upon one electron-transfer process, radical cation is formed and is amongst the most stable organic radicals. This stability is attributable to the delocalisation of the radical electron throughout the π-framework of the bipyridyl nucleus, the 1- and 1’-substituents normally bearing some of the charge [1,2]. This radical cation is intensely coloured, exhibiting high molar absorption coefficients according to an intense intramolecular optical charge-transfer. The colour is mostly dependent of the substituent type and length on the nitrogen, the type of anion and the solvent [1,2]. The di-reduced species is formed by one-electron reduction of the respective radical cation or may also be formed by direct two-electron reduction process of the di-cation [1]. This neutral species showed a lower intensity of colour, since no optical charge-transfer or internal transition corresponding to visible wavelengths is accessible [1]. In addition, the electrical potential required to promote the electron-transfer process also depends on both the substituents at nitrogen and on the bipyridyl core (*“nuclear substituted”* compounds) [1].

The 4,4’-bipyridinium salts have also been extensively investigated for electrochromic devices. One interesting example was reported by Diamond and co-workers (2013) [21]. These authors tested an innovative approach to the design of solid-state electrochromic device, in which an IL acts as electrolyte and electrochromic material simultaneously (see Figure 2.1). They synthetize an IL based on phosphonium core bearing a viologen unit. Therefore, this IL was encapsulated within a hybrid sol-gel by *in situ* photo-polymerization to build the electrochromic device.

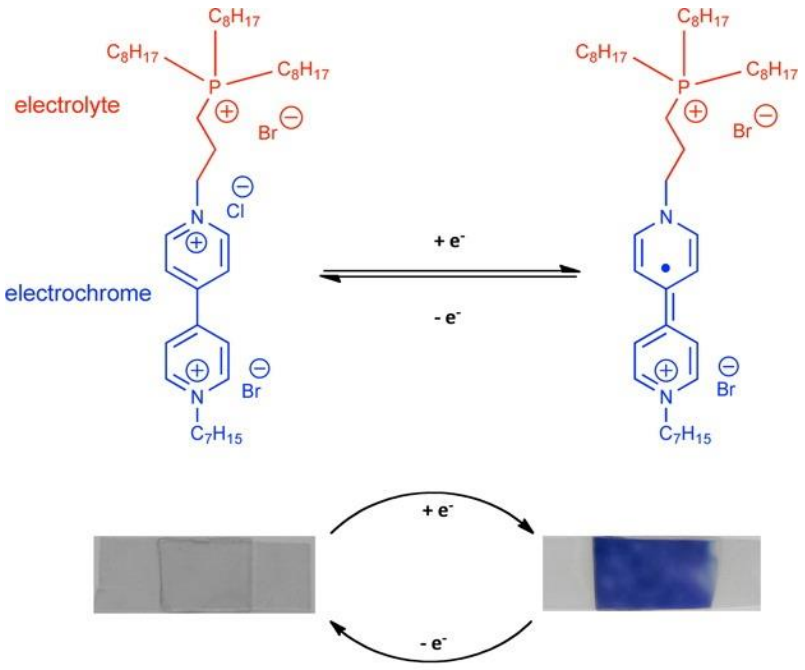

Figure 2.1 – Example of an electrochromic device, where the electrochromic IL act as electrolyte and electrochromic material simultaneously. The phosphonium cation is covalently linked to bipyridinium cation and encapsulated in sol-gel matrix [21]. (Source: *ACS Appl. Mater. Interfaces*, 2013, **5**, 55–62).

Despite of the rather viscous nature of the material, the device showed a colouration efficiency of 10.72 cm^2 C^{-1}, a varied optical output as a function of the incident current and a faster switching times, when compared to previously reported electrochromic ILs [21,22].

In this year, an interesting application of 4,4'-bipyridinium derivative salt is reported by Velayutham and co-workers [23]. They reported that the 1,1'-diethyl-4,4'-bipyridinium di-bromide based on redox active electrolyte in 1.0 M H_2SO_4 as novel electrolyte for supercapacitor application. The performance of the supercapacitor containing that 4,4'-bipyridinium salt was significantly improved by the synergic effect of cathodic (bipyridinium cation) and anodic (bromide anion) redox behaviour, when compared with neat H_2SO_4 and tri-ethylbutylammonium bromide $[N_{2,2,2,4}]$Br electrolytes [23].

2. Electrochromic Organic salts: 4,4’ – Bipyridinium Derivatives

2.2. 4,4’- Bipyridinium Salts

Herein, electrochromic organic salts based on mono- or di-substituted-4,4’-bipyridinium by incorporation with different functional groups (alkyl and ether units) have been explored (Scheme 2.3). The first approach involves the introduction of alkyl chain in 4,4’-bipyridinium scaffold, followed by the introduction of oxygen units as alternative substituents, once oxygen unit can contribute to reduce the toxicity of the salt [24–27]. It can also contribute to decrease the melting point as well as improve the solubility of the salt. An anion exchange reaction is also required, in particular using suitable organic anions such as bis(trifluoromethanesulfonyl)imide [NTf_2] and docusate [AOT] (Scheme 2.3).

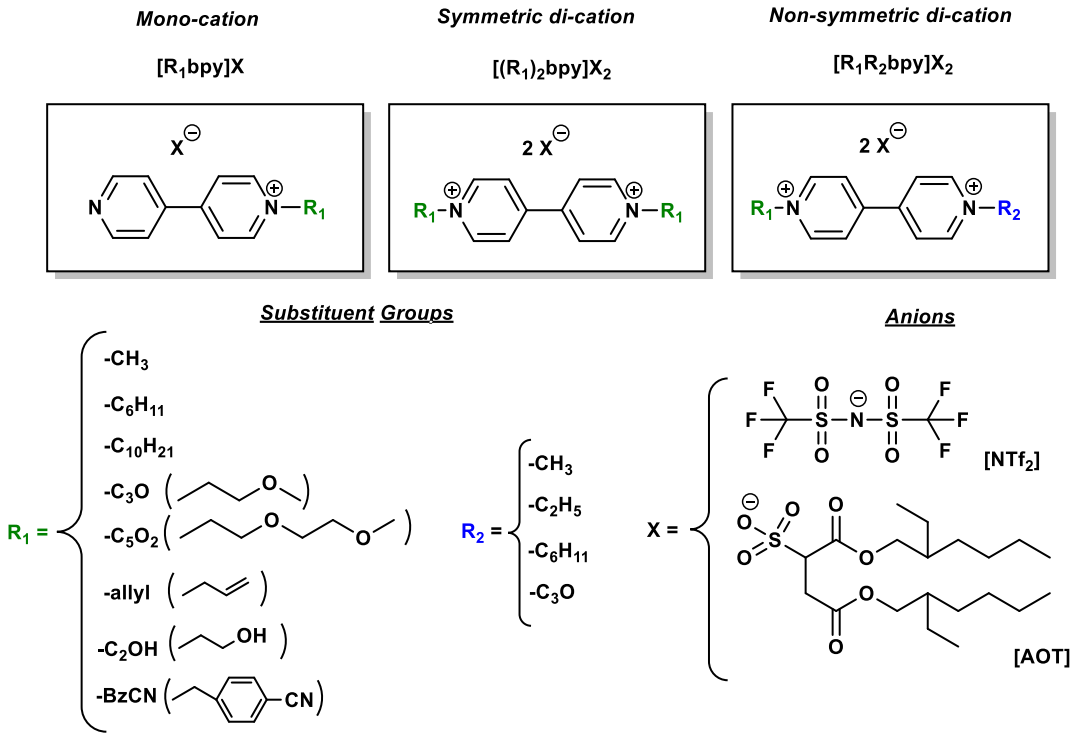

Scheme 2.3 – Mono-substituted-, symmetric di-substituted- and non-symmetric di-substituted-4,4’-bipyridinium salts prepared.

The anion selection was, mainly, focused by the fact that bis(triflyl)amides have attractive properties, such as its hydrophobicity, high thermal and electrochemical stability and conductivity, reduced viscosity and very low melting point [28,29]. In the case of docusate anion ([AOT]), which is an emollient with reduced toxicity and it is also considered a biocompatible anion [30,31]. Indeed, it was possible obtain salts with low melting point, including RTILs.

Further evaluation of the functional groups and anions effects in the physical, thermal and electrochemical properties of the final salt were tested.

In the case of [AOT] based salts, it is possible to determine the proportion between anion and cation by comparison of both integral areas from specific protons in ^{1}H NMR spectra. Whereas in [NTf_2] salts the presence of fluorine atoms in the structure is check by ^{19}F NMR spectroscopy.

2.2.1. Mono-substituted-4,4'-bipyridinium salts

The preparation of mono-substituted-4,4'-bipyridinium salts was performed in two synthetic steps: alkylation reaction and anion exchange reaction from halide to bis(trifluoromethanesulfonyl)imide ([NTf_2]) or docusate ([AOT]).

In the first step, mono-substituted-4,4'-bipyridinium salts were obtained through nucleophilic substitution reaction of 4,4'-bipyridine unit, using an appropriate alkylating agent and specific reaction conditions in order to obtain the desired mono-cation. The reactional conditions such as temperature, solvent and reagent equivalents were optimized according with the literature and the reactivity of functional groups. In this specific case of mono-substituted salts, ethyl acetate or acetonitrile are selected as reaction media. The second step involved an anion exchange reaction using Li[NTf_2] or Na[AOT] in methanol or aqueous media was performed (Scheme 2.4).

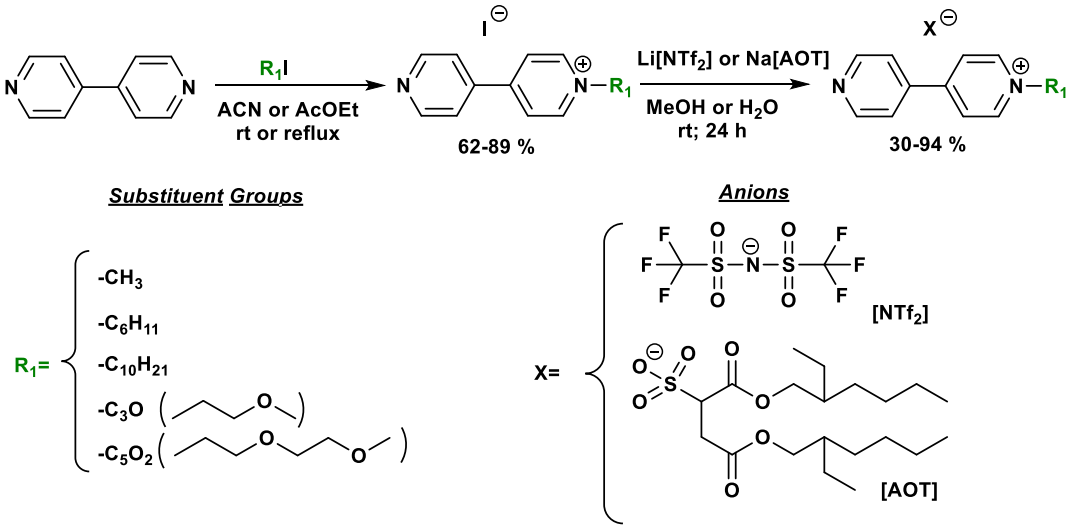

Scheme 2.4 – Synthetic route for preparation of mono-substituted-4,4'-bipyridinium salts.

Di-cation salts can also be formed during the nucleophilic substitution reaction depending on the reaction conditions. For example, in one of the reactions to prepare [C_{10}bpy]I, the di-cation formation was also observed by ^{1}H NMR analysis (Figure 2.2). From ^{1}H NMR spectra, it is possible to determine the proportion between both salts by comparison of the integration areas of aromatic protons, in particular 1:0.38 (mono:di), as illustrated in Figure 2.2. Therefore, it was possible to isolate the mono- from the di-cation with higher purity levels through recrystallization method using acetone as solvent. These purity levels for mono-cation (see Figure 2.3) and di-cation (see Figure 2.6 in the section 2.2.2.) were confirmed by ^{1}H NMR analysis. Similar recrystallization procedures were done for others mono-cations using acetone or ethanol as solvents.

Thereby, mono-substituted-4,4'-bipyridinium iodide or bromide salts (see Scheme 2.4) were obtained with higher purity levels (after mono and di-cation separation) in moderate to high yields (62 to 89%). In other hand, the final salts combined with [NTf_2] or [AOT] anions were obtained in low to high yields (30 to 94%) due to the purification step in order to remove any halide residues.

2. Electrochromic Organic salts: 4,4’ – Bipyridinium Derivatives

In general, the anion exchange reaction from halide to [NTf_2] anion was performed in water, facilitating the purification step. In the others cases, methanol was selected as reaction media and additional purification steps such as precipitation or liquid/liquid extraction with water were required. All prepared salts are analysed by ^{1}H NMR, ^{13}C NMR and ^{19}F NMR for the particular case of [NTf_2] based salts.

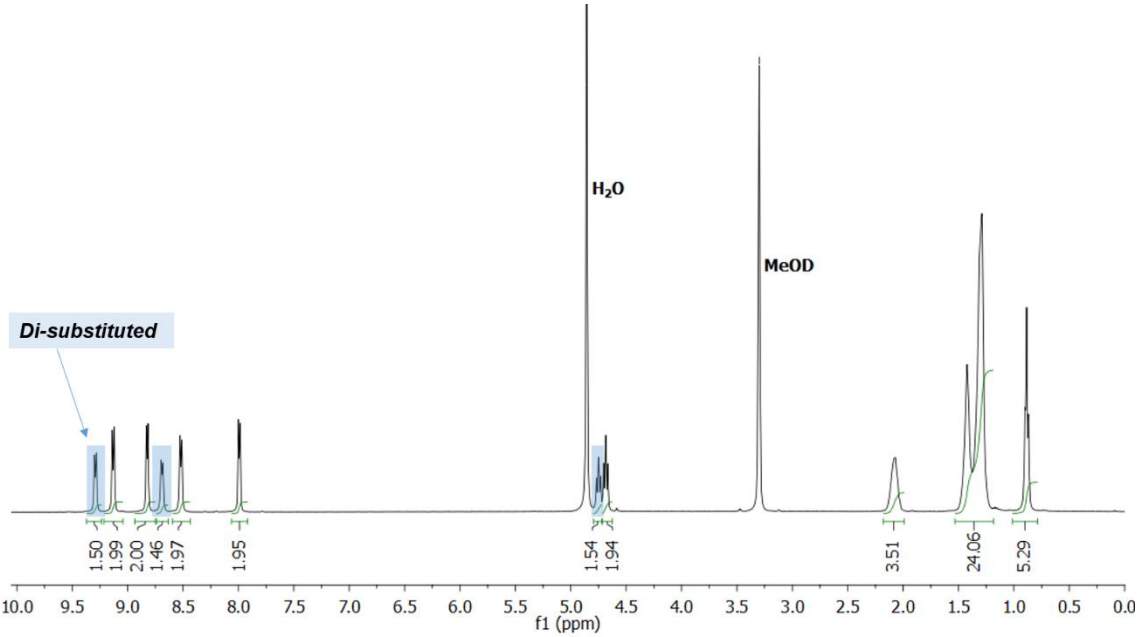

Figure 2.2 – ^{1}H NMR spectra of the product from the reaction to produce [C_{10}bpy]I in CH_3OD.

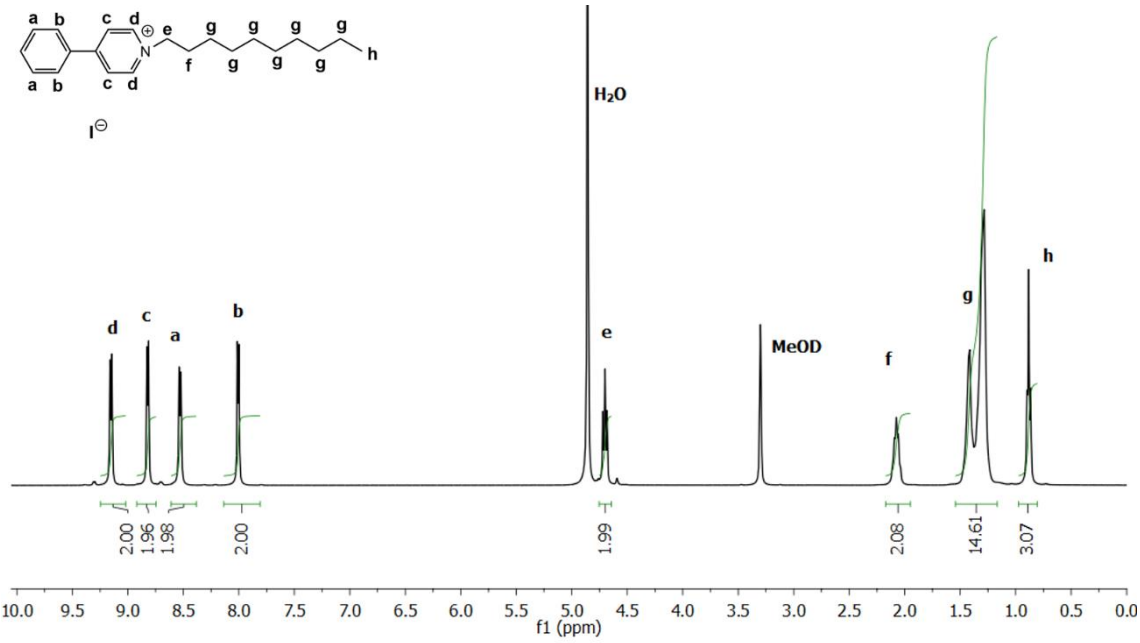

Figure 2.3 – ^{1}H NMR spectra of [C_{10}bpy]I in CH_3OD upon recrystallization in acetone.

All [NTf_2] salts showed the presence of fluorine atoms, which are detected by ^{19}F NMR. In the case of [AOT] based salts, it is possible to determine the proportion between anion and cation by ^{1}H NMR. In this way, the proportion between cation:anion for [C_{10}bpy][AOT], [C_3Obpy][AOT],

[C_5O_2bpy][AOT], [(allyl)bpy][AOT] is 1:1.03, 1:1.05, 1:1.1, 1:1.0, respectively. It should be mentioned that those values are affected by 10 % error from ^{1}H NMR analysis.

FTIR is also performed to check the structure of the salts. Additionally, [NTf_2] and [AOT] based salts are analysed by elemental analysis (C, H, N). Thermal properties such as melting points and glass transition (T_g, only using differential scanning calorimetry – DSC) for different prepared organic salts have been studied (Table 2.1).

Table 2.1 – Yield, physical state and thermal properties of mono-substituted-4,4'-bipyridinium salts prepared.

Salts	Yield (%)	Physical State	m.p. (T_g) (ºC)
[C_1bpy]I	89	Orange solid	240 [a]
[C_1bpy][NTf_2]	71	White solid	70 [a]
[C_6bpy]I	62	Orange solid	190 [a]
[C_6bpy][NTf_2]	90	Brown solid	56 [a] (-40.6) [b]
[C_{10}bpy]I	64	Yellow solid	124 [a]
[C_{10}bpy][NTf_2] [c]	94	Brown liquid	RTIL (-38.4) [b]
[C_{10}bpy][AOT]	59	Brown liquid	RTIL (-20.9) [b]
[C_3Obpy]I	66	Yellow solid	72 [a]
[C_3Obpy][NTf_2]	83	Pale brown solid	90 [a]
[C_3Obpy][AOT]	30	Brown liquid	RTIL (-15.9) [b]
[C_5O_2bpy]I	57	Brown liquid	RTIL (4.5) [b]
[C_5O_2bpy][NTf_2]	87	Pale brown solid	79 [a]
[C_5O_2bpy][AOT]	83	Brown liquid	RTIL [a]
[(allyl)bpy]I	70	Yellow solid	149 [a]
[(allyl)bpy][NTf_2]	89	Brown liquid	RTIL (-39.2) [b]
[(allyl)bpy][AOT]	32	Brown liquid	RTIL (-15.4) [b]
[(C_2OH)bpy]I	76	Yellow solid	196 [a]
[(C_2OH)bpy][NTf_2]	34	Pale brown solid	86.2 (-6.2) [b]

[a] Melting point (m.p.) was measured using a melting point apparatus. [b] Melting point and Glass transition temperature (T_g) was determined by DSC analysis with heating/cooling rate of 10 or 20 ºC/min. [c] Density: 1.216 g/cm^3 (26.5 ºC), measured by picnometer.

In general, the mono-substituted-4,4'-bipyridinium salts combined with [NTf_2] showed significantly lower melting points than correspondent iodide salts, since [NTf_2] is a well-known anion to depress the melting point of ILs, possibly due to its lower symmetry and bulky nature, i.e. its inability to hydrogen bonding, extensive charge delocalization and flexibility [11,29,32,33].

However, [C_3Obpy][NTf_2] and [C_2O_5bpy][NTf_2] have higher melting points than correspondent iodide salts that could be explained by cation-anion interactions. When iodide is changed to [AOT] anion, it is also observed a decrease in melting point, due to [AOT] anion is considered a large and asymmetrical anion. In particular, for mono-alkyl 4,4'-bipyridinium cations combined with [NTf_2] anion, it is observed that longer alkyl chains (hexyl and decyl) contribute to reduce their melting points (Table 2.1).

From these anion exchange reactions, it was possible to obtain eleven ILs, which six are RTILs. In general, all mono-substituted iodide salts are water miscible, whereas the corresponding [NTf_2] salts are water immiscible.

Some of these salts have been studied by differential scanning calorimetry (DSC) to evaluate in more detailed their thermal properties, such as glass transition (Table 2.1). For example, the DSC analysis of the mono-cation [C_{10}bpy][NTf_2] is presented in Figure 2.4.

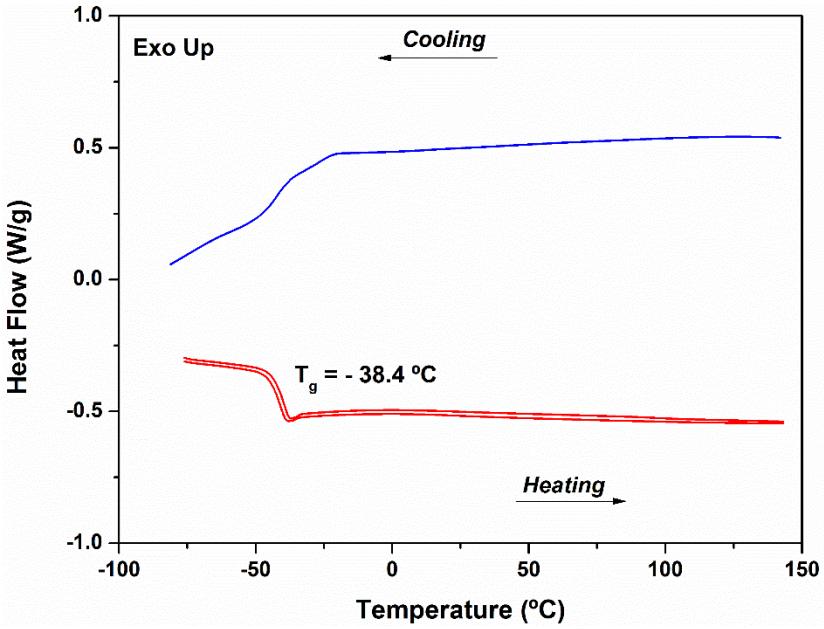

Figure 2.4 – Heat flow thermogram for [C_{10}bpy][NTf_2] obtained at 20 ºC/min (heating/cooling rate), where glass transition temperature (T_g as midpoint) was determined on the second heating.

As expected, the thermogram confirms that in this selected conditions (-90 to 150 ºC at 20 ºC/min), the salt is liquid at room temperature. Besides that, it indicates that this salt has a glass transition (T_g) with a midpoint located at -38.4 ºC; a similar behaviour was found in the two following cycles. This behaviour is also observed for other salts. In the case of [(C_2OH)bpy][NTf_2], the thermogram indicates that originally the salt is a crystalline solid, once only the melting point is detected on the 1st cycle. Upon cooling, it avoids crystallization and the salt becomes a supercooled liquid, since only glass transition is detected in heating (see Figure A. 7.1.48 in annex). In some of the cases, it was additionally detected a sharp exothermic peak in the cooling run, which could be attributed to the energy release derived from the cracking of the glassy structure (for example, see Figure A. 7.1.44 in annex) [34].

Mono-substituted-4,4'-bipyridinium iodide salts presents a yellow, orange or brown colour in solid state due to the strong optical charge-transfer with the iodide anion. When the anion is changed to [NTf_2] or [AOT] a white or brown colour is observed (Figure 2.5). These colours are dependent of the type of substituents on *N*-position of bipyridinium core and the counter-ion. This anion exchange leads to a red shift in the maximum wavelength value of the salts in acetonitrile solution. The UV-Vis spectra of the salts are presented in annex. These mono-substituted-4,4'-bipyridinium salts are very useful precursors for the preparation of non-symmetric di-substituted-4,4'-bipyridinium salts.

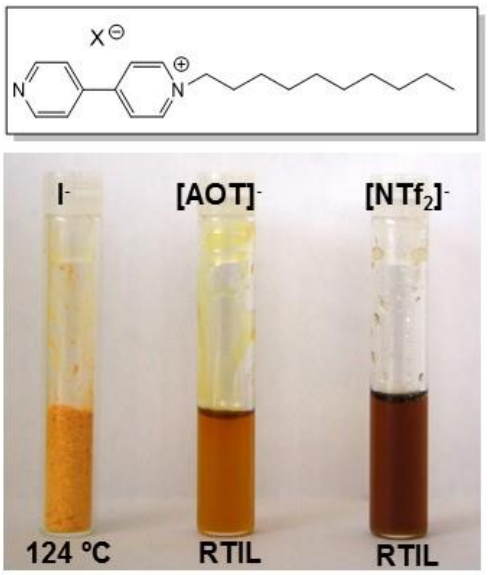

Figure 2.5 – Colour of mono-substituted-4,4'-bipyridinium salts: [C_{10}bpy]I, [C_{10}bpy][AOT] and [C_{10}bpy][NTf_2], respectively.

2.2.2. Di-substituted-4,4'-bipyridinium salts

According to the literature, 4,4'-bipyridinium di-cations are the most stable species and colourless, unless optical charge-transfer with the anion or other charge-donating species occurs [1]. The first electron-transfer process attracted attention due to possibility to observe clearly a colour switch between di-cation and radical cation scaffolds. Essentially, this colour switch is depending from the type and length of the substituent on the nitrogen, the type of anion and the solvent [1,2].

Thereby, it is possible to prepare 4,4'-bipyridinium salts with the same substituent (symmetric) or different groups (non-symmetric) at *N*-position on bipyridinium scaffold. We have explored both alternatives as described in detail below. The preparation of di-substituted-4,4'-bipyridinium salts was performed in two synthetic steps. Firstly, synthesis of symmetric or non-symmetric 4,4'-bipyridinium salts, which can be prepared directly from 4,4'-bipyridine (symmetric salt) or using a mono-substituted-4,4'-bipyridinium salt as precursor previously prepared (non-symmetric salt). Then, a second step was related to anion exchange reaction using Li[NTf_2] or Na[AOT] as selected anions.

2.2.2.1. Synthesis of Symmetric Salts

The preparation of symmetric salts involved the recrystallization of mono-cation or directly from 4,4'-bipyridine by nucleophilic substitution reaction with appropriate alkylating agent in excess. After optimization of the reactional conditions, acetonitrile as suitable solvent was selected allowing the precipitation of desired di-cation salt during the reaction. The ^{1}H NMR of the di-cation recrystallized from the reactional mixture previously mentioned is presented in Figure 2.6.

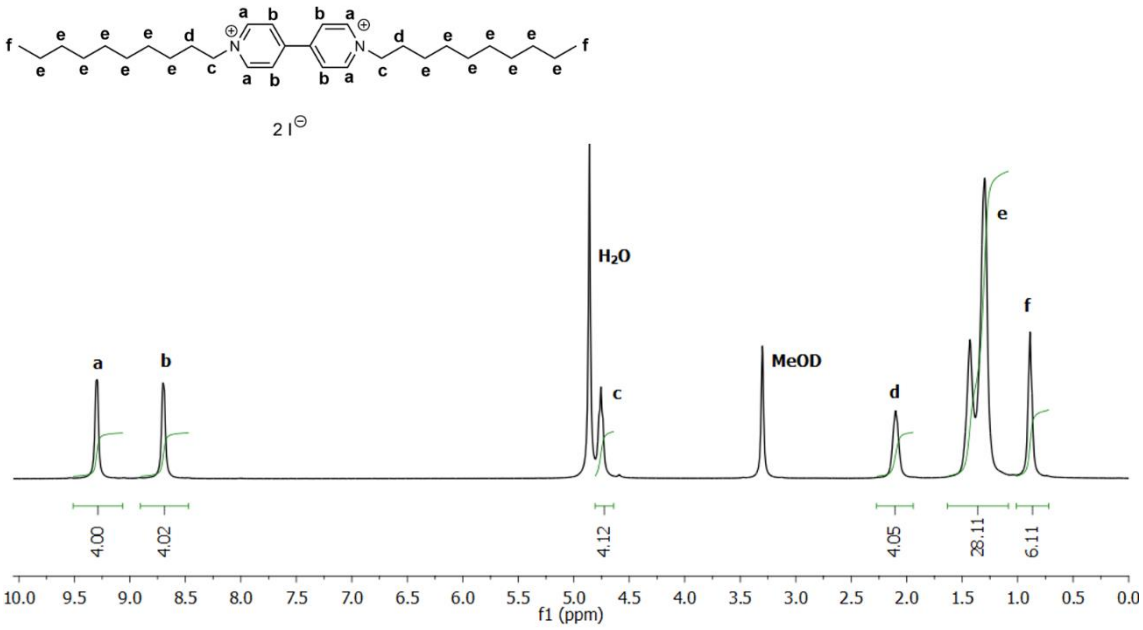

Figure 2.6 – ^{1}H NMR spectra of $[(C_{10})_2bpy]I_2$ in CH_3OD upon recrystallization in acetone.

Di-substituted-4,4'-bipyridinium di-iodide salts were obtained in moderate to high yields (50 to 94 %) as well as high purity levels. A second synthetic step, which is related to an anion exchange reaction, was further performed using $Li[NTf_2]$ and Na[AOT] in methanol or aqueous media, from room temperature to 60 ºC (Scheme 2.5).

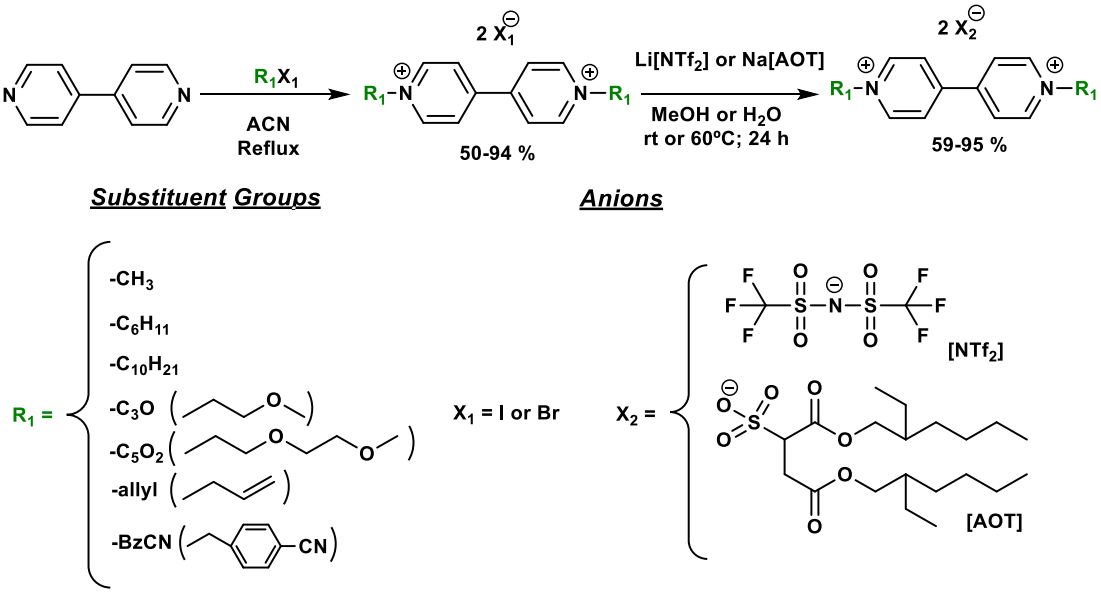

Scheme 2.5 –Synthetic route for preparation of symmetric di-substituted-4,4'-bipyridinium salts.

In general, the $[NTf_2]$ and [AOT] based salts were obtained in moderate to high yields (59 to 95 %) due to the purification step in order to remove any residual halides. Similar to the mono-cations, the anion exchange reaction from halide to $[NTf_2]$ anion was performed in water, facilitating the purification step. In the others cases, methanol was selected as reaction media and additional purification steps such as precipitation or liquid/liquid extraction with water were required.

All prepared salts are analysed by ^{1}H NMR, ^{13}C NMR and ^{19}F NMR for $[NTf_2]$ based salts. In the case of [AOT] salts, it is also possible to determine the proportion between anion and cation by ^{1}H NMR, particularly for $[(C_5O_2)_2bpy][AOT]_2$ as 1:2.15 (cation:anion). Fluorine atoms are detected by ^{19}F NMR in the case of $[NTf_2]$ based salts.

FTIR was also used to check the structure of the salts. The most promising salts are analysed by elemental analysis (C, H, N). Melting points and glass transition (by DSC) for different prepared organic salts were determined (Table 2.2).

Table 2.2 – Yield, physical state and thermal properties of symmetric di-substituted-4,4'-bipyridinium salts prepared.

Salts	Yield (%)	Physical State	m.p. (T_g) (ºC)
$[(C_1)_2bpy]I_2$	n.d.[a]	Orange solid	>290 [b]
$[(C_1)_2bpy][NTf_2]_2$	68	White solid	130 [b]
$[(C_6)_2bpy]I_2$	n.d [a]	Red solid	256 [b]
$[(C_6)_2bpy][NTf_2]_2$	86	Yellow solid	75 [b]
$[(C_{10})_2bpy]I_2$	n.d.[a]	Red solid	290 [b]
$[(C_{10})_2bpy][NTf_2]_2$	95	Yellow solid	161 [b]
$[(C_3O)_2bpy]I_2$	50	Orange solid	248 [b]
$[(C_3O)_2bpy][NTf_2]_2$	91	White solid	109.3 (-22.6) [c]
$[(C_5O_2)_2bpy]I_2$	80	Orange solid	148 [b]
$[(C_5O_2)_2bpy][NTf_2]_2$	89	White solid	99.7 (-27.4) [c]
$[(C_5O_2)_2bpy][AOT]_2$	59	Pale brown liquid	RTIL (-21.7) [c]
$[(allyl)_2bpy]Br_2$	95	Yellow solid	215 [b]
$[(allyl)_2bpy][NTf_2]_2$	90	Cream solid	87 [b]
$[(bzCN)_2bpy]Br_2$	94	Pale yellow solid	[a]
$[(bzCN)_2bpy][NTf_2]_2$	93	White solid	[a]

[a] n.d. – not determined. These salts were obtained by recrystallization of mono-cation. [b] Melting point (m.p.) was measured using a melting point apparatus. [c] Melting point and glass transition temperature (T_g) was determined by DSC analysis with heating/cooling rate of 10 or 20 ºC/min.

In general, symmetric di-substituted-4,4'-bipyridinium combined with $[NTf_2]$ or [AOT] anions showed significantly lower melting point than their iodide or bromide salts analogues. Overall, it was possible to obtain three ILs, including one RTIL, $[(C_5O_2)_2bpy][AOT]_2$.

Thermal analysis was performed for some $[NTf_2]$ and [AOT] salts using DSC and the obtained parameters are summarized also in Table 2.2. In some cases, cold-crystallization is observed; this corresponds to the crystallization occurring when the amorphous material is heated above its glass transition [35].

In the case of $[(C_5O_2)_2bpy][AOT]_2$, it was possible to confirm that salt is a liquid at room temperature and only glass transition was detected under the applied experimental conditions (-60 to 120 ºC at 20 ºC/min). While $[(C_3O)_2bpy][NTf_2]_2$ presents a particular behaviour, only a melting peak centred at 109.3 ºC is detected (1st cycle, - 90 to 150 ºC at 10 ºC/min). During the subsequent cooling run, the sample partially undergoes melt crystallization (exothermic peak at 14.4 ºC) where some fraction remains amorphous. This amorphous fraction undergoes cold-crystallization

upon further heating that is observed as an exothermic peak at 8.1 ºC, followed by melting at 109.3 ºC. A concomitant variation of the areas under the melt and cold-crystallization peak occurs in such a way that the melting enthalpy remains almost invariant (Figure 2.7). In the case of $[(C_5O_2)_2bpy][NTf_2]_2$, only a melting at the 1st heating run (1st cycle, - 90 to 150 ºC at 10 ºC/min) is observed. In the subsequent runs, glass transition is detected with a midpoint at -27.4 ºC, followed by cold-crystallization (17.5 ºC) and melting (99.7 ºC).

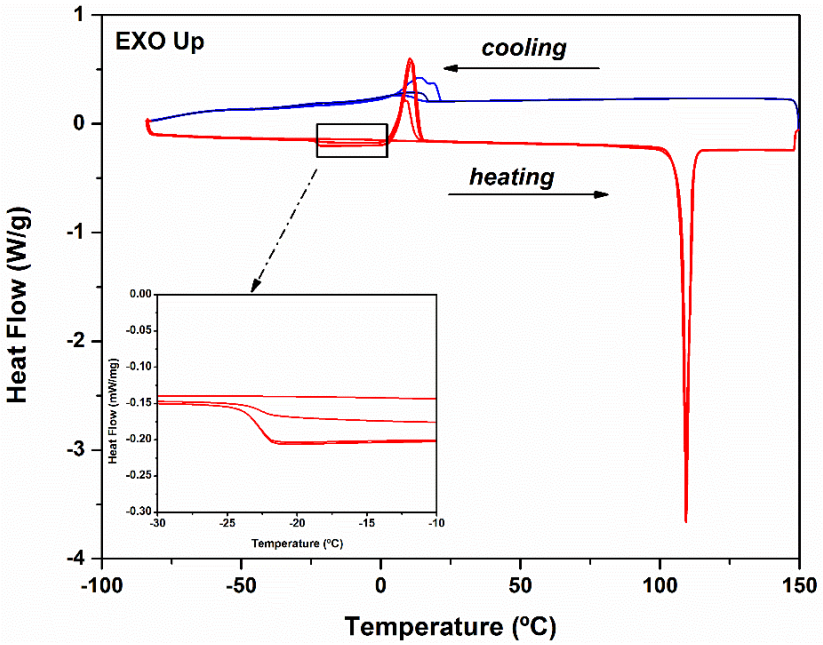

Figure 2.7 – Heat flow thermogram for $[(C_3O)_2bpy][NTf_2]_2$ obtained at 10 ºC/min (heating/cooling rate), where glass transition temperature (T_g as midpoint) was determined on the last heating run. Inset: the thermogram was enlarged to visualize the glass transition.

Herein, it is also observed an optical charge-transfer according to selected anion, in particular orange or red colour in solid state for di-iodide and yellow colour for di-bromide are observed. When the anion is changed to $[NTf_2]$ or [AOT] anion, a white, cream or pale brown colours were observed (Figure 2.8). In general, associated to this anion exchange the maximum wavelength value of the salts in acetonitrile solution exhibited a characteristic redshift. The UV-Vis spectra are presented in annex.

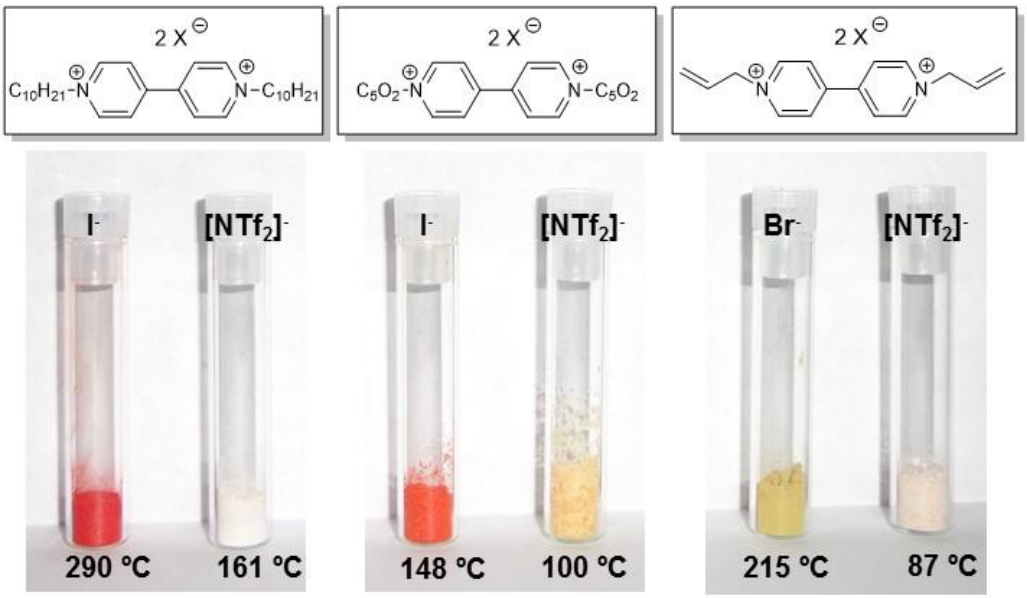

Figure 2.8 – Colour of symmetric di-substituted-4,4'-bipyridinium salts: $[(C_{10})_2bpy]I_2$, $[(C_{10})_2bpy][NTf_2]_2$, $[(C_5O_2)_2bpy]I_2$, $[(C_5O_2)_2bpy][NTf_2]_2$, $[(allyl)_2bpy]Br_2$, $[(allyl)_2bpy][NTf_2]_2$, respectively.

2.2.2.2. Synthesis of Non-Symmetric Salts

The non-symmetric salts obtained from nucleophilic substitution using the mono-cation previously prepared as precursor with appropriate reaction conditions, where the alkylating agent is added in excess. In this way, a variety of combinations of substituent groups can be obtained (Scheme 2.6).

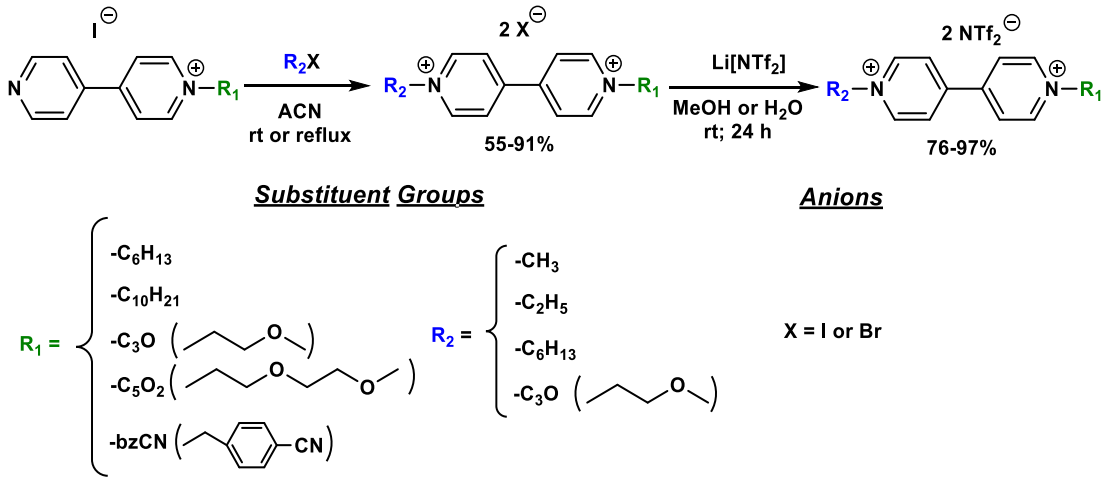

Scheme 2.6 – Synthetic route for preparation of non-symmetric di-substituted-4,4'-bipyridinium salts.

Acetonitrile as preferential reaction media in order to improve the reaction efficiency and facilitate further purification of the desired non-symmetric salt was selected. These non-symmetric salts are obtained with higher purity levels in moderate to high yield (55 to 91%). Then, an optimized anion exchange reaction using $Li[NTf_2]$ in methanol or aqueous media is performed. The final pure 4,4'-bipyridinium salts are obtained in high yields (76 to 97%) after the purification step. All prepared salts are analysed by ^{1}H NMR, ^{13}C NMR and ^{19}F NMR in the case of $[NTf_2]$ based salts

(Figure 2.9). For all cases, it was confirmed the presence of fluorine atoms in [NTf_2] salts by ^{19}F NMR.

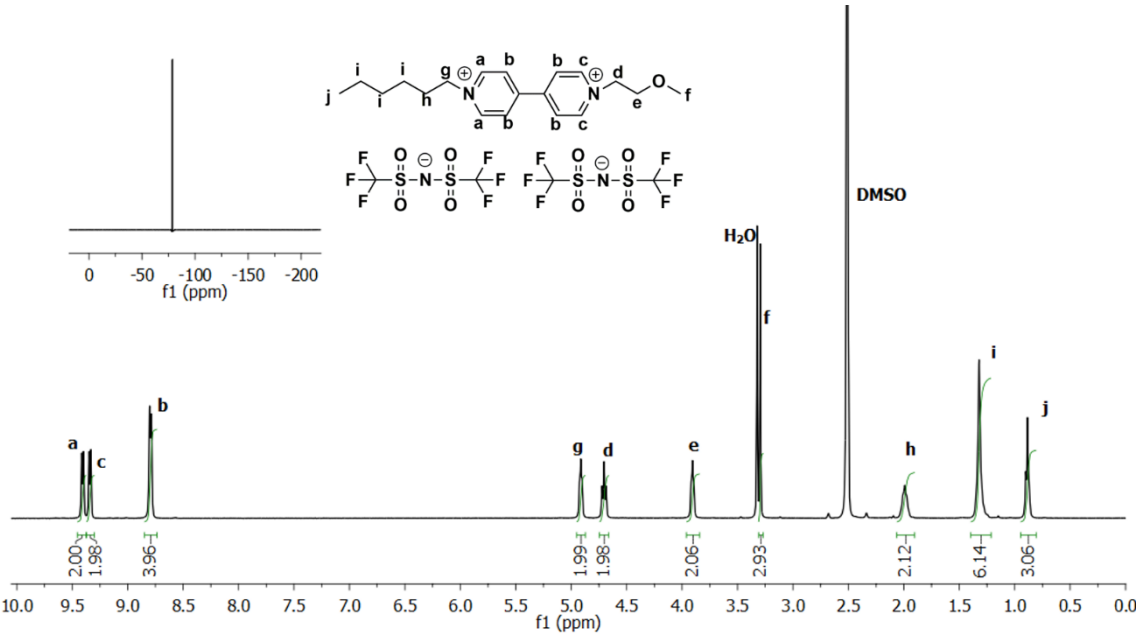

Figure 2.9 – ^{1}H NMR spectra of [C_6C_3Obpy][NTf_2]$_2$ in $(CD_3)_2SO$. Inset: ^{19}F NMR spectra of this salt.

FTIR has been also used to check the structure of the salt and the most promising salts were analysed by elemental analysis (C, H, N). Thermal properties were also determined for different prepared organic salts (Table 2.3).

Table 2.3 – Yield, physical state and thermal properties of non-symmetric di-substituted-4,4'-bipyridinium salts prepared.

Salts	Yield (%)	Physical State	m.p. (T_g) (ºC)
[C_1C_{10}bpy]I_2	90	Red solid	225 [a]
[C_1C_{10}bpy][NTf_2]$_2$	83	Brown solid	48.0 (-22.1) [b]
[(C_2C_6bpy]IBr	55	Red solid	241[a]
[(C_2C_6bpy][NTf_2]$_2$	97	Brown solid	48.0 (-28.3) [b]
[C_1C_3Obpy]I_2	85	Red solid	245 [a]
[C_1C_3Obpy][NTf_2]$_2$	89	Brown solid	80.8 (-17.5) [b]
[C_6C_3Obpy]I_2	79	Orange solid	>250 [a]
[C_6C_3Obpy][NTf_2]$_2$	88	Brown solid	57.9 (-25.9) [b]
[$C_1C_5O_2$bpy]I_2	91	Orange solid	195 [a]
[$C_1C_5O_2$bpy][NTf_2]$_2$	76	Brown liquid	RTIL (-22.1) [b]
[$C_6C_5O_2$bpy]I_2	81	Red solid	182 [a]
[$C_6C_5O_2$bpy][NTf_2]$_2$	87	Brown liquid	RTIL (-30.1) [b]
[(bzCN)C_3Obpy]BrI	58	Dark orange solid	n.d. [c]
[(bzCN)C_1bpy]BrI	62	Orange solid	n.d. [c]

[a] Melting point (m.p.) was measured using a melting point apparatus. [b] Melting point (m.p.) and Glass transition temperature (T_g) was determined (mid-point) by DSC analysis with heating/cooling rate of 5, 10 or 20 ºC/min, [c] n.d. – not determined.

Similar to the previous examples, the anion exchange reaction from halide to [NTf_2] leads to a significantly decrease in the melting points. In this context, six ILs are obtained, including two RTILs.

Some of these salts were studied by DSC. In the case of [$C_1C_5O_2$bpy][NTf_2]$_2$ and [$C_6C_5O_2$bpy][NTf_2]$_2$ it was possible to confirm for this selected conditions (-90 to 150 ºC at 10 ºC/ min), that these salts are liquid at room temperature and showed a glass transition with a midpoint around to -22.1 ºC and -30.1 ºC, respectively. In the case of [(C_2C_6)bpy][NTf_2]$_2$, a melting around 48.0 ºC at the first cycle was detected under the applied experimental conditions (-130 to 100 ºC at 10 ºC/min). In the subsequently cycle, a glass transition is observed with a midpoint around -28.3 ºC and this amorphous fraction undergoes cold-crystallization (31.3 ºC) upon further heating, followed by melting at 48.0 ºC. In the case of [C_1C_{10}bpy][NTf_2]$_2$, [C_1C_3Obpy][NTf_2]$_2$ and [C_6C_3Obpy][NTf_2]$_2$ (see Figure 2.10) only a melting point is observed at first cycle under the applied experimental conditions (- 90 to 150 ºC at 10 ºC/min). In the subsequent cooling run, the crystallization it is avoided and the salt becomes a supercooled liquid, since only glass transition is detected with a midpoint around -22.1 ºC, -17.5 ºC and -25.9 ºC, respectively.

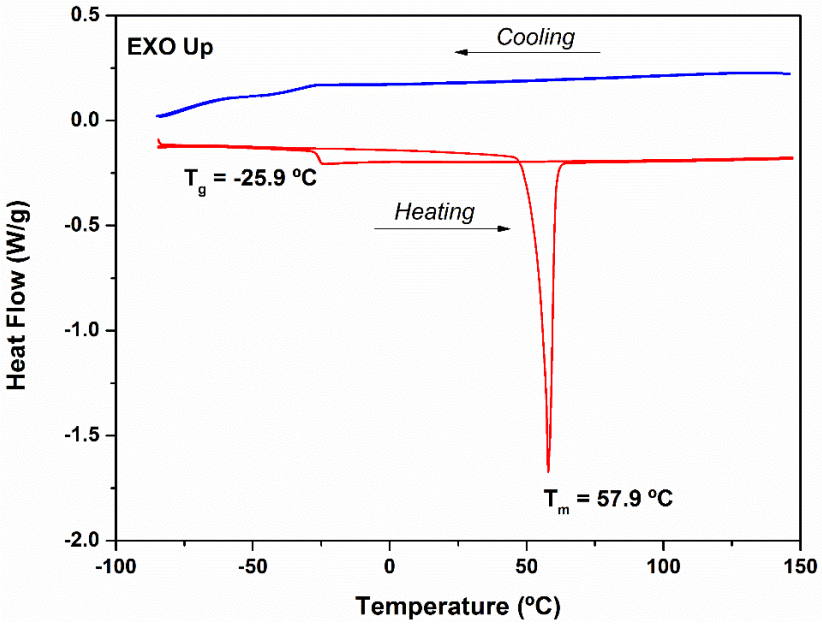

Figure 2.10 – Heat flow thermogram for [C_6C_3Obpy][NTf_2]$_2$ obtained at 10 ºC/min (heating/cooling rate), where glass transition temperature (T_g as midpoint) was determined on the last heating run.

It also observed an optical charge-transfer with anion, the halide salts are red or orange in solid state and a brown colour is observed for [NTf_2] based salts (Figure 2.11).

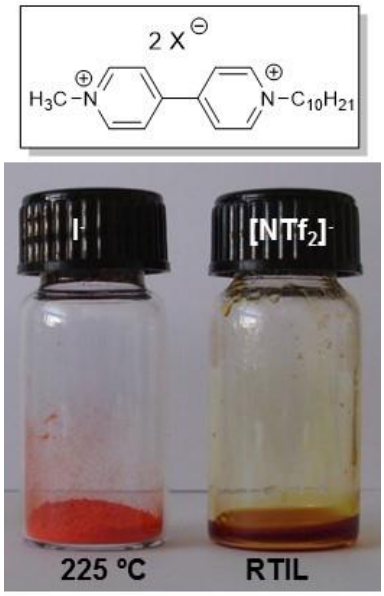

Figure 2.11 – Colour of non-symmetric di-substituted-4,4'-bipyridinium salts: (a) $[C_1C_{10}bpy]I_2$ and (b) $[C_1C_{10}bpy][NTf_2]_2$.

2.3. Rheological Studies

Viscosity is an important property in the case of IL applications such as electrochromic devices. It is also known as *"internal friction"* and it is considered a measure of "*resistance to flow*", i.e. "*the property of a material to resist deformation increasingly with increasing rate of deformation*" [36].

Detailed rheological studies for the initial prepared ILs, $[C_{10}bpy][NTf_2]$, $[C_{10}bpy][AOT]$ and $[C_1C_{10}bpy][NTf_2]_2$ were performed. These studies allowed to evaluate the type of fluid as Newtonian or Non-Newtonian. Newtonian fluids are fluids that obey Newton's linear law of friction (Equation 2.1).

$$\sigma = \eta\dot{\gamma}$$

Equation 2.1

Where, σ is shear stress (Pa), η is viscosity (Pa. s) and $\dot{\gamma}$ is shear rate (s^{-1}). Non-Newtonian Fluids are fluids that do not follow the linear law and are usually highly viscous fluids [36].

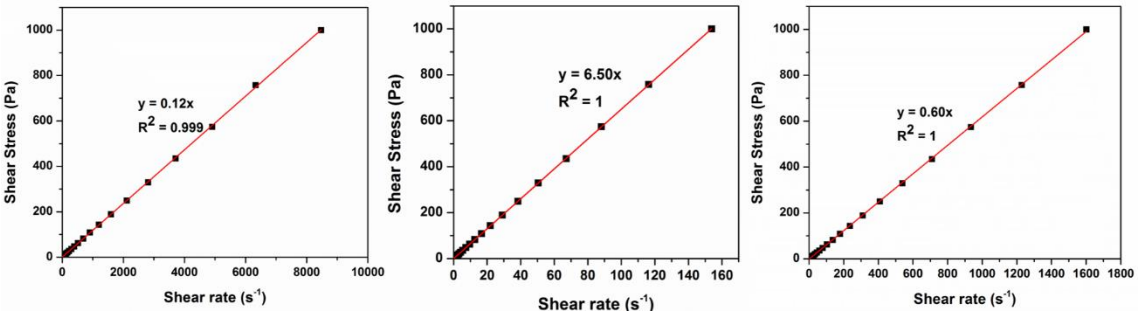

Figure 2.12 – Shear rate in function of shear stress for $[C_{10}bpy][NTf_2]$ (25 ºC), $[C_{10}bpy][AOT]$ (25 ºC) and $[C_1C_{10}bpy][NTf_2]_2$ (60 ºC).

In these viscosity studies, the previous plots of shear rate *versus* shear stress revealed that 4,4'-bipyridinium salts act as Newtonian fluid. From these plots, it is possible to determine the viscosity

at experimental temperature, which corresponds to the slope of the linear fitting. In the case of $[C_{10}bpy][NTf_2]$ and $[C_{10}bpy][AOT]$, the studies were performed at 25 ºC, while for $[C_1C_{10}bpy][NTf_2]_2$ was 60 ºC, in order to ensure that both salts are in the liquid state. These studies have been done in duplicate and the viscosity value is obtained by average values of both experiments. The dependence of viscosity with temperature was also studied for the previous salts. The heating and cooling profiles are represented in Figure 2.13 and Figure 2.14.

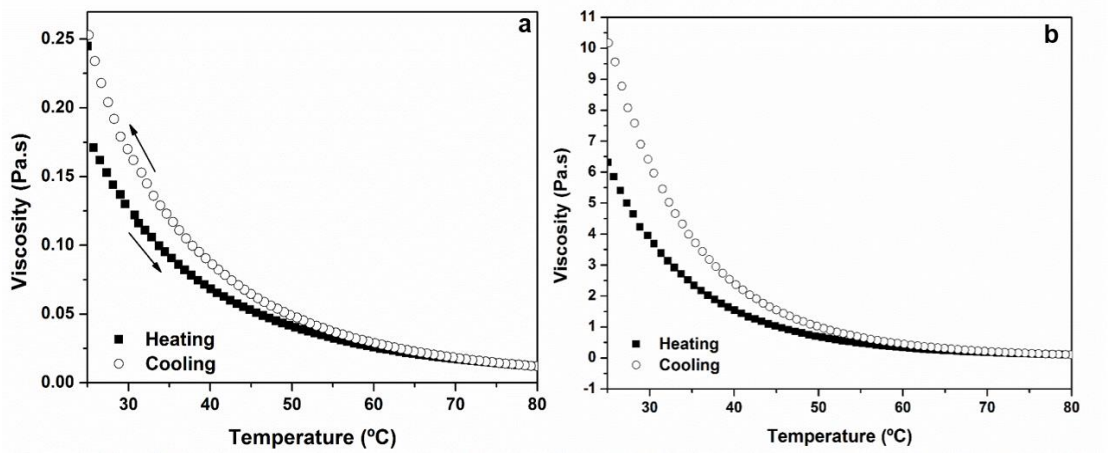

Figure 2.13 – Profile of the dependence of viscosity with temperature: heating and cooling profile of (a) $[C_{10}bpy][NTf_2]$ and (b) $[C_{10}bpy][AOT]$ from 25 ºC to 60 ºC (0.9 ºC/min).

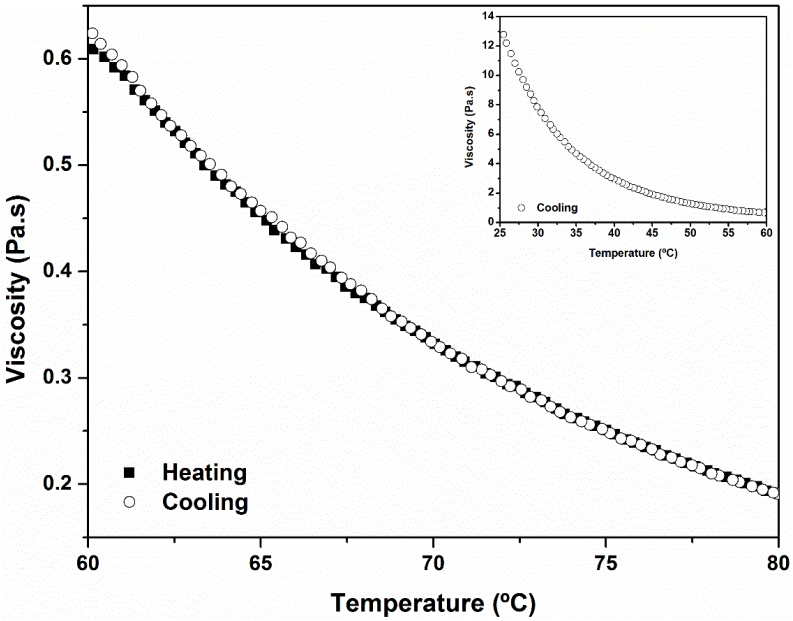

Figure 2.14 – Profile of the dependence of viscosity with temperature: (a) heating and cooling profiles of $[C_1C_{10}bpy][NTf_2]_2$ from 60 ºC to 80 ºC (1.0 ºC/min). Inset: cooling profile of $[C_1C_{10}bpy][NTf_2]_2$ from 60 ºC to 25 ºC (5.0 ºC/min).

The viscosity values obtained from the steady-state flow measurements and the viscosity values obtained from profile of the heating and cooling processes are presented in Table 2.4.

The viscosity of the RTILs is strongly dependent on the nature of the anion and cation and their tendency to form hydrogen bonds and the strength of van der Waals interactions (dispersion and repulsion) [28,29].

Table 2.4 – Rheological properties of $[C_{10}bpy][NTf_2]$, $[C_{10}bpy][AOT]$ and $[C_1C_{10}bpy][NTf_2]_2$.

Salts	Viscosity (Pa. s) [a]			Activation energy ($kJ.mol^{-1}$) [b]	
	25 ºC	60 ºC [c]	80 ºC [c]	E_h	E_c
$[C_{10}bpy][NTf_2]$	0.118 [d]	0.027	0.012	45.96 [e]	51.50 [f]
$[C_{10}bpy][AOT]$	6.458 [d]	0.403	0.120	72.28 [e]	75.98[f]
$[C_1C_{10}bpy][NTf_2]_2$	n.d. [g]	0.625 [d]	0.194	58.35 [h]	59.34 [i]

[a] Viscosity values were measured by using a rheometer with control of temperature ± 0.5 ºC. [b] Activation energy calculated with Arrhenius model, with r^2>0.999. [c] Viscosity values were determined by single point of temperature profile. [d] Newtonian fluid. [e] Heating profile (25 ºC to 80 ºC) with heating rate of 0.9 ºC/min [f] Cooling profile (80 ºC to 25 ºC) with cooling rate of 0.9 ºC/min. [g] n.d. – not determined. [h] Heating profile (60 ºC to 80 ºC), with heating rate of 1.0 ºC/min. [i] Cooling profile (80 ºC to 60 ºC), with cooling rate of 1.0 ºC/min.

Usually, the delocalization of the charge over the anion seems to reduce the viscosity values due to their weak hydrogen bonding with cation, in particular in the cases of $[NTf_2]$ based salts [29,37]. In the case of imidazolium, longer alkyl chains on the cation lead to an increase in viscosity value due to stronger van der Waals interactions [28]. Besides that, fluorinated chains and alkyl chain ramification, from butyl to isobutyl, lead also to an increase in viscosity value due to the reduction of rotation freedom [29].

In our case, $[C_1C_{10}bpy][NTf_2]_2$ is significantly more viscous than $[C_{10}bpy][NTf_2]$ and $[C_{10}bpy][AOT]$ at 60 ºC and 80 ºC. Comparing the anion nature effect for the same cation, $[C_{10}bpy][AOT]$ seems to be more viscous than $[C_{10}bpy][NTf_2]$. This can be explained by the nature of [AOT] anion, which it is a large and asymmetrical anion. The activation energies are obtained from the fitting of the heating and cooling profiles for the salts. As expected $[C_1C_{10}bpy][NTf_2]_2$ showed higher activation energies for the heating and cooling processes (E_h and E_c) comparing to $[C_{10}bpy][NTf_2]$. The salt $[C_{10}bpy][AOT]$ showed also higher activation energies for heating and cooling processes than those for $[C_{10}bpy][NTf_2]$. As expected, in all cases the viscosity values decrease with increasing temperature. In particular, $[C_1C_{10}bpy][NTf_2]_2$ showed the same profile of heating and cooling processes, indicating that the fluid returns to its initial state. Whereas, in the case of $[C_{10}bpy][NTf_2]$ and $[C_{10}bpy][AOT]$ the values of viscosity in the cooling process are higher than those found in the heating process, indicating that the reversibility of the fluid viscosity is relatively slow.

2.4. Electrochemical Studies

Electrochemical studies in solution using a three-electrode cell containing working electrode, reference electrode and auxiliary electrode have been performed [38,39]. The working electrode is in contact with the electroactive species and after applied with an adequate potential, the transfer of electrons between electrode and electroactive species occurs and the redox process take place on working electrode surface. Usually, the working electrode can be made from inert materials such as gold, silver, platinum, and glassy carbon, among others. While the auxiliary or counter electrode is an electrode that helps to carry out the current flowing through the cell [38–40]. Therefore, the current passes between the working electrode and the counter electrode. Typically, inert conducting materials such platinum or graphite are used [38–40]. The reference electrode has a stable and well-known electrode potential and the potential difference is measured between working electrode and the reference electrode. The most common reference electrode is silver/silver chloride (Ag/AgCl) and the saturated calomel. In order to avoid the contamination of the sample solution, it can be insulated from the sample reaction using an intermediate bridge [38].

As already mentioned in the introduction of this chapter, 4,4'-bipyridinium salts may exhibit three redox states: a di-cation, a radical cation and a neutral compound (di-reduced species) achieved by two successive electron-transfer processes [1,2]. One of the interests of these salts is related to the possibility to tune the colour switch between the di-cation and the radical cation through adequate selection of substituents, type and length, at *N*-position of bipyridinium cation and type of anion [1,2].

In our case, the 4,4'-bipyridinium salts are dissolved in dry acetonitrile (1 mM) with 0.1 M of tetrabutylammonium perchlorate (TBAP) as supporting electrolyte in three-electrode cell under inert atmosphere, using a glassy carbon (GC) as a working electrode, a platinum wire as a counter electrode and an aqueous saturated calomel electrode (SCE) as a reference electrode. The electrochemical measuring techniques as cyclic voltammetry (CV), pulsed voltammetry (DPV) and square-wave voltammetry (SWV) were used to evaluate the electrochemical behaviour.

Square-wave voltammetry (SWV) of one di-substituted-4,4'-bipyridinium salt, $[(C_5O_2)_2bpy]I_2$, is represented in Figure 2.15. Two successive one electron-transfer processes in the cathodic scan are observed. The first electron-transfer process (more positive peak) corresponds to the reduction of di-cation to radical cation, followed by the reduction of the radical cation to the neutral species.

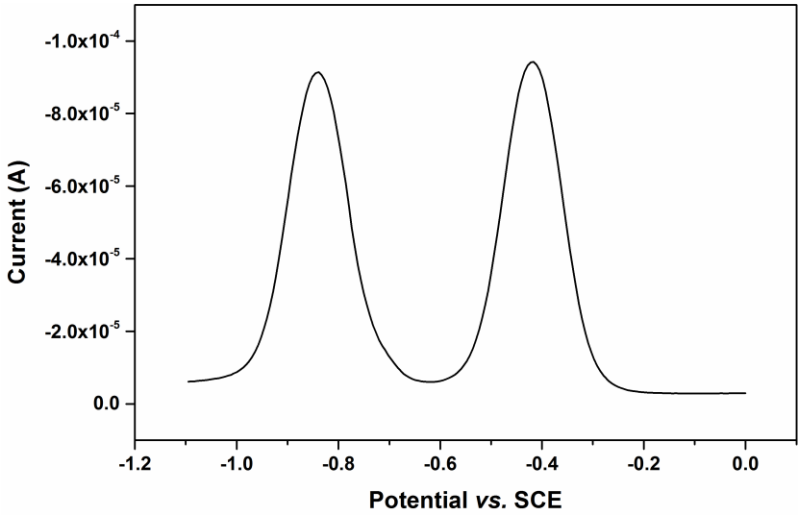

Figure 2.15 – Square-wave voltammetry (SWV) of 1 mM solutions of $[(C_5O_2)_2bpy]I_2$, in acetonitrile containing 0.1 M TBAP, at a glassy carbon working electrode *versus* SCE; 6 mV step potential, 60 mV pulse amplitude, 20 Hz.

Cyclic voltammetry of the previous di-substituted-4,4'-bipyridinium salt, $[(C_5O_2)_2bpy]I_2$, is illustrated in Figure 2.16.

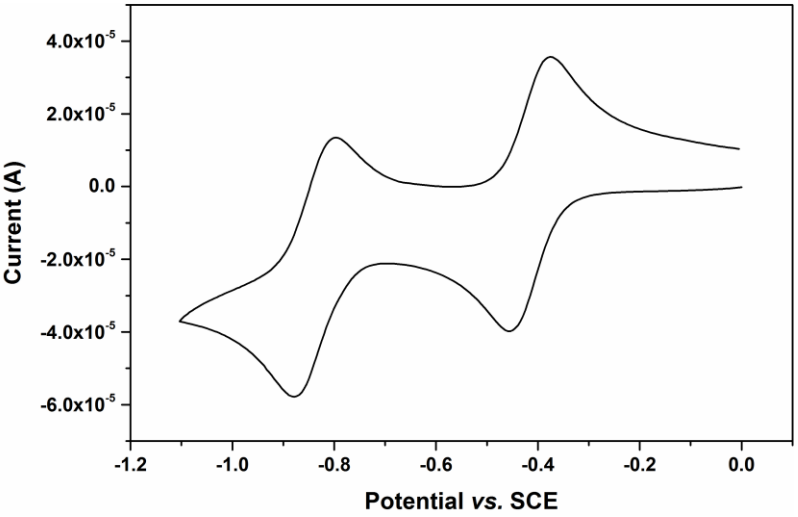

Figure 2.16 – Cyclic Voltammetry (CV) of 1 mM solution of $[(C_5O_2)_2bpy]I_2$ in acetonitrile containing 0.1 M TBAP at a glassy carbon working electrode *versus* SCE at 0.250 $V.s^{-1}$, 0/-1.1/0 V.

From the previous voltammogram it is possible to observe two electron-transfer processes, as expected for di-substituted-4,4'-bipyridinium salts. The first electron-transfer process, which is mono-electronic process, corresponds to the reduction of di-cation to radical cation. Then, the radical cation undergoes a second one electron-transfer process leading to the formation of neutral compound. These cyclic voltammetry studies allowed the determination of redox potentials as well as the evaluation of its reversibility. In this case, both reduction waves seem to be reversible.

In the context of this thesis, the first electron-transfer process is the most important redox process, due to the fact that is accompanied by a change of colour. Thus, it can be applied to electrochromic devices.

This electron-transfer process was studied in detail and an example of cyclic voltammetry is illustrated in Figure 2.17.

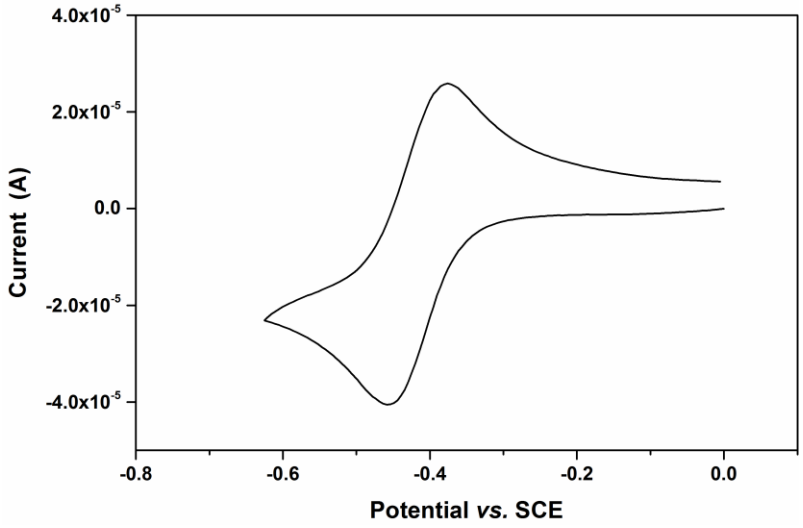

Figure 2.17 – Cyclic voltammetry (CV) of 1 mM of $[(C_5O_2)_2bpy]I_2$ in acetonitrile containing 0.1 M TBAP at a glassy carbon working electrode *versus* SCE at 0.250 $V.s^{-1}$, 0/-0.61/0V.

In general, all di-substituted-4,4'-bipyridinium salts showed a reversible wave that corresponds to the reduction of the di-cation to radical cation. From these studies, it was possible to determine the redox potential of the first and second electron-transfer processes of mono- and di-substituted-4,4'-bipyridinium salts and these results are discussed above. The redox potential for the first (E_{pc1}) and second (E_{pc2}) electron-transfer processes of mono- and di-substituted-4,4'-bipyridinium salts are presented in Table 2.5.

Table 2.5 – Cathodic peaks potential of mono-substituted-4,4'-bipyridinium salts [a].

Salts	E_{pc1} [V *vs.* SCE]	E_{pc2} [V *vs.* SCE]
$[C_6bpy]I$	-0.86	n.d. [b]
$[C_6bpy][NTf_2]$	-0.98	-1.68
$[C_{10}bpy]I$	-0.96	n.d. [b]
$[C_{10}bpy][NTf_2]$	-0.98	-1.59
$[C_{10}bpy][AOT]$	-0.98	-1.68

[a] Square-wave voltammetry (SWV) and cyclic voltammetry (CV) studies were performed in order to check the redox peaks of mono-substituted-4,4'-bipyridinium salt in dry acetonitrile (1 mM) with 0.1M TBAP. Acquisition parameters: SWV at 20 Hz, CV at 0.200 $V.s^{-1}$ scan rate; working, auxiliary, and reference electrodes of Pt, Pt wire, and SCE, respectively. [b] n.d. – not determined.

Two waves in direct cathodic scan were observed, corresponding to the reduction of mono-cation to radical cation, followed the reduction of radical cation to neutral compound. In general, the reduction of the radical cation to neutral compound exhibited higher redox potential (-1.59 to -1.68 V *vs* SCE) than the corresponding electrochemical generation of radical cation (-0.86 to -0.98 V *vs* SCE). The electrochemical studies of mono-substituted-4,4'-bipyridinium salts were not studied in detail.

Similar behaviour was also detected in the case of di-substituted-4,4'-bipyridinium salts. The standard redox potentials of symmetric di-substituted-4,4'-bipyridinium salts are presented in Table 2.6.

Table 2.6 – Standard cathodic potential of symmetric di-substituted-4,4'-bipyridinium salts.

Salts	E^0_1 [V *vs.* SCE]	E^0_2 [V *vs.* SCE]
$[(C_1)_2bpy]I_2$ [a]	-0.44 [c]	-0.85 [c]
$[(C_1)bpy][NTf_2]_2$ [a]	-0.44 [c]	-0.85 [c]
$[(C_{10})bpy]I_2$ [b]	-0.433	-0.867
$[(C_{10})bpy][NTf_2]_2$ [b]	-0.440	-0.874
$[(C_5O_2)_2bpy]I_2$ [b]	-0.415	-0.839
$[(C_5O_2)_2bpy][NTf_2]_2$ [b]	-0.410	-0.834
$[(C_5O_2)_2bpy][AOT]_2$ [b]	-0.417	-0.842
$[(C_3O)_2bpy]I_2$ [b]	-0.409	-0.837
$[(C_3O)_2bpy][NTf_2]_2$ [b]	-0.406	-0.834
$[(allyl)_2bpy]Br_2$ [b]	-0.401	-0.805
$[(allyl)_2bpy][NTf_2]_2$ [b]	-0.385	-0.800

[a] Square-wave voltammetry (SWV) and cyclic voltammetry (CV) studies were performed in order to check the redox peaks of di-substituted-4,4'-bipyridinium salt in dry acetonitrile (1 mM) with 0.1M TBAP. Acquisition parameters: SWV at 20 Hz, CV at 0.200 $V.s^{-1}$ scan rate; working, auxiliary, and reference electrodes of Pt, Pt wire, and SCE, respectively. [b] Cyclic Voltammetry (CV) studies were performed in order to check the standard redox potentials of di-substituted-4,4'-bipyridinium salts in dry acetonitrile (1 mM) with 0.1M TBAP. Acquisition parameters: SWV at 20 Hz, CV at 0.250 $V.s^{-1}$ scan rate; working, auxiliary and reference electrodes of glassy carbon (GC), Pt wire and *SCE*, respectively. [c] Cathodic potential peak.

As expected, in direct cathodic scan of the CV, two reversible waves are detected, which correspond to the first and second electron-transfer processes characteristic from di-cation 4,4'-bipyridinium salts. The first wave corresponds to the reversible one electron-transfer process (-0.39 to -0.44 V *vs* SCE) that was accompanied by an intensely coloured radical cation formation. Whereas, the second wave that is also one electron-transfer process (-0.80 to -0.85 V *vs* SCE) leads to the formation of neutral compound. The observed shift in the standard potential (E^0) is due to the length and type of the side chain as well as the effect of the anion.

In general, in the first electron-transfer process, the di-cation salts combined with $[NTf_2]$ anion showed a lower standard potential, i.e. they are easier to reduce. In particular, the cation $[(allyl)_2bpy]$ seems to be the easiest cation to reduce when combined either bromide or $[NTf_2]$ anions. On the other side, the salt combined with [AOT] seems to stabilise the di-cation species, and consequently, is difficult to reduce than the corresponding iodide salt.

Table 2.7 summarizes the electrochemical properties of non-symmetric di-substituted-4,4'-bipyridinium salts. Similar to the symmetric 4,4'-bipyridinium salts, two reversible waves in direct cathodic scan and a shift in the standard potential are also detected. In general, at the first electron-transfer process, the non-symmetric di-cation salts combined with $[NTf_2]$ anion are also easier to reduce.

Table 2.7 – Standard cathodic potential of non-symmetric di-substituted-4,4'-bipyridinium salts.

Salts	E^0_1 [V *vs. SCE*]	E^0_2 [V *vs. SCE*]
$[C_2C_6bpy]IBr$ [a]	-0.47 [c]	-0.89 [c]
$[C_2C_6bpy][NTf_2]_2$ [a]	-0.40 [c]	-0.84 [c]
$[C_1C_{10}bpy]I_2$ [a]	-0.43 [c]	-0.86 [c]
$[C_1C_{10}bpy][NTf_2]_2$ [a]	-0.44 [c]	-0.86 [c]
$[(C_1C_5O_2)Bpy]I_2$ [b]	-0.426	-0.846
$[(C_1C_5O_2)Bpy][NTf_2]_2$ [b]	-0.417	-0.833
$[(C_6C_5O_2)Bpy]I_2$ [b]	-0.423	-0.850
$[(C_6C_5O_2)Bpy][NTf_2]_2$ [b]	-0.422	-0.850
$[(C_1C_3O)Bpy]I_2$ [b]	-0.427	-0.844
$[(C_1C_3O)Bpy][NTf_2]_2$ [b]	-0.421	-0.844
$[(C_6C_3O)Bpy]I_2$ [b]	-0.421	-0.847
$[(C_6C_3O)Bpy][NTf_2]_2$ [b]	-0.420	-0.845

[a] Square-wave voltammetry (SWV) and cyclic voltammetry (CV) studies were performed in order to check the redox peaks of di-substituted-4,4'-bipyridinium salt in dry acetonitrile (1 mM) with 0.1M TBAP. Acquisition parameters: SWV at 20 Hz, CV at 0.200 $V.s^{-1}$ scan rate; working, auxiliary, and reference electrodes of Pt, Pt wire, and SCE, respectively. [b] Cyclic Voltammetry (CV) studies were performed in order to check the standard redox potentials of di-substituted-4,4'-bipyridinium salts in dry acetonitrile (1 mM) with 0.1M TBAP. Acquisition parameters: SWV at 20 Hz, CV at 0.250 $V.s^{-1}$ scan rate; working, auxiliary and reference electrodes of glassy carbon (GC), Pt wire and SCE, respectively. [c] Cathodic potential peak.

Cyclic voltammetry of symmetric and non-symmetric di-substituted-4,4'-bipyridinium salts are presented in Figure 2.18, where a redox potentials shift correspondent to the first electron-transfer process are observed.

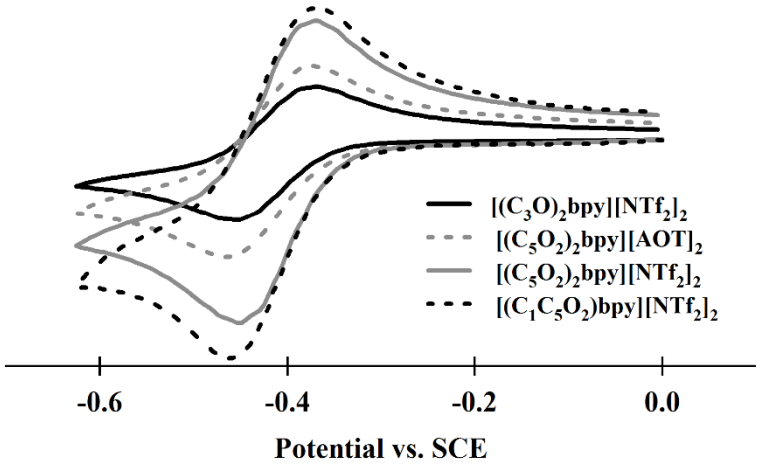

Figure 2.18 – Cyclic voltammetry (CV) of 1 mM solutions of di-substituted-4,4'-bipyridinium salts in acetonitrile containing 0.1 M TBAP, at a glassy carbon working electrode *versus* SCE, at 0.250 $V.s^{-1}$, showing the reversibility of the first reduction process (di-cation to radical cation) in detail. All voltammograms are normalised for a better comparison of the shift in the potentials for the different di-substituted-4,4'-bipyridinium salts, and then multiplied by a correction factor.

In conclusion, in the case of symmetric and non-symmetric di-substituted-4,4'-bipyridinium, the reduction potentials are more positive than the corresponding mono-cation (see Table 2.5, Table

2.6 and Table 2.7). As result of that, di-substituted-4,4’-bipyridinium salts were studied in more detail in accordance with their higher electrochemical stability as well as their potential electrochromic applications (Chapter 3 – Electrochromic application in Devices).

2.5. Conclusions

In general, the anion exchange to [AOT] and [NTf_2] allowed a decrease of the melting point of the salts comparing to halide precursor salts. In the case of mono- or di-substituted-4,4'-bipyridinium salts, it was possible to obtain examples of ILs, including RTILs.

The preparation of mono-substituted-4,4'-bipyridinium salts seems to be very interesting in order to facilitate the final preparation of non-symmetric salts.

It was possible to observe an effect on substituent groups (length and type) on *N*-position of 4,4'-bipyridinium scaffold, as well as the type of anion in thermal, rheological and electrochemical properties of the 4,4'-bipyridinium salts.

According to electrochemical data, di-substituted-4,4'-bipyridinium salts exhibited two reversible one electron-transfer processes and showed good electrochemical stability. In general, the reduction potentials are higher than correspondent mono-substituted 4,4'-bipyridinium salts. From an electrochemical point of view, it seems possible to use di-substituted-4,4'-bipyridinium based on [NTf_2] or [AOT] anions for electrochromic applications.

2.6. Experimental Section

Solvent and Reagents for synthesis

All solvents and reagents were used as supplied. Acetonitrile (J.T. Baker), methanol (Carlo Erba Reagents), ethyl acetate (Carlo Erba Reagents), dichloromethane (Sigma-Aldrich) and acetone (Sigma-Aldrich). 4,4'-bipyridine (Alfa-Aesar, 98 %), 2-methoxyethanol (Alfa-Aesar, 99 %), iodomethane (B.D.H laboratory reagent, > 98 %), 1-iododecane (Sigma-Aldrich, 98 %), 1-bromoethane (Sigma-Aldrich, 98 %), 1-iodohexane (Sigma-Aldrich, 98 %), 1-Allyl iodide (Sigma-Aldrich, 98 %), lithium bis(trifluoromethanesulfonyl)imide (Alfa-Aesar, > 98 %), sodium docusate (Acros Organics, 96%). 2-Methoxyethyl iodide and 2-(2-methoxyethoxy)ethyl iodide were prepared in two steps according to the synthetic method reported previously [41].

NMR Spectroscopy

NMR spectra were done on a Bruker AMX 400 instrument operating at 400.13 MHz (^{1}H), 100.61 MHz (^{13}C) and 376.50 MHz (^{19}F). The NMR spectrometers are part of The National NMR Facility supported by Fundação para a Ciência e a Tecnologia (RECI/BBB-BQB/0230/2012).

Elemental analysis

Elemental analysis was obtained on a Thermofinnigan Flash EA 1112 Series instrument and was performed by the Laboratório de Análises at LAQV/UCIBIO – REQUIMTE.

Thermal analysis

Melting points were determined with capillary on Electrothermal Melting Point apparatus (uncorrected). DSC analysis is carried out using Setaram DSC 131 by the Laboratório de Análises at LAQV/UCIBIO – REQUIMTE. As alternative, TA Instruments Q-series TM Q2000 DSC with a refrigerated cooling system was also used. The sample is continuously purged with 50 ml/min nitrogen. About 2-15 mg of salt was crimped in an aluminium hermetic sample pan with lid. The melting point and glass transition temperature were determined in the second or third heating run.

FTIR spectroscopy

FTIR spectra were recorded on a Buker Tensor 27, using KBr pellet for the solids and NaCl cells for the liquids.

Rheology studies

The viscosity measurements were done using a Rheometer (RS-300, Haake, Germany). A steady-state flow measurements were carried out using a controlled-stress rheometer fitted with a sensor PP20. The torque amplitude was imposed using a logarithmic ramp of shear stress increasing in 30 min from 0.01 to 1000 Pa. The temperature of the mono-cations, $[C_{10}bpy][NTf_2]$, $[C_{10}bpy][AOT]$ and the di-cation, $[C_1C_{10}bpy][NTf_2]_2$, were maintained at 25±0.5 °C and 60±0.5 °C respectively, using a circulating water bath. Another study made was the temperature dependence of viscosity. The mono-cations $[C_{10}bpy][NTf_2]$, $[C_{10}bpy][AOT]$ and di-cation $[C_1C_{10}bpy][NTf_2]_2$ were heated from 25 to 80 ºC (0.91ºC/min) and 60 to 80 ºC (1.00 ºC/min) respectively, using a constant shear rate of 20 Pa. All the measurements were performed in duplicate and the viscosity were determined based on average of these two measurements.

Electrochemical studies

For electrochemical studies acetonitrile (J.T. Baker) and methanol (Carlo Erba) were of gradient-HPLC grade and acetonitrile was dried over CaH_2 and distilled under argon. Tetrabutylammonium perchlorate (TBAP) puriss electrochemical grade was purchased from Fluka, and was dried overnight at 80 ºC before use. Type I water was obtained from a Watermax purification station (Diwer Technologies). All glassware was cleaned with a mixture of concentrated H_2SO_4:H_2O_2 (1:1), thoroughly rinsed, oven dried and cooled in a desiccator prior to use. Prior to use, the working electrode was polished in aqueous suspensions of 1.0 and 0.3 μm alumina (Beuhler) over 2-7/8" micro-cloth (Beuhler) polishing pads, then rinsed with water and methanol or acetonitrile.

UV-Visible spectroscopy

UV-Visible spectroscopy was done using Varian Cary 100 Bio spectrophotometer at room temperature.

Density

The density measurement was done using a micropycnometer. The density of the $[C_{10}bpy][NTf_2]$ was measured by an indirect method in the presence of n-heptane to complete the volume of the micropycnometer.

Synthesis of mono-substituted-4,4'-bipyridinium salts

1-methyl-4,4'-bipyridinium iodide [C_1bpy]I

To a solution of 4,4'-bipyridine (0.503 g, 3.22 mmol) in ethyl acetate and iodomethane (1.10 mL, 17.67 mmol) was slowly added. The mixture was stirred at room temperature for 78 hours. After that, the precipitate was filtered and washed with diethyl ether. After purified by recrystallization with ethanol, the desired product was isolated and dried in vacuum to give an orange solid (0.850 g, 89 %). m.p. = 240 ºC (dec.). ^{1}H NMR (400.13 MHz, DMSO-d6, 25 ºC) δ = 9.15 (d, J = 6.6 Hz, 2H), 8.85 (d, J = 6.0 Hz, 2H), 8.62 (d, J = 6.6 Hz, 2H), 8.03 (d, J = 6.1 Hz, 2H), 4.39 (s, 3H). ppm. ^{13}C NMR (100.61 MHz, DMSO-d6, 25 ºC) δ = 151.8, 151.0, 146.1, 140.8, 124.9, 121.8, 47.6 ppm. FTIR (KBr): $\tilde{\upsilon}$ = 3022, 1643, 1539, 1412, 1331, 1188, 808, 710 cm^{-1}.

1-methyl-4,4'-bipyridinium bis(trifluoromethanesulfonyl)imide [C_1bpy][NTf_2]

The salt [C_1bpy]I (0.214 g, 0.72 mmol) was dissolved in water and lithium bis(trifluoromethanesulfonyl)imide (Li[NTf_2]) (0.248 g, 0.86 mmol) was added. The reaction mixture was stirred during 24 hours at room temperature. The precipitate was filtered and dried to give a white solid (0.229 g, 71%). m.p. = 70 ºC. ^{1}H NMR (400.13 MHz, DMSO-d6, 25 ºC) δ = 9.12 (d, J = 6.7 Hz, 2H), 8.86 (d, J = 6.1 Hz, 2H), 8.60 (d, J = 6.8 Hz, 2H), 8.02 (d, J = 6.2 Hz, 2H), 4.37 ppm (s, 3H). ^{19}F NMR (376.50 MHz, DMSO-d6, 25 ºC) δ = -78.73 ppm. ^{13}C NMR (100.61 MHz, DMSO-d6, 25 ºC) δ = 151.9, 151.0, 146.1, 140.9, 124.9, 121.8, 47.5 ppm. FTIR (KBr): $\tilde{\upsilon}$ = 3098, 3054, 2133, 1960, 1650, 1606, 1528, 1359, 1179, 1051, 877, 821, 788, 718 cm^{-1}. Elemental analysis calcd (%) for $C_{13}H_{11}F_6N_3O_4S_2$: C 34.59, H 2.46, N 9.30; found C 34.78, H 2.07, N 9.24.

1-hexyl-4,4'-bipyridinium iodide [C_6bpy]I

To a solution of 4,4'-bipyridine (0.572 g, 3.66 mmol) in dried acetonitrile was added slowly 1-iodohexane (0.92 mL, 6.23 mmol). The solution was heated at 60 ºC for 26 hours in argon atmosphere. The product was precipitate and washed with diethyl ether. After purified by recrystallization with acetone, the desired product was isolated as orange solid (0.839 g, 62 %). m.p. = 190 ºC (dec.). ^{1}H NMR (400.13 MHz, MeOD, 25ºC) δ = 9.18 (d, J = 6.8 Hz, 2H), 8.82 (d, J = 6.2 Hz, 2H), 8.54 (d, J = 6.6 Hz, 2H), 8.02 (d, J = 6.2 Hz, 2H), 4.72 (t, J = 7.6 Hz, 2H), 2.15-2.03 (m, 2H), 1.53 – 1.29 (m, 6H), 0.92 ppm (t, J = 7.0 Hz, 3H). ^{13}C NMR (100.61 MHz, MeOD, 25 ºC) δ = 154.9, 151.8, 146.6, 143.6, 127.2, 123.6, 62.8, 32.4, 26.9, 23.5, 14.3 ppm. FTIR (KBr): υ = 3030, 2926, 2858, 1637, 1539, 1458, 1412, 1223, 1169, 829, 729 cm^{-1}.

1-hexyl-4,4'-bipyridinium bis(trifluoromethanesulfonyl)imide [C_6bpy][NTf_2]

The salt [C_6bpy]I (0.096 g, 0.30 mmol) was dissolved in water and Li[NTf_2] (0.080 g, 0.28 mmol) was added and stirred during 24 hours at room temperature. The product was isolated by extraction with water/dichloromethane as brown solid (0.122 g, 90%). T_g = - 40.6 ºC. m.p. = 56 ºC. ^{1}H NMR (400.13 MHz, DMSO-d6, 25 ºC) δ= 9.22 (d, J = 6.8 Hz, 2H), 8.86 (d, J = 6.1 Hz, 2H), 8.62 (d, J = 6.8 Hz, 2H), 8.03 (d, J = 6.2 Hz, 2H), 4.61 (t, J=7.4 Hz, 2H), 2.02 – 1.87 (m, 2H), 1.39 – 1.20 (m, 6H), 0.86 ppm (t, J = 6.8 Hz, 3H). ^{13}C NMR (100.61 MHz, DMSO-d6, 25 ºC) δ = 152.3, 151.0, 145.3, 140.9, 125.4, 121.9, 60.4, 30.6, 30.6, 25.1, 21.8, 13.8 ppm. ^{19}F NMR (376.50 MHz, DMSO-d6, 25 ºC) δ = -78.7 ppm. FTIR (NaCl): υ = 3128, 3070, 2934, 2864, 1645, 1539, 1524, 1464, 1412 1352, 1194, 1057, 816, 789, 739 cm^{-1}. Elemental analysis calcd (%) for $C_{18}H_{21}F_6N_3O_4S.0.5H_2O$: C 40.75, H 4.18, N 7.92; found C 40.86, H 4.06, N 7.77.

1-decyl-4,4'-bipyridinium iodide [C_{10}bpy]I

To a solution of 4,4'-bipyridine (0.500 g, 3.23 mmol) in dried acetonitrile was added slowly 1-iododecane (1.30 mL, 6.09 mmol). The mixture was heated at 60 ºC for 23 hours, in argon atmosphere. The product was precipitated and washed with diethyl ether. After purified by recrystallization with acetone, the desired product was obtained as a yellow solid (0.877 g, 64 %). m.p. = 124 ºC. ^{1}H NMR (400.13 MHz, MeOD, 25 ºC) δ = 9.15 (d, J = 6.6 Hz, 2H), 8.82 (d, J = 6.1 Hz, 2H), 8.53 (d, J = 6.4 Hz, 2H), 8.01 (d, J = 6.1 Hz, 2H), 4.70 (t, J = 7.6 Hz, 2H), 2.16 – 2.00 (m, 2H), 1.50 – 1.20 (m,14H), 0.88 ppm (t, J = 6.5 Hz, 3H). ^{13}C NMR (100.61 MHz, MeOD, 25 ºC) δ = 155.5, 151.8, 146.5, 143.7, 127.2, 123.6, 62.8, 33.0, 32.5, 31.0, 30.5, 30.4, 30.1, 27.2, 23.7,14.4 ppm. FTIR (KBr): υ = 3038, 2920, 2853, 1641, 1543, 1462, 1412, 1217, 1178, 812, 727 cm^{-1}.

1-decyl-4,4'-bipyridinium bis(trifluoromethanesulfonyl)imide [C_{10}bpy][NTf_2]

The salt [C_{10}bpy]I (0.454 g, 1.07 mmol) was dissolved in methanol and Li[NTf_2] (0.367 g, 1.28 mmol) was added and stirred during 24 hours at room temperature. The solvent was removed and the product was isolated by extraction with water/dichloromethane as brown liquid (0.582 g, 94%). T_g = -38.4 ºC. ^{1}H NMR (400.13 MHz, DMSO-d6, 25 ºC) δ = 9.24 (d, J = 6.5 Hz, 2H), 8.88 (d, J = 5.7 Hz, 2H), 8.65 (d, J = 6.5 Hz, 2H), 8.05 (d, J = 5.9 Hz, 2H), 4.63 (t, J = 7.3 Hz, 2H), 2.03-1.90 (m, 2H), 1.38-1.15 (m, 14H), 0.85 ppm (t, J = 6.5 Hz, 3H). ^{13}C NMR (100.61 MHz, DMSO-d6, 25 ºC) δ = 152.7, 151.5, 145.8, 141.4, 125.9, 122.4, 60.9, 31.7, 31.2, 29.3, 29.3, 29.1,

28.9, 25.9, 22.6, 14.4 ppm. ^{19}F NMR (376.50 MHz, MeOD, 25 ºC) δ = -80.6 ppm. FTIR (NaCl): ῡ = 3072, 2928, 2856, 1643, 1607, 1549, 1524, 1464, 1348, 1188, 1055, 816,789, 741 cm^{-1}. Elemental analysis calcd (%) for $C_{22}H_{29}F_6N_3O_4S_2$: C 45.75, H 5.07, N 7.27; found C 45.52, H 4.50, N 6.99.

1-decyl-4,4'-bipyridinium docusate[C_{10}bpy][AOT]

The salt [C_{10}bpy]I (0.103 g, 0.24 mmol) was dissolved in water and sodium docusate (Na[AOT]) (0.124 g, 0.28 mmol) was added and stirred during 24 hours at room temperature. The product was recovered by extraction with water/dichloromethane and dried in vacuum to give a brown liquid (0.102 g, 59 %). T_g = -20.9 ºC. [cation:anion = 1:1.03]. ^{1}H NMR (400.13 MHz, DMSO-d6, 25ºC) δ = 9.22 (d, J = 6.5 Hz, 2H), 8.86 (d, J = 5.6, 2H), 8.63 (d, J = 6.5 Hz, 2H), 8.04 (d, J = 6.0 Hz, 2H), 4.61 (t, J = 7.4 Hz, 2H), 3.96 – 3.79 (m, 4H), 3.67 – 3.56 (m, 1H), 2.93 – 2.48 (m, 2H), 2.03 – 1.87 (m, 2H), 1.55 – 1.11 (m, 32H), 0.95 – 0.71 (m, 15H) ppm. ^{13}C NMR (100.61 MHz, DMSO-d6) δ = 171.0, 168.4, 152.2, 151.0, 145.3, 140.9, 125.4, 121.9, 66.1, 66.0, 61.4, 60.4, 38.2, 38.1, 31.3, 28.9, 28.8, 28.6, 28.4, 28.3, 25.4, 23.2, 23.1, 23.0, 22.4, 22.1, 13.9, 10.8, 10.7 ppm. FTIR (NaCl): ῡ = 3123, 3059, 2926, 2858, 1736, 1643, 1601, 1547, 1464, 1412, 1038, 820, 725 cm^{-1}. Elemental analysis calcd (%) for $C_{40}H_{66}N_2O_7S.2H_2O$: C 63.63, H 9.34, N 3.71; found (%) C 64.19, H 8.93, N 3.28.

1-(2-methoxyethyl)-4,4'-bipyridinium iodide [C_3Obpy]I

To a solution of 4, 4'-bipyridine (0.718 g, 4.60 mmol) in ethyl acetate was added slowly to 2-methoxyethyl iodide (1.434 g, 7.71 mmol) previously prepared. The reaction mixture was refluxed for ca. of 99 hours. After this period of time, the precipitate was filtered and washed with diethyl ether. The desired product was isolated and dried in vacuum to give a yellow solid (1.040 g, 66%). m.p. = 72 ºC. ^{1}H NMR (400.13 MHz, $CDCl_3$, 25 ºC) δ = 9.49 (d, J = 6.8 Hz, 2H), 8.91 (dd, J = 4.5, 1.6 Hz, 2H), 8.33 (d, J = 6.8 Hz, 2H), 7.74 (dd, J = 4.5, 1.6 Hz, 2H), 5.25 (t, 4.7 Hz, 2H), 4.00 (t, J = 4.7 Hz, 2H), 3.39 (s, 3H) ppm. ^{13}C NMR (100.61 MHz, D_2O, 25 ºC) δ = 154.2, 150.0, 145.2, 142.5, 125.9, 122.5, 70.1, 60.6, 58.4 ppm. FTIR (KBr): ῡ = 3036, 1642, 1546, 1406, 1218, 1178, 1108, 1012, 816, 708 cm^{-1}.

1-(2-methoxyethyl)-4,4'-bipyridinium bis(trifluoromethanesulfonyl)imide [C_3Obpy][NTf_2]

The salt [C_3Obpy]I (0.305 g, 0.89 mmol) was dissolved in water and Li[NTf_2] (0.334 g, 1.16 mmol) was added. After addition, the reaction was stirred during ca. 28 hours at room temperature. The precipitate was filtered, washed with water and dried in vacuum to give a pale brown solid (0.397 g, 81%). m.p. = 90 ºC. ^{1}H NMR (400.13 MHz, DMSO-d6, 25 ºC) δ = 9.17 (d, J = 5.7 Hz, 2H), 8.87 (d, J = 4.4 Hz, 2H), 8.63 (d, J = 5.8 Hz, 2H), 8.04 (d, J = 4.4, 2H), 4.87-4.80 (m, 2H), 3.91-3.83 (m, 2H), 3.28 (s, 3H) ppm. ^{19}F NMR (376.50 MHz, DMSO-d6, 25 ºC) δ = -76.51 ppm. ^{13}C NMR (100.61 MHz, DMSO-d6, 25 ºC) δ = 153.1, 151.5, 146.2, 141.4, 125.64, 122.41, 121.54, 118.34, 70.53, 60.36, 58.72 ppm. FTIR (KBr): ῡ = 3134, 3076, 2957, 2918, 1647, 1553, 1354, 1200, 1140, 1055, 814, 735, 613 cm^{-1}.

1-(2-methoxyethyl)-4,4'-bipyridinium docusate [C$_3$Obpy][AOT]

The salt [C$_3$Obpy]I (0.531 g, 1.55 mmol) was dissolved in methanol and Na[AOT] (0.790 g, 1.78 mmol) was added. After addition, the reaction was stirred during ca. 24 hours at room temperature. The solvent was evaporated and the product was recovered by extraction with water/ethyl acetate. The organic layer was dried over anhydrous magnesium sulfate and the desired product was obtained as brown liquid (0.295 g, 30%). [cation:anion = 1:1.05]. T_g = -15.9 ºC. ^{1}H NMR (400.13 MHz, DMSO-d6, 25 ºC) δ = 9.16 (d, J = 6.9 Hz, 2H), 8.87 (dd, J = 4.5, 1.6 Hz, 2H), 8.62 (d, J = 6.8 Hz, 2H), 8.03 (dd, J = 4.5,1.7 Hz, 2H), 4.82 (t, J = 4.9 Hz, 2H), 3.94 – 3.79 (m, 6H), 3.65 – 3.56 (m, 1H), 3.27 (s, 3H), 2.96 – 2.72 (m, 2H), 1.55 – 1.14 (m, 18H), 0.92 – 0.76 (m, 12H) ppm. ^{13}C NMR (100.61 MHz, DMSO-d6, 25 ºC) δ = 171.5, 168.8, 153.1, 151.5, 146.2, 141.4, 125.7, 122.4, 70.5, 66.6, 66.5, 61.9, 60.4, 58.7, 38.6, 34.6, 30.2, 30.1, 30.0, 28.8, 23.7, 23.6, 23.5, 22.9, 14.4, 11.3, 11.2 ppm. FTIR (NaCl): υ = 3123, 3057, 2959, 2930, 2866, 1732, 1643, 1549, 1460, 1410, 1240, 1038, 820, 729 cm^{-1}.

1-(2-(2-methoxyethoxy)ethane)-4,4'-bipyridinium iodide [C$_5$O$_2$bpy]I

To a solution of 4,4'-bipyridine (0.546 g, 3.50 mmol) in dried acetonitrile, 2-(2-methoxyethoxy)ethyl iodide (1.188 g, 5.16 mmol) was slowly added and the reaction mixture was stirred at 55 ºC during ca. 34 hours. The product was precipitated with diethyl ether and dried in vacuum to give a brown solid (0.419 g, 31 %). m.p. = 85 ºC. ^{1}H NMR (400 MHz, $CDCl_3$, 25 ºC) δ = 9.44 (d, J = 6.3 Hz, 2H), 8.82 (d, J = 5.2 Hz, 2H), 8.23 (d, J = 6.3 Hz, 2H), 7.64 (d, J = 5.3 Hz, 2H), 5.25 – 5.10 (m, 2H), 4.14 – 3.97 (m, 2H), 3.65 – 3.57 (m, 2H), 3.47 – 3.39 (m, 2H), 3.26 (s, 3H) ppm. FTIR (KBr) υ = 3034, 2924, 2878, 2820, 1640, 1460, 1410, 1178, 1098, 816, 706 cm^{-1}.

1-(2-(2-methoxyethoxy)ethane)-4,4'-bipyridinium bis(trifluoromethanesulfonyl)imide [C$_5$O$_2$bpy][NTf$_2$]

The salt [C$_5$O$_2$bpy]I (0.170 g, 0.44 mmol) dissolved in dichloromethane was mixed with Li[NTf$_2$] (0.152 g, 0.53 mmol) dissolved in methanol. The reaction mixture was stirred during 26 hours at room temperature. The solvents were removed and the product was recovered by addition of water. Then, the dried desired product was obtained as pale brown solid (0.197 g, 87%). m.p. = 79 ºC. ^{1}H NMR (400.13 MHz, $CDCl_3$, 25 ºC) δ = 8.98 (d, J = 6.4 Hz, 2H), 8.90 (d, J = 5.2 Hz, 2H), 8.24 (d, J = 6.3 Hz, 2H), 7.70 (d, J = 5.4 Hz, 2H), 4.83 (t, J = 4.1 Hz, 2H), 4.02 (t, J = 4 Hz, 2H), 3.70-3.62 (m, 2H), 3.54-3.47 (m, 2H), 3.34 (s, 3H) ppm. ^{13}C NMR (100.61 MHz, $CDCl_3$, 25 ºC) δ = 154.8, 151.5, 145.7, 141.1, 125.6, 121.5, 71.5, 70.5, 68.7, 61.5, 58.9 ppm. ^{19}F NMR (376.50 MHz, $CDCl_3$, 25 ºC) δ = -78.83 ppm. FTIR (KBr): υ = 3134, 3074, 2998, 2900, 2836, 1648, 1356, 1198, 1058, 932, 856, 814, 786, 738 cm^{-1}.

1-(2-(2-methoxyethoxy)ethane)-4,4'-bipyridinium docusate [C$_5$O$_2$bpy][AOT]

To a solution of [C$_5$O$_2$bpy]I (0.130 g, 0.34 mmol) in methanol, Na[AOT] (0.161 g, 0.36 mmol) was slowly added and the reaction mixture was stirred during 48 hours at room temperature. The solvent was removed and the product was recovered by extraction with dichloromethane/water. The organic layer was dried over anhydrous magnesium sulfate, filtered and the solvent was evaporated to give a brown liquid (0.190 g, 83%). [cation:anion = 1:1.1]. ^{1}H NMR (400.13 MHz,

DMSO-d6, 25 ºC) δ = 9.17 (d, J = 6.6 Hz, 2H), 8.88 (d, J = 5.8 Hz Hz, 2H), 8.66 (d, J = 6.6 Hz, 2H), 8.06 (d, J = 5.8 Hz, 2 H), 4.83 (m, 2H), 4.04 – 3.93 (m, 2H), 3.94 – 3.80 (m, 4H), 3.66 – 3.60 (m, 1 H), 3.59 – 3.53 (m, 2H), 3.16 (s, 3H), 3.02 – 2.72 (m, 2H), 1.57 – 1.12 (m, 18 H), 0.97 – 0.77 (m, 12H) ppm. FTIR (NaCl): ῡ = 3120, 3056, 2924, 2928, 2872, 1730, 1642, 1548, 1462, 1220, 1038, 818, 728 cm^{-1}.

1-allyl-4,4'-bipyridinium iodide [(allyl)bpy]I

To a solution of 4, 4'-bipyridine (0.499 g, 3.20 mmol) in ethyl acetate was added slowly to 1-allyl iodide (0.919 g, 5.47 mmol). The reaction mixture was stirred at room temperature for ca. of 29 hours. After this period of time, the precipitate was filtered and washed with diethyl ether. The desired product was isolated and dried in vacuum to give a yellow solid (0.728 g, 70%). m.p. = 149 ºC. ^{1}H NMR (400.13 MHz, D_2O, 25 ºC) δ = 8.86 (d, J = 6.9 Hz, 2H), 8.66 (dd, J = 4.7, 1.6 Hz, 2H), 8.31 (d, J = 6.8 Hz, 2H), 7.81 (dd, J = 4.6, 1.6 Hz, 2H), 6.18 – 6.03 (m, 1H), 5.55 – 5.38 (m, 2H), 5.19 (d, J = 6.3 Hz, 2H) ppm. FTIR (KBr): ῡ = 3118, 3036, 1638, 1602, 1546, 1412, 1220, 1166, 994, 956, 814, 748, 716 cm^{-1}.

1-allyl-4,4'-bipyridinium bis(trifluoromethanesulfonyl)imide [(allyl)bpy][NTf_2]

The salt [(allyl)bpy]I (0.232 g, 0.72 mmol) was dissolved in water and Li[NTf_2] (0.244 g, 0.85 mmol) was added. After addition, the reaction was stirred during ca. 25 hours at room temperature. The product was recovered by extraction with water/dichloromethane. The organic layer was dried over anhydrous magnesium sulfate, filtered and the solvent was evaporated to give a brown liquid (0.305 g, 89%). T_g = -39.2 ºC. ^{1}H NMR (400.13 MHz, DMSO-d6, 25 ºC) δ = 9.17 (d, J = 6.9 Hz, 2H), 8.87 (dd, J = 4.5, 1.6 Hz, 2H), 8.64 (d, J = 6.9 Hz, 2H), 8.02 (d, J = 4.5, 1.6 Hz, 2H), 6.28 – 6.11 (m, 1H), 5.51 – 5.38 (m, 2H), 5.29 (d, J = 6.1 Hz, 2H) ppm. ^{19}F NMR (376.50 MHz, DMSO-d6, 25 ºC) δ = -78.70 ppm. ^{13}C NMR (100.61 MHz, DMSO-d6, 25 ºC) δ = 153.2, 151.5, 145.9, 141.3, 132.1, 126.1, 122.4, 122.4, 62.5 ppm. FTIR (NaCl): ῡ = 3130, 3070, 1642, 1600, 1548, 1522, 1464, 1412, 1354, 1192, 1058, 994, 956, 814, 740, 654 cm^{-1}.

1-allyl-4,4'-bipyridinium docusate [(allyl)bpy][AOT]

The salt [(allyl)bpy]I (0.414 g, 1.28 mmol) was dissolved in methanol and Na[AOT] (0.667 g, 1.50 mmol) was added. After addition, the reaction was stirred during 24 hours at room temperature. The solvent was evaporated and the product was recovered by extraction with water/ethyl acetate. The organic layer was dried over anhydrous magnesium sulfate, filtered and the solvent was evaporated to give the product as brown liquid (0.250 g, 32%). [cation:anion = 1:1]. T_g = -15.4 ºC. ^{1}H NMR (400.13 MHz, DMSO-d6, 25 ºC) δ = 9.19 (d, J = 6.6 Hz, 2H), 8.89 (dd, J = 4.5, 1.6 Hz, 2H), 8.66 (d, J = 6.9 Hz, 2H), 8.05 (dd, J = 4.5, 1.6 Hz, 2H), 6.32-6.12 (m, 1H), 5.55 – 5.38 (m, 2H), 5.31 (d, J = 6.2 Hz, 2H), 4.03 – 3.79 (m, 4H), 3.67 – 3.59 (m, 1H), 3.00 – 2.73 (m, 2H), 1.57 – 1.17 (m, 18H), 0.93 – 0.74 (m, 12H) ppm. ^{13}C NMR (100.61 MHz, DMSO-d6, 25 ºC) δ = 171.1, 168.3, 152.7, 151.0, 145.4, 140.8, 131.7, 125.6, 121.9, 121.9, 66.1, 66.1, 66.0, 62.0, 61.4, 38.1, 34.1, 29.7, 29.6, 29.5, 28.3, 23.2, 23.1, 23.0, 22.4, 13.9, 10.8, 10.7 ppm. FTIR (NaCl): ῡ = 3117, 3055, 2964, 2928, 2864, 1730, 1641, 1601, 1547, 1462, 1412, 1240, 1038, 818, 725 cm^{-1}.

1-(2-hydroxylethyl)-4,4'-bipyridinium iodide [(C_2OH)bpy]I

To a solution of 4, 4'-bipyridine (0.681 g, 4.36 mmol) in ethyl acetate was added slowly to 1-iodoethanol (0.919 g, 5.47 mmol). The reaction mixture was refluxed for ca. of 96 hours. After this period of time, the solid was filtered and washed with diethyl ether. The desired product was recrystallized with acetonitrile and the desired product was obtained as yellow solid (0.788 g, 55 %). m.p. = 196 ºC (dec.). ^{1}H NMR (400.13 MHz, DMSO-d6, 25 ºC) δ = 9.14 (d, J = 6.5 Hz, 2H), 8.87 (d, J = 5.8 Hz, 2H), 8.63 (d, J = 6.5 Hz, 2H), 8.03 (dd, J = 5.9 Hz, 2H), 5.25 (t, J = 5.2 Hz, 1H), 4.69 (t, J = 4.7 Hz, 2H), 3.98-3.80 (m, 2H) ppm. ^{13}C NMR (100.61 MHz, DMSO-d6, 25 ºC) δ = 152.4, 151.0, 145.7, 140.9, 125.0, 121.9, 62.7, 60.0 ppm. FTIR (KBr): υ = 3267, 3113, 3005, 2866, 1637, 1543, 1462, 1402, 1175, 1063, 866, 812, 714 cm^{-1}.

1-(2-hydroxylethyl)-4,4'-bipyridinium bis(trifluoromethanesulfonyl)imide [(C_2OH)bpy][NTf_2]

The salt [C_2OHbpy]I (0.480 g, 1.46 mmol) was dissolved in water (with 20 % ACN (v/v)) and Li[NTf_2] (0.511 g, 1.78 mmol) was added. After addition, the reaction was stirred during ca. 68 hours at room temperature. The acetonitrile was evaporated and the product was recovered by extraction with water/ethyl acetate. The organic layer was dried over anhydrous magnesium sulfate, filtered and the solvent was evaporated to give a pale brown solid (0.240 g, 34%). m.p. = 86.21 ºC. T_g = -6.19 ºC. ^{1}H NMR (400.13 MHz, DMSO-d6, 25 ºC) δ = 9.13 (d, J = 6.4 Hz, 3H), 8.62 (d, J = 6.4 Hz, 3H), 8.16 – 8.01(m, 2H), 5.26 (t, J = 5.2 Hz, 1H), 4.68 (t, J = 4.7 Hz, 2H), 3.94 – 3.85 (m, 2H) ppm. ^{19}F NMR (376.50 MHz, DMSO-d6, 25 ºC) δ = -78.70 ppm. ^{13}C NMR (100.61 MHz, DMSO-d6, 25 ºC) δ = 152.5, 151.0, 145.7, 140.8, 125.0, 121.0, 117.8, 62.7, 60.0 ppm. FTIR (KBr): υ = 3132, 3068, 2864, 1648, 1614, 1532, 1364, 1194, 1140, 1050, 824, 790, 612 cm^{-1}.

Synthesis of di-substituted-4,4'-bipyridinium salts

1,1'-di-methyl-4,4'-bipyridinium di-iodide [(C_1)$_2$bpy]I_2

This salt was obtained by recrystallization of mono-cation [C_1bpy]I to give the desired product as an orange solid. m.p. > 290 ºC (dec.). ^{1}H NMR (400.13 MHz, DMSO-d6, 25 ºC) δ = 9.29 (d, J = 6.6 Hz, 4H), 8.77 (d, J = 6.6 Hz, 2H), 4.44 ppm (s, 3H). ^{13}C NMR (100.61 MHz, DMSO-d6, 25 ºC) δ = 148.1, 146.6, 126.0, 48.1 ppm. FTIR (KBr): υ = 3009, 1636, 1556, 1448, 1350,1269, 1178, 820 cm^{-1}.

1,1'-di-methyl-4,4'-bipyridinium di-[bis(trifluoromethanesulfonyl)imide] [(C_1)$_2$bpy][NTf_2]$_2$

The salt [(C_1)$_2$bpy]I_2 (0.101 g, 0.23 mmol) was dissolved in water and Li[NTf_2] (0.151, 0.52 mmol) was added and stirred during 24 hours at room temperature. The precipitate was filtered and dried in vacuum to give a white solid (0.116, 68 %). m.p. = 130 ºC. ^{1}H NMR (400.13 MHz, DMSO-d6, 25 ºC) δ = 9.27 (d, J = 6.4 Hz, 4H), 8.74 (d, J = 6.4 Hz, 4H), 4.42 ppm (s, 3H). ^{13}C NMR (100.61 MHz, DMSO-d6, 25 ºC) δ = 148.2, 146.6, 126.0, 48.0 ppm. ^{19}F NMR (376.50 MHz, DMSO-d6, 25 ºC) δ = -78.73 ppm. FTIR (KBr): υ = 3138, 3072, 1645, 1574, 1508, 1439, 1358,1190, 1136, 1051, 833, 795, 741 cm^{-1}. Elemental analysis calcd (%) for $C_{16}H_{14}F_{12}N_4O_8S_4$: C 25.74, H 1.89, N 7.51; found: C 25.94, H 1.46, N 7.07.

1,1'-di-hexyl-4,4'-bipyridinium di-iodide [$(C_6)_2$bpy]I_2

This salt was obtained by recrystallization of monocation [C_6bpy]I to give the desired product as red solid. m.p. = 256 ºC (dec.). ^{1}H NMR (400.13 MHz, MeOD, 25 ºC) δ = 9.30 (d, J = 5.7 Hz, 4H), 8.70 (d, J = 4.8 Hz, 4H), 4.76 (t, J = 7.3 Hz, 4H), 2.20 – 2.00 (m, 4H), 1.59 – 1.26 (m, 12H), 0.93 ppm (t, J = 6.5 Hz, 6H). ^{13}C NMR (100.61 MHz, MeOD, 25 ºC) δ = 151.2, 147.1, 128.4, 63.2, 32.5, 32.3, 26.9, 23.5, 14.3 ppm. FTIR (KBr): $\breve{\upsilon}$ = 3015, 2928, 2856, 1636, 1553, 1508, 1454, 1371, 1234, 1173, 829 cm^{-1}.

1,1'-di-hexyl-4,4'-bipyridinium di-[bis(trifluoromethanesulfonyl)imide] [$(C_6)_2$bpy][NTf_2]$_2$

The salt [$(C_6)_2$bpy]I_2 (0.234 g, 0.40 mmol) was dissolved in water and Li[NTf_2] (0.268 g, 0.93 mmol) was added and stirred during 24 hours at room temperature. The precipitate was filtered and dried to give a pale yellow solid (0.308 g, 86%). m.p. = 75 ºC. ^{1}H NMR (400.13 MHz, MeOD, 25 ºC) δ = 9.27(d, J = 6.4 Hz, 4H), 8.66 (d, J = 5.9 Hz, 4H), 4.76 (t, J = 7.5 Hz, 4H), 2.14 – 2.07 (m, 4H),1.47 – 1.40 (m, 12H), 0.97 – 0.94 ppm (t, 6H). ^{13}C NMR (100.61 MHz, DMSO-d6, 25ºC) δ = 148.7, 145.7, 126.6, 61.0, 30.7, 30.6, 25.1, 21.9,13.8 ppm. ^{19}F NMR (376.50 MHz, MeOD, 25 ºC) δ = -80.66 ppm. FTIR (KBr): $\breve{\upsilon}$ = 3128, 3074, 2949, 2870, 1643,1564,1512, 1458, 1354, 1192, 1136, 1055, 847, 789, 735 cm^{-1}. Elemental analysis calcd (%) for $C_{26}H_{34}F_{12}N_4O_8S_4$: C 35.21, H 3.86, N 6.32; found C 35.91, H 3.37, N 6.30.

1,1'-di-decyl-4,4'-bipyridinium di-iodide [$(C_{10})_2$bpy]I_2

This salt was obtained by recrystallization of mono-cation of [C_{10}bpy]I to give the desired product as a red solid. m.p. = 290 ºC (dec.). ^{1}H NMR (400.13 MHz, MeOD, 25ºC) δ = 9.29 (d, J = 5.7 Hz, 4H), 8.69 (d, J = 5.2 Hz, 4H), 4.75 (t, J = 7.4 Hz, 4H), 2.15 – 2.03 (m, 4H), 1.51-1.22 (m, 28H), 0.88 ppm (t, J = 6.8 Hz, 3H). ^{13}C NMR (100.61 MHz, MeOD, 25 ºC) δ = 151.2, 147.3, 128.3, 128.3, 63.3, 33.0, 32.6, 30.6, 30.5, 30.4, 30.2, 27.2, 23.7, 14.4 ppm. FTIR (KBr): $\breve{\upsilon}$ = 3011, 2920, 2853, 1634, 1555, 1454, 1371, 1230, 1175, 831, 723 cm^{-1}.

1,1'-di-decyl-4,4'-bipyridinium di-[bis(trifluoromethanesulfonyl)imide] [$(C_{10})_2$bpy][NTf_2]$_2$

The salt [$(C_{10})_2$bpy]I_2 (0.252 g, 0.36 mmol) was dissolved in water and Li[NTf_2] (0.268g, 0.93 mmol) was added and stirred during 24 hours at room temperature. The precipitate was recovered by extraction with water/dichloromethane, filtered and dried in order to give a pale yellow solid (0.344 g, 95 %). m.p. = 161 ºC. ^{1}H NMR (400.13 MHz, DMSO-d6, 25 ºC) δ = 9.37(d, J = 6.8 Hz, 4H), 8.76 (d, J = 6.8 Hz, 4H), 4.67 (t, J = 7.3 Hz, 4H), 2.04-1.90 (m, 4H),1.38 – 1.14 (m, 28H), 0.84 ppm (t, J = 6.7 Hz, 6H). ^{13}C NMR (100.61 MHz, MeOD, 25 ºC) δ = 148.6, 145.7, 126.6, 124.3, 60.9, 31.2, 30.7, 28.9, 28.8, 28.6, 28.4, 25.4, 22.1, 13.9 ppm. ^{19}F NMR (376.50 MHz, DMSO-d6, 25 ºC) δ = -78.76 ppm. FTIR (KBr): $\breve{\upsilon}$ = 3138, 3076, 2928, 2860, 1645, 1570, 1510, 1460, 1352, 1190, 1134, 1053, 837, 795, 735 cm^{-1}. Elemental analysis calcd (%) for $C_{34}H_{50}F_{12}N_4O_8S_4$: C 40.88, H 5.04, N 5.61; found C 41.42, H 4.45, N 5.58.

1,1'-di-[2-methoxyethyl]-4,4'-biyridinium di-iodide [$(C_3O)_2$bpy]I_2

To a solution of 4,4'-bipyridine (0.685 g, 4.34 mmol) in dried acetonitrile was added slowly 2-methoxyethyl iodide in excess (2.380 g, 12.80 mmol) previously prepared. The reaction mixture

was refluxed for ca. of 48 hours in nitrogen atmosphere. After this period of time, the solid was filtered and washed with diethyl ether. The desired product was dried in vacuum to give an orange solid (1.154 g, 50 %). m.p. = 248 ºC. ^{1}H NMR (400.13 MHz, D_2O, 25 ºC) δ = 9.03 (d, J = 5.6 Hz, 4H), 8.48 (d, J = 5.6 Hz, 4H), 4.90 – 4.80 (m, 4H), 4.01 – 3.89 (m, 4H), 3.31 (s, 6H) ppm.^{13}C NMR (100.61 MHz, D_2O, 25 ºC) δ = 150.3, 145.9, 126.9, 70.0, 61.2, 58.5 ppm. FTIR (KBr): υ = 3130, 3084, 3009, 2893, 1637, 1556, 1502, 1443, 1377, 1223, 1115, 1074, 1015, 820, 710 cm^{-1}.

1,1'-di-[2-methoxyethyl]-4,4'-biyridinium di-[bis(trifluoromethanesulfonyl)imide] [$(C_3O)_2$bpy][NTf_2]$_2$

The salt [$(C_3O)_2$bpy]I_2 (0.506 g, 0.96 mmol) was dissolved in water and Li[NTf_2] (0.634 g, 2.21 mmol) was added. After addition, the reaction was stirred during 48 hours at room temperature. The desired product was filtered, washed with water and dried in vacuum to give a white solid (0.728 g, 91 %). m.p. = 109.3 ºC. T_g = -22.6 ºC. ^{1}H NMR (400.13 MHz, DMSO-d6, 25 ºC) δ = 9.33 (d, J = 5.9 Hz, 4H), 8.77 (d, J = 5.9 Hz, 4H), 4.99 – 4.83 (m, 4H), 3.95 – 3.84 (m, 4H), 3.29 (s, 6H) ppm. ^{19}F NMR (376.50 MHz, DMSO-d6, 25 ºC) δ = -78.71 ppm. ^{13}C NMR (100.61 MHz, DMSO-d6, 25 ºC) δ = 149.6, 146.6, 127.0, 121.5, 118.3, 70.5, 60.9, 58.7 ppm. FTIR (KBr): υ = 3142, 3074, 3945, 1643, 1562, 1452, 1354, 1196, 1057, 835, 795, 741, 615 cm^{-1}. Elemental analysis calcd (%) for $C_{20}H_{22}F_{12}N_4O_{10}S_4$: C 28.78, H 2.66, N 6.71; found. C 28.90, H 2.69, N 6.57.

1,1'-di-[2-(2-methoxyethoxy)ethane]-4,4'-bipyridinium di-iodide [$(C_5O_2)_2$bpy]I_2:

To a solution of 4, 4'-bipyridine (0.522 g, 3.34 mmol) in acetonitrile was slowly added 2-(2-methoxyethoxy)ethyl iodide in excess (2.318g, 10.08 mmol) previously prepared. The solution was vigoursly stirred in reflux for ca. 30 hours. After cooling the reaction mixture, the solid was filtered, washed with diethyl ether and dried in vacuum to give an orange solid (1.645 g, 80 %). m.p. = 148 ºC. ^{1}H NMR (400.13 MHz, DMSO-d6, 25 ºC) δ = 9.31 (d, J = 6.3 Hz, 4H), 8.80 (d, J = 6.2 Hz, 4H), 4.93 – 4.84 (m, 4H), 4.02 – 3.92 (m, 4H), 3.62 – 3.51 (m, 4H), 3.42 – 3.34 (m, 4H), 3.16 (s, 6H) ppm. ^{13}C NMR (100.61 MHz, D_2O, 25 ºC) δ = 150.3, 146.1, 126.9, 70.9, 69.9, 68.6, 61.4, 58.1 ppm. FTIR (KBr): υ = 3034, 2986, 2930, 2882, 1636, 1556, 1446, 1354, 1142, 1106, 1018, 834, 716 cm^{-1}.

1,1'-di-[2-(2-methoxyethoxy)ethane]-4,4'-bipyridinium di-[bis(trifluoromethanesulfonyl)imide] [$(C_5O_2)_2$bpy][NTf_2]$_2$

The salt [$(C_5O_2)_2$bpy]I_2 (0.514 g, 0.83 mmol) was dissolved in water and Li[NTf_2] (0.551 g, 1.92 mmol) was added and stirred during ca. 24 hours at room temperature. The product was recovered by filtration, washed with water and dried in vacuum to give a white solid (0.688 g, 89 %). m.p. = 99.7 ºC. T_g = -27.4 ºC. ^{1}H NMR (400.13 MHz, DMSO-d6, 25 ºC) δ = 9.30 (d, J = 6.4 Hz, 4H), 8.78 (d, J = 6.2 Hz, 4H), 4.93-4.83 (m, 4H), 4.02-3.92 (m, 4H), 3.62-3.52 (m, 4H), 3.42-3.34 (m, 4H), 3.16 (s, 6H) ppm. ^{19}F NMR (376.50 MHz, DMSO-d6, 25 ºC) δ = -78.72 ppm. ^{13}C NMR (100.61 MHz, DMSO-d6, 25 ºC) δ = 149.4, 146.7, 126.7, 121.6, 118.4, 71.5, 69.9, 69.1, 61.0, 58.6 ppm. FTIR (KBr): υ = 3140, 3102, 3070, 2990, 2938, 2898, 1640, 1450, 1354, 1208, 1144, 1060, 834, 790, 740 cm^{-1}. Elemental analysis calcd (%) for $C_{24}H_{30}F_{12}N_4O_{12}S_4$: C 31.24, H 3.28, N 6.07; found. C 30.93, H 3.23, N 5.99.

1,1'-di-[2-(2-methoxyethoxy)ethane]-4,4'-bipyridinium di-docusate [$(C_5O_2)_2$bpy][AOT]$_2$

The salt [$(C_5O_2)_2$bpy]I_2 (0.113g, 0.18 mmol) was dissolved in ethanol and Na[AOT] (0.174 g, 0.39 mmol) was added. After addition, the reaction was stirred during ca. 24 hours at 60 ºC. Then, the solvent was evaporated and the product was recovered by extraction with water/dichloromethane. The organic layer was dried over anhydrous magnesium sulfate, filtered and the solvent was evaporated to give a pale brown liquid (0.130 g, 59 %). [cation:anion = 1:2.15]. T_g = -21.7 ºC. ^{1}H NMR (400.13 MHz, DMSO-d6, 25 ºC) δ = 9.30 (d, J = 6.4 Hz, 4H), 8.78 (d, J = 6.4 Hz, 4H), 4.96 – 4.80 (m, 4H), 4.04 – 3.80 (m, 12H), 3.64 – 3.51 (m, 6H), 3.43 – 3.33 (m, 4H), 3.20 – 3.10 (m, 6H), 2.98 – 2.71 (m, 4H), 1.58 – 1.16 (m, 36H), 0.95 – 0.73 (m, 24H) ppm. ^{13}C NMR (100.61 MHz, DMSO-d6, 25 ºC) δ = 171.0, 168.3, 148.9, 146.2, 126.3, 71.0, 69.4, 68.6, 68.5, 66.1, 66.0, 61.4, 60.5, 58.1, 38.2, 38.1, 34.1, 29.7, 29.6, 29.5, 28.3, 23.2, 23.1, 23.0, 22.4, 13.9, 10.8, 10.7 ppm. FTIR (NaCl): $\breve{\upsilon}$ = 3130, 3058, 2960, 2928, 2874, 1732, 1640, 1560, 1506, 1456, 1210, 1038, 842, 726 cm^{-1}. Elemental analysis calcd (%) for $C_{60}H_{104}N_2O_{18}S_2.2H_2O$: C 58.04, H 8.77, N 2.26; found. C 58.41, H 8.84, N 2.05.

1,1'-di-allyl-4,4'-bipyridinium di-bromide [(allyl)$_2$bpy][Br]$_2$

To a solution of 4,4'-bipyridine (0.531 g, 3.40 mol) in dried acetonitrile, 1-allyl bromide (2.097 g, 17.33 mol) was slowly added and the reaction was stirred at 70 ºC during 21 hours, in nitrogen atmosphere. The solid was filtered and washed with diethyl ether to give a yellow solid (1.286 g, 95 %). ^{1}H NMR (400.13 MHz, D_2O, 25 ºC) δ = 9.04 (d, J = 6.0 Hz, 4H), 8.49 (d, J = 5.6 Hz, 4H), 6.20 – 6.05 (m, 2H), 5.60 – 5.43 (m, 4H), 5.27 (d, J = 5.9 Hz, 4H) ppm. ^{13}C NMR (100.61 MHz, DMSO-d6, 25ºC) δ = 150.4, 145.5, 129.5, 127.0, 123.7, 121.5, 63.7 ppm. FTIR (KBr): $\breve{\upsilon}$ = 3130, 3070, 1642, 1600, 1548, 1522, 1464, 1412, 1354, 1192, 1058, 994, 956,814, 740, 654 cm^{-1}.

1,1'-di-allyl-4,4'-bipyridinium di-bis(trifluoromethanesulfonyl)imide [(allyl)$_2$bpy][NTf$_2$]$_2$

The salt [(allyl)$_2$bpy]Br_2 (0.512 g, 1.29 mmol) was dissolved in water and Li[NTf_2] (0.855 g, 2.98 mmol) was added. After addition, the reaction was stirred during ca. 28 hours at room temperature. The solid was filtered, washed with water and dried in vacuum to give a pale pink solid (0.928 g, 90 %). m.p. = 87 ºC. ^{1}H NMR (400.13 MHz, DMSO-d6, 25 ºC) δ = 9.31 (d, J = 5.8 Hz, 4H), 8.76 (d, J = 5.8 Hz, 4H), 6.29 – 6.11 (m, 2H), 5.59 – 5.5.39 (m, 4H), 5.35 (d, J = 5.6 Hz, 4H) ppm. ^{19}F NMR (376.50 MHz, DMSO-d6, 25 ºC) δ = -78.70 ppm. ^{13}C NMR (100.61 MHz, DMSO-d6, 25ºC) δ = 149.5, 146.3, 131.9, 127.3, 122.7, 121.5, 63.0 ppm. FTIR (KBr): $\breve{\upsilon}$ = 3136, 3074, 1640, 1566, 1508, 1458, 1348, 1186, 1138, 1060, 994, 944, 842, 812, 794, 740, 620 cm^{-1}.

1-methyl-1'-decyl-4,4'-bipyridinium di-iodide [C_1C_{10}bpy]I_2

To a solution of [C_{10}bpy]I (0.850 g, 2.00 mmol) in dried acetonitrile was added 1-iodomethane (0.62 mL, 9.96 mmol). The mixture was stirred at room temperature during 42 hours, in argon atmosphere. The precipitate was filtered and washed with diethyl ether. The desired product was isolated and dried in vacuum as a red solid (1.03 g, 90 %). m.p. = 225 ºC (dec.). ^{1}H NMR (400.13 MHz, DMSO-d6, 25 ºC) δ = 9.40 (d, J = 6.6 Hz, 2H), 9.30 (d, J = 6.6 Hz, 2H), 8.79 (dd, J = 6.7 Hz, 4H), 4.69 (t, J = 7.3 Hz, 2H), 4.44 (s, 3H), 2.03-1.89 (m, 2H), 1.39-1.13 (m, 14H), 0.85-0.82 ppm (m, 3H). ^{13}C NMR (100.61 MHz, DMSO-d6, 25 ºC) δ = 148.4, 148.1, 146.6, 145.7, 126.5,

126.1, 60.8, 48.1, 31.2, 30.7, 28.80, 28.6, 28.4, 25.4, 22.1, 13.9 ppm. FTIR (KBr): ῡ = 3015, 2922, 2853, 1637, 1555, 1456, 1364, 1273, 1178, 829, 719 cm^{-1}.

1-methyl-1'-decyl-4,4'-bipyridinium di-bis(trifluoromethanesulfonyl)imide $[C_1C_{10}bpy][NTf_2]_2$

The salt $[C_1C_{10}bpy]I_2$ (0.153g, 0.27 mmol) was dissolved in methanol and $Li[NTf_2]$ (0.268g, 0.93 mmol) was added and stirred during 24 hours at room temperature. The solvent was removed and the product was recovered by extraction with water/dichloromethane and dried in vacuum, to give a brown solid (0.195 g, 83 %). m.p. = 46 ºC. T_g = -26.5 ºC. ^{1}H NMR (400 MHz, DMSO-d6, 25 ºC) δ = 9.36 (d, J = 6.8 Hz, 2H), 9.27 (d, J = 6.7 Hz, 2H), 8.75 (dd, J =6.8 Hz, J = 6.9 Hz, 4H), 4.66 (t, J=7.4 Hz, 2H), 4.43 (s,3H), 2.05 – 1.90 (m, 2H),1.38 – 1.15 (m, 14H), 0.84 ppm (t, J = 6.7 Hz, 3H); ^{13}C NMR (100.61 MHz, MeOD, 25 ºC) δ = 148.6, 148.2, 146.6, 145.8, 126.5, 126.1, 121.1, 117.9, 60.9, 48.0,31.3, 30.8, 28.9, 28.8, 28.6, 28.4, 25.4, 22.1, 13.9 ppm. ^{19}F NMR (376.50 MHz, DMSO-d6, 25 ºC) δ = -78.75 ppm. FTIR (NaCl): ῡ = 3128, 3070, 2930, 2860, 1641,1564, 1508, 1456, 1350, 1192, 1140, 1057, 831, 793, 735 cm^{-1}. Elemental analysis calcd (%) for $C_{25}H_{32}F_{12}N_4O_8S_4$: C 34.40, H 3.70, N 6.42; found: C 35.20, H 3.26, N 6.18

1-ethyl-1'-hexyl-4,4'-bipyridinium iodide bromide$[C_2C_6bpy]IBr$

To a solution of $[C_6bpy]I$ (0.260 g, 0.71 mmol) in dried acetonitrile was slowly added 1-bromoethane (0.65 mL, 8.70 mmol). The mixture was heated at 55 ºC for 120 hours, in argon atmosphere. The product was filtered and washed with diethyl ether and dried to give a red solid (0.184 g, 55 %). m.p. = 241 ºC. ^{1}H NMR (400.13 MHz, DMSO-d6, 25 ºC) δ = 9.45 (d, J = 5.8 Hz, 4H), 8.84 (d, J = 6.0 Hz, 4H), 4.78 – 4.70 (m, 4H), 2.05 – 1.90 (m, 2H), 1.59 (t, J = 7.2 Hz, 3H), 1.38 –1.20 (m, 6H), 0.94 – 0.78 ppm (m, 3H). ^{13}C NMR (100.61 MHz, DMSO-d6, 25 ºC) δ = 148.5, 145.7, 145.6, 126.6, 60.8, 56.5, 30.7, 30.6, 25.1, 21.9, 16.3, 13.8 ppm. FTIR (KBr): ῡ = 3007, 2928, 2857, 1638, 1558, 1509, 1450, 1360, 1232, 1175, 829, 718 cm^{-1}.

1-ethyl-1'-hexyl-4,4'-bipyridinim di-bis(trifluoromethanesulfonyl)imide $[C_2C_6bpy][NTf_2]_2$

The salt $[C_2C_6bpy]IBr$ (0.415 g, 0.87 mmol) was dissolved in water and $Li[NTf_2]$ (0.612 g, 2.13 mmol) was added and stirred during 87 hours at room temperature. The product was recovered by extraction with water/ethyl acetate and dried to give a pale brown solid (0.698 g, 97 %). m.p. = 48 ºC. T_g = -28.3 º C. ^{1}H NMR (400.13 MHz, DMSO-d6, 25 ºC) δ = 9.40 (dd, J = 4.4 Hz, J = 4.3 Hz, 4H), 8.78 (d, J = 6.8 Hz, 4H), 4.77 – 4.64 (m, 4H), 2.05 – 1.92 (m, 2H), 1.61 (t, J = 7.3 Hz, 3H), 1.37 – 1.24 (m, 6H), 0.87 ppm (t, J = 7.0 Hz, 3H).^{13}C NMR (100.61 MHz, DMSO-d6, 25 ºC) δ = 148.6, 148.6, 145.7, 145.6, 126.6, 126.5, 124.3, 121.1, 117.9, 60.9, 56.6, 30.7, 30.6, 25.1, 21.9, 16.3, 13.8. ^{19}F NMR (376.50 MHz, DMSO-d6, 25 ºC) δ = -78.73 ppm. FTIR (NaCl): ῡ = 3130, 3069, 2961, 2934, 2864, 1639, 1560, 1508, 1450, 1348, 1194, 1136, 1055, 833, 789, 741 cm^{-1}. Elemental analysis calcd (%) for $C_{22}H_{26}F_{12}N_4O_8S_4$: C 31.81, H 3.15, N 6.74; found: C 32.27, H 2.27, N 6.63.

1-methyl-1'-[2-methoxyethyl]-4,4'-bipyridinium di-iodide $[C_1C_3Obpy]I_2$

The salt $[C_3Obpy]I$ (0.500 g, 1.46 mmol) previously prepared was dissolved in acetonitrile and 1-iodomethane (1.140 g, 8.03 mmol) was slowly added to the solution. The reaction mixture was

vigorously stirred at room temperature during ca. 48 hours. In the end of the reaction, the solid was filtered, washed with diethyl ether and dried in vacuum to give a red solid (0.598 g, 85 %). m.p. = 245 ºC. ^{1}H NMR (400.13 MHz, D_2O, 25 ºC) δ = 9.02 (d, J = 5.6 Hz, 4H), 8.57 – 8.33 (m, 4H), 4.88 – 4.78 (m, 2H), 4.41 (s, 3H), 3.99 – 3.85 (m, 2H), 3.30 (s, 3H) ppm. ^{13}C NMR (100.61 MHz, D_2O, 25 ºC) δ = 150.4, 149.7, 146.3, 145.9, 126.8, 126.7, 70.0, 61.1, 58.5, 48.4 ppm. FTIR (KBr): $\breve{\upsilon}$ = 3094, 3049, 3001, 1636, 1555, 1504, 1447, 1354, 1271, 1223, 1178, 1117, 1009, 816, 708 cm^{-1}.

1-methyl-1'-[2-methoxyethyl]-4,4'-bipyridinium di-[bis(trifluoromethanesulfonyl)imide] [C_1C_3Obpy][NTf_2]$_2$

The salt [C_1C_3Obpy]I_2 (0.499 g, 1.03 mmol) was dissolved in water and Li[NTf_2] (0.708 g, 2.47 mmol) was added. After addition, the reaction was stirred during ca. 48 hours at room temperature. The aqueous phase was decanted and the organic phase was washed with water, dried in vacuum to give a brown solid (0.727 g, 89 %). m.p. = 80.8 ºC. T_g = -17.5 ºC. ^{1}H NMR (400.13 MHz, DMSO-d6, 25 ºC) δ = 9.36 – 9.25 (m, 4H), 8.81 – 8.72 (m, 4H), 4.90 (t, J = 4.8 Hz, 2H), 4.44 (s, 3H), 3.89 (t, J = 4.8 Hz, 2H), 3.29 (s, 3H) ppm.^{19}F NMR (376.50 MHz, DMSO-d6, 25 ºC) δ = -78.71 ppm. FTIR (NaCl): $\breve{\upsilon}$ = 3138, 3072, 2940, 1642, 1562, 1452, 1350, 1192, 1138, 1056, 834, 790, 740, 618 cm^{-1}. Elemental analysis calcd (%) for $C_{18}H_{18}F_{12}N_4O_9S_4$: C 27.35, H 2.30, N 7.09; found. C 28.18, H 2.22, N 6.91.

1-hexyl-1'-[2-methoxyethyl]-4,4'-bipyridinium di-iodide [C_6C_3Obpy]I_2

The salt [C_3Obpy]I (0.412 g, 1.20 mmol) was dissolved in acetonitrile and iodohexane (1.078 g, 5.08 mmol) was slowly added to the solution. The reaction mixture was stirred in reflux ca. of 64 hours. In the end of the reaction, diethyl ether was added to precipitate the product. Then, the solid was filtered, washed with diethyl ether and dried in vacuum to give an orange solid (0.526 g, 79 %). m.p. > 250 ºC. ^{1}H NMR (400.13 MHz, DMSO-d6, 25 ºC) δ = 9.41 (d, J = 6.4 Hz, 2H), 9.34 (d, J = 6.4, 2H), 8.85 – 8.75 (m, 4H), 4.91 (t, J = 4.5, 2H), 4.70 (t, J = 7.4 Hz, 2H), 3.91 (t, J = 4.4 Hz, 2H), 3.29 (s, 3H), 2.08 – 1.92 (m, 2H), 1.40 – 1.22 (m, 6H), 0.97 – 0.80 (m, 3H) ppm. ^{13}C NMR (100.61 MHz, DMSO-d6, 25 ºC) δ = 149.6, 149.1, 146.6, 146.3, 127.2, 126.9, 70.5, 61.4, 60.9, 58.8, 31.2, 31.0, 25.6, 22.3, 14.3 ppm. FTIR (KBr): $\breve{\upsilon}$ = 3007, 2926, 2858, 1637, 1556, 1504, 1445, 1375, 1221, 1178, 1117, 1076, 1015, 820, 712 cm^{-1}.

1-hexyl-1'-[2-methoxyethyl]-4,4'-bipyridinium di-bis(trifluoromethanesulfonyl)imide [C_6C_3Obpy][NTf_2]$_2$

The salt [C_6C_3Obpy]I_2 (0.405 g, 0.73 mmol) was dissolved in water and Li[NTf_2] (0.453 g, 1.58 mmol) was added. After addition, the reaction was stirred during ca. 24 hours at room temperature. The aqueous phase was decanted and the product was recovered by extraction with water/dichloromethane. The organic layer was dried over anhydrous magnesium sulfate, filtered and the solvent was evaporated to give a brown solid (0.546 g, 88 %). m.p. = 57.9 ºC. T_g = -25.9 ºC. ^{1}H NMR (400.13 MHz, DMSO-d6, 25 ºC) δ = 9.37 (d, J = 6.4 Hz, 2H), 9.30 (d, J = 6.4, 2H), 8.79 – 8.72 (m, 4H), 4.88 (t, J = 4.5, 2H), 4.67 (t, J = 7.3 Hz, 2H), 3.88 (t, J = 4.5 Hz, 2H), 3.27 (s, 3H), 2.05 – 1.88 (m, 2H), 1.37 – 1.21 (m, 6H), 0.91 – 0.80 (m, 3H) ppm. ^{19}F NMR (376.50

MHz, DMSO-d6, 25 ºC) δ = -78.71 ppm. ^{13}C NMR (100.61 MHz, DMSO-d6, 25 ºC) δ = 149.5, 149.2, 146.6, 146.2, 127.2, 126.9, 121.5, 118.3, 70.5, 61.4, 60.9, 58.7, 31.2, 31.0, 25.6, 22.3, 14.3 ppm. FTIR (NaCl): ῡ = 3134, 3070, 2936, 2868, 1640, 1562, 1508, 1450, 1348, 1192, 1136, 1056, 830, 790, 742, 618 cm^{-1}.

1-methyl-1'-[2-(2-methoxyethoxy)ethane]-4,4'-bipyridinium di-bis(trifluoromethanesulfonyl)imide [$C_1C_5O_2$bpy]I_2

The salt [C_5O_2bpy]I (0.588 g, 1.52 mmol) previously prepared was dissolved in acetonitrile and 1-iodomethane (1.094 g, 7.71 mmol) was slowly added to the reaction. After addition, the reaction was stirred during ca. 64 hours at room temperature. The desired product was precipitated, washed with diethyl ether, and dried in vacuum to give an orange solid (0.593 g, 91 %). m.p. = 195 ºC. ^{1}H NMR (400.13 MHz, D_2O, 25 ºC) δ = 9.02 (d, J = 6.3 Hz, 2H), 8.95 (d, J = 6.2 Hz, 2H), 8.45(dd, J = 5.9, 5.9 Hz, 4H), 4.87 – 4.78 (m, 2H), 4.40 (s, 3H), 4.03 – 3.94 (m, 2H), 3.64 – 3.55 (m, 2H), 3.51 – 3.42 (m, 2H), 3.20 (s, 3H) ppm. ^{13}C NMR (100.61 MHz, DMSO-d6, 25 ºC) δ = 150.5, 149.7, 146.4, 146.0, 126.8, 126.7, 70.9, 69.7, 68.6, 61.4, 58.0, 48.4 ppm. FTIR (KBr): ῡ = 3034, 2986, 2930, 2882, 1636, 1556, 1446, 1354, 1142, 1106, 1018, 834, 716 cm^{-1}.

1-methyl-1'-[2-(2-methoxyethoxy)ethane]-4,4'-bipyridinium di-bis(trifluoromethanesulfonyl)imide [$C_1C_5O_2$bpy][NTf_2]$_2$

The salt [$C_1C_5O_2$bpy]I_2 (0.480 g, 0.91 mmol) was dissolved in water and Li[NTf_2] (0.613 g, 2.14 mmol) was added and the reaction mixture was stirred during 25 hours at room temperature. The aqueous phase was decanted and the organic phase was washed with water and dried in vacuum to give a brown liquid (0.577 g, 76 %). T_g = -22.1 ºC. ^{1}H NMR (400.13 MHz, DMSO-d6, 25 ºC) δ = 9.34-9.23 (m, 4H), 8.83-8.70 (m, 4H), 4.93-4.83 (m, 2H), 4.42 (s, 3H), 4.01-3.88 (m, 2H), 3.62-3.52 (m, 2H), 3.44-3.35 (m, 2H), 3.04 (s, 3H) ppm. ^{13}C NMR (100.61 MHz, DMSO-d6, 25 ºC) δ = 148.9, 148.2, 146.6, 146.2, 126.2, 126.1, 121.1, 117.9, 71.0, 69.4, 68.6, 60.5, 58.1, 48.0 ppm. ^{19}F NMR (376.50 MHz, DMSO-d6, 25 ºC) δ = -78.72 ppm. FTIR (KBr): ῡ = 3032, 2986, 2870, 1638, 1560, 1438, 1356, 1224, 1092, 830, 706 cm^{-1}.

1-hexyl-1'-[2-(2-methoxyethoxy)ethane]-4,4'-bipyridinium di-iodide [$C_6C_5O_2$bpy]I_2

The salt [$C_6C_5O_2$bpy]I_2 (0.479 g, 1.24 mmol) was dissolved in dried acetonitrile and iodohexane (1.052 g, 4.96 mmol) was slowly added and the reaction mixture was vigoursly stirred in reflux during during 64 hours. The desired product was precipitated, washed with diethyl ether and dried in vacuum to give a red solid (0.364 g, 81%). m.p. 182 ºC. ^{1}H NMR (400.13 MHz, D_2O, 25 ºC) δ = 9.19 – 9.09 (m, 4H), 8.63 – 8.52 (m, 4H), 4.99 – 4.89 (m, 2H), 4.74 (t, J = 7.2 Hz, 2H), 4.16 – 4.05 (m, 2H), 3.75 – 3.66 (m, 2H), 3.62 – 3.53 (m, 2H), 3.32 (s, 3H), 2.16 – 2.04 (m, 2H), 1.48 – 1.21 (m, 6H), 0.87 (t, J = 6.5 Hz, 3H) ppm. ^{13}C NMR (100.61 MHz, D_2O, 25 ºC) δ = 150.4, 149.8, 146.0, 145.5, 127.1, 126.9, 70.9, 69.7, 68.6, 62.3, 61.4, 58.1, 30.6, 30.3, 24.9, 21.7, 13.2 ppm. FTIR (KBr): ῡ = 3036, 2928, 2856, 1640, 1438, 1208, 1086, 830, 718 cm^{-1}.

1-hexyl-1'-[2-(2-methoxyethoxy)ethane]-4,4'-bipyridinium di-[bis(trifluoromethanesulfonyl)imide] [$C_6C_5O_2$bpy][NTf_2]$_2$

The salt [$C_6C_5O_2$bpy]I_2 (0.496 g, 0.83 mmol) was dissolved in water and Li[NTf_2] (0.588 g, 2.05 mmol) was added. The reaction mixture was stirred at room temperature during 26 hours. After this time, the water was decanted and the product was dissolved in dichloromethane and washed with water. The organic layer was dried over anhydrous magnesium sulfate, filtered and the solvent was evaporated to give a brown liquid (0.662 g, 87 %). T_g = -30.1 ºC. ^{1}H NMR (400.13 MHz, DMSO-d6, 25 ºC) δ = 9.37 (d, J = 5.8 Hz, 2H), 9.30 (d, J =5.9 Hz, 2H), 8.77 (d, J = 5.7 Hz, 4H), 4.91 – 4.82 (m, 2H), 4.66 (t, J = 7 Hz, 2H), 4.00 – 3.92 (m, 2H), 3.61 – 3.51 (m, 2H), 3.16 (s, 3H), 2.03 – 1.91 (m, 2H), 1.36 – 1.23 (m, 6H), 0.92 – 0.80 (m, 3H) ppm. ^{19}F NMR (376.50 MHz, DMSO-d6, 25 ºC) δ = -78.72 ppm. ^{13}C NMR (100.61 MHz, DMSO-d6, 25 ºC) δ = 149.4, 149.1, 146.7, 146.2, 127.1, 126.7, 121.5, 118.3, 71.5, 69.9, 69.1, 61.4, 61.0, 58.6, 31.2, 31.0, 25.5, 22.4, 14.3 ppm. FTIR (NaCl): $\tilde{\upsilon}$ = 3132, 3066, 2934, 2872, 1634, 1454, 1336, 1184, 1054, 832, 788, 740 cm^{-1}. Elemental analysis calcd (%) for $C_{25}H_{32}F_{12}N_4O_{10}S_4$: C 33.19, H 3.57, N 6.19; found. C 33.29, H 3.91, N 6.02.

1,1'-di-[4-cyanobenzyl]-4,4'-bipyridinium di-bromide [(bzCN)$_2$bpy]Br$_2$

To a solution of 4, 4'-bipyridine (0.364 g, 2.33 mmol) in acetonitrile was slowly added a solution of 4-(Bromomethyl)benzonitrile (1.012 g, 5.16 mmol) in acetonitrile. The solution mixture was stirred in reflux for ca. 4 days. After cooling the reaction mixture, the solid was filtered, washed with diethyl ether and dried in vacuum to give a pale yellow solid (1.201 g, 94 %). ^{1}H NMR (400.13 MHz, DMSO-d6, 25 ºC) δ = 9.59 (d, J = 6.6 Hz, 4H), 8.83 (d, J = 6.0 Hz, 4H), 7.98 (d, J = 8.2 Hz, 4H), 7.82 (d, J = 8.2 Hz, 4H), 6.11 (s, 4H) ppm. ^{13}C NMR (100.61 MHz, DMSO-d6, 25ºC) δ =149.77, 146.51, 139.65, 133.56, 130.29, 127.79, 118.76, 112.64, 62.93 ppm.

1,1'-di-[4-cyanobenzyl]-4,4'-bipyridinium di-[bis(trifluoromethanesulfonyl)imide] [(bzCN)$_2$bpy][NTf_2]$_2$

To a solution of [(bzCN)$_2$bpy]Br_2 (0.408 g, 0.75 mmol) in water:methanol (1:4), Li[NTf_2] (0.453 g, 1.61 mmol) in methanol was slowly added and stirred during 3 days at 60 ºC. After this time, the solvent was evaporated and the product was recovered by addition of water. The solid was filtered and washed with water, dried in vacuum to give a white solid (0.657 g, 93 %). ^{1}H NMR (400.13 MHz, DMSO-d6, 25ºC) δ = 9.49 (d, J = 6.6 Hz, 4H), 8.76 (d, J = 6.6Hz, 4H), 7.99 (d, J = 8.2 Hz, 4H), 7.76 (d, J = 8.2 Hz, 4H), 6.11 (s, 4H) ppm. ^{19}F NMR (376.50 MHz, DMSO-d6, 25ºC) δ =-78.70 ppm. ^{13}C NMR (100.61 MHz, DMSO-d6, 25ºC) δ =149.86, 146.54, 139.58, 133.58, 130.16, 127.77, 121.54, 118.72, 118.34, 112.69, 63.22 ppm.

1-[4-cyanobenzyl]-1'-[2-methoxyethyl]-4,4'-bipyridinium bromide iodide [(bzCNC$_3$O)bpy]BrI

To a solution of mono-cation [C_3Obpy]I (0.536 g, 1.6 mmol) in acetonitrile, 4-(Bromomethyl)benzonitrile (0.428 g, 2.2 mmol) in acetonitrile solution was slowly added and the reaction was stirred at reflux during 72 hours. The solid was filtered and washed with diethyl ether to give a dark orange solid (0.509 g, 58 %). ^{1}H NMR (400.13 MHz, DMSO-d6, 25ºC) δ = 9.58 (d,

J = 6.2 Hz, 2H), 9.37 (d, J = 6.4 Hz, 2H), 8.85 (d, J = 6.3 Hz, 2H), 8.80 (d, J = 6.3 Hz, 2H), 7.99 (d, J = 8.1 Hz, 2H), 7.81 (d, J = 8.1 Hz, 2H), 6.10 (s, 2H), 4.93 (t, J = 4.3 Hz, 2H), 3.90 (t, J = 4.3 Hz, 2H), 3.29 (s, 3H) ppm. ^{13}C NMR (100.61 MHz, DMSO-d6, 25ºC) δ =149.89, 149.39, 146.61, 146.48, 139.65, 133.57, 130.26, 127.78, 126.98, 118.75, 112.65, 70.49, 62.97, 60.85, 58.75 ppm.

1-[4-cyanobenzyl]-1'-[2-methoxyethyl]-4,4'-bipyridinium di-[bis(trifluoromethanesulfonyl)imide] [(bzCNC$_3$O)bpy]BrI

To a solution of mono-cation [C1bpy]I (0.786 g, 2.6 mmol) in acetonitrile, 4-(Bromomethyl)benzonitrile (0.680 g, 3.4 mmol) in acetonitrile solution was slowly added and the reaction was stirred at reflux during 72 hours. The solid was filtered and washed with diethyl ether to give an orange solid (g, 62 %). ^{1}H NMR (400.13 MHz, DMSO-d6, 25ºC) δ = 9.59 (d, J = 6.2 Hz, 2H), 9.33 (d, J = 6.2 Hz, 2H), 8.82 (d, J = 6.2 Hz, 2H), 8.79 (d, J = 6.2 Hz, 2H), 7.98 (d, J = 8.2 Hz, 2H), 7.82 (d, J = 8.0 Hz, 2H), 6.11 (s, 2H), 4.46 (m, 2H) ppm. ^{13}C NMR (100.61 MHz, DMSO-d6, 25ºC) δ =149.78, 148.54, 147.10, 146.53, 139.68, 133.55, 130.26, 127.63, 126.68, 118.76, 112.62, 62.84, 48.54 ppm.

2.7. References

1 P. M. S. Monk, R. J. Mortimer and D. R. Rosseinsky, *Electrochromism and Electrochromic Devices*, Cambridge University Press, Cambridge, 2007.

2 P. M. S. Monk, *The viologens: physicochemical properties, synthesis, and applications of the salts of 4,4'-bipyridine*, Wiley, 1998.

3 L. Michaelis and E. S. Hill, *J. Gen. Physiol.,* 1933, **16**, 859–873.

4 M. C. Grenier, R. W. Davis, K. L. Wilson-Henjum, J. E. LaDow, J. W. Black, K. L. Caran, K. Seifert and K. P. C. Minbiole, *Bioorg. Med. Chem. Lett.*, 2012, **22**, 4055–4058.

5 L. E. Ator, M. C. Jennings, A. R. McGettigan, J. J. Paul, W. M. Wuest and K. P. C. Minbiole, *Bioorg. Med. Chem. Lett.*, 2014, **24**, 3706–3709.

6 R. O. Lezna and S. A. Centeno, *Langmuir*, 1996, **12**, 591–593.

7 M. Gratzel, *Acc. Chem. Res.*, 1981, **14**, 376–384.

8 A. J. Bard and M. A. Fox, *Acc. Chem. Res.*, 1995, **28**, 141–145.

9 P. Bhowmik, H. Han, I. Nedeltchev and J. Cebe, *Mol. Cryst. Liq. Cryst.*, 2004, **419**, 27–46.

10 P. K. Bhowmik, H. Han, J. J. Cebe, R. A. Burchett, B. Acharya and S. Kumar, *Liq. Cryst.*, 2003, **30**, 1433–1440.

11 V. Causin and G. Saielli, *J. Mater. Chem.*, 2009, **19**, 9153–9162.

12 C. J. Schoot, J. J. Ponjee, H. T. van Dam, R. A. van Doorn and P. T. Bolwijn, *Appl. Phys. Lett.*, 1973, **23**.

13 C. L. Bird and A. T. Kuhn, *Chem. Soc. Rev.*, 1981, **10**, 49–82.

14 L. Pospíšil, J. Kůta and J. Volke, *J. Electroanal. Chem. Interfacial Electrochem.*, 1975, **58**, 217–227.

15 G. Casella, V. Causin, F. Rastrelli and G. Saielli, *Liq. Cryst.*, 2016, **43**, 1161–1173.

16 G. Casella, V. Causin, F. Rastrelli and G. Saielli, *Phys. Chem. Chem. Phys.*, 2014, **16**, 5048–5051.

17 M. Bonchio, M. Carraro, G. Casella, V. Causin, F. Rastrelli and G. Saielli, *Phys. Chem. Chem. Phys.*, 2012, **14**, 2710–2717.

18 G. Saielli, *J. Phys. Chem. A*, 2008, **112**, 7987–7995.

19 E. Marotta, F. Rastrelli and G. Saielli, *J. Phys. Chem. B*, 2008, **112**, 16566–16574.

20 R. J. Mortimer, A. L. Dyer and J. R. Reynolds, *Displays*, 2006, **27**, 2–18.

21 A. Kavanagh, K. J. Fraser, R. Byrne and D. Diamond, *ACS Appl. Mater. Interfaces*, 2013, **5**, 55–62.

22 A. Branco, L. C. Branco and F. Pina, *Chem. Commun.*, 2011, **47**, 2300–2302.

23 S. Sathyamoorthi, M. Kanagaraj, M. Kathiresan, V. Suryanarayanan and D. Velayutham, *J. Mater. Chem. A*, 2016, **4**, 4562–4569.

24 R. F. M. Frade, A. Matias, L. C. Branco, C. A. M. Afonso and C. M. M. Duarte, *Green Chem.*, 2007, **9**, 873–877.

25 R. F. M. Frade, A. A. Rosatella, C. S. Marques, L. C. Branco, P. S. Kulkarni, N. M. M. Mateus, C. A. M. Afonso and C. M. M. Duarte, *Green Chem.*, 2009, **11**, 1660–1665.

26 C. Samorì, D. Malferrari, P. Valbonesi, A. Montecavalli, F. Moretti, P. Galletti, G. Sartor,

E. Tagliavini, E. Fabbri and A. Pasteris, *Ecotoxicol. Environ. Saf.*, 2010, **73**, 1456–1464.

27 S. P. F. Costa, V. D. Justina, K. Bica, M. Vasiloiu, P. C. A. G. Pinto and M. L. M. F. S. Saraiva, *J. Hazard. Mater.*, 2014, **265**, 133–141.

28 Z.-B. Zhou, H. Matsumoto and K. Tatsumi, *Chem. Eur. J.*, 2004, **10**, 6581–6591.

29 P. Bonhôte, A.-P. Dias, N. Papageorgiou, K. Kalyanasundaram and M. Grätzel, *Inorg. Chem.*, 1996, **35**, 1168–1178.

30 F. Alves, F. S. Oliveira, B. Schröder, C. Matos and I. M. Marrucho, *J. Pharm. Sci.*, 2016, **102**, 1504–1512.

31 D. J. Smith, J. K. Shah and E. J. Maginn, *Mol. Pharm.*, 2015, **12**, 1893–1901.

32 W. A. Henderson, M. Herstedt, V. G. Young, S. Passerini, H. C. De Long and P. C. Trulove, *Inorg. Chem.*, 2006, **45**, 1412–1414.

33 J. Sun, M. Forsyth and D. R. MacFarlane, *J. Phys. Chem. B*, 1998, **102**, 8858–8864.

34 E. Dudognon, F. Danède, M. Descamps and N. T. Correia, *Pharm. Res.*, 2008, **25**, 2853–2858.

35 J. D. Menczel, L. Judovits, R. B. Prime, H. E. Bair, M. Reading and S. Swier, in *Thermal Analysis of Polymers*, John Wiley & Sons, Inc., 2008, pp. 7–239.

36 H. A. Barnes, J. F. Hutton and K. Walters, in *An introduction to rheology*, Elsevier Science Publishers, 1989.

37 P. S. Kulkarni, L. C. Branco, J. G. Crespo, M. C. Nunes, A. Raymundo and C. A. M. Afonso, *Chem. Eur. J.*, 2007, **13**, 8478–8488.

38 G. Li and P. Miao, in *Electrochemical Analysis of Proteins and Cells*, Springer Berlin Heidelberg, 2013, pp. 5–18.

39 C. G. Zoski, in *Handbook of electrochemistry*, Elsevier, 2007.

40 A. J. Bard and L. R. Faulkner, in *Electrochemical methods: fundamentals and applications*, John Wiley & Sons. Inc., 2nd edn., New York, 2001.

41 M. Döbbelin, I. Azcune, M. Bedu, A. Ruiz de Luzuriaga, A. Genua, V. Jovanovski, G. Cabañero and I. Odriozola, *Chem. Mater.*, 2012, **24**, 1583–1590.

3. Electrochromic Organic Ionic Oligomers and Polymers

3. Electrochromic Organic Ionic Oligomers and Polymers

3.1. Introduction

In the literature, it was reported that the electrochromic devices (ECD) containing aqueous methyl viologen (MV) displayed lower write-erase (colouration-bleaching) efficiency values, once both the di-cation and radical cation are very soluble in polar solvents [1]. The use of anionic polyelectrolyte such as poly(2-acrylamido-2-methylpropane-sulfonic acid), also designed as Poly(AMPS) or sulfonated perfluorinated polyether (Nafion®) can be a possible approach to improve this behaviour [1]. Once, the rate of radical cation species is obtained upon one electron-transfer process diffuses away from the electrode is retarded. Mortimer and Dillingham reported the electrostatic incorporation of 1,1'-di-alkyl-4,4'-bipyridinium salts into Nafion® films to produce electrochromic electrodes [2]. They observed different radical cation colours, from purple to pink depending on alkyl chain length used. Also, they observed that the response times for colouration are shorter than for bleaching process, owing to the slower physical diffusion of the radical cation dimers [2]. Alternative approaches such as surface modification of an electrode using silanisation methodology [3], a polymer complex based on poly(viologen)-poly(styrenesulfonate) modified electrodes [4], oxidative electropolymerization of pyrrole *N*-substituted by an aliphatic chain bearing the viologen group [5], poly(pyrrole-bound viologen) [6] or preparation of polyelectrolyte multilayers using poly(butyl viologen) (PBV) di-bromide and poly(styrene sulfonate) sodium salt [7] have been explored [1]. In conclusion, those chemically modified electrodes and immobilising the viologen species within a semi-solid electrolyte seems to improve the performance of the electrochromic devices. Besides that, it is also reported in the literature an alternative approach that consist in the use of non-aqueous and rigorously dried solvents, in which viologen salts shows very high write-erase efficiency [8].

There is reported in the literature the application of viologen dimers (tetra-substituted-4,4'-bipyridinium salts) as host-guest complexes [9,10]. It was also reported the use of viologen dimer as ionic liquid crystals by Saielli and co-workers [11,12]. They reported several tetra-substituted-4,4'-bipyridinium salts, which contains alkyl chains as linker and [NTf_2] as anion. These systems showed a rich mesomorphism and they studied the dependence of that with the length of both linker and lateral chains. The electrochemical reduction of several viologen dimers and trimers linked by different alkyl chains have been also explored [13,14].

Recently, Poly(ionic liquids), also known as polymerized or polymeric ionic liquids (PILs) as innovative polyelectrolytes have been intensely investigated [15,16]. In general, PILs are constituted by a polymeric backbone, where each repeated unit (ionic liquid monomer) can be positively (cation) or negatively (anion) charged (see Figure 3.1) [15,16]. This strategy can be relevant to take advantage for suitable combination between the unique properties of ILs and polymeric materials, in particular, their improvement of ionic conductivity, thermal and chemical stability as well as durability [15,16].

PILs are permanent and strong polyelectrolytes, once they are solvent-independent ionization state of the IL species and frequently it is reported that PILs present a rather broad glass transition ranges, despite of their high charge density [15].

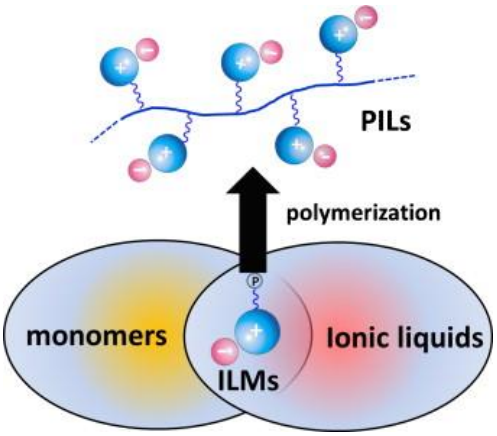

Figure 3.1 – Illustration of the preparation of PILs through IL monomers containing a polymerizable group "P" [15]. (Source: *Prog. Polym. Sci.*, 2013, **38**, 1009–1036).

In general, most of PILs are not soluble in water but in organic solvents, from polar to less polar depending on the chemical nature of the PIL, contrarily to classic polyelectrolytes [15,16]. Thus, the chemical nature of the PILs, specially the nature of anion plays an important role to control their solubility [15].

PILs can be classified as Poly(cation) if the polymer backbone is bearing a cationic group or Poly(anion) if it bearing an anionic group [16]. Different possible combinations of anions such as tetrafluoroborate [BF_4], hexafluorophosphate [PF_6], bis(trifluoromethanesulfonyl)imide [NTf_2], dicyanamide [DCA], trifluoromethanesulfonate [OTf], among others as well as organic cations such as imidazolium, pyrrolidinium, ammonium, pyridinium, can be selected (Figure 3.2) [17]. In this way, PILs can undergo structural variation by adequate selecting of counter-ion as well as the backbone type [15]. The macromolecular architecture of the polymer backbone can be linear, star-shaped or hyperbranched. It is also possible to prepare different types of co-polymers containing PILs covalently bonded to other types of polymers, such as random, alternating and block [15,16].

There are reported in the literature that PILs are commonly prepared through direct polymerization of ILs monomers but chemical modification of existing polymers can be also used as an alternative approach [15,18]. The preparation of PILs was mostly focused on the conventional free-radical polymerization of ILs monomers. More recently, different polymerization techniques such as *"living"* radical polymerization, ring opening metathesis polymerization, step-growth polymerization and others have been explored for preparation of PILs [18]. For example, the *"living"* radical polymerization such as Atom Transfer Radical Polymerization (ATRP) and Reversible Addition/Fragmentation Chain Transfer Polymerization (RAFT) allowed to design and to control macromolecular architecture (e.g. that includes molecular weight (M_w), molecular weight distribution (polydispersity index, PDI), functionality and composition) of IL species on meso-/nanoscale within a polymer matrix [18].

There reported in the literature different examples containing poly(cations) and poly(anions) combined with different counter-ions.

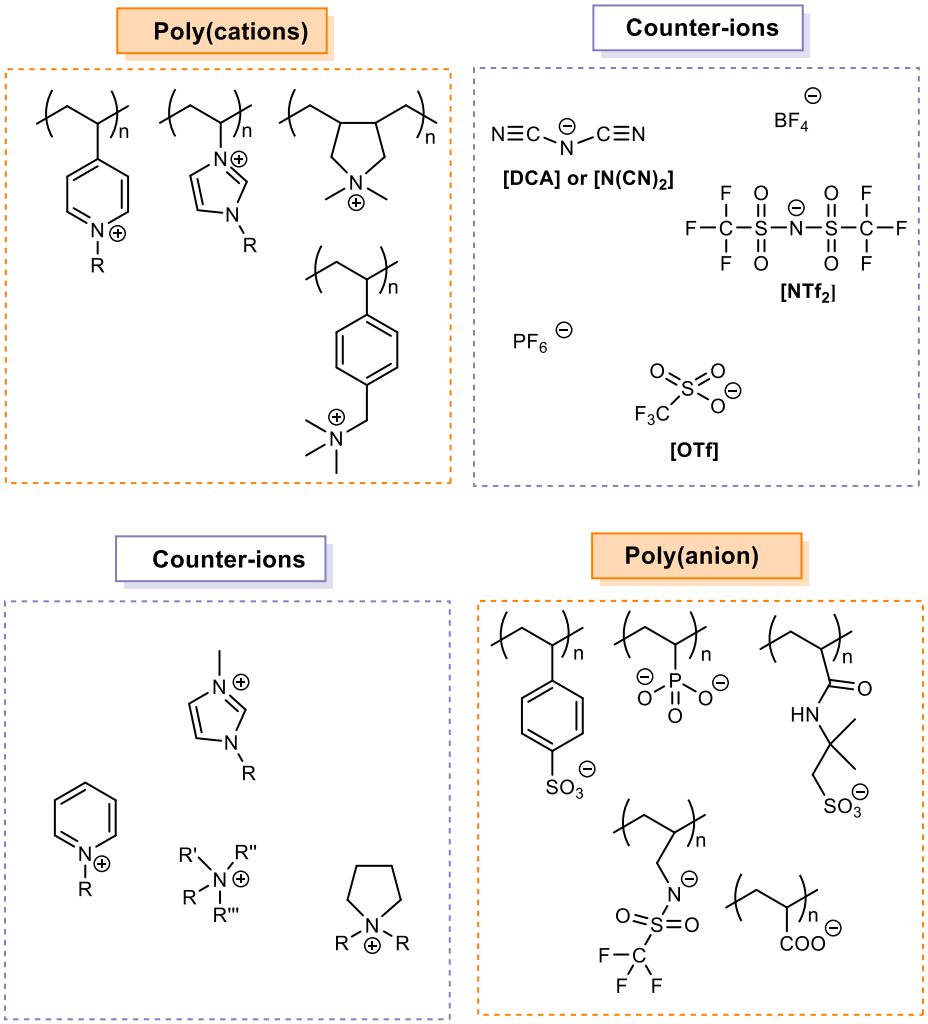

Figure 3.2 – Possible combinations between poly(cation), poly(anion) and respective counter-ions [16]. (Source: *Prog. Polym. Sci*., 2011, **36**, 1629–1648).

One of the most studied PILs are based on vinyl-imidazolium derivatives. Ohno and co-workers firstly reported the synthesis and bulk ionic conductivity of PILs based on vinyl polymers bearing either imidazolium or sulfonamide group in the side chain [19,20]. There is described in the literature two possible approaches in order to prepare vinyl-imidazolium PILs [16]. The first approach (Scheme 3.1, Route 1) was adapted from the synthesis of ILs and consists in the preparation of different IL monomers by anion exchange reaction of a cationic 1-vinyl-3-alkyl imidazolium halide monomer with different anions [16,21]. Herein, the IL monomer can be isolated using similar methodologies applied to the purification of ILs, such as liquid/liquid phase separation in water, after anion exchange with a hydrophobic anion [16]. Then, the PILs were prepared through direct polymerization of each different IL monomer. An alternative approach consists firstly on polymerization of the imidazolium monomer combined with halide anion, followed by anion exchange reaction directly into the PILs (Scheme 3.1, Route 2) [16,22]. It is also reported that the final PILs can be isolated through precipitation in water of the solid PIL obtained after anion exchange reaction to a more hydrophobic anion [16,22].

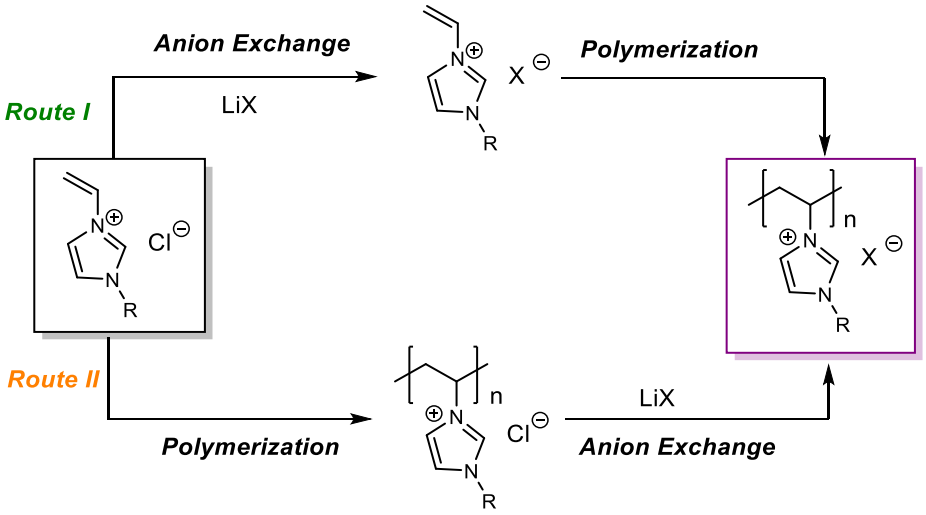

Scheme 3.1 – Possible synthetic routes to prepare vinyl-imidazolium PILs [16]. (Source: *Prog. Polym. Sci*., 2011, **36**, 1629–1648).

Similar approaches (Route I and II) can be applied to prepare a variety of PILs. The first approach, which consists on direct polymerization of IL monomers enables the preparation of homopolymers and co-polymers. However, the large number of organic synthesis and purification steps at the monomer level as well as the need of controlling the polymerization conditions of each individual monomer can be significant disadvantages for this process [16]. Despite of the second approach only involve one type of monomer purification and polymerization step. Some limitations can be observed in cases where the anion exchange reaction is not quantitative, random co-polymers or more complicated polymer architectures are explored [16].
Interestingly, it is described the use of step-growth polymerization method to prepare PILs derived from poly(alkyl imidazolium), poly(alkyl pyridinium) through direct quaternization of a di-halide with di-imidazole or di-pyridine molecule. Then, an anion exchange reaction to produce the corresponding PIL can be performed [16,23,24].

As already mentioned the anion nature has a strong influence on the PIL solubility and this effect is more evident in the case of poly(cations) combined with different anions. In this way, Mecerreyes and co-workers studied the effect of anion nature on solubility of Poly(vinyl-imidazolium) derivatives. For that, they polymerized vinylimidazolium halides (monomer) and then an anion exchange reaction was performed with different anions. They observed that poly(1-vinyl-3-ethylimidazolium) when combined with bromide as anions is soluble in water similar to the conventional polyelectrolytes. When the anions were replaced by [BF_4] or [PF_6], the PIL became practically insoluble in water and soluble in methanol and polar aprotic solvents such as acetone, dimethylsulfoxide (DMSO) and *N,N*-dimethylformamide (DMF) [16]. Whereas, the anions were substituted by fluorinated anion such as [NTf_2] or hydrophobic anions like dodecylbenezenesulphonate, the PIL became soluble in less polar solvents, in particular tetrahydrofuran (THF) and toluene [16].

Yuan and co-workers reported that the most PILs reported until 2013 are solids, with a relatively low glass transition and showed a similar behaviour to usual polymers, contrarily to the

solid polyelectrolytes, which are usually glassy until decomposition [15]. They also mentioned that there are some examples of PILs possessing liquid/fluidic properties at room temperature, in particular in the cases of non-polar polymers, whose chemical structure consisted of unsaturated groups and lacked polar groups like as poly(1,4-butadiene) [15].

In the last years, different applications of PILs have been reported, in particular their use as thermo-responsive materials, carbon materials, specific catalysts, porous polymers, separation and absorption materials, task-specific materials for energy and biotechnology fields [15,16]. Additionally, this type of polymers receives attention for electrochemical device applications due to their high ionic conductivity, good compatibility, improved electrochemical and thermal stability comparing to other reported polymer electrolytes (see Figure 3.3) [17].

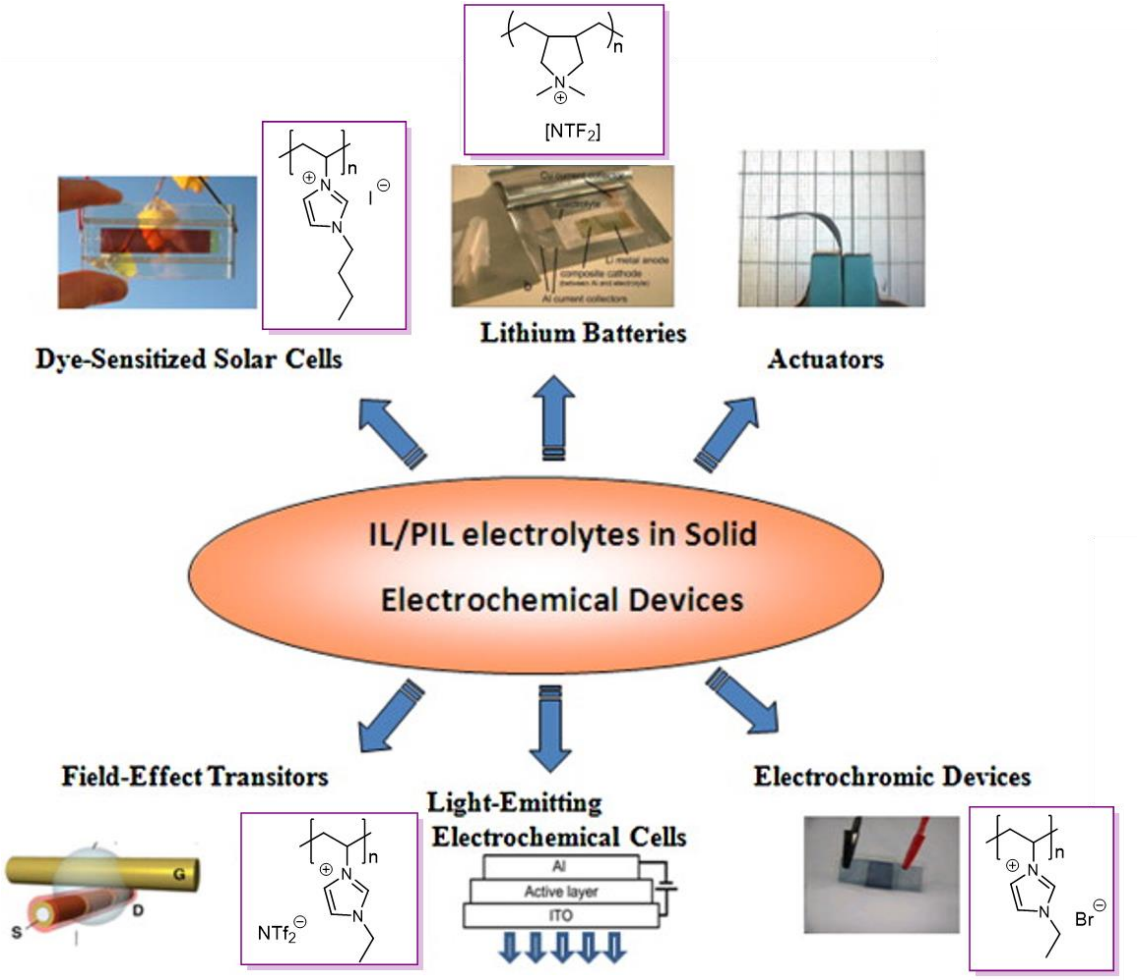

Figure 3.3 – Possible application of PILs as electrolytes in different solid electrochemical devices, including a representative chemical structure used [16]. (Source: *Prog. Polym. Sci., 2011*, **36**, 1629–1648).

Mecerreyes and co-workers firstly reported the preparation of ion gels based on the mixture of imidazolium-based on PILs and conventional imidazolium ILs and their use as polymer electrolyte in electrochromic devices containing poly(3,4-ethylenedioxythiophene) (PEDOT) [25]. Stable polymer electrolytes are obtained using the following ILs: 1-butyl-3-methylimidazolium bis(trifluoromethanesulfonimide) [bmim][NTf_2], 1-butyl-3-methylimidazolium tetra-fluoroborate [bmim][BF_4] and 1-butyl-3-methylimidazolium bromide [bmim][Br] combined with poly[1-vinyl-

ethyl-imidazolium] bearing similar anions, [NTf_2], [BF_4] and Br, respectively [25]. They observed that the ionic conductivity of all these electrolyte polymers are between 10^{-2} and 10^{-5} $S.cm^{-1}$ at room temperature and these values increase with addition of more IL quantity. The electrochromic device (1.5 cm^2) was symmetrical built with a thin layer of polymer electrolyte deposited by casting onto a poly(ethylene terephtalate) film covered with poly(3,4-ethylenedioxythiophene) (PEDOT) (Orgacon EL-350 foils commercialized by AGFA). Then, a second Orgacon EL-350 foil on top of the electrolyte layer is added [17,25]. The cycle life of these electrochromic devices is significantly improved (up to 70 000 cycles) comparing to previously poly(ethylene oxide) electrolytes [25].

Later, Pozo-Gonzalo and co-workers described the preparation of switchable optical attenuator in the near infrared (NIR) ion gels as electrolyte. These ion gels are based on poly(1-vinyl-ethyl-imidazolium) and 1-ethyl-3-methylimidazolium ILs combined with different anions ([NTf_2], [BF_4] or [PF_6]) [17,26]. The symmetrical electrochromic device was prepared using poly(ethylene terephthalate) foils covered with indium tin oxide (ITO) and PEDOT from above electrodes. These solid state devices were switched between 0 to 2 V with an optical contrast up to 50.5 % in the visible region and up to 44 % at 1971 nm (IR region). They also reported that the switching times of the devices are in the order of few seconds with a colouration time of 2.7 s and a bleaching time of 3.8 s. Additionally, the best results were achieved when the polymer electrolyte containing [BF_4] anion is used [17,27].

Recently, Shaplov and co-workers published the use of PILs as single solid polymer electrolyte in electrochromic devices without addition of any IL or lithium salts, since the IL species are grafted on the polymer backbone [28,29]. They used a symmetrical electrochromic device built, PET-ITO/PEDOT/electrolye/PEDOT/PET-ITO and poly[1-(2-(2-(2-(methacryloyloxy)ethoxy)ethoxy)-ethyl)-3-methylimidazolium][NTf_2] as electrolyte. The electrochromic devices showed a fast switching time (3 s), high colouration efficiency (390 $cm^2.C^{-1}$ at 620 nm), optical contrast up to ΔT = 22 % and the possibility of application in open air and under vacuum [28].

In conclusion, PILs can be very attractive for industrial field. Taking into account their polymeric nature, they can be easily manipulated using classical polymer processing methods, such as spin coating, electrospinning, and extrusion. This allows to control the morphology of the material, which need to have distinctive and stable shapes for fabrication and assembly with other components into functional devices [15]. However, similar to ILs, PILs have the tendency to absorbing water, mainly attributed to their hydrophobic nature [15]. This moisture sensitivity can cause problems in processing and practical applications of PILs, once that can affect dramatically some properties such as ionic conductivity. In addition, this ionic conductivity can be also dramatically affected by additives or impurities, including moisture or the environmental humidity [15]. In the case of PILs, the purification step can be more easily comparing to ILs, once established purification techniques for polymers can be used [15].

3.2. Tetra-substituted-4,4'-bipyridinium Salts

Tetra-substituted-4,4'-bipyridinium or bis(bipyridinium) salts, where one bipyridinium unit is covalently linked to another unit by a specific linker (spacer) have been developed. These tetra-cations can also be symmetric or non-symmetric, if they have the same functional group (symmetric) or different functional groups (non-symmetric) as side chain of bipyridinium scaffold. Herein, different bis(bipyridinium) salts linked by ether units have been prepared. Then, an anion exchange reaction using Li[NTf_2] was performed (Scheme 3.2).

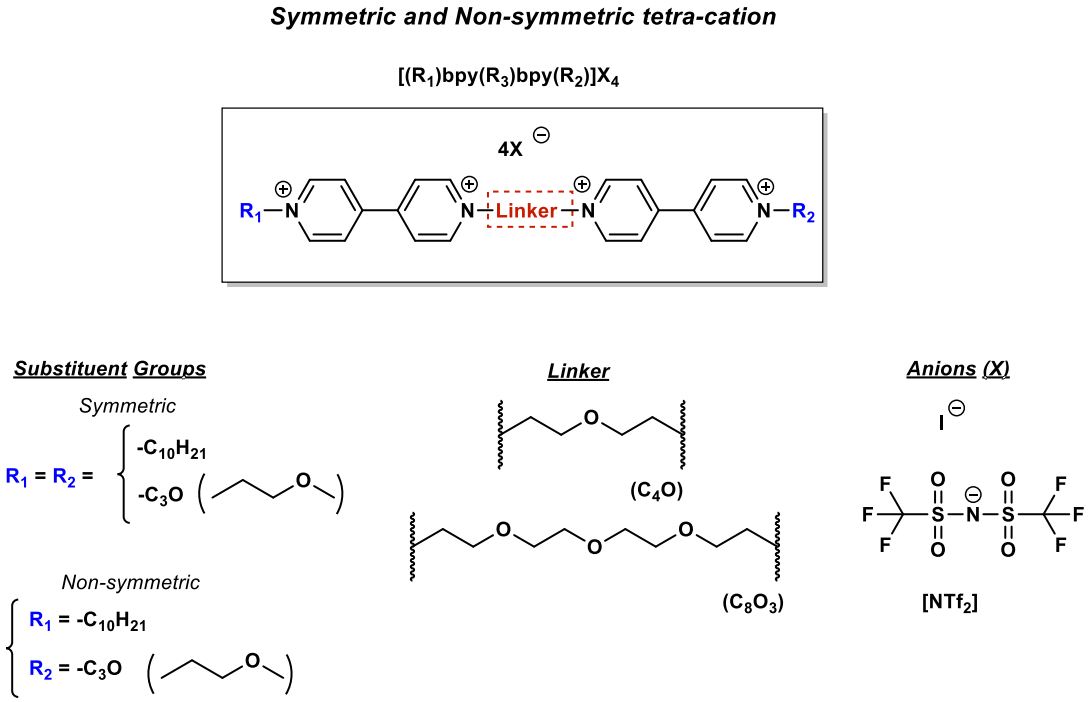

Scheme 3.2 – Bis(bipyridinium) salts prepared to build electrochromic devices.

According to all possible substituent pendant groups from bipyridinium cation scaffold, the length of linkers as well as the selected organic or inorganic anions, it is possible to obtain salts based on ILs, including RTILs.

Different synthetic routes in order to prepare these type of salts have been tested. In particular, the synthesis includes three steps: 1) preparation of mono-cations with adequate functional group, 2) introduction of the spacer for formation of di-cations, 3) preparation of tetra-cations with the same or different functional groups. This synthetic route seems to facilitate the purification of the desired intermediate product as well as their solubility profiles.

In order to achieve the desired tetra-cation based on bis(bipyridinium) scaffolds, an optimized methodology already described for the preparation of mono-substituted-4,4'-bipyridinium salts was firstly followed. Then, symmetrical oxo-bis(bipyridinium) tetra-iodides are prepared using a direct functionalization with bis[2-(2-iodoethoxy)ethyl]ether and 2-iodoethyl ether as linkers through nucleophilic substitution reaction (Scheme 3.3, Route I).

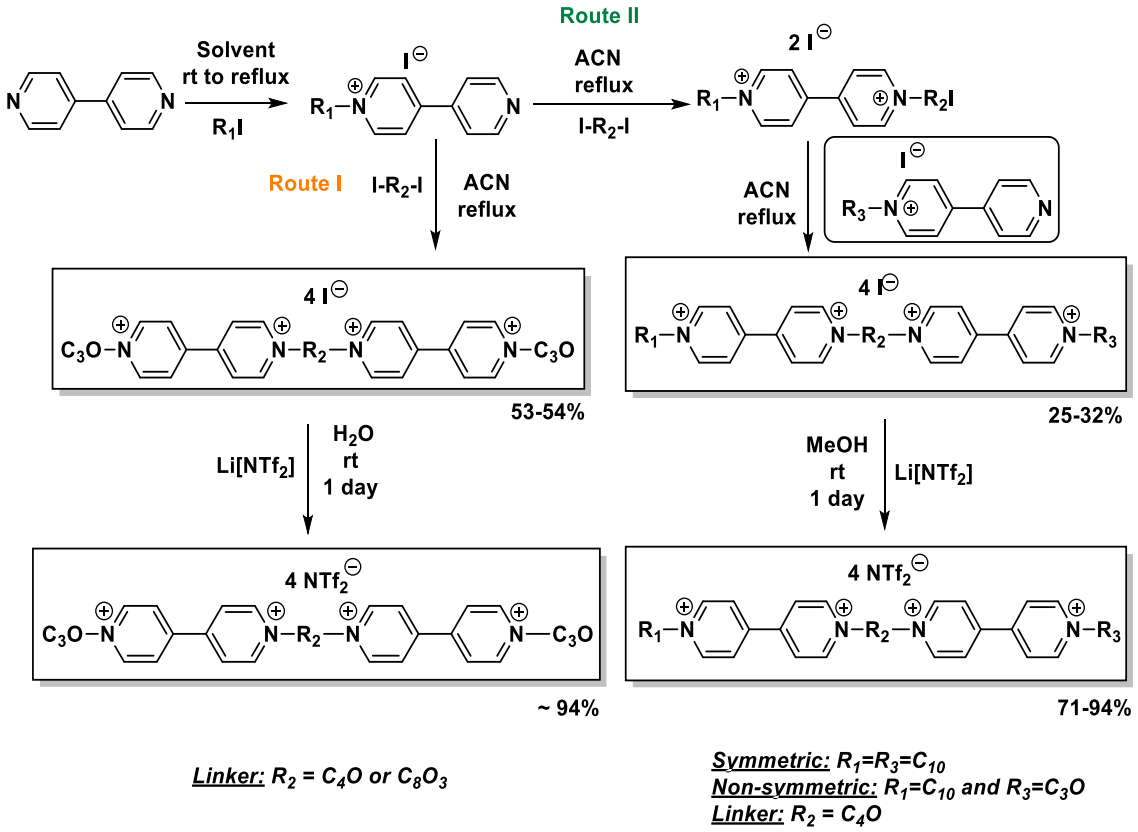

Scheme 3.3 – Synthetic route for preparation of symmetric and non-symmetric bis(bipyridinium) salts.

Alternatively, di-decyl and non-symmetrical bis(bipyridinium) tetra-iodide salts required an additional synthetic step of di-cation scaffold formation (Scheme 3.3, Route II). After preparation of the different tetra-iodide salts, an anion exchange reaction using Li[NTf_2] in aqueous and methanol solution at room temperature have been performed.

In general, the desired bis(bipyridinium) tetra-iodide salts were obtained after precipitation in acetonitrile and further recrystallization in acetone, with low to moderate yields (25 to 54 %) is achieved. Whereas, [NTf_2] salts were obtained in high yields (71 to 94 %), but a purification step by simple water addition and phase separation (Scheme 3.3, Routes I and II) in order to eliminate inorganic salts is required.

All of these prepared 4,4'-bipyridinium salts were analysed by ^{1}H, ^{13}C and ^{19}F NMR (only in the case of [NTf_2] salts). In general, ^{19}F NMR spectra of all [NTf_2] salts showed the presence the fluorine atoms as demonstrate in inset of the Figure 3.4. However, it was not possible to determine the cation/anion proportion by NMR spectra.

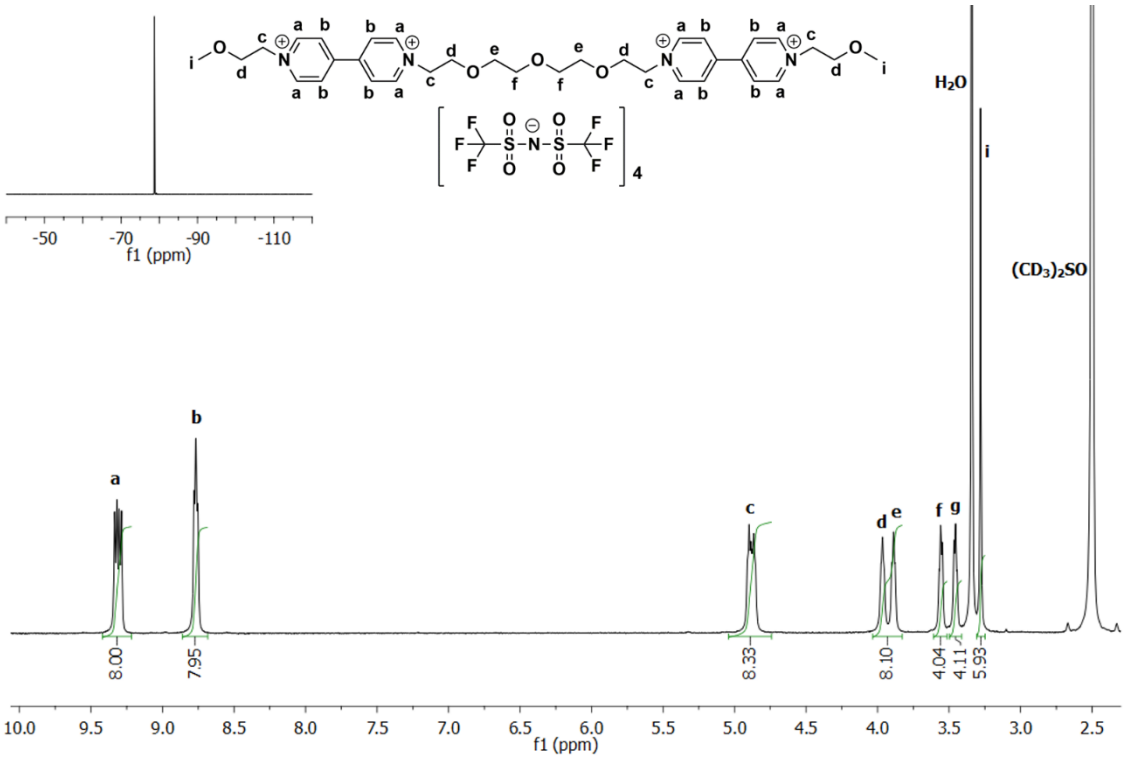

Figure 3.4 – ^{1}H NMR spectra of $[(C_3O)bpy(C_8O_3)bpy(C_3O)][NTf_2]_4$ in $(CD_3)_2SO$. Inside: the correspondent ^{19}F NMR spectra.

Elemental analysis and differential scanning calorimetry (DSC) have also been performed. In particular, for the case of $[(C_3O)bpy(C_4O)bpy(C_3O)]I_4$, $[(C_3O)bpy(C_8O_3)bpy(C_3O)]I_4$ and $[(C_{10})bpy(C_4O)bpy(C_3O)]I_4$ simultaneous TGA and DSC measurements (TGA/DSC) were performed. The physical state and thermal analysis of all prepared bis(bipyridinium) salts are described in Table 3.1.

Table 3.1 – Yield, physical state and thermal properties of bis(bipyridinium) salts prepared.

Bis(bipyridinium) Salts	Yield (%)	Physical State	m.p. (T_g) [ºC] [a]	T_d [ºC] [d, g]
$[(C_{10})bpy(C_4O)bpy(C_{10})]I_4$	32	Red solid	58.9 [b]	-
$[(C_{10})bpy(C_4O)bpy(C_{10})][NTf_2]_4$	84	Yellow solid	67.8 (n.d.) [c]	-
$[(C_3O)bpy(C_4O)bpy(C_3O)]I_4$	53	Pale orange solid	n.d.[d]	241.2
$[(C_3O)bpy(C_4O)bpy(C_3O)][NTf_2]_4$	94	Brown gel	RTIL (4.5) [e]	-
$[(C_3O)bpy(C_8O_3)bpy(C_3O)]I_4$	54	Orange solid	183.6 [d]	215.2
$[(C_3O)bpy(C_8O_3)bpy(C_3O)][NTf_2]_4$	94	Brown solid	85.3 (-6.9) [f]	-
$[(C_{10})bpy(C_4O)bpy(C_3O)]I_4$	25	Brown solid	190.2 [d]	213.5
$[(C_{10})bpy(C_4O)bpy(C_3O)][NTf_2]_4$	71	Brown gel	RTIL (6.0) [c]	-

[a] Melting point (m.p.) was determined by DSC analysis using a heating/cooling rate of 10 ºC/min at 2nd cycle. Glass transition temperature (T_g) was determined on 2nd or 3rd cycle. [b] Crystallization (T_c) were determined at 18.6, 50.0 ºC by DSC analysis using a heating/cooling rate of 10ºC/min at 2nd cycle). [c] Crystallization (T_c) were determined at 36.3, 64.2 ºC by DSC analysis using a heating/cooling rate of 10 ºC/min at 2nd cycle. [d] Melting point detected by TGA/DSC experiments from 25 ºC to 300 ºC at 10 ºC/min. [e] Glass transition temperature was determined at 2nd cycle by DSC analysis using a heating/cooling rate of 20 ºC/min. [f] Melting point was only detected on the 1st cycle, determined by DSC analysis using a heating/cooling rate of 10 ºC/min. [g] The decomposition temperature was determined as onset temperature from TGA/DSC experiments (25 ºC to 300 ºC at 10 ºC/min).

In general, the prepared tetra-iodide salts showed melting points higher than 150 ºC, except in the case of [(C_{10})bpy(C_4O)bpy(C_{10})] (58.9 ºC). These melting points as well as the decomposition temperatures have been checked by simultaneous TGA/DSC experiments. Contrarily to iodide salts, [NTf_2] based salts were obtained as ILs, including two RTILs, [(C_3O)bpy(C_4O)bpy(C_3O)] and [(C_{10})bpy(C_4O)bpy(C_3O)], respectively. These anion exchange reactions allowed a significantly decrease of the melting points comparing to the correspondent iodide salts.

All tetra-substituted-4,4'-bipyridinium salts have been studied by DSC technique. In general, for iodide salts were not detected any glass transition in the selected experimental conditions (-90 to 150 ºC at 10 ºC/min). In the case of three of the [NTf_2] salts, a glass transition between -6.9 to 6.0 ºC were detected. It is relevant to focus that those glass transition range values were higher than all values already described for di-cation 4,4'-bipyridinium salts (-17.5 to -30.0 ºC).
In the case of [(C_{10})bpy(C_4O)bpy(C_3O)][NTf_2]$_4$, a glass transition (6.0 ºC) is also observed and in the following cooling run it is observed an exothermic peak, which could be attributed to the energy release derived from the cracking of the glassy structure occurring below to glass transition detected in heating [30]. The [(C_3O)bpy(C_8O_3)bpy(C_3O)][NTf_2]$_4$ presented a particular behaviour, once only a melting peak is detected (85.3 ºC) in the first cycle. During the subsequent cooling and heating runs, a glass transition (-6.9 ºC) is detected, indicating that this salt became a supercooled liquid (Figure 3.5).

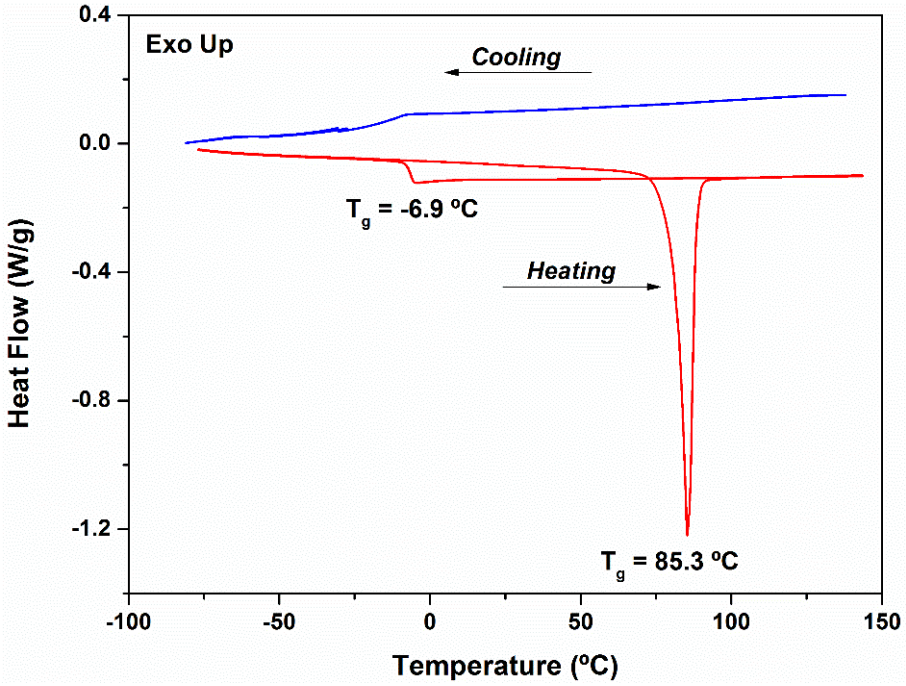

Figure 3.5 – Heat flow thermogram for [(C_3O)bpy(C_8O_3)bpy(C_3O)][NTf_2]$_4$ obtained at 10 ºC/min (heating /cooling rate), where glass transition temperature (T_g as midpoint) was determined on the third heating run.

An interestingly thermal behaviour is observed in the cases of [(C_{10})bpy(C_4O)bpy(C_{10})]I_4 and [(C_{10})bpy(C_4O)bpy(C_{10})][NTf_2]$_4$ that could be attributed to the formation of ionic liquid crystals. However, complementary analysis should be required in order to proof this thermal behaviour.
According to the literature, di- and tetra-substituted-4,4'-bipyridinium salts can be obtained as liquid crystals, including ILCs as indicated in the introduction of this chapter. It is known that the

development of ILCs is dependent to the length and type of the alkyl chains as well as the appropriate selection of anions. The di-substituted-4,4'-bipyridinium salts are considered rod-like molecules with high structural similarity and tendency to form ILCs [11,12,31]. The iodide and bromide di-substituted-4,4'-bipyridinium salts are found to be crystalline up to the decomposition temperature [32–34].

The electrochromic properties of all these bis(bipyridinium) tetra-iodide salts have been investigated and it is presented in the next chapter.

3.3. Ionic Polymers

Polymers consist in a sequence of molecules that are arranged in a simple repeating structure, also known as monomer, to form a macromolecular architecture with a distribution of molecular weight. These macromolecules can be linear, slightly branched or highly interconnected (large three-dimensional network) [35].

In general, the most reported electrochromic polymers are neutral species and taking in account the properties of the PILs, electrochromic ionic polymers have been explored.

There is reported in the literature an interesting example of the use of ionic polymer based on bipyridinium cation for redox-active polyelectrolyte multilayers [36,37]. Firstly, they used an electrostatic layer by layer approach to achieve multilayers of polyelectrolytes containing redox active sites. For that, they used a linear poly(cation) derived from viologen units, where the bipyridinium units are connected together by alkyl chain, combined with a poly(anion), poly(styrene sulfonate) (PSS) and deposited as film on conducting substrates by electrochemical methods. Also, they demonstrated that multilayers system showed elecrochromism and electrocatalytic activity [36].

Later, Schlenoff and co-workers reported again polyelectrolyte multilayers but now using a Poly(vinyl benzyl) bearing viologen units [37]. There is also reported the preparation of poly(cations) based on 4,4'-bipyridinium, which is found in the main chain [16,24]. These polymers were prepared by step-growth polymerization, where a direct quaternization of a di-halide with di-pyridinium unit occurs [16,24]. Subsequently, an anion exchange reaction can be done.

Herein, some ionic polymers bearing a bipyridinium units have been prepared by thermal free-radical polymerization (Figure 3.6, approach A). Additional ionic polymers, where Poly(anion) or Poly(cation) are combined with an electrochromic counter-ion have been also performed (Figure 3.6, approach B).

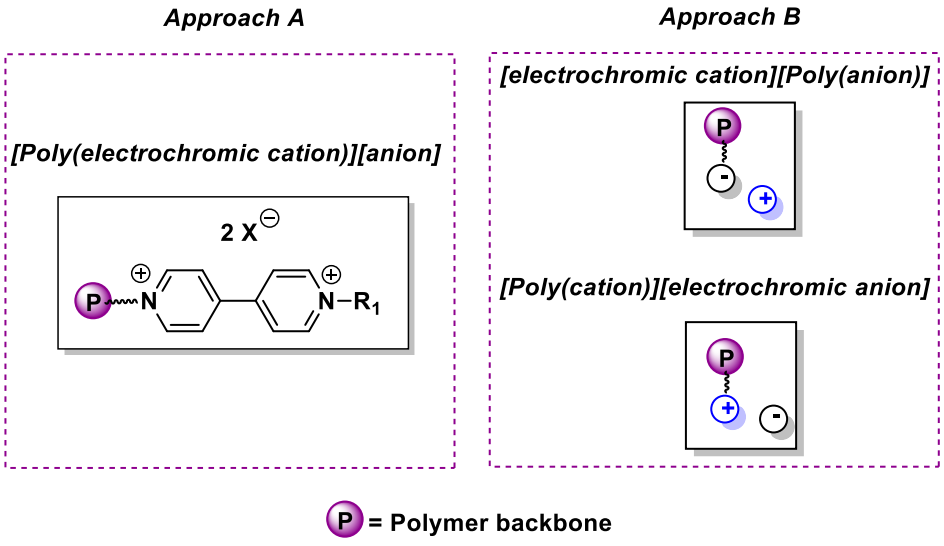

Figure 3.6 – Different approaches used to prepare electrochromic ionic polymers.

3.3.1. Ionic polymers by thermal polymerization

All ionic polymers have been prepared using free-radical polymerization, which proceeds via chain mechanism involving free radicals (Scheme 3.4).

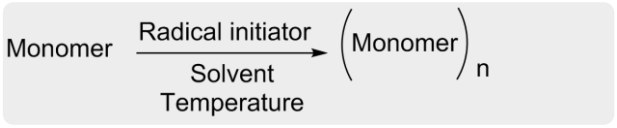

Scheme 3.4 – Scheme of free-radical polymerization.

This type of polymerization consists in the following steps: initiation, propagation, chain transfer and termination. In addition, azobisisobutyronitrile (AIBN) is normally used as radical initiator.

Two different synthetic procedures have been tested to prepare ionic polymers based on bipyridinium scaffolds. Firstly, the introduction of polymerizable groups in bipyridinium scaffolds (monomers) and then thermal polymerization. However, this approach failed but will be briefly discussed, followed by a more detailed description of the second synthetic approach. This alternative approach was performed in two steps: 1) preparation of the polymer having a free leaving group such as chloride or iodide and 2) functionalization of the polymer with mono-substituted-4,4'-bipyridinium salt previously prepared through nucleophilic substitution reaction.

3.3.1.1. Approach I

The synthetic route used in order to prepare ionic polymers based on 4,4'-bipyridinium salts has been adapted from imidazolium PILs preparation, which is well-described in the literature. Firstly, preparation of the di-substituted-4,4'-bipyridinium salts containing a polymerizable groups and then thermal polymerization as illustrated in Scheme 3.5. The preparation of non-symmetric di-substituted-4,4'-bipyridinium salts containing only one polymerizable group (Scheme 3.5, Route A) or containing two polymerizable groups (symmetric di-substituted 4,4'-bipyridinium salts), which can lead to a cross-linked polymer (Scheme 3.5, Route A).

The polymerization of the salt 1,1'-di-allyl-4,4'-bipyridinium combined with bromide or [NTf_2] have been tested through free-radical polymerization but it was unsuccessful. Thus, a more reactive polymerizable group based on vinyl scaffold was chosen.
These di-substituted-4,4'-bipyridinium salts were prepared using similar synthetic route for symmetric and non-symmetric salts as previously discussed in Chapter 1.

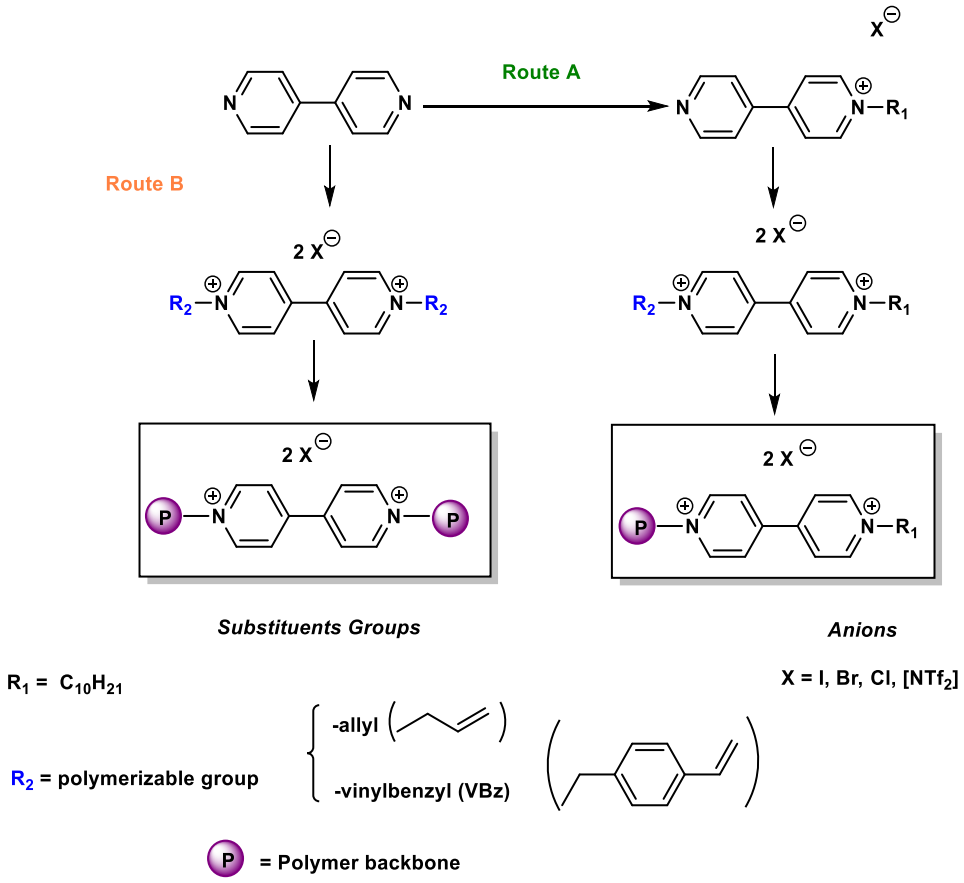

Scheme 3.5 – Possible approaches to prepare symmetric and non-symmetric ionic polymers based on 4,4'-bipyridinium scaffold.

Anion exchange reactions to $[NTf_2]$ have been also performed. The yields and physical states for the prepared salts are summarized in Table 3.2.

Table 3.2 – Symmetric and non-symmetric di-substituted-4,4'-bipyridinium salts prepared, containing a polymerizable group.

Salts	Yield (%)	Physical State
$[C_{10}VBzbpy]ICl$	85	Brown solid
$[C_{10}VBzbpy][NTf_2]_2$	100	Red solid
$[(VBz)_2bpy]Cl_2$	81	Pale yellow solid
$[(VBz)_2bpy][NTf_2]_2$	93	Yellow solid

In general, all salts were prepared in high yields and analysed by ^1H NMR spectroscopy. Then, a free-radical polymerization using AIBN as initiator was performed for the cases of $[C_{10}VBzbpy]ICl$, $[C_{10}VBzbpy][NTf_2]_2$ and $[(VBz)_2bpy][NTf_2]_2$. All polymerization failed and it was confirmed by ^1H NMR spectroscopy. In the case of $[C_{10}VBzbpy]ICl$, this salt seems to have solubility problems and different solvents, such as ethanol:methanol (1:1), methanol (pressure tube), ethyl lactate, poly(ethylene glycol) 400 have been tested. In order to improve the solubility problems of the halide salts, the polymerization of $[NTf_2]$ salts have been tested. However, the ^1H NMR spectroscopy showed that the polymerization did not occurred and one possible explanation is the anion effect during the polymerization steps.

In the literature, there are reported two synthetic routes to prepare PILs as already mentioned in the introduction of this chapter: (1) anion exchange reaction and then polymerization or (2) polymerization and then anion exchange reaction [16]. The most common route described in the literature to prepare Poly(imidazolium derivatives) bis(trifuoromethanesulfonyl)imide is firstly polymerized, followed by the anion exchange reaction [22,38–40].

Despite of all problems to prepare ionic polymer through directly free-radical polymerization of the di-substituted-4,4'-bipyridinium salts, it could be more explored and the solubility problems could be improved by testing a variety of anions.

3.3.1.2. Approach II

Schlenoff and co-workers reported the functionalization of a commercial polymer, poly(vinyl benzyl chloride) with 1-methyl-4,4'-bipyridinium chloride as side chain [37]. A similar approach has been adapted from their work. This approach consists in the preparation of polymer backbone using 4-vinylbenzyl chloride as monomer and halide exchange reaction to more reactive leaving group (chloride to iodide), followed by functionalization using mono-substituted-4,4'-bipyridinium salt through nucleophilic substitution reaction (Figure 3.7).

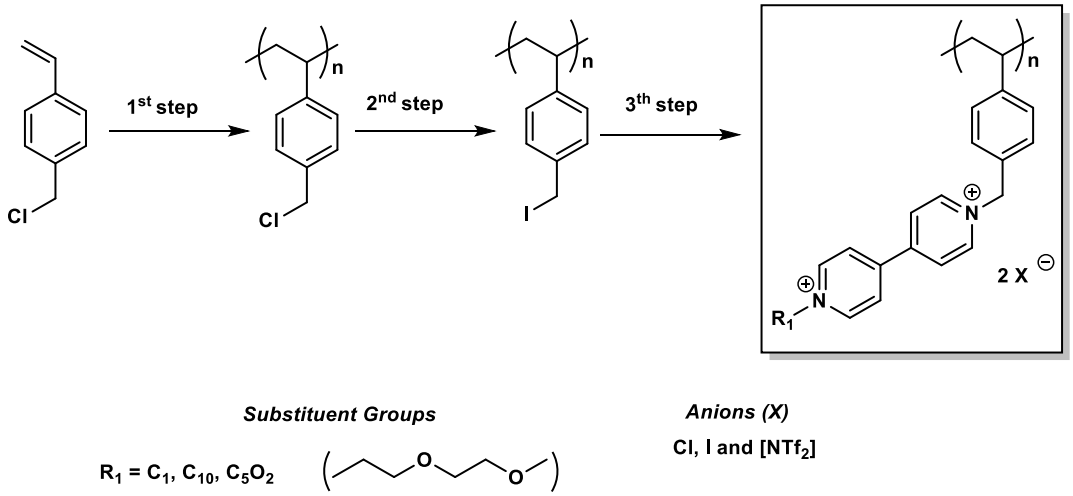

Figure 3.7 – Synthetic route used to prepare ionic polymers bearing 4,4'-bipyridinium units.

The polymer Poly(4-vinylbenzyl chloride) **PVBz1** was polymerized by free-radical polymerization (Scheme 3.6).The polymerization was performed in DMF at 80 ºC during 24 hours using AIBN as initiator.

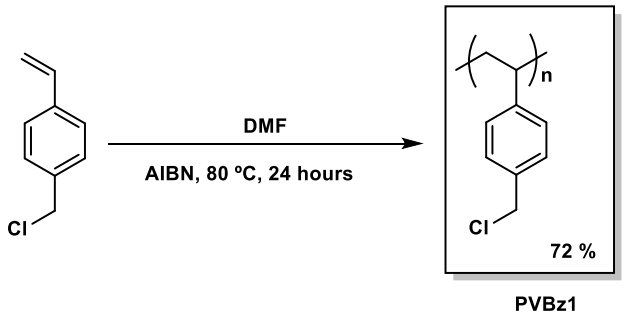

Scheme 3.6 – Polymerization to obtain Poly(4-vinylbenzyl chloride) (**PVBz1**).

The ^{1}H NMR spectra showed the correspondent protons of the polymer **PVBz1** (see Figure 3.8).

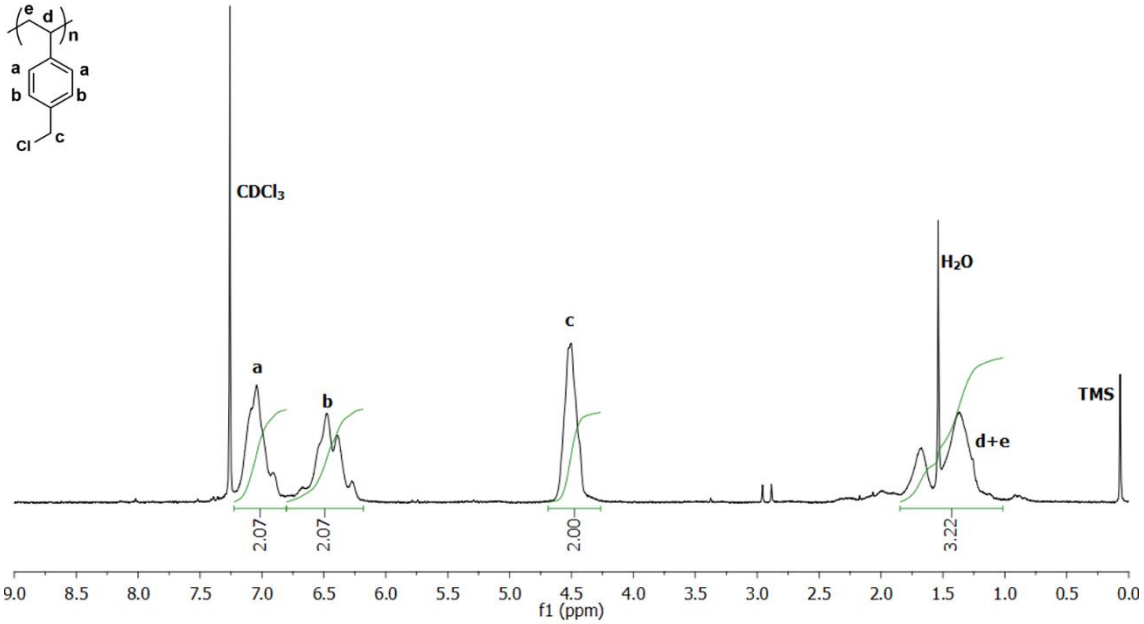

Figure 3.8 – ^{1}H NMR spectra of **PVBz1** in $CDCl_3$.

The functionalization of **PVBz1** with the mono-cation [C_1bpy]I similar to the reported by Schlenoff and co-workers have been performed. However, it was not possible to analyse this polymer by ^{1}H NMR spectroscopy due to solubility problems. For example, using deuterated DMSO a second phase (gel) was formed after few minutes (Figure 3.9) and unclearly ^{1}H NMR spectra was obtained.

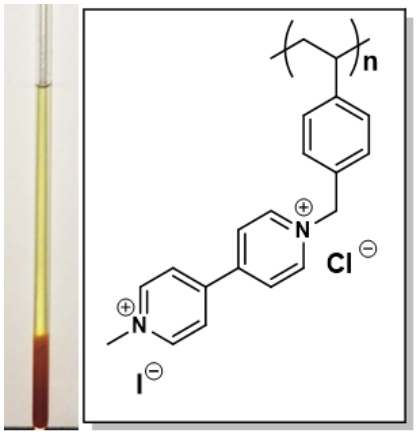

Figure 3.9 – Polymer **PVBz1** functionalized with 1-methyl-4,4'-bipyridinium iodide in deuterated DMSO-d6.

Additional analysis should be done in order to check the structure of the polymer, as well as to evaluate the degree of functionalization (if possible). According to the similar polymers from the literature, the molecular weight distribution of this polymer (was not evaluated) as well as the anion effect could explained the unsuccessful ^{1}H NMR analysis [37,41].

An attempt to overcome this observation was performed, for that the halide exchange reaction from chloride to iodide, using sodium iodide in acetone (Scheme 3.7) for further functionalization with mono-substituted-4,4'-bipyridinium salt was done.

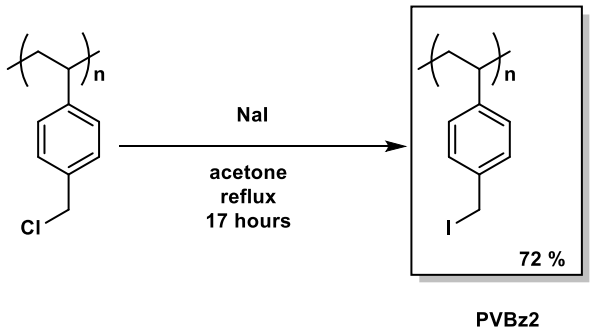

PVBz2

Scheme 3.7 – Synthetic route to prepare the poly(4-vinylbenzyl iodide) **PVBz2**.

The functionalization using an alternative mono-substituted-4,4'-bipyridinium salt, [(C_5O_2)bpy]I (more polar group as side chain) was performed in DMF at 100 ºC, during *ca.* 48 hours (Scheme 3.8).

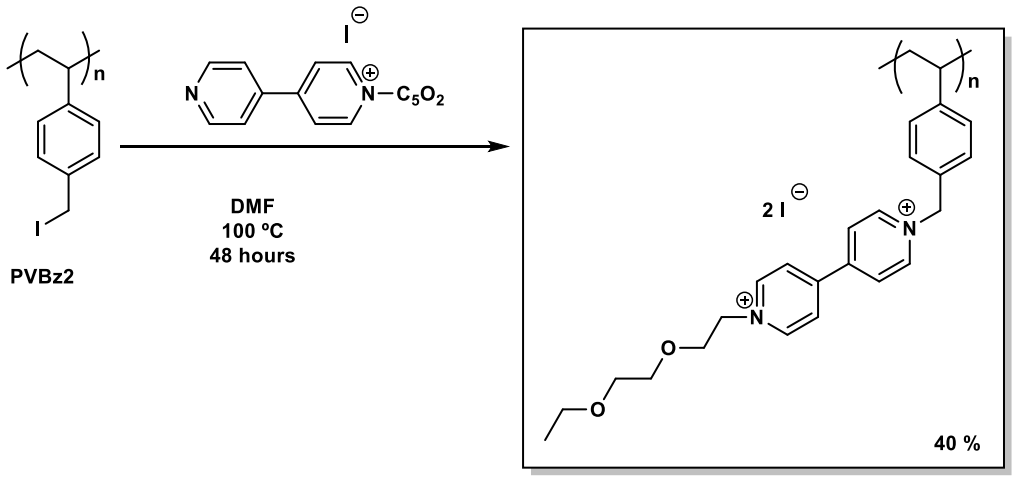

PVBz3

Scheme 3.8 – Synthetic route to prepare the ionic polymer bearing a 4,4'-bipyridinium unit, **PVBz3**.

The ^{1}H NMR analysis was not successful performed due to the fact that the final product showed lower solubility in the common deuterated solvents and became a gel after few minutes as mentioned before. Additional analysis such as solid NMR spectroscopy or mass spectrometry is required to check the polymer structure. Similar behaviour was observed for ionic polymer bearing mono-substituted-4,4'-bipyridinium salt with longer alkyl chain (C_{10}). It seems the anion and molecular weight distribution of the polymer are important parameters for the polymer structure analyse and an alternative attempt could be realized in order to optimize this synthetic step.

In order to facilitate the solubility in common solvents an anion exchange with Li[NTf_2] in DMF have been performed (see Scheme 3.9).

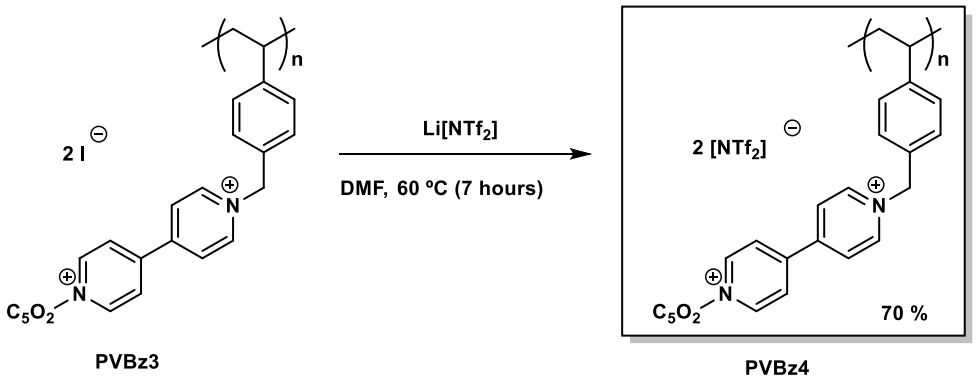

Scheme 3.9 – Synthetic route to prepare the ionic polymer bearing a 4,4'-bipyridinium unit with [NTf_2] anion, **PVBz4**.

However, the ^{1}H NMR was also difficult to perform and it seems to be inconclusive. Alternative analysis should be performed (elucidation of the structure using solid state NMR or mass spectrometry). However, this polymer PVBz4 was tested in electrochromic device to check the presence of electrochrome species and their electrochromic performance. These preliminary studies are important to evaluate if this approach is attractive for future applications.

3.3.2. Poly(cation)/Poly(anion) with electrochromic counter-ion

3.3.2.1. Synthesis of [Poly(cation)][anion]

The commercial Poly(Diallyl Dimethyl Ammonium Chloride) (20 wt % H_2O, average M_w: 200 000 to 350 000) was combined with vanadate (VO_3) and cobalt EDTA complex (Co[EDTA]) anions as electrochromic units (Figure 3.10).

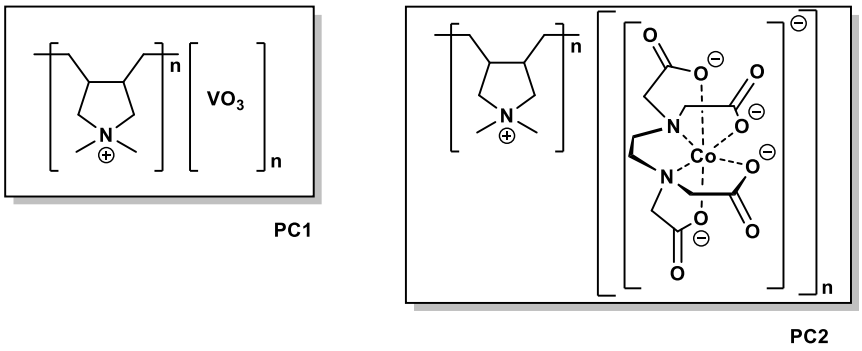

Figure 3.10 – Poly(diallyl dimethyl ammonium vanadate) (**PC1**) and Poly(diallyl dimethyl ammonium Co[EDTA]) prepared.

In the case of **PC1** the anion exchange reaction was performed in water at room temperature during 72 hours (Scheme 3.10).

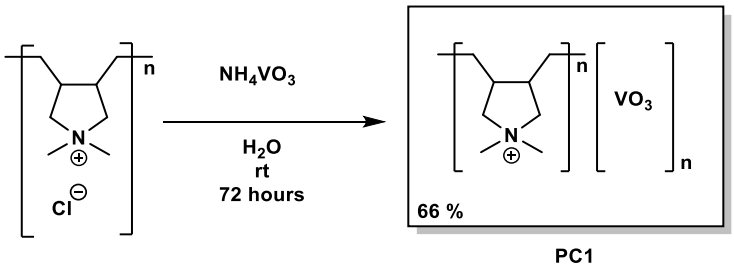

PC1

Scheme 3.10 – Synthetic route to prepare the poly(diallyl dimethyl ammonium vanadate) **PC1**.

However, ^{1}H NMR was not possible to perform due to the lower solubility of the final polymer. Alternative analytical techniques should be used, namely solid NMR spectroscopy.

In the case of **PC2**, the anion exchange reaction was performed in water at 80 ºC during 27 hours (Scheme 3.11). The ^{1}H NMR spectra is presented in Figure 3.11.

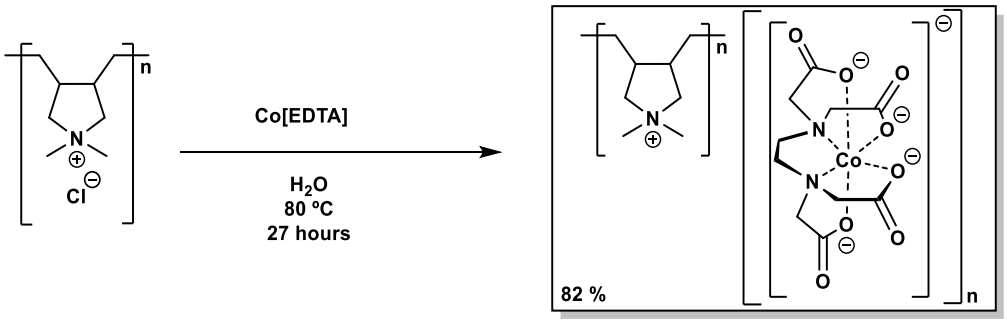

PC2

Scheme 3.11 – Synthetic route to prepare the poly(diallyl dimethyl ammonium Co[EDTA]) **PC2**.

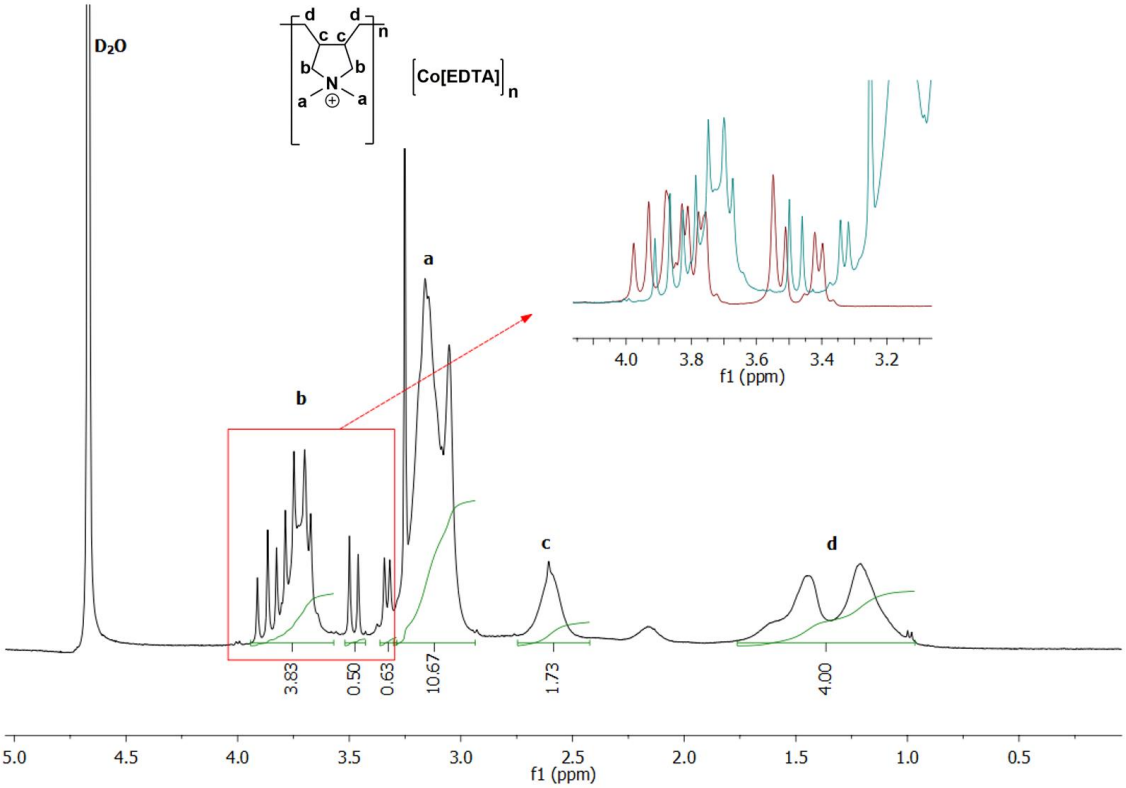

Figure 3.11 – ^{1}H NMR spectra in D_2O of **PC2**. The 3.1 – 4.0 ppm region has been expanded to visualize the signals corresponding of the poly(diallyl dimethyl ammonium) overlap with Co[EDTA] anion. Also, the spectrum of Co[EDTA] is superimposed (red line).

From ^{1}H NMR spectra, it is possible to identify the protons from the cation and anion but its proportion is not clear. Additional analysis should be required to clarify the cation/anion proportion.

3.3.2.2. Synthesis of [cation][Poly(anion)]

The commercial Poly(sodium 4-styrenesulfonate) (30 wt % solution in water, average M_w: 70 000) was combined with mono-substituted-4,4'-bipyridinium salt, $[(C_5O_2)_2bpy]$, as electrochromic cation (Figure 3.12).

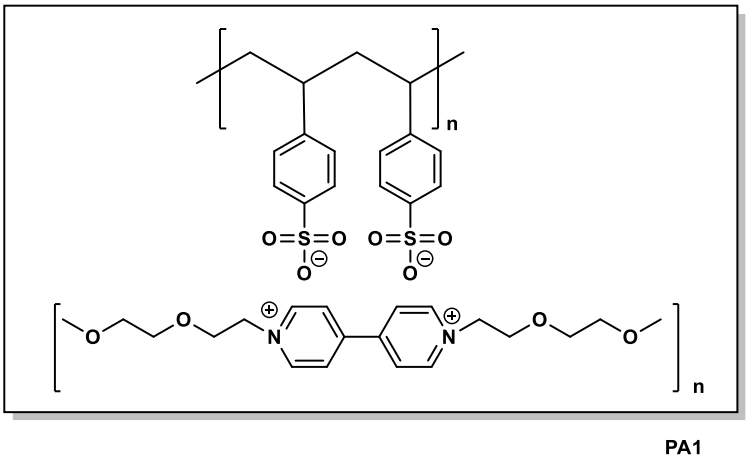

PA1

Figure 3.12 – Poly(4-styrene sulfonate) combined with $[(C_5O_2)_2bpy]$ as electrochromic cation.

The preparation of the polymer **PA1** was performed in two steps. Firstly, cation exchange reaction from sodium to silver, using silver nitrate in order to facilitate the further isolation and purification of the desired product. Then, cation exchange reaction with $[(C_5O_2)_2bpy)]I_2$ (see Figure 3.12).

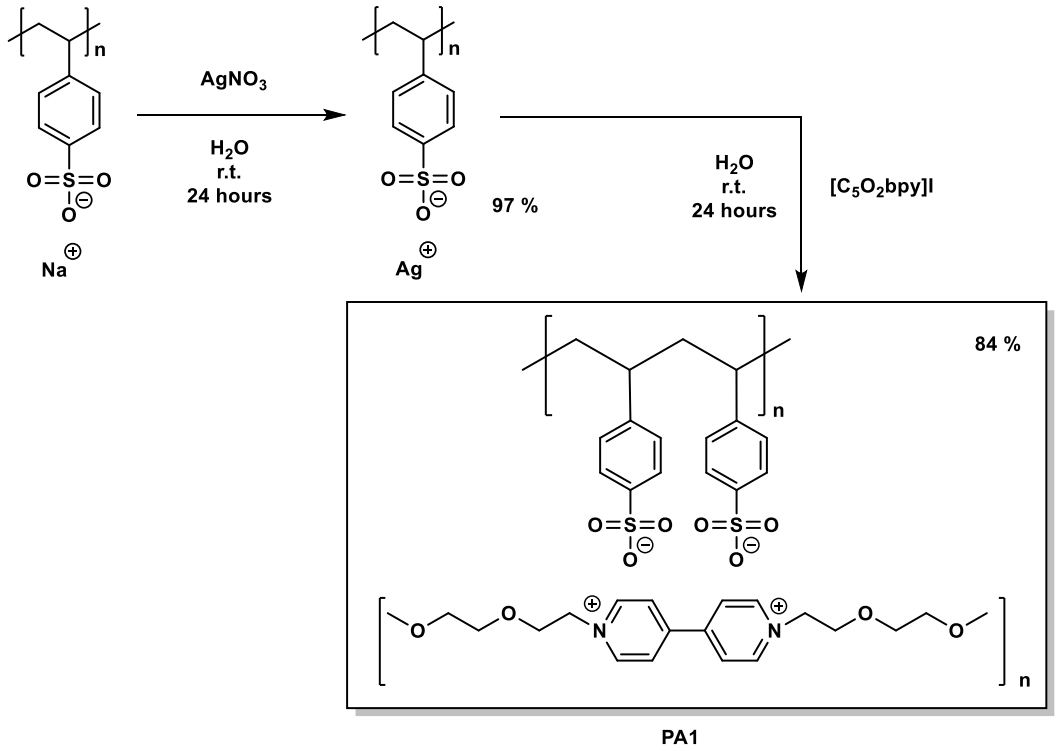

PA1

Scheme 3.12 – Synthetic procedure used to prepare the poly(4-styrene sulfonate) combined with $[(C_5O_2)_2bpy]$ as electrochromic cation.

From the ^{1}H NMR spectra, it is possible to identify the protons from the polymer (cation) but also the cation (Figure 3.13). The proportion between cation and anion can be determined by comparison of integral areas of specific protons of both. It was found to be 1:0.9 (cation:anion) by comparison of the aromatic proton from $[(C_5O_2)_2bpy]$ (proton **2**) and the aromatic proton of poly(anion) (proton **a**).

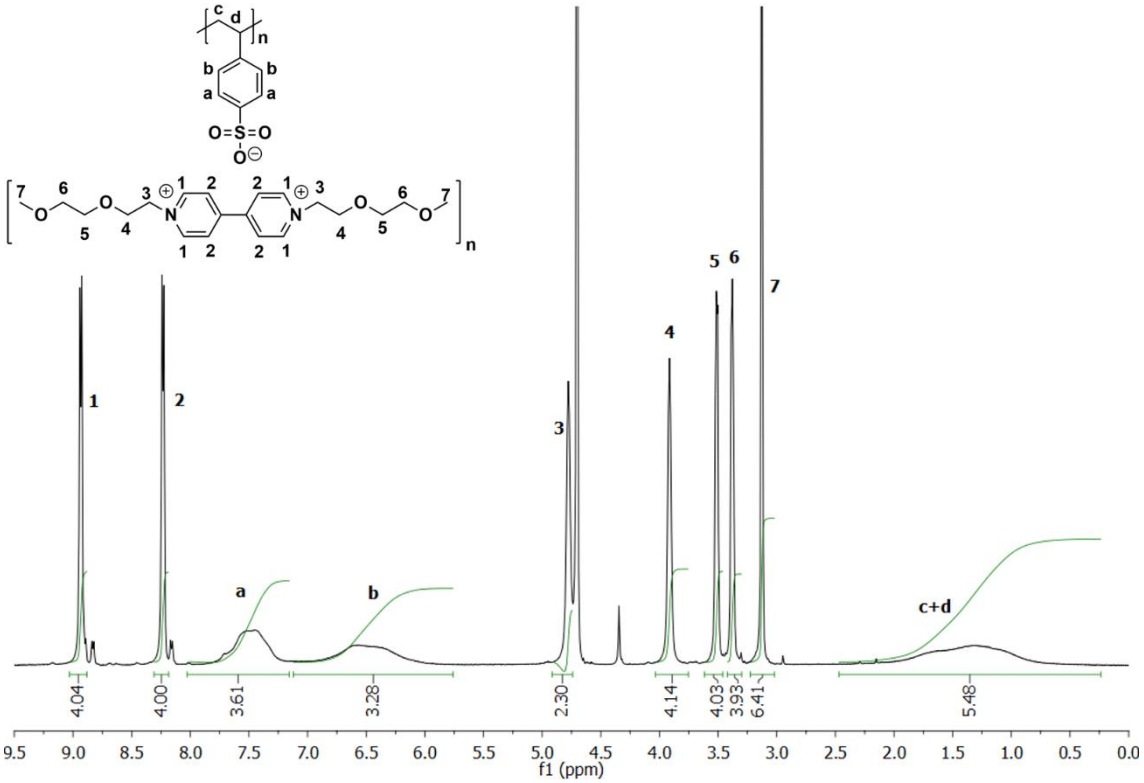

Figure 3.13 – ^{1}H NMR spectra in D_2O of the polymer **PA1**.

All these approaches can be more explored and the synthetic route as well as the purification step needs to be improved.

Herein, we demonstrated that is possible to develop electrochromic ionic polymers based on well-known molecules.

3.4. Conclusions

Different tetra-substituted and ionic polymers based on 4,4'-bipyridinium as well as electrochromic ionic polymers have been developed.

Tetra-substituted-4,4'-bipyridinium tetra-iodide salts have been prepared, where two 4,4'-bipyridinium units are covalently linked to other 4,4'-bipyridinium unit by a specific linker. Subsequently, an anion exchange reaction using $Li[NTf_2]$ have been performed. It allowed to obtain four ILs, including two RTILs. The thermal properties of all salts were evaluated and the electrochromic properties were also studied and discussed in the next chapter. This type of approach is useful to prepare linear polymers and control the length of the polymer.

Electrochromic ionic polymers were prepared using two different approaches: the functionalization of a prepared polymer, where a backbone chain is bearing an electrochromic unit as side chain as well as the combination of a poly(cation) or poly(anion) with electrochromic counter-ion. In the case of the functionalization of a prepared polymer, it was possible to prepare the polymer by free-radical thermal polymerization of 4-vinylbenzyl chloride using AIBN as radical initiator. However, the resulting polymer after functionalization step showed solubility problems to performed ^1H NMR spectroscopy and it was difficult to check the introduction of the 4,4'-bipyridinium unit as well as the degree of functionalization. Additional analysis is required in order to analyse the resulting polymer. An anion exchange reaction was also performed. One of the resulting polymers has been tested as electrochromic material and it will be discussed in the next chapter. This approach could be more explored and the synthetic procedure as well as the purification step could be more improved.

Similar strategy to prepare PILs based on commercial poly(cation) or poly(anion) combined with adequate electrochromic counter-ions have been explored. The resulting polymers seem to be interesting to use as electrochromic material and the electrochromic properties need to be investigated.

3.5. Experimental Part

Solvent and Reagents for synthesis

Dimethylformamide (Carlo Erba), Acetonitrile (Carlo Erba). 4,4'-bipyridine (Alfa Aesar, 98 %), 1-Iododecane (Sigma-Aldrich, > 98 %), 1-Iodomethane (Sigma-Aldrich, > 98 %), 1-bromoallyl (Sigma-Aldrich, > 98 %), 4-Vinylbenzyl chloride (Sigma-Aldrich, ≥ 90 %), azobisisobutyronitrile (AIBN, Fluka, 98 %), sodium iodide (Alfa Aesar, 99.9 + %), silver nitrate (Sigma Aldrich,>> 99.9 %), Poly(Diallyl Dimethyl Ammonium Chloride) (Aldrich, 20 wt % in H_2O), Poly(sodium 4-styrenesulfonate) (Aldrich, 30 wt % solution in H_2O), lithium bis(trifluoromethanesulfonyl)imide (Sigma-Aldrich, > 98 %), Ammonium vanadate (Merck, > 98 %), 2-chloroethylether (Sigma-Aldrich, > 98 %), bis[2-(2-chloroethoxy)ethyl]ether (Aldrich, 99 %), 2-Methoxyethanol (Alfa Aesar, 99 %), 2-(2-methoxyethoxy)ethanol (Sigma Aldrich, > 98 %) were used as supplied.

2-Methoxyethyl iodide, 2-(2-methoxyethoxy)ethyl iodide, bis[2-(2-iodoethoxy)ethyl]ether and 2-iodoethyl ether were prepared in two steps according to the synthetic method reported previously [40]. The mono-substituted-4,4'-bipyridinium salts are prepared according to the synthetic method described in the previous chapter. Sodium Co[EDTA] was prepared according to the synthetic method described in the literature [42,43].

NMR Spectroscopy

NMR spectra were done on a Bruker AMX 400 instrument operating at 400.13 MHz (^{1}H), 100.61 MHz (^{13}C) and 376.50 MHz (^{19}F). The NMR spectrometers are part of The National NMR Facility supported by Fundação para a Ciência e a Tecnologia (RECI/BBB-BQB/0230/2012).

Elemental analysis

Elemental analysis was obtained on a Thermofinnigan Flash EA 1112 Series instrument and was performed by the Laboratório de Análises at LAQV/UCIBIO – REQUIMTE.

Thermal analysis

DSC: TA Instruments Q-series TM Q2000 DSC with a refrigerated cooling system was used. The sample is continuously purged with 50 ml/min nitrogen. About 2-15 mg of salt was crimped in an aluminium hermetic sample pan with lid. And the melting point and glass transition temperature were determined in the second or third heating run.

TGA/DSC:

Setaram Labsys EVO was used. The sample (4 – 10 mg) is continuously purged with argon from 25 ºC to 300 ºC at 10 ºC/min.

FTIR spectroscopy

FTIR spectra were recorded on a Buker Tensor 27, using KBr pellet for the solids and NaCl cells for the liquids.

Synthesis of tetra-substituted-4,4'-bipyridinium salts

1-decyl-1'-[2-(2-iodoethoxy)ethyl]-4,4'-bipyridinium di-iodide [(C_{10})bpy(C_4O)I]I_2

The monocation [C_{10}bpy]I (0.687 g, 1.62 mmol) already prepared was dissolved in acetonitrile and stirred at reflux in nitrogen atmosphere. The 2-iodoethylether (1.522 g, 4.67 mmol) was slowly added and the reaction mixture was stirred during ca. 4.5 days. After cooling the reaction mixture, the solid was filtered, washed with diethyl ether and dried in vacuum to give a red solid (1.061 g, 87 %). ^{1}H NMR (400.13 MHz, DMSO-d6, 25 ºC) δ = 9.40 (d, J = 5.4 Hz, 4 H), 9.36 (d, J = 5.3 Hz, 4 H), 5.03 – 4.85 (m, 2 H), 4.83 – 4.61 (m, 2 H), 4.13 – 3.96 (m, 2 H), 3.82 – 3.64 (m, 2 H), 3.32 –3.24 (m, 2 H), 2.09 – 1.91 (m, 2 H), 1.46 – 1.15 (m, 14 H), 0.96 – 0.75 (m, 3 H) ppm. ^{13}C NMR (100.61 MHz, DMSO-d6, 25 ºC) δ = 149.4, 149.0, 146.8, 146.2, 127.1, 126.8, 70.8, 68.4, 61.4, 60.9, 31.7, 31.2, 29.4, 29.3, 29.1, 28.9, 25.9, 22.6, 14.4, 5.8 ppm.

[(C_{10})bpy(C_4O)bpyC_{10}]I_4:

The salt [C_{10}bpy(C_4O)I]I_2 (0.212 g, 0.28 mmol) previously prepared was dissolved in dried acetonitrile and stirred at reflux in nitrogen atmosphere. The mono-cation [C_{10}bpy]I (0.152 g, 0.36 mmol) was dissolved in dried acetonitrile and slowly added to the previous reaction mixture. The reaction mixture was stirred in reflux during ca. 7 days. After cooling the reaction mixture, the solid was filtered, washed with diethyl ether and dried in vacuum to give a red solid (0.107 g, 32 %). m.p. = 58.9 ºC. T_c = 18.6 and 50.0 ºC. ^{1}H NMR (400.13 MHz, DMSO-d6, 25 ºC) δ = 9.43 (d, J = 5.5 Hz, 4 H), 9.35 (d, J = 5.5 Hz, 4 H), 8.82 (d, J = 4.4 Hz, 8 H), 5.00 – 4.85 (m, 4 H), 4.72 (t, J = 6.5 Hz, 4 H), 4.13 – 3.95 (m, 4 H), 2.09 – 1.91 (m, 4 H), 1.46 – 1.15 (m, 28 H), 0.93-0.80 (m, 6 H) ppm. ^{13}C NMR (100.61 MHz, DMSO-d6, 25 ºC) δ = 148.8, 148.4, 146.2, 145.7, 126.7, 126.4, 68.5, 60.9, 60.2, 31.2, 30.8, 28.9, 28.8, 28.6, 28.4, 25.4, 22.1 ppm. FTIR (KBr): $\breve{\upsilon}$ = 3105, 3038, 2920, 2853, 1637, 1553, 1443, 1348, 1215, 1178, 1115, 831, 718 cm^{-1}. Elemental Analysis calcd (%) for $C_{44}H_{66}I_4N_4.3H_2O$: C 43.01, H 5.91, N 4.56; found C 42.69, H 5.81, N 4.58.

[C_{10}bpy(C_4O)bpyC_{10}][NTf_2]$_4$

To a solution of [C_{10}bpy(C_4O)bpyC_{10}]I_4 (0.104 g, 0.09 mmol) in methanol Li[NTf_2] (0.143 g, 0.50 mmol) was slowly added and stirred during 5 days at room temperature. After this time, the solvent was evaporated and the product was recovered by addition of water. Then, the solid was filtered and dried in vacuum to give a yellow solid (0.133 g, 84 %). An additional step was performed to remove any halides salts by addition of acetone. m.p.= 67.8 ºC, T_c = 36.3 and 64.2 ºC. ^{1}H NMR (400.13 MHz, DMSO-d6, 25 ºC) δ = 9.38 (d, J = 6.6 Hz, 4 H), 9.29 (d, J = 6.6 Hz, 4 H), 8.76 (d, J = 4.4 Hz, 8 H), 4.91 – 4.81 (m, 4 H), 4.68 (t, J = 7.3 Hz, 4 H), 4.05 – 3.95 (m, 4 H), 2.03 - 1.91 (m, 4 H), 1.38 – 1.15 (m, 28 H), 0.84 (t, J = 6.5 Hz, 6 H) ppm. ^{19}F NMR (376.50 MHz, DMSO-D6, 25 ºC) δ = -78.70 ppm. ^{13}C NMR (100.61 MHz, DMSO-d6, 25 ºC) δ = 149.4, 145.0, 146.7, 127.1, 126.8, 121.5, 118.3, 69.1, 61.5, 60.8, 31.7, 31.3, 29.3, 29.1, 28.9, 25.9, 22.5, 14.4 ppm.
FTIR (KBr): $\breve{\upsilon}$ = 3132, 3055, 2926, 2856, 1643, 1564, 1448, 1348, 1198, 1138, 1059, 831, 791, 739 cm^{-1}. Elemental analysis calcd (%) for $C_{52}H_{66}F_{24}N_8O_{17}S_8.2C_3H_6O$: C 36.59, H 4.13, N 5.89; found C 36.29, H 4.19, N 5.92.

[C_3Obpy(C_4O)bpyC_3O]I_4

The salt [C_3Obpy]I (0.889 g, 2.6 mmol) previously prepared was dissolved in acetonitrile. The 2-iodoethylether (0.968 g, 3.0 mmol) was slowly added and the reaction mixture was stirred at reflux during ca. 6 days. After cooling the reaction mixture, the solid was filtered, washed with acetonitrile and diethyl ether, dried in vacuum to give a pale orange solid (0.367 g, 53 %). T_d = 241.2 ºC. ^{1}H NMR (400.13 MHz, D_2O, 25 ºC) δ = 9.06 (dd, J = 4.6, 9.5 Hz, 8 H), 8.51 (dd, J = 4.6, 8.3 Hz, 8 H), 4.90-4.81 (m, 8 H), 4.05 (t, J = 3.2 Hz, 4 H), 3.96 (t, J = 3.2 Hz, 4 H), 3.33 (s, 6 H) ppm. ^{13}C NMR (100.61 MHz, DMSO-d6, 25 ºC) δ =149.6, 149.4, 146.7, 146.6, 126.9, 121.5, 118.3, 70.5, 69.1, 61.0, 60.8, 58.8, 31.2 ppm. Elemental analysis calcd (%) for $C_{30}H_{38}I_4N_4O_9$.(2.5H_2O): C 34.14, H 4.11, N 5.31; found C 33.70, H 3.80, N 5.27.

[C_3Obpy(C_4O)bpyC_3O][NTf_2]$_4$

The salt [C_3Obpy(C_4O)bpyC_3O]I_4 (0.400 g, 0.40 mmol) was dissolved in water and Li[NTf_2] (0.562 g, 1.96 mmol) was slowly added and stirred during 1 day at room temperature. After this time, the solvent was decanted and the product was washed with water, dried in vacuum to give a brown gel (0.607 g, 94 %). T_g = 4.5 ºC. ^{1}H NMR (400.13 MHz, DMSO-d6, 25 ºC) δ = 9.32 (dd, J = 6.8, 15.9 Hz, 8 H), 8.76 (dd, J = 3.3, 6.5 Hz, 8 H), 4.92 (t, J = 4.5 Hz, 8 H), 4.89 – 4.82 (m, 4 H), 4.05 – 3.98 (m, 4 H), 3.91 (t, J = 45 Hz, 4 H), 3.30 (s, 6 H) ppm. ^{19}F NMR (376.50 MHz, DMSO-D6, 25 ºC) δ = -78.70 ppm. ^{13}C NMR (100.61 MHz, DMSO-d6, 25 ºC) δ =146.0, 127.1, 127.0, 70.00, 68.9, 61.3, 61.2, 58.5, 31.2 ppm. Elemental analysis calcd (%) for $C_{38}H_{38}F_{24}N_8O_{19}S_8$: C 28.12, H 2.36, N 6.90; found C 28.06, H 2.34, N 6.50.

[C_3Obpy(C_8O_3)bpyC_3O]I_4

The salt [C_3Obpy]I (1.834 g, 5.36 mmol) previously prepared was dissolved in acetonitrile. The bis[2-(2-chloroethoxy)ethyl] ether (1.527 g, 3.69 mmol) was slowly added and the reaction mixture was stirred at reflux during ca. 6 days. After cooling the reaction mixture, the solid was filtered, washed with acetonitrile and diethyl ether. The solid was recrystallized in acetonitrile and dried in vacuum to give an orange solid (0.756 g, 54 %). m.p. = 183.6 ºC. T_d = 215.2 ºC. ^{1}H NMR (400.13 MHz, D_2O, 25 ºC) δ = 9.06 (t, J = 6.7 Hz, 8 H), 8.51 (d, J = 5.8 Hz, 8 H), 4.86 (t, J = 4.4Hz, 8 H), 4.03 (t, J = 4.3Hz, 4 H), 3.96 (t, J = 4.5 Hz, 4 H), 3.70 – 3.51 (m, 8 H), 3.33 (s, 6 H) ppm. ^{13}C NMR (100.61 MHz, D_2O, 25 ºC) δ =150.3, 150.3, 146.0, 146.0, 126.9, 126.9, 70.0, 69.8, 69.5, 68.6, 61.3, 61.2, 58.5 ppm. Elemental analysis calcd (%) for $C_{34}H_{46}I_4N_4O_5$: C 37.18, H 4.22, N 5.10; found C 36.78, H 4.15, N 5.03.

[C_3Obpy(C_8O_3)bpyC_3O][NTf_2]$_4$

The salt [C_3Obpy(C_8O_3)]I_4 (0.444 g, 0.40 mmol) was dissolved in water and Li[NTf_2] (0.545 g, 1.90 mmol) was slowly added and stirred during 1 day at room temperature. After this time, the solvent was decanted and the product was washed with water, dried in vacuum to give a brown solid (0.647 g, 94%). m.p. =85.3 ºC and T_g = -6.9 ºC. ^{1}H NMR (400.13 MHz, DMSO-d6, 25 ºC) δ = 9.38 –9.26 (m, 8H), 8.87 – 8.69 (m, 8H), 4.94 – 4.84 (m, 8 H), 4.89 – 4.82 (m, 4 H), 4.05 – 3.98 (m, 4 H), 3.91 (t, J = 4.5 Hz, 4 H), 3.29 (s, 6 H) ppm. ^{19}F NMR (376.50 MHz, DMSO-d6, 25 ºC) δ = -78.70 ppm. ^{13}C NMR (100.61 MHz, DMSO-d6, 25 ºC) δ = 149.5, 149.5, 146.6, 126.9, 126.8,

121.5, 118.3, 70.5, 70.1, 70.0, 69.1, 60.9, 58.7 ppm. Elemental analysis calcd (%) for $C_{42}H_{46}F_{24}N_8O_{21}S_8$: C 29.48, H 2.71, N 6.55; found C 29.55, H 2.76, N 6.44.

[C_{10}bpy(C_4O)bpyC_3O]I_4

The salt [C_{10}bpy(C_4O)I]I_2 (0.847 g, 1.13 mmol) previously prepared was dissolved in acetonitrile and the salt [C_3Obpy]I (0.470 g, 1.37 mmol) was slowly added. The reaction mixture was stirred at reflux during ca. 4 days. After cooling the reaction mixture, the solid was filtered, washed with acetonitrile and diethyl ether, dried in vacuum to give a brown solid (0.303 g, 25 %). mp = 190.2 ºC. Td = 213.5 ºC. ^{1}H NMR (400.13 MHz, DMSO-d6, 25 ºC) δ = 9.67 – 9.37 (m, 8 H), 9.10 – 8.59 (m, 8 H), 5.35 – 4.45 (m, 8 H), 4.30 – 3.68 (m, 8 H), 3.29 (s, 3 H, overlapped with H_2O), 2.19 – 1.82 (m, 2 H), 1.57 – 1.02 (m, 14 H), 0.99 – 0.60 (m, 3 H) ppm. ^{13}C NMR (100.61 MHz, DMSO-d6, 25 ºC) δ = 149.4, 149.3, 148.9, 146.7, 146.2, 70.5, 69.2, 61.4, 60.9, 60.7, 58.8, 55.4, 31.7, 31.3, 29.4, 29.3, 29.1, 28.9, 25.9, 22.6, 14.4 ppm. Elemental analysis calcd (%) for $C_{37}H_{52}I_4N_4O_2$: C 40.68, H 4.80, N 5.13; found C 40.28, H 4.91, N 4.78.

[C_{10}bpy(C_4O)bpyC_3O][NTf_2]$_4$

The salt [C_{10}bpy(C_4O)bpyC_3O]I_4 (0.202 g, 0.19 mmol) was dissolved in methanol and Li[NTf_2] (0.250 g, 0.87 mmol) was slowly added and stirred during 1 day at room temperature. After this time, the solvent was removed and the product was recovered by extraction with water/ethyl acetate and dried in vacuum to give a brown gel (0.222 g, 71%). An additional step was performed to remove any halides salt by addition of acetone. T_g = 6.0 ºC. ^{1}H NMR (400.13 MHz, DMSO-d6, 25 ºC) δ = 9.47-9.27 (m, 8 H), 8.76 (d, J = 6.6Hz, 8 H), 4.97 – 4.60 (m, 8 H), 4.07 – 3.84 (m, 8 H), 3.29 (s, 3 H, overlapped with H_2O), 2.04 – 1.90 (m, 2H), 1.38 – 1.15 (m, 14 H), 0.91 – 0.81 (m, 3 H) ppm. ^{19}F NMR (376.50 MHz, DMSO-d6, 25 ºC) δ = -78.71 ppm. ^{13}C NMR (100.61 MHz, DMSO-d6, 25 ºC) δ = 149.6, 149.5, 149.4, 149.0, 146.7, 146.6, 146.2, 127.1, 126.9, 126.8, 124.7, 121.5, 118.3, 115.1, 70.5, 69.1, 61.5, 61.0, 60.8, 58.7, 31.7, 31.3, 29.3, 29.1, 28.9, 25.9, 22.5, 14.4 ppm. Elemental analysis calcd (%) $C_{45}H_{52}F_{24}N_8O_{18}S_8.3C_3H_6O$: C 34.51 H 3.75, N 5.96; found C 34.11, H 3.78, N 5.82.

<u>Synthesis of monomers: di-substituted-4,4'-bipyridinium salts</u>

1-decyl-1'-[4-vinylbenzyl]-4,4'-bipyridinium iodide chloride [C_{10} (BzV) bpy]ICl

To a solution of [(C_{10})bpy]I (0.527 g, 1.24 mmol) in acetonitrile was slowly added 4-vinylbenzly chloride (0.379 g, 2.48 mmol) with 2.5 wt % of hydroquinone. The solution was stirred at 70 ºC for ca. 48 hours and the product was recovered by filtration and washed with diethyl ether and dried to give a brown solid (0.609 g, 85 %). ^{1}H NMR (400.13 MHz, DMSO-d6, 25 ºC) δ = 9.53 (d, *J* = 6.1 Hz, 2 H), 9.38 (d, *J* = 6.0 Hz, 2 H), 8.76 (d, *J* = 9.5 Hz, J = 6.6 Hz, 4 H), 7.58 (dd, *J* = 8.2 Hz, J = 8.6 Hz, 4 H), 6.82 – 6.67 (m, 1 H), 6.00 – 5.82 (m, 3 H), 5.32 (d, J = 10.9 Hz, 1 H), 4.67 (t, J = 7.2 Hz, 2 H), 2.04 – 1.85 (m, 2 H), 1.42 – 1.14 (m, 14 H), 0.84 (t, J = 6.3 Hz, 3 H) ppm. ^{13}C NMR (100.61 MHz, DMSO-d6, 25 ºC) δ = 149.6, 149.1, 146.2, 138.8, 136.3, 134.1, 129.9, 127.6, 127.4, 127.2, 116.3, 63.5, 61.3, 31.7, 31.2, 29.4, 29.3, 29.1, 28.9, 25.9, 22.6, 14.4 ppm.

1-decyl-1'-[4-vinylbenzyl]-4,4'-bipyridinium di-[bistrifluoromethanesulfonyl]imide [C_{10}(VBz) bpy][NTf_2]$_2$

The salt [(VBzC_{10}bpy)] (0.451g, 0.78 mmol) previously prepared was dissolved in methanol and Li[NTf_2] (0.517 g, 1.80 mmol) was added. After addition, the reaction was stirred during ca. 27 hours at room temperature. The solvent was evaporated and the product was recovered by addition of dried acetone. Then, acetone was removed under vacuum to give a red solid (0.768 g, 100%). ^{1}H NMR (400.13 MHz, DMSO-d6, 25 ºC) δ = 9.50 (d, *J* = 6.1 Hz, 2 H), 9.37 (d, *J* = 6.0 Hz, 2 H), 8.81 – 8.70 (m, 4 H), 7.69 – 7.49 (m, 4 H), 6.82 – 6.71 (m, 1 H), 6.00 – 5.82 (m, 3 H), 5.34 (d, J = 10.9 Hz, 1 H), 4.68 (t, J = 7.3 Hz, 2 H), 2.04 – 1.85 (m, 2 H), 1.42 – 1.14 (m, 14 H), 0.86 (t, J = 6.4 Hz, 3 H) ppm. ^{19}F NMR (376.50 MHz, DMSO-d6, 25 ºC) δ = -78.70 ppm. ^{13}C NMR (100.61 MHz, DMSO-d6, 25 ºC) δ = 149.2, 148.6, 145.7, 138.3, 135.7, 133.5, 129.3, 127.1, 126.9, 126.7, 121.1, 117.9, 115.8, 63.2, 60.9, 31.2, 30.7, 30.7, 28.8, 28.8, 28.6, 28.4, 25.4, 22.1, 14.00 ppm.

1,1'-di-[4-vinylbenzyl]-4,4'-bipyridinium di-chloride [(VBz)$_2$bpy]Cl_2

To a solution of 4,4'-bipyridine (0.556 g, 3.56 mmol) in acetonitrile was slowly added 4-vinylbenzly chloride (2.383 g, 15.62 mmol) with 3.8 wt % of hydroquinone. The solution was stirred at 70 ºC for ca. 96 hours. The solid was filtered and washed with diethyl ether and dried to give a pale yellow solid (1.336 g, 81 %). ^{1}H NMR (400.13 MHz, DMSO-d6, 25 ºC) δ = 9.55 (d, *J* = 6.2 Hz, 4 H), 8.76 (d, *J* = 5.9 Hz, 4 H), 7.60 (q, J = 8.2 Hz, J = 9.7 Hz, 8 H), 6.81 – 6.70 (m, 2 H), 5.98 – 5.86 (m, 6 H), 5.34 (d, J = 10.9 Hz, 2 H) ppm. ^{13}C NMR (100.61 MHz, DMSO-d6, 25 ºC) δ = 149.6, 146.2, 138.8, 136.3, 134.1, 129.9, 127.7, 127.3, 116.3, 63.5 ppm.

1,1'-di-[4-vinylbenzyl]-4,4'-bipyridinium di-[bis(trifluoromethanesulfonyl)imide] [(VBz)$_2$bpy][NTf_2]$_2$

The salt [(VBz)$_2$bpy]Cl_2 (1.023 g, 2.22 mmol) previously prepared was dissolved in methanol and Li[NTf_2] (1.465 g, 5.10 mmol) was added. After addition, the reaction was stirred during ca. 72 hours at room temperature. The solvent was evaporated and the product was recovered by precipitation with water to give a yellow solid (1.950 g, 93 %). ^{1}H NMR (400.13 MHz, DMSO-d6, 25 ºC) δ = 9.48 (d, *J* = 6.4 Hz, 4H), 8.72 (d, *J* = 6.4 Hz, 4H), 7.73 – 7.54 (m, 8 H), 6.81 – 6.70 (m, 2 H), 5.95 – 5.86 (m, 6 H), 5.34 (d, J = 10.9 Hz, 2 H) ppm. ^{19}F NMR (376.50 MHz, DMSO-d6, 25 ºC) δ = -78.70 ppm. ^{13}C NMR (100.61 MHz, DMSO-d6, 25 ºC) δ = 149.2, 145.6, 138.3, 135.7, 133.4, 129.3, 127.2, 126.9, 121.3, 115.9, 63.4 ppm.

Synthesis of polymers

Poly(4-vinylbenzyl chloride) PVBz1

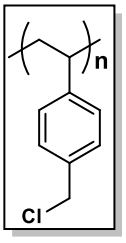

The monomer 4-vinylbenzyl chloride (1.19 g) was dissolved in DMF and the polymerization was carried out at 80 ºC with AIBN (1.3 mg) in nitrogen atmosphere, after nitrogen-vacuum cycles. After 24 hours, the polymerization was stopped by addition of a hydroquinone solution (MeOH). The polymer was recovered by addition of the reaction mixture into to the methanol solution. Then, the polymer was

filtered, dissolved in dichloromethane and added to methanol solution. After this purification step, the polymer was dried in vacuum to give a white solid (0.87 g, 72 %). ^{1}H NMR (400.13 MHz, $CDCl_3$, 25 ºC) δ = 7.17 – 6.76 (m, 2 H), 6.68 – 6.06 (m, 2 H), 4.66 – 4.21 (m, 2 H), 1.81 – 0.98 (m, 3 H) ppm.

Poly(4-vinyl benzyl iodide) PVBz2

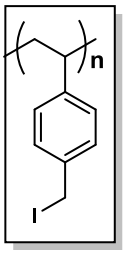

The polymer PVBz1 (0.308 g, 2.02 mmol) was dissolved in acetone and sodium iodide (0.843 g, 5.63 mmol) was added. The suspension was stirred at reflux during ca. 17 hours. The desired product was obtained as viscous a gel and washed with acetone. Additional purification step using chloroform has been performed in order to remove any sodium iodide. After, drying in vacuum the final product was obtained as yellow solid (0.416 g, 72 %). ^{1}H NMR (400.13 MHz, $CDCl_3$, 25 ºC) δ = 7.16 – 6.69 (m, 2 H), 6.67 – 5.99 (m, 2 H), 4.59 – 4.11 (m, 2H), 1.78 – 1.05 (m, 3H) ppm.

PVBz3

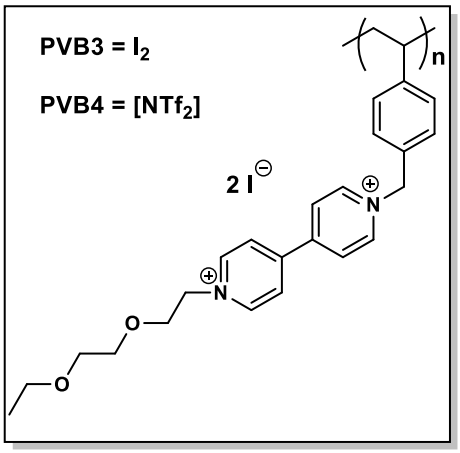

The polymer PVBz2 (0.304 g, 1.25 mmol) and $[C_5O_2bpy]I$ (0.434 g, 1.12 mmol) were dissolved in dimethylformamide and stirred at 100 ºC during 48 hours. The solvent was removed by distillation and the desired product was precipitated using acetone. Then, the desired product was dried in vacuum to give a brown solid (0.283 g, 40 %).

PVBz4

The polymer PVBz3 (0.163 g, 0.56 mmol) and $Li[NTf_2]$ (0.172 g, 0.60 mmol) were dissolved in dimethylformamide. The solution was stirred at 60 ºC during 7 hours and stirred at room temperature during 2 days. The desired product was precipitation with water. Then, the dried product was obtained as a pale brown solid (0.169 g, 70 %).

PVBz5

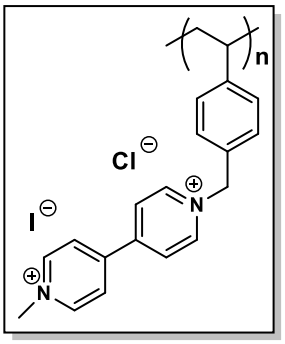

The polymer PVBz2 (0.210 g, 1.38 mmol) and $[C_1bpy]I$ (0.504 g, 1.69 mmol) were dissolved in dimethylformamide. The solution was stirred at 100 ºC during 4 hours and the product was recovered by precipitation using ethyl acetate. Then, the mixture was centrifugated in order to isolated the desired product. The final product was washed with methanol and dried in vacuum to give a brown solid.

PVBz6

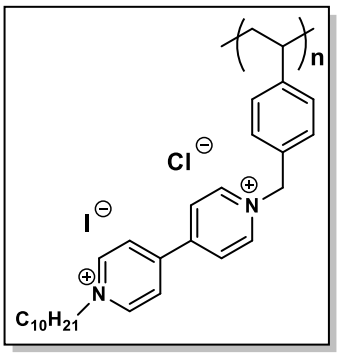

The polymer PVBz2 (0.153 g, 0.63 mmol) and [C_{10}bpy]I (0.357 g, 0.84 mmol) were dissolved in dimethylformamide. The solution was stirred at 100 ºC during ca. 3 days and the product was recovered by precipitation using water. Then, the mixture was centrifugated in order to isolated the desired product. The final product was dried in vacuum to give a brown solid (0.148 g, 35%).

Poly(diallyl dimethyl ammonium vanadate) PC1

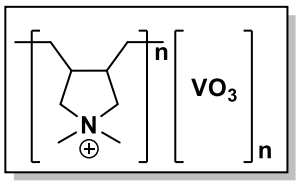

Ammonium vanadate (0.47 g, 4.00 mmol) was dissolved in hot water and aqueous solution of poly(diallyl dimethyl ammonium chloride) (20 wt % in water, 4.26 g, 26.40 mmol) was added. The solution was stirred at room temperature during 72 hours and an immiscible phase was formed. The immiscible phase was washed desired product was dried in vacuum to give a white solid (0.87 g, 66%).

Poly(diallyl dimethyl ammonium Co[EDTA]) PC2

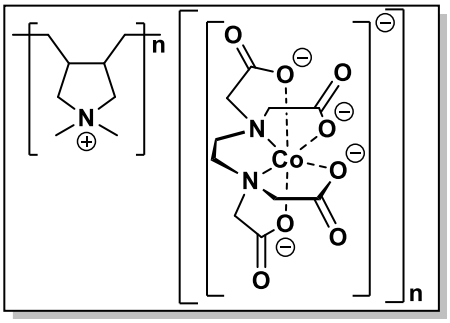

Sodium Co[EDTA] (0.40 g, 1.10 mmol) was dissolved in water and poly(diallyl dimethyl ammonium chloride (20 wt % in water, 1.25 g, 7.70 mmol) was added. The solution was stirred at 80 ºC during 27 hours. The solvent was removed and methanol was added. The desired product was recovered by centrifugation. Then the solvent was removed, dried in vacuum to give the desired product as pink solid (0.42 g, 82 %). Additional analysis shloud be required to check the proportion between cation and anion. ^{1}H NMR (400.13 MHz, D_2O, 25 ºC) δ = 3.95 – 3.58 (m, overlap of signals from anion and cation), 3.52 – 3.42 (m, 1H), 3.36 – 3.30 (m, 1H), 3.25 –2.95 (m, 6 H), 2.72 – 2.48 (m, 1 H), 2.26 – 2.05 (m, 1 H), 1.72 – 0.92 (m, 3 H).

PA1

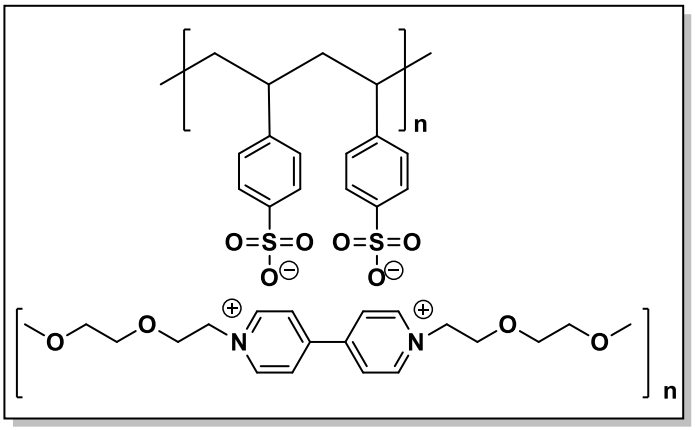

Silver nitrate (0.47 g, 2.50 mmol) was dissolved in water and poly(sodium 4-styrene sulfonate) (30 wt % in water, 1.74 g, 2.50 mmol) was added. The solution was stirred at room temperature during 24 hours. Then, acetone was added to precipitate the product, it was washed with acetone and dried in vacuum to give a pink solid (0.72 g, 97%). [(C_5O_2)bpy]I (0.36 g, 0.59 mmol) was dissolved in water and added to the aqueous

suspension containing the previous product (0.35 g, 1.20 mmol). The suspension was stirred at room temperature during 24 hours. The product was recovered by centrifugation and the solvent was removed. The desired product was dried to give an orange solid (0.37 g, 84 %).^{1}H NMR (400.13 MHz, D_2O, 25 ºC) δ = 8.93 (d, J = 6.3 Hz, 8H), 8.23 (d, J = 6.2 Hz, 8H), 7.80 – 7.16 (m, 4H), 6.92 – 5.84 (m, 4H), 4.86 – 4.73 (m, 4 H), 3.99 – 3.85 (m, 4H), 3.57 – 3.46 (m, 4H), 3.44 – 3.33 (m, 4H), 3.13, (s, 6 H), 2.13 – 0.69 (m, 6H) ppm.

3.6. References

1 R. J. Mortimer, A. L. Dyer and J. R. Reynolds, *Displays*, 2006, **27**, 2–18.

2 R. J. Mortimer and J. L. Dillingham, *J. Electrochem. Soc.,* 1997, **144**, 1549–1553.

3 R. N. Dominey, T. J. Lewis and M. S. Wrighton, *J. Phys. Chem.*, 1983, **87**, 5345–5354.

4 H. Akahoshi, S. Toshima and K. Itaya, *J. Phys. Chem.*, 1981, **85**, 818–822.

5 G. Bidan, A. Deronzier and J.-C. Moutet, *J. Chem. Soc., Chem. Commun.*, 1984, 1185–1186.

6 T. Komura, T. Yamaguchi, K. Furuta and K. Sirono, *J. Electroanal. Chem.*, 2002, **534**, 123–130.

7 J. Stepp and J. B. Schlenoff, *J. Electrochem. Soc.,* 1997, **144**, L155–L158.

8 P. M. S. Monk, R. J. Mortimer and D. R. Rosseinsky, *Electrochromism and Electrochromic Devices*, Cambridge University Press, Cambridge, 2007.

9 S. Deroo, U. Rauwald, C. V Robinson and O. A. Scherman, *Chem. Commun.*, 2009, 644–646.

10 D.-S. Guo, L.-H. Wang and Y. Liu, *J. Org. Chem.*, 2007, **72**, 7775–7778.

11 G. Casella, V. Causin, F. Rastrelli and G. Saielli, *Liq. Cryst.*, 2016, **43**, 1161–1173.

12 G. Casella, V. Causin, F. Rastrelli and G. Saielli, *Phys. Chem. Chem. Phys.*, 2014, **16**, 5048–5051.

13 S.-I. Imabayashi, N. Kitamura, S. Tazuke and K. Tokuda, *J. Electroanal. Chem. Interfacial Electrochem.*, 1988, **239**, 397–403.

14 M. Passon, A. Ruff, P. Schuler, B. Speiser and W. Leis, *J. Solid State Electrochem.*, 2015, **19**, 85–101.

15 J. Yuan, D. Mecerreyes and M. Antonietti, *Prog. Polym. Sci.*, 2013, **38**, 1009–1036.

16 D. Mecerreyes, *Prog. Polym. Sci.*, 2011, **36**, 1629–1648.

17 A. S. Shaplov, R. Marcilla and D. Mecerreyes, *Electrochim. Acta*, 2015, **175**, 18–34.

18 J. Yuan and M. Antonietti, *Polymer,* 2011, **52**, 1469–1482.

19 H. Ohno and K. Ito, *Chem. Lett.*, 1998, **27**, 751–752.

20 A. S. Shaplov, P. S. Vlasov, E. I. Lozinskaya, D. O. Ponkratov, I. A. Malyshkina, F. Vidal, O. V Okatova, G. M. Pavlov, C. Wandrey, A. Bhide, M. Schönhoff and Y. S. Vygodskii, *Macromolecules*, 2011, **44**, 9792–9803.

21 K. Ito, N. Nishina and H. Ohno, *Electrochim. Acta*, 2000, **45**, 1295–1298.

22 R. Marcilla, J. Alberto Blazquez, J. Rodriguez, J. A. Pomposo and D. Mecerreyes, *J. Polym. Sci. Part A Polym. Chem.*, 2004, **42**, 208–212.

23 M. Watanabe, S. Yamada and N. Ogata, *Electrochim. Acta*, 1995, **40**, 2285–2288.

24 N. Ogata, K. Sanui, M. Rikukawa, S. Yamada and M. Watanabe, *Synth. Met.*, 1995, **69**, 521–524.

25 R. Marcilla, F. Alcaide, H. Sardon, J. A. Pomposo, C. Pozo-Gonzalo and D. Mecerreyes, *Electrochem. Commun.*, 2006, **8**, 482–488.

26 C. Pozo-Gonzalo, D. Mecerreyes, J. A. Pomposo, M. Salsamendi, R. Marcilla, H. Grande, R. Vergaz, D. Barrios and J. M. Sánchez-Pena, *Sol. Energ. Mater. Sol. Cells*, 2008, **92**,

101–106.

27 C. Pozo-Gonzalo, M. Salsamendi, A. Viñuales, J. A. Pomposo and H.-J. Grande, *Sol. Energ. Mater. Sol. Cells*, 2009, **93**, 2093–2097.

28 A. S. Shaplov, D. O. Ponkratov, P.-H. Aubert, E. I. Lozinskaya, C. Plesse, F. Vidal and Y. S. Vygodskii, *Chem. Commun.*, 2014, **50**, 3191–3193.

29 A. S. Shaplov, D. O. Ponkratov, P.-H. Aubert, E. I. Lozinskaya, C. Plesse, A. Maziz, P. S. Vlasov, F. Vidal and Y. S. Vygodskii, *Polymer,* 2014, **55**, 3385–3396.

30 E. Dudognon, F. Danède, M. Descamps and N. T. Correia, *Pharm. Res.*, 2008, **25**, 2853–2858.

31 K. Binnemans, *Chem. Rev.*, 2005, **105**, 4148–4204.

32 E. Marotta, F. Rastrelli and G. Saielli, *J. Phys. Chem. B*, 2008, **112**, 16566–16574.

33 P. K. Bhowmik, H. Han, J. J. Cebe, R. A. Burchett, B. Acharya and S. Kumar, *Liq. Cryst.*, 2003, **30**, 1433–1440.

34 P. Bhowmik, H. Han, I. Nedeltchev and J. Cebe, *Mol. Cryst. Liq. Cryst.*, 2004, **419**, 27–46.

35 J. W. Nicholson, in *The Chemistry of Polymers (3)*, The Royal Society of Chemistry, 2006, pp. 1–22.

36 J. B. Schlenoff, D. Laurent, H. Ly and J. Stepp, *Adv. Mater.*, 1998, **10**, 347–349.

37 A. Reisch, M. D. Moussallem and J. B. Schlenoff, *Langmuir*, 2011, **27**, 9418–9424.

38 T. Inoue, A. Matsumoto and K. Nakamura, *Macromolecules*, 2013, **46**, 6104–6109.

39 T. K. Carlisle, W. M. McDanel, M. G. Cowan, R. D. Noble and D. L. Gin, *Chem. Mater.*, 2014, **26**, 1294–1296.

40 M. Döbbelin, I. Azcune, M. Bedu, A. Ruiz de Luzuriaga, A. Genua, V. Jovanovski, G. Cabañero and I. Odriozola, *Chem. Mater.*, 2012, **24**, 1583–1590.

41 Y. Tsou, H. Liu and A. J. Bard, *J. Electrochem. Soc.,* 1988, **135**, 1669–1675.

42 A. Branco, L. C. Branco and F. Pina, *Chem. Commun.*, 2011, **47**, 2300–2302.

43 *Synthesis of iron(III) EDTA complex, Na[Fe(EDTA].3H$_2$O (http://www.rsc.org/learn-chemistry)*, 2016.

4. Application of Electrochromic Salts in Devices

Publications associated with this chapter:

N. Jordão, L. Cabrita, F. Pina and L. C. Branco, *Chem. Eur. J.*, 2014, **20**, 3982–3988.

N. Jordão, H. Cruz, A. Branco, F. Pina and L. C. Branco, *ChemPlusChem*, 2015, **80**, 202–208.

N. Jordão, H. Cruz, A. Branco, C. Pinheiro, F. Pina and L. C. Branco, *RSC Adv.*, 2015, **5**, 27867–27873.

4. Application of Electrochromic Salts in Devices

4.1. Introduction

Electrochromic materials are a class of responsive materials that change colour as a result of redox process (oxidation or reduction) when an appropriate electric potential is applied [1]. In other words, electrochromic materials comprise electroactive species, which exhibits a colour change resulting from an electron-transfer process at electrode, it is entitled as electrochrome [2].

In 2001, Rosseinsky and Mortimer reported that *"electrochromic materials are currently attracting much interest in academia and industry for both their fascinating spectroelectrochemical properties and their commercial applications"* [2].

Some electrochromic materials can be integrated in devices, allowing the control of their transmission, reflection, absorption and emission properties [3]. These devices have been applied for antiglare car mirrors; sun-roofs of cars, smart windows (Figure 4.1) for use in cars, aircraft and buildings; electrochromic strips as battery state-of-charge indicators and electrochromic sunglasses [2,4,5]. Also, there are proposed applications, including devices for frozen-food monitoring, camouflage materials, among others [2,4].

Figure 4.1 – Switching sequence of a laminated electrochromic glass manufactured by Gesimat GmbH, Berlin (Germany). This electrochromic device uses tungsten oxide and Prussian blue as complementary electrochromic layers and ion-conducting poly(vinylbutyral) as polymer electrolyte [5–7]. (Source: www.gesimat.de, accessed in August of 2016).

The term "*smart windows*" was firstly introduced in 1984 by Svensson and Granqvist [8]. An example is illustrated in Figure 4.1, where some properties such as solar factor and the transmission of radiation in the solar spectrum can be changed according to control of the light intensity that passes through the windows. Thus, a reversible switching between transparent and blocking state, in response to an electric current or to the changing environmental conditions is also observed [5,9].

The development of smart windows could be an important application for economic and environmental point of views, once it can prevent solar radiation entering into the highly glazed buildings. As a consequence, a significant reduction of energy consumption of the building, for example for heating, ventilation and air conditioning processes can be achieved [5,9]. In 2002, Lee and DiBartolomeo reported that electrochromic windows "*may not be able to fulfil both energy-efficiency and visual comfort objectives when low winter direct sun is present*" [1,10]. However, they suggested that the windows and architectural design as well as the electrochromic control options could be used to broaden the applicability for commercial buildings [10].

The most successful commercial application of electrochromic materials in devices was developed by Gentex as anti-dazzle car mirrors and the adjustable-darkening windows of the Boeing Dreamliner aircraft (Figure 4.2) [11].

Figure 4.2 – Examples of commercial application of electrochromic materials in anti-dazzle car mirrors (upon) and adjustable-darkening windows of the Boeing Dreamliner aircraft manufactured by Gentex [12]. (Source: www.gentex.com, accessed in August of 2016).

For example, in the case of adjustable-darkening windows of the Boing Dreamliner aircraft, the windows of the passenger cabins switch from a bright (clear state) to an extreme dark state or to an intermediate level, through at the touch of a button [12].

There are a few companies such as Acreo®, Ynvisible® and Ntera® that use electrochromic materials as a component in the field of printed electronics, for example, as sensors and indicators incorporated in packages, matrix-addressed displays used for advertising purposes and electroluminescent lighting (see Figure 4.3)[13]. These printed electronics use functional inks printed in thin layers of paper and plastic as flexible materials.

Figure 4.3 – Examples of printed electronics of Acreo® and Ynvisible® (Sata Boarding Pass) [13,14]. (Source: www.acreo.se and www.ynvisible.com, accessed in August of 2016).

The generic sensor platform Acreo® uses electrically conductive materials as inks to print battery, sensor and displays that are integrated with a silicon chip [13]. In particular, the integrated biosensor platform from Acreo® exemplified in Figure 4.3 is integrated with glucose sensor to demonstrate

the possibilities of those platform. Ynvisible® developed a printed electronic boarding pass for *SATA* (Portuguese airline Company).

Electrochromic devices (ECD) are electrochemical cells composed by a minimum of two electrodes separated through an electrolyte, with high ionic conductivity [1,2]. An illustrative scheme of electrochromic device is presented in Scheme 4.1.

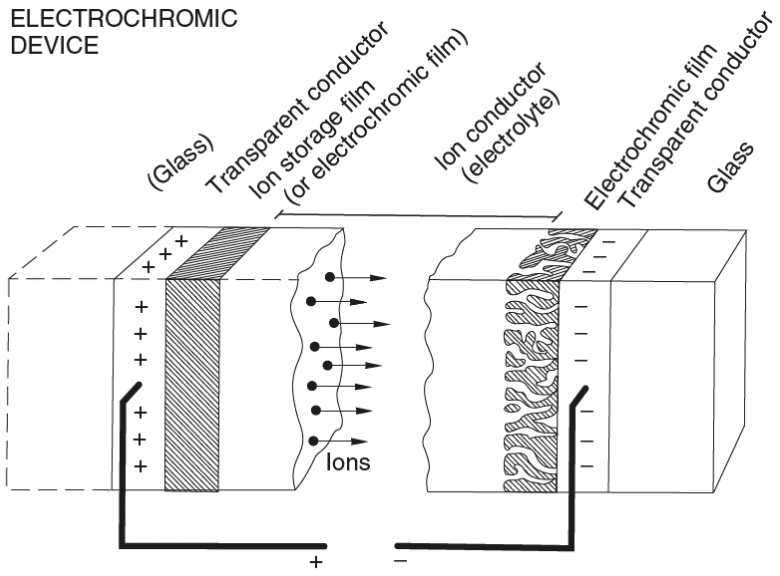

Scheme 4.1 – Example of electrochromic device, where arrows indicate the movement of ions in the selected applied potential [3]. (Source: C. G. Granqvist, in Electrochromic Materials and Devices, Wiley VCH, pp. 1–40).

This electrochromic device is built layer by layer and contains mainly three different types of layered materials: the electrolyte, the electrochromic films (or one ion storage film combined with an electrochromic film) and the transparent conductors (electrodes) [3]. The electrolyte providing only ionic not electronic conduction and separates the electrochromic films or separates one electrochromic film from an optically passive ion storage film [1–3]. The electrochromic films conduct both ions and electrons. Finally, the transparent conductors (electrodes) are working as pure electron conductors [3]. When adequate potential is applied, the electrons move into the electrochromic film(s) from the electrodes along with charge-balancing ions incoming from the electrolyte and consequently a colour change is observed due to redox reaction [3].

Mortimer and co-workers described that there are many types of chemical species that exhibit electrochromism but they emphasized that only those with favourable electrochromic performance parameters are potentially useful for commercial applications [15]. Thus, the electrochromic materials include their high contrast ratio, colouration efficiency, cycle life as well as write-erase efficiency [15]. However, some performance parameters are dependent of the application, for example displays require low response times, while smart windows can use response times of up to several minutes [15].

The contrast ratio (CR) quantifies the intensity change between the bleached and coloured states, or between two coloured states [16]. It is the luminance ratio of the brightest colour against

the darkest colour. This CR parameter is used to quantify the intensity of colour electrochemically formed, as seen by eye (Equation 4.1) [1].

$$CR = \left(\frac{R_0}{R_x}\right)$$

Equation 4.1

Where R_x is the intensity of light reflected diffusely thought the coloured state of an electrochromic material or device (ECD) and R_o is the intensity reflected from a non-shiny white card at a specific wavelength, usually at the wavelength of maximum absorbance (λ_{max}) of the coloured state. For electrochromic materials and EDCs that operating in transmission mode, the CR can be determined using the following equation (Equation 4.2) [16].

$$CR = \left(\frac{T_b}{T_c}\right)$$

Equation 4.2

Where, T_b and T_c is the transmittance in the bleach and coloured states, respectively. When CR values are used it is important to explain the details of the experimental conditions. Alternatively, the colour contrast can also be expressed as the change in absorbance (ΔA) or the percentage change in transmittance (ΔT %) between the bleach and coloured states [16].

Response time is defined as the required time for an electrochromic material or ECD to change from bleach to coloured state (or vice-versa) or between two distinct coloured states. In general, the response time of colouration is unlikely the same of the bleach process [16]. However, there is no consistency in the reporting and determination of response time in the literature. For example, response time may represent the time for some fraction of the colour (defined or arbitrary) in order to form or to bleach. Also, it can be related to the required time for an amount of charge (defined or arbitrary) to be consumed in forming or bleaching colour [1,16].

The write-erase efficiency is the fraction (or percentage) of the initially formed colouration that can be subsequently electro-bleached or vice-versa and must be around 100 % for a successful ECD [16]. For example, the write-erase efficiency of an ECD of aqueous methyl viologen (MV^{2+}) will always be low on a realistic time scale due to the slowness of diffusion to and from the electrode through solution. As already mentioned, this electrochrome is extremely soluble either its di-cationic and radical cation forms, as consequence the kinetic associated to diffusion process is considered complex [1].

The cycle life also commonly known as cycling, is defined as the number of write-erase cycles that can be performed by the electrochromic material or ECD, without any significant degradation. This parameter indicates the durability of the electrochromic material or ECD, the idea is obtaining the maximum of the cycle life as possible and 10^5 cycles is often stipulated as number minimum of cycle life [16]. Another important parameter is the colouration efficiency (CE), which represents the amount of colour formed or bleached by the charge consumed at specific wavelength, usually correspond to the maximum (λ_{max}) of the optical absorption band [16].

The colouration efficiency is described by the following equation:

$$\Delta A = (CE)\ Q$$

Equation 4.3

Where, ΔA is the absorbance change on passing a charge density of Q, i.e. inserted charge per unit of area. If absorbance is plotted in function of charge density, the colouration efficiency is given as the gradient. The ideal electrochromic material or EDC should exhibit higher absorbance change leading to a high colouration efficiency [16]. In general, the fails of the electrochromic device can be attributed to the degradation of conductive electrodes, electrolyte layer as well as electrochromes [1].

One of the most common classes of organic electrochromic materials is viologen, also classified as di-substituted-4,4'-bipyridinium salts. They undergo two successive electron-transfer processes and may exhibit three redox states: the di-cation, the radical cation and the neutral compound. Of these three redox states, it is known that di-cation is the most stable and colourless species, unless optical charge-transfer with the anion occurs. On the other hand, the radical cation is intensely coloured exhibiting high molar absorption coefficients related with an intense intramolecular optical charge-transfer. Therefore, the first reduction process (one electron-transfer process) of the di-cation leads to an intensely coloured radical cation, which it is considered paramagnetic viologen radical cation (Equation 4.4).

$$V^{2+} + e^{-} \rightarrow V^{+}$$

Equation 4.4

This reduction can be achieved electrochemically or chemically, through the application of the desired electrochemical potential or chemical reductant addition such as zinc dust or dithionite ion. The radical cation is particular stable and its colour persist in the absence of oxidising agents such as oxygen [17].

The colours of radical cations are depending on the substituents (type and length) on the *N*-position and their impact on the molecular orbital levels [1,18,19]. For example, alkyl groups can promote a blue-violet colour while aryl and other groups with electron-withdrawing substituents can lead to a green colour [1,18,19]. According to the selection of substituents at *N*-position of 4,4'-bipyridinium cation as well as the type of anion, the desired colour can be tuned. There is also reported in the literature that the colours of 4,4'-bipyridinium radical cation species are dependent of the concentration [20]. For example, in the case of 4,4'-bipyridinium salts with short alkyl chains, the radical cation achieves an intense blue colour in solution and becomes blue-purple by increasing of the concentration. Contrarily, radical cation of 4,4'-bipyridinium salt with long alkyl chains shows a crimson colour largely due to the contribution of dimerized radical cation, where the monomer of alkyl-substituted radical cation is blue and the respective dimer is red [20].

The electrolyte used to fabricate the gel and solid-state electrochromic devices, was provide us from Ynvisible® [21].

4.2. Liquid electrochromic devices

Firstly, all prepared di-alkyl-4,4'-bipyridinium salts were studied in solution in order to evaluate the electrochemical behaviour, particularly the first electron-transfer process. The most promising di-alkyl-4,4'-bipyridinium salts have been tested in liquid electrochromic device. In this sequence, the $[C_1C_{10}bpy][NTf_2]_2$ and $[C_2C_6bpy][NTf_2]_2$ salts were placed in a U-tube system for application as liquid electrochromic devices, previously reported by Photochemistry and Supramolecular Chemistry Group from FCT/UNL [22].

The $[C_1C_{10}bpy][NTf_2]_2$ was dissolved in acetonitrile (0.025 M) or RTIL $[EMIM][NTf_2]$ containing 34 wt % of acetonitrile (0.01 M). Whereas, the $[C_2C_6bpy][NTf_2]_2$ was dissolved in RTIL $[EMIM][NTf_2]$ (0.01 M), with 5 wt % of acetonitrile. In the acetonitrile pure system, the di-alkyl-4,4'-bipyridinium salt worked simultaneously as electrochrome and electrolyte. For the others cases, $[EMIM][NTf_2]$ acted as additional electrolyte. However, due to the viscosity of the system, acetonitrile was added in order to improve the diffusion of electroactive species in the electrochromic device. Two-sides of a U-tube were filled with the appropriate mixtures and platinum wires as working electrode placed at each side and connected to a commercial battery (potential > ± 0.5 V) (Figure 4.4).

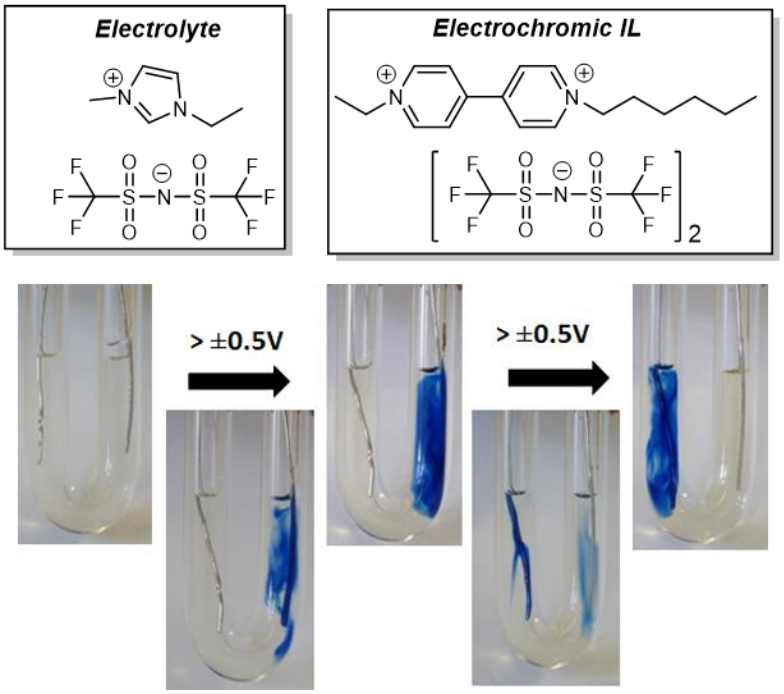

Figure 4.4 – A liquid electrochromic device containing $[C_2C_6bpy][NTf_2]_2$ in $[EMIM][NTf_2]$ (with 34 wt % CH_3CN) (0.01 M).

In this case, the liquid electrochromic device can reversibly switch between pale yellow to blue and vice-versa upon changing the signal of the applied potential. This blue colour can be attributed to the radical cation formation upon one electron-transfer process. Similar behaviour is also observed for the other cases and the colour switch of these three systems is present in Figure 4.5.

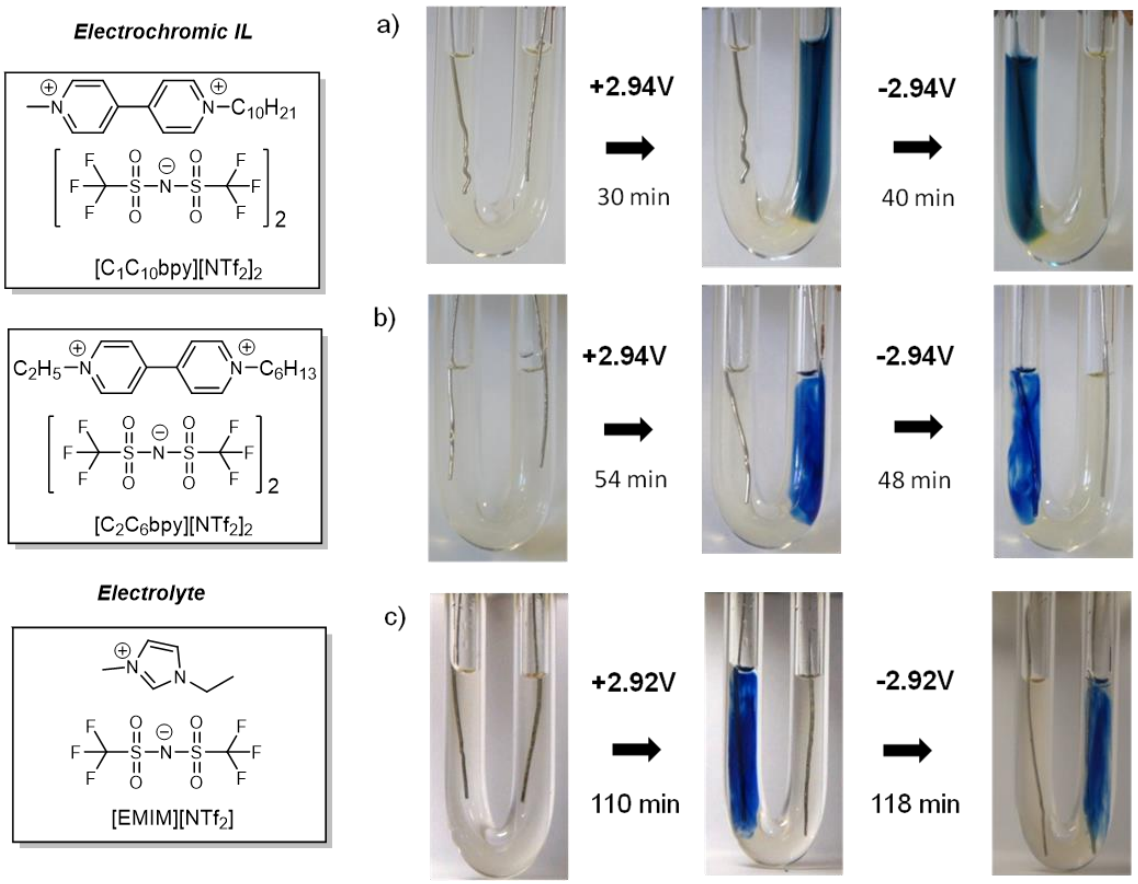

Figure 4.5 – A liquid electrochromic device containing: a) $[C_1C_{10}bpy][NTf_2]_2$ in dried ACN (0.025 M); b) $[C_2C_6bpy][NTf_2]_2$ in [EMIM][NTf_2] (0.01M) (with 34 wt % ACN); c) $[C_2C_6bpy][NTf_2]_2$ in [EMIM][NTf_2] (0.01M) (with 5 wt % ACN).

In general, all of these liquid electrochromic devices showed a reversible switch of colours that can be tuned by changing the viscosity of the media and the applied redox potential. In this context, $[C_1C_{10}bpy][NTf_2]_2$ in dried ACN as lower viscosity system showed the faster reversible redox process.

4.3. Gel electrochromic devices

The gel electrochromic devices are built using layer by layer protocols, where the electrochromic salt were dissolved in adequate electrolyte and the mixture were placed between two conductive layers, like PET-ITO (see Scheme 4.2). In this way, two PET-ITO layers are separated by a thickness of, approximately 0.23 mm spacer using a double sided adhesive tape. The conductive face of PET-ITO layer, possessing ca. 2 x 1.5 cm^2 as electroactive area was coated with di-substituted-4,4'-bipyridinium salt dissolved in adequate gel electrolyte. Finally, the devices were sealed with another PET-ITO layer, where the conductive face is in contact with the gel (composed by electrochromic material and the electrolyte). These symmetric electrochromic devices are easy to construct, once the electrochrome is incorporated in the gel electrolyte and no film deposition is required.

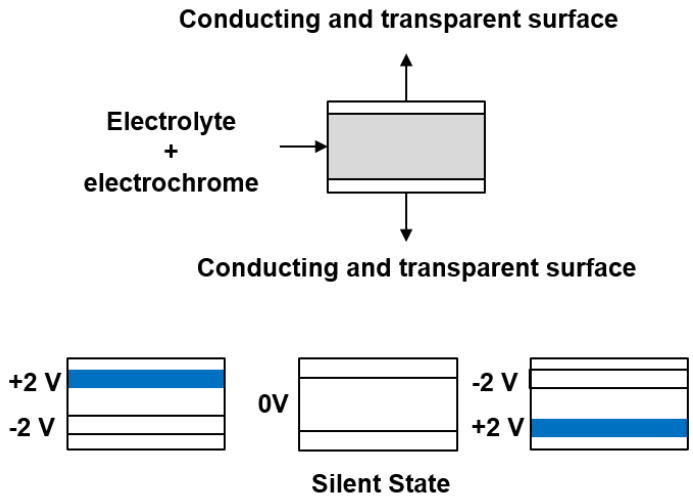

Scheme 4.2 – Symmetric electrochromic device with the electrochrome incorporated in the gel electrolyte. The oxidized form is transparent or pale yellow, while the reduced one is blue as occurring in many viologens.

These electrochromic devices are studied by cyclic voltammetry (CV) and a symmetrical response can be observed due to the fact the potential alternates between two identical electrodes, where one working as anode and the other as a cathode (Scheme 4.2). For example, when the potential of -2 V is applied in an electrochromic device containing an electrochromic probe, such as methyl viologen (MV), combined with a transparent electrolyte, the colour appears in both sides of the device. Reverting the potential from 0 to +2 V, the same behaviour is observed. The signal of the current depends on the face where reduction takes place in this specific case of viologen family. When the potential is reverted, the process occurs in the other face and the signal is opposite independently if it is an anodic or cathodic current.

However, it is possible to make the electrolyte opaque and white by addition of a specific pigment such as titanium or zinc dioxide. This addition can facilitate to understand the working of the device and allow us to visualize the switch of colours in both sides of the device (no colour mixture between oxidize and reduced side). Considering the same example, if the potential of – 2 V is applied to the device, the colour changes is more visible in the cathode, which become more coloured and the anode become slightly coloured. When the potential is from 0 to + 2 V, identical behaviour is observed, but now in the other face of the device. At 0 V a state equivalent to the open circuit is reached, which is designed by silent state.

4.3.1. Di-substituted 4,4'-bipyridinium salts

The most promising symmetric and non-symmetric di-substituted-4,4'-bipyridinium salts, including iodide or bromide salts, for the assembly of electrochromic devices were studied.

In particular, the di-iodide and di-bromide salts, $[(C_{10})_2bpy]I_2$, $[(C_5O_2)_2bpy]I_2$ and $[(allyl)_2bpy]Br_2$ were tested in electrochromic devices. In the case of $[(C_{10})_2bpy]I_2$ the cyclic voltammetry as well as the switch of colours associated to different redox states is illustrate in Figure 4.6. It is observed two switches of colours between yellow to blue, corresponding to the radical cation formation and blue to red, which can be explained by dimer formation. It is already described the possible

dimerization of viologen radical cations (spin-pair) in aqueous solutions leading a colour change between blue (monomer) and red (dimer) [17,19,23–25]. Monk and co-workers (1992) reported that the immediate product of the 4,4'-bipyridinium comproportionation reaction is a spin-paired radical cation dimer [17]. The following equation described the formation of the dimer from radical cation species (Equation 4.5).

$$2\,V^{+\bullet} = V_2^{2+}$$

Equation 4.5

The dimer is diamagnetic species since opposing spins are paired and the usual configuration stated for the dimer is a sandwich-type structure, with the two bipyridinium planes lying parallel and face-to-face [17]. Often the presence of both monomer and dimer radical cations species can be observed by UV-Vis spectroscopy, once the dimer presents some different spectral properties comparing to monomer [17,19,23–25]. It is also reported that the electro-oxidation of the radical cation dimer is not very fast and the bleaching of the coloured state is delayed with a negative impact on its switching time [19,23]. The radical cation dimer/ di-cation redox couple is known to be *quasi reversible* [25]. However, it reported that dimerization is particularly prevalent for viologens in aqueous solution and at low temperatures in non-aqueous solutions [17,19,23–25].

The cyclic voltammetry of the electrochromic device containing $[(C_{10})_2bpy]I_2$ and the respective colour switches are illustrated in Figure 4.6.

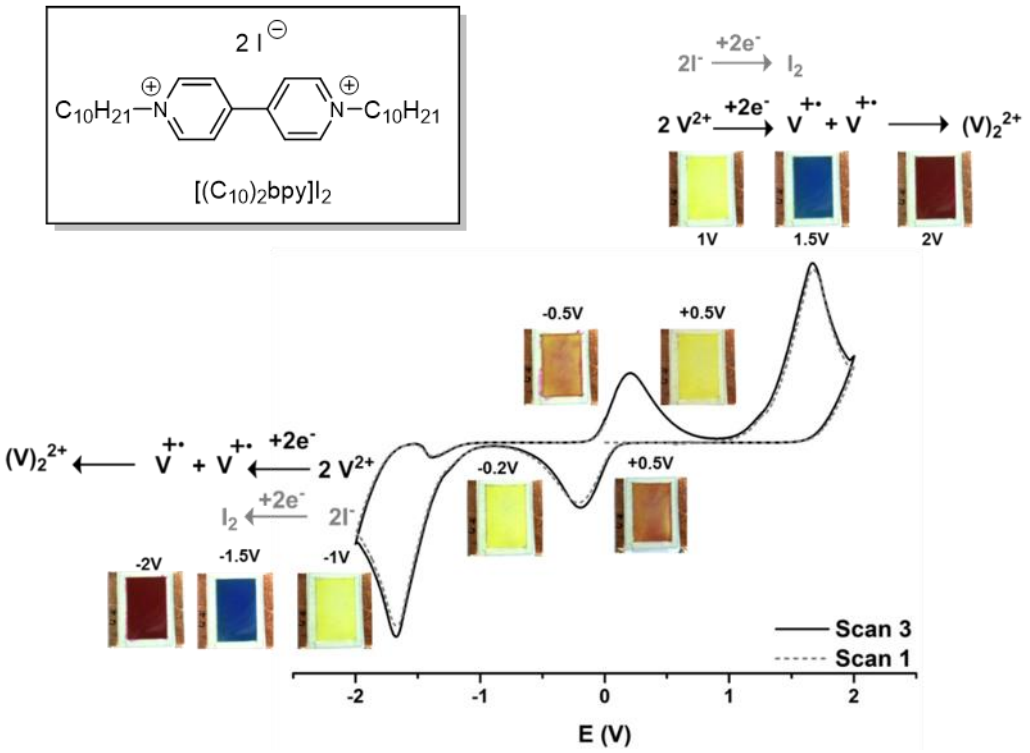

Figure 4.6 – Voltammogram of $[(C_{10})_2bpy]I_2$ in electrochromic device with respective switch of colours at scan range between 0/+2/-2/0 at 0.2 Vs^{-1}.

Starting the cyclic voltammetry in the direct anodic scan (from 0 to +2 V) no response is observed until ca. + 1.5 V (1st cycle), where the blue colour starts to appear. This process can be attributed to the first electron-transfer of di-substituted-4,4'-bipyridinium salts, the electrogenerated radical

cation. Then, after reach + 2 V the red dimer is clearly observed and seems to be thermally formed. Once when the potential is hold at + 1.5 V, electrolysis at a controlled potential, the dimer appears slowly. In the reverse anodic back scan (+2 to 0 V) the oxidation occurs firstly for the radical cation, followed by the dimer (after *ca.* + 0.5 V) corresponding to the change back to di-cationic species (V^{2+}), accompanied by a change of colour back to yellow (initial colour, V^{2+}). Identical behaviour takes place in the other face of the device, due to its symmetry. This redox process seems to be fully reversible during three cycles as observed in Figure 4.6.

Indeed, Monk and co-workers studied spin pairing (dimerization) of the viologen radical cation in aqueous solution [17]. They concluded that the kinetic data showed that the rate-limiting reaction during radical dimerization occurs between an anion and a radical cation monomer to form an association pair. They also suggested that the dimerization process is two-step mechanism: firstly, a radical cation monomer associates slowly with an anion (Equation 4.6).

$$V^{+\bullet} + X^{-} \rightarrow V^{+\bullet}X^{-}$$

Equation 4.6

Then, a spin-pairing reaction (Equation 4.7) occurs and it is faster than the previous one.

$$2\,V^{+\bullet}X^{-} \rightarrow (V)_2^{2+}\,2\,X^{-}$$

Equation 4.7

However, it is possible that spin-pairing reaction could proceed with only one of the radicals existing as an ion-paired monomer and the other can be free (Equation 4.8) [17].

$$V^{+\bullet} + \ V^{+\bullet}X^{-} \rightarrow (V)_2^{2+}\,2\,X^{-}$$

Equation 4.8

During the comproportionation reaction, it is expected a dimer having an anion (X) placed between the two viologen units $(V\text{-}X\text{-}V)^{2+}$, once viologen di-cations are quite electron poor and readily form charge-transfer complexes [17].

In our case, the oxidation of the dimer can be more difficult than the one of the radical cation. This behaviour can be explained considering that the dimer is stabilised by the covalent bond involving the two unpaired electron (Scheme 4.3).

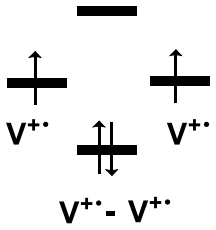

Scheme 4.3 – Representation of the molecular orbital diagram for the viologen dimer ($V^{+\bullet}$ - $V^{+\bullet}$) from the radical cations ($V^{+\bullet}$).

A possible kinetic approach for the oxidation process for this system is shown in Scheme 4.4.

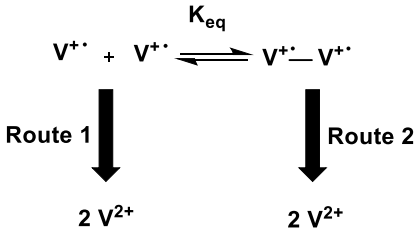

Scheme 4.4 – Kinetic representation of the possible oxidation process that occurs in the device containing $[(C_{10})_2bpy]I_2$.

During the oxidation process, route 1, which correspond to the radical cation oxidation process, occurs before route 2 that is relate to the dimer oxidation process. As consequence, the blue colour disappears before the red. This red colour only vanishes when a sufficiently high potential, to oxidize the dimer, is reached. The proposed oxidation process in the device can be possible if the dimer equilibrium process is slower than route 1 and 2, which it is a reasonable assumption in gel state.

In the case of $[(C_5O_2)bpy]I_2$ a similar behaviour relative to the previous one is observed (see Figure 4.7). A complete reversible electrochromic behaviour and a switch of colours between yellow to blue, formation of radical cation ($V^{+\bullet}$) and from blue to violet, which can be attributed to the dimer formation ($V^{+\bullet}$ - $V^{+\bullet}$), is detected.

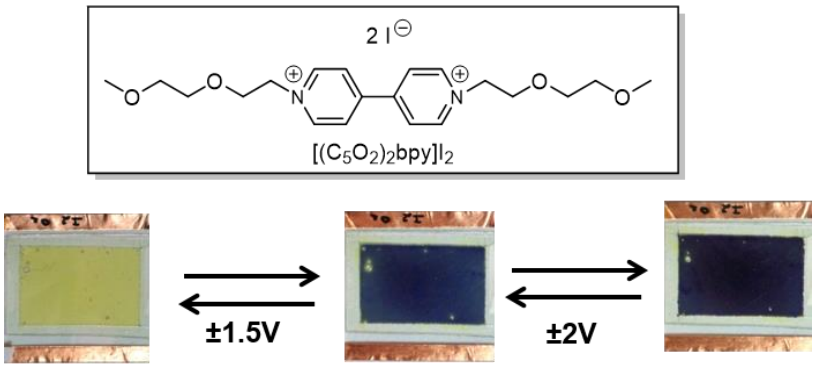

Figure 4.7 – Electrochromic device containing the electrochromic 4,4'-bipyridinium salt $[(C_5O_2)bpy]I_2$ in gel electrolyte (0.07 M) between two PET-ITO layers.

Starting from initial state (V^{2+}, yellow colour, 0 V) and applying +1.5 V, the blue colour appears, due to the formation of the radical cation, followed, possibly the formation of the dimer ($V^{+\bullet}$ - $V^{+\bullet}$, violet colour, +2 V). When the current is reversed the colour changes back to blue by oxidation of the radical cation. As reported in the literature, dissociation of the dimer species produces the characteristic colour of the radical cation monomer [25]. At 0 V the colour returns to the original state (V^{2+}, yellow colour) by oxidation of the dimer. This electrochromic device was studied by cyclic voltammetry and the system is fully reversible during three cycles.

Other example of symmetric di-substituted-4,4'-bipyridinium salts studied is $[(allyl)_2bpy]Br_2$. In this case, a switch of colour between transparent to slight blue and then, from slight blue to an intense blue is observed (Figure 4.8).

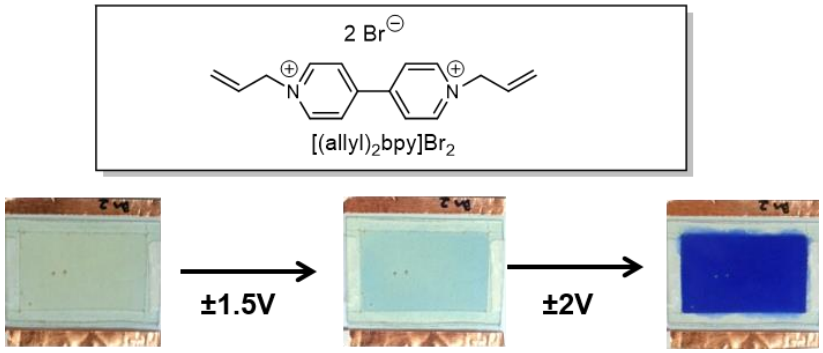

Figure 4.8 – Electrochromic device containing the electrochromic 4,4'-bipyridinium salt $[(allyl)_2bpy]Br_2$. in gel electrolyte (0.07 M) between two PET-ITO layers.

When started from 0 to 1.5 V, a pale blue colour appears, which can be explained by the radical cation formation. After this reduction, an intense blue colour is observed probably due to the dimer formation. During the cyclic voltammetry studies it was observed that the oxidation of dimer is not complete and some dimer remained in the device, giving a blue colour. It is also observed that the device became darker upon a new cycle, maybe due to the formation of the more dimer, i.e. accumulation of dimer on the device. The device was submitted a five redox cycles and only after five days in open circuit that recovered the initial colour. This redox process seems to be not complete reversible, once the fully oxidation of the dimer only occurs in open circuit (thermally).
Interestingly, Monk and co-workers reported that in aqueous solution of radical cation were blue-purple for small alkyl chain, while more reddish is observed to longer alkyl chain. It means that the dimerization process increase with the length of the alkyl chain [17].

The most interesting 4,4'-bipyridinium based on $[NTf_2]$ salts are also tested in symmetric electrochromic device, as illustrated in Figure 4.9.
These electrochromic devices are completely reversible between pale yellow and blue in short periods of time upon application of redox potential cycles of -2 to 0 V, except in the case of $[(allyl)_2bpy][NTf_2]_2$.In the case of $[(allyl)_2bpy][NTf_2]_2$ the colour change from transparent to slightly blue and the systems seem to be not complete reversible, similar to the $[(allyl)_2bpy]Br_2$. It is also observed that the fully oxidation of the dimer only occurs in open circuit, leading to the initial colour of the device (pale yellow).
The appearance of the blue colour can be attributed to the formation of the radical cation. When the potential is increased to + 2 V, the blue colour became more intense, possibly due to an increase on radical cation concentration. Besides that, the radical cation concentration increases with the increase on the number of cycles and allowing the dimerization process. In the cyclic voltammetry studies on the 3rd cycle an oxidation peak (*ca.* 0 V) appears, which can be attributed to the oxidation of the dimer.

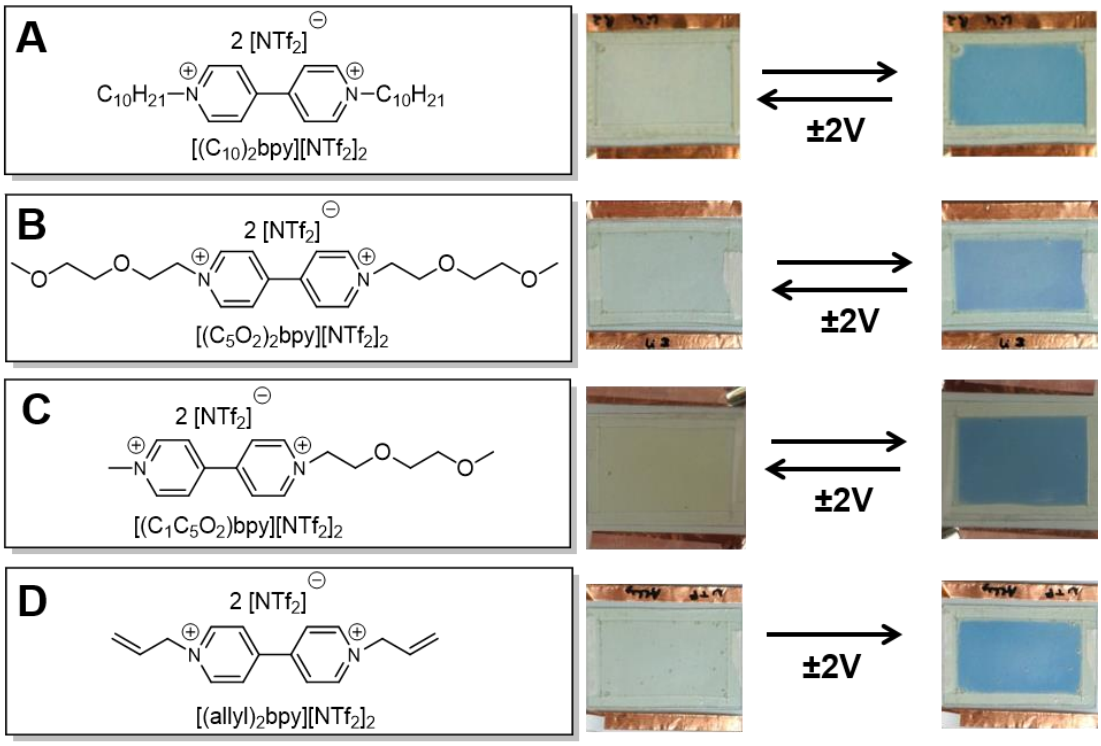

Figure 4.9 – Electrochromic device containing the electrochromic di-substituted-4,4'-bipyridinium salt (a) $[(C_{10})_2bpy][NTf_2]_2$, (b) $[(C_5O_2)_2bpy)][NTf_2]_2$, (c) $[C_1C_5O_2bpy][NTf_2]_2$, (d) $[(allyl)_2bpy][NTf_2]_2$ in gel electrolyte (0.06 – 0.07 M) between two PET-ITO layers.

Monk and co-workers reported also the anion effect in the dimer formation, also known as comproportionation reaction [17]. They explained when the anion (X) incorporated on the dimer (two viologen planes parallel) were smaller such as chloride, allows to two radical planes to get closer leading to a sufficiently large overlap to provide the observed dimer stability and hence the colour of dimer. Whereas, if the anion is large, such as $[Fe(CN)_6]^{4-}$, the two viologen radicals are too far apart for the viologen orbitals to overlap, as required for spin pairing. In this case, when a dimer species incorporating this anion is formed, it must either dissociate immediately, as consequence the only colour observed is from the radical monomer or have radical cation planes positioned sufficiently far apart that no spin pairing is possible [17]. They also explained the absence of comproportionation reaction, where two monomer species approach and orbital overlap occurs without anion incorporation between the two radical cation ($V^{+\bullet}$) units. The expected coulombic repulsion between the two radical cations units will be greater, as well as the spin pairing energy because they will be closer without an intercalated anion.

Electrochromic performance

The electrochromic performance of some of these devices was studied through the following parameters: colour coordinates, chromatic contrast, colouration efficiency and stability.

The colour space coordinates (L*a*b*) of each electrochromic device was determined by spectroelectrochemistry studies. In general, CIE ("*Commission Internationale de l'éclairage*") L*a*b represents colours by using the coordinates in a uniform colour space and is defined by lightness variable (*L*) and chromaticity indices *a** and *b** (Figure 4.10).

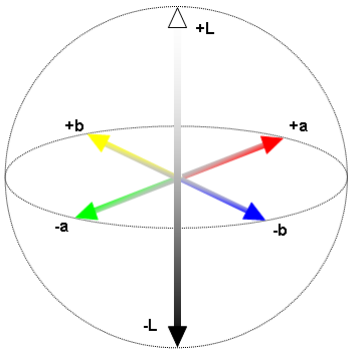

Figure 4.10 – Representation of CIE Lab coordinates [26].

The *L* variable represent the lightness of the colour and if L* = 0 has no lightness (absolute black) and L* = 100 indicates maximum lightness (absolute white). The chromaticity indices a* represents the red/green coordinate and at one extremity is red (+a), whereas at the other is green (-a). While the chromaticity indices b* represents the yellow/blue coordinate. The b* axis has blue at one extremity (-b) and yellow at the other (+b) [27].

The CIE L*a*b coordinates can be determined through absorption or transmittance spectra or from an image using adequate software program, such as *Matlab* and a Colour Checker as calibrate. From the absorption spectra obtained in the visible range (400 to 700 nm) it is possible calculate the colour coordinates using the Standard Iluminant CIE D65, which simulates daylight and calculating the trichromatic individual coordinates, tristimulus values, (X, Y, Z) [28,29] (Equation 4.9).

$$X = \sum E_i x_i T_i$$

Equation 4.9

Where, E_i is the coefficient of the Standard Illuminat CIE, x_i is the coefficient of the tristimulus value and T_i is the optical transmittance all for a given wavelength λ_i. Similar calculations have been done for Y and Z coordinates by adjustment of Equation 4.9. Then, X, Y and Z values can then be converted to L*a*b* colour coordinates [1,28,29] (Equation 4.10, Equation 4.11 and Equation 4.12).

$$L^* = 116 \left(\frac{Y}{Y_n}\right)^{1/3} - 16$$

Equation 4.10

$$a^* = 500 \left[\left(\frac{X}{X_n}\right)^{1/3} - \left(\frac{Y}{Y_n}\right)^{1/3}\right]$$

Equation 4.11

$$b^* = 200 \left[\left(\frac{Y}{Y_n}\right)^{1/3} - \left(\frac{Z}{Z_n}\right)^{1/3}\right]$$

Equation 4.12

Where X_n, Y_n and Z_n are the tristimulus values of a perfect transmitting diffuser, calculated from the background measurement using the same illuminat. These equations are valid as long as the quotients X/X_n, Y/Y_n and Z/Z_n are greater than 0.0008856 [28,29].

In this case, all colour space coordinates were determined using spectroelectrochemistry studies between 0 to +2.0 V and 0 to -2.0 V. The CIE L*a*b coordinates for $[(C_{10})_2bpy]I_2$, $[(C_{10})_2bpy][NTf_2]_2$, $[(C_5O_2)_2bpy]I_2$ and $[(C_5O_2)_2bpy][NTf_2]_2$ are presented in Table 4.1.

Table 4.1 – Colour space coordinates (CIE L*a*b*) of the devices [a].

Salts	E_{app} (V)	L*	*a	*b
$[(C_{10})_2bpy]I_2$	0	86.4	-7.9	18.7
	-1.4	69.9	-10.5	-0.6
	-1.8	22.1	38.6	-4.5
$[(C_{10})_2bpy][NTf_2]_2$	0	90.7	-3.0	5.5
	-2	73.0	-6.7	-17.5
$[(C_5O_2)_2bpy]I_2$	0	90.4	-9.2	30.3
	-1.4	44.3	20.2	-4.4
	-2	2.5	30.7	-6.8
$[(C_5O_2)_2bpy][NTf_2]_2$	0	90.1	-2.8	4.7
	-2	44.0	23.0	-35.9

[a] E_{app}: Applied Electrical Potential (in volts); L: represents lightness; a: positive values indicate amounts of red while negative values indicate amounts of green; b: yellow is positive and blue is negative.

The RGB colour space was also determined based on CIE L*a*b coordinates using adequate software program. The RGB colours obtained for the different prepared devices are demonstrated in Figure 4.11.

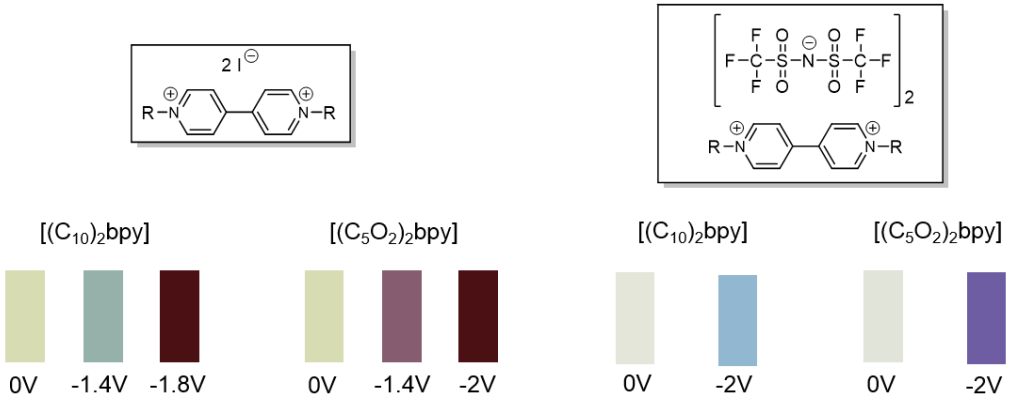

Figure 4.11 – RGB colour space determined by spectroelectrochemistry studies for different electrochromic devices.

In general, the RGB colours obtained from the electrochemistry studies are similar to those observed in previous photography images of the devices.

The chromatic contrast (ΔT, %), transition times between the bleached and coloured states, the colouration efficiency (CE) are determined through spectroelectrochemical studies for $[(C_{10})_2bpy]I_2$, $[(C_{10})bpy][NTf_2]_2$, $[(C_5O_2)_2bpy]I_2$ and $[(C_5O_2)_2bpy][NTf_2]_2$ (Table 4.2).

In general, the introduction of oxygen in the bipyridinium cation scaffold ($[(C_5O_2)_2bpy]$) seems to reduce transmittance contrasts and colouration efficiencies of the devices. The di-iodide salts showed faster transition times between the bleached and coloured states then the correspondent

[NTf_2] salts. The higher colouration efficiency is observed in the case of [$(C_{10})_2$bpy][NTf_2]$_2$, which present 186.9 $cm^2.C^{-1}$ (605 nm).

Table 4.2 – Chromatic contrast, transition time and colouration efficiency of the devices [a].

Salts	E_{app} (V)	ΔT (%)	t_{90} [t_{70}] (s)	CE ($cm^2.C^{-1}$) [λ, nm]
[$(C_{10})_2$bpy]I_2	1.8	72.7	13 [7]	102.6 [550]
	1.4	45.3	53 [33]	45.9 [605]
[$(C_{10})_2$bpy][NTf_2]$_2$	2	66.9	109 [46]	186.9 [605]
[$(C_5O_2)_2$bpy]I_2	1.8	71.3	10 [5]	100.5 [521]
[$(C_5O_2)_2$bpy][NTf_2]$_2$	2	51.1	93 [37]	95.3 [605]

[a] E_{app}: applied electrical potential (in volts); ΔT: transmittance contrast; t_{90} or t_{70}: time taken for the transmittance change by 90 or 70% of the total difference between the bleached and coloured states (in seconds); CE: colouration efficiency (in $cm^2.C^{-1}$); λ: wavelength of reduced coloured species (in nanometers).

There are examples of electrochromic devices based on 4,4'-bipyridinium salts reported in the literature, which present similar colouration efficiency. For example, electrochromic devices based on methyl viologen is reported with 176 $cm^2.C^{-1}$ (604 nm) [1]. Ho and co-workers reported an electrochromic device (ECD) based on poly(butyl viologen) (PBV) and Prussian blue (PB) confined to the electrode surfaces [30]. This EDC contains a solid-state electrolyte, which is prepared by adding lithium tetrafluoroborate to succinonitrile. The electrochromic device showed good optical contrast with a colouration efficiency of ca. 163 $cm^2.C^{-1}$ (650 nm). The transmittance of the ECD at 650 nm changed from 73% (bleached) to 8% (darkened), with an applied potential of 1.7 V across the two electrodes. Fitzmaurice and co-workers reported the construction of an electrochromic window based on a modified transparent nanostructured metal oxide film (TiO_2) supported on conducting glass [31]. This nanostructured TiO_2 film is modified by adsorption of a monolayer of the redox chromophore bis-(2-phosphonoethyl)-4,4-bipyridinium di-chloride, the electrolyte is 0.05 M $LiClO_4$ and 0.05 M ferrocene in γ-butylrolactone. The authors reported 170 $cm^2.C^{-1}$ (608 nm) as colouration efficiency of this device. Other example is reported by Pozo-Gonzalo and co-workers [32]. They described two materials based on viologen (1,1'-di-ethyl-4,4'-bipyridinium di-perchlorate and 1,1'-di-octadecyl-4,4'-bipyridinium di-perchlorate) where the maximum transparency of the device was 80% in the bleach state and a colouration efficiency (CE) of 136.6 $cm^2.C^{-1}$.

Preliminary on/off cycling studies for the [$(C_{10})_2$bpy]I_2 and [$(C_5O_2)_2$bpy][NTf_2]$_2$ have been performed in order to evaluate the stability of these devices (Figure 4.12). These studies consist in on/off cycling by alternating between the bleach and coloured states of the devices and the absorbance change is measured at a specific wavelength. The associated degradation is determined by the difference between the colour contrast in the first cycle and after a specific number of cycles.

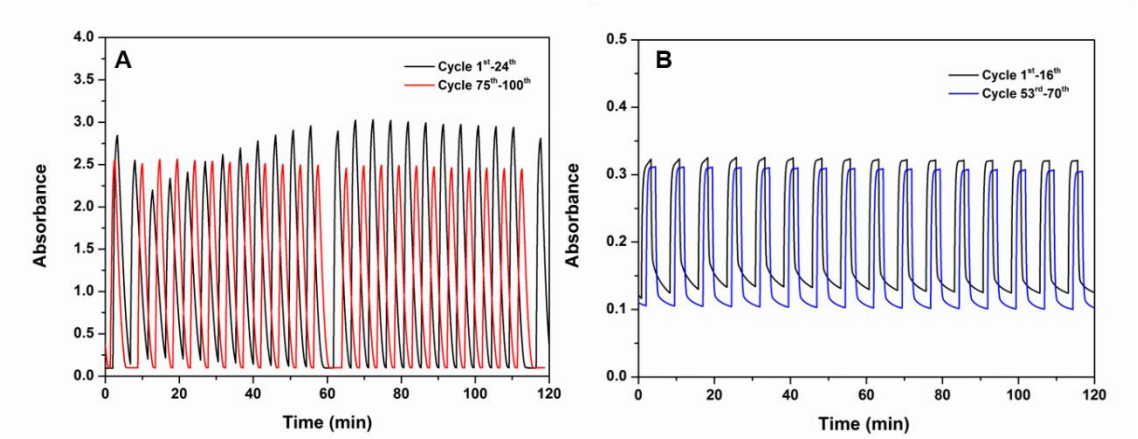

Figure 4.12 – Preliminary on/ off cycling studies of: (a) $[(C_{10})_2bpy]I_2$ by alternating the potential between 1.8 V/0V and monitoring the absorbance at 550 nm (~ 100 cycles), (b) by alternating the potential between 2 V/0V and monitoring the absorbance at 605 nm (~ 70 cycles).

In the case of iodide salt, these preliminary studies indicate us a modest stability performance, with around 20 % of decrease in the absorbance value between 1st and 100th cycles. Whereas, in the case of $[NTf_2]$ salt showed a good cycling stability during 70 cycles performed.

4.3.2. Tetra-substituted-4,4'-bipyridinium salts

All tetra-substituted-4,4'-bipyridinium salts have been dissolved into gel electrolyte and the respective electrochromic device was built as previously explained. These devices are studied by cyclic voltammetry and their electrochromic performance was evaluated.

Electrochromic performance

The electrochromic performance of these devices was studied through the following parameters: colour coordinates, chromatic contrast, colouration efficiency and stability.

The colour space coordinates (L*a*b*) of each electrochromic device was determined by spectroelectrochemistry studies. The CIE L*a*b coordinates were determined for each device as indicated in Table 4.3.

Table 4.3 – Colour space coordinates (CIE L*a*b*) of the devices [a].

Salts	Initial			E_{app} (-2 V)		
	L*	a*	b*	L*	a*	b*
$[(C_{10})bpy(C_4O)bpy(C_{10})]I_4$	90.2	-10.3	29.6	33.4	41.8	-19.4
$[(C_{10})bpy(C_4O)bpy(C_{10})][NTf_2]_4$	92.0	-3.6	7.8	27.5	57.6	-49.6
$[(C_3O)bpy(C_4O)bpy(C_3O)]I_4$	90.5	-4.4	10.1	34.5	46.3	-27.2
$[(C_3O)bpy(C_4O)bpy(C_3O)][NTf_2]_4$	91.4	-3.0	4.3	65.1	14.9	-26.1
$[(C_3O)bpy(C_8O_3)bpy(C_3O)]I_4$	90.7	-4.0	11.1	36.7	39.5	14.2
$[(C_3O)bpy(C_8O_3)bpy(C_3O)][NTf_2]_4$	90.1	-2.9	4.7	60.7	23.5	-16.9
$[(C_{10})bpy(C_4O)bpy(C_3O)]I_4$	78.3	-3.4	51.5	30.7	36.8	6.3

[a] E_{app}: Applied Electrical Potential (in volts); L: represents lightness; a: positive values indicate amounts of red while negative values indicate amounts of green; b: yellow is positive and blue is negative.

The RGB colour space was also determined based on CIE L*a*b coordinates using adequate software program. The RGB colours obtained for the different prepared devices are demonstrated in Figure 4.13 .

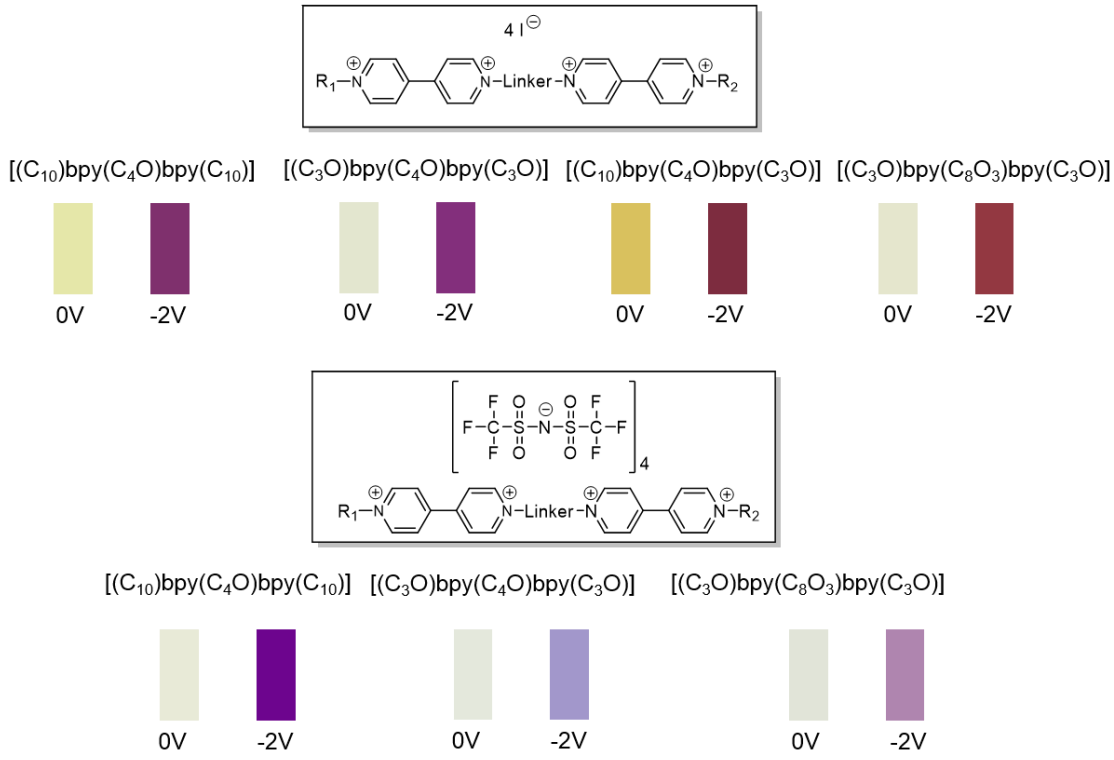

Figure 4.13 – RGB colour space obtained through spectroelectrochemistry studies for electrochromic devices based on tetra-substituted 4,4'-bipyridinium salts.

In general, all RGB colours spaces are similar to the obtained previously for di-substituted 4,4'-bipyridinium salts.

The chromatic contrast (ΔT, %), transition times between the bleached and coloured states, the colouration efficiency (CE) are determined through spectroelectrochemical studies. These values are compared to the previous di-substituted-4,4'-bipyridinium salts: $[(C_{10})_2bpy]I_2$, $[(C_{10})_2bpy][NTf_2]_2$, $[(C_5O_2)_2bpy]I_2$ and $[(C_5O_2)_2bpy][NTf_2]_2$ (Table 4.4).

Table 4.4 – Chromatic contrast, transition time and colouration efficiency of the devices [a].

Salts	E_{app} (V)	ΔT (%)	t_{90} [t_{70}] (s)	CE ($cm^2.C^{-1}$) [λ, nm]
$[(C_{10})bpy(C_4O)bpy(C_{10})]I_4$	-2.0	97.8	22 [8]	81.4 [540]
$[(C_{10})bpy(C_4O)bpy(C_{10})][NTf_2]_4$	-2.0	97.0	39 [14]	105.2 [550]
$[(C_3O)bpy(C_4O)bpy(C_3O)]I_4$	-1.7	90.6	24 [10]	80.6 [545]
$[(C_3O)bpy(C_8O_3)bpy(C_3O)]I_4$	-2.0	97.1	24 [9]	88.1 [515]
$[(C_{10})bpy(C_4O)bpy(C_3O)]I_4$	-2.0	99.0	26 [8]	82.2 [540]

[a] E_{app}: applied electrical potential (in volts); ΔT: chromatic contrast; t_{90} or t_{70}: time taken for the transmittance change by 90 or 70% of the total difference between the bleached and coloured states (in seconds); CE: colouration efficiency (in $cm^2.C^{-1}$); λ: wavelength of reduced coloured species (in nanometers).

From Table 4.4, it can be observed that the switching time correspondents to the bleached to coloured states as well as the correspondent colouration efficiency are very similar between them mainly in the case of tetra-iodide salts.

The device stability of $[C_3ObpyC_4ObpyC_3O]I_4$ was tested by on/off cycling through alternating the potential between two different states, i.e. bleached and coloured and monitoring the colour contrast (Δ E) with time through CIE L*a*b coordinates.

The electrochromic device and a Colour Checker accessory are placed in an isolated box and several photographs are taken using a digital camera under diffuse light during the electrochromic transitions as described in experimental section. Then, the images were treated with a *Matlab* software and the RGB coordinates obtained from the images were converted into L*a*b coordinates, taking in account a Colour Checker (colour pattern) as calibrate. The degradation of the device is measured as the variation of the colour from CIE L*a*b coordinates. These colour contrast, while the device switched between the reduced and oxidized state, respectively is calculated from Equation 4.13 [28,33].

$$\Delta E = \sqrt{(\Delta L^*)^2 + (\Delta a^*)^2 + (\Delta b^*)^2}$$

Equation 4.13

Where:

$$\Delta L^* = |L\ reduction - L\ oxidation|$$

Equation 4.14

$$\Delta a^* = |a\ reduction - a\ oxidation|$$

Equation 4.15

$$\Delta b^* = |b\ reduction - b\ oxidation|$$

Equation 4.16

The difference between the three coordinates (ΔL*, Δa*, Δb*) as well as the total colour difference (ΔE*) are present in Table 4.5.

Table 4.5 – Differences in colour space coordinates CIE L*a*b (ΔL*, Δa*, Δb*), total colour difference between the three coordinates (ΔE*) and the respective colour retention (ΔR) obtained for the electrochromic device containing $[C_3ObpyC_4ObpyC_3O]I_4$ [a].

Number of cycles	ΔL*	Δa*	Δb*	ΔE*	ΔR (%)
1	55.1	27.6	41.7	74.4	100
864	56.0	28.1	41.7	75.3	101
1724	55.7	27.8	43.3	75.8	102
2592	54.2	26.4	42.0	73.5	99
5184	50.4	26.2	41.9	70.6	95
8640	39.2	21.2	35.9	57.2	77

[a] The L*a*b coordinates obtained from a long cycling measurements of the electrochromic device by alternating the potential between 0 and -1.7 V (bleached and coloured) for 60 (bleached) and 30 (coloured) seconds, during 8640 cycles on/off. L: represents lightness; a: positive values indicate amounts of red while negative values indicate amounts of green; b: yellow is positive and blue is negative. ΔR (%) is the colour retention between the initial state and upon a specific number of cycles.

The device containing [C_3ObpyC$_4$ObpyC$_3$O]I$_4$ lost ca. of 23 % of the initial colour after 8640 redox cycles and showed a very good cycling stability when compared with the previously di-iodide salts.

4.4. Solid-State Electrochromic device

This device is built layer by layer with film deposition using spray technique and its architecture is illustrated in Figure 4.14.

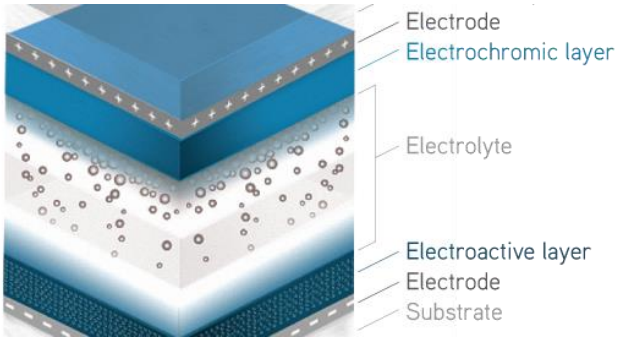

Figure 4.14 – Solid-State Electrochromic device used in this work [14]. (Source: www.ynvisible.com, accessed in August 2016)

Herein, the conductive layer (protective layer plus electrode) was PET-ITO and the electroactive layer corresponds to the PET-ITO layer covered with an electrochrome film, where a specific area of the film was previously cleaned, to allow to observe the switching of colours. The two PET-ITO layers are separated by a thickness of, approximately 0.23 mm spacer using a double sided adhesive tape and the electroactive area is around ca. 2.5 x 2.5 cm^2.

4.4.1. Ionic Polymers

An optimized experimental conditions were used and the spray deposition was made using 8 mg/mL of electrochrome in acetone and it was repeated 15 times (layers) upon drying the PET-ITO layer, to ensure total evaporation of acetone. The ionic polymer PVBz4 (Figure 4.15), where a polymer backbone has 4,4'-bipyridinium unit has pendent group previously prepared has been studied in electrochromic device to evaluate their possible electrochromic properties. Their colour switch is presented in Figure 4.15.

The system seems to be reversible and showed a colour switching between yellow to pink in the circle drawn in the middle of the electrochromic device. This suggested the presence of electrochromic species in the polymer structure.

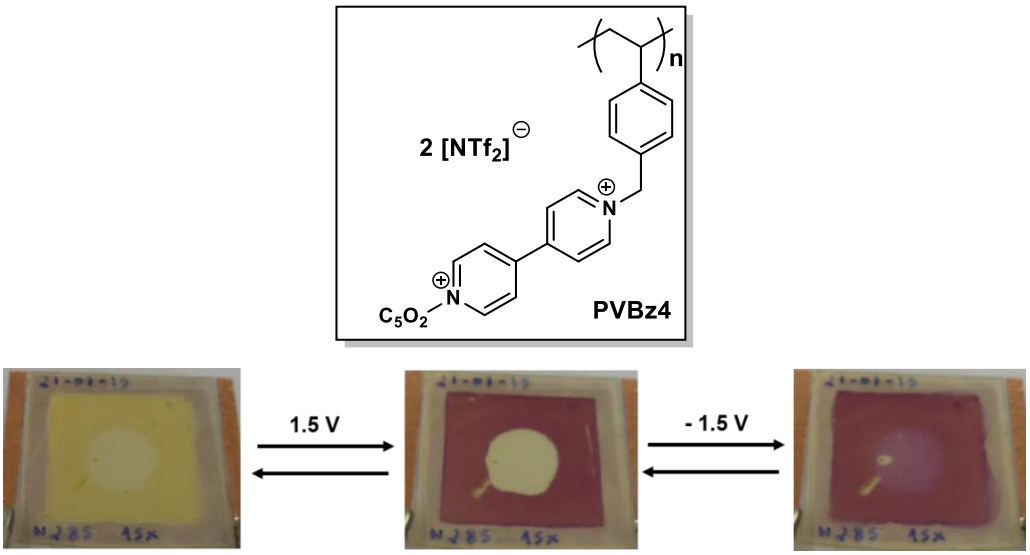

Figure 4.15 – Electrochromic device containing the polymer PVBz4 by spray deposition between two PET-ITO layers.

The electrochromic performance of this device was studied through the following parameters: chromatic contrast, colouration efficiency, colour coordinates and stability. The chromatic contrast (ΔT, %), transition times between the bleached and coloured states, the colouration efficiency (CE) are determined through spectroelectrochemical studies (Table 4.6).

Table 4.6 – Chromatic contrast, transition time and colouration efficiency of the device [a].

Salts	E_{app} (V)	ΔT (%)	t_{90} [t_{70}] (s)
PVBz4	-1.5	31	47 [34]

[a] E_{app}: applied electrical potential (in volts); ΔT: chromatic contrast; t_{90} or t_{70}: time taken for the transmittance change by 90 or 70% of the total difference between the bleached and coloured states (in seconds) followed at 527 nm.

The colour space coordinates (L*a*b*) of the electrochromic device was determined by spectroelectrochemistry studies. All colour space coordinates were determined between 0 to + 1.5 V and 1.5 to – 1.7 V. These values posteriorly are converted into RGB colour coordinate. The CIE L*a*b and respective RGB colour are presented in Table 4.7.

Table 4.7 – Colour space coordinates (CIE L*a*b*) of the device [a].

Salts	E_{app} (V)	L*	*a	*b	RGB colour
PVBz4	0	90.2	-2.9	10.9	
	+ 1.5	90.6	-2.9	10.2	
	- 1.5	65.3	22.2	-9.5	
	- 1.7	63.8	23.6	-10.7	

[a] E_{app}: Applied Electrical Potential (in volts); L: represents lightness; a: positive values indicate amounts of red while negative values indicate amounts of green; b: yellow is positive and blue is negative.

The device stability was also tested by on/off cycling through alternating the potential between two different states (bleached and coloured) and monitoring the colour contrast (Δ E) against time through CIE L*a*b coordinates. The electrochromic device and a Colour Checker accessory are placed in an isolated box and several photographs are taken using a digital camera under diffuse light during the electrochromic transitions as described in experimental section. Then, the images

were treated with a *Matlab* software and the RGB coordinates obtained from the captured images were converted into L*a*b coordinates, taking in account a Colour Checker (colour pattern) as calibrate. The difference between the three coordinates (ΔL*, Δa*, Δb*) as well as the total colour difference (ΔE*) are presented in Table 4.8.

Table 4.8 – Differences in colour space coordinates CIE L*a*b (ΔL*, Δa*, Δb*), total colour difference between the three coordinatews (ΔE*) and the respective colour retention obtained for the electrochromic device containing the polymer PVBz4 [a].

Number of cycles	ΔL*	Δa*	Δb*	ΔE*	ΔR (%)
1	8.5	2.0	2.0	9.0	100
320	8.4	2.0	2.0	8.9	99
1100	7.4	2.2	2.6	8.2	91
1500	7.0	2.5	2.0	7.7	86

[a] The L*a*b coordinates obtained from a long cycling measurements of the electrochromic device by alternating the potential between 1.5 and – 1.5 V (bleached and coloured) for 20 seconds each, during 1500 cycles on/off. L: represents lightness; a: positive values indicate amounts of red while negative values indicate amounts of green; b: yellow is positive and blue is negative.

The degradation of the device is calculated based on the loss of colour upon successive reduction and oxidation cycles through the difference between the colour contrast in the first cycle (ΔE^*_1) and the contrast after 1500 cycles (ΔE*(1500 cycles)). The electrochromic species seems to be degraded around 14 % upon 1500 redox cycles. In conclusion, the device showed a good performance, once presents a colour contrast of 31 % (Δ T) and it seems to be stable upon 1500 redox cycles.

Taking in account these preliminary electrochromic results, the ionic polymer, where the polymer backbone is bearing a 4,4'-bipyridinium unit, should be more explored in order to investigate the possibility to improve their electrochromic performance parameters as well as different colour switches. Besides that, this device architecture can be also attractive for future applications.

4.5. Conclusions

The di-substituted- and tetra-substituted-4,4'-bipyridinium salts as well as an ionic polymer bearing bipyridinium unit as pendant group have been tested in electrochromic devices and some electrochromic parameters were also investigated.

Initially, a liquid electrochromic device, which has previously reported by our group was used. The most promising di-substituted-4,4'-bipyridinium [NTf_2] salts using a RTIL, [EMIM][NTf_2] as electrolyte and platinum wires as working electrode have been tested. However, some amount of acetonitrile is added to system due to their intrinsic viscosity. All systems tested showed a reversible colour switch between transparent or pale yellow to blue, which can be attributed to the first electron-transfer process, typically from 4,4'-bipyiridinium salts derivatives, also known as viologen.

After this approach, a gel electrochromic devices containing di-substituted 4,4'-bipyridinium salts have been developed and different colour switches were achieved. In general, the iodide di-substituted-4,4'-bipyridinium salts showed two different colour switches that can be explained by radical cation formation (first electron-transfer process), followed by a dimerization process.

In contrast, the [NTf_2] derivative salts showed a colour switch between transparent to pale yellow to blue. The salt [$(C_{10})_2$bpy][NTf_2]$_2$ showed higher chromatic contrast (ΔT = 66.9 %) and colouration efficiency (186.9 $cm^2.C^{-1}$ at 605 nm) than the other [NTf_2] salts. Two of these salts [$(C_{10})_2$bpy]I_2 and [$(C_5O_2)_2$bpy][NTf_2]$_2$ were analysed by preliminary on/off cycling studies. In this context, [$(C_{10})_2$bpy]I_2 showed a modest stability performed, with around 20 % of decrease in absorbance value, while [$(C_5O_2)_2$bpy][NTf_2]$_2$ salt showed a good cycling stability during 70 cycles. In general, different colour switches were obtained for the tetra-substituted-4,4'-bipyridinium salts. In particular, the [(C_{10})bpy(C_4O)bpy(C_{10})][NTf_2]$_4$ salt showed higher chromatic contrast (ΔT = 38.4 %) and colouration efficiency (105.2 $cm^2.C^{-1}$ at 550 nm). The salt [C_3ObpyC_4ObpyC_3O]I_4 was also studied by on/off cycling studies and lost ca. of 23 % of the initial colour after almost 9000 redox cycles. In conclusion, this salt indicated us a very good cycling stability as well as a colour contrast of 23.8 % (ΔT) and a colouration efficiency of 80.6 $cm^2.C^{-1}$ at 545 nm.

The ionic polymer was tested in different architecture solid-state electrochromic devices and they showed a colour switch between pale yellow to pink. The colour contrast obtained was 31 % (ΔT). This device was also submitted an on/off cycling studies and showed a good performed, once it lost ca. 14 % of initial colour upon 1500 redox cycles. This preliminary studies open good perspectives about the potential of the application of this kind of ionic polymers in electrochromic devices.

4.6. Experimental Part

Spectroelectrochemistry

Spectroelectrochemistry studies were performed using UV-Vis-NIR spectrophotometer Varian Cary 5000. The potential was controlled with a device potentiostat/galvanostat Model 20 Autolab. The device was placed in the spectrophotometer compartment perpendicularly to the light beam. The potentiostat/galvanostat applied an electric potential appropriated and previous selected potentials from CV, and the spectrophotometer registered the absorbance in the UV-Vis and then at the wavelengths selected for each experiment within the range of the equipment.

Electrochemical Studies

Electrochemical studies were performed on an Autolab PGSTAT 12 potentiostat/galvanostat, controlled with GPES software version 4.9 (Eco-Chemie), using the PET-ITO layers as electrodes.

Cycling

Cycling stability tests were also performed in the same setup of spectroelectrochemistry. For long cycling experiments the followed procedure was used. A camera, a lamp (to control the luminosity) and a Colour Checker accessory (colour pattern) were placed inside an isolated box (chamber). The electrochromic device is placed inside this set-up (box) and connected to a function generator. While the function generator applies a selected potential square waveform (changing from positive to negative), the camera is recording, from time to time, 150 pictures during a calculated period of time, enough to see a complete redox (oxidation–reduction) cycle of the device. The pictures are then treated with a *Matlab* software converting RGB coordinates obtained from the film into L*a*b* coordinates.

4.7. References

1 P. M. S. Monk, R. J. Mortimer and D. R. Rosseinsky, *Electrochromism and Electrochromic Devices*, Cambridge University Press, Cambridge, 2007.

2 D. R. Rosseinsky and R. J. Mortimer, *Adv. Mater.*, 2001, **13**, 783–793.

3 C.-G. Granqvist, in *Electrochromic Materials and Devices*, Wiley-VCH Verlag GmbH & Co. KGaA, 2013, pp. 1–40.

4 R. J. Mortimer, *Annu. Rev. Mater. Res.*, 2011, **41**, 241–268.

5 R. Baetens, B. P. Jelle and A. Gustavsen, *Sol. Energ. Mater. Sol. Cells*, 2010, **94**, 87–105.

6 R. J. Mortimer, *Annu. Rev. Mater. Res.*, 2011, **41**, 241–268.

7 *Gesimat (www.gesimat.de)*, 2016.

8 C. G. Granqvist, *Handbook of Inorganic Electrochromic Materials*, Elsevier Science B.V., Amsterdam, 1995.

9 Y. Wang, E. L. Runnerstrom and D. J. Milliron, *Annu. Rev. Chem. Biomol. Eng.*, 2016, **7**, 283–304.

10 E. S. Lee and D. L. DiBartolomeo, *Sol. Energ. Mater. Sol. Cells*, 2002, **71**, 465–491.

11 R. J. Mortimer, D. R. Rosseinsky and P. M. S. Monk, in *Electrochromic Materials and Devices*, Wiley-VCH Verlag GmbH & Co. KGaA, 2015, pp. I–XXVIII.

12 *Gentex (www.gentex.com)*, 2016.

13 *Acreo (www.acreo.se)*, 2016.

14 *Ynvisible (www.ynvisible.com)*, 2016.

15 R. J. Mortimer, A. L. Dyer and J. R. Reynolds, *Displays*, 2006, **27**, 2–18.

16 R. J. Mortimer, P. M. S. Monk and D. R. Rosseinsky, in *Electrochromic Materials and Devices*, Wiley-VCH Verlag GmbH & Co. KGaA, 2015, pp. 623–626.

17 P. M. S. Monk, N. M. Hodgkinson and S. A. Ramzan, *Dye. Pigment.*, 1999, **43**, 207–217.

18 P. M. S. Monk, *The viologens: physicochemical properties, synthesis, and applications of the salts of 4,4'-bipyridine*, John Wiley & Sons, Inc., 1998.

19 V. Ramamurthy and K. S. Schanze, *Semiconductor photochemistry and photophysics*, Marcel Dekker Inc., 2003.

20 P. M. S. Monk, D. R. Rosseinsky and R. J. Mortimer, in *Electrochromic Materials and Devices*, Wiley-VCH Verlag GmbH & Co. KGaA, 2013, pp. 57–90.

21 A. C. L. Marques, C. A. P. Baptista and J. Araujo, *Electrolyte solution, printing method thereof and resulting solid electrolyte - US20140361211*, 2014.

22 A. Branco, L. C. Branco and F. Pina, *Chem. Commun.*, 2011, **47**, 2300–2302.

23 R. J. Mortimer, *Electrochim. Acta*, 1999, **44**, 2971–2981.

24 D. R. Rosseinsky and P. M. S. Monk, *J. Chem. Soc. Faraday Trans.*, 1993, **89**, 219–222.

25 P. M. S. Monk, R. D. Fairweather, M. D. Ingram and J. A. Duffy, *J. Chem. Soc., Perkin Trans. 2*, 1992, 2039–2041.

26 *The Known Colors Palette Tool (www.codeproject.com/Articles/243610/The-Known-Colors-Palette-Tool-Final-Revision-Hopef#toc_bookmark_4)*, 2016.

27 M. L. Gulrajani, *Colour measurement principles, advances and industrial applications*,

Woodhead Pub, 2010.

28 C. Costa, C. Pinheiro, I. Henriques and C. A. T. Laia, *ACS Appl. Mater. Interfaces*, 2012, **4**, 5266–5275.

29 R. J. Mortimer and J. R. Reynolds, *J. Mater. Chem.*, 2005, **15**, 2226–2233.

30 T.-H. Kuo, C.-Y. Hsu, K.-M. Lee and K.-C. Ho, *Sol. Energ. Mater. Sol. Cells*, 2009, **93**, 1755–1760.

31 R. Cinnsealach, G. Boschloo, S. Nagaraja Rao and D. Fitzmaurice, *Sol. Energ. Mater. Sol. Cells*, 1998, **55**, 215–223.

32 C. Pozo-Gonzalo, M. Salsamendi, A. Viñuales, J. A. Pomposo and H.-J. Grande, *Sol. Energ. Mater. Sol. Cells*, 2009, **93**, 2093–2097.

33 P. Tehrani, L.-O. Hennerdal, A. L. Dyer, J. R. Reynolds and M. Berggren, *J. Mater. Chem.*, 2009, **19**, 1799–1802.

5. Development of Diarylethene salts

5. Development of Diarylethene Salts

5.1. Introduction

A diaryethene is a derivative of stilbene, in which the phenyl groups of stilbene are replaced with five-membered heterocyclic rings of low aromatic stabilization energy such as thiophenes and furans. These photochromic molecules belong to the thermally irreversible (P-type) photochromic systems and show high-sensitivity and fatigue-resistant properties [1–3]. They can also display rapid response and reactivity in solid state, i.e. many diarylethenes undergo photochromic reactions in the single crystalline phase [2]. All these properties have contributed to convey diarylethenes as rather promising molecules for applications in photonic devices [3].

These photochromic compounds undergo a reversible 6π-electron photocyclization reaction, between the generally colourless open-ring isomer (hexatriene structure) and the coloured closed-ring isomer (cyclohexadiene structure) by alternate irradiation with UV and visible light, respectively (Scheme 5.1).

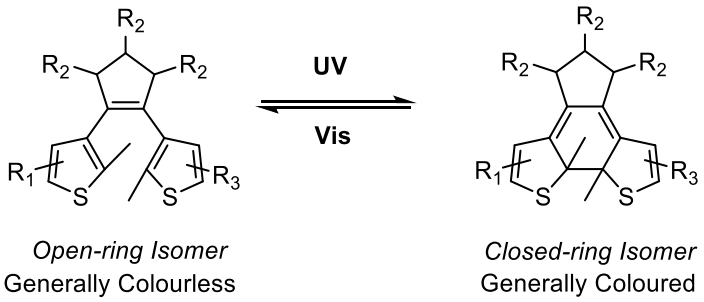

Scheme 5.1 – General photochromic reaction of diarylethenes [1]. (Source: *J. Photochem. Photobiol. C Photochem. Rev.*, 2004, **5**, 169–182).

The coloured ring-closed isomers can acquire different hues such as yellow, red or blue, depending on the substituents, as shown in Figure 5.1 for systems in the liquid phase and in Figure 5.2 for systems in the solid state [1,3].

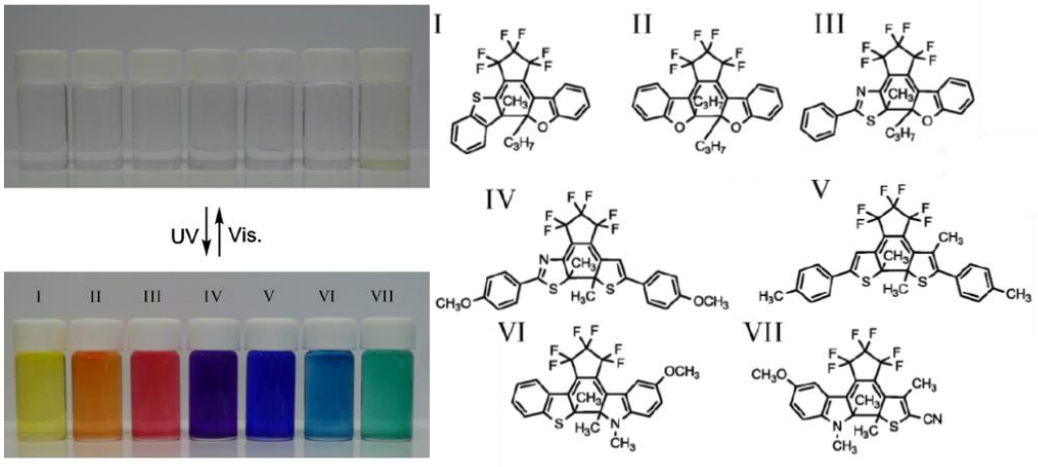

Figure 5.1 – Colour change of diarylethene derivatives in toluene solutions upon photoirradiation [3]. (Source: *Chem. Rev*., 2014, **114**, 12174–12277).

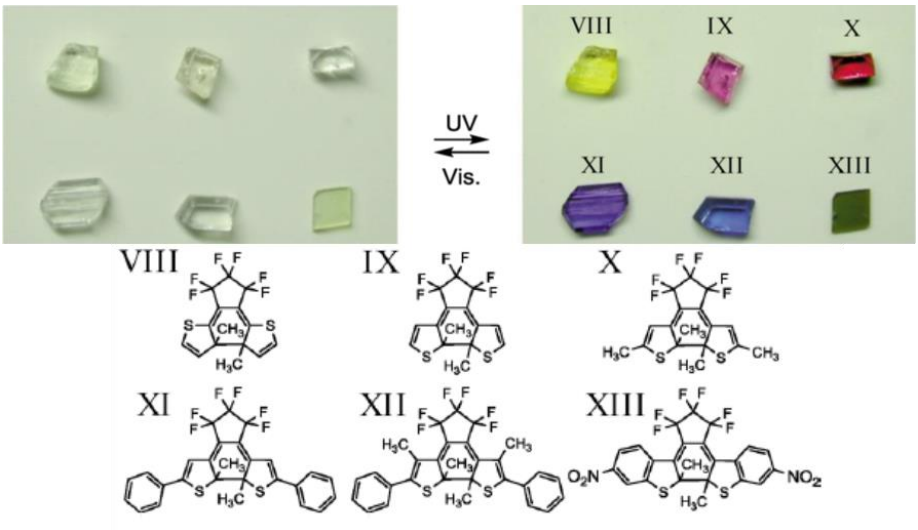

Figure 5.2 – Colour change of diarylethene derivatives in the single crystalline phase upon photoirradiation [3]. (Source: *Chem. Rev*., 2014, **114**, 12174–12277).

In the case of open-ring isomers, a free rotation between ethene moiety and the aryl groups occurs. As consequence, the isomer is non-planar and the π-electrons are localized in the two aryl groups. Furthermore, the rotational energy barrier allows for the existence of two conformations in the open-ring isomers, with the two rings in mirror symmetry (photo-inactive, parallel conformation) or in C_2 symmetry (photo-active, anti-parallel conformation) [1,3].

According to the Woodward-Hoffmann rules, photochemical electrocyclic reactions involving (4n+2) π-electron systems proceed in a *conrotatory mode*, while thermal electrocyclic reactions proceed in *disrotatory mode*. In *conrotatory motion*, the terminal *p*-orbitals can rotate in the same direction. In the case of *disrotatory motion*, they rotate in opposite directions. The *conrotatory* photocyclization reaction can only take place in the photo-active conformation, i.e. anti-parallel conformation (Scheme 5.2) [1].

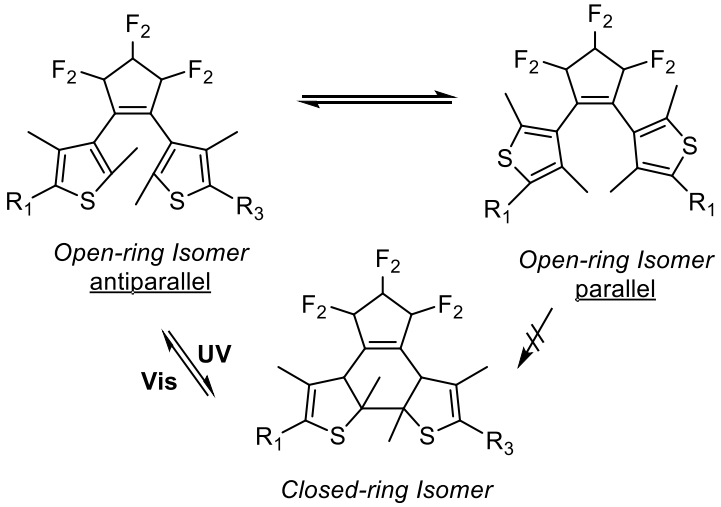

Scheme 5.2 – Diarylethene open-ring isomer conformations: anti-parallel and parallel conformations, with two groups aryl in C_2 symmetry (photo-active) or in mirror symmetry (photo-inactive), respectively [3]. (Source: *Chem. Rev*., 2014, **114**, 12174–12277).

On the other hand, the closed-ring isomer has a planar structure with asymmetrically arranged carbon atoms at the reaction site, originating two enantiomers (*R, R* and *S, S*). It has a bond alternation polyene structure and the π -electrons are delocalized throughout the molecule [1].
As already mentioned, the structural differences between open-ring and closed-ring isomers lead to changes in the physical properties.

For photochromic molecules, the thermal stability in both isomers, is one of the most important parameters in the practical application point of view (e.g. photonic devices). In this context, diarylethenes have received considerable attention and a variety of new diarylethene derivatives have been synthesized. The challenge is to achieve a thermally irreversible molecular system but photochemically reversible [2,3]. The thermal stability of the photogenerated close-ring isomer is mainly dependent on the type of aryl groups from the molecule. Also, to control this thermal stability it is necessary taking into account mainly the aromatic stabilization energy and electron-withdrawing substituents of the aryl groups as well as steric hindrance of the substituents at the reactive carbons [3]. In particular, the energy barrier, which correlates with the ground-state energy difference between the open- and the closed-ring isomers, controls the stability of the closed-ring isomers. When the energy difference is large, the energy barrier becomes small and the cycloreversion reaction occurs. When the energy difference is small, the reaction barrier becomes large. This kind of information is particularly relevant to molecular design principle in order to obtain thermally irreversible diarylethenes [2]. Therefore, when the aryl groups are pyrrolyl, indolyl or phenyl rings, which have high aromatic stabilization energies, the photogenerated closed-ring isomers are thermally unstable. This can be explained by the increase in the energy level of the closed-ring isomers due to the loss of the aromatic stabilization energy [3]. The thermal stability of the photogenerated closed-ring isomers is achieved by introduction of aryl groups with low aromatic stabilization energies, such as furan, thiophene, selenophene or thiazole. Those photogenerated closed-ring isomers are thermally stable and remain stable even at 100 ºC [2,3]. When electron-withdrawing substituents are present at the aryl groups, the closed-ring isomers become thermally unstable, because the central carbon-carbon bonds (closed-ring isomers) are weakened by the electron-withdrawing substituents [3]. Also, when bulky substituents at the reacting positions are present, a thermally unstable closed-ring isomers are obtained [3]. In conclusion, the thermal stability of open- and closed-ring isomers can be attained by introducing aryl groups, preferably with low aromatic stabilization energies.

The quantum yield is an important property of photochromic compounds and it is defined for a photochemical reaction as the amount of reactant consumed or product formed per amount of photons absorbed. In the case of diarylethenes, the open-ring isomer has two conformations with two aryl rings in mirror symmetry (parallel conformation) and in C_2 symmetry (anti-parallel conformation). These two conformations can interconvert with each other in solution. However, the *conrotatory* cyclization reaction can only proceed from the anti-parallel conformation (see Scheme 5.2) [2,3]. In general, the population of these two conformations is 1:1, so the cyclization quantum yield cannot exceed 0.5 [2,3]. If the population ratio of the anti-parallel conformation is increased than the cyclization quantum yield is also expected to increase. In this way, different

approaches to increase the population of anti-parallel conformers have been proposed [2,3]. For example, the introduction of bulky substituents [4] or long alkyl groups [5] at reactive carbons were found to increase the population of the anti-parallel conformers and consequently, the cyclization quantum yields.

Alternative approaches to improve the quantum yield have been reported by introducing these chromophores into cyclodextrin cavities [6–8], covalently link them to polymers [9], incorporating pyridinium cations at both sides of the diarylethene structure [10], making a bridge structure between two thiophene rings [11–14] or introducing multiple intramolecular noncovalent interactions [15]. In addition, it is expected an increase of the cyclization quantum yield by an increase of the ratio of anti-parallel conformers in the photoexcited state because the photo-inactive parallel conformation can transfer the photoexcited energy to photoactive anti-parallel conformation [3].

The photocyclization reactions of some diarylethene derivatives can be dependent on the solvent polarity, as reported by Irie and co-workers [16]. Thereby, an increase in the solvent polarity leads to a decrease in the photocyclization reaction quantum yield while practically it does not affect the photocycloreversion reaction quantum yield [3,16]. This solvent effect can be explained by twisted intramolecular charge-transfer (TICT). In the case of the photocycloreversion reaction, the quantum yield is dependent of the substituents on the aryl groups. When diarylethenes have long π-conjugated aryl groups they show low cycloreversion quantum yields [3,17,18]. The photocycloreversion quantum yield is strongly suppressed through introduction of electron-donating substituents, such as methoxy groups in reactive carbons. The introduction of electron-withdrawing substituents, such as cyano groups lead to an increase of the photocycloreversion quantum yield [3]. In conclusion, the range of the cyclization and cycloreversion quantum yield values are reported to be between 0.01 to 0.86 [2].

Fatigue-resistant is another important property for practical applications. There are several photochromic compounds reported, that can repeat colouration and decolouration cycles induced by light more than 1000 times. However, this number of cycles can be considered limited. The difficulty in obtaining fatigue-resistant photochromic compounds can be easily understood through the fact that photochromic reactions are always accompanied by rearrangement of chemical bonds. During these rearrangement, undesirable side reactions can occur [2,3]. So, it is necessary to understand the fatigue mechanism in order to improve the fatigue-resistant properties. Diarylethenes incorporated with suitable aryl groups, such as benzothiophene or 2,4-dimethyl-5-phenylthiophene are reported as low fatigue-resistant examples, where the colouration and decolouration cycles were repeated more than 14 000 cycles in solution [19] and 30 000 cycles in the single crystalline phase [20], without significant loss of performance.

As already mentioned, reversible photo-isomerisation between two isomers, leads to a change in the electronic structure that influences the fluorescence properties. Usually, diarylethenes are non-fluorescent in both open- and closed-ring isomers. However, in diarylethenes having benzothiophene as aryl groups, a weak fluorescence in both isomers is observed [21–23]. In order to improve its fluorescence, it is possible to attach fluorescent units, such as indole, pyrrole, coumarin, naphthalene as the aryl group in diarylethene structure [24–28].

In this case, for inherently fluorescent diarylethenes, the fluorescence emission and the photoisomerisation reaction compete with each other. Consequently, when the fluorescence quantum yield is high, the photoisomerisation reaction is suppressed. For example, Yagi and Irie reported two diarylethenes containing a fluorescent indole ring as the aryl group and the fluorescence quantum yields of the open-ring isomers are between 4.6 to 6.3%, while almost zero for closed-ring isomer. They observed that the fluorescence quantum yields decreased with the increase in the photocyclization quantum yields [24].

Another possible alternative to improve the fluorescent properties of diarylethenes, i.e. efficient photochromic reactivity and high fluorescence quantum yield, is the introduction of fluorescent chromophores in the diarylethene unit. Several diarylethenes containing fluorophores such as anthracene, rhodamine, fluorescein, have been reported [29–32].

In addition to light, electricity can be also applied to molecular isomerisation reactions. Some examples of diarylethenes that undergo cyclization and cycloreversion reactions chemically or by electrochemical oxidation or reduction have been reported [3].

Branda and co-workers reported that when several dithienylethene derivatives, e.g. diarylethenes with thiophene rings, are chemically or electrochemically oxidized, they presented the same ring-opening and ring-closing reactions already described for light activated process [33]. There are several works reporting dithienylethenes that can be ring-closed when oxidized or reduced, or ring-opened upon oxidation [34].

In the case of dithienyethene derivatives containing electron-withdrawing substituents, the open-ring isomer can be obtained electrochemically from the corresponding closed form [35,36]. In a first step, an electron-transfer process corresponding to the oxidation of the closed-ring isomer into its cation radical is observed. Then, the obtained radical cation evolves thermally to its open-ring isomer radical cation, which is later reduced into the neutral open isomer. Interestingly, a large difference in the redox potential of the open- and closed-ring isomers it is observed with the open couple being more anodic that the closed one. So, the ring-opening of the closed-ring isomer radical cation produces the open-ring form of the radical cation and this one is the most stronger oxidizing species relative to the closed isomer [36].

Kawai and co-workers reported the optical and electrochemical properties of a diarylethene derivative, *cis*-1,2-Dicyano-1,2-bis(2,4,5-trimethyl-3-thienyl)ethane (CMTE). They observed that CMTE showed irreversible oxidation current waves and the open-ring form, which is a thermodynamically stable form, presented higher oxidation potential than closed-ring form. They also reported that the electrochemical oxidation of the closed form of CMTE resulted in the neutral open-form isomer [37]. Branda and co-workers demonstrated the electrochemical reduction of the ring-open isomer of a diarylethene derivative incorporating two *N*-methylpyridinium groups results in the ring-closed isomer, the same as generated photochemically. However, this electrochemical reaction also produces a sub-product, which is photochemically unattainable [33]. Later on, Branda and co-workers realized that all examples of redox-triggered switching of hexatriene architectures were limited by the fact that in these reactions only one of the two reactions (unidirectional), cyclization or cycloreversion, can be triggered electrochemically. In order to obtain redox control

in both directions, a combination of optical and electrical inputs is required [34]. They demonstrated the first examples of dithienylethene derivatives, which presented both directional photochromic and electrochromic behaviour as illustrated in Figure 5.3 [34].

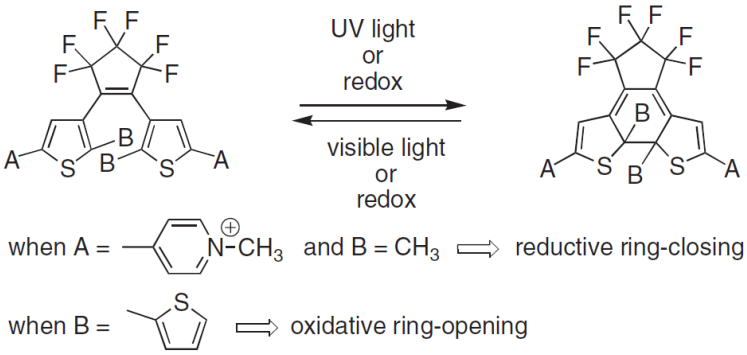

Figure 5.3 – Photo- and electroswitching of the dithienylethene architecture [34]. (Source: *Adv. Funct. Mater.*, 2007, **17**, 786–796.)

The diarylethenes undergo oxidative cyclization reactions, when the radical cations of the closed-ring isomer are more stable relative to the open-ring isomers. On the other side, the diarylethenes undergo oxidative cycloreversion reactions when the radical cations of the open-isomer are more stable than the closed-ring isomers [3].

There is also reported in the literature molecular memory devices based on indium tin oxide (ITO) electrodes modified with a dithienyethene switch, presenting reversible opening- or closing-ring isomer by photo- and electro-chemically stimuli with non-destructive electrochemical readout [38]. Willner and co-workers also reported an example of photo- and electrochromic diarylethene derivatives in modified electrodes. They presented an electroactive and photoisomerizable monolayer assembled in gold (Au) electrodes allowing sequential photo- and electrochemical storage of information [39]. More recently, Lee and co-workers developed molecular-scale electronic devices with a photo-switching diarylethene derivative on flexible substrates, through self-assembly monolayers on gold (Au) and titanium (Ti) electrodes [40].

Gated photochromic reactivity is also an important property for memory media application, since photochromic reactions usually occur in direct proportion to the number of photons absorbed by the molecule, i.e., a linear response is observed. As a consequence, the recorded memories may be destroyed during readout of the absorbance or fluorescence. In this way, gated photochromic reactivity appears as a possible approach to avoid that. So, additional external stimuli such as photons with a different energy, chemicals or heat can be used in order to control the photochromic reactions [3]. In the literature there are several approaches to attain the gated reactivity of the diarylethenes [41–57].

In conclusion, the best performance of diarylethenes as well-designed derivatives with half-life time at room temperature longer than 400 000 years (thermally stable) have been reported. Additionally, the quantum yield of colouration is close to 1, colouration and decolouration cycles can be repeated more than 10 000 times and both reactions occurs in picosecond time region [3].

5.2. Diarylethenes Salts

Several molecular designs of diarylethene derivatives, incorporating different functional groups have been developed [3]. These functional groups can contribute to obtain different colours (closed-ring isomer) and to improve their quantum yields, fluorescence, thermal stability and fatigue-resistant.

In general, the most common reported diarylethene molecules are neutral. In 2003, Irie and co-workers reported the incorporation of an *N*-methylpyridinium cation at one and at both thiophene rings of the dithienylethene architecture. The diarylethene having two *N*-methylpyridinium scaffolds showed higher cyclization quantum yield than diarylethene with only one *N*-methylpyridinium cation as well as the original neutral structure [10].

In 2009, Kawai and co-workers reported cationic diarylethenes containing an imidazolium ring directly connected to the central ethene unit as aryl group with [NTf_2] used as counter-ion (Scheme 5.3) [58]. In their experimental section, it is indicated that one of these compounds (compound 1) is obtained as an oily product, which probably is an intrinsically photochromic IL. However, no remarks about this possibility appear in the paper [58,59]. These systems undergo reversible photochromic reactions in a wide range of solvents, including ILs.

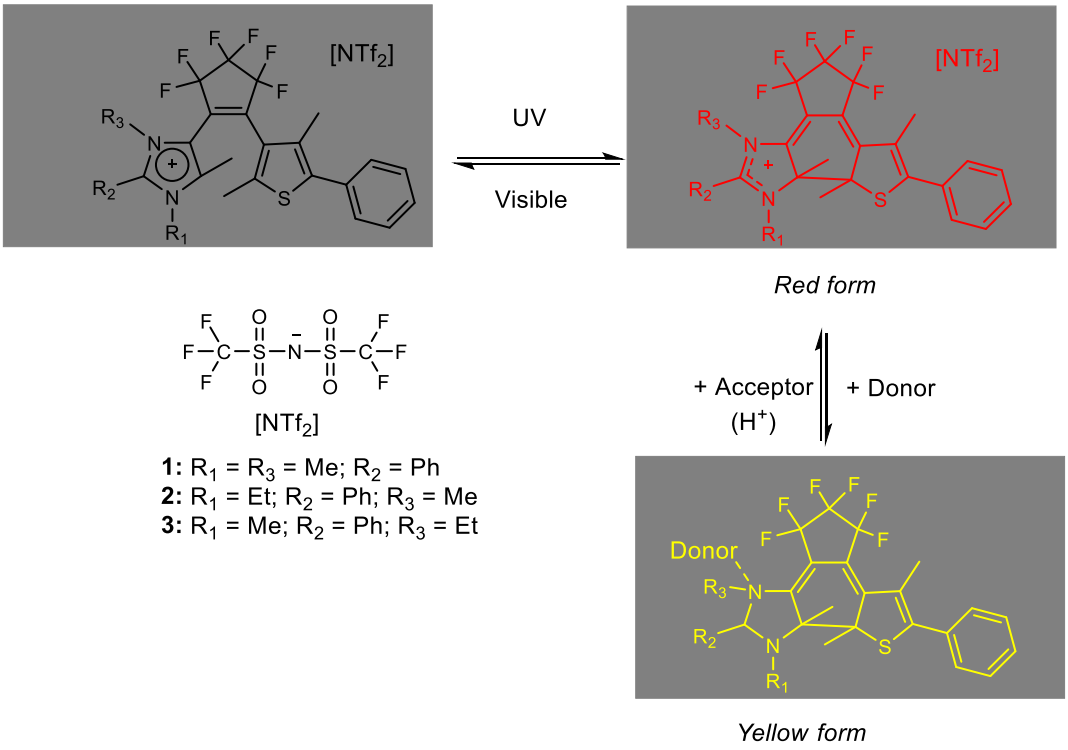

Scheme 5.3 – Cationic diarylethenes containing imidazolium ring directly connected to the central ethane unit as aryl group and [NTf_2] was used as counter-ion [58]. (Source: *Chem. Eur. J.*, 2009, **15**, 1977–1984).

When the solvatochromic behaviour of compound 1 was studied in two ILs, [EMIM][NTf_2] and [EMIM][$EtSO_4$], different closed-ring isomer absorption spectra were obtained depending on the nature of the anion [58,59]. The red form is stabilised in [EMIM][$EtSO_4$], whereas the yellow form in [EMIM][NTf_2]. This behaviour was explained on the basis of the different donor-acceptor

properties of the ILs [58,59]. The presence of positively a charged nitrogen directly on the conjugated π-system leads to solvent- and anion-dependent absorption profiles similar to 11-*cis*-retinal [58].

Yam and co-workers reported a similar approach; they prepared a variety of diarylethene containing *N*-heterocyclic carbenes, in particular the Arduengo-type, which was complexed with gold (I), silver (I) and palladium (II) [60]. Several counter-ions have been tested and when bis(trifluoromethane)sulfonimide [NTf_2] was used, a RTIL (melting point below 20 ºC) was obtained [60]. The authors claim that RTIL is an intrinsically photochromic IL but no experimental studies focusing photochromic behaviour is available in the communication or in the supplementary material [59,60].

Later on, Yam and co-workers also reported a variety of dithienylethenes containing imidazolium cations, where a series of substituents on the 2-position of the imidazolium ring combined with [PF_6] as anion [61].

Herein, we are interested to develop diarylethene derivatives as anionic units (di-acid compound) and then combined with appropriate organic cations, in particular ammonium and phosphonium units (Figure 5.4).

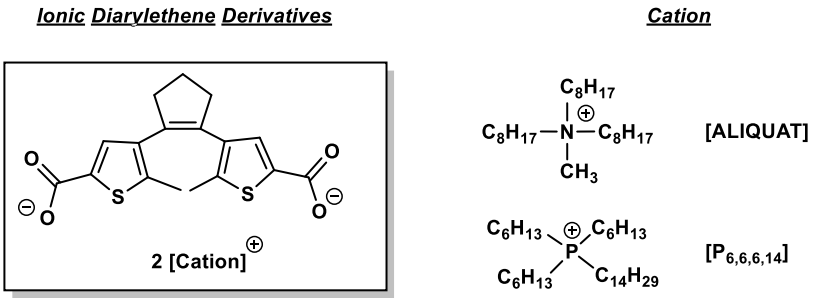

Figure 5.4 – Ionic diarlyethene derivatives developed through adequate combination of an anionic diarylethene with different organic cations.

The selection of these large organic cations allowed the preparation of novel ILs incorporating the diarylethene derivative anion. At this moment, only the diarylethene (**DAE**) combined with tri-octyl methylammonium ([ALIQUAT]) cation was suitably obtained as pure RTIL.

5.2.1. Synthesis of an ionic diarylethene derivative

The synthesis of an ionic diarylethene derivative as IL involved two synthetic stages, the preparation of a di-carboxylic acid dithienyethene derivative (di-acid), followed by an acid-base reaction in order to obtain diarylethene carboxylate salt.

In the first stage, the di-carboxylic acid dithienyethene derivative (di-acid) is synthesized through four steps (Scheme 5.4) according with literature [35,62].

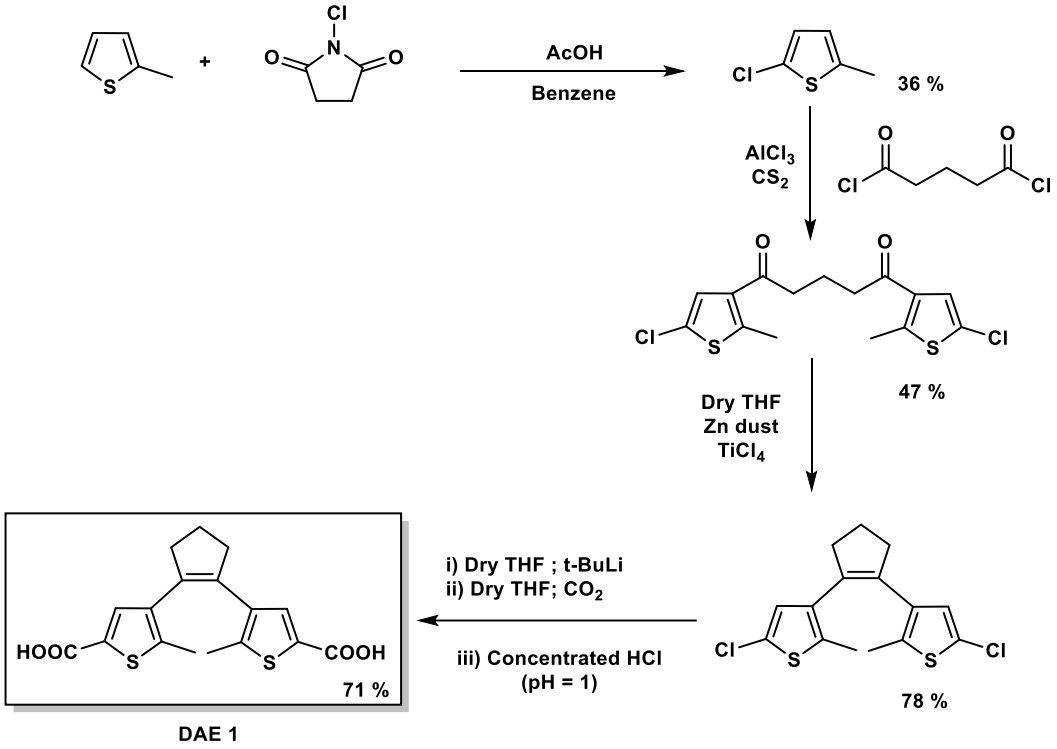

Scheme 5.4 – Synthesis of di-carboxylic acid diarylethene derivative (**DAE 1**) [35,62].

Firstly, a chlorination of 2-methylthiophene is performed using *N*-chlorosuccinimide and 2-chloro-5-methylthiophene is obtained in 36 % yield. The following step is a Friedel-Craft acylation with aluminium chloride ($AlCl_3$) and glutaryl dichloride in carbon disulfide (CS_2) at 0 ºC to obtain 1,5-bis(5-chloro-2-methylthien-3-yl)pentane-1,5-dione, which is obtained in 47 % yield. The third step involved a McMurry cyclization using the previous diketone and titanium tetrachloride ($TiCl_4$) in tetrahydrofuran (THF) solution and using zinc as reducing agent to prepare the Ti^0 species *in situ* [62]. The desired product, 1,2-bis(5-chloro-2-methylthien-3-yl)cyclopentene, is obtained in 78% yield. The final step involves the formation of a carbanion using *tert*-butyl lithium in dry THF (chlorine to lithium exchange process). This carbanion as prepared *in situ* reacted with CO_2-saturated THF solution to give the desired di-carboxylic acid. Then, after adequate work-up in order to remove any impurity from the previous reaction, the di-carboxylic acid is recovered by acidification of the aqueous solution in 71 % of yield [35].

The structure of the 1,2-bis(5'-carboxy-2'-methylthien-3'-yl)-cyclopentene (**DAE 1**) was confirmed by ^1H NMR analysis (Figure 5.5) and elemental analysis (C, H, N).

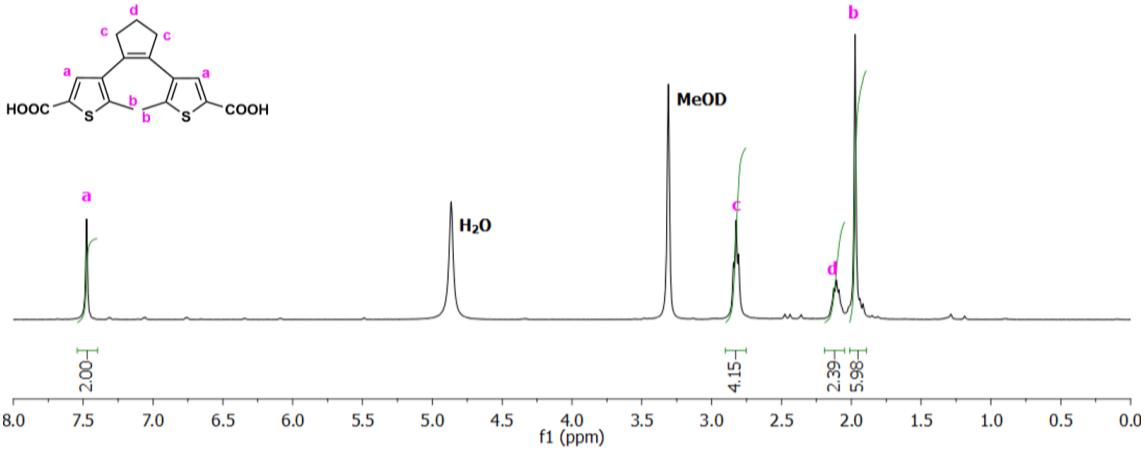

Figure 5.5 – ^{1}H NMR spectra in CD_3OD of **DAE 1**.

The presence of typical protons of the final product in the ^{1}H NMR spectra proofs the preparation of **DAE 1** in high purity levels.

In the second stage, an additional step to prepare the basic form of the selected organic cation is required, through an anion exchange resin method. Then, neutralization acid-base reaction using the carboxylic acid (**DAE 1**) prepared in stage 1 and this organic cation in basic form allowed the preparation of the desired ionic diarylethene derivative salt (**DAE 2**) (Scheme 5.5).

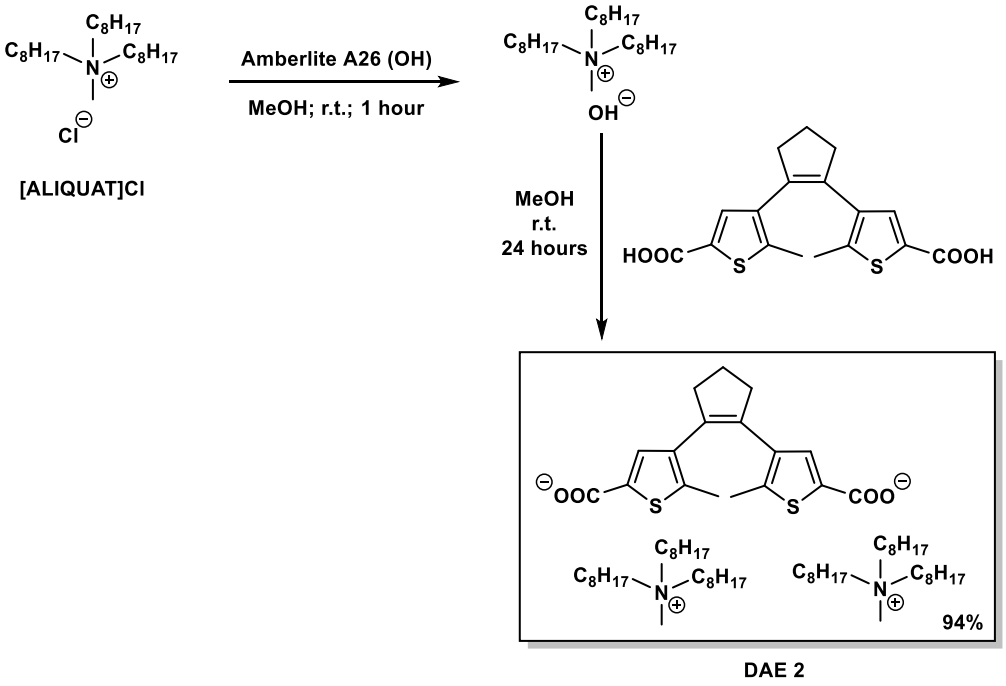

Scheme 5.5 – Preparation of **DAE 2** in two steps: hydroxide anion exchange and neutralization acid-base reaction.

In the first step hydroxide anion exchange is performed using amberlyst A26 (OH) as basic anion-exchange resin to replace the chloride anion in [ALIQUAT]Cl by hydroxide. Then, a neutralization acid-base reaction involving slow addition (dropwise) of this diluted methanol solution containing the organic cation with hydroxide counter-ion to a solution of the di-carboxylic acid dithienylethene compound has been performed. After complete addition and further purification, the desired salt

(**DAE 2**) is obtained as a brown viscous liquid, i.e. room temperature ionic liquid (RTIL). ^{1}H NMR (see Figure 5.6) and ^{13}C NMR and elemental analysis were performed in order to check the product structure.

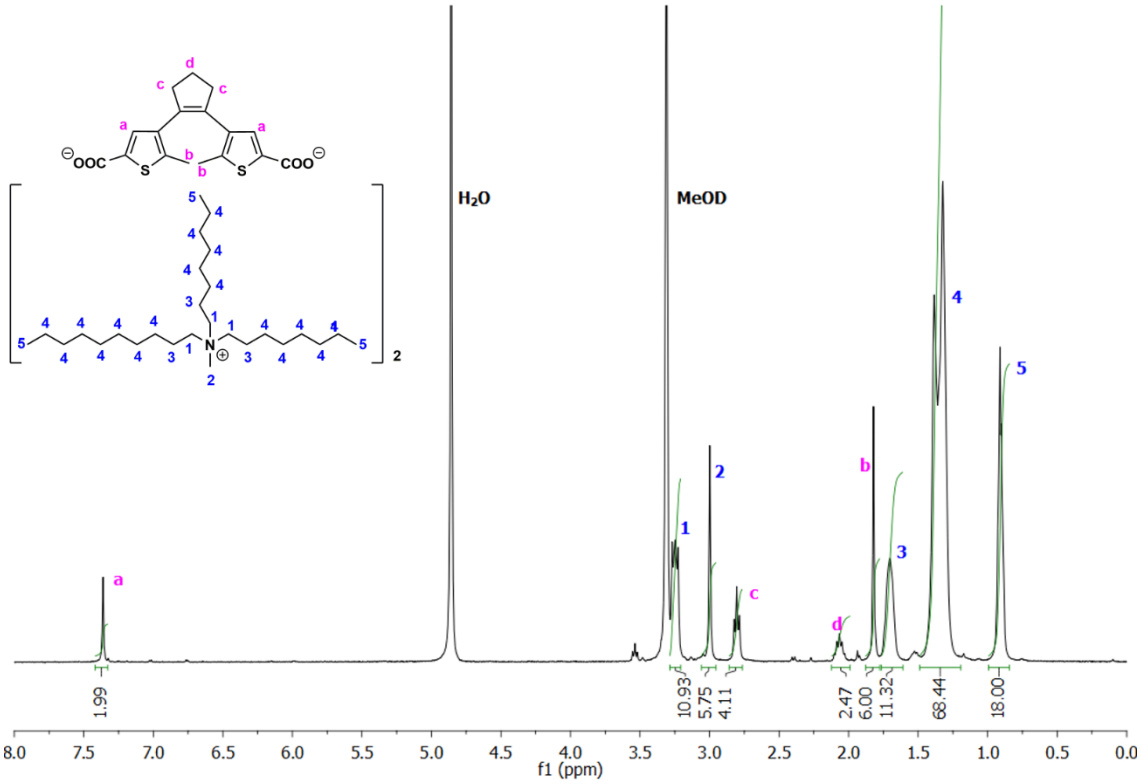

Figure 5.6 – ^{1}H NMR spectra in CD_3OD of **DAE 2**.

^{1}H NMR analysis of **DAE 2** showed the typical signals of the ALIQUAT cation considering a mixture of octyl (C_8) and decyl (C_{10}) chains, with octyl chain (C_8) predominating and di-COOH dithienylethene. As a consequence, it is possible to determine the adequate proportion between anion and cation by comparing the integration areas, for example, from the aromatic proton of the anion (~7.36 ppm, a) and the terminal protons of aliphatic chains of ALIQUAT cation (~0.9 ppm, 5). Hence, the proportion is close to 2:1 (cation:anion), as expected.

Differential scanning calorimetry (DSC) was also performed in order to evaluate the thermal behaviour of the prepared **DAE2** (Figure 5.7).

In the first cycle, a broad endothermal event above 50 ºC is observed due to solvent evaporation, possibly water. The following cycles are practically identical and it is possible to observe in the cooling run close to – 50 ºC the presence of exothermic peaks, which could be attributed to the energy release derived from the cracking of the glassy structure, an indication that the glass transition occurs somehow at a higher temperature [63]. In fact, a step in the heat flux, however ill-defined, emerges near 0 ºC coherent with the usual discontinuity associated with the glass transition.

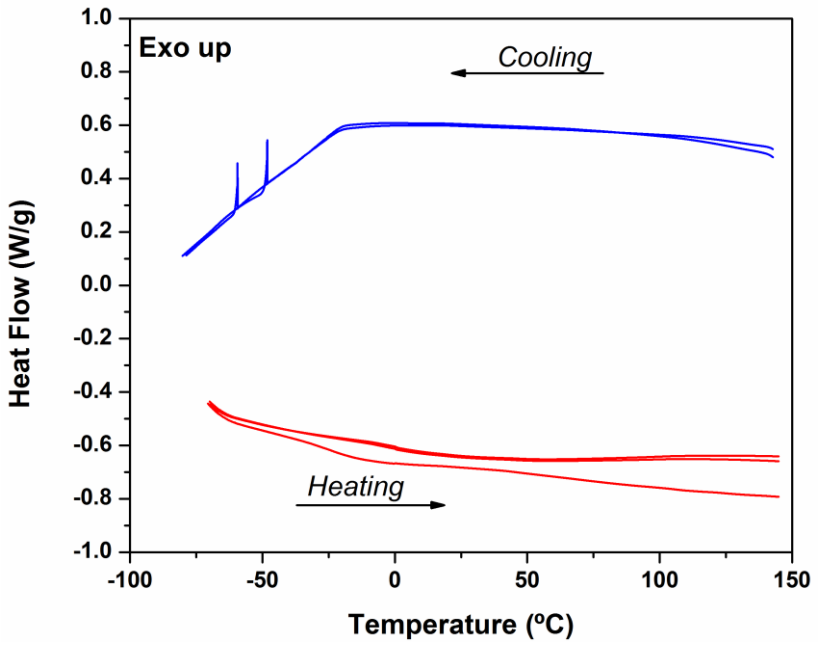

Figure 5.7 – Heat flow thermogram for **DAE 2** obtained at 20 ºC/min (heating/cooling rate), after the sample subjected to thermal cycling treatment to remove solvent content (1st cycle).

Additional studies could be carried out to confirm the assignment of that event to a glass transition, namely ageing experiments, i.e. annealing the sample during a certain time at a given temperature below to the possible glass transition. If the thermal event is a true glass transition, an overshoot due to structural relaxation should be couplet to the heat flux step detected upon further heating.

Phosphonium based on di-COOH dithienyethene (**DAE 3**) was also prepared through the same synthetic routes described before (Figure 5.8), which ^{1}H NMR spectra was analysed (Figure 5.9).

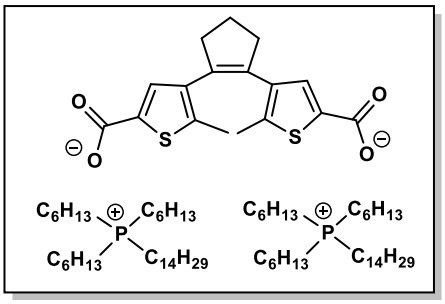

DAE 3

Figure 5.8 – Phosphonium based on di-COOH diarylethene derivative (**DAE 3**).

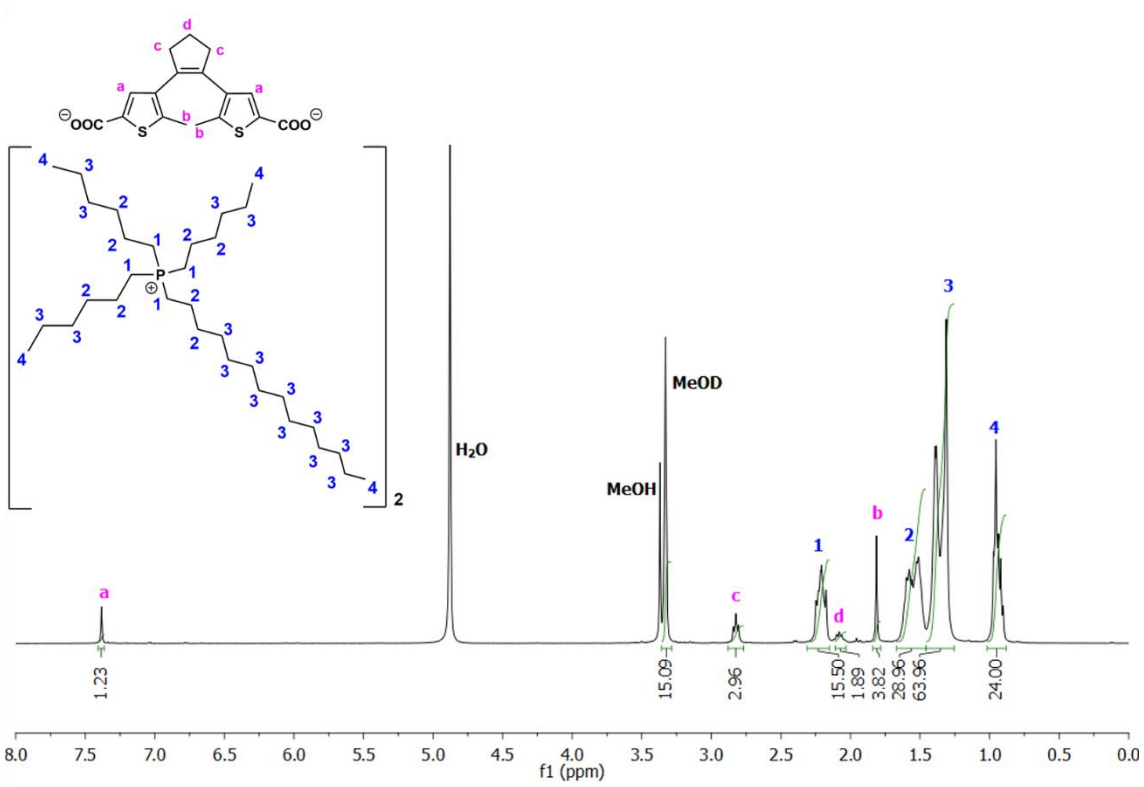

Figure 5.9 – ^{1}H NMR spectra in CD_3OD of **DAE 3**.

The analysis of the ^{1}H NMR spectrum reveals an excess of phosponium cation relative to the diarylethene anion. Comparison of the integration areas of the aromatic proton of di-COOH diarylethene anion (~7.38 ppm, **a**) and of the terminal protons of alkyl chains of phosponhium cation (~0.95 ppm, **4**) gives a proportion cation:anion of *ca.* 2:0.62. It may be possible to complete the acid-base reaction by addition of the adequate amount of di-COOH dithienyethene derivative to fulfil the required 2:1 stoichiometry.

5.2.2. Photochemical Behaviour

The photochemical behaviour of the di-acid compound (**DAE 1**) is well-described by Coudret and co-workers [64]. They studied quantitatively the gated photochromism and the acidity photomodulation properties of the neutral di-carboxylic acid dithienylethene compound. They observed that the photocyclization quantum yield of the di-acid species was around 90%, decreasing to 67 % after neutralization in order to obtain di-anion. They also reported a considerable difference in acidity with the closed-ring isomer being more acidic than the open-ring isomer by more than one pK_a unit [64].

Herein, a preliminary study of the photochemical behaviour in methanol solution and pure **DAE 2** IL was performed.

The solution of **DAE 2** in methanol was kept at 20 ºC during, approximately, 5 min before the irradiation, in order to stabilise the temperature of the sample. Then, it was irradiated at 248 nm, following the evolution of the system by UV-Vis spectroscopy (Figure 5.10).

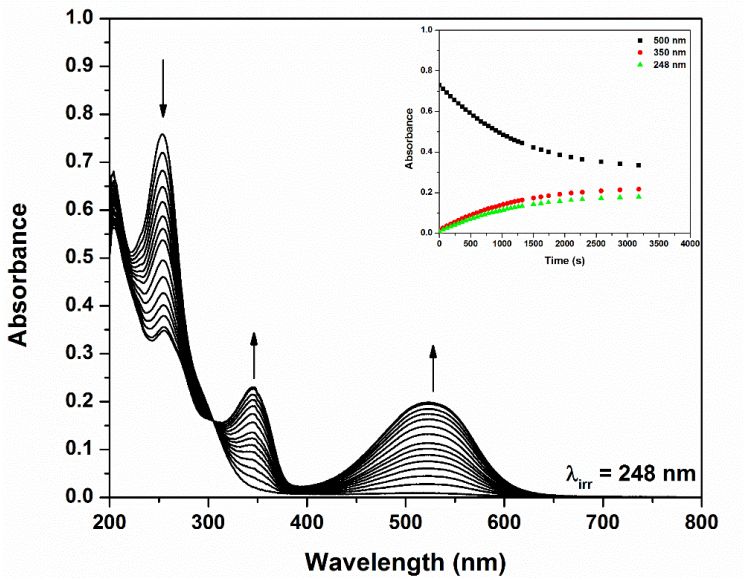

Figure 5.10 – Spectral variations upon irradiation of the solution of **DAE 2** in methanol, with baseline correction. Conditions: [**DAE 2**] = 2.7x10^{-5} M, T = 20 ºC, λ_{irr} = 248 nm. Irradiation times (s): 0, 60, 120, 240, 360, 480, 600, 720, 840, 1080, 1320, 1620, 1920, 2280, 2880, and 3180, until photostationary state is reached.

The spectrum of the open-ring form of **DAE 2** showed two characteristic bands, one at lower wavelength (well-defined peak at 256 nm) and other at higher wavelength band, which occurs under the form of a small shoulder close to 300 nm (Figure 5.10). The closed-ring form is obtained by irradiation at 248 nm until a photostationary state is reached. This closed-ring form showed three main bands: at higher wavelength a broad peak is clearly visible at 528 nm; a second peak is observed at 350 nm and it is also possible to observe a residual band at lower wavelength (~260 nm), which could be attributed to the open-ring form and thus, a slight red-shift is observed. The solution of **DAE 2** was kept in the dark for *ca.* 35 minutes (Figure 5.11) after conversion from open-ring form to closed-ring form and this experiment allowed us to proof the thermal stability of **DAE 2** over that time period.

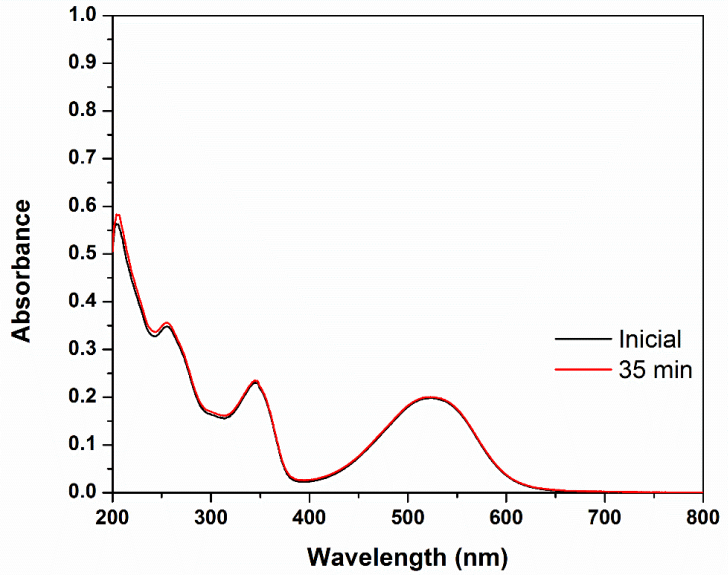

Figure 5.11 – Spectral variations of the solution of **DAE 2** in methanol after the photostationary state is reached (initial) and then ca. of 30 minutes in the dark (with baseline correction). Conditions: [**DAE 2**] = 2.7x10^{-5} M, T = 20 ºC.

The closed-ring form can be irradiated at *ca.* 350 nm (higher energetic band) or 528 nm (less energetic band). In this case, the solution of **DAE 2** was irradiated in the visible region at 500 nm and practically all closed form turned back to open form (Figure 5.12).

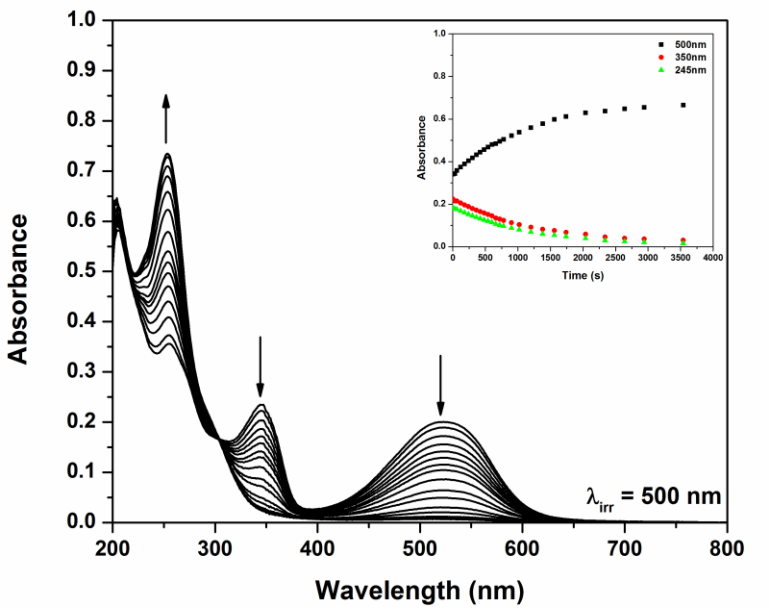

Figure 5.12 – Spectral variations upon irradiation of the solution of **DAE 2** in methanol, with baseline correction. Conditions: [**DAE 2**] = 2.7x10^{-5} M, T = 20 ºC, λ_{irr} = 500 nm. Irradiation times (s): 0, 60, 180, 300, 420, 540, 660, 780, 1020, 1380, 1740, 2340, 2940, 4140, 5340, and 7140. Inset: change in absorbance values at specified wavelengths with irradiation time.

The switch of colour of **DAE 2** in methanol solution upon irradiation at 248 nm during ca. 20 minutes is shown in Figure 5.13.

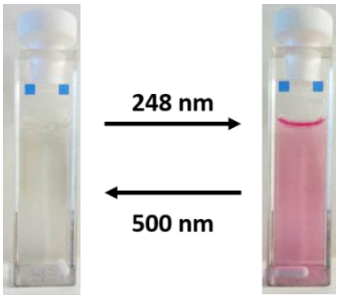

Figure 5.13 – Photo-switch of **DAE 2** in methanol (2.7x10^{-5} M) upon irradiation at 248 nm during 20 minutes. Previous studies showed that the system can turn back to initial state (reversible switch) upon irradiation at 500 nm.

The initial colour of **DAE 2** in methanol solution is transparent, corresponding to the open-ring form and upon irradiation at 248 nm a pink colour appears, due to the formation of the closed-ring form. This system seems to be totally reversible based on the previous results (Figure 5.12).

A preliminary study allowed to estimate the quantum yields for ring-closure (photocyclization) under UV irradiation (248 nm) and ring-opening (photocycloreversion) under visible light irradiation (500 nm) of the **DAE 2** IL in methanol solution. The quantum yields were determined using the "initial slope method", which considers only the first 10 % of the conversion between open-ring to closed-ring (or *vice-versa*) [65]. For the quantum yields based on ring-closure it is considered that in the beginning only open-ring isomers are present. It is assumed that the overall

absorbance at the irradiation wavelength is constant and the UV-light that would induce the back reaction can be neglected because only a very small amount of closed-ring isomer is formed during this period [65]. As a consequence, a linear relationship to estimate the quantum yield (Equation 5.1) can be used.

$$\phi = \frac{3 \times \frac{dA^{obs}(t)}{dt}}{1000 \times I_{abs} \times \Delta\varepsilon^{obs}} \quad and\ I_{abs} = I_0 \times (1 - 10^{-\overline{Abs}})$$

Equation 5.1

Where, ϕ is the quantum yield, I_{abs} corresponds to light intensity absorbed by the reagent (Einstein. min^{-1}), I_0 correspond to light intensity (Einstein. min^{-1}), $\Delta\varepsilon^{obs}$ corresponds to the difference in molar absorptivity of the product and reagent at the observed wavelength (L. mol^{-1}. cm^{-1}), Abs^{obs} corresponds to the absorbance at the observed wavelength and $\overline{Abs}$ corresponds to the average absorbance at the irradiation wavelength. Considering the absorbance recorded in the visible range ($Abs^{obs}(t)$) under steady-state light irradiation where only the ring-closed isomer absorbs and plotting that against irradiation time, the slope can be determined through a linear regression.

For the case of **DAE 2**, additional assumptions were used to estimate the cyclisation and cycloreversion quantum yields values: 1) the selected light intensity (I_0) value is close to the irradiation wavelength and 2) the extinction coefficient was determined as a single point measurement. Table 5.1 summarizes these results as well as those reported in the literature for similar systems, where the di-carboxylic acid dithienylethene compound acts as di-anion species.

Table 5.1 – Quantum yields for ring-closure (photocyclisation) and ring-opening (photocycloreversion) for the reported **DAE 1** as di-anion species [64] and **DAE 2**.

	DAE 1 [λ_{irr}] [a]	**DAE 2** [λ_{irr}] [b]
$\phi_{o\rightarrow c}$ [c]	0.67 [247 nm]	0.23 [248 nm] [d]
$\phi_{c\rightarrow o}$ [e]	0.025 [332 nm]	0.18 [500 nm] [f]

[a] in acetonitrile solution upon deprotonation with tetrabutylammonium hydroxide. [b] in methanol solution. [c] photocyclization quantum yield. [d] I_0 was determined using ferrioxalate as chemical actinometer at 255 nm. [e] photocycloreversion quantum yield. [f] I_0 was determined using ferrioxalate as chemical actinometer at 500 nm.

The **DAE 2** seems to have lower photocyclization quantum yield than di-acid **DAE 1**, which could be explained according to the anion effect during the photo-cyclization reaction but also the polarity effect from the solvent as reported in the literature [3,16]. On the contrary, the photocycloreversion quantum yield seems to be higher than that of **DAE 2**. As expected, the quantum yield of photocycloreversion is found to be smaller than that for the photocyclization. The quantum yield values obtained for **DAE 2** IL are very similar to those reported in the literature when imidazolium is incorporated in diarylethene structure and then combined with [PF_6] as anion [61]. In addition, non-linear regression for quantum yields calculation is also reported as alternative method for the “initial slope method” [64,65].

An extremely small amount of pure **DAE 2** IL was put between two lamellae of quartz and a thin film was obtained by pressing them. Two main bands, a well-defined peak at 256 nm with a small

shoulder close to 300 nm were observed. These results are similar to those obtained in methanol solution. The closed-ring form could be obtained upon irradiation of this film at 248 nm (Figure 5.14).

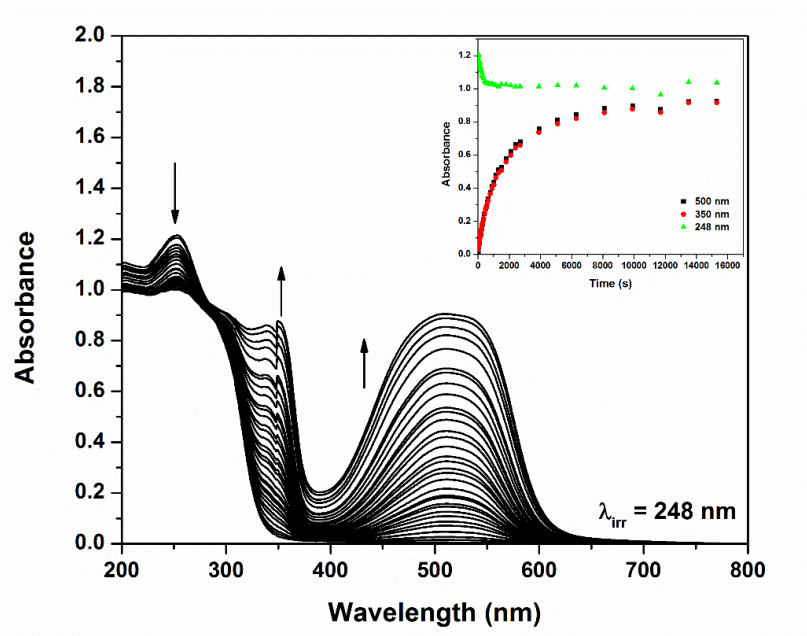

Figure 5.14 – Spectral variations upon irradiation of pure **DAE 2**, with baseline correction. Conditions: λ_{irr} = 248 nm, T = 20 ºC. Irradiation times (s): 0, 15, 30, 60, 120, 150, 180, 210, 240, 270, 300, 360, 420, 480, 540, 600, 660, 780, 900, 1020, 1140, 1320, 1500, 1800, 2100, 2400, 2700, 3900, 5100, 6300, 8100 and 9900. Inset: change in absorbance values at specified wavelengths with irradiation time.

The closed-ring form has two main bands at higher wavelengths, ca. 350 and 515 (broadly band). A residual band at lower wavelength, assignable to the open-ring form was also observed.

This film was kept in the dark overnight and a change in the spectrum was observed, i.e. an absorbance increment (Figure 5.15).

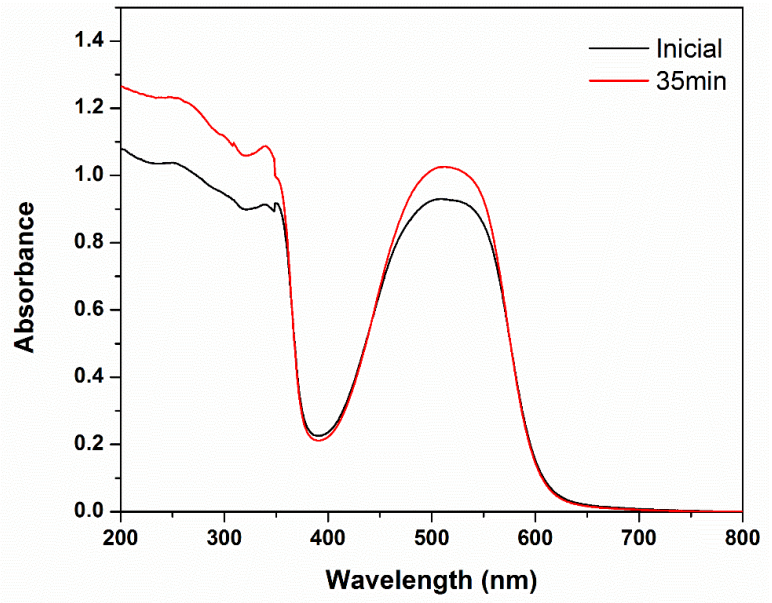

Figure 5.15 – Spectral variations of the solution of pure **DAE 2** when photostationary state is reached (initial) and after ca. of 35 minutes in the dark (with baseline correction).

The most reasonable explanation is related to heterogeneities in the film with the light beam passing through another area. This can in principle be improved by changing the deposition method, for example by the use of a volatile solvent for deposition of the **DAE 2** IL in the quartz lamellae.

The film was irradiated in the visible region (500 nm) and the closed-ring form was converted into open-ring form (Figure 5.16). The system seems to not totally recover to the initial state and some closed-ring form remains.

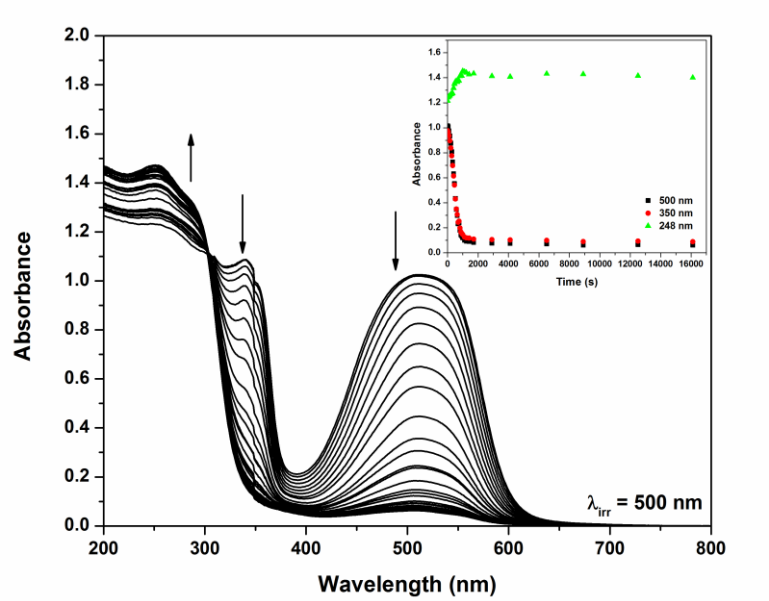

Figure 5.16 – Spectral variations upon irradiation of pure **DAE 2**, with baseline correction. Conditions: T = 20 ºC, λ_{irr} = 500 nm. Irradiation times (s): 0, 30, 90, 150, 210, 270, 330, 390, 450, 510, 570, 630, 690, 750, 810, 870, 930, 990, 1110, 1230, 1410, 1710, 2910, 4110, 6510, 8910, 12510 and 16110. Inset: change in absorbance values at specified wavelengths with irradiation time.

5.2.3. Electrochemical Behaviour

The electrochemical behaviour of the di-acid compound **DAE 1** was reported by Coudret and co-workers [36]. The open-ring isomer converts into the closed-ring isomer upon UV-light irradiation and the back reaction can be induced by visible-light irradiation or constant potential electrolysis as illustrated in Figure 5.17.

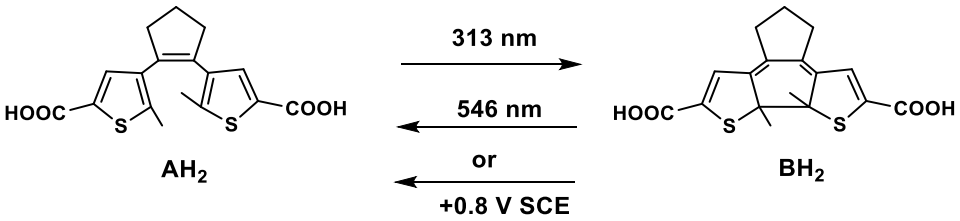

Figure 5.17 – Photo- and electrochemical interconversion processes between the open-ring isomer (AH_2) and the closed-ring isomer (BH_2) of di-carboxylic acid **DAE 1** in acetonitrile solution [36]. (Source: *Chem. Eur. J.*, 2013, **19**, 12435–12445.)

The authors investigated the electrochemical mechanism of the opening-ring (cycloreversion process) reaction through cyclic voltammetry at high scan rates and electrochemical simulation techniques [36]. They described that the electron-transfer process is mono-electronic (one electron)

and all the closed-ring isomer derivatives, independently of their protonation states, undergo fast oxidation at the electrode surface and then, a first-order chemical reaction occurs. This oxidation process is accompanied by a decolouration of the sample [36]. So, the electrochemical behaviour of open- and closed-ring isomers for the di-acid, mono-anion and di-anion were studied. In addition, the authors reported no dependence for any of the closed-ring isomers of di-acid derivatives between the anodic peak potential value and the logarithm of the concentration, i.e. the Nernst equation it is not followed [36].

A preliminary electrochemical study of the **DAE 2 IL** in solution was performed and the anodic peak potentials of the open- and closed-ring isomers as well as those reported for **DAE 1** (di-acid, mono-anion and di-anion) [36] are presented in Table 5.2.

Table 5.2 – Anodic peak potentials of **DAE 1** [36] and **DAE 2**.

Compound (protonation states)	E_{pa} vs SCE [V]	
	DAE 1[a]	**DAE 2** [b]
Closed/ closed$^{\bullet+}$ (di-acid)	0.85	[c]
Closed^{-}/ closed$^{\bullet}$ (mono-anion)	0.57	[c]
Closed $^{2-}$/ closed$^{\bullet-}$ (di-anion)	0.33	0.42
Open/ open$^{\bullet+}$ (di-acid)	1.44	1.32
Open^{-}/ open$^{\bullet}$ (mono-anion)	1.12	1.09
Open $^{2-}$/ open$^{\bullet-}$ (di-anion)	0.87	0.82

[a] **DAE 1** was dissolved in acetonitrile (10^{-3} M) with tetrabutylammonium tetrafluoroborate [TBA][BF_4] (0.1 M).The working, auxiliary and reference electrodes of glassy carbon (GC), platinum disk and saturated calomel electrode (SCE), respectively were used [36]. The closed^{-}/closed^{2-} (mono to di-anion) were obtained by titration of the closed protonated **DAE 1** form by using a solution of tetrabutylammonium hydroxide (70 mM) in acetonitrile [36]. [b] **DAE 2** was dissolved in acetonitrile with *ca.* 5-10 % of methanol (10^{-3} – 10^{-4} M) and tetrabutylammonium tetrafluoroborate [TBA][BF_4] (0.1M). CV was acquired at 0.1 V.s^{-1}.The working, auxiliary and reference electrodes of glassy carbon (GC), Pt wire and saturated calomel electrode (SCE), respectively were used [36]. [c] Anodic peaks detected were vestigial. +

The **DAE 2** showed lower solubility in pure acetonitrile and for that reason a small amount of methanol was added. Although, methanol could perturb the **DAE 2** electrochemical behaviour, since it is reported that the radical species can react in the presence of solvents able to transfer hydrogen atom [36,66,67] or through a Kolbe-type mechanism [36,68]. The open-ring isomer of **DAE 2** was studied and three oxidation waves, which can be attributed to the di-anion, mono-anion and di-acid species, were detected. One possible explanation for this behaviour is the presence of methanol in the solution, which can act as hydrogen-atom donor and consequently can react with radical species upon oxidation process.

Additional electrochemical studies are required in order to elucidate this indication and other alternative solvents should be tested. In the case of closed-ring isomer, oxidation wave close to 0.82 V (*vs.* SCE), which can be attributed to the di-anion species was detected. However, residual oxidation waves are also detected, which can correspond to another species. It is important to mention that additional studies will be required in order to clarify the electrochemical behaviour of **DAE 2**.

5.3. Conclusions

In this work, ionic diarylethene derivatives possessing two carboxylic acid units were prepared. The diarylethene scaffold is used as anion and then combined with appropriate organic cations to obtain ILs. In this context, it was possible to obtain a RTIL, using tri-octyl methylammonium as cationic unit.

The photochemical behaviour in solution was investigated and similar behaviour to the free di-acid compound, already published in the literature, was observed. Upon irradiation with UV light, the open-ring isomer converts into the closed-ring one with its characteristic bands in the visible range. Preliminary studies on the thermal stability of this isomer have shown that the IL is stable in the dark. The back reaction was induced by irradiation in the visible with practically full recovery of the initial state. The quantum yields of ring-closure and ring-opening have been estimated through “initial slope method”. The quantum yield of photocyclization is smaller than that reported in the literature for the di-anion species. As expected, the quantum yield for photocyclization is found to be smaller than photocycloreversion. The pure IL was also studied as a thin film and it showed a photochromic behaviour identical to observed in solution.

A preliminary electrochemical study of this IL in solution was performed and oxidation waves were detected according to those reported in the literature.

It was then possible to develop RTILs based on diarylethene derivatives, which can present response to electric and light stimuli, obtaining dual stimuli-responsive material. The development of ionic diarylethene derivatives opens good perspectives for appropriate combination between anions (different anionic units) and cations (with or without additional functionality) in order to improve their properties and obtain a multi stimuli-responsive material.

5.4. Experimental Part

Solvent and Reagents for synthesis

Benzene (Merck), methanol (Sigma-Aldrich), tetrahydrofuran (THF) (Scharlau), diethyl ether (LabChem), *n*-hexane (LabChem), ethyl acetate (LabChem), dichloromethane (LabChem), Acetic Acid (Merck), sodium hydroxide (Eka), sodium sulfate anhydrous (Carbo Erba), Potassium carbonate (K_2CO_3, Riedel-de Haen). 2-Methyltiophene (Alfa Aesar, 98 %), *N*-chlorosuccinimide (Aldrich, 98 %), Glutaryl Chloride (Aldrich, 97 %), Diphenylacetic acid (Aldrich, 99 %), Aluminium Chloride ($AlCl_3$, Sigma Aldrich, ≥ 99 %), carbon disulfide (Aldrich, > 99.9 %), Zn dust (Fluka, ≥ 99 %), titanium tetrachloride (Aldrich, ≥ 99 %), *tert*-butyl lithium (Pentane solution, Aldrich), hydrochloric acid (Sigma-Aldrich), [ALIQUAT]Cl (Aldrich, > 98 %), $[P_{6,6,6,14}]Cl$ (Cytec, > 98 %) were used as received. The basic anion-exchange resin Amberlyst A26-(OH) (ion-exchange capacity 1.4 eq. mL^{-1}, Alfa Aesar) and Flash Chromatography (230-400 mesh, Sigma-Aldrich) was used as received.

NMR Spectroscopy

NMR spectra were done on a Bruker AMX 400 instrument operating at 400.13 MHz (^1H), 100.61 MHz (^{13}C). The NMR spectrometers are part of The National NMR Facility supported by Fundação para a Ciência e a Tecnologia (RECI/BBB-BQB/0230/2012).

Elemental analysis

Elemental analysis was obtained on a Thermofinnigan Flash EA 1112 Series instrument and was performed by the Laboratório de Análises at LAQV/UCIBIO – REQUIMTE.

Thermal analysis

TA Instruments Q-series TM Q2000 DSC with a refrigerated cooling system was also used. The sample is continuously purged with 50 ml/min nitrogen. About 2.610 mg of salt was crimped in an aluminium hermetic sample pan with a lid.

Electrochemical studies

Acetonitrile (Sigma-Aldrich, HPLC grade) and methanol (Sigma-Aldrich) were used as received. Tetrabutylammonium tetrafluoroborate ([TBA][BF_4]) was purchased from Sigma-Aldrich (99 %) and was dried overnight at 100 ºC before use. Cyclic voltammetry (CV) measurements were performed on an Autolab PGSTAT 12 potentiostat/galvanostat, controlled with GPES software version 4.9 (Eco-Chemie), using a cylindrical three electrode cell of 5 mL. A glassy carbon (BAS inc.) electrode was used as the working electrode and Pt wire was used as an auxiliary electrode. All potentials refer to an SCE (3 M KCl) reference electrode (Metrohm). Prior to use, the working electrode was polished in aqueous suspensions of 1.0 and 0.3 µm alumina (Beuhler) over 2-7/8" micro-cloth (Beuhler) polishing pads, then rinsed with water and methanol or acetonitrile.

Photochemical studies

Photo-excitation in continuous irradiation experiments was carried out with a Xe lamp (450W) using a monochromator. The photochromic solution was stirred with a magnetic bar in a 1 cm^{-1} x 1 cm^{-1} quartz cell.

UV-Visible spectroscopy

UV-Visible spectroscopy was done using Varian Cary 100 Bio spectrophotometer at room temperature or using a thermostatized bath to keep the sample at the selected temperature.

Synthesis

2-Chloro-5-methylthiophene

This compound was prepared according to a synthetic procedure previously reported in the literature [62]. 2-Methylthiophene (12.3 mL, 0.11 mol) and *N*-chlorosuccinimide (15.529 g, 0.12 mol) were added to a stirred solution of benzene (40 mL) and acetic acid (40 mL). The suspension was stirred for *ca.* 30 minutes at room temperature and then heated in reflux for *ca.* 1.5 hours. After that, the cooled mixture was poured into a 3 M aqueous sodium hydroxide solution (30 mL). The organic phase was washed with 3 M sodium hydroxide aqueous solution (5 x 30 mL), dried over anhydrous sodium sulfate (Na_2SO_4), filtered and the solvent evaporated. The product was dried under vacuum yielding a slightly yellow liquid (4.977 g, 36 %). ^{1}H NMR (400.13 MHz, $CDCl_3$, 25 ºC) δ = 6.69 (d, J = 3.6 Hz, 1 H), 6.57-6.48 (m, 1 H), 2.41 (s, 6 H) ppm. ^{13}C NMR (100.61 MHz, $CDCl_3$, 25 ºC) δ = 138.5, 126.5, 126.2, 125.8, 124.4, 15.5 ppm.

1,5-Bis(5-chloro-2-methylthien-3-yl)pentane-1,5-dione

This compound was prepared according to a synthetic procedure previously reported in the literature [62]. Under vigorous stirring aluminium chloride, $AlCl_3$ (2.237 g, 16.78 mmol) was slowly added in portions and to an ice-cooled solution of 2-chloro-5-methylthiophene (1.5 mL, 13.69 mmol) and glutaryl dichloride (0.89 mL, 6.97 mmol) in carbon disulphide CS_2 (14 mL). The reaction mixture was then stirred for 2.5 h at room temperature. Ice-cold water (10 mL) was carefully added to the reaction mixture and the water layer extracted with diethyl ether (3 x 15 mL). The combined organic phases were washed with water (1 x 10 mL), dried over anhydrous sodium sulfate (Na_2SO_4) and the solvent removed. The product was dried under vacuum to yield a brown tar. This tar can be purified by flash chromatography, using *n*-hexane/ethyl acetate (9:1) to provide a white solid (0.245 g, 47 %). ^{1}H NMR (400.13 MHz, $CDCl_3$, 25 ºC) δ =7.18 (s, 2 H), 2.86 (t, J = 6.9 Hz, 2 H), 2.66 (s, 6 H), 2.12 - 2.01 (m, 2 H) ppm. ^{13}C NMR (100.61 MHz, $CDCl_3$, 25 ºC) δ = 194.9, 147.8, 134.9, 126.8, 125.3, 40.5, 18.2, 16.1 ppm.

1,2-Bis(5-chloro-2-methylthien-3-yl)cyclopentene

This compound was prepared according to a synthetic procedure previously reported in the literature [62]. Dried THF (15 mL) and Zn dust (0.879 g, 13.45 mmol) were placed in a two-necked flask under nitrogen atmosphere, upon vacuum-nitrogen cycles. Titanium tetrachloride $TiCl_4$ (0.72 mL, 6.55 mmol) was carefully and slowly added to the suspension after, which it was heated to reflux for ca. 1 hour. Then the reaction mixture was cooled in an ice bath and a solution of 1,5-bis(5-chloro-2-methylthien-3-yl)pentane-1,5-dione (1.685 g, 4.66 mmol) in THF (9 mL) was slowly added under nitrogen atmosphere. After that, the mixture was refluxed for ca. 2.5 hours, subsequently quenched with 10 % aqueous solution of potassium carbonate (K_2CO_3) (35 mL) and extracted with diethyl ether (8 x 80 mL). The combined organic layers were washed with water

(two times) and dried over anhydrous sodium sulfate (Na_2SO_4). The desired product was dissolved in dichloromethane and purified by column chromatography using *n*-hexane as eluent to give a pale yellow solid (1.195 g, 78 %). ^{1}H NMR (400.13 MHz, $CDCl_3$, 25 ºC) δ =6.57 (s, 2 H), 2.71 (t, J = 7.4 Hz, 4 H), 2.09 – 1.97 (m, 2 H), 1.89 (s, 6 H) ppm.^{13}C NMR (100.61 MHz, $CDCl_3$, 25 ºC) δ = 134.8, 134.4, 133.3, 126.7, 125.2, 38.3, 22.8, 14.2 ppm.

1,2-Bis(5'-carboxy-2'-methylthien-3'-yl)-cyclopentene (DAE 1)

This compound was prepared according to a synthetic procedure previously reported in the literature [35]. Previously, to the reaction, the *tert*-butyl lithium concentration was determined through a titration using diphenylacetic acid in dried THF. It was found to be *ca*. 1.5 M in *n*-pentane solution. To a solution of 1,2-bis(5′-chloro-2′-methylthien-3′-yl)-cyclopentene (0.406 g, 1.23 mmol) in THF (20 mL) cooled to -78 ºC (acetone-liquid nitrogen slash), *tert*-butyl lithium (2.6 mL of a 1.5 M solution in pentane) was carefully and slowly added under nitrogen atmosphere. At the same time, an ice-cooled solution of THF was saturated with CO_2. After 1.5 hour the reaction mixture was transferred under nitrogen using a cannula to 160 mL of the CO_2-THF saturated solution. The reaction was allowed to warm to room temperature and stirred during 2.5 hours. The THF was removed and dichloromethane (100 mL) was added to the residue. The residue was partitioned and washed with 5 % sodium hydroxide aqueous solution (4 x 100 mL). The combined aqueous layers were acidified by dropwise addition of concentrated hydrochloric acid (HCl) until pH = 1. The resulting white precipitate was collected by filtration and washed twice with cold dichloromethane to remove the monoacid, then dried in vacuum affording the pure di-acid as a white solid (0.304 g, 71 %). ^{1}H NMR (400.13 MHz, CD_3OD, 25 ºC) δ = 7.48 (s, 2 H), 2.82 (t, J = 7.1 Hz, 4 H), 2.16 – 2.04 (m, 2 H), 1.97 (s, 6 H) ppm. ^{13}C NMR (100.61 MHz, MeOD, 25 ºC) δ = 163.8, 142.7, 136.6, 134.9, 134.3, 130.1, 34.0, 22.5, 13.4 ppm. Elemental Analysis calcd (%) for $C_{17}H_{16}O_4S_2.1H_2O$: C 55.72, H 4.95; found C 55.73, H 4.45.

DAE 2

Amberlyst A26 (OH) (~ 3mL; 2.7 equivalents) was added to [ALIQUAT]Cl (0.353 g, 0.87 mmol) in methanol solution (40 mL) and the suspension was stirred at room temperature during 1 hour. The resin was removed by filtration and [ALIQUAT]OH was slowly added to **DAE 1** (0.150 g, 0.43 mmol) in methanol solution (30 mL) and stirred at room temperature during ca. 21 hours in the dark. The solvent was removed and the desired product was dried at 40 ºC in vacuum to give a brown liquid (0.440 g, 94 %). ^{1}H NMR (400.13 MHz, MeOD, 25 ºC) δ = 7.36 (s, 2 H), 3.29 - 3.19 (m, 12 H), 3.00 (s, 6 H), 2.80 (t, J = 7.4 Hz, 4H), 2.12 – 2.02 (m, 2 H), 1.82 (s, 6 H), 1.77 – 1.60 (m, 12 H), 1.47-1.22 (m, 64 H), 1.22 (s, 18 H) ppm. ^{13}C NMR (100.61 MHz, MeOD, 25 º C) δ = 138.7, 138.2, 136.1, 134.4, 130.8, 61.3, 38.4, 31.6, 31.5, 29.2, 29.1, 29.0, 28.8, 26.0, 22.3, 21.7, 13.4, 13.0 ppm. Elemental Analysis calcd (%) for $C_{17}H_{122}N_2O_4S_2.3H_2O$: C 70.72, H 11.34, N 2.46; found C 70.91, H 11.05, N 2.27.

DAE 3

Amberlyst A26 (OH) (~ 5mL; 4.6 equivalents) was added to $[P_{6,6,6,14}]Cl$ (0.456 g, 0.88 mmol) in methanol solution (40 mL) and the suspension was stirred at room temperature during 1 hour. The resin was removed by filtration and $[P_{6,6,6,14}]OH$ was slowly added to **DAE 1** (0.150 g, 0.431 mmol) in methanol solution (45 mL) and stirred at room temperature during ca. 22 hours in the dark. The solvent was removed and the desired product was dried at 40 ºC in vacuum to give a brown liquid. The ^1H NMR analysis showed an excess of $[P_{6,6,6,14}]OH$ relative to **DAE 1** and futher purification should be performed. ^1H NMR (400.13 MHz, MeOD, 25 ºC) δ = 7.36 (s), 2.80 (t, J = 7.4 Hz), 2.29 – 2.12 (m), 1.79 (s), 1.68 – 1.21 (m), 1.01 – 0.82 ppm.

5.5. References

1 K. Matsuda and M. Irie, *J. Photochem. Photobiol. C Photochem. Rev.*, 2004, **5**, 169–182.

2 M. Irie, *Chem. Rev.*, 2000, **100**, 1685–1716.

3 M. Irie, T. Fukaminato, K. Matsuda and S. Kobatake, *Chem. Rev.*, 2014, **114**, 12174–12277.

4 K. Uchida, E. Tsuchida, Y. Aoi, S. Nakamura and M. Irie, *Chem. Lett.*, 1999, 63–64.

5 T. Yamaguchi and M. Irie, *J. Photochem. Photobiol. A Chem.*, 2006, **178**, 162–169.

6 M. Takeshita and M. Irie, *Chem. Commun.*, 1997, 2265–2266.

7 M. Takeshita, N. Kato, S. Kawauchi, T. Imase, J. Watanabe and M. Irie, *J. Org. Chem.*, 1998, **63**, 9306–9313.

8 M. Takeshita, M. Yamada, N. Kato and M. Irie, *J. Chem. Soc., Perkin Trans. 2*, 2000, 619–622.

9 F. Stellacci, C. Bertarelli, F. Toscano, M. C. Gallazzi, G. Zotti and G. Zerbi, *Adv. Mater.*, 1999, **11**, 292–295.

10 K. Matsuda, Y. Shinkai, T. Yamaguchi, K. Nomiyama, M. Isayama and M. Irie, *Chem. Lett.*, 2003, **32**, 1178–1179.

11 M. K. Hossain, M. Takeshita and T. Yamato, *Tetrahedron Lett.*, 2005, **46**, 431–433.

12 M. Takeshita, C. Tanaka, T. Miyazaki, Y. Fukushima and M. Nagai, *New J. Chem.*, 2009, **33**, 1433–1438.

13 M. K. Hossain, M. Takeshita and T. Yamato, *Eur. J. Org. Chem.*, 2005, 2771–2776.

14 M. Takeshita and S. Yamaguchi, *Chem. Lett.*, 2011, **40**, 646–647.

15 S. Fukumoto, T. Nakashima and T. Kawai, *Angew. Chem., Int. Ed.*, 2011, **50**, 1565–1568.

16 M. Irie and K. Sayo, *J. Phys. Chem.*, 1992, **96**, 7671–7674.

17 M. Irie, T. Eriguchi, T. Takada and K. Uchida, *Tetrahedron*, 1997, **53**, 12263–12271.

18 A. T. Bens, D. Frewert, K. Kodatis, C. Kryschi, H. Martin and H. P. Trommsdorff, *Eur. J. Org. Chem.*, 1998, 2333–2338.

19 M. Hanazawa, R. Sumiya, Y. Horikawa and M. Irie, *J. Chem. Soc., Chem. Commun.*, 1992, 206–207.

20 H. Jean-Ruel, R. R. Cooney, M. Gao, C. Lu, M. A. Kochman, C. A. Morrison and R. J. D. Miller, *J. Phys. Chem. A*, 2011, **115**, 13158–13168.

21 M.-S. Kim, T. Kawai and M. Irie, *Chem. Lett.*, 2001, **30**, 702–703.

22 K. Yagi and M. Irie, *Chem. Lett.*, 2003, **32**, 848–849.

23 M.-S. Kim, T. Kawai and M. Irie, *Opt. Mater.*, 2003, **21**, 271–274.

24 K. Yagi and M. Irie, *Bull. Chem. Soc. Jpn.*, 2003, **76**, 1625–1628.

25 V. F. Traven, A. Y. Bochkov, M. M. Krayushkin, V. N. Yarovenko, V. A. Barachevsky and I. P. Beletskaya, *Mendeleev Commun.*, 2010, **20**, 22–24.

26 N. I. Makarova, P. V Levchenko, E. N. Shepelenko, A. V Metelitsa, V. S. Kozyrev, V. P. Rybalkin, V. A. Bren' and V. I. Minkin, *Russ. Chem. Bull.*, 2011, **60**, 1899–1905.

27 S. Pu, G. Liu, L. Shen and J. Xu, *Org. Lett.*, 2007, **9**, 2139–2142.

28 R. Wang, S. Pu, G. Liu, S. Cui and W. Liu, *J. Photochem. Photobiol. A Chem.*, 2012, **243**,

47–55.

29 T. Kawai, M.-S. Kim, T. Sasaki and M. Irie, *Opt. Mater.*, 2003, **21**, 275–278.

30 A. E. Keirstead, J. W. Bridgewater, Y. Terazono, G. Kodis, S. Straight, P. A. Liddell, A. L. Moore, T. A. Moore and D. Gust, *J. Am. Chem. Soc.*, 2010, **132**, 6588–6595.

31 N. Soh, K. Yoshida, H. Nakajima, K. Nakano, T. Imato, T. Fukaminato and M. Irie, *Chem. Commun.*, 2007, 5206–5208.

32 H. Zheng, W. Zhou, M. Yuan, X. Yin, Z. Zuo, C. Ouyang, H. Liu, Y. Li and D. Zhu, *Tetrahedron Lett.*, 2009, **50**, 1588–1592.

33 B. Gorodetsky, H. D. Samachetty, R. L. Donkers, M. S. Workentin and N. R. Branda, *Angew. Chem., Int. Ed.*, 2004, **43**, 2812–2815.

34 B. Gorodetsky and N. R. Branda, *Adv. Funct. Mater.*, 2007, **17**, 786–796.

35 G. Guirado, C. Coudret, M. Hliwa and J.-P. Launay, *J. Phys. Chem. B*, 2005, **109**, 17445–17459.

36 J. Massaad, J.-C. Micheau, C. Coudret, C. L. Serpentini and G. Guirado, *Chem. Eur. J.*, 2013, **19**, 12435–12445.

37 T. Koshido, T. Kawai and K. Yoshino, *J. Phys. Chem.*, 1995, **99**, 6110–6114.

38 J. Areephong, W. R. Browne, N. Katsonis and B. L. Feringa, *Chem. Commun.*, 2006, 3930–3932.

39 R. Baron, A. Onopriyenko, E. Katz, O. Lioubashevski, I. Willner, S. Wang and H. Tian, *Chem. Commun.*, 2006, 2147–2149.

40 D. Kim, H. Jeong, H. Lee, W.-T. Hwang, J. Wolf, E. Scheer, T. Huhn, H. Jeong and T. Lee, *Adv. Mater.*, 2014, **26**, 3968–3973.

41 H. Miyasaka, M. Murakami, T. Okada, Y. Nagata, A. Itaya, S. Kobatake and M. Irie, *Chem. Phys. Lett.*, 2003, **371**, 40–48.

42 H. Miyasaka, M. Murakami, A. Itaya, D. Guillaumont, S. Nakamura and M. Irie, *J. Am. Chem. Soc.*, 2001, **123**, 753–754.

43 M. Murakami, H. Miyasaka, T. Okada, S. Kobatake and M. Irie, *J. Am. Chem. Soc.*, 2004, **126**, 14764–14772.

44 Y. Ishibashi, K. Tani, H. Miyasaka, S. Kobatake and M. Irie, *Chem. Phys. Lett.*, 2007, **437**, 243–247.

45 S. Ryo, Y. Ishibashi, M. Murakami, H. Miyasaka, S. Kobatake and M. Irie, *J. Phys. Org. Chem.*, 2007, **20**, 953–959.

46 K. Tani, Y. Ishibashi, H. Miyasaka, S. Kobatake and M. Irie, *J. Phys. Chem. C*, 2008, **112**, 11150–11157.

47 Y. Ishibashi, M. Mukaida, M. Falkenstrom, H. Miyasaka, S. Kobatake and M. Irie, *Phys. Chem. Chem. Phys.*, 2009, **11**, 2640–2648.

48 Y. Ishibashi, K. Okuno, C. Ota, T. Umesato, T. Katayama, M. Murakami, S. Kobatake, M. Irie and H. Miyasaka, *Photochem. Photobiol. Sci.*, 2010, **9**, 172–180.

49 J. Piard, Y. Ishibashi, H. Saito, R. Métivier, K. Nakatani, G. Gavrel, P. Yu and H. Miyasaka, *J. Photochem. Photobiol. A Chem.*, 2012, **234**, 57–65.

50 M. Ohsumi, T. Fukaminato and M. Irie, *Chem. Commun.*, 2005, 3921–3923.

51 F. Nourmohammadian, T. Wu and N. R. Branda, *Chem. Commun.*, 2011, **47**, 10954–10956.

52 J. Kühni and P. Belser, *Org. Lett.*, 2007, **9**, 1915–1918.

53 V. Lemieux and N. R. Branda, *Org. Lett.*, 2005, **7**, 2969–2972.

54 K. Yumoto, M. Irie and K. Matsuda, *Org. Lett.*, 2008, **10**, 2051–2054.

55 H.-H. Liu and Y. Chen, *J. Photochem. Photobiol. A Chem.*, 2010, **215**, 103–107.

56 B. Song, H. Li, L. Yang, C. Zhao, H. Sai, S. Zhang, F. Zhang and J. Xiang, *J. Photochem. Photobiol. A Chem.*, 2012, **241**, 21–25.

57 Y. Kutsunugi, C. Coudret, J. C. Micheau and T. Kawai, *Dye. Pigment.*, 2012, **92**, 838–846.

58 T. Nakashima, K. Miyamura, T. Sakai and T. Kawai, *Chem. Eur. J.*, 2009, **15**, 1977–1984.

59 F. Pina and L. Branco, in *Ionic Liquids: Theory, Properties, New Approaches*, ed. A. Kokorin, InTech, 2011, pp. 139–166.

60 V. W.-W. Yam, J. K.-W. Lee, C.-C. Ko and N. Zhu, *J. Am. Chem. Soc.*, 2009, **131**, 912–913.

61 G. Duan, N. Zhu and V. W.-W. Yam, *Chem. Eur. J.*, 2010, **16**, 13199–13209.

62 L. N. Lucas, J. J. D. de Jong, J. H. van Esch, R. M. Kellogg and B. L. Feringa, *Eur. J. Org. Chem.*, 2003, 155–166.

63 E. Dudognon, F. Danède, M. Descamps and N. T. Correia, *Pharm. Res.*, 2008, **25**, 2853–2858.

64 J. Massaad, J.-C. Micheau, C. Coudret, R. Sanchez, G. Guirado and S. Delbaere, *Chem. Eur. J.*, 2012, **18**, 6568–6575.

65 M. Herder, PhD Thesis, Mathematisch-Naturwissenschaftliche Fakultät der Humboldt-Universität zu Berlin, 2015.

66 F. M'Halla, J. Pinson and J. M. Saveant, *J. Am. Chem. Soc.*, 1980, **102**, 4120–4127.

67 C. P. Andrieux, J. Badoz-Lambling, C. Combellas, D. Lacombe, J. M. Saveant, A. Thiebault and D. Zann, *J. Am. Chem. Soc.*, 1987, **109**, 1518–1525.

68 C. P. Andrieux, F. Gonzalez and J.-M. Savéant, *J. Electroanal. Chem.*, 2001, **498**, 171–180.

6. Multi stimuli-responsive Polymer

Publications associated with this chapter:

N. Jordão, R. Gavara and A. J. Parola, *Macromolecules*, 2013, **46**, 9055 – 9063.

6. Multi stimuli-responsive Polymer

6.1. Introduction

Polymers as multi stimuli-responsive materials have attracted much interest due to their ability to respond to external stimuli (e.g. pH, temperature, light, ionic strength, electron-transfer and host-guest interactions), even small environmental variations by changing their properties [1-4].

In this context, the incorporation of different functional moieties within one polymer can be efficiently explored in order to obtain dual or multi stimuli-responsive materials as well as to be the starting point to more sophisticated applications [2]. Hence, the adequate combination of responsive groups can contribute to design of a multi-functional polymer, which exhibits a stimuli-responsive behaviour according to our demands [2].

6.1.1. Poly(N-isopropylacrylamide)

In last decades, thermo-responsive polymers have been explored due to their ability to respond to temperature changes, occurring modification of the solvation state (change of volume phase). They can become insoluble upon heating exhibit a lower critical solution temperature (LCST) or become soluble upon heating exhibit an upper critical solution temperature (UCST) [2,4].

One of the most commonly and successfully thermo-responsive polymer is Poly(*N*-isopropylacrylamide) (PNIPAm) (see Figure 6.1), which exhibit a lower critical solution temperature (LCST) in water around 32 ºC [5]. This LCST value depends on several factors such as molecular weight [6] and concentration [7].

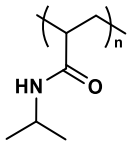

Figure 6.1 – Poly(*N*-isopropylacrylamide) (PNIPAm).

LCST is defined as the critical temperature at which a polymer solution undergoes phase transition from a soluble (T<LCST) to an insoluble state (T>LCST) [6]. Below the LCST, the polymer is solvated in water due to the hydrogen bonding interactions with the surrounding water molecules and the amide groups of the polymeric chains. Heating the polymer above the LCST, hydrogen bonding with water is disrupted, consequently collapsing and precipitation of the polymer occurs (see Figure 6.2) [8].

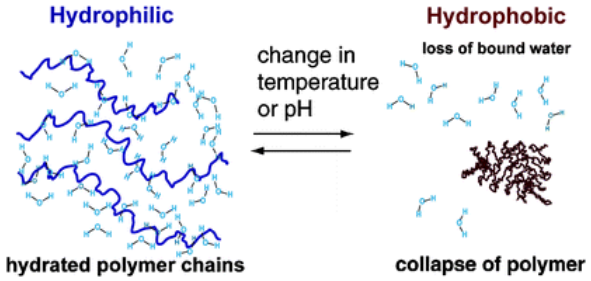

Figure 6.2 – LCST of PNIPAm in water [9]. (Source: *Chem. Soc. Rev*., 2005, **34**, 276–85).

PNIPAm have attracted much research interest over the years, mainly because its LCST occurs close to the human body temperature. This feature made this neutral water soluble polymer very promising for biotechnological applications, such as drug delivery, tissue engineering and cell sheet engineering [10–12]. Also, for tunable optical devices and chromatographic separations [13,14]. If the temperature of PNIPAm solution in water is changed, its solubility behaviour can be modified from soluble to insoluble or vice-versa, and it can, thus, be triggered externally [11]. Different examples have been reported in the literature, in particular the preparation of amphiphilic block co-polymers prepared with PNIPAm, which can form a stable core-shell-type micelle in aqueous solution. When heating the solution to a higher temperature over LCST of PNIPAm, the micellar structures collapses and the drug is released [15–18]. Okano and co-workers also reported the use of PNIPAm hydrogel for thermo-responsive drug delivery systems. The drug can be released from the hydrogel matrix during the shrinking of PNIPAm hydrogel by heating the system above the LCST [15,19]. Recently, the application of PNIPAm in regenerative medicine have been explored in particular examples where PNIPAm is modified on substrate, from that a reversible cell attachment and detachment in response to temperature can be observed [15]. In addition, it is possible to adjust the LCST of PNIPAm by co-polymerization with hydrophilic or hydrophobic monomers for several biomedical applications [9].

Light as stimulus has also become interesting in the field of stimuli-responsive polymers, once it can also be triggered from outside of the system. Indeed, the light-responsive behaviour can be started or stopped when the light is switched on or off and generate only limited amount of by-products, since no additional reagents are required [11,20]. It is also possible adjust different parameters such as light intensity and its wavelength, which enables good control over the reaction.

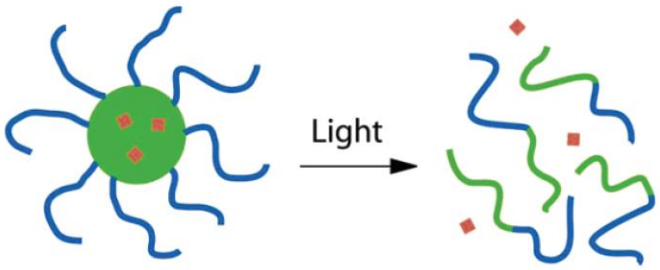

Figure 6.3 – Schematic illustration of drug release triggered by light. An encapsulated agent is released as a result of the photo-induced dissociation of the polymer micelles [21]. (Source: *Macromolecules*, 2006, **39**, 4633–4640).

In addition, even one light-responsive unit incorporated into the polymer can be enough to influence the properties of the whole polymer chain [11]. This light-responsive unit can be attached to the polymeric backbone or terminal chain contributing to reversible or irreversible light-responsive behaviour dependent of selected chromophore [11].

In general, an irreversible light-responsive behaviour can be achieved by incorporating photo-cleavable units instead of photochromic units. If this light-responsive polymer is irradiated, then the light-responsive units would be cleaved into a more polar species through an irreversible

transformation. One of the most common example is the o-nitrobenzyl ester (ONB), that showed an irreversible light-responsive behaviour and the photo-cleavage reaction is usually initiated by UV-light but under certain conditions NIR-light can also be used [22–27]. Other example of light-responsive behaviour in polymeric systems can be extended to reversible or irreversible cross-linking reactions based on coumarin dimerization has been reported [11,20].

In the case of reversible light-responsive behaviour, different photochromic molecules have been commonly used. These photochromic molecules undergo a reversible isomerisation, typically accompanied by a polarity change as well as colour switch, induced by light. The most common families include azobenzene, spiropyran, salicylideneaniline, among others [11]. In general, upon irradiation, the light-responsive polymer system can turn back to initial state by a thermal or photo re-isomerisation process. Typically, UV-light between 300 and 400 nm is used to induce the isomerisation process, while visible light (>400 nm) is used to the re-isomerisation process [11].

Recently, different stimuli-responsive polymers systems with dual or even multi-responsive polymers have been reported. These materials have attracted attention due to the possibility to tune their properties in multiple ways [11]. In particular, thermo-responsive polymers incorporating photochromic, photo-cleavable or photo-crosslinking units have been explored for the fine-tuning of LCST using light as stimulus have been explored.

Other stimuli such as pH and electron-transfer processes (redox) have also been investigated [11]. The first example of a thermo- and light-responsive polymer was reported by Kungwatchakun and Irie. The idea of this work is related to the photocontrol of the phase separation temperature of aqueous solutions of PNIPAm by introducing azobenzene moieties into the pendant groups. They prepared a dual-responsive polymer by co-polymerization of *N*-isopropylacrylamide with *N*-(4-phenylazophenyl)acrylamide [11,28]. They demonstrated for a co-polymer system containing 2.7 mol % azobenzene groups, a shift in the LCST from 21 ºC (initial value) to 27 ºC after UV-light irradiation [11,28]. This can be explained by the change in the dipole moment that is due to the *trans*-to-*cis* isomerisation of the azobenzene moieties. The co-polymer system returns to the initial phase transition temperature (21 ºC) by irradiation with visible light. They also found a direct correlation between the light-induced shift in the LCST and the amount of azobenzene incorporated into the co-polymer. At higher azobenzene amounts (>3.4 % mol) incorporated into the co-polymer, the hydrophobic character is decreased and it was not enough to weaken the existing inter- and intra-molecular interactions, consequently LCST remained constant after UV-light exposure [11,29]. Other interesting example to control the LCST of PNIPAm using azobenzene as light-responsive unit was reported by Akiyama and Tamaoki [30]. They used an azobenzene derivative substituted with a 2-chloropropionyl group as an initiator for atom transfer radical polymerization of *N*-isopropylacrylamide. They change the polymerization conditions (time and proportion between NIPAm and initiator) and the final polymers, which has a single terminal azobenzene end-group, showed different molecular weight (1.7 to 12.0 kDa). Aqueous solutions of these polymers showed that LCST alternated reversibly through light irradiation due to terminal azobenzene moieties. The LCST shift increased linearly up to a value of over 10 ºC upon decreasing the molecular weight of the polymer. In other words, there was an increasing influence

of the azobenzene end-groups effect on LCST of the polymer [11,30]. PNIPAm combined with azobenzene derivatives have been intensely investigated and several works have been reported in the literature over the years, including, the addition of third stimulus such as pH changes. For example, Liu and co-workers prepared co-polymer hydrogels that respond to temperature, light and pH [31]. Also, an alternative thermo-responsive polymers have been explored containing azobenzene derivatives have been reported.

Thermo-responsive polymers containing other photochromic units, such as salicylideneaniline, spiropyrane, fulgimide have also been investigated. Jochum and Theato reported a polyacrylamides containing different amounts of salicylideneaniline moieties, which were synthesized using a double polymer analogous reaction of poly(pentafluorophenyl acrylate), i.e. forming *in situ* salicylideneaniline side group within PNIPAm co-polymers [32]. The polymers exhibit LCST in aqueous solution, which is dependent on the amount of incorporated salicylideneaniline group and the isomerisation state of salicylideneaniline, respectively. Higher LCST values were obtained for UV-irradiated solutions of the co-polymers, when compared with non-irradiated co-polymer solutions [11,32]. Mattiasson and co-workers reported a co-polymer of *N*-isopropylacrylamide and methacryloyl derivative of spirobenzopyran by a free-radical polymerization. The final co-polymer contains 1.9 % mol of spiropyran units and exhibits a LCST in water in the temperature range of 30 – 50 ºC. The spiropyran unit incorporated into the polymer is then converted into their coloured merocyanine form by light. The LCST of the irradiated polymer did not increase as expected by polymer structure but decrease after the light exposure. Additionally, the re-isomerisation process takes more than 20 days, once the open zwitterionic merocyanine form is stabilised in a polar environment [11,33].

In conclusions, thermo-responsive polymers for a wide variety of applications have rapidly grown over the last decade. Although many advances in the thermo-responsive polymers, it is expected a numerous challenges and opportunities.

6.1.2. Flavylium salts

Flavylium salts are synthetic compounds similar to natural anthocyanins, an important family of natural compounds responsible for most of the colour of flowers and fruits. Synthetic flavylium have been used as model compounds for anthocyanins, allowing to elucidate several aspects of the structural transformations that occurred in the ground state of both families [34]. They gained attention due to their attractive photochemical properties. Also, they have been used to explore the possibility of designing optical memory systems with multiple storage and non-destructive readout capacity, i.e. molecular devices capable of undergoing write-lock-read-unlock-erase cycles [34]. In other words, optical memory systems where the record can be erased when necessary, but not destroyed by readout [35].

Flavylium salts can readily interconvert into different species in aqueous solution, using different controlled stimuli, such as pH jumps and light (see Figure 6.4 and Scheme 6.1) [36,37].

They can be classified as Type T photochromic molecules with potential application into the design photochromic systems as well as models of optical memories, as already mentioned [36,38].

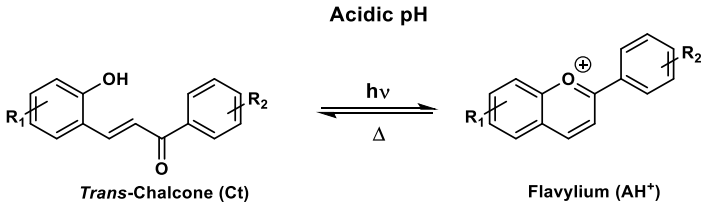

Figure 6.4 – General photochromic reaction of Flavylium/ *trans*-chalcone systems [39]. (Source: *J. Phys. Chem. A*, 2014, **118**, 4723–4731).

At very acidic pH values flavylium cation (**AH⁺**) is the most stable species. When pH is increased a hydration reaction occurs, i.e. the nucleophilic attack of water at position 2, leading to the formation of the hemiketal (**B**). This species subsequently reorganizes by means of a ring-chain tautomerization reaction to give a *cis*-chalcone (**Cc)**. Finally, the *cis*-to-*trans* isomerisation of the double bond results on the *trans*-chalcone species (**Ct**). Moreover, if hydroxyl substituents are present in the compound, usually at position 7 and/or 4', the deprotonation reaction of the flavylium cation gives rise to the formation of the quinoidal base (**A**). This reaction competes with hydration and is by far the fastest process taking place in the network. Thus, when the pH is increased from very acidic to higher pH values, the quinoidal base is the kinetic product, but usually disappears with time because the equilibrium network shifts to the formation of the *trans*-chalcone, the most stable species at moderately acidic and neutral pH values (Scheme 6.1).

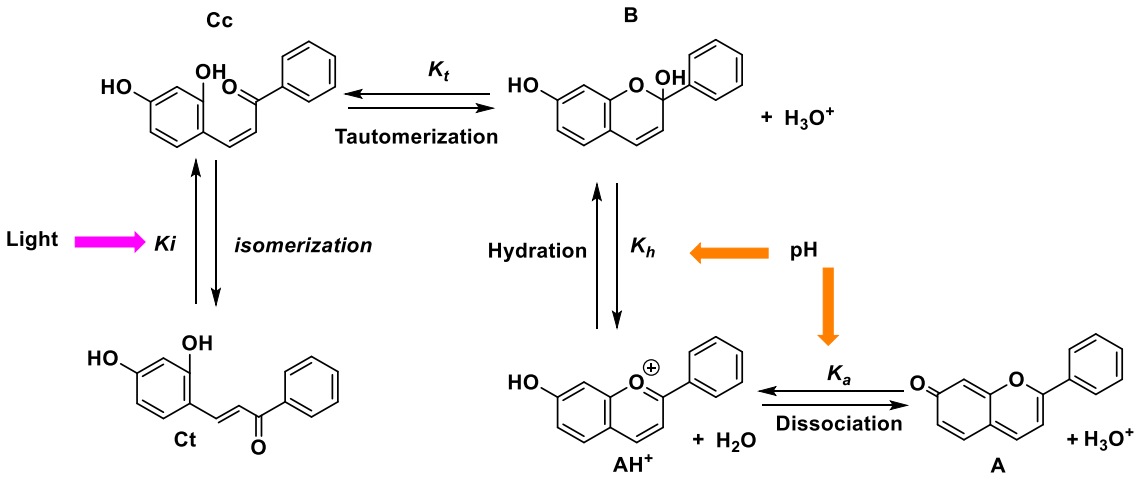

Scheme 6.1 – Network of chemical reactions of 7-hydroxyflavylium in aqueous media.

In general, the network of flavylium compounds in water (acid to moderately acid) allows to distinguish at the equilibrium five species: the flavylium cation (**AH⁺**), the quinoidal base (**A**) obtained from the previous one by proton transfer (Scheme 6.1), the hemiketal (**B**) formed from **AH⁺** by hydration reaction (Equation 6.2), the *cis*-chalcone (**Cc**) obtained from the hemiketal by tautomerization process (Equation 6.3) and the *trans*-chalcone (**Ct**) by isomerisation process of the **Cc** (Equation 6.4).

$$AH^+ + H_2O \rightleftharpoons A + H_3O^+ \qquad K_a$$

Equation 6.1

$$AH^+ + H_2O \rightleftharpoons B + H_3O^+ \qquad K_h$$

Equation 6.2

$$B \rightleftharpoons Cc \qquad K_t$$

Equation 6.3

$$Cc \rightleftharpoons Ct \qquad K_i$$

Equation 6.4

The Equations 1 to 4 can be replaced by a single acid-base equilibrium (Equation 6.5).

$$AH^+ + H_2O \rightleftharpoons CB + H_3O^+ \qquad K_a'$$

Equation 6.5

Where the conjugate base (**CB**) represents the sum of all the other species in the network, i.e. quinoidal base (**A**), hemiketal (**B**), *cis*-chalcone (**C*c***) and *trans*-chalcone (**C*t***) (Equation 6.6).

$$[CB] = [A] + [B] + [Cc] + [Ct]$$

Equation 6.6

The apparent equilibrium constant K'_a (Equation 6.1) relates with those describing the other equilibria (see Scheme 6.1) according to Equation 6.7.

$$K_a' = K_a + K_h + K_h K_t + K_h K_t K_i$$

Equation 6.7

One interesting feature of flavylium networks is the photochemical reactivity exhibited by the *trans*-chalcone (**Ct**) that photoisomerizes to give the *cis*-chalcone (**Cc**). At appropriate pH values, Cc subsequently evolves to give the coloured species in the network namely **AH$^+$** and **A**, then the system reverts back to the equilibrium with a rate that depends on the substituents present on the flavylium compound.

The flavylium network has been extensively investigated in homogenous solutions. Taking in account that synthetic flavylium have been used as model compound for anthocyanins and it is recognised that in nature the anthocyanins exist in heterogeneous environments, namely in the presence of membranes and biomolecules. Therefore, flavylium in heterogeneous media appeared as a logical follow up and different systems, such as biphasic water/ionic liquid mixtures, micelles and reverse micelles, polymers, gels and solids (namely, zeolites and clays) have been explored [36].

Pina and Hatton described an incorporation of two flavylium compounds, 7,4'-dihydroxyflavylium and 7-(*N,N*-diethylamino)-4-hydroxyflavylium into Pluronic F-127 matrixes, non-ionic tri-block co-polymer, PEO-PPO-PEO, poly(ethylene oxide) (PEO), poly(propylene oxide) (PPO), with a nominal molecular weight of 12 500 and a PEO/PPO ratio of 2:1 by weight. This incorporation leads to efficient and versatile photochromic gels, which the quantum yield and the thermal back reaction can be tuned by the pH control and then different switching colours are obtained, depending on the substituents on the flavylium backbone [40]. Later on, Pina and co-workers described in detail the photochromism of the 4′-*N,N*-dimethylamino-7-hydroxyflavylium incorpored in Pluronic F127 micelles and gels [41]. Matsushima and Suzuki also described the incorporation of flavylium/chalcone photochromic system into polymers. They studied a series of substituted 2-hydroxychalcones in solution and polymer films. Poly(methylmethacrylate) (PMMA),

poly(styrene) (PS), poly(acrylic acid) (PAA) and a co-polymer of styrene and maleic anhydride (SMA) have been tested as polymer films. They observed a good contrast and reversibility, although lower and slower when compared to solution [36,42]. Later on, Matsushima and co-workers described the incorporation of substituted 2-hydroxychalcone in solid hydrogel matrices. They used a solid agar-gel and silica sol-gel matrices and the results showed good reversibilities for the chalcone-flavylium interconversion. In the case of agar-gel matrix, the colouration-decolouration cycles could be repeated over 50 cycles, without significant fatigue. While, in silica sol-gel matrix, a fairly good reversibility was obtained until 30 cycles, after that a significant degradation was observed [36,43]. Pina and co-workers reported the incorporation of the 4',7-dihydroxyflavylium in poly(2-hydroxyethylmethacrylate) (PHEMA), a water-permeable crosslinked matrix. This matrix was prepared by co-polymerization of 2-hydroxyethylmethacrylate (HEMA) and ethylene glycol dimethacrylate (EGDMA) by free-radical co-polymerization, using AIBN as initiator. The water-permeable and the transparency of the polymeric matrix allowed the use of pH and light stimulus to attain different states on the flavylium network (see Figure 6.5) [38,44].

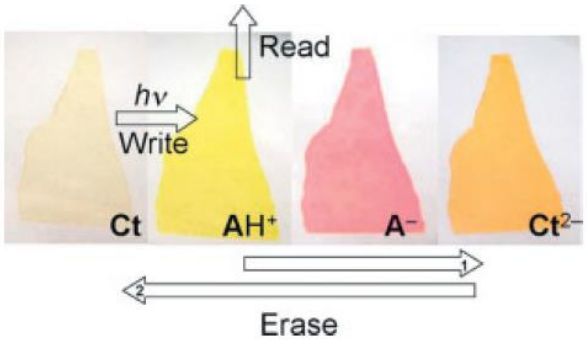

Figure 6.5 – Example of flavylium salt encapsulated in polymeric matrix. A cycle to write-read-erase in solid state of 4'-7-dihydroxyflavylium in PHEMA.The first step (write) are based on the irradiation of the film containing the Ct form in acidic medium (metastable). The read step can be achieved using a wavelength at which the Ct species does not absorb light, for example 470 nm. To erase the system, a sequence of two pH jumps is necessary: the first one to basic medium produces the Ct^{2-}species and followed a second one back to acidic medium, restores the original Ct species [44]. (Source: *Adv. Funct. Mater*., 2005, **15**, 541–545).

The results of 4',7-dihydroxyflavylium incorporated in PHEMA showed a thermal barrier between the *cis*-to-*trans* chalcones, a necessary requirement for write-read-erase cycle, contrarily to 4',7-dihydroxyflavylium in aqueous solution [44]. It is known the synthetic flavylium salts containing hydroxyl substituents shows efficient intermolecular excited state proton transfer (ESPT), i.e. display fluorescence emission, which is quenched upon dissolution in water [34,36]. The encapsulation of these flavylium salts in cross-linked PHEMA hydrogel, which show ability of to concentrate water from the surrounding atmosphere, were shown to perform well as humidity sensor with high sensitivity [36,45]. The encapsulation of the flavylium without any covalent bonding to the polymeric matrix has the advantage of allowing the exploitation of well-known network of this compound. However, the system shows several limitations, such as the involvement of ion mass transfer between states and the long-time need at present to erase the system that can be manipulated by suitable hydroxyl-ion concentration [44]. Also, it is not possible to avoid the partition of the flavylium salt between the polymeric hydrophase and the bulk water, if an external reservoir

is used to change the pH of the system. This partition is also depending on the solubility of the flavylium salt [44].

In conclusion, flavylium salts showed interesting photochromic properties and respond to different stimuli such as pH and light. In the last years, the flavylium network has been largely investigated. Heterogeneous media become an interesting research topic to explore, for that several works have been reported using biphasic water/ionic liquid mixtures, micelles and reverse micelles, polymers, gels and solids (namely zeolites and clays) have been recently reported [36].

6.2. Flavylium-supported Poly(*N*-isopropylacrylamide)

Several stimuli-responsive polymers incorporating functional moieties within or on a polymer chain have been reported. These responses can be tuned by the type of stimuli-responsive group. Indeed, it is possible to obtain dual or multi-responsive polymers [2,11].

In this context, we developed a novel multi stimuli-responsive polymer, where the 7-hydroxy-4'-vinylflavylium hydrogen sulfate (as photochromic unit) was co-polymerized with *N*-isopropylacrylamide (as thermo-responsive polymer) via free-radical co-polymerization (see Figure 6.6).

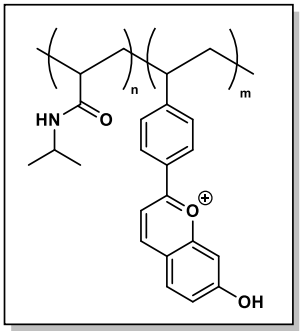

Figure 6.6 – Polymer **P1** obtained from co-polymerization between 7-hydroxy-4'-vinylflavylium hydrogen sulfate and *N*-isopropylacrylamide.

It is expected that the chemical and photochemical of flavylium network can be affected by the covalent linkage of flavylium salt to the polymer, contrarily to the encapsulation of the flavylium salt in polymeric matrix, without covalent bonding. This last approach has the advantage of allowing the exploitation of the well-known network of the flavylium salt but it shows several limitations. The most important are related to the involvement of ion mass transfer between states and the long time needed at present to erase the system [44].

6.2.1. Synthesis of the Polymers

The synthesis of the multi stimuli-responsive polymer **P1** was performed in two stages: i) preparation of polymerizable 7-hydroxy-4'-vinylflavylium hydrogen sulfate monomer and ii) polymerization of this monomer in order to obtain **P1**. In the first stage, the polymerizable 7-hydroxy-4'-vinylflavylium hydrogensulfate monomer (**1**) was synthesized by acidic condensation between 2,4-dihydroxybenzaldehyde and 4-vinylacetophenone at room temperature. Previously, the 4-vinylacetophenone was obtained by palladium-catalyzed Hiyama reaction of vinyltrimethoxysilane and 4-bromoacetophenone (see Scheme 6.2) [46].

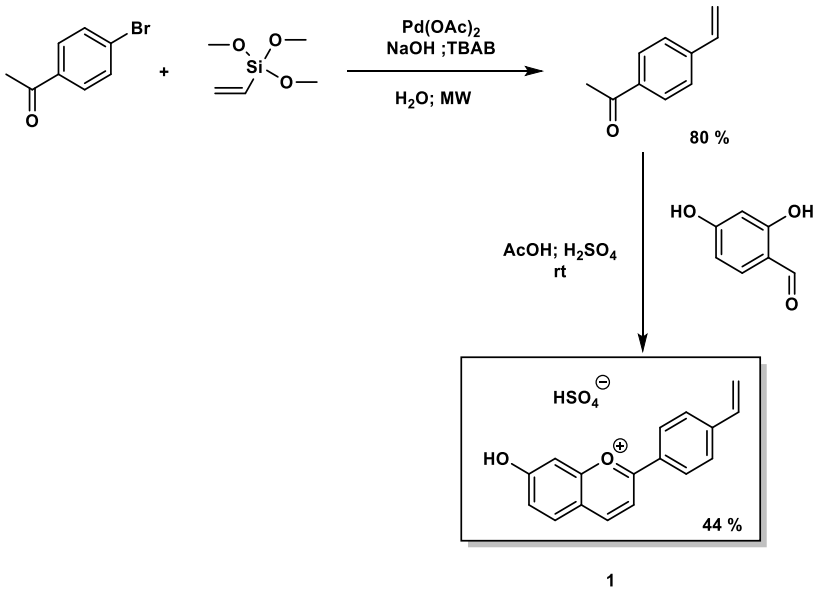

Scheme 6.2 – Synthesis of the polymerizable monomer 7-hydroxy-4'-vinylflavylium hydrogen sulfate monomer.

In the second stage, the polymer **P1** was obtained by thermal free-radical polymerization involving previous flavylium salt **1** (1.8% mol) and *N*-isopropylacrylamide (NIPAM, 98.2% mol) (see Scheme 6.3).

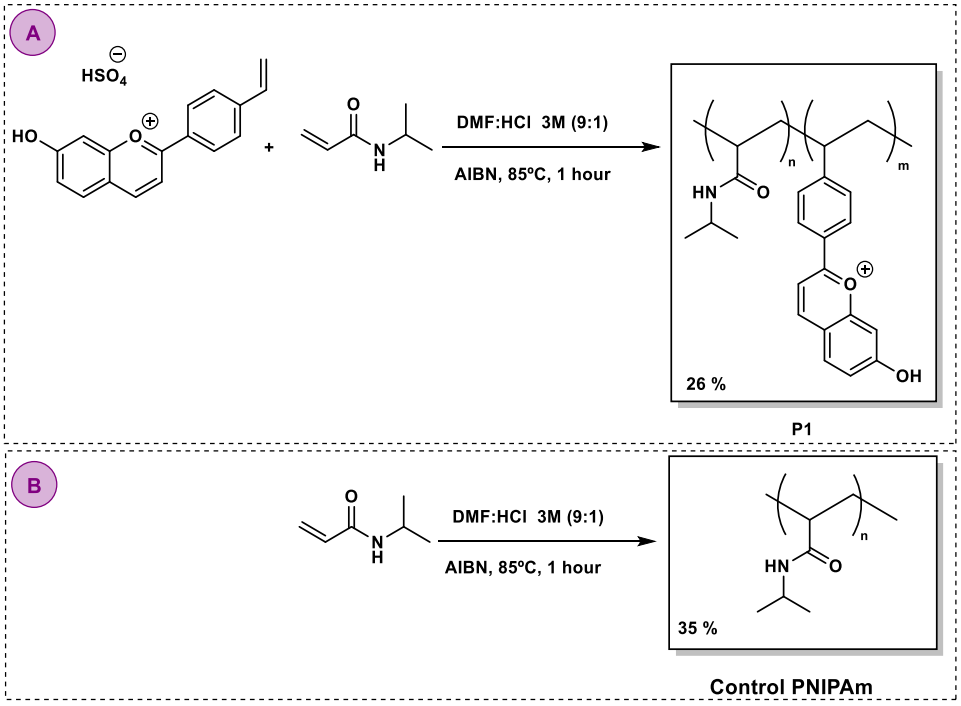

Scheme 6.3 – Polymerization to obtain (A) **P1**; (B) **Control PNIPAm**.

The polymerization was performed in short reaction time and acidic conditions, in order to avoid the evolution of the flavylium cation to the *cis*- and *trans*-chalcone species, which could introduce some cross-linking, affecting different polymeric chains through the reaction of the second double bond (see Scheme 6.1). For comparative studies, a control polymer (**PNIPAm**), without flavylium salt (**1**), was also prepared at the same conditions.

The polymerization was followed by UV-vis spectroscopy and after one hour (1 h) a blue shift of the absorption maximum of the flavylium salt (**1**), from 452 nm to 437 nm, has been observed (see Figure 6.7).

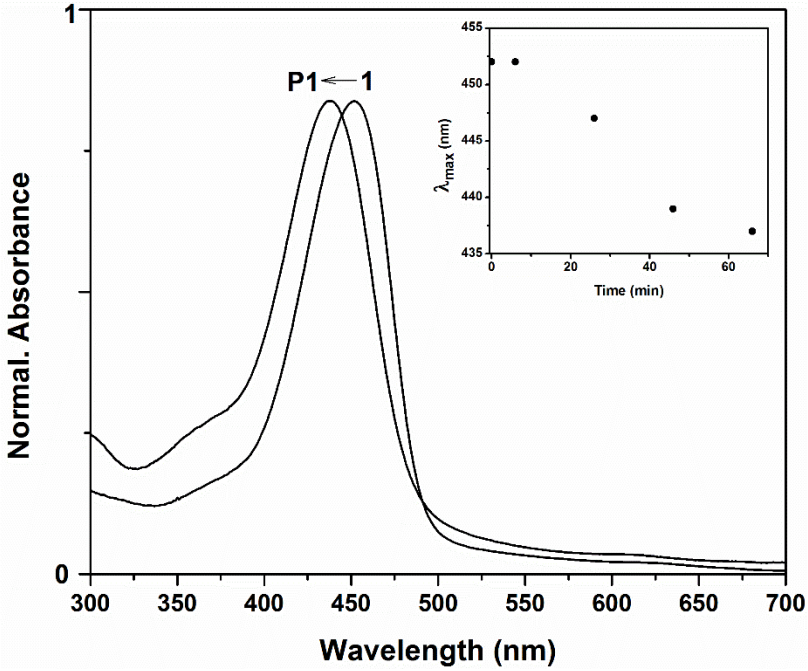

Figure 6.7 – The blue shift of the absorption maximum on going from monomer 1 to polymer **P1** was used to monitor the polymerization reaction (inset). Monitorization of the polymerization reaction by UV-Vis was carried out by taking 10 µL aliquots from the reaction vessel and diluting to 3 mL with 0.3 M HCl; the solutions were allowed to equilibrate before recording the spectra at room temperature.

This shift of the band can be explained by a loss of electronic conjugation in the flavylium molecule by reaction of the double bound, indicating that polymerization is occurring. In addition, the maximum absorption of the flavylium cation after the polymerization is similar to the 7-hydroxy-4'-methylflavylium (426 nm), which containing a methyl substituent in the 4' position (see Figure 6.8) [47]. This salt can be used as model in solution for the thermodynamic and kinetic flavylium network studies of **P1**.

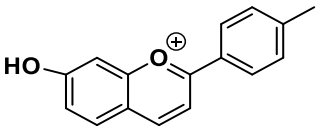

Figure 6.8 – Chemical structure of 7-hydroxy-4'-methylflavylium [47]. (Source: *Chem. Eur. J*., 2011, 17, 6359–6368).

The control polymer (**control PNIPAm**) and the isolated polymer (**P1**) were characterized by ^{1}H NMR. In both cases it was possible to identify the typical signals correspondent to poly(*N*-isopropylacrylamide) (see Figure 6.9 and Figure 6.10) [48].

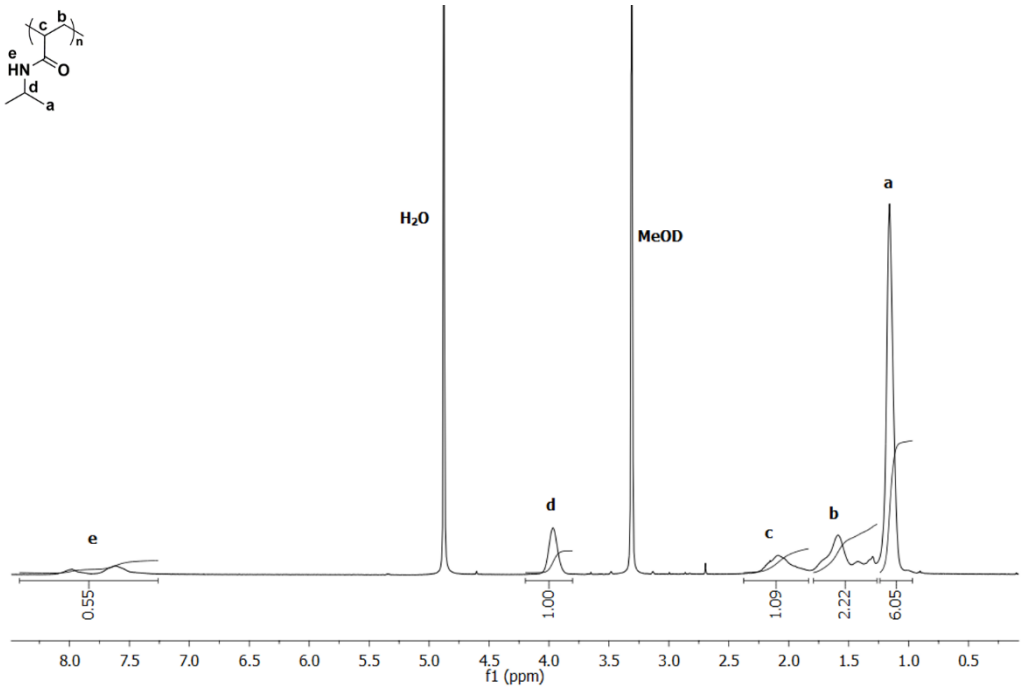

Figure 6.9 –^{1}H NMR spectra in CD_3OD of the polymer control PNIPAm.

In the case of the isolated polymer (**P1**) the aromatic region has been expanded and it was possible to determine that about 0.4% mol of flavylium was incorporated into the polymer by comparison between the integration areas of the most deshielded proton in the flavylium moiety (H4, δ=9.35 ppm) and the proton corresponding to -CH- in the isopropyl side group of *N*-isopropylacrylamide (δ=3.97 ppm) (see Figure 6.10).

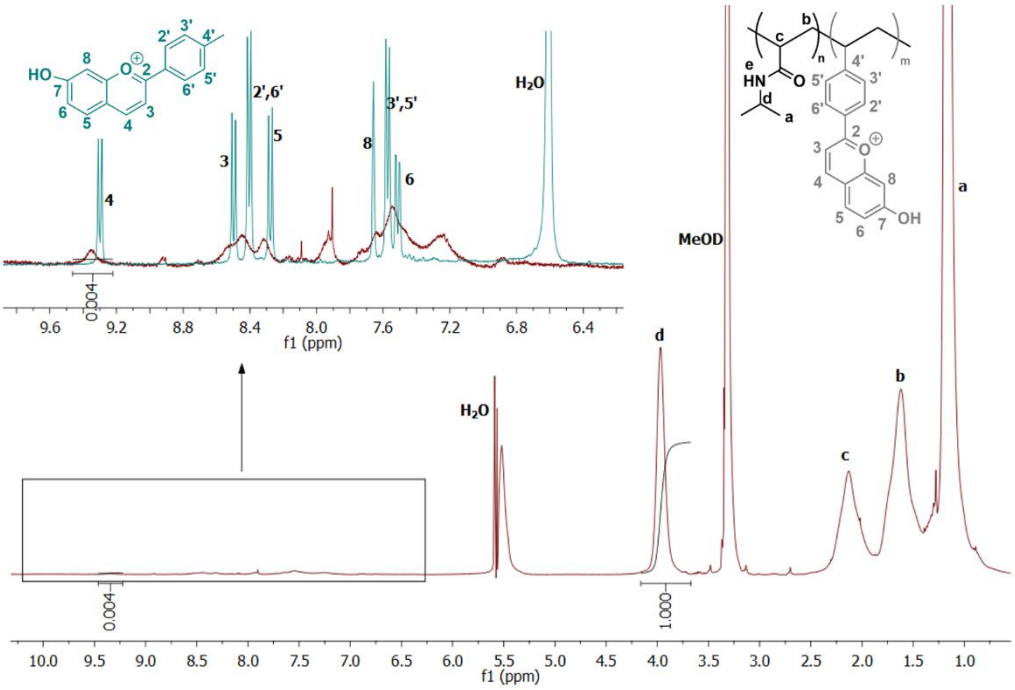

Figure 6.10 – ^{1}H NMR spectrum in CD_3OD with DCl (pD<1) of the isolated polymer **P1.** The 9.6 to 6.4 ppm region has been expanded to visualize the signals corresponding of the flavylium moieties. Also, the spectrum of model flavylium salt (**2**) is superimposed. The integration values corresponding to the proton H4 of the flavylium moiety and the proton in the isopropyl side group ("d") from NIPAM side chain are indicated.

However, ^{1}H NMR analysis showed some additional peaks in the aromatic region besides those of the flavylium moieties in the isolated polymer (**P1**). This suggests that the flavylium partially evolves to the other species of the network (hemiketal and *cis* or *trans*-chalcones) in this solvent and/or during the polymerization occurs some partial evolution of the flavylium to the *trans*-chalcone, confirmed by UV-vis spectroscopy and, consequently the *trans*-chalcone can react through its middle double bond, leads to aromatic moieties on the polymer.

FTIR analysis of control polymer (PNIPAm) and isolated polymer **P1** have been performed and was practically identical (see Figure A. 7.4.2 in annex), due to the low content of the flavylium moiety incorporate into the polymer **P1.** In this way, it was possible to identify their characteristic bands at 3298 cm^{-1} (secondary amide N-H stretching), 2972 cm^{-1} (-CH_3 asymmetric stretching), 1651 cm^{-1} (amide I bond) and 1547 cm^{-1} (amide II bond) [49].

The molecular weight distribution was analyzed by means of GPC/SEC and MALDI-TOF MS [50] measurements. GPC/SEC measurements for the control polymer and **P1** give us molecular weight about 2800 g mol^{-1}, using THF as eluent and narrow linear polystyrene standards ranging in molecular weight from 238700 to 370 g mol^{-1} as calibrate mode. However, the reproducibility of the measurements was reduced, and, moreover, the selected standards used are not the most appropriate for PNIPAm samples. MALDI-TOF MS measurements for the control polymer (PNIPAm) give us M_w= 7842 g mol^{-1} and M_n=7842 g mol^{-1}, which has a relatively narrow polydispersity index, PDI =1.2 (see Figure A. 7.4.3 in annex). However, it was not possible to obtain a reliable signal for **P1**, probably because the sample did not desorb well from the MALDI matrix. Once, the reaction conditions for the synthesis of both polymers are similar, it is reasonable to assume a molecular weight distribution of **P1** close to that found for the control polymer. Nowadays, MALDI-TOF is described as a usual technique for the analysis of the molecular weight distributions of synthetic polymers. This technique can offer several advantages such as the determination of absolute molecular weights for polymers with narrow polydispersity contrarily to chromatographic techniques, does not required polymer standards to assign molecular weights to oligomers, lower sample of material consumption and shorted analytical time is required. In addition, MALDI-TOF can determine the molecular weight independently of the polymer structure [51]. In this sequence, we considered that the values obtained by MALDI-TOF-MS are more reliable.

6.2.2. Thermodynamics of the Flavylium Network

The thermodynamic equilibria of flavylium salts can be described as the global acid-base equilibrium between flavylium cation and a conjugate base (**CB**), which can be defined as the sum of all the other species in the network, as illustrated earlier by Equation 6.1 to Equation 6.7. The flavylium cation (**AH^+**), which is the most stable species at very acidic pH values, and the chalcones can be interconverted by pH changes. Therefore, it is possible to determine the value of the acidity constant (**K_a**) associated with the equilibrium between the flavylium cation, (**AH^+**), and the quinoidal base (**A**).

The spectral variations occurring immediately after a series of pH jumps, from pH = 1 to higher pH, of the polymer **P1** are shown in Figure 6.11.

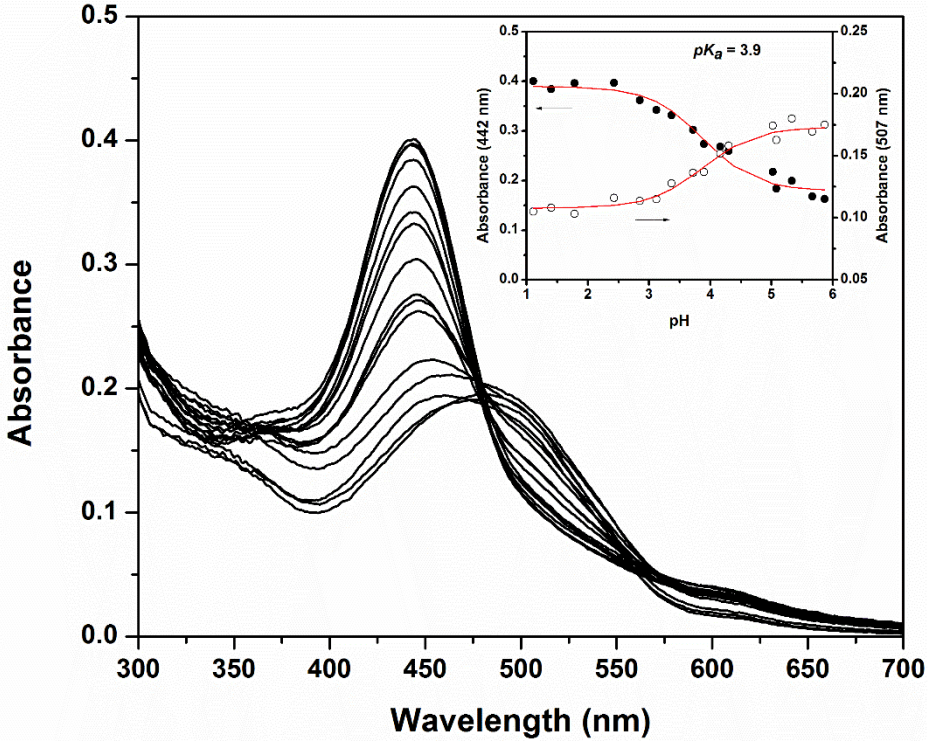

Figure 6.11 – Spectral variations taking place immediately after a series of pH jumps from pH = 1 to higher pH values of **P1** (1.7% MeOH, ionic strength = 0.1 M ($NaClO_4$ or $HClO_4$), **[P1]** = 0.017 wt %, T = 21ºC). Inset: fittings of the absorbance values at the specified wavelengths allowed the determination of pK_a.

The calculated value of the acidity constant ($\mathbf{K_a}$) associated to the equilibrium between the flavylium cation (**AH**$^+$, λ_{max} ~ 442 nm) and the quinoidal base (**A**, λ_{max} ~ 480 nm) is $K_a = 10^{-3.9}$, compares with $K_a = 10^{-4.1}$ for the model compound [47].

The absorption of the solutions was measured 24 hours after the pH jumps and no significant changes in absorption were observed, indicating that solutions are equilibrated.

The pH-dependent absorption of the equilibrated solutions shows that at acidic pH values the flavylium moiety is basically in the form of the flavylium cation while at moderately acidic pH values two species are dominant, namely the *trans*-chalcone (λ_{max} ~ 360 nm) and the quinoidal base (λ_{max} ~ 480 nm) (see Figure 6.12 A).

The absorbance at 442 nm as a function of pH was plotted and the data cannot be fitted with a sigmoid function (see inset in Figure 6.12 A). Consequently, it is not possible to determine a single global acidity constant (see Equation 6.1 to Equation 6.7). This suggests that several microenvironments are present in the polymer that influence the equilibrium between flavylium cation (**AH**$^+$) and the other species (**CB**) in the network. Indeed, the fittings become increasingly better when two or more pK'_a values are used.

According to literature, stretched exponential functions and scaling functions such as the power law are often used to describe polymer properties, e.g. dielectric relaxation and rheological parameters that show up with a distribution function behavior due to microheterogeneities in the system [52–54].

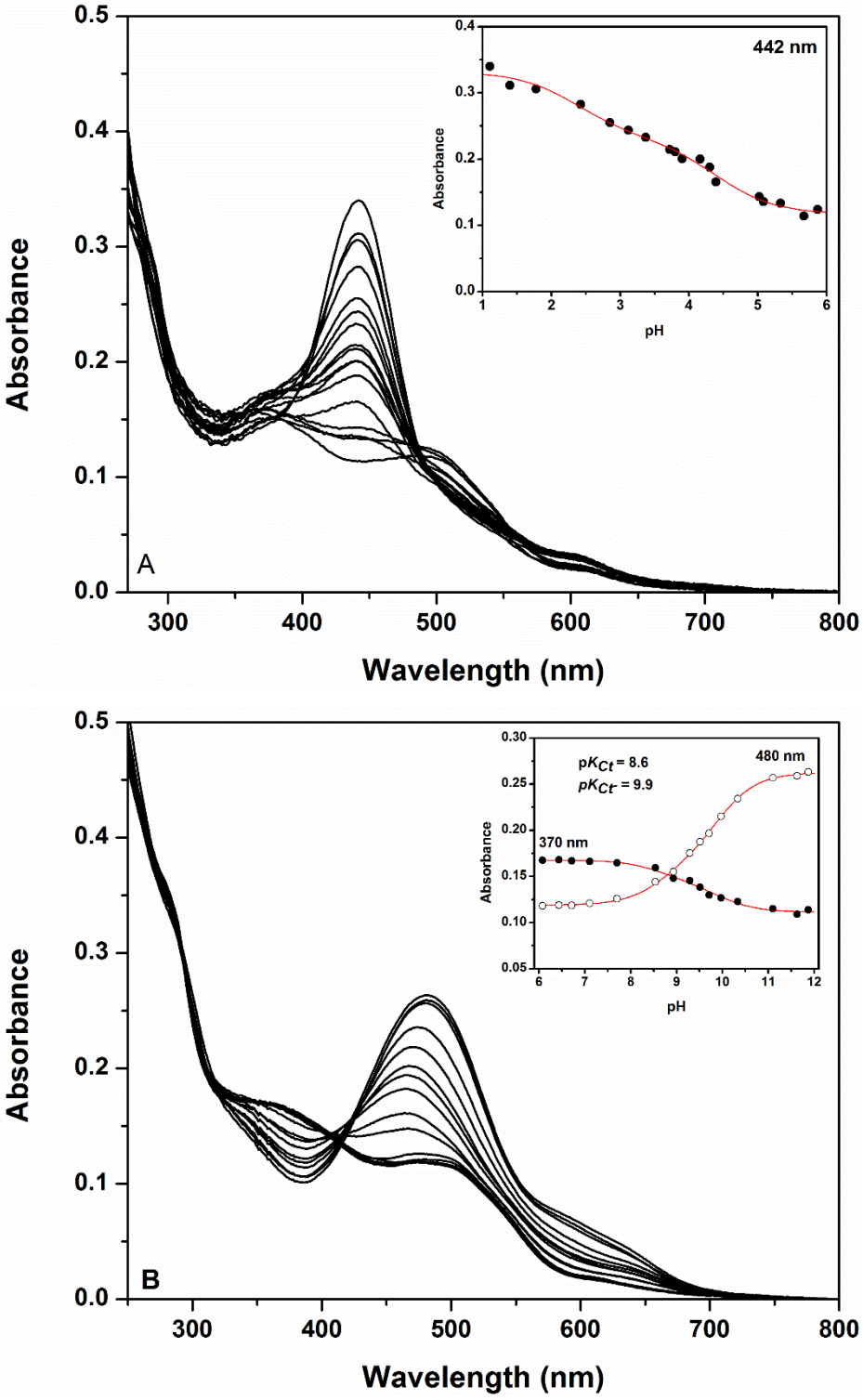

Figure 6.12 – Spectral variations of equilibrated aqueous solutions (1.7% MeOH, ionic strength = 0.1 M ($NaClO_4$ or $HClO_4$)) of **P1** at different pH values, [**P1**] = 0.017 wt %, T = 21 °C. (A) pH ranges from 1 to 6; the absorbance variations at 442 nm were fitted using a power law model (inset). (B) pH ranges from 6 to 12; data fitted with normal sigmoid curve (inset).

An adjusted power law model for our case are described in Equation 6.8, where A is the absorbance, $[H^+]$ is the proton concentration, K'_a is the apparent equilibrium constant, *a* and *b* are constants. The constant *a* can be considered a normalization constant for the absorbance, *b* can be interpreted as an indication of the heterogeneity degree of the system.

$$A = a\left(\frac{[H^+]}{[H^+] + K'_a}\right)^b$$

Equation 6.8

When b = 1, Equation 6.8 reduces to the usual sigmoid function on pH. When 0<*b*<1, the smaller *b* is the more stretched is the sigmoid. In that sense, a value closer to 1 would be indicative of a homogeneous system.

The data trend was adequately fitted using a power law model and the apparent equilibrium constant (K'_a) between **AH$^+$** and **CB** was obtained. The calculated values were $K'_a = 10^{-2.1}$, a = 0.33 and b = 0.12. This constant *b* seems to indicate a relatively important number of microenvironments affecting the global acid-base equilibrium relating **AH$^+$** and the other species. From spectral variations of equilibrated aqueous solutions (Figure 6.12) reveals that the fraction of quinoidal base (**A)** at the equilibrium at pH ~ 6 is significantly larger (~55%) than that observed for the model compound [47] and in general for the majority of flavylium compounds in water, which is usually less than 10% [36]. This fact can be explained by the stabilization of the quinoidal base, neutral form, relatively to the positively charged **AH$^+$** species in the polymer backbone, when compared to water. Moreover, aggregation can occur more easily in the case of the quinoidal base due to its planar and non-charged structure, stabilizing this species against the other species in the flavylium network. This phenomenon is well known for anthocyanins, the natural analogs of flavylium compounds, where the quinoidal base is present at the equilibrium in large quantities (up to 50% or more, depending on the concentration), stabilised by self-aggregation [55].

Direct pH jumps to pH ≥ 12 leads to the formation of the species Ct^{-2} in a few minutes, due to the hydroxyl nucleophilic attack to quinoidal base [56] (**A**) and this species can be titrated back to acidic pH values to give the species ionized *trans*-chalcone (**Ct$^-$**) and *trans*-chalcone (**Ct)** (see Scheme 6.4).

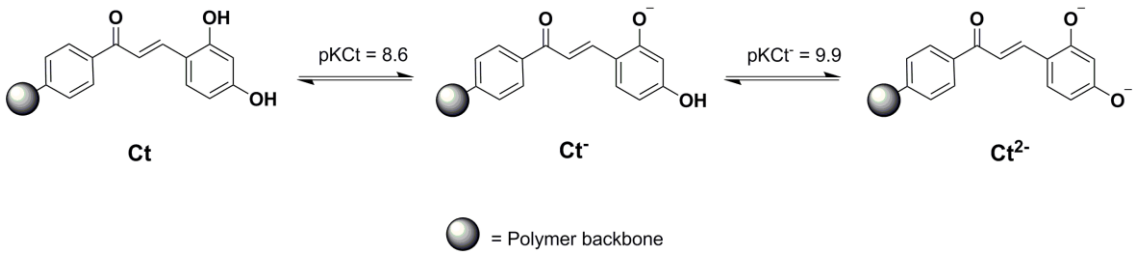

Scheme 6.4 – Acidity constants of the *trans*-chalcones attached to the polymer backbone (deprotonation order was not confirmed).

The spectral variations from this titration are shown in Figure 6.12B. The absorbance at 370 and 480 nm as a function of pH was plotted and the data can be fitted with normal sigmoid curve (inset of Figure 6.12 B). The calculated acidity constants for the protonation process corresponding to the formation of ionized *trans*-chalcone (Ct^-) and *trans*-chalcone (Ct) are $pKCt^-$ = 9.9 and pKCt = 8.6, respectively. These values are slightly higher those found for the model compound, namely $pKCt^-$ = 9.4 and pKCt = 7.9, respectively [47]. This difference can be explained by the polymeric environment stabilises neutral/less charged species against more charged species. It must be

noted in Figure 6.12 B, that at the end of the titration a significant percentage of quinoidal base (**A**) is already in equilibrium with the neutral *trans*-chalcone, which remarks the high stabilisation of the quinoidal base in the polymer.

The polymerization method used to obtain **P1**, thermal free-radical polymerization and short times, probably leading to a significant heterogeneity in polymeric chain, namely in the distribution of the flavylium moieties regarding to the local concentration and number of flavylium units per chain, among other factors. These heterogeneities can induce different microenvironments that can affect the attainment of the equilibrium. Although the acid-base processes regarding to both the formation of the quinoidal base, as well as, the consecutive deprotonation equilibria of the *trans*-chalcone can be well-fitted with individual constants. Additionally, we cannot exclude the presence of several equilibrium conditions corresponding to slightly different chemical environments in the polymer. It can simply happen that we don't reach the experimental resolution to distinguish between these slight differences. In fact, it is difficult to detect two pK_a values that differ in less than one unit. [57]

Comparing with the global acid-base equilibrium, which implies several reactions (acid-base, hydration, tautomerization and isomerisation), it can be more affected by small differences in the micro-environment than a single protonation-deprotonation process and thus it is easier the establishment and detection of different equilibrium conditions. The protonation-deprotonation processes take place in the microseconds (μs) timescale while the hydration, tautometization and isomerisation reactions occur in longer timescales (often in the second (s), millisecond (ms) and hour (h) timescales, respectively). The overall equilibria leading to K'a (Scheme 6.1) may then discriminate the several microenvironments present in the polymer, which is reflected in the large non-sigmoidal mole fraction *vs.* pH distribution curve (inset Figure 12 A) comprising a series of close equilibrium constants.

6.2.3. Steady-state fluorescence emission

The polymer **P1** was also studied by steady-state fluorescence emission. For these studies equilibrated solutions were used and can be observed at pH = 1.2 and pH = 8.0 (see Figure 6.13), the emission spectra are very similar and it can be assigned to the emission of the quinoidal base (λ_{max} = 610 nm). Other evidence is related to the characteristic vibrational resolved band from quinoidal base [36]. This behaviour can be explained by an excited state proton transfer process (ESPT), i.e. a reversible adiabatic transfer of a proton between an excited acid and its conjugate base. The acid-base properties in the excited state are often different from that in the ground state and as result of that a large change in its acidity can be often observed [34].

Herein, the acidity of the flavylium cation is much higher in the excited state than in the ground state and as consequence the emission of the quinoidal base is collected when exciting a solution of the flavylium cation (see Figure 6.14).

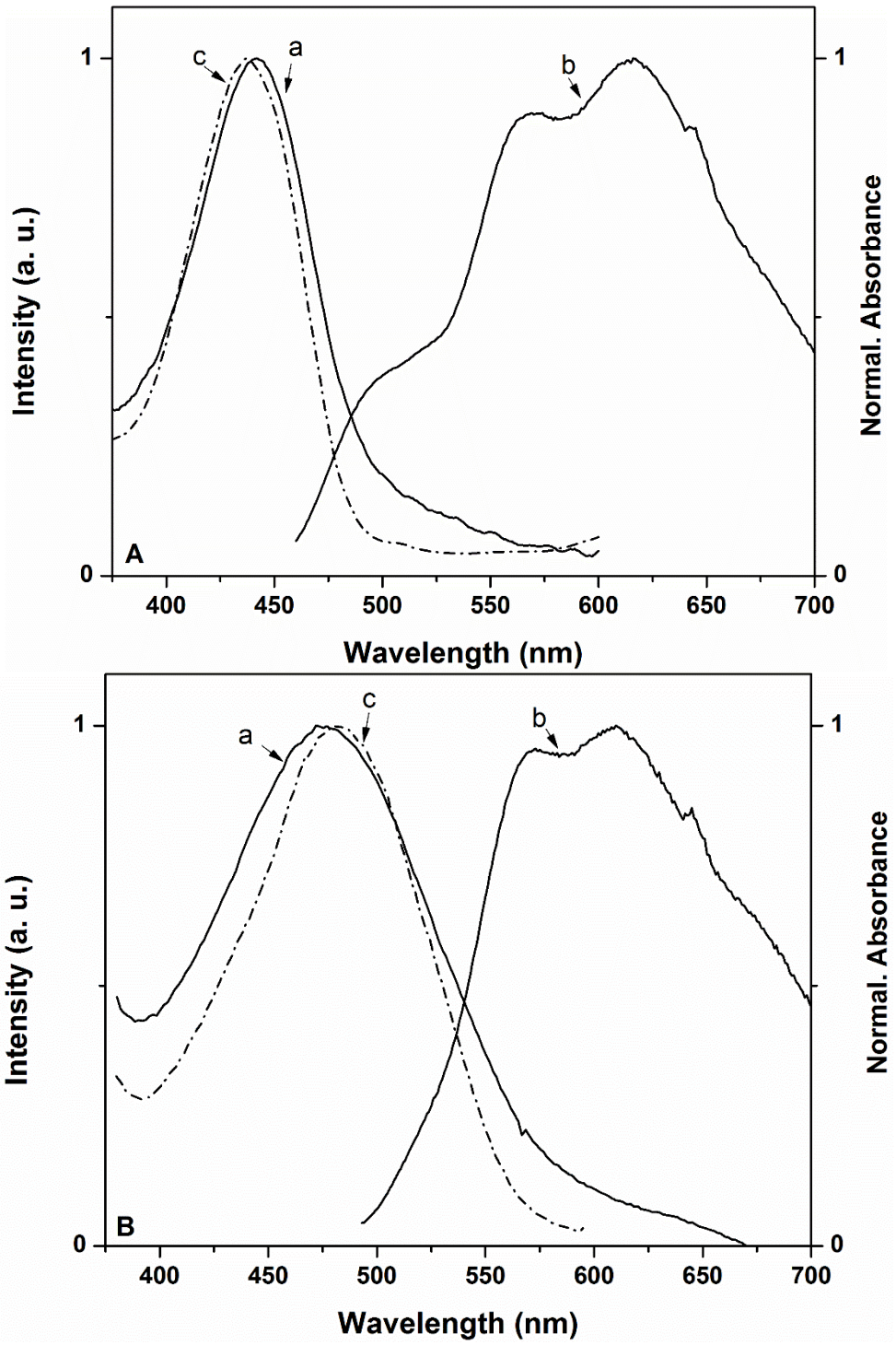

Figure 6.13 – Steady-state fluorescence of equilibrate solutions of **P1** (1.7% MeOH, ionic strength = 0.1M ($NaClO_4$ or $HClO_4$), [**P1**] = 0.007 wt %, T = 21 ^oC). (A) Normalized absorption (a), emission (b, λ_{exc} = 442 nm) and excitation (c, λ_{em} = 615 nm) spectra at pH = 1.2. (B) Normalized absorption (a), emission (b, λ_{exc} = 476 nm) and excitation (c, λ_{em} = 610 nm) spectra at pH = 8.0.

At pH = 1.2 (see Figure 6.13 and Figure 6.14), an additional contribution centred at *ca.* 500 nm is observed, that can be attributed to the emission of the flavylium cation itself. At pH = 5.3 (Figure 6.14) together with the emission of the quinoidal base, it is possible to observe a new emission band centred at 488 nm that is assigned to the *trans*-chalcone.

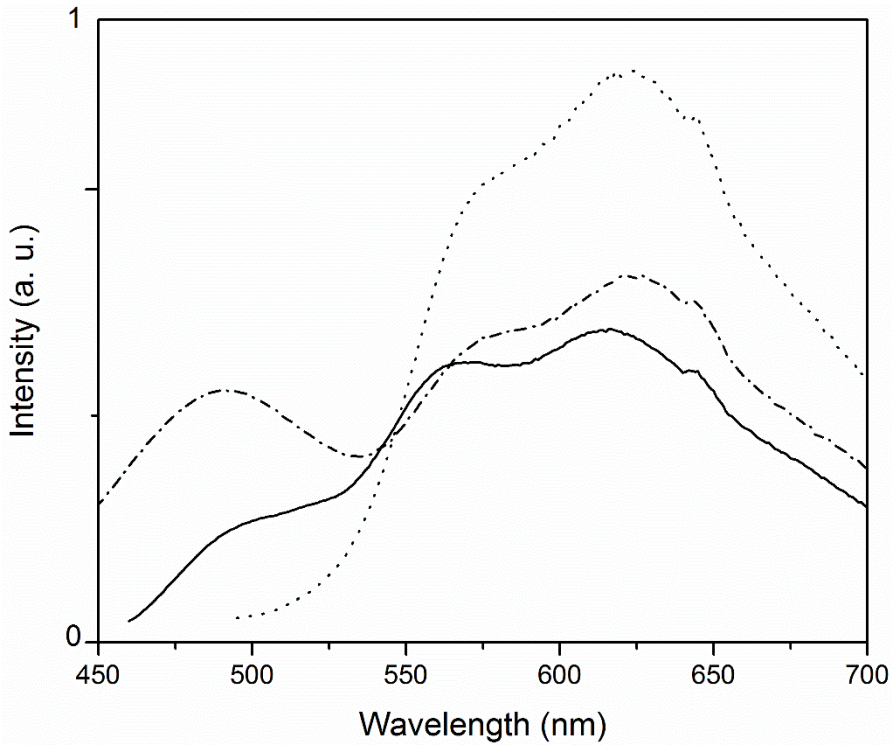

Figure 6.14 – Steady state fluorescence emission spectra of **P1** (1.7 % MeOH, ionic strength 0.1M ($NaClO_4$ or $HClO_4$), [**P1**] = 0.007 wt %). Full line: at pH 1.2 and (λ_{exc} = 442 nm, dashed line: at pH = 5.3 and λ_{exc} = 370 nm and pointed line: at pH = 5.3 and λ_{exc} = 476 nm.

As expected, when the equilibrated solutions at pH = 1.2 and pH = 5.3 were irradiated under 366 nm UV light an orange and yellow colour can be observed, respectively (Figure 6.15).

Figure 6.15 – Image of the solutions at pH=1.2 (left) and at pH=5.3 (right) under 366 nm UV light.

6.2.4. Kinetics of the Flavylium Network

The network of chemical reactions involving synthetic flavylium compounds (Scheme 6.1) can be separated into four processes taking in account their timescales [36,38]: 1) fast proton transfer equilibria (microseconds) [58]; 2) pseudo-equilibrium between flavylium cation and hemiketal during the hydration reaction (seconds to minutes) [58,59]; 3) ring opening and closing processes during tautomerization process (sub-seconds) [56,60] and 4) the slowest process, *cis-trans* isomerisation (seconds to days) [56,60]. In most cases, it is possible to separate if not all, at least three of this four kinetics processes using appropriate techniques, in order to obtain the respective rate constants. The overall kinetic process is very dependent on the magnitude of the *cis-trans* isomerisation

barrier. In the case of the barrier is higher, *cis-trans* isomerisation is the rate-determining step and the four processes can be separated [38].

As already mentioned above the proton transfer reaction is a very fast process, as consequence conventional spectrophotometry, including stopped flow analysis, is useless. The respective kinetics can be obtained, for example, by means of temperature jump techniques, because the transfer of a proton from flavylium cation to water is exothermic [58,61] or flash photolysis when excited state proton transfer between flavylium cation and quinoidal base occurs [62]. Relatively to the other kinetics of the system, they can be easily access by pH jumps. Typically, an equilibrated solution where the flavylium cation is dominant species (very acidic pH values) is made less acidic by addition of base to higher pH values or vice-verse (reverse pH jumps). The spectral variations can be monitored by stopped-flow or, when the kinetic processes are sufficiently slow by a spectrophotometer.

In general, after a pH jump and depending on pH, the flavylium cation, **AH⁺**, can be partially or completely transformed into the quinoidal base (**A**, kinetic product). This proton transfer process is very fast and for this reason cannot be followed by conventional spectrophotometer, as already mentioned below. This first (pseudo) equilibrium is exponentially attained and can be described by Equation 6.9.

$$k_1 = k_a + k_{-a}([H^+])$$

Equation 6.9

Where the rate constant, $\mathbf{k_1}$, results from the sum of the forward and backward reactions (second order process) [38,62]. After this process, a hydration reaction of **AH⁺** to give **B** occurs, followed by tautomerization of **B** leading to formation of *cis*-chalcone (**Cc**). During the hydration process, the kinetic product **A** disappears at the same rate of **AH⁺**, once **AH⁺** and **A** behave as single species, since their formation. Once **B** is formed, rapidly equilibrates with **Cc** and this pair behave kinetically also as single species. Thus, the tautomerization process is considered much more rapid than the hydration process, unless for very acidic pH values. For this reason, the hydration process is the rate-determining step and a second (pseudo) equilibrium exponentially is achieved by the system (Equation 6.10) [38,62].

$$k_2 = \frac{[H^+]}{[H^+] + K_a} k_h + \frac{1}{1 + K_t} k_{-h}[H^+]$$

Equation 6.10

Finally, the isomerisation process of *cis*-chalcone (**Cc**) to *trans*-chalcone (**Ct**). This process occurs in a timescale much slower process than all the other processes. The respective rate constant results from the sum of the direct step multiplied by the mole fraction available of *cis*-chalcone available to convert in *trans*-chalcone and the reverse isomerisation process (Equation 6.11) [62].

$$k_3 = \frac{[H^+]}{[H^+] + K_a + K_h + K_h K_t} k_i + k_{-i}$$

Equation 6.11

The spectra variations taken immediately after a pH jump from equilibrated solutions of **P1** at pH=1 to moderately acidic and neutral pH values as indicated in Figure 6.16.

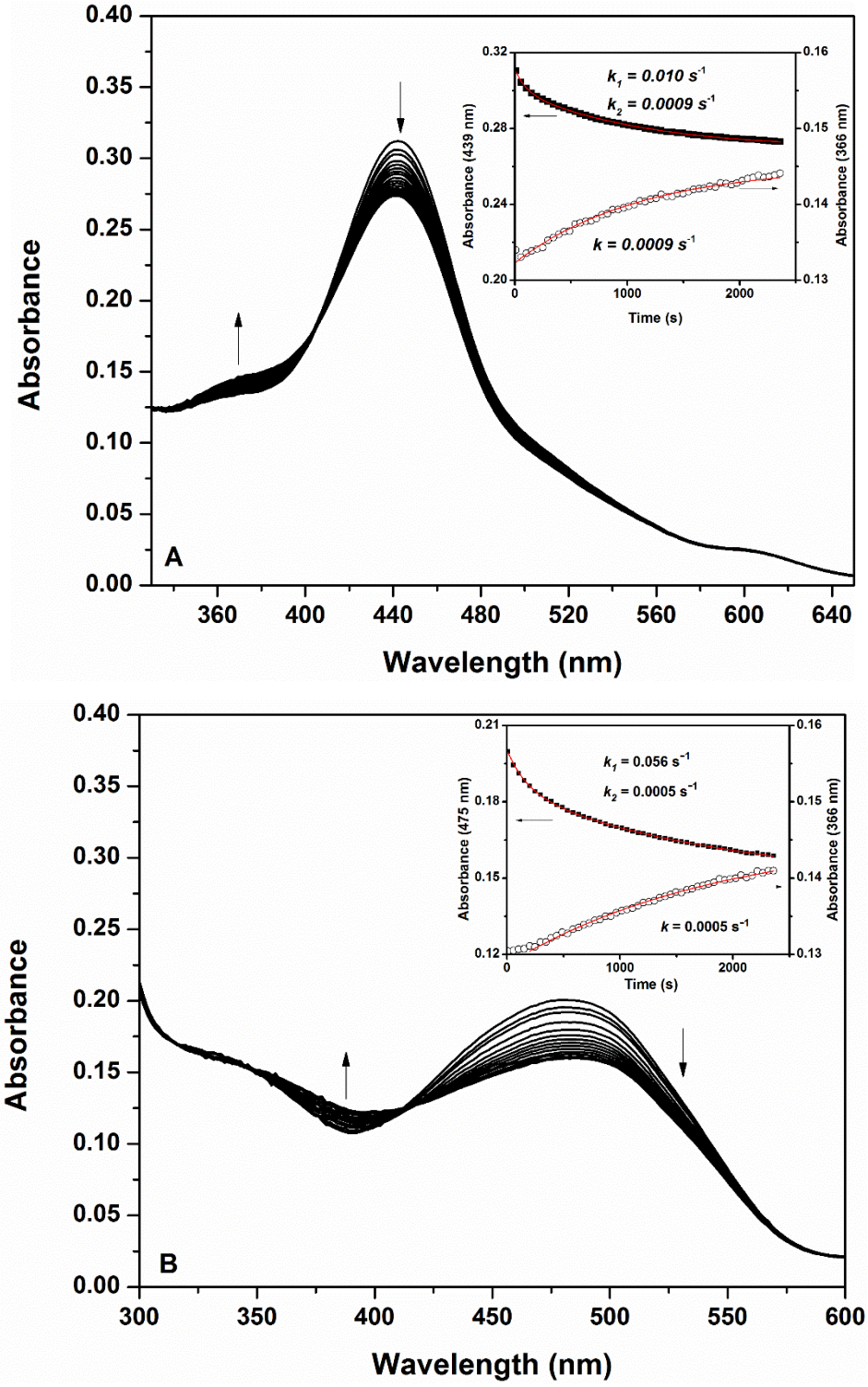

Figure 6.16 – Time evolution of UV-Vis spectra upon a pH jump from a stock aqueous solution of **P1** (1.7% MeOH, ionic strength = 0.1M ($NaClO_4$ or $HClO_4$), [**P1**] = 0.007 wt %, T = 21 ºC) (A) at pH = 1 to pH = 3.4 and (B) at pH=1 to pH = 6.2. Insets: Fittings of the absorbance values to the specified wavelengths to a single or double exponential.

The spectral variations that occurs in **P1** (see Figure 6.16) at the absorption wavelength of $\mathbf{AH^+}$ and/or **A** reveal a bi-exponential process, whereas the trace at 366 nm (absorption of **Ct**) can be fitted as a mono-exponential growth, with a delay during the first seconds. In the last case, the observed rate constant is coincident with the slowest rate calculated for the bi-exponential decay

of **AH^+/A**. This behaviour is in fact compatible with the attainment of the pseudo-equilibrium involving **AH^+**/**A**, **B** and **Cc** previously to the formation of **Ct**. On the other hand, in flavylium cations possessing hydroxyl groups in position 7, the hydration and tautomerization reactions are often too fast to be observed by conventional spectrophotometers for pH < 4, and monoexponential kinetic laws are observed [35]. Thus, the bi-exponential behaviour in Figure 6.16A (pH = 3.4) seems to indicate that the polymer backbone slows down the hydration process because the tautomerization reaction is an intramolecular process, and therefore less prone to be affected.

The kinetics of the formation of the equilibrium species after direct pH jumps from pH = 1 to pH = 3.4 and pH = 6.2, revealed the lack of a high *cis*-to-*trans* isomerisation barrier for the formation of **Ct**, as expected for flavylium compounds bearing a hydroxyl substituent in position 7 [35]. This behaviour indicates that the polymeric chains are averagely solvated, facilitating the reaction of the flavylium moieties.

6.2.5. Temperature Dependence behaviour

As already mentioned, lower critical solution temperature, LCST, is defined as the critical temperature at which a polymer solution undergoes phase transition from a soluble (T<LCST) to an insoluble state (T>LCST) [6].

This phase separation behaviour can be studied by different techniques, namely, differential scanning calorimetry (DSC), optical cloud point and turbidimetry [7]. PNIPAm undergo a sharp and reversible thermal transition closed to 32 ºC [5].

6.2.5.1. Cloud Point

The lower critical solution temperature (LCST) of **P1** and **PNIPAM** control was determined for several equilibrated solutions at different pH values by measuring the optical density of the solutions at 700 nm (see Figure 6.17 A for **P1** at pH = 1).

The LCST for the polymer **PNIPAM** control increases with increasing pH (Figure 6.17B), going from 31.7 °C to 34.0 °C when the pH changes from 1 to 7. It is known that the addition of salts generally lowers the phase transition temperature of **PNIPAM** [63–65]. This behaviour could be related to interactions of the ions with the hydration water molecules in the polymer and to the increase of the surface tension on the cavity around the isopropyl side chains as well as the polymeric backbone (hydrophobic effect) [63,64,66]. Similar effects can take place in the presence of hydronium ions (H_3O^+), especially the first one, due to the singular and cooperative hydrogen-bond network that solvates protons in bulk water, which should compete and weaken the solvation of the polymeric chains.

In the case of **P1**, the LCST decreases as well in acidic media but the effect is higher than for **PNIPAM**. At pH = 1, the value is 28.2 °C (about 3.5 ºC lower than in the control) and increases with higher pH up to 32.2 °C (pH = 6.4; Figure 6.17B). Interestingly, for **P1** the pH dependence of the LCST can be fitted to a sigmoid curve with an inflection point at pH = 3.6 that corresponds to a mole fraction of **AH^+**~0.5, previously determined through the data from in Figure 6.12 A. This

behaviour indicates that the presence of **AH⁺** in the polymer leads to a reduction in the value of the LCST. This effect can be explained by the hydrophobic character of the flavylium cation that could prevent to a certain extension of the hydrogen bonding network between the amide groups in the polymer and the water molecules and consequently facilitate the collapse of the polymer at lower temperatures.

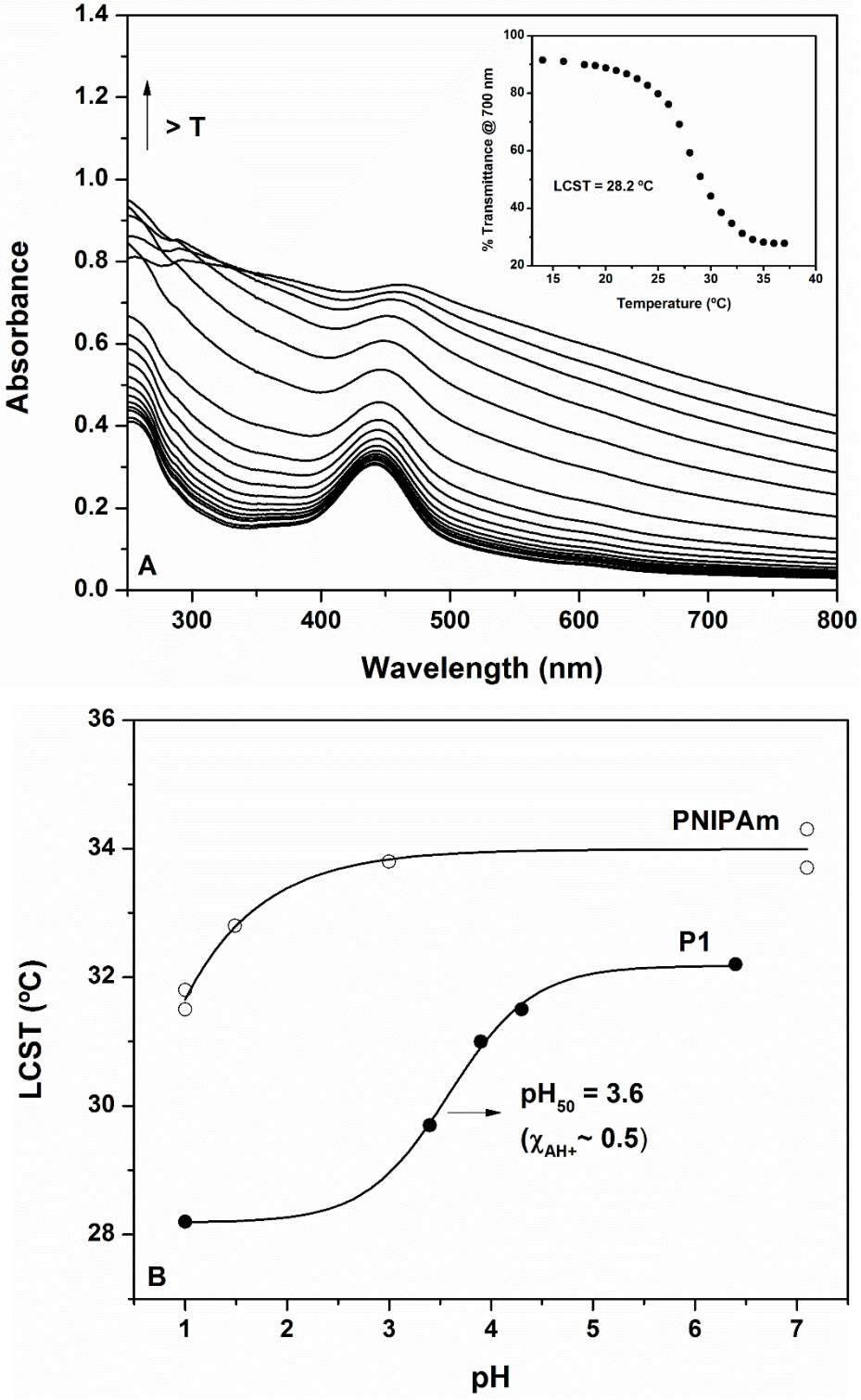

Figure 6.17 – (A) Spectral variations of a solution of **P1** at pH = 1 upon increase of the temperature (inset: transmittance changes at 700 nm and determination of the LCST value by the inflection point method). (B) pH dependence of the LCST of **P1** and **pNIPAM** control.

6.2.5.2. Differential Scanning Calorimetry

Physical processes such as phase transformations, including first order transitions and glass transition can be studied by Differential Scanning Calorimetry (DSC). It is the most popular thermal analysis technique and measures the difference in heat flow between a sample and an inert reference, when they are submitted to a linear change in temperature with time [67]. In other words, this thermal analysis instrument measures the heat flow variation with temperature allowing to determine temperatures and enthalpies associated to physical transitions of the material.

In this work, a polymer control (**control PNIPAm**) in aqueous solutions (without any buffer addition) with 40.3 wt % of polymer content have been studied by conventional DSC. The sample was submitted to a cooling run (25 ºC to -90 ºC), where an exothermic peak was observed (Figure 6.18 A) and can be explained by *o-ring* from pan effect. In the subsequent heating run, a glass transition was observed at -43.7 ºC (mid-point temperature), similar to the values reported in the literature [69]. This low glass transition temperature reflects a significant plastificant effect, since the glass transition of dried PNIPAm is 140.4 ºC, previously determined (see Figure A. 7.4.1 in annex) and the value is according with literature [69].

After the glass transition, it is also observed an exothermic peak corresponding to a cold-crystallization (-17.8 ºC) of the mixture, following the melting (-0.7 ºC). The enthalpy values of cold-crystallization and melting (calculated from the integration of the corresponding peaks) are different (38.4 and 55.3 J/g), suggesting that some crystallization could be occurred upon cooling. In fact, that could be overlapped with *o-ring* effect, previously mentioned.

After, the melting an endothermic peak with minimum at 33.1 ºC is detected that can be associated to LCST process. As expected, the heating and cooling rate influence the LCST position, changing the temperature of collapse of the polymer (Figure 6.18). It is also possible observed in Figure 6.18B that the demixing (collapse of the polymer) is higher than remixing (dissolution of the polymer). This observation can be explained based on kinetic constant rates of the both processes.

Additionally, DSC combined with Modulated Temperature DSC (MTDSC) experiments reveals potential alternative to study LCST behaviour, as well as, to evaluate the kinetics parameters associated to this physical transition, as reported in the literature [68–70]. MTDSC is a recent extension of the conventional DSC technique, in which a sinusoidal (or modulated) run is superimposed to the linear temperature run. This procedure allows simultaneous measurement of heat flow, heat capacity, and heat flow phase, and as a consequence it is possible to decompose the heat capacity component (reversing signal) from the kinetic component (non-reversing signal) of the total heat flow [68]. MTDSC can be a useful tool to study the LCST behavior and the phase separation kinetics of polymer/water solutions over the entire composition range, as reported in the literature [68–70].

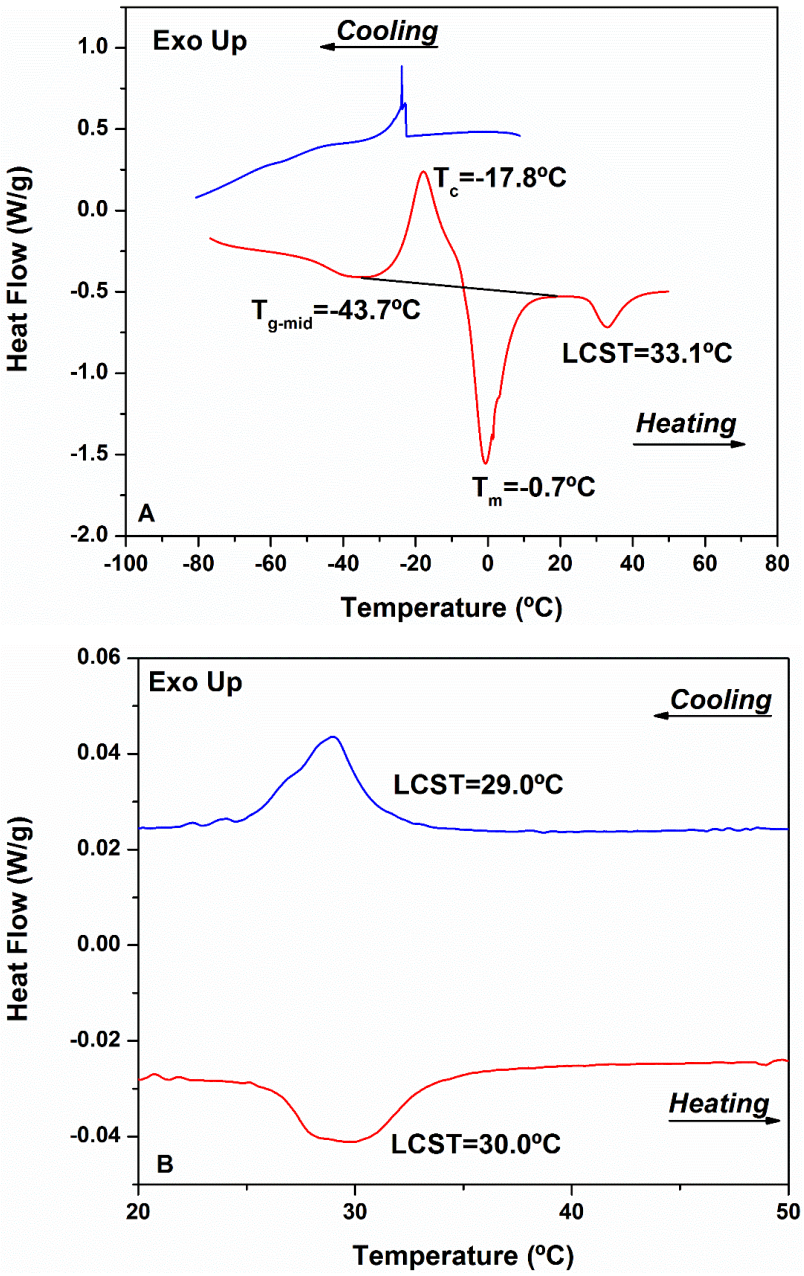

Figure 6.18 – (A) Heat flow thermograms for aqueous solution of PNIPAm (40.3 wt %) obtained upon heating and cooling at rate of 10 ºC/min. (B) LCST obtained upon heating and cooling rate at 0.5 ºC/min (right).

Different thermal-responsive polymers have been studied by DSC and MTDSC [68–72]. One of the examples is the Poly(methyl vinyl ether), that shows a type III LCST demixing behavior in water, contrarily to PNIPAm, that showed a type II demixing behavior according to a classification of polymer/solvent phase diagrams. Since, demixing process primarily consist of breaking hydrogen bonds between polymer chains and water, an endothermic heat effect can be observed by conventional DSC. However, in the case of Poly(methyl vinyl ether) a complex thermal behavior with two overlapping endothermic peaks is observed upon heating. These endothermic peaks can be separated through MTDSC by deconvolution of the endothermic heat effect in a reversing and nonreversing contribution, allowing to characterize the temperature at the three-phase equilibrium [69,71].

6.2.6. Photochemical behaviour

The introduction of flavylium moieties in the polymer reduces the value of the LCST, so it is expected to be possible to induce the photochemical collapse of **P1** by irradiating a solution at appropriate pH and temperature values.

In the flavylium system the photoactive species is the *trans*-chalcone (**Ct**). When a solution of **Ct** is irradiated, the photoproduct, *cis*-chalcone (**Cc**) is formed in picoseconds and then two competitive thermal processes occur, namely the back isomerisation to **Ct** and the formation of $\mathbf{AH^+}$ through the hemiketal **B**. The dehydration of **B** to give $\mathbf{AH^+}$ is pH-dependent becoming slower at higher pH values, and at a certain point, when the pH is too high, the dehydration is too slow and **Ct** is recovered from the mixture of **Cc** and **B** without formation of $\mathbf{AH^+}$ [36]. Taking in account these factors we can estimate that a good pH to photoproduce $\mathbf{AH^+}$, should be one high enough to permit the existence of a significant amount of **Ct** at the equilibrium and low enough to allow **B** to dehydrate and give $\mathbf{AH^+}$.

In the case of the polymer **P1**, we selected for the irradiation an equilibrated solution at pH = 3.9 because at this pH value a significant amount of *trans*-chalcone is present at the equilibrium and it is acidic enough to permit the formation of $\mathbf{AH^+}$ from **B**. On the other hand, the temperature selected for the experiment was 29 °C since in these conditions the formation of $\mathbf{AH^+}$ is expected to produce a collapse of the polymer, as the comparison of the LCST values for pH =1 (28.2 ºC) and pH = 3.9 (31.0 ºC) suggests (see Figure 6.19).

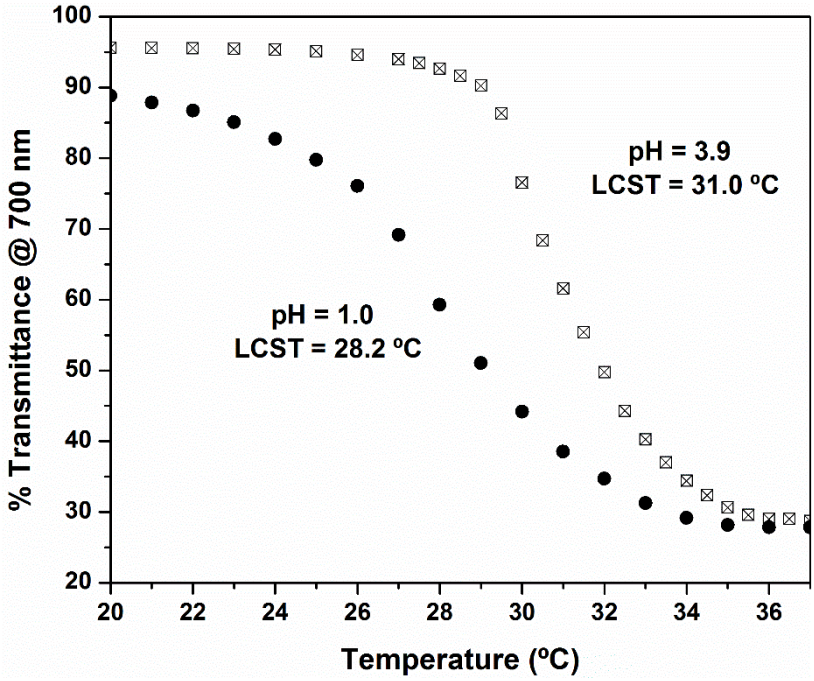

Figure 6.19 – Comparison between the transmittance changes at 700 nm as a function of temperature for **P1** at pH = 1.0 and pH = 3.9.

The equilibrated solutions of **P1** at pH = 3.9 was kept at 29 ºC during 10 min before the irradiation, to stabilise the temperature on the sample and then was irradiated with a Xe lamp (450W) at 370 nm. The evolution of the system was followed by absorption spectroscopy (Figure 6.20).

At the beginning of the irradiation, the baseline did not change but after a certain time the baseline started to rise, indicating that the polymer was collapsing due to the consumption of *trans*-chalcone and appearance of flavylium cation (and quinoidal base). This effect can be clearly observed when the baseline is corrected (Figure 6.20 B). Comparison of both figures makes clear that after the formation of a certain percentage of flavylium cation the polymer started to collapse. After approximately 1 hour of exposition to light, the system started to degrade and the irradiation was stopped. The recovery of the system was followed by absorption spectroscopy at 29 ºC (see Figure 6.21).

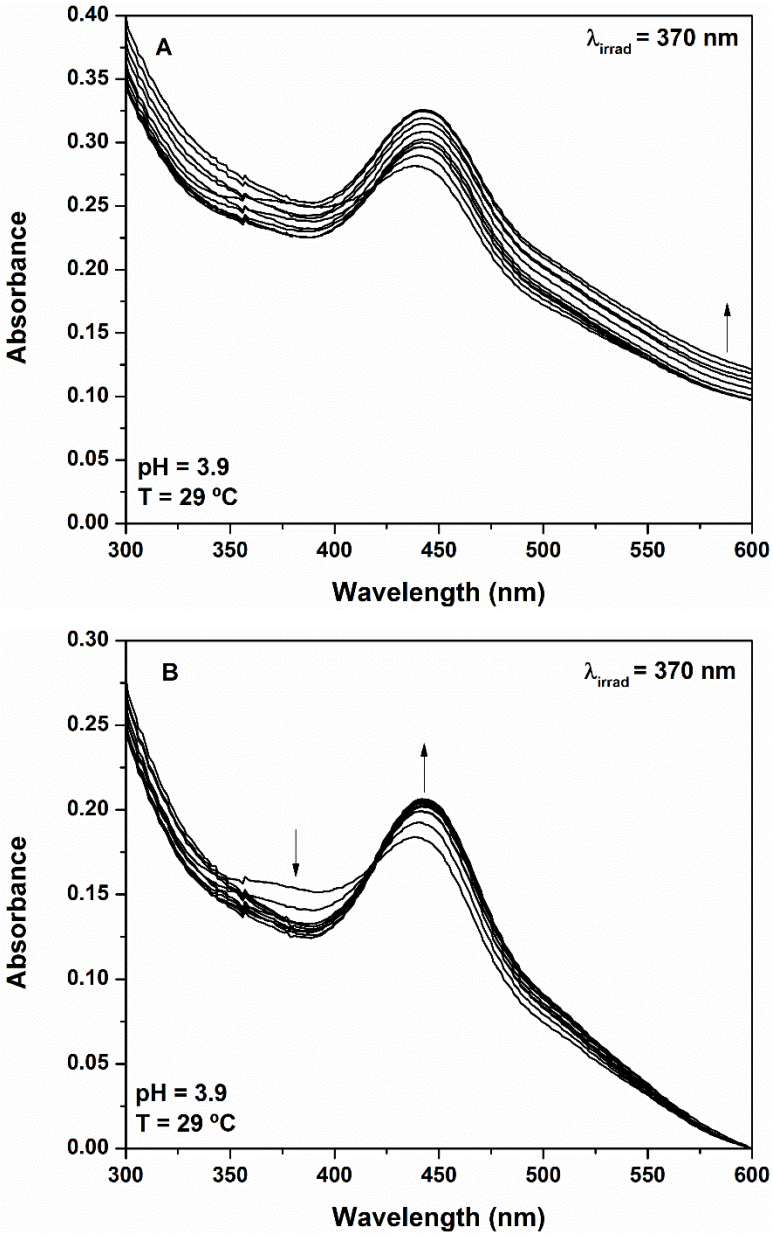

Figure 6.20 – (A) Spectral variations upon irradiation of a solution of **P1** at pH = 3.9 and T = 29 ºC (λ_{irr} = 370 nm, [**P1**] = 0.017 wt %, 1.7% MeOH, [$NaClO_4$] = 0.1 M). The arrow indicates the rise of the baseline due to the collapsing of the polymer. Irradiation times (s): 0, 20, 80, 140, 260, 560, 1160, 1760, 2360, 2960 and 3260. (B) The same as **A** with the baseline corrected showing the consumption of **Ct** (arrow down) and the formation of **AH^+/A** (arrow up).

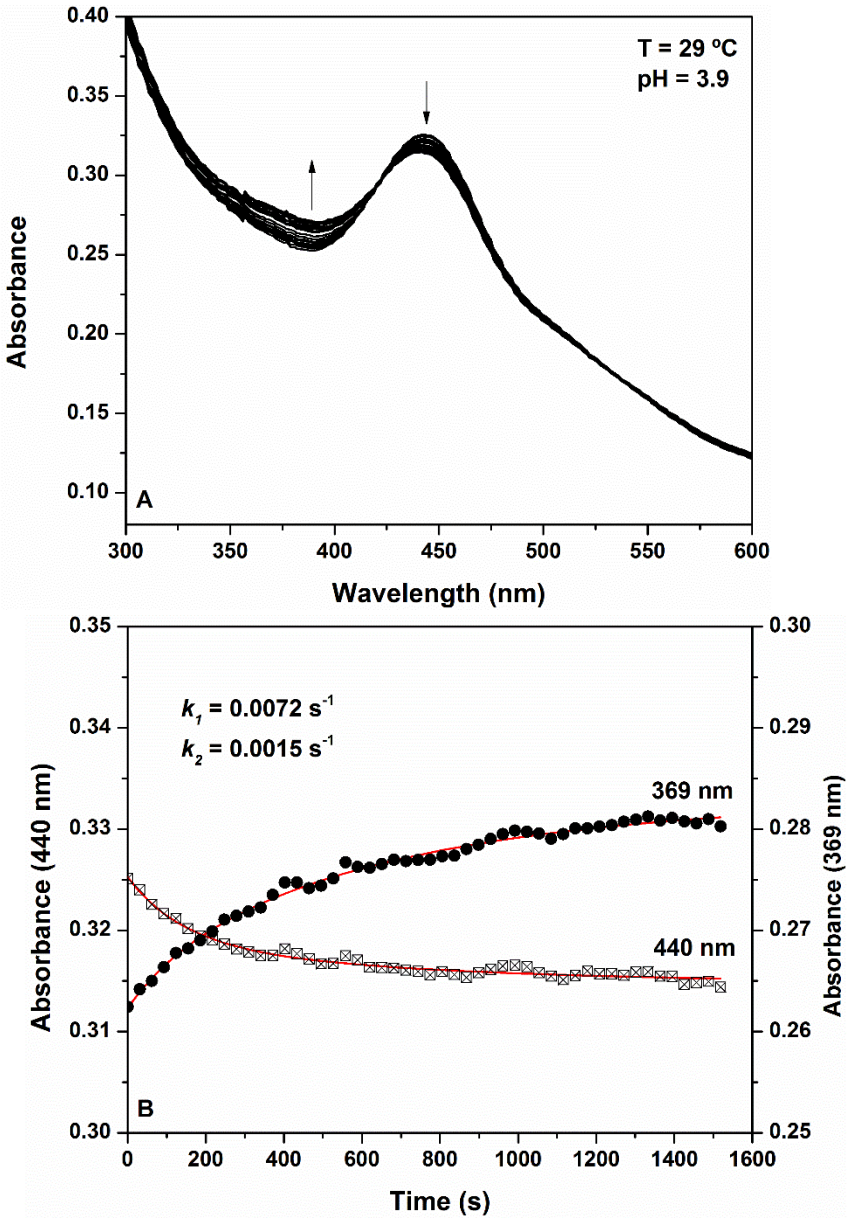

Figure 6.21 – Recovery in the dark of Ct after the irradiation at 29 ºC: (A) Spectral variations. (B) Traces at 369 nm and 440 nm as a function of time.

The subsequent monitoring of the absorbance changes at 29 ºC showed the slow recovery of **Ct**; nevertheless, the collapsed polymer remained precipitated during much more time (several hours) until the polymeric chains could be re-solvated.

6.3. Conclusions

A new multi stimuli-responsive polymer with response to temperature, pH and light was synthesized. The polymer is obtained by co-polymerization of *N*-isopropylacrylamide, which is thermo-responsive polymer (temperature-induces changes) and a vinyl flavylium derivative, which is chromophore that respond to pH and light.

The polymer followed the typical pH-dependent network of reactions of flavylium compounds in water and it showed an unusual large stabilization of the quinoidal base. The incorporation of flavylium cation in the polymer reduces the lower critical solution temperature, LCST, (pH=1, 28.2 ºC) when compared to the PNIPAm control (pH =1, 31.7 ºC), due to the hydrophobic character of the species that may prevent at a certain extension the formation of hydrogen bonds between the polymer and water. It is possible to take profit of this behaviour to photo-collapse partially the polymer, by irradiating a solution at the appropriate pH and temperature. Under suitable irradiation conditions, the *trans*-chalcone leads to the formation of the flavylium cation and the polymer precipitates.

Due to the chemical versatility of flavylium compounds, we believe that this application on the development of multi stimuli-responsive polymers opens a wide range of attractive possibilities.

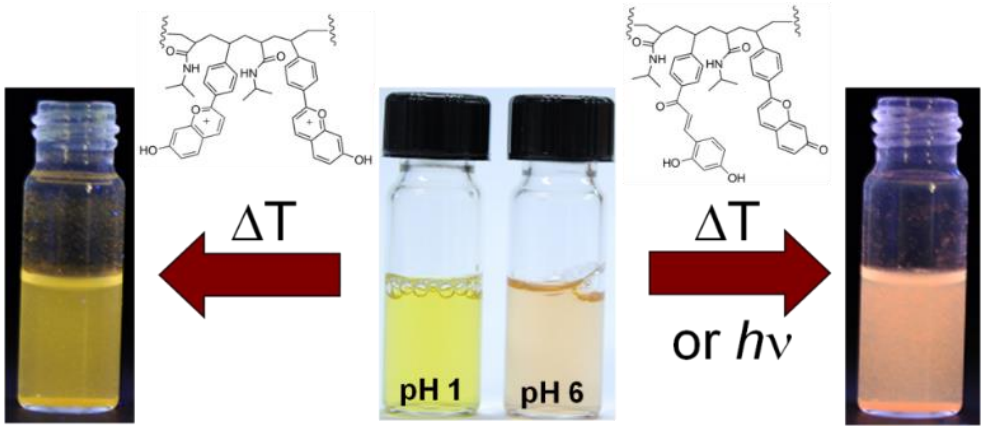

Figure 6.22 – Flavylium-Supported in poly(*N*-isopropylacrylamide) [73]. (Source: *Macromolecules*, 2013, **46**, 9055–9063).

6.4. Experimental Section

General

All reagents and solvents from analytical grade were used. NMR spectra were performed in the Bruker ARX 400 instrument operating at 400.13 MHz (^{1}H) or a Bruker Avance III 400 operating at 400.15 MHz (^{1}H) and 100.62 MHZ (^{13}C). Signals of deuterated solvents were used as internal references. FTIR analyses were carried out using a Nicolet Nexus spectrophotometer coupled to a Continuum microscope (15x objective) with a MCT-A detector cooled by liquid nitrogen. The spectra were collected in transmission mode, in 50 –100 mm areas; resolution set to 4 cm^{-1} and 128 or 256 scans, using a Thermo diamond anvil compression cell. ESI-TOF HRMS mass spectra were performed on a Bruker microTOF (Bruker Corporation). MALDI-TOF MS analyses were performed on a Voyager-DETM PROBiospectrometry Workstation model (Applied Biosytems) and data were analysed with Voyager V5.1 software. Dithranol was employed as the matrix and $NaBF_4$ was added to improve the ionization. Samples and matrix were dissolved in acetone and the spectra were recorded on the positive linear mode. Solutions were prepared in Millipore water containing 1.7 % of spectroscopic MeOH. Polymeric concentration was set at 0.017 wt %. The pH of the solutions was adjusted by the addition of $HClO_4$, NaOH and the universal buffer of Theorell and Stenhagen and it was measured on a Radiometer Copenhagen PHM240 pH/ion meter. In all measurements, the ionic strength was kept constant at 0.1 M by the addition of $NaClO_4$. UV-vis absorption spectra were recorded on a Varian Cary 100 Bio spectrophotometer. Emission spectra were registered on a Jobin Yvon Spex, Fluorolog FL3-22. Photo-excitation in continuous irradiation experiments was carried out with a Xe lamp (450W) using a monochromator to select the 370 ± 7 nm window and a thermostatized bath was employed to keep the sample at the selected temperature. LCST values were determined by measuring the transmittance at 700 nm on a Varian Cary 100 Bio spectrophotometer and using the inflection point method. The temperature of the cell was regulated to ± 0.1 °C by a circulating water bath.

Synthesis of 4'-vinylacetophenone

The compound was prepared according to the Hiyama coupling reaction as described previously in the literature, using sodium hydroxide as activating agent, palladium(II) acetate and tetra-*n*-butylammonium bromide (TBAB) as catalyst and phase transfer catalyst, respectively [46]. In a high pressure glass vessel with septum, *p*-bromoacetophenone (10.12 mmol; 2.01 g), vinyltrimethoxysilane (20.37 mmol; 3.02 g), palladium acetate (0.06 mmol; 0.01 g) and TBAB (0.01 mmol; 4.06 g) were mixed, and then water (20 mL) was added and the mixture deoxygenated with argon. Next, 2 mL of a previously deoxygenated 50 wt % NaOH aqueous solution was added dropwise to the mixture under argon atmosphere, and the vessel was locked, while a white-off solid appeared. After that, the reaction was carried out on a microwave reactor by performing 8 consecutive cycles of 5 min duration with 80 Watts power and *ca.* 1.4 bar pressure. After every cycle, the mixture was cooled with an air stream during 2 min. Afterwards, the reaction mixture was let to cool at room temperature. The product was extracted with diethyl ether (8 x 75 mL), and then washed with 2 M NaOH (2 x 60 mL), 2 M HCl (2 x 60 mL) and water

(2 x 60 mL). The ether extract was then dried with anhydrous sodium sulfate and the solvent evaporated. The product was dried under vacuum yielding a yellow oil (1.18 g, 80 %). ^{1}H NMR (400.13 MHz, 25 ºC, $CDCl_3$) δ = 7.92 (d, 2H, J = 7.2 Hz), 7.48 (d, 2H, J = 7.3 Hz), 6.76 (dd, 1H, J = 17.6 and 10.8 Hz), 5.88 (d, 1H, J = 17.6 Hz,), 5.40 (d, 1H, J = 10.8 Hz), 2.60 (s, 3H) ppm.

Synthesis of 7-hydroxy-4'-vinylflavylium hydrogensulfate (1)

This compound was prepared by condensation of 4'-vinylacetophenone (3.54 mmol; 520 mg) with 2,4-dihydroxybenzaldehyde (3.54 mmol; 490 mg) in acidic medium. The reagents were dissolved in 7.1 mL of acetic acid and 1.8 mL of sulfuric acid and the reaction mixture was stirred at room temperature overnight. Then, the product was precipitated using ethyl acetate and the solid washed with this solvent several times. The compound was dried under vacuum yielding a brownish powder (530 mg, 44 %). ^{1}H NMR (400.15 MHz, 25 ºC, CD_3OD/DCl, pD < 1, **AH$^+$** species) δ = 9.32 (d, 1H, J = 8.5 Hz, H4), 8.54 (d, 1H, J = 8.6 Hz, H3), 8.49 (d, 2H, J = 8.4 Hz, H2', H6'), 8.29 (d, 1H, J = 9.0 Hz, H5), 7.82 (d, 2H, J = 8.4 Hz, H3', H5'), 7.67 (d, 1H, J = 1.9 Hz, H8), 7.52 (dd, 1H, J = 9.0 and 2.1 Hz, H6), 6.91 (dd, 1H, J = 17.6 and 11.0 Hz, CH=CH_2), 6.14 (d, 1H, J = 17.6 Hz, CH=CH(*trans*)), 5.57 (d, 1H, J = 10.9 Hz, CH=CH(*cis*)) ppm. ^{13}C NMR (400.15 MHz, 25 ºC, CD_3OD/DCl, pD < 1, **AH$^+$** species) δ = 172.8, 171.5, 161.3, 156.2, 146.6, 136.7, 134.5, 131.0, 129.5, 128.9, 123.6, 121.5, 119.9, 114.3, 103.8 ppm. ESI-TOF HRMS: *m/z* (%) calcd for $C_{17}H_{13}O_2^+$: 249.0910; found: 249.0909 [M^+] (100).

Synthesis of poly(*N*-isopropylacrylamide-co-7-hydroxy-4'-vinylflavylium) (P1)

The synthesis was carried out by free-radical polymerization in a solvent mixture DMF/H_2O (90/10; v/v) in the presence of 0.3 M HCl and employing 2,2'-azobisisobutyronitrile (AIBN) as the initiator. First, the solvent mixture was deoxygenated during 15 minutes with argon. Then, *N*-isopropylacrylamide (NIPAM, 2.23 mmol; 250 mg), 7-hydroxy-4'-vinylflavylium hydrogensulfate (0.04 mmol; 13 mg) and AIBN (2.6 mg, 1 wt % with respect to the monomers) were dissolved in 1.67 mL of the solvent mixture. The flask was sealed with a rubber septum, the temperature was raised to 85 °C, and the mixture let to react during one hour. The reaction mixture was then cooled at room temperature and the product was precipitated in ethyl acetate. The polymer was dissolved in 0.5 M HCl, and re-precipitated by warming at 50 °C. The precipitate was isolated by filtration and washed carefully with hot water. A last precipitation was carried out by dissolving the polymer in methanol, precipitating with hot water and washing with diethyl ether. The polymeric solid was recovered from the sintered glass funnel by dissolving in methanol, the solvent was evaporated and the brown polymeric solid dried under vacuum (70 mg; 26 %). The mole fraction content of the flavylium moiety in the polymer is ~ 0.4% from comparison between the ^{1}H NMR integrations of proton H4 of the flavylium and the proton corresponding to -CH- in the isopropyl group of NIPAM. ^{1}H NMR (400.15 MHz, 25 ºC, CD_3OD/DCl, pD < 1, **AH$^+$** species for flavylium): δ = 9.35 (br, 1H, H4), 8.61 – 8.22 (br, 4H, H3, H2', H6', H5), 7.71 – 7.34 (br, 4H, H8, H3', H5', H6), 3.97 (br, 1H, $(CH_3)_2CH$ from NIPAM), 2.13 (br, 1H, CH in polymeric backbone), 1.62 (br, 2H, CH_2 in polymeric backbone), 1.17 (br, 6H, $(CH_3)_2CH$ from NIPAM) ppm. FTIR (solid): $\tilde{\upsilon}$ = 3298 cm^{-1}

(secondary amide N-H stretching), 2972 cm^{-1} (-CH_3 asymmetric stretching), 1651 cm^{-1} (amide I bond), 1547 cm^{-1} (amide II bond).

Synthesis of poly (N-isopropylacrylamide) (PNIPAM)

N-isopropylacrylamide (2.23 mmol; 250 mg) was polymerized in the presence of AIBN (2.5 mg; 1 wt % with respect to the monomers) using the same reaction and purification conditions that in the case of **P1**. The polymer was isolated as a white powder (88 mg; 35 %). ^{1}H NMR (400.13 MHz, 25ºC, CD_3OD) δ = 8.16 – 7.16 (br, 1H, N*H*), 3.97 (br, 1H, $(CH_3)_2CH$), 2.09 (br, 1H, C*H* in polymeric backbone), 1.80 – 1.27 (br, 2H, CH_2 in polymeric backbone), 1.16 (br, 6H, $(CH_3)_2CH$) ppm. FTIR (solid): υ = 3286 cm^{-1} (secondary amide N-H stretching), 2972 cm^{-1} (-CH_3 asymmetric stretching), 1651 cm^{-1} (amide I bond), 1549 cm^{-1} (amide II bond). MALDI-TOF MS: M_w = 7842 g/mol, M_n = 6521 g/mol, PDI = M_w/M_n = 1.2.

6.5. References

1 J. Thévenot, H. Oliveira, O. Sandre and S. Lecommandoux, *Chem. Soc. Rev.*, 2013, **42**, 7099–116.

2 P. Schattling, F. D. Jochum and P. Theato, *Polym. Chem.*, 2014, **5**, 25–36.

3 H. R. Schneider, in *Chemoresponsive Materials: Stimulation by Chemical and Biological Signals*, The Royal Society of Chemistry, 2015, pp. 1–9.

4 D. Schmaljohann, *Adv. Drug Deliv. Rev.*, 2006, **58**, 1655–1670.

5 H. G. Schild, *Prog. Polym. Sci.*, 1992, **17**, 163–249.

6 E. S. Gil and S. M. Hudson, *Prog. Polym. Sci.*, 2004, **29**, 1173–1222.

7 C. Boutris, E. G. Chatzi and C. Kiparissides, *Polymer,* 1997, **38**, 2567–2570.

8 D. Roy, W. L. Brooks and B. S. Sumerlin, *Chem. Soc. Rev.*, 2013, **42**, 7214–7243.

9 C. Alarcon, S. Pennadam and C. Alexander, *Chem. Soc. Rev.*, 2005, **34**, 276–85.

10 A. Halperin, M. Kröger and F. M. Winnik, *Angew. Chem., Int. Ed.*, 2015, **54**, 15342–15367.

11 F. D. Jochum and P. Theato, *Chem. Soc. Rev.*, 2013, **42**, 7468–7483.

12 L. Klouda, *Eur. J. Pharm. Biopharm.*, 2015, **97**, 338–349.

13 T. Yakushiji, K. Sakai, A. Kikuchi, T. Aoyagi, Y. Sakurai and T. Okano, *Anal. Chem.*, 1999, **71**, 1125–1130.

14 J. Kim, M. J. Serpe and L. A. Lyon, *Angew. Chem., Int. Ed.*, 2005, **44**, 1333–1336.

15 Z. Tang, Y. Akiyama and T. Okano, *J. Polym. Sci., Part B: Polym. Phys.*, 2014, **52**, 917–926.

16 M. Nakayama and T. Okano, *J. Drug Deliv. Sci. Technol.*, 2006, **16**, 35–44.

17 H. Jean-Ruel, M. Gao, M. A. Kochman, C. Lu, L. C. Liu, R. R. Cooney, C. A. Morrison and R. J. D. Miller, *J. Phys. Chem. B*, 2013, **117**, 15894–15902.

18 J. Akimoto, M. Nakayama, K. Sakai and T. Okano, *Biomacromolecules*, 2009, **10**, 1331–1336.

19 T. Okano, Y. H. Bae, H. Jacobs and S. W. Kim, *J. Control. Release*, 1990, **11**, 255–265.

20 J.-M. Schumers, C.-A. Fustin and J.-F. Gohy, *Macromol. Rapid Commun.*, 2010, **31**, 1588–1607.

21 J. Jiang, X. Tong, D. Morris and Y. Zhao, *Macromolecules*, 2006, **39**, 4633–4640.

22 H. Zhao, W. Gu, E. Sterner, T. P. Russell, E. B. Coughlin and P. Theato, *Macromolecules*, 2011, **44**, 6433–6440.

23 H. Zhao, E. S. Sterner, E. B. Coughlin and P. Theato, *Macromolecules*, 2012, **45**, 1723–1736.

24 O. Bertrand, J.-M. Schumers, C. Kuppan, J. Marchand-Brynaert, C.-A. Fustin and J.-F. Gohy, *Soft Matter*, 2011, **7**, 6891–6896.

25 S. Kumar, Y. L. Dory, M. Lepage and Y. Zhao, *Macromolecules*, 2011, **44**, 7385–7393.

26 J.-M. Schumers, O. Bertrand, C.-A. Fustin and J.-F. Gohy, *J. Polym. Sci., Part A: Polym. Chem.*, 2012, **50**, 599–608.

27 B. Yan, J.-C. Boyer, N. R. Branda and Y. Zhao, *J. Am. Chem. Soc.*, 2011, **133**, 19714–19717.

28 D. Kungwatchakun and M. Irie, *Makromol. Chem., Rapid Commun.*, 1988, **9**, 243–246.
29 M. Irie and D. Kungwatchakun, *Proc. Japan Acad. Ser. B*, 1992, **68**, 127–132.
30 H. Akiyama and N. Tamaoki, *Macromolecules*, 2007, **40**, 5129–5132.
31 L. Li, X. Xing and Z. Liu, *J. Appl. Polym. Sci.*, 2012, **124**, 1128–1136.
32 F. D. Jochum and P. Theato, *Macromolecules*, 2009, **42**, 5941–5945.
33 A. E. Ivanov, N. L. Eremeev, P.-O. Wahlund, I. Y. Galaev and B. Mattiasson, *Polymer*, 2002, **43**, 3819–3823.
34 F. Pina, M. J. Melo, H. Santos, J. C. Lima, I. Abreu, R. Ballardini and M. Maestri, *New J. Chem.*, 1998, **22**, 1093–1098.
35 A. Roque, J. C. Lima, A. J. Parola and F. Pina, *Photochem. Photobiol. Sci.*, 2007, **6**, 381–385.
36 F. Pina, M. J. Melo, C. A. T. Laia, A. J. Parola and J. C. Lima, *Chem. Soc. Rev.*, 2012, **41**, 869.
37 F. Pina, *J. Agric. Food Chem.*, 2014, **62**, 6885–6897.
38 F. Pina, V. Petrov and C. A. T. Laia, *Dye. Pigment.*, 2012, **92**, 877–889.
39 R. Gavara, S. Gago, N. Jordão and F. Pina, *J. Phys. Chem. A*, 2014, **118**, 4723–4731.
40 F. Pina and T. A. Hatton, *Langmuir*, 2008, **24**, 2356–2364.
41 R. Gomes, C. A. T. Laia and F. Pina, *J. Phys. Chem. B*, 2009, **113**, 11134–11146.
42 R. Matsushima and M. Suzuki, *Bull. Chem. Soc. Jpn.*, 1992, **65**, 39–45.
43 R. Matsushima, K. Kato and S. Ishigai, *Bull. Chem. Soc. Jpn.*, 2002, **75**, 2079–2080.
44 F. Galindo, J. C. Lima, S. V. Luis, A. J. Parola and F. Pina, *Adv. Funct. Mater.*, 2005, **15**, 541–545.
45 F. Galindo, J. C. Lima, S. V Luis, M. J. Melo, A. J. Parola and F. Pina, *J. Mater. Chem.*, 2005, **15**, 2840–2847.
46 E. Alacid and C. Nájera, *J. Org. Chem.*, 2008, **73**, 2315–2322.
47 A. M. Diniz, C. Pinheiro, V. Petrov, A. J. Parola and F. Pina, *Chem. Eur. J.*, 2011, **17**, 6359–6368.
48 Y. Kotsuchibashi, Y. Kuboshima, K. Yamamoto and T. Aoyagi, *J. Polym. Sci., Part A: Polym. Chem.*, 2008, **46**, 6142–6150.
49 D. Li, X. Zhang, J. Yao, G. P. Simon and H. Wang, *Chem. Commun.*, 2011, **47**, 1710–1712.
50 T. Schulte, K. O. Siegenthaler, H. Luftmann, M. Letzel and A. Studer, *Macromolecules*, 2005, **38**, 6833–6840.
51 L. Fernandes, R. Rial-Otero, M. Temtem, C. V. Macedo, A. Aguiar-Ricardo and J. L. Capelo, *Talanta*, 2008, **77**, 882–888.
52 P. G. de Gennes, in *Scaling Concepts in Polymer Physics*, Cornell University Press, Ithaca, NY, 1979.
53 G. Williams and D. C. Watts, *Trans. Faraday Soc.*, 1970, **66**, 80–85.
54 E. Klüver and M. Meyer, *J. Appl. Polym. Sci.*, 2013, **128**, 4201–4211.
55 Y. Leydet, R. Gavara, V. Petrov, A. M. Diniz, A. J. Parola, J. C. Lima and F. Pina,

Phytochemistry, 2012, **83**, 125–135.

56 R. A. McClelland and G. H. McGall, *J. Org. Chem.*, 1982, **47**, 3730–3736.

57 J. T. Edsall and J. Wyman, *Biophysical Chemistry*, Academic Press, New York, 1958.

58 R. Brouillard and J.-E. Dubois, *J. Am. Chem. Soc.*, 1977, **99**, 1359–1364.

59 R. Brouillard and B. Delaporte, *J. Am. Chem. Soc.*, 1977, **99**, 8461–8468.

60 R. A. McClelland and S. Gedge, *J. Am. Chem. Soc.*, 1980, **102**, 5838–5848.

61 F. Pina, *J. Chem. Soc. Faraday Trans.*, 1998, **94**, 2109–2116.

62 F. Pina, J. Oliveira and V. de Freitas, *Tetrahedron*, 2015, **71**, 3107–3114.

63 R. Freitag and F. Garret-Flaudy, *Langmuir*, 2002, **18**, 3434–3440.

64 Y. Zhang, S. Furyk, D. E. Bergbreiter and P. S. Cremer, *J. Am. Chem. Soc.*, 2005, **127**, 14505–14510.

65 H. Du, R. Wickramasinghe and X. Qian, *J. Phys. Chem. B*, 2010, **114**, 16594–16604.

66 Y. Hiruta, Y. Nagumo, Y. Suzuki, T. Funatsu, Y. Ishikawa and H. Kanazawa, *Colloids Surf., B,* 2015, **132**, 299–304.

67 G. Höhne, W. F. Hemminger and H.-J. Flammersheim, *Differential Scanning Calorimetry*, Springer-Verlag Berlin Heidelberg, 2nd edn., 2003.

68 J. Zhao, J. Shan, G. Van Assche, H. Tenhu and B. Van Mele, *Macromolecules*, 2009, **42**, 5317–5327.

69 K. Van Durme, G. Van Assche and B. Van Mele, *Macromolecules*, 2004, **37**, 9596–9605.

70 K. Van Durme, S. Verbrugghe, F. E. Du Prez and B. Van Mele, *Macromolecules*, 2004, **37**, 1054–1061.

71 K. Van Durme, G. Van Assche, H. Rahier and B. Van Mele, *J. Therm. Anal. Calorim.*, 2009, **98**, 495–505.

72 K. Van Durme, S. Verbrugghe, F. E. Du Prez and B. Van Mele, *Macromolecules*, 2004, **37**, 1054–1061.

73 N. Jordão, R. Gavara and A. J. Parola, *Macromolecules*, 2013, **46**, 9055–9063.

7. Annexes

7.1. Electrochromic Organic Salts: 4,4'-Bipyridinium Derivatives

7.1.1. NMR spectra

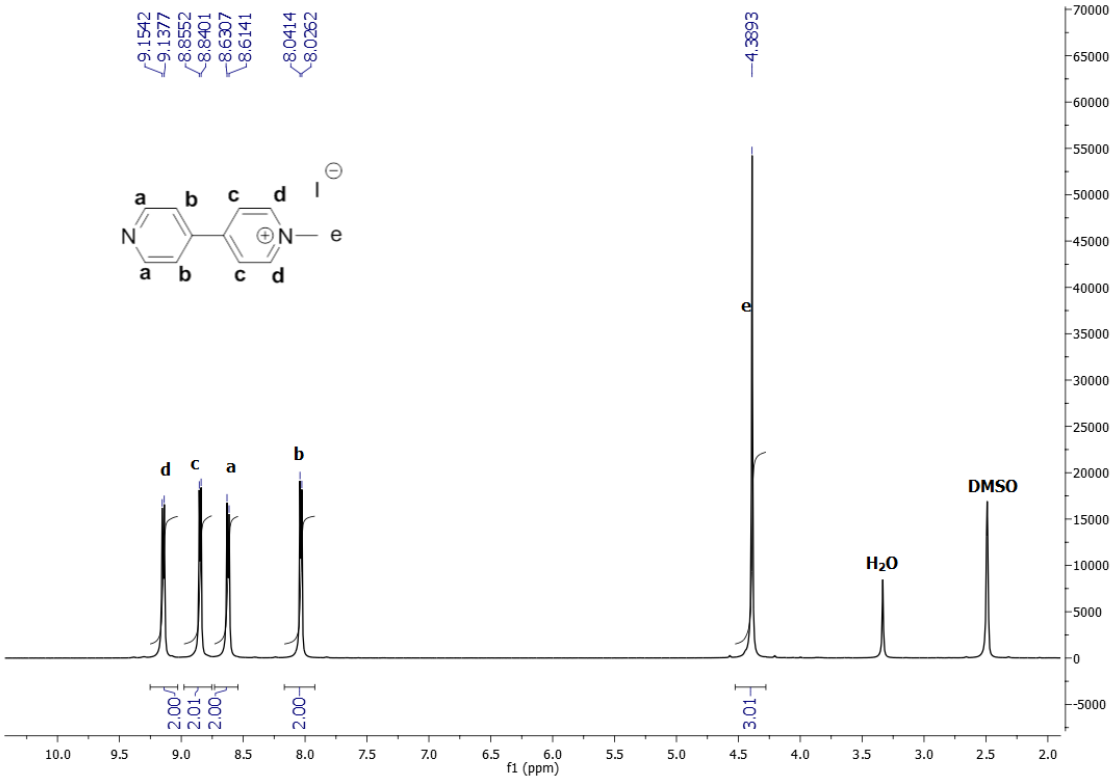

Figure A. 7.1.1 – ^{1}H NMR (DMSO-d6, 400.13 MHz, 25 ºC, ppm) of [C_1bpy]I.

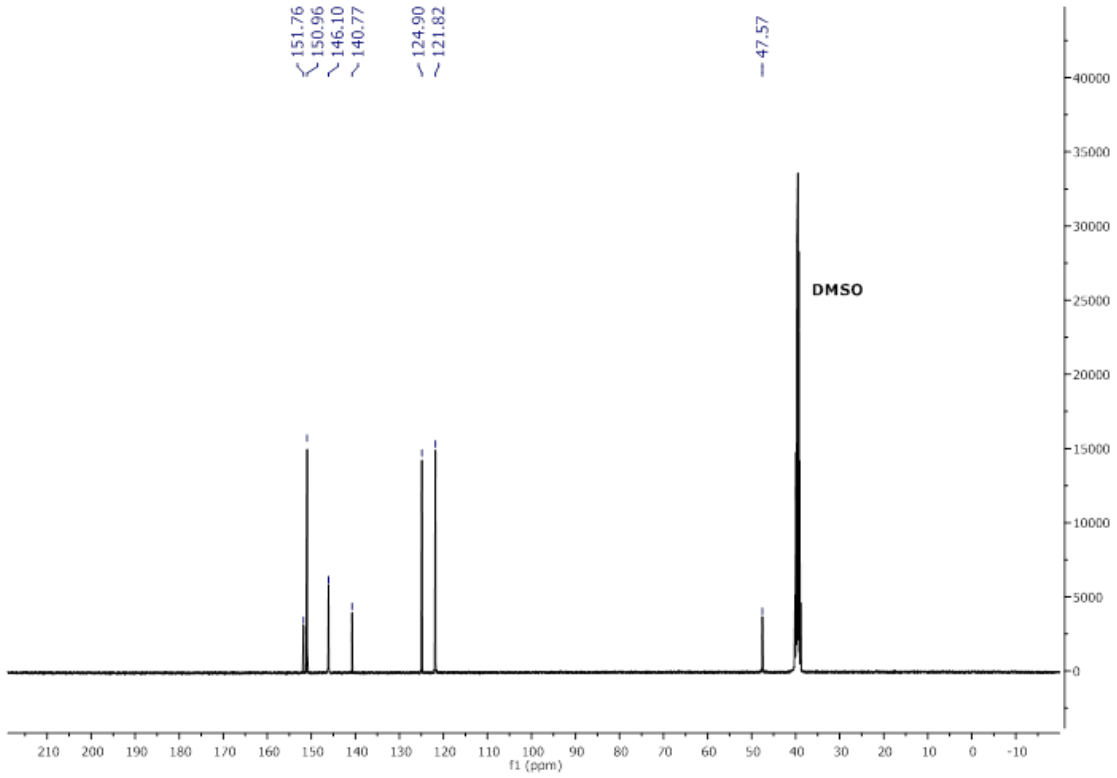

Figure A. 7.1.2 – ^{13}C NMR (DMSO-d6, 100.61 MHz, 25 ºC, ppm) of [C_1bpy]I.

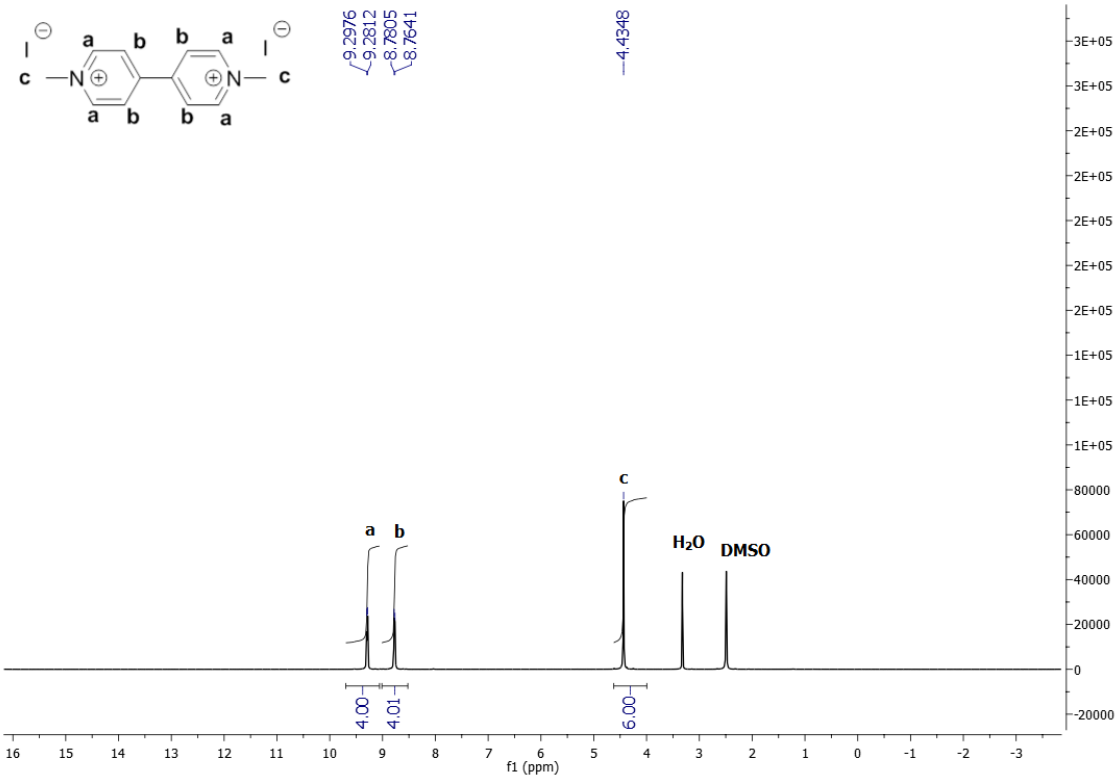

Figure A. 7.1.3 – ^{1}H NMR (DMSO-d6, 400.13 MHz, 25 ºC, ppm) of $[(C_1)_2bpy]I_2$.

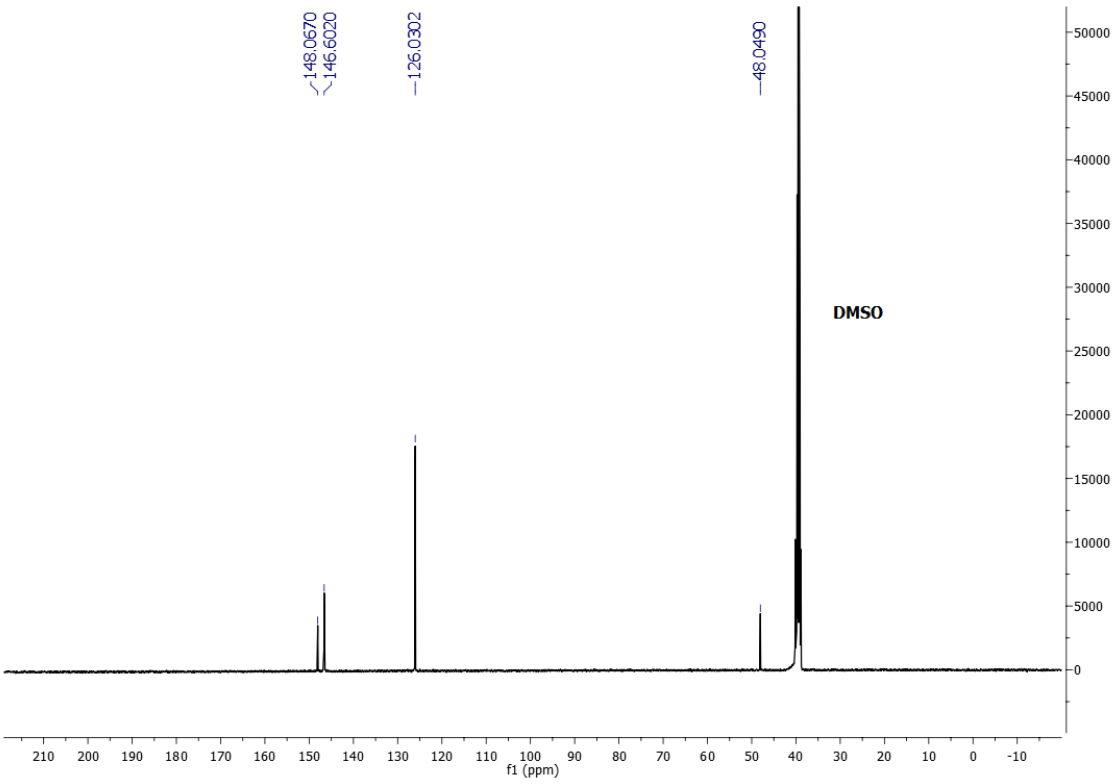

Figure A. 7.1.4 – ^{13} C NMR (DMSO-d6, 100.61 MHz, 25 ºC ppm) of $[(C_1)_2bpy]I_2$.

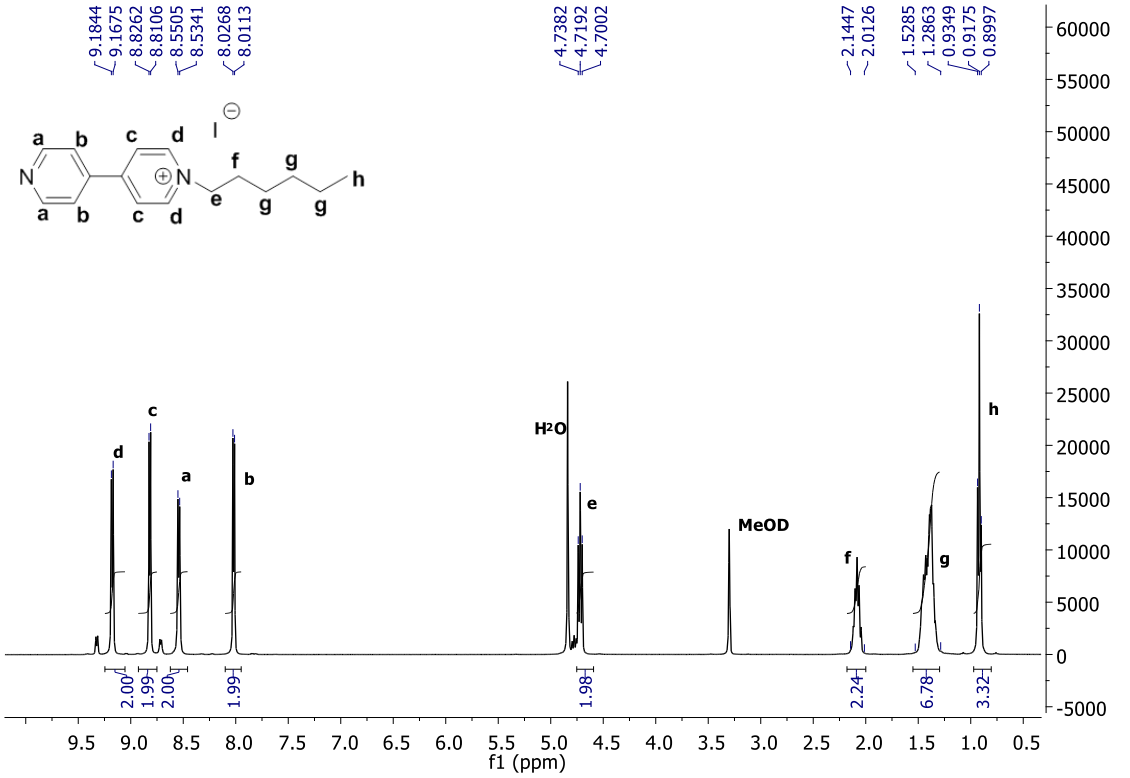

Figure A. 7.1.5 – ^{1}H NMR (MeOD, 400.13 MHz, 25 ºC, ppm) of [C$_6$bpy]I.

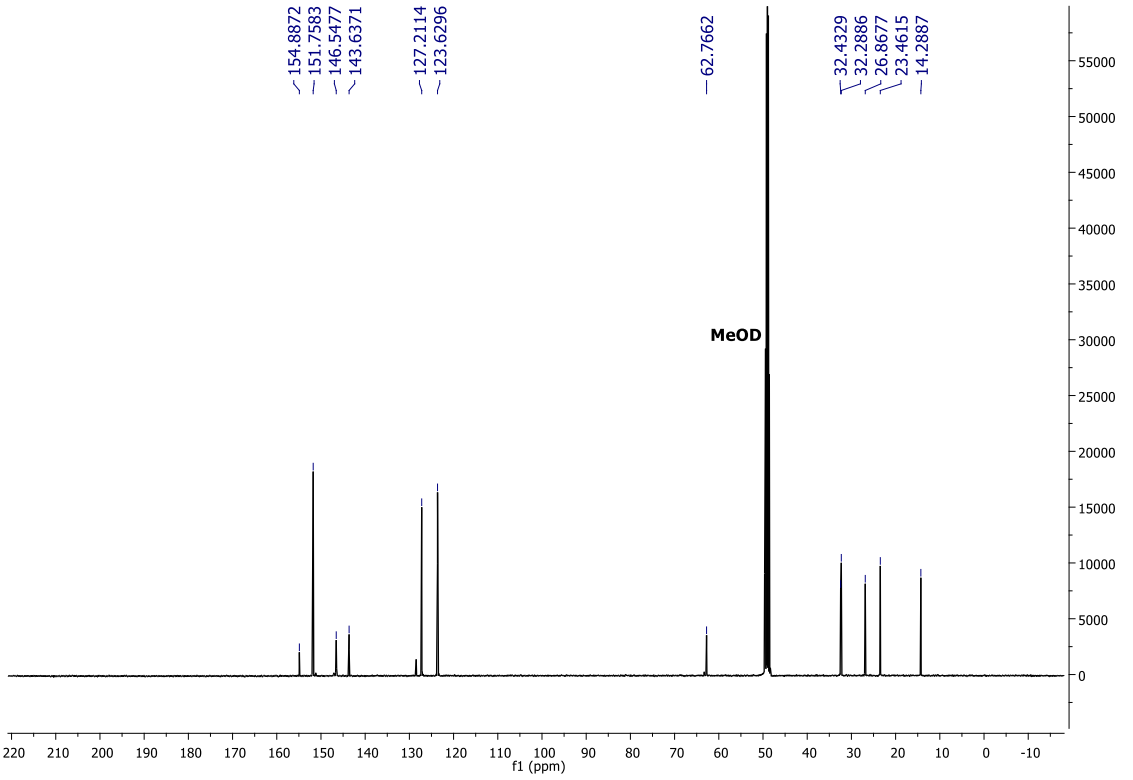

Figure A. 7.1.6 – ^{13}C NMR (MeOD, 100.61 MHz, 25 ºC, ppm) of [C$_6$bpy]I.

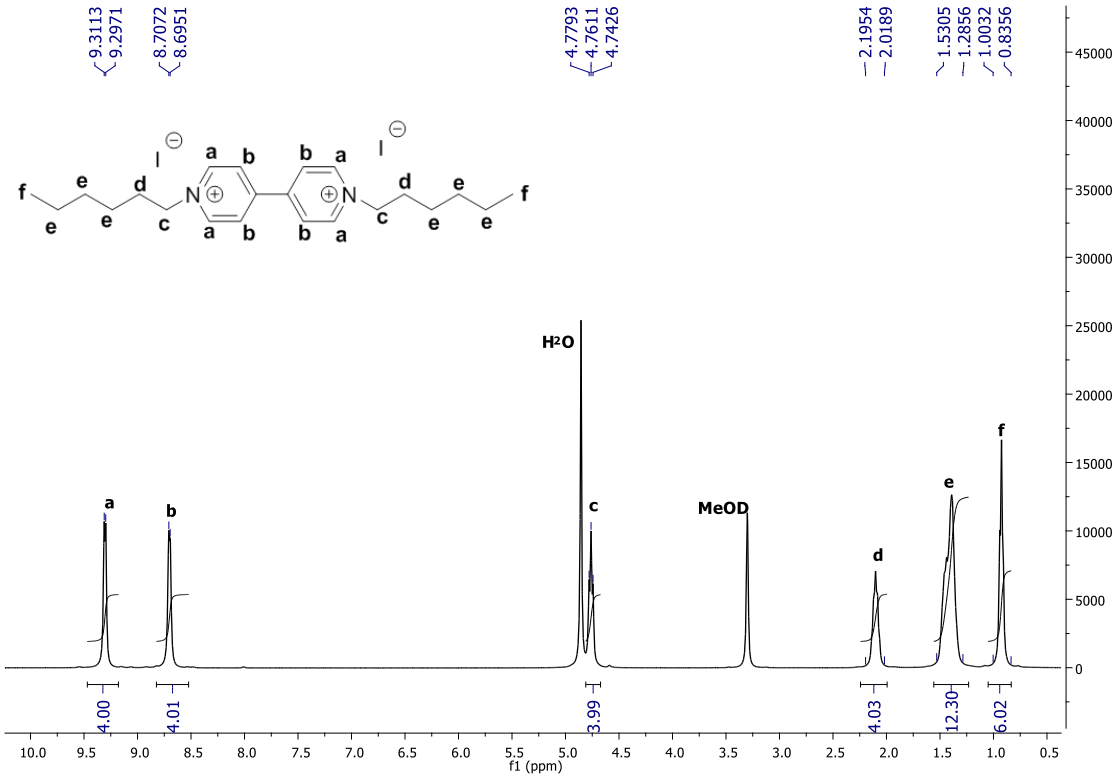

Figure A. 7.1.7 – ^{1}H NMR (MeOD, 400.13 MHz, 25 ºC, ppm) of $[(C_6)_2bpy]I_2$.

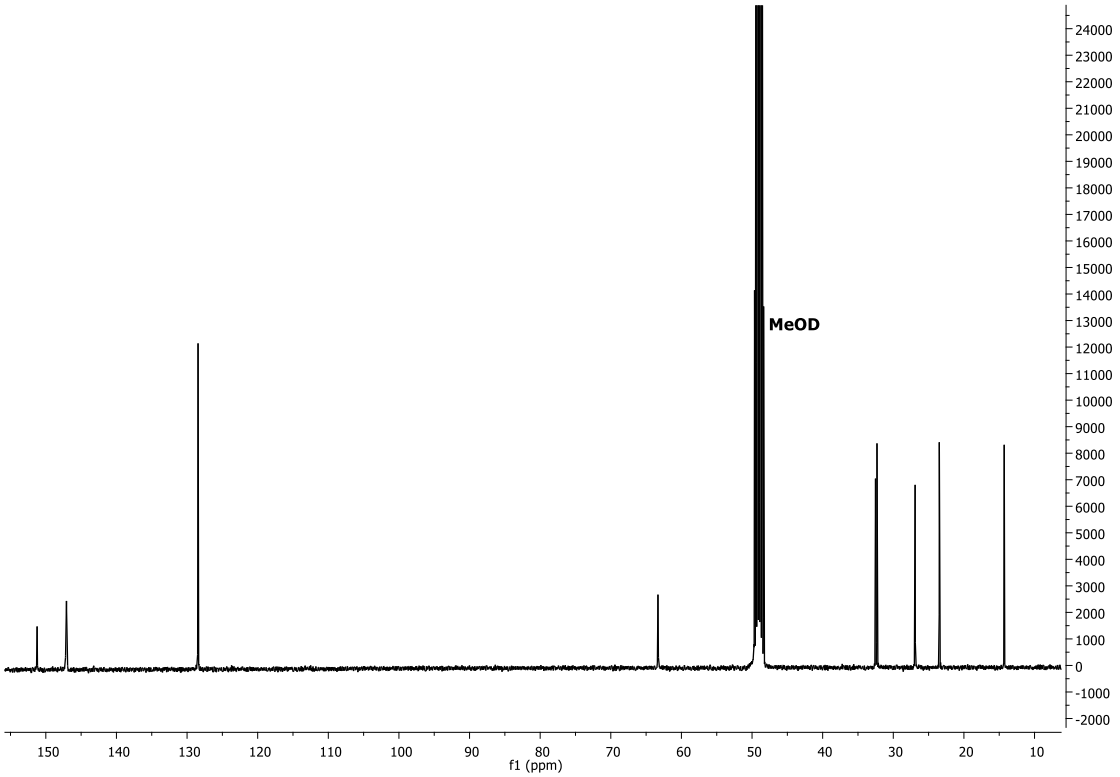

Figure A. 7.1.8 – ^{13}C NMR (MeOD, 100.61 MHz, 25 ºC, ppm) of $[(C_6)_2bpy]I_2$.

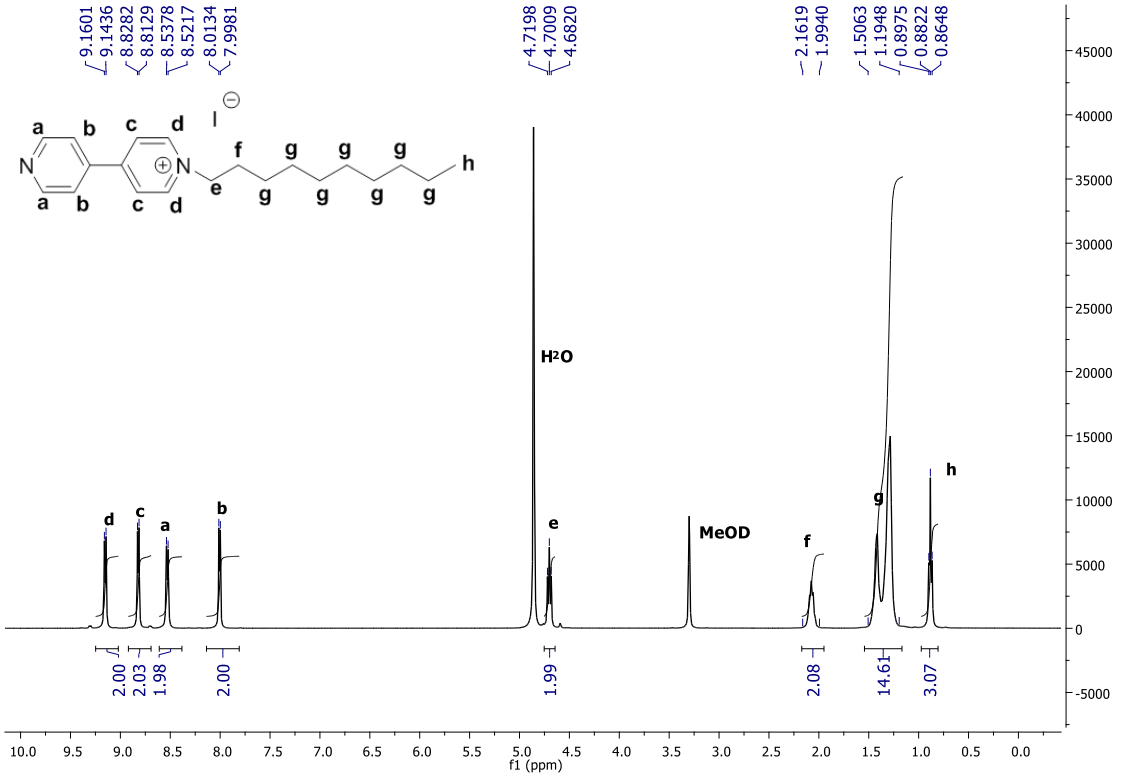

Figure A. 7.1.9 – ^{1}H NMR (MeOD, 400.13 MHz, 25 ºC, ppm) of [C_{10}bpy]I.

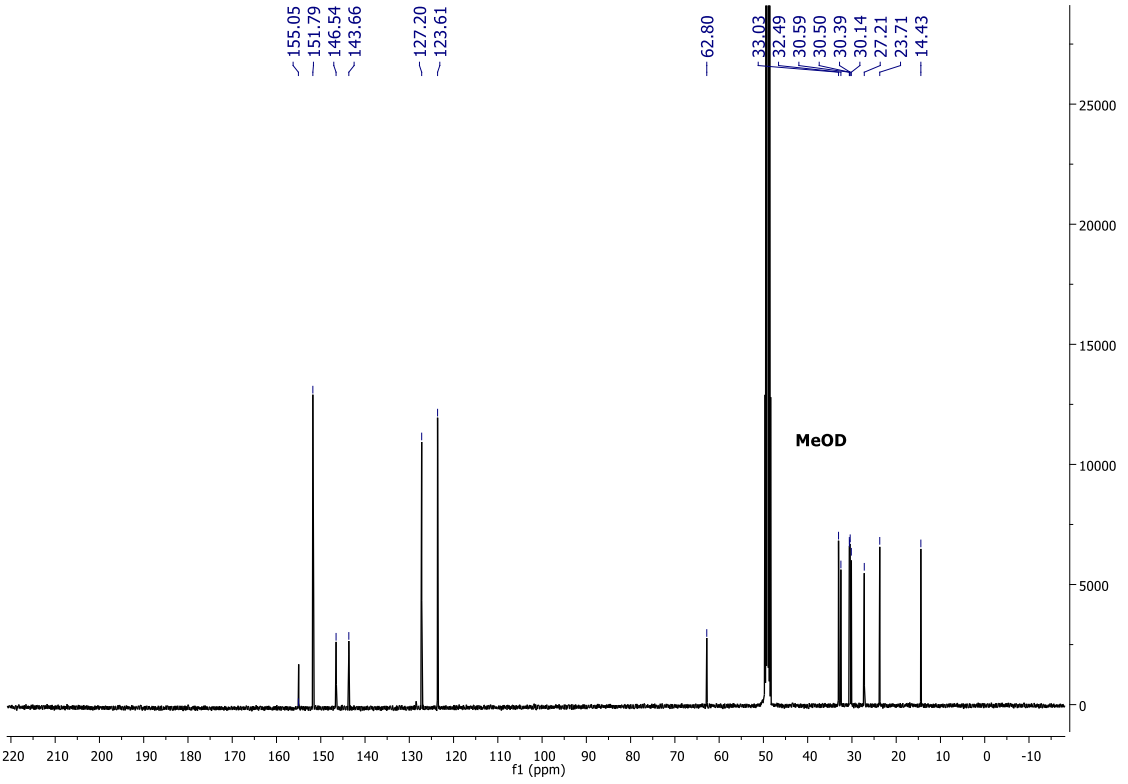

Figure A. 7.1.10 – ^{13}C NMR (MeOD, 100.61 MHz, 25 º C, ppm) of [C_{10}bpy]I.

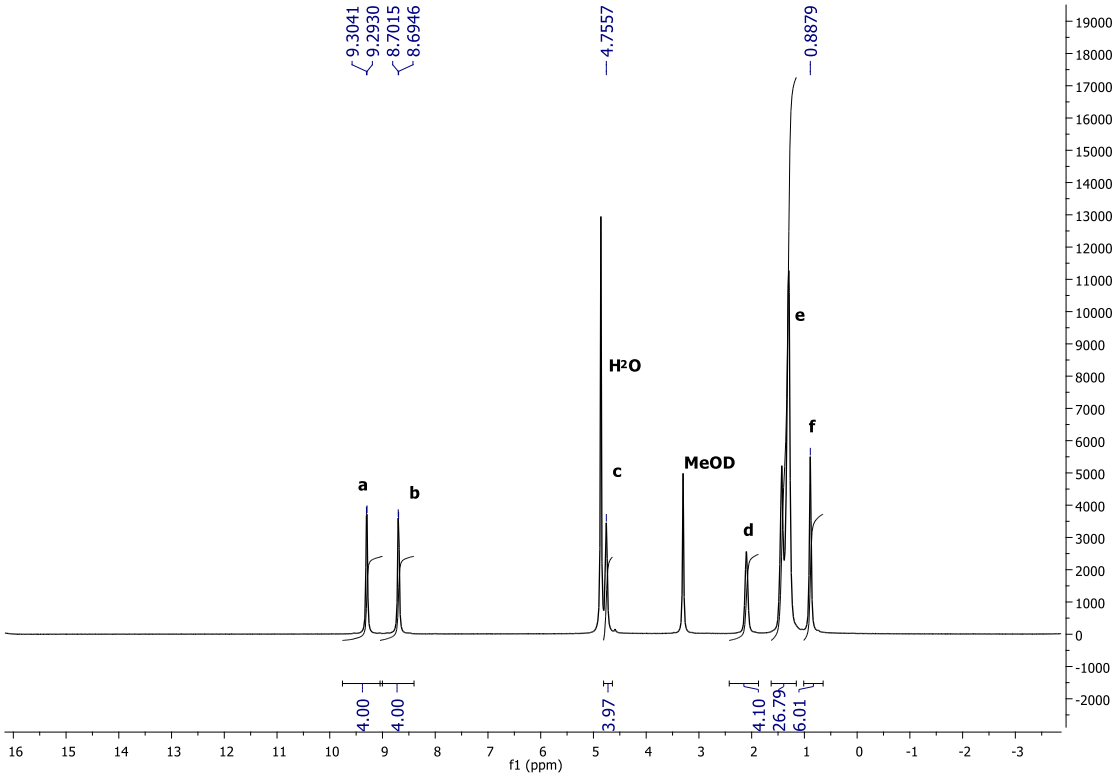

Figure A. 7.1.11 – ^{1}H NMR (MeOD, 400.13 MHz, 25 ºC, ppm) of $[(C_{10})_2bpy]I_2$.

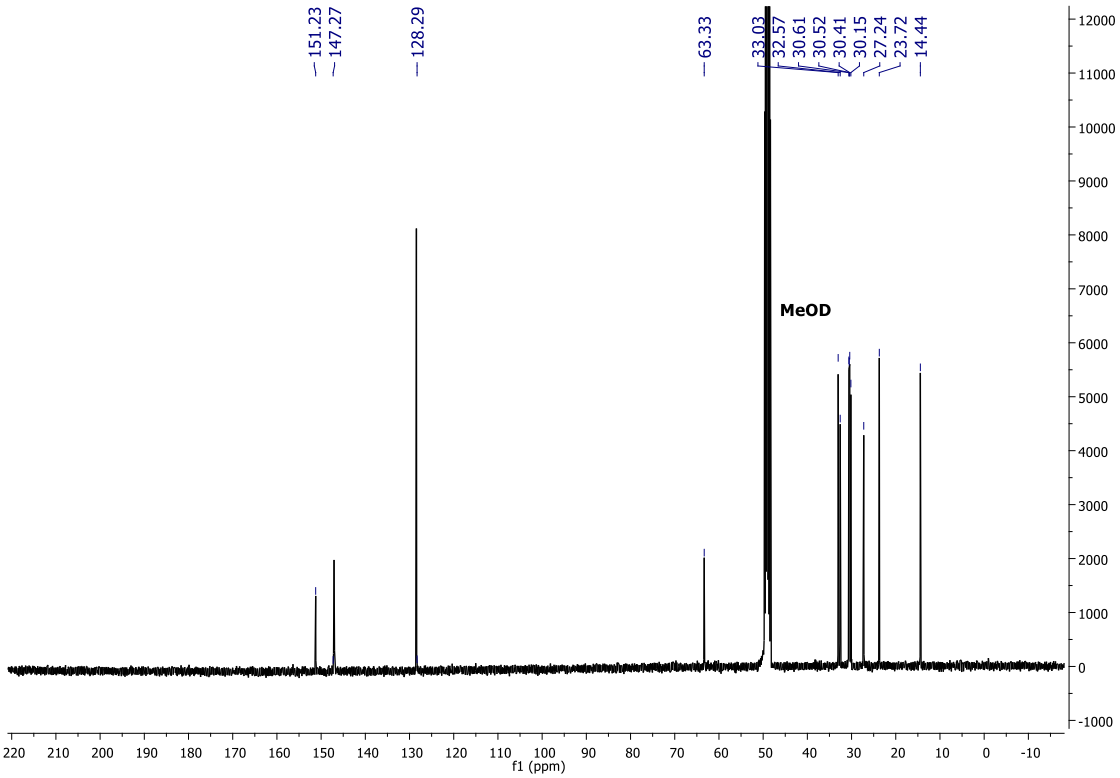

Figure A. 7.1.12 – ^{13}C NMR (MeOD, 100.61 MHz, 25 ºC, ppm) of $[(C_{10})_2bpy]I_2$.

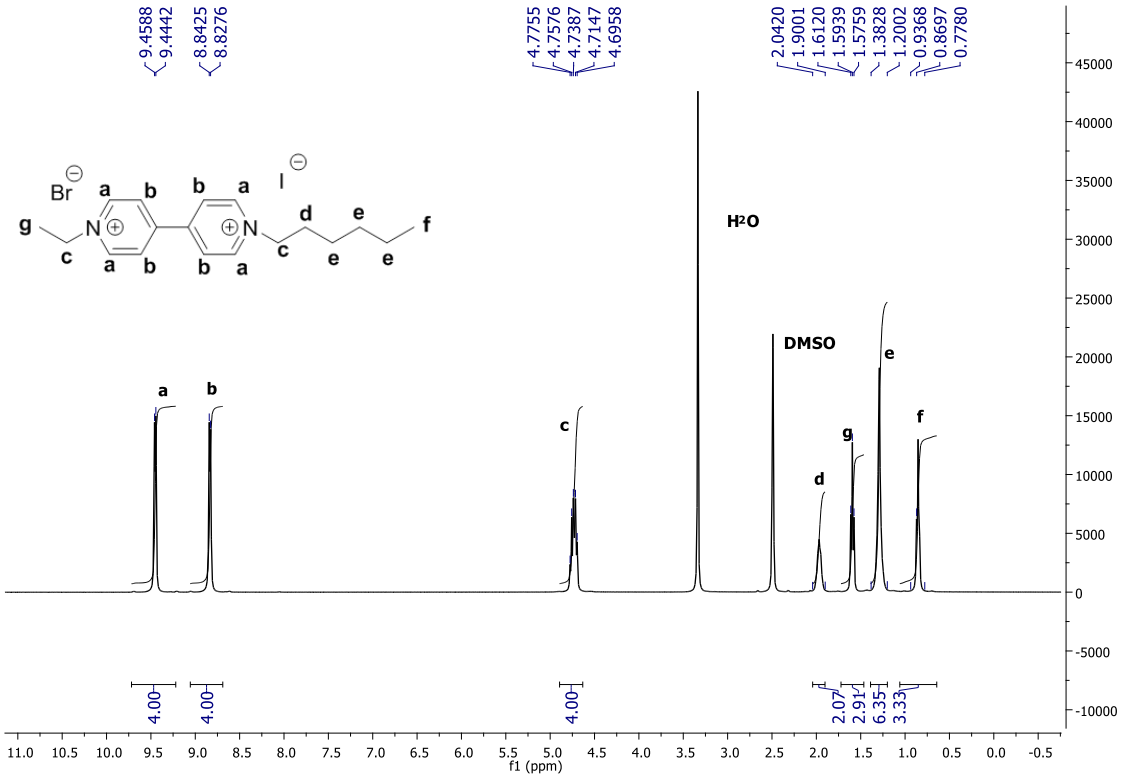

Figure A. 7.1.13 – ^{1}H NMR (DMSO-d6, 400.13 MHz, 25 ºC, ppm) of [C_2C_6bpy]BrI.

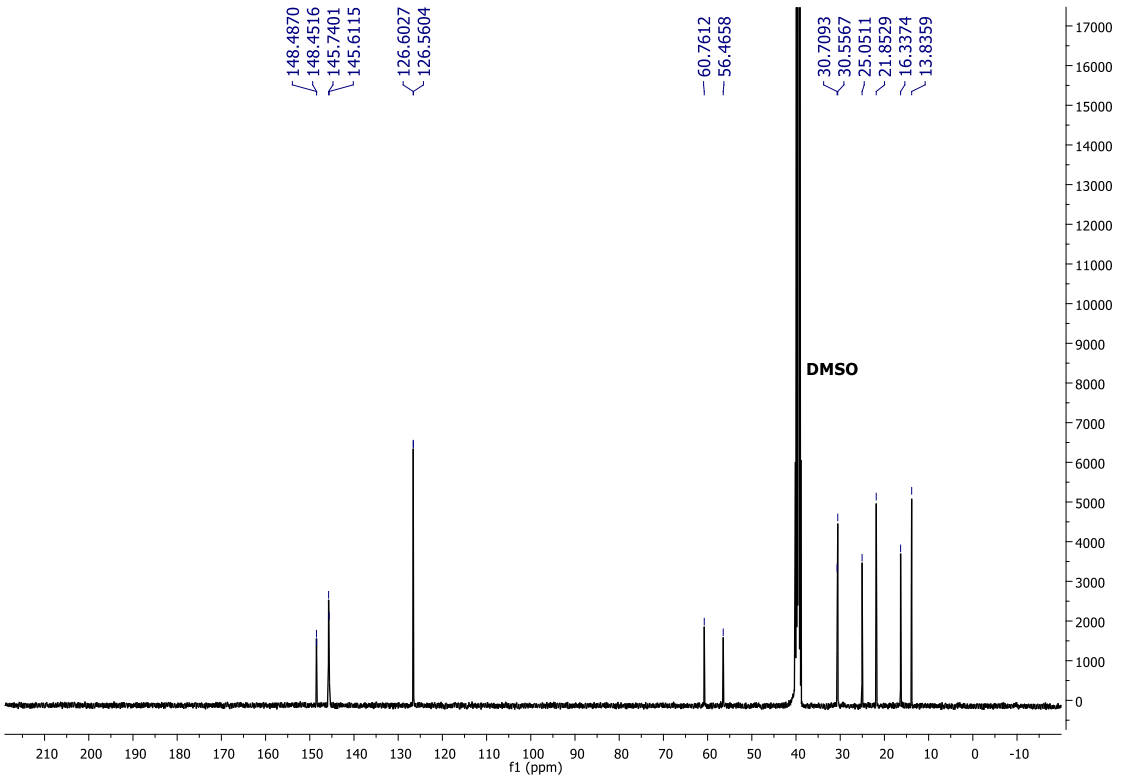

Figure A. 7.1.14 – ^{13}C NMR (DMSO-d6, 100.61 MHz, 25 ºC, ppm) of [C_2C_6bpy]BrI.

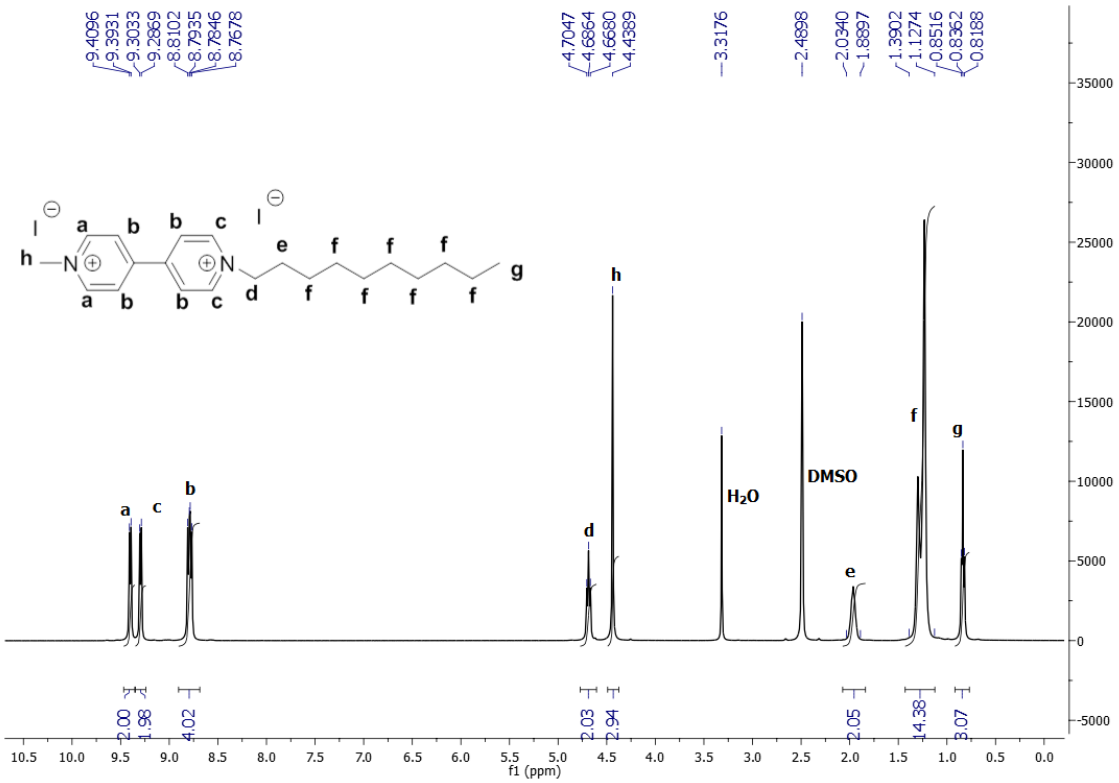

Figure A. 7.1.15 – ^{1}H NMR (DMSO-d6, 400.13 MHz, 25 ºC, ppm) of $[C_1C_{10}bpy]I_2$.

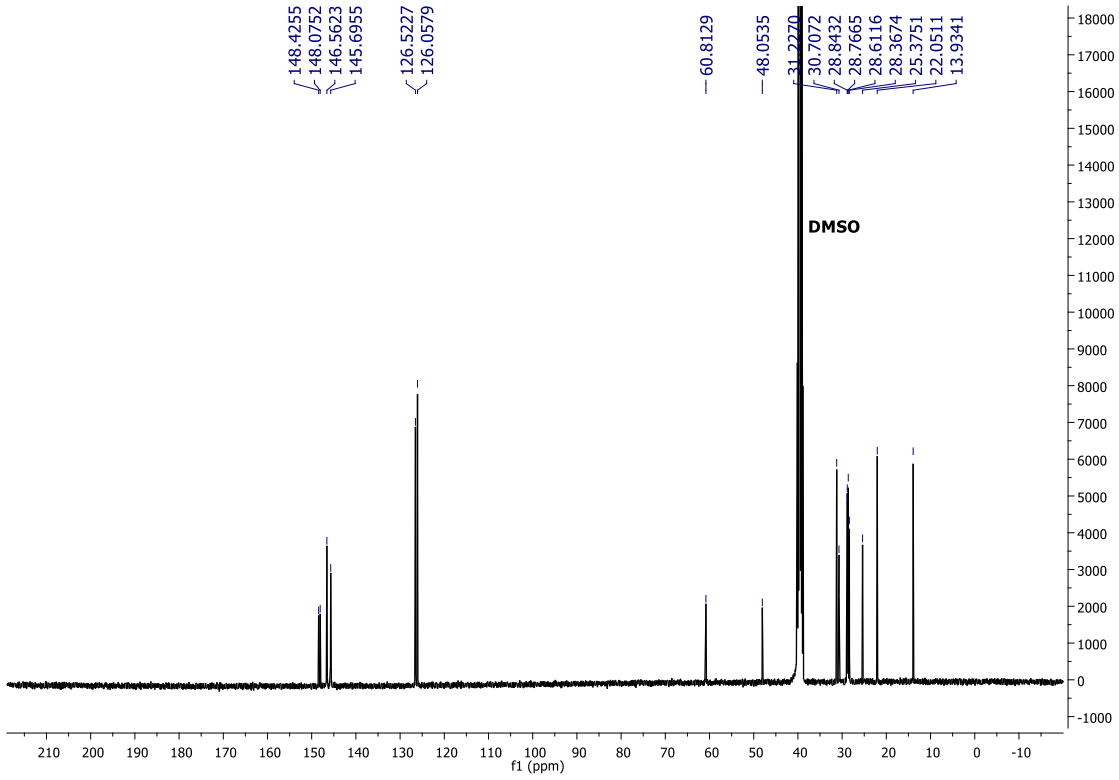

Figure A. 7.1.16 – ^{13}C NMR (DMSO-d6, 100.61 MHz, 25 ºC, ppm) of $[C_1C_{10}bpy]I_2$.

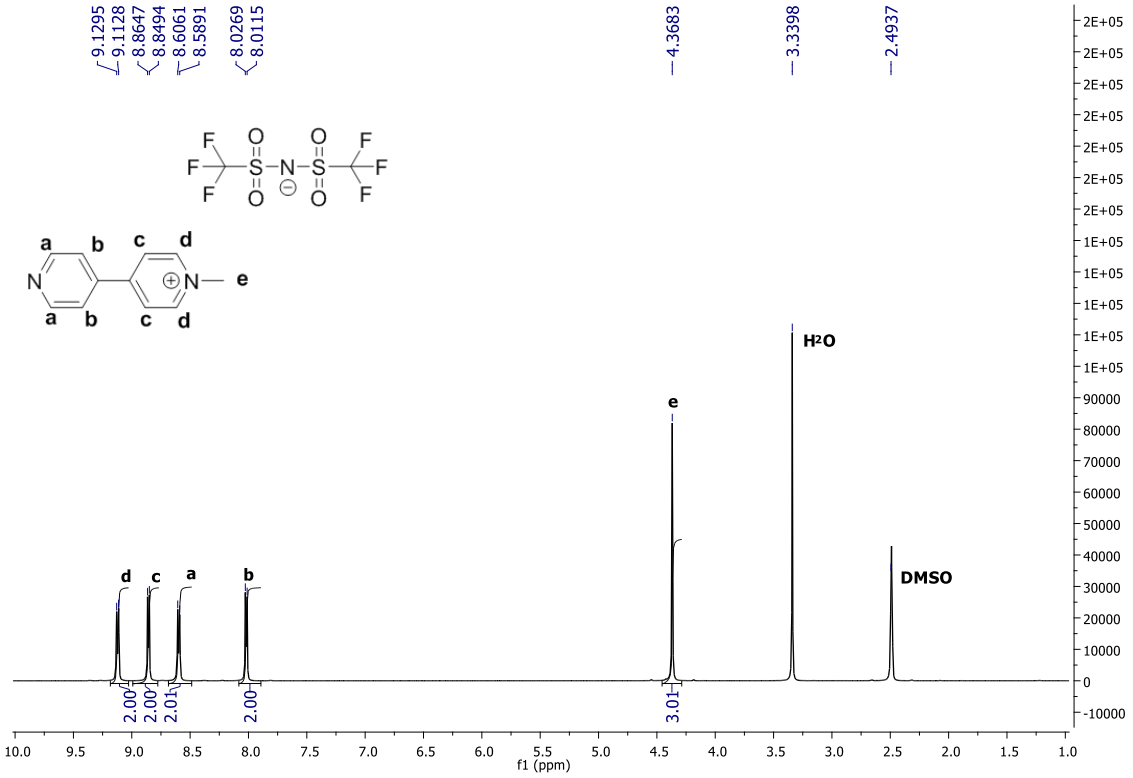

Figure A. 7.1.17 – ^{1}H NMR (DMSO-d6, 400.13 MHz, 25 ºC, ppm) of [C_1bpy][NTf_2].

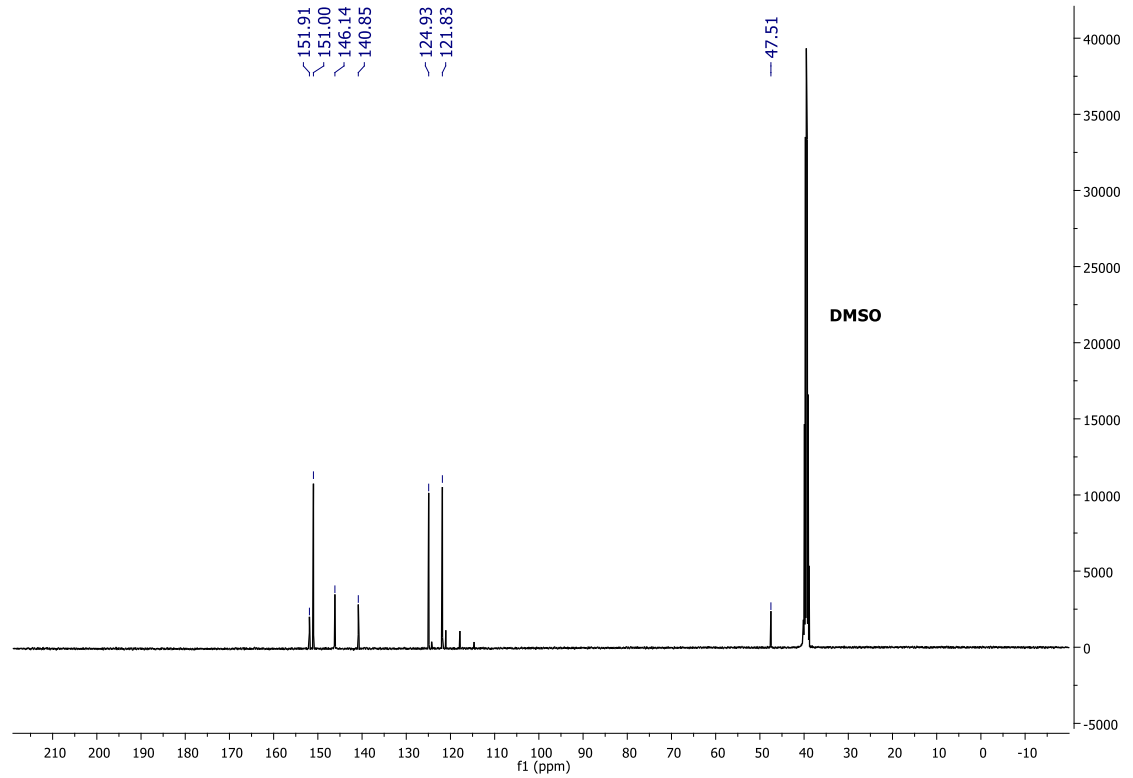

Figure A. 7.1.18 – ^{13}C NMR (DMSO-d6, 100.61 MHz, 25 ºC, ppm) of [C_1bpy][NTf_2].

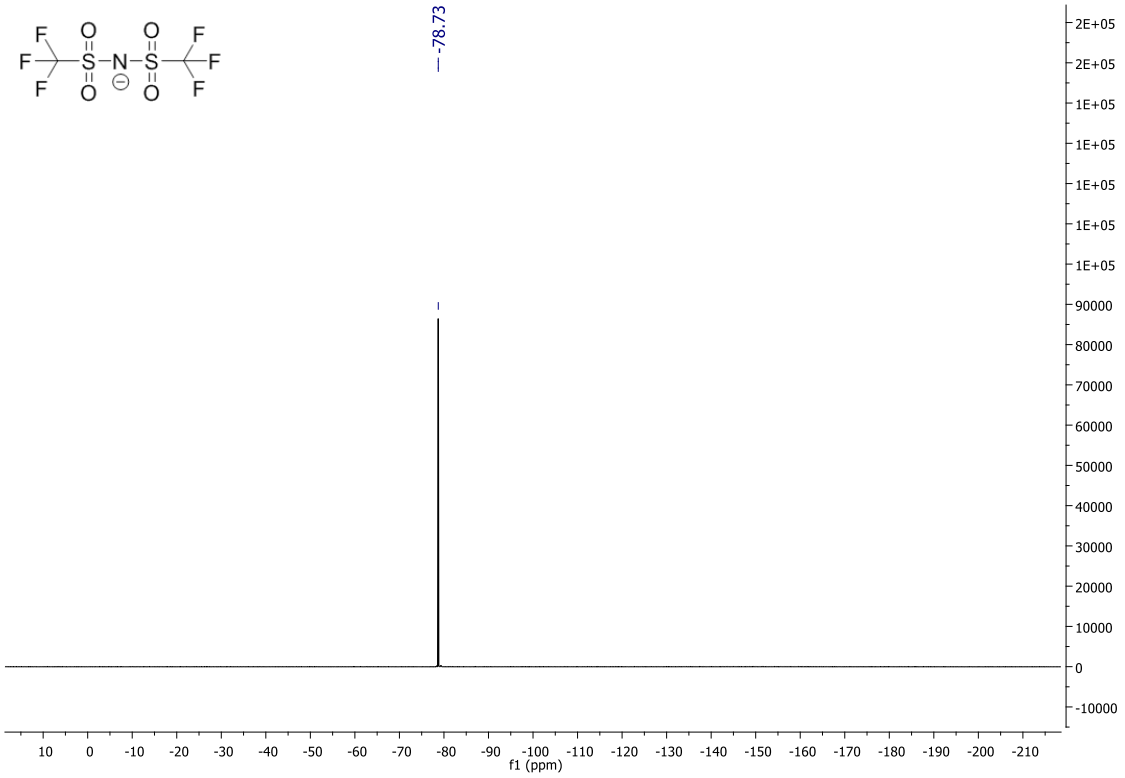

Figure A. 7.1.19 – ^{19}F NMR (DMSO-d6, 376.50 MHz, 25 ºC, ppm) of [C_1bpy][NTf_2].

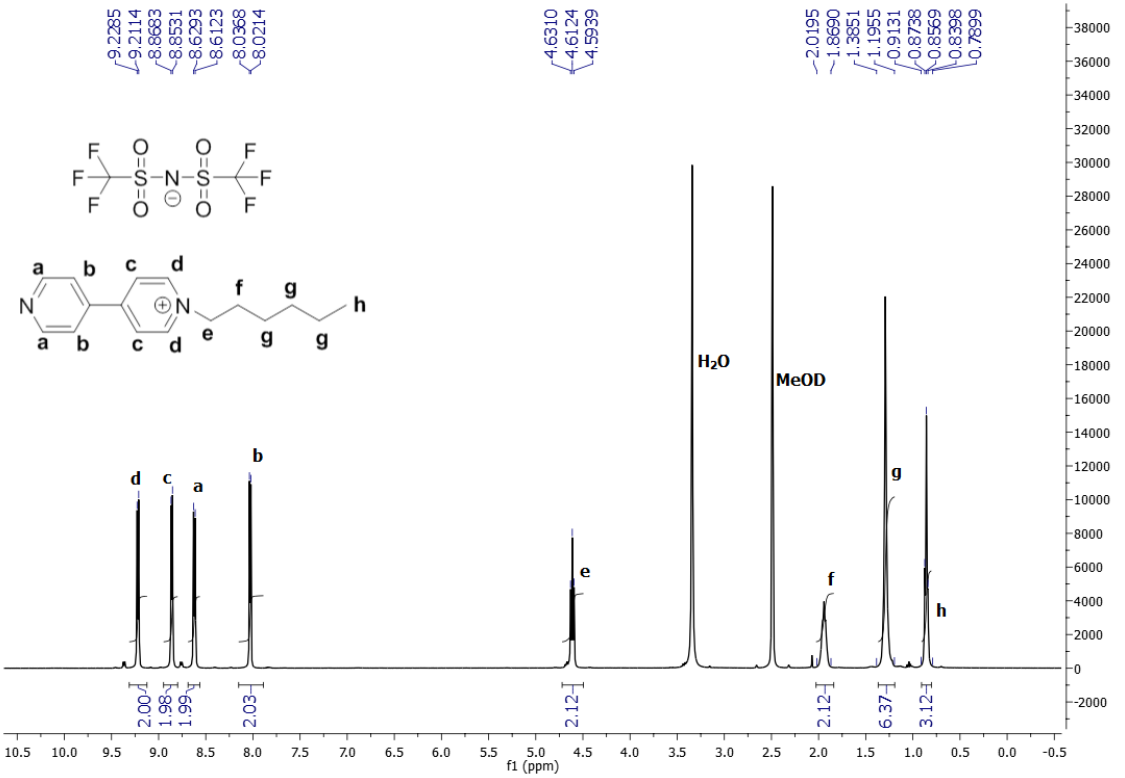

Figure A. 7.1.20 – ^{1}H NMR (MeOD, 400.13 MHz, 25 ºC, ppm) of [C_6bpy][NTf_2].

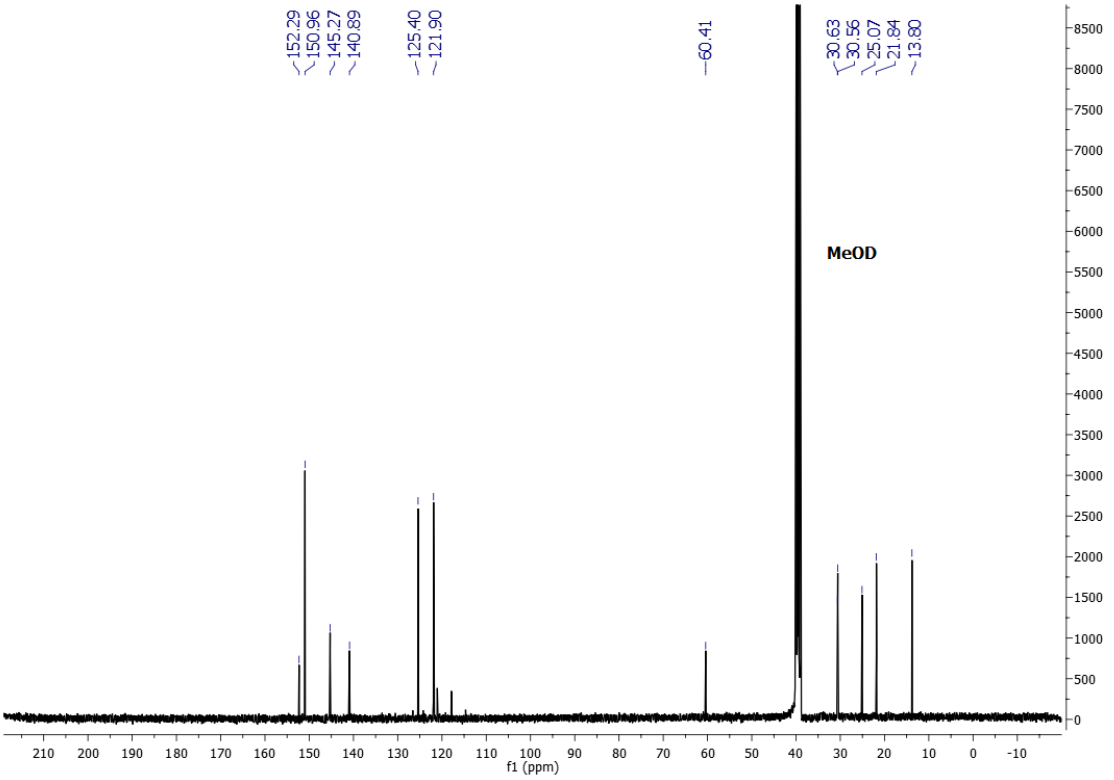

Figure A. 7.1.21 – ^{13}C NMR (MeOD, 100.61 MHz, 25 ºC, ppm) of $[C_6bpy][NTf_2]$.

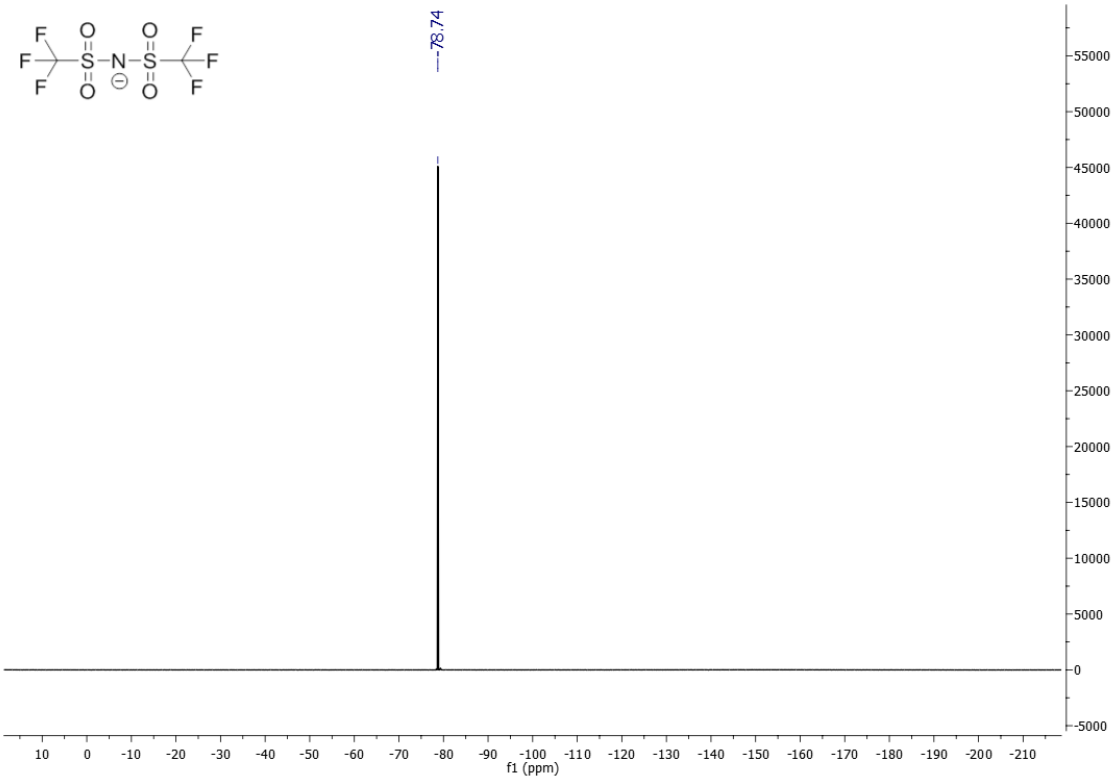

Figure A. 7.1.22 – ^{19}F NMR (MeOD, 376.50 MHz, 25 ºC, ppm) of $[C_6bpy][NTf_2]$.

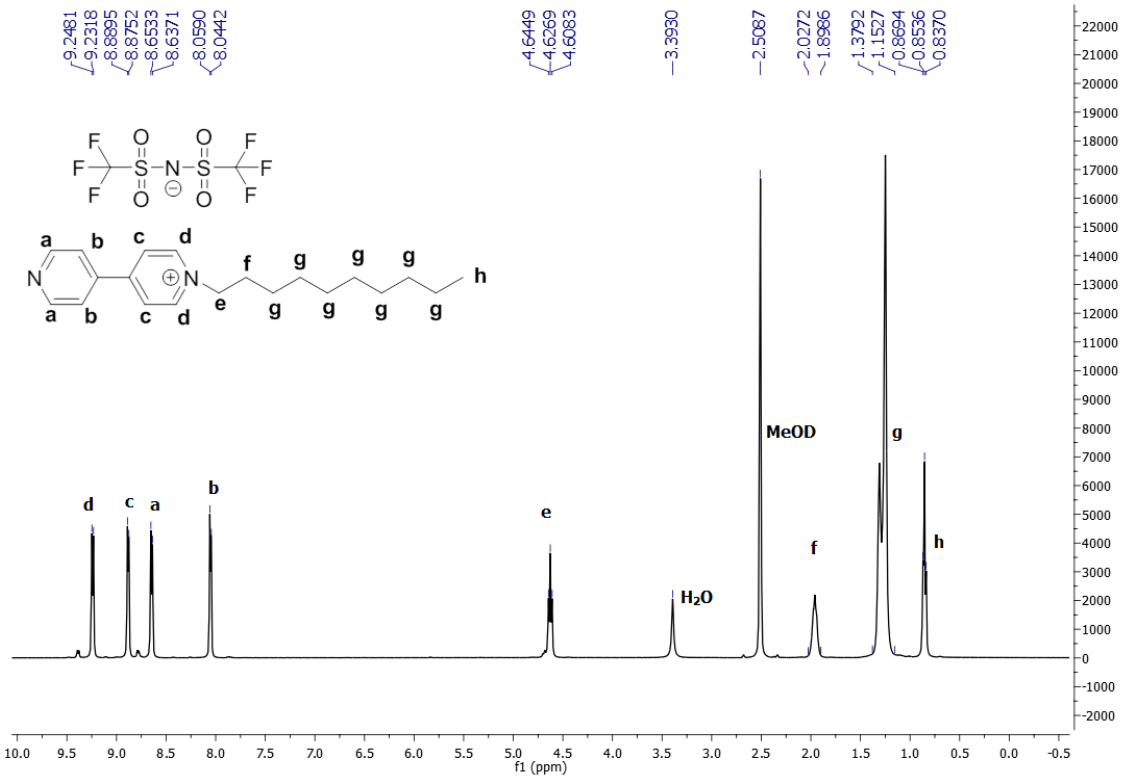

Figure A. 7.1.23 – ^{1}HNMR (MeOD, 400.13 MHz, 25 ºC, ppm) of [C_{10}bpy][NTf_2].

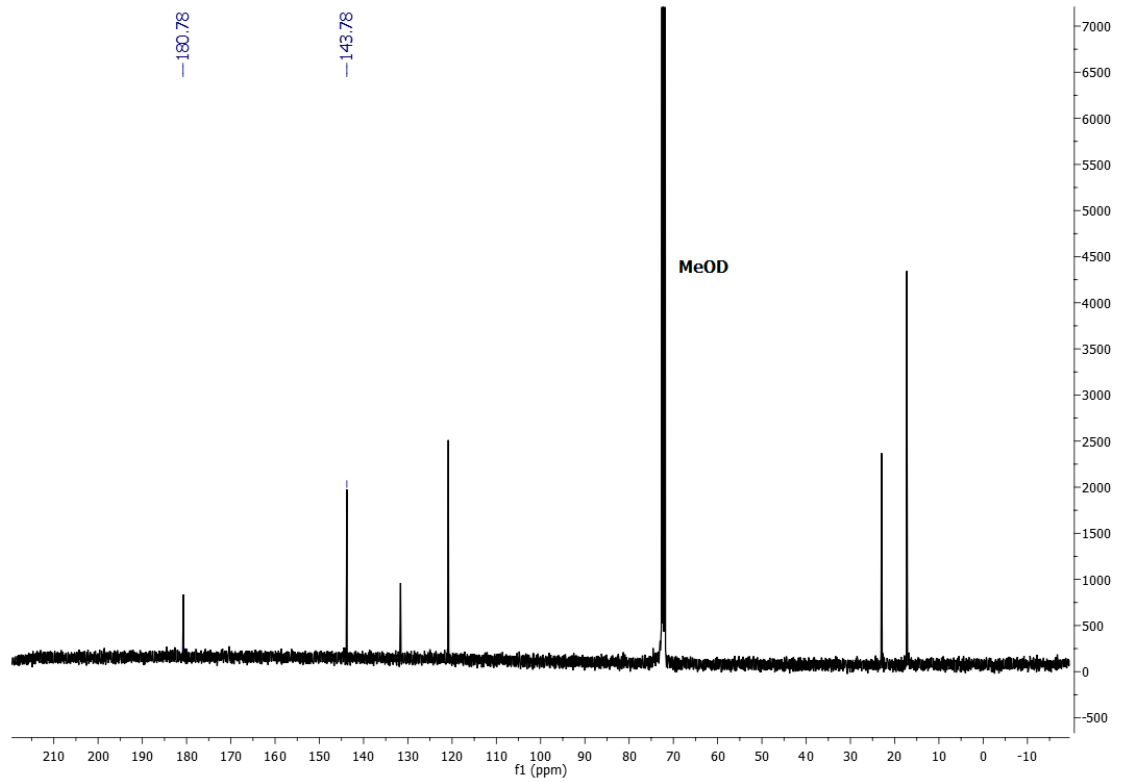

Figure A. 7.1.24 – ^{13}C NMR (MeOD, 100.61 MHz, 25 ºC, ppm) of [C_{10}bpy][NTf_2].

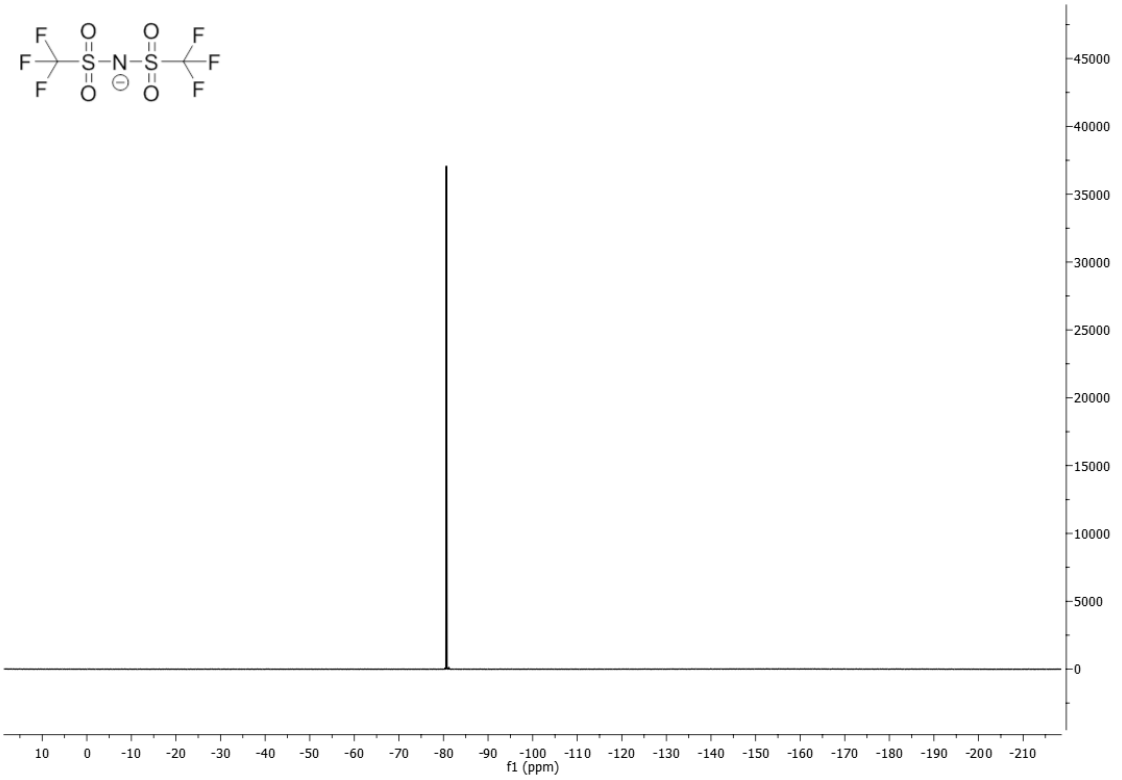

Figure A. 7.1.25 – ^{19}F NMR (MeOD, 376.50 MHz, 25 ºC, ppm) of $[C_{10}bpy][NTf_2]$.

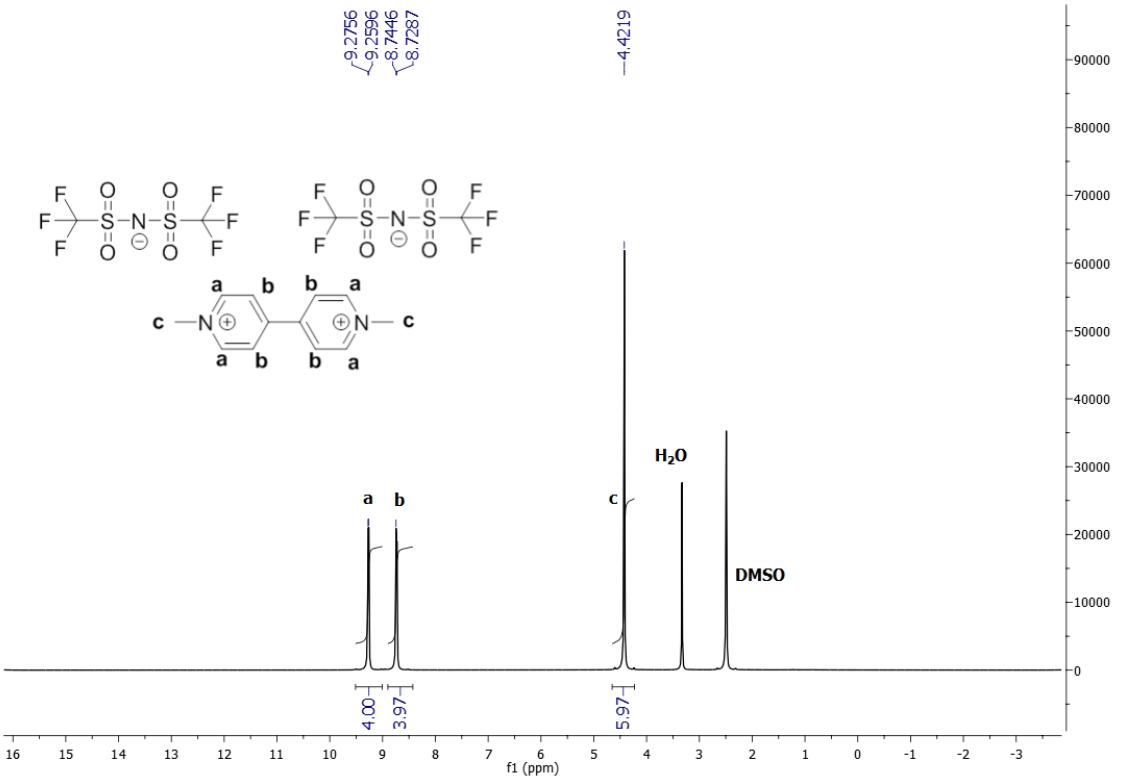

Figure A. 7.1.26 – ^{1}H NMR (DMSO-d6, 400.13 MHz, 25 ºC, ppm) of $[(C_1)_2bpy][NTf_2]_2$.

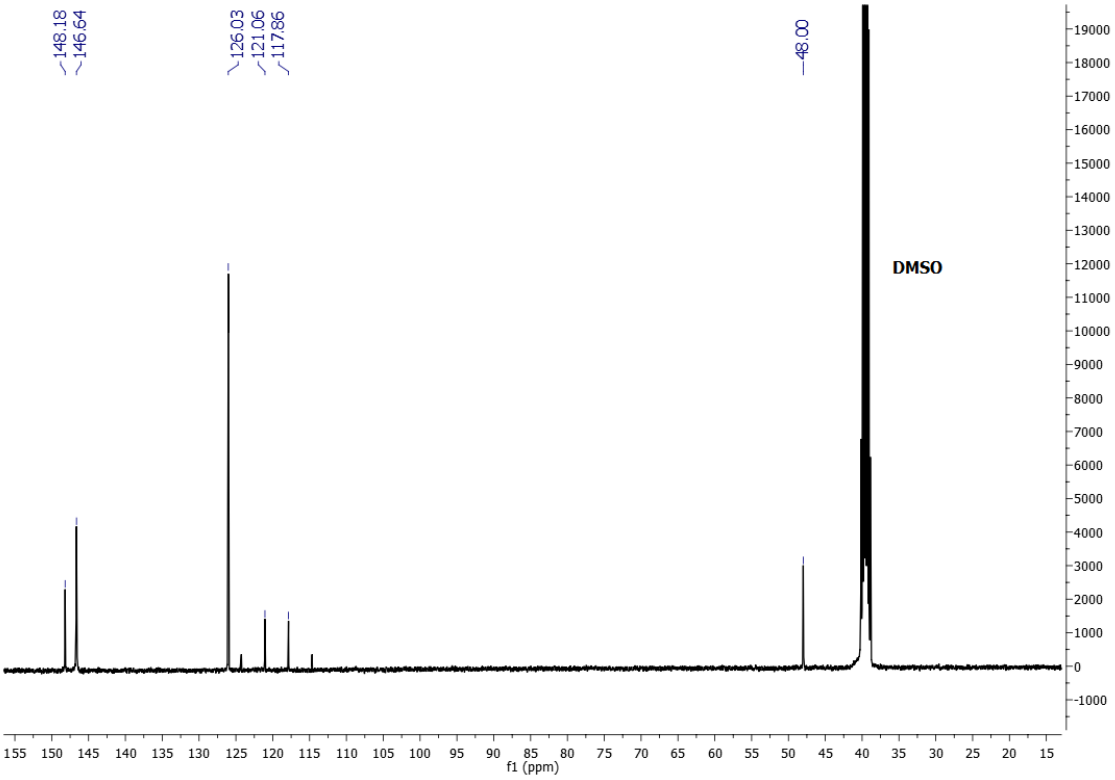

Figure A. 7.1.27 – ^{13}C NMR (DMSO-d6, 100.61 MHz, 25 ºC, ppm) of $[(C_1)_2bpy][NTf_2]_2$.

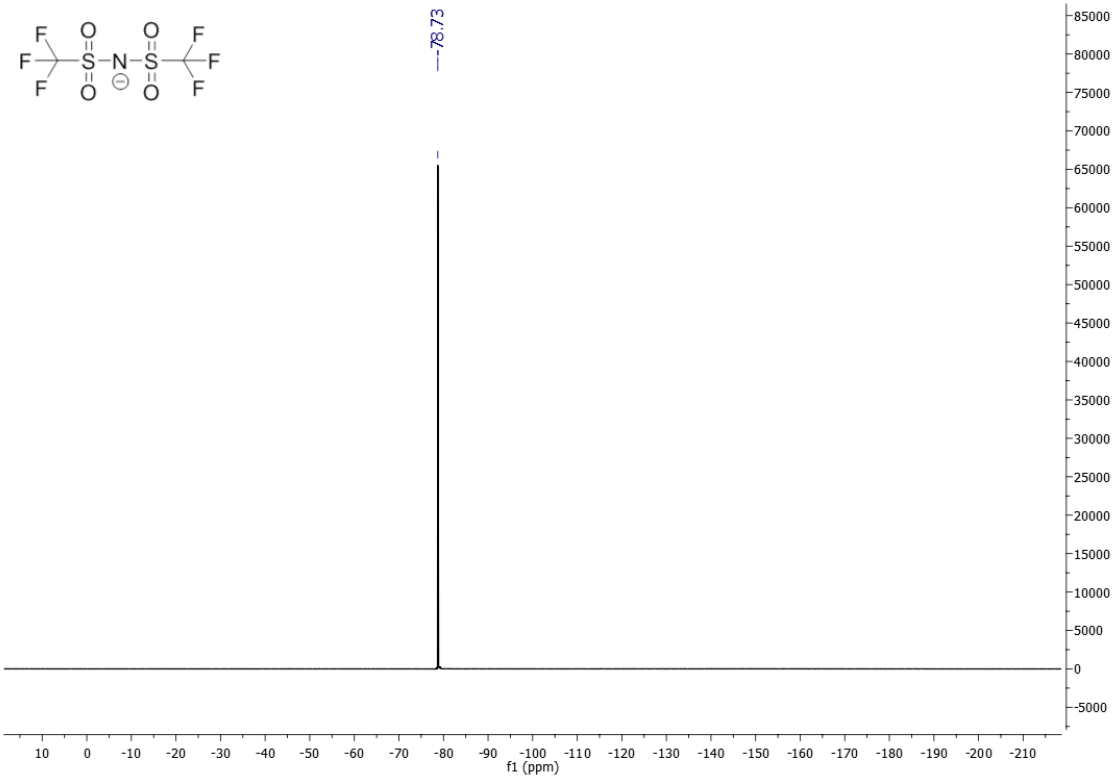

Figure A. 7.1.28 – ^{19}F NMR (DMSO-d6, 376.50 MHz, 25 ºC, ppm) of $[(C_1)_2bpy][NTf_2]_2$.

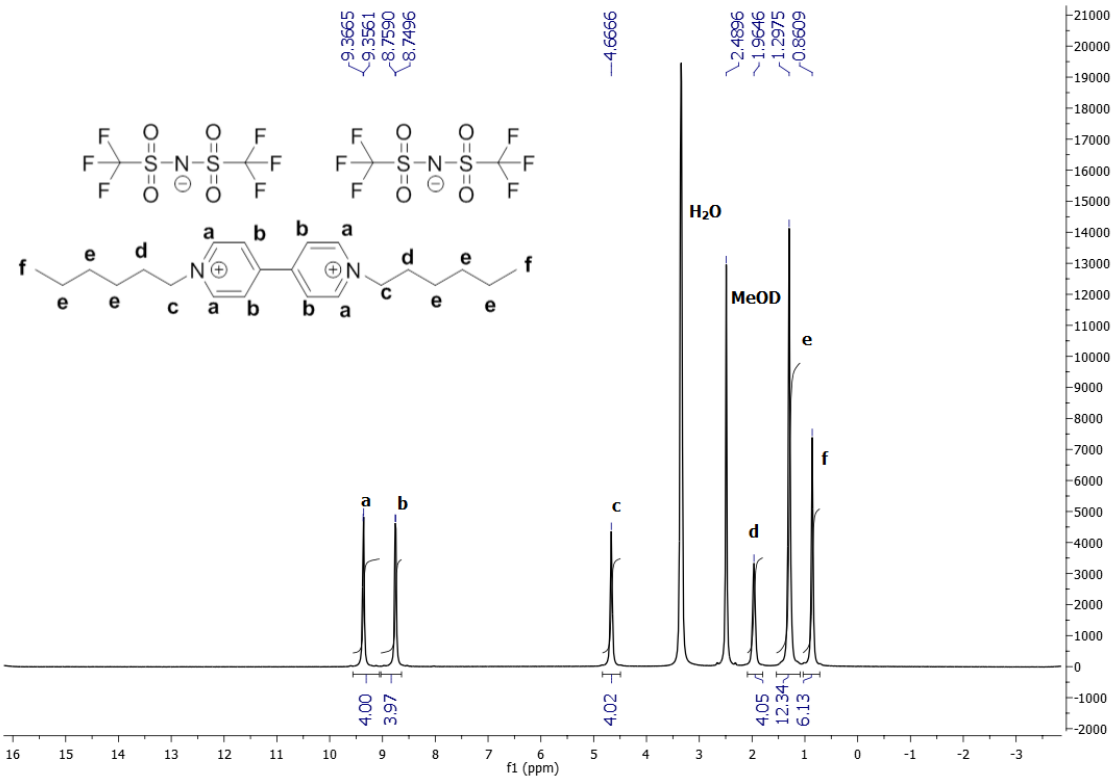

Figure A. 7.1.29 – ^{1}H NMR (MeOD, 400.13 MHz, 25 ºC, ppm) of $[(C_6)_2bpy][NTf_2]_2$.

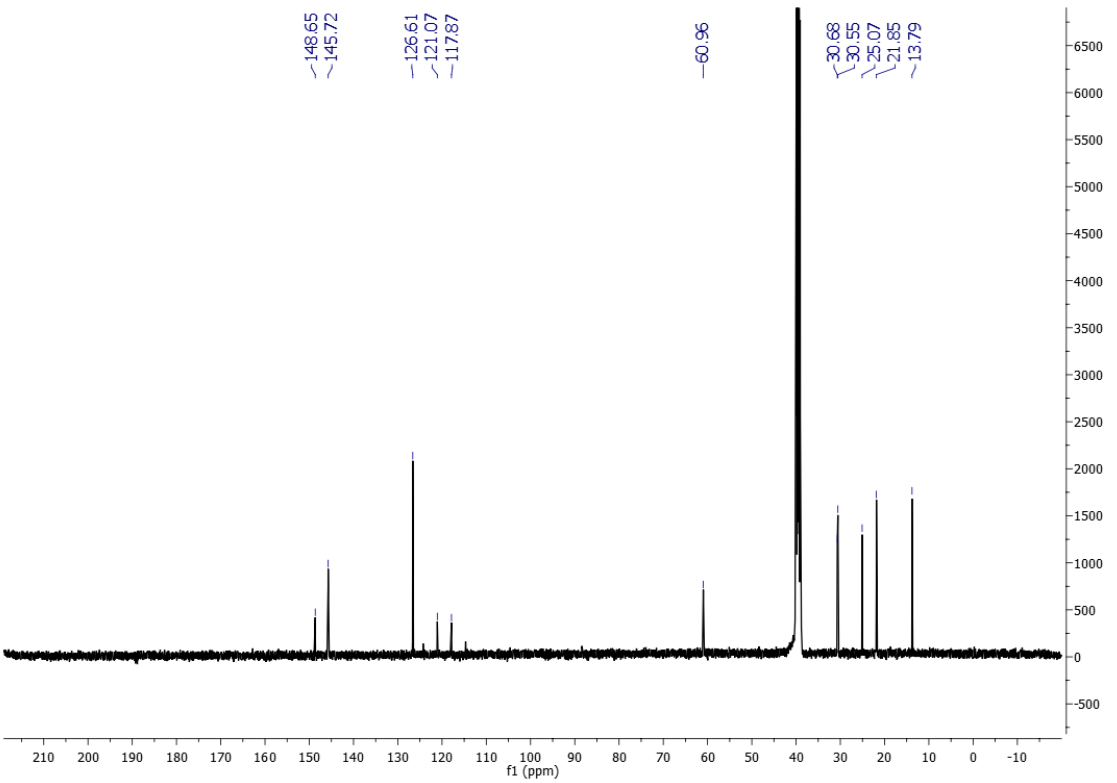

Figure A. 7.1.30 – ^{13}C NMR (MeOD, 100.61 MHz, 25 ºC, ppm) of $[(C_6)_2bpy][NTf_2]_2$.

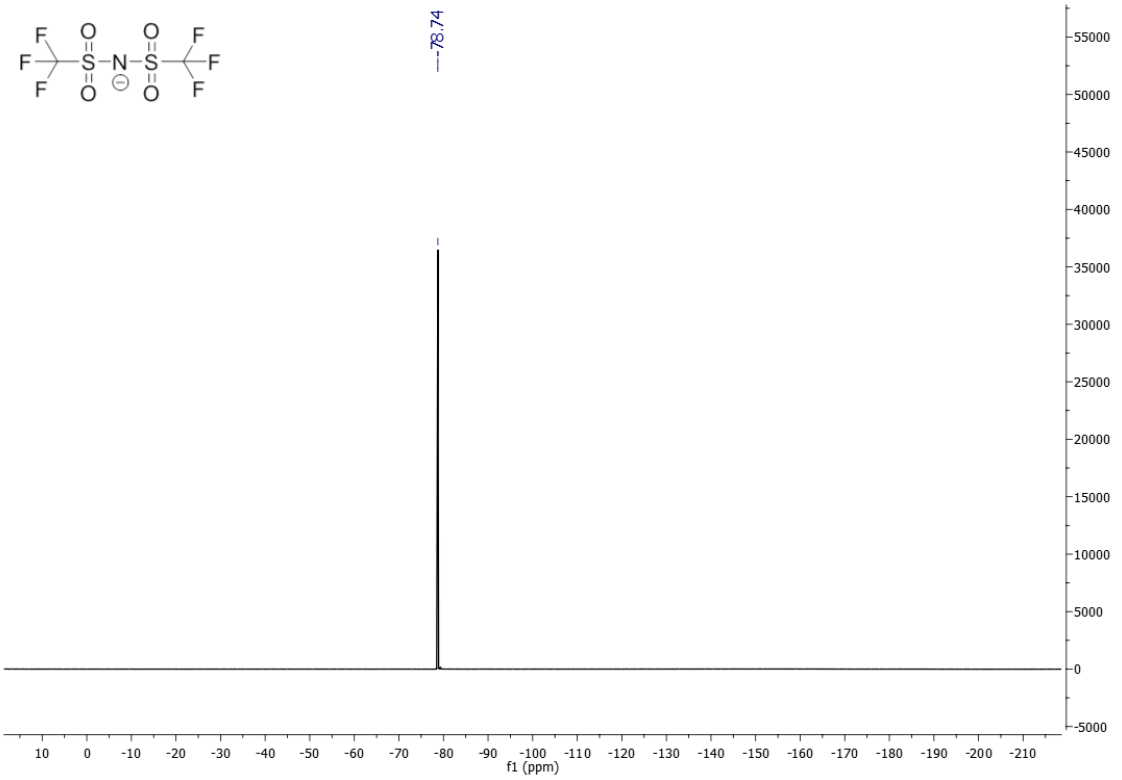

Figure A. 7.1.31 – ^{19}F NMR (MeOD, 376.50 MHz, 25 ºC, ppm) of $[(C_6)_2bpy][NTf_2]_2$.

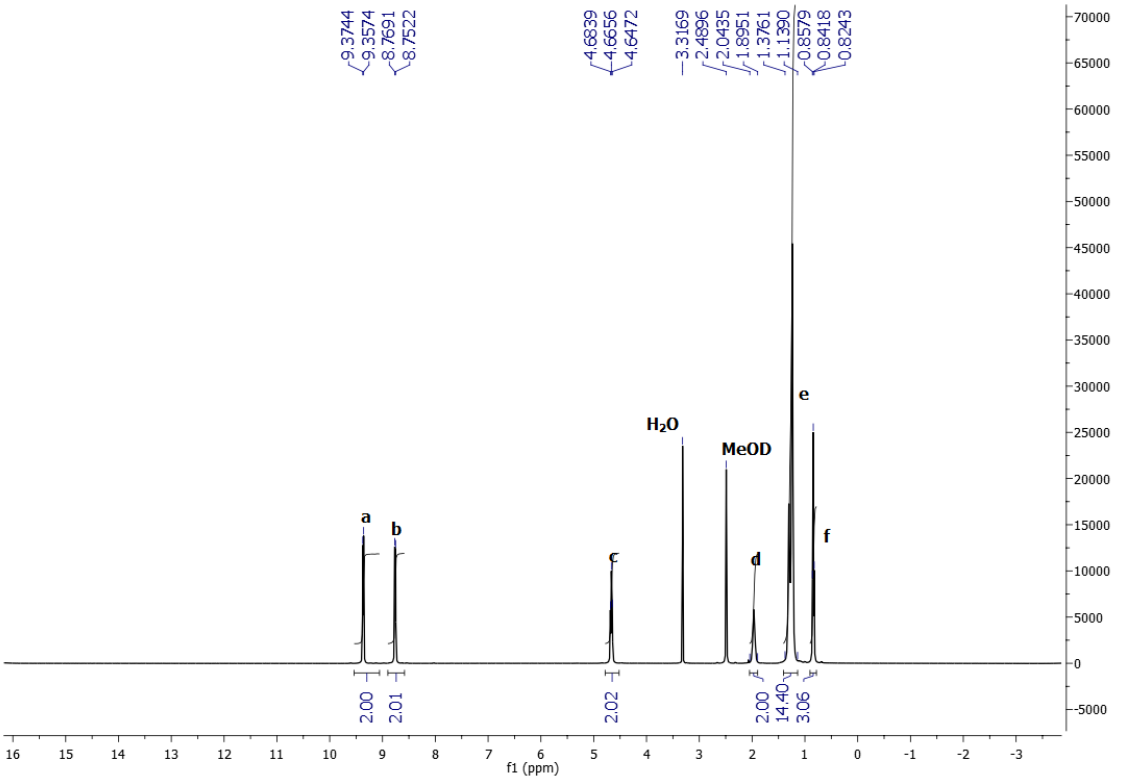

Figure A. 7.1.32 – ^{1}H NMR (MeOD, 400.13 MHz, 25 ºC, ppm) of $[(C_{10})_2bpy][NTf_2]_2$.

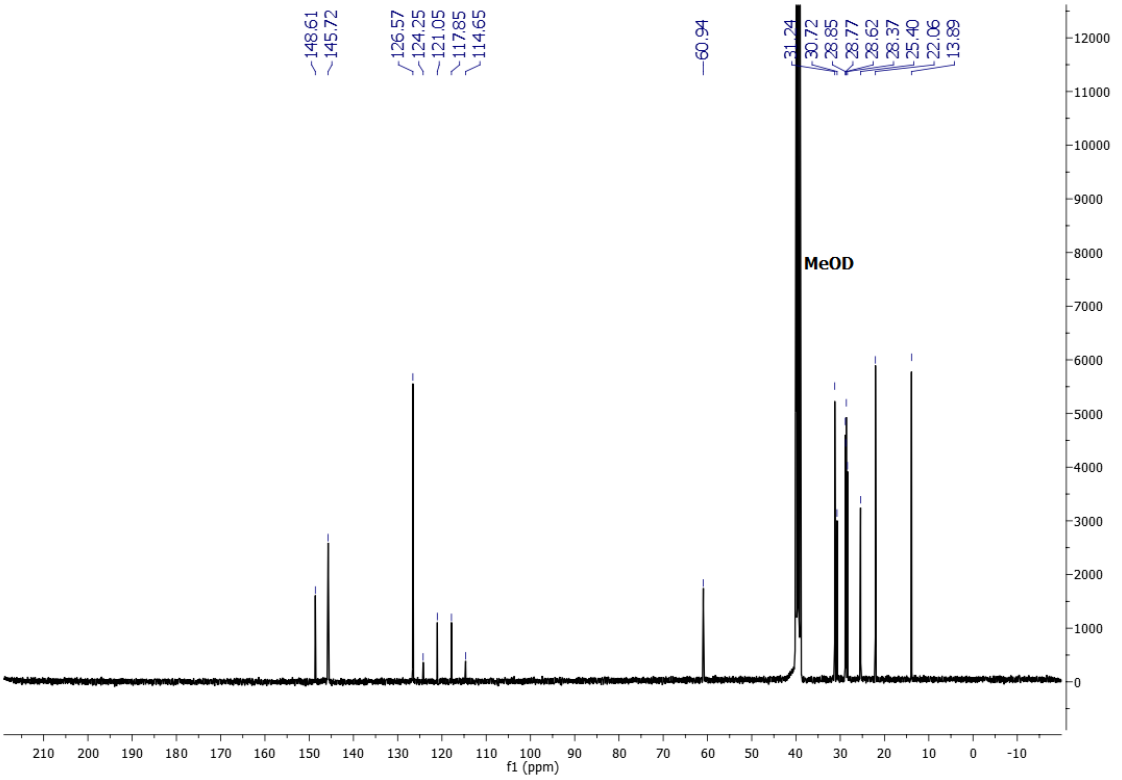

Figure A. 7.1.33 – ^{13}C NMR (MeOD, 100.61 MHz, 25 ºC, ppm) of $[(C_{10})_2bpy][NTf_2]_2$.

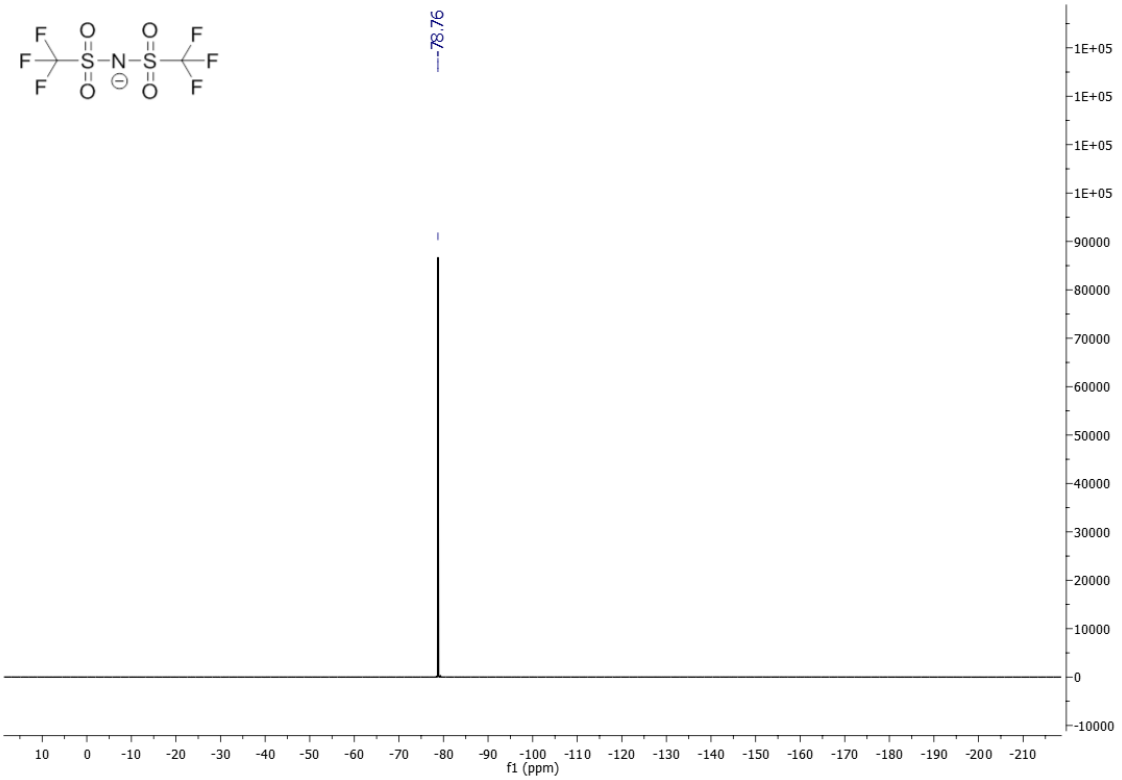

Figure A. 7.1.34 – ^{19}F NMR (MeOD, 376.50 MHz, 25 ºC, ppm) of $[(C_{10})_2bpy][NTf_2]_2$.

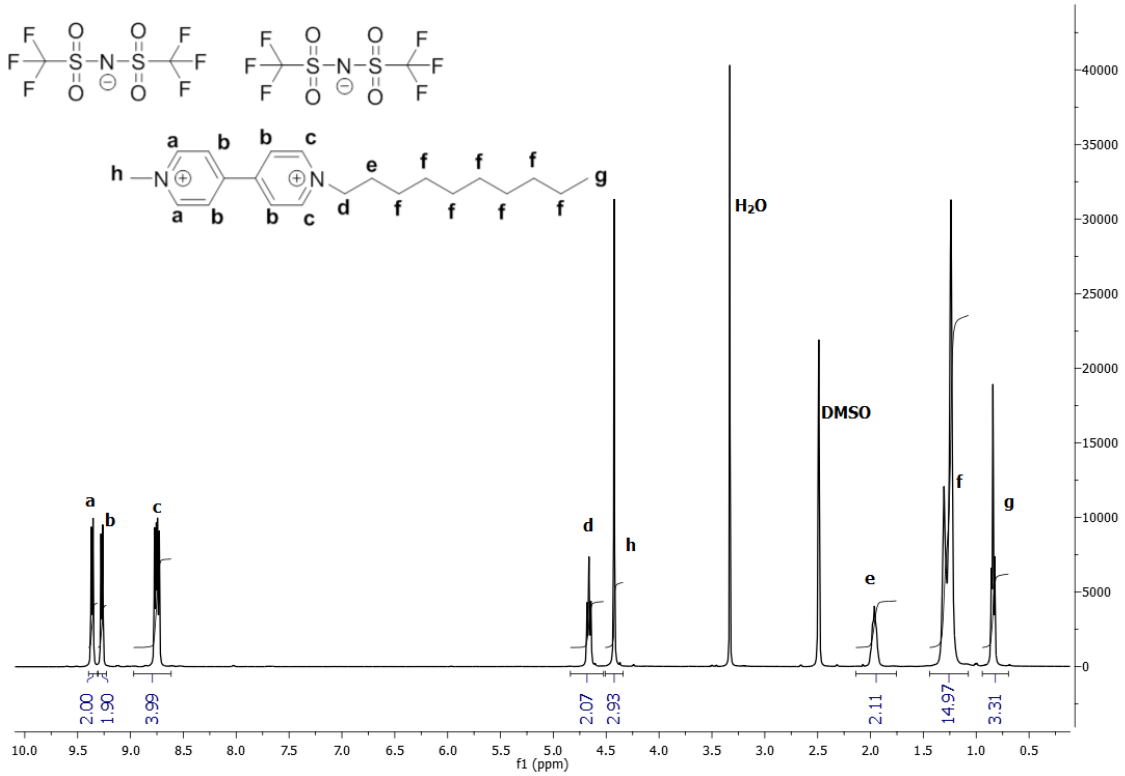

Figure A. 7.1.35 – ^{1}H NMR (DMSO-d6, 400.13 MHz, 25 ºC, ppm) of $[C_1C_{10}bpy][NTf_2]_2$.

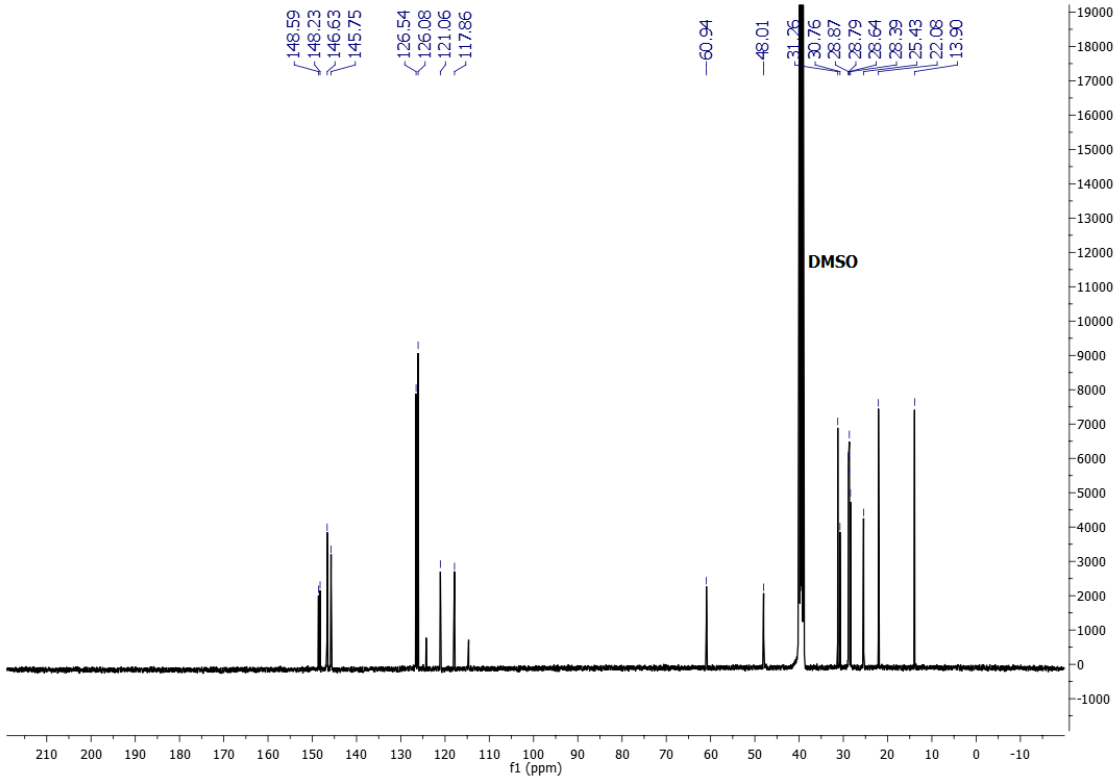

Figure A. 7.1.36 – ^{13}C NMR (DMSO-d6, 100.61 MHz, 25 ºC, ppm) of $[C_1C_{10}bpy][NTf_2]_2$.

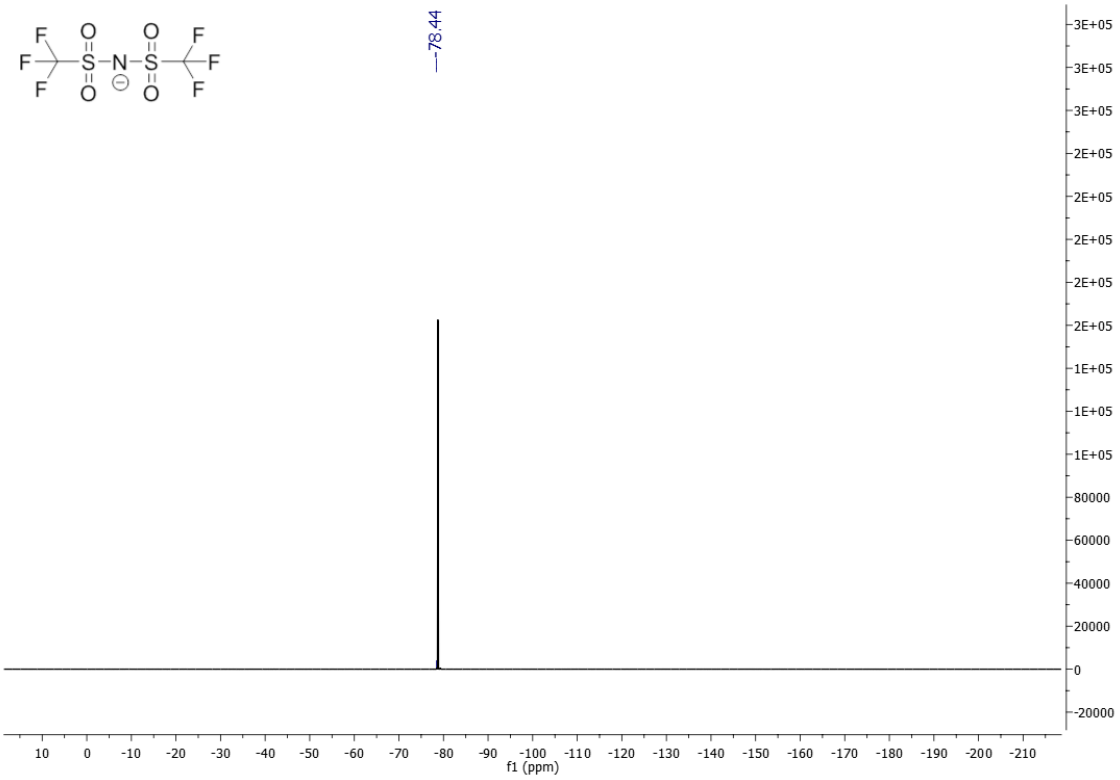

Figure A. 7.1.37 – ^{19}F NMR (DMSO-d6, 376.50 MHz, 25 ºC, ppm) of $[C_1C_{10}bpy][NTf_2]_2$.

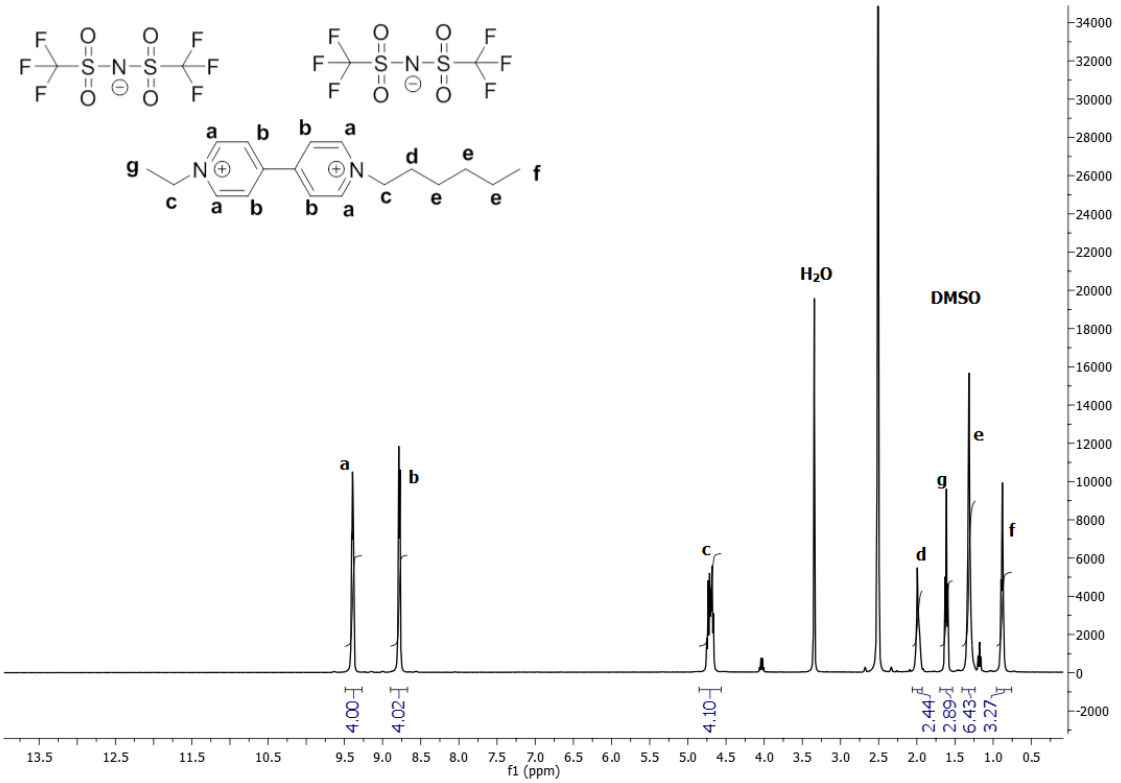

Figure A. 7.1.38 – ^{1}H NMR (DMSO-d6, 400.13 MHz, 25 ºC, ppm) of $[C_2C_6bpy][NTf_2]_2$.

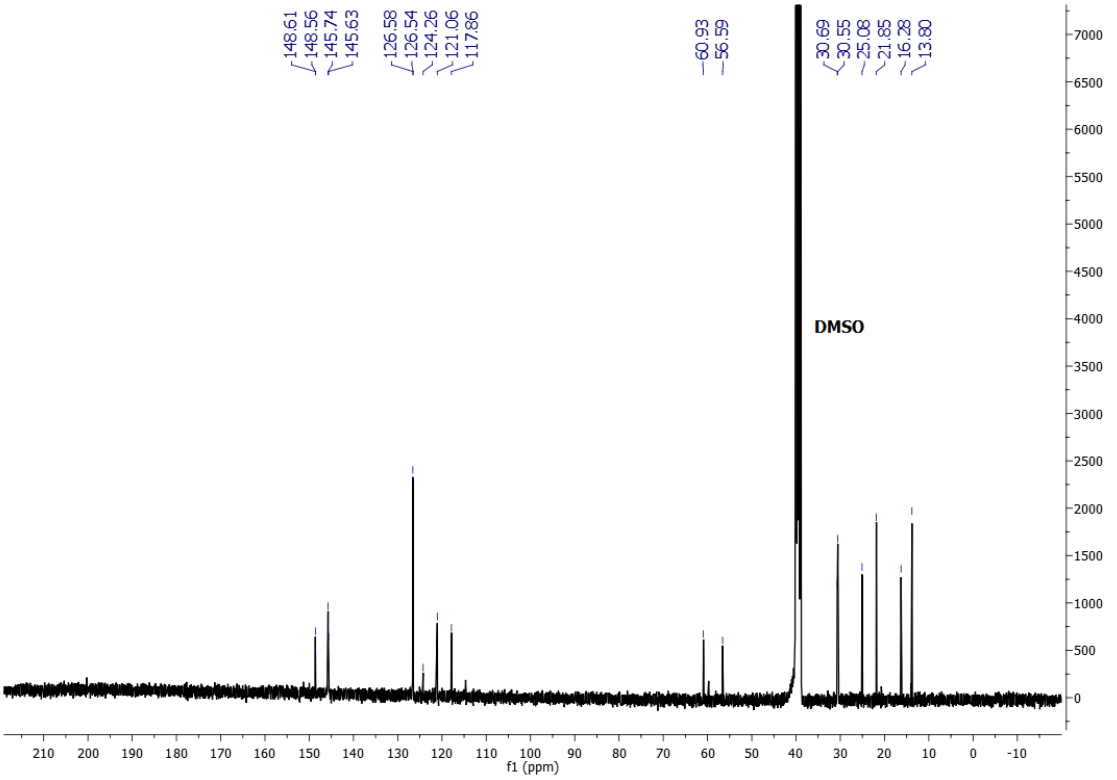

Figure A. 7.1.39 – ^{13}C NMR (DMSO-d6, 100.61 MHz, 25 ºC, ppm) of $[C_2C_6bpy][NTf_2]_2$.

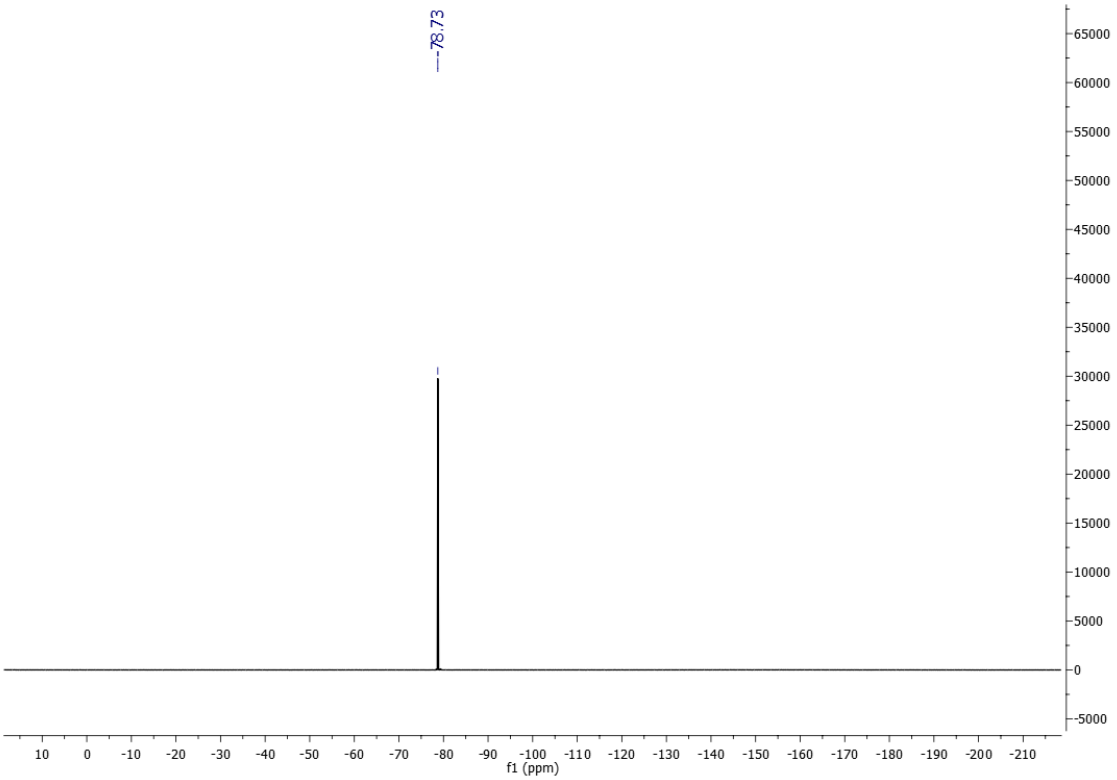

Figure A. 7.1.40 – ^{19}F NMR (DMSO-d6, 376.50 MHz, 25 ºC, ppm) of $[C_2C_6bpy][NTf_2]_2$.

7.1.2. DSC

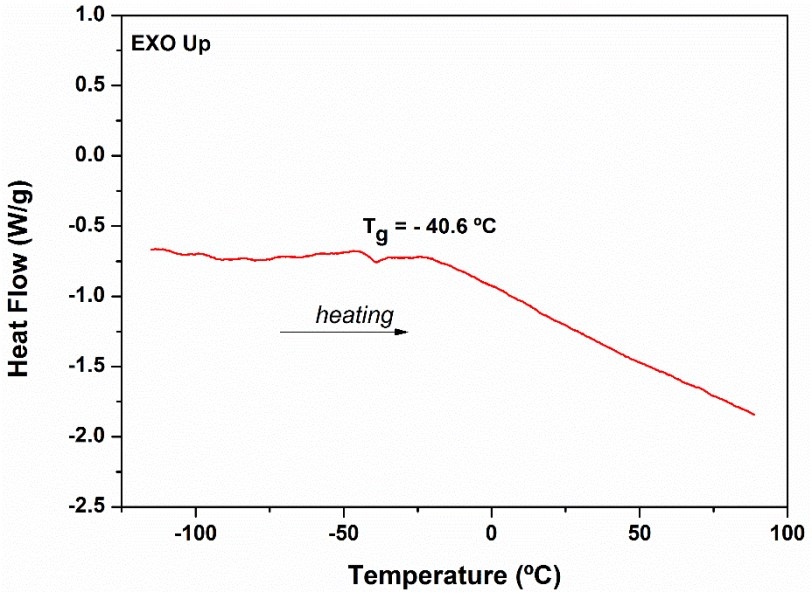

Figure A. 7.1.41 – Thermogram of [C_6bpy][NTf_2] was obtained with heating/cooling rate of 10 ºC/min, where glass transition temperature (T_g) was determined as midpoint on the second heating.

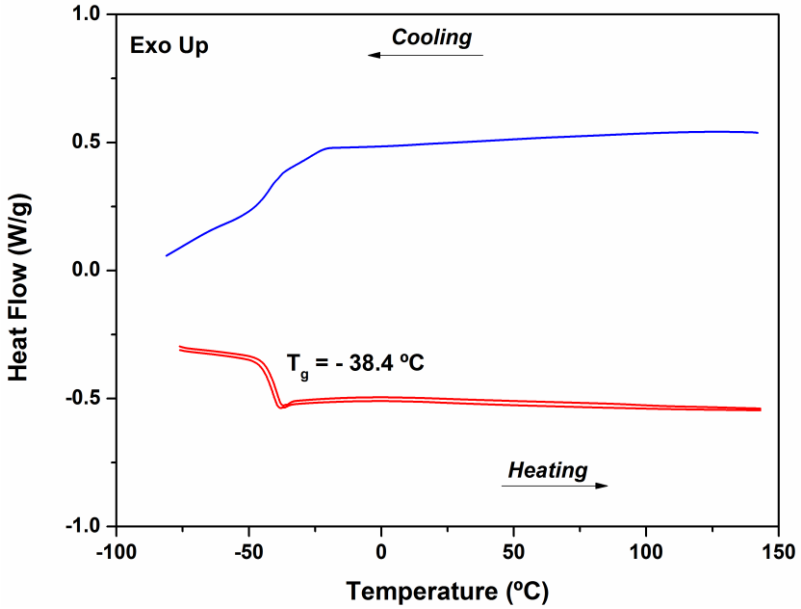

Figure A. 7.1.42 – Thermogram of [C_{10}bpy][NTf_2] was obtained with heating/cooling rate of 20 ºC/min, where glass transition temperature (T_g) was determined as midpoint on the second heating.

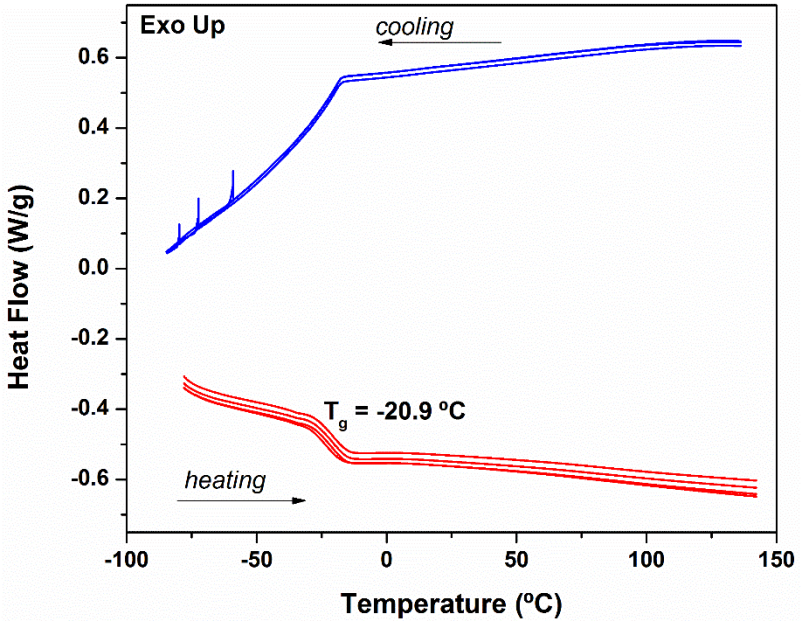

Figure A. 7.1.43 – Thermogram of [C_{10}bpy][AOT] was obtained with heating/cooling rate of 20 ºC/min, where glass transition temperature (T_g) was determined as midpoint on the last heating.

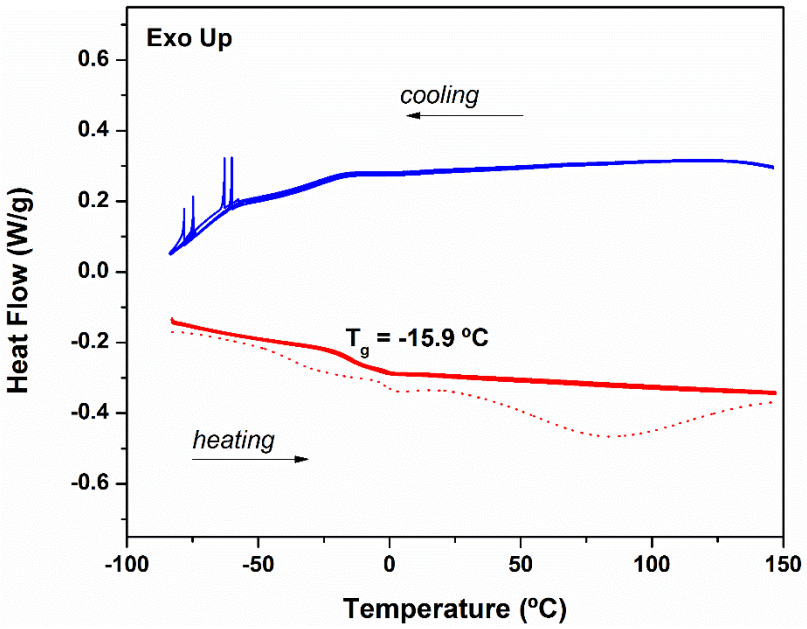

Figure A. 7.1.44 – Thermogram of [C_3O][AOT] was obtained with heating/cooling rate of 10 ºC/min. Glass transition temperature (T_g) was determined as midpoint on the last heating. The dot line corresponds to the first cycle, where a solvent evaporation process as broadly endothermic peak is observed.

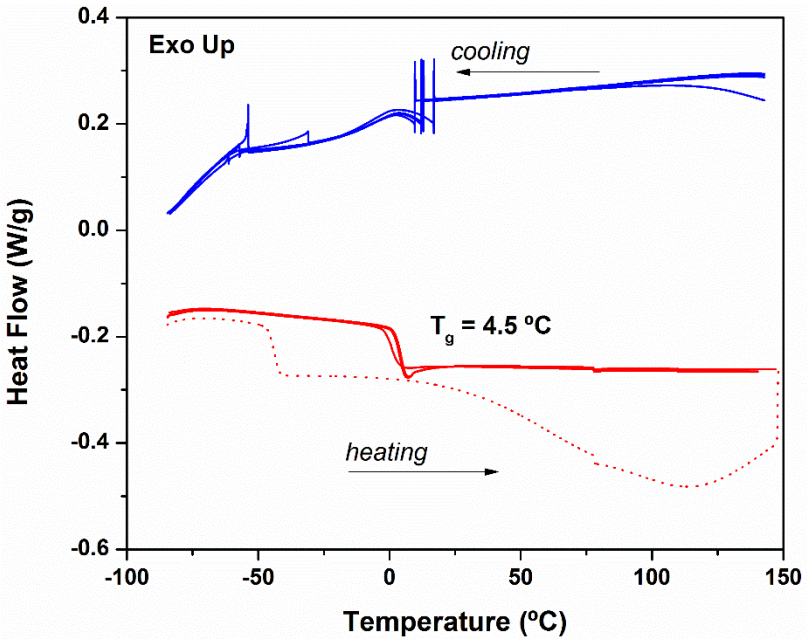

Figure A. 7.1.45 – Thermogram of $[C_5O_2bpy]I_2$ was obtained with heating/cooling rate of 10 ºC/min. Glass transition temperature (T_g) was determined as midpoint on the last heating. The dot line corresponds to the first cycle, where a solvent evaporation process as broadly endothermic peak is observed.

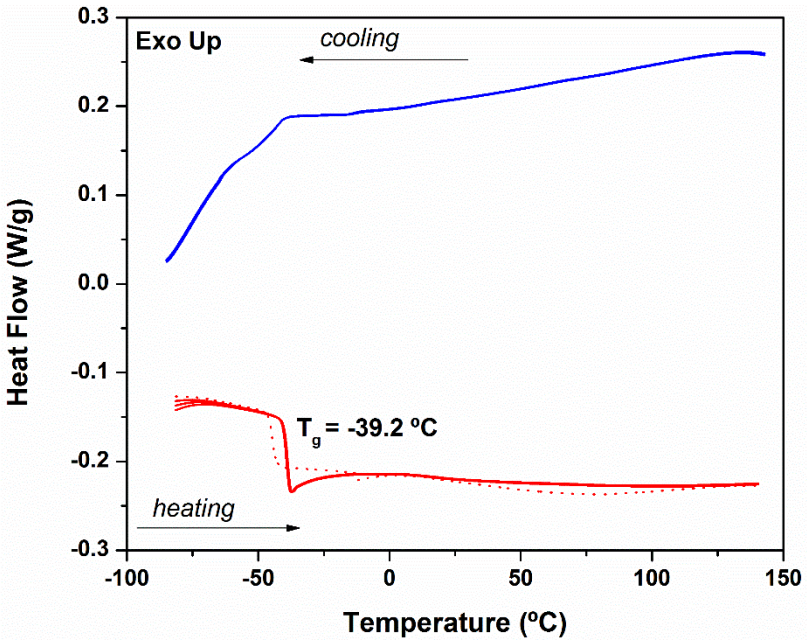

Figure A. 7.1.46 – Thermogram of [(allyl)bpy][NTf_2] was obtained with heating/cooling rate of 10 ºC/min. Glass transition temperature (T_g) was determined as midpoint on the last heating. The dot line corresponds to the first cycle, where a solvent evaporation process as broadly endothermic peak is observed.

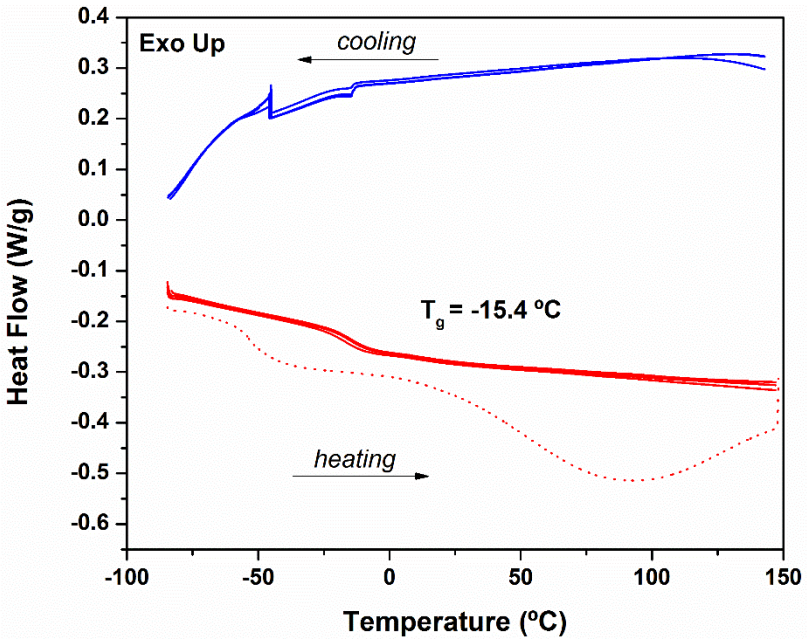

Figure A. 7.1.47 – Thermogram of [(allyl)bpy][AOT] was obtained with heating/cooling rate of 10 ºC/min. Glass transition temperature (T_g) was determined as midpoint on the last heating. The dot line corresponds to the first cycle, where a solvent evaporation process as broadly endothermic peak is observed.

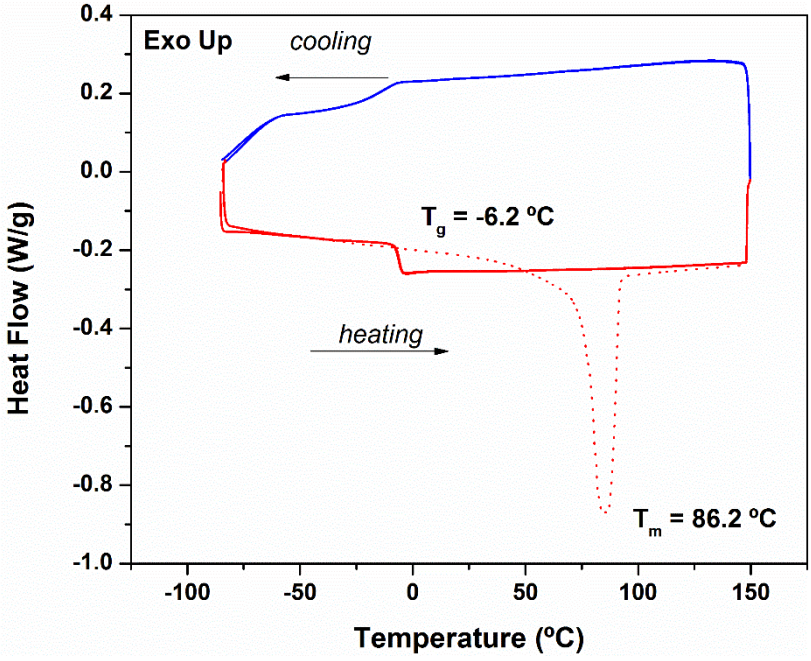

Figure A. 7.1.48 – Thermogram of [C_2OHbpy][NTf_2] was obtained with heating/cooling rate of 10 ºC/min. Glass transition temperature (T_g) was determined as midpoint on the last heating. The dot line corresponds to the first cycle, where a melting as endothermic peak is observed.

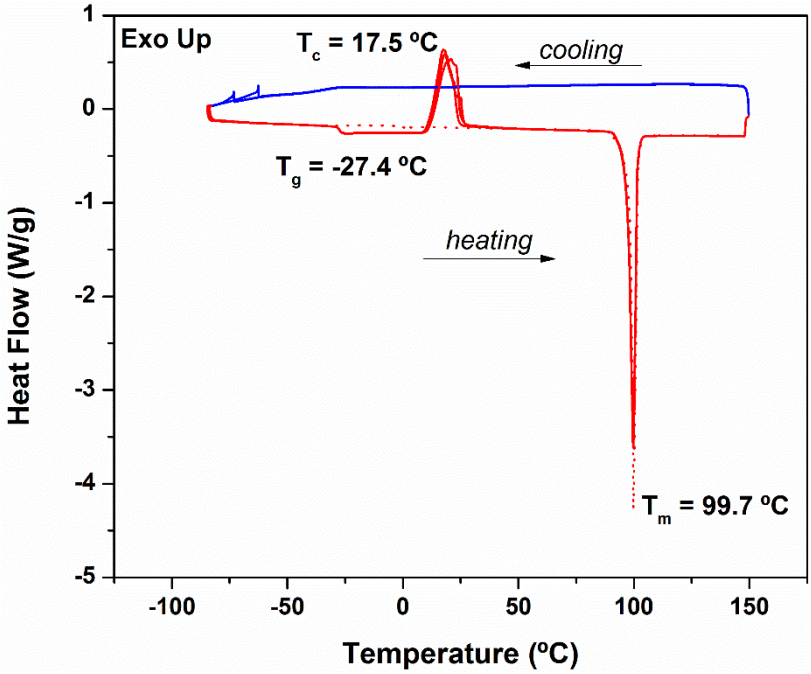

Figure A. 7.1.49 – Thermogram of $[(C_5O_2)_2bpy][NTf_2]_2$ was obtained with heating/cooling rate of 10 ºC/min. Glass transition temperature (T_g) was determined as midpoint on the last heating. The dot line corresponds to the first cycle, where a melting as endothermic peak is observed.

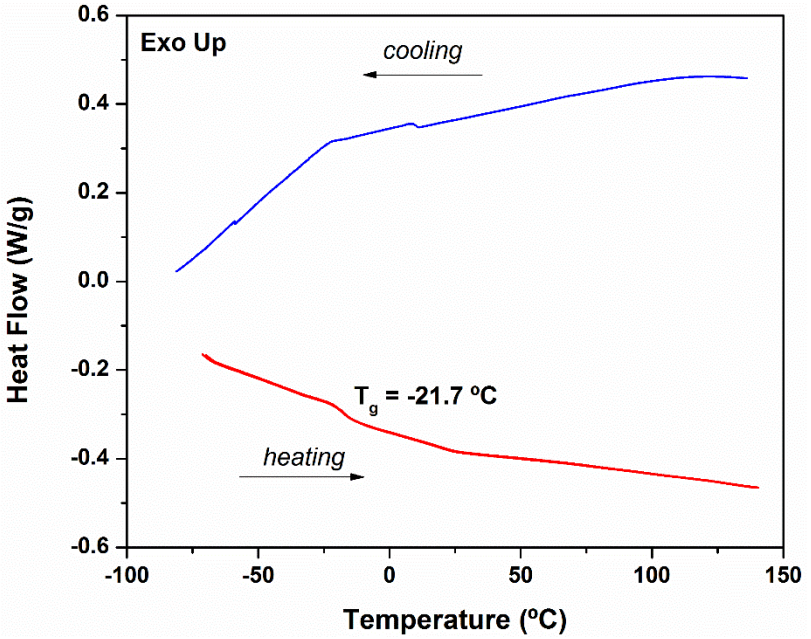

Figure A. 7.1.50 – Thermogram of $[(C_5O_2)_2bpy][AOT]_2$ was obtained with heating and cooling rate of 20 ºC/min. Glass transition temperature (T_g) was determined as midpoint on the last heating.

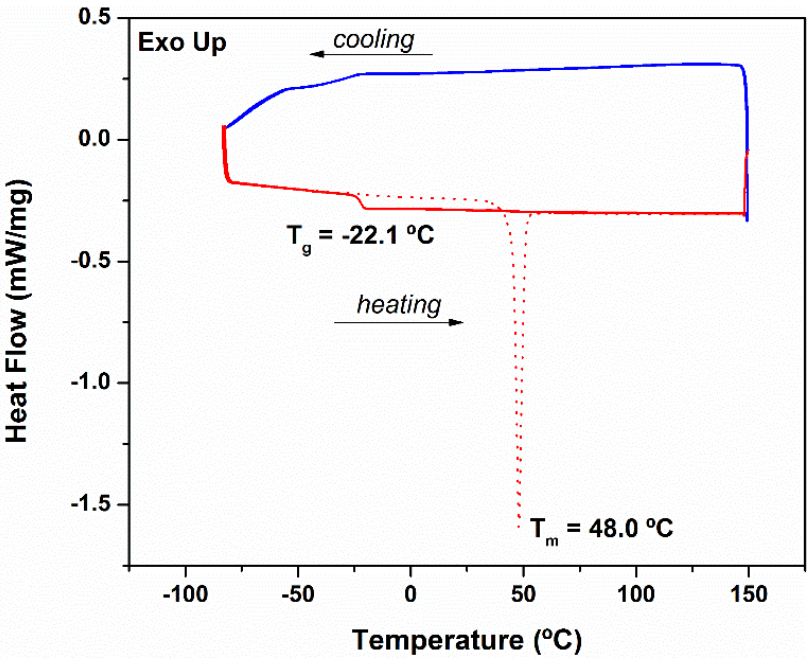

Figure A. 7.1.51 – Thermogram of $[(C_1C_{10}bpy][NTf_2]_2$ was obtained with heating and cooling rate of 10 ºC/min. Glass transition temperature (T_g) was determined as midpoint on the last heating. The dot line corresponds to the first cycle, where a melting is observed as endothermic peak.

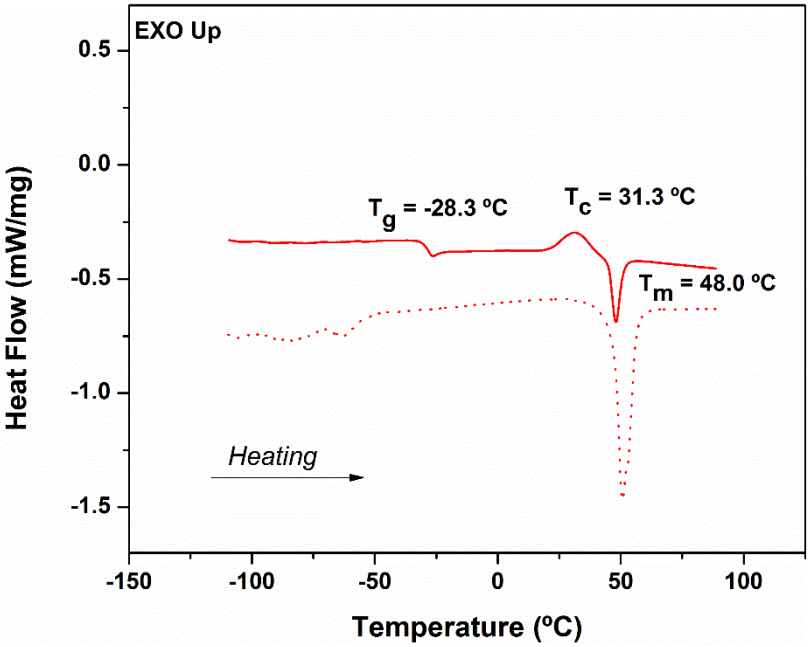

Figure A. 7.1.52 – Thermogram of $[(C_2C_6bpy][NTf_2]_2$ was obtained with heating/cooling rate of 10 ºC/min. Glass transition temperature (T_g) was determined as midpoint on the last heating. The dot line corresponds to the first cycle, where a melting is observed as endothermic peak.

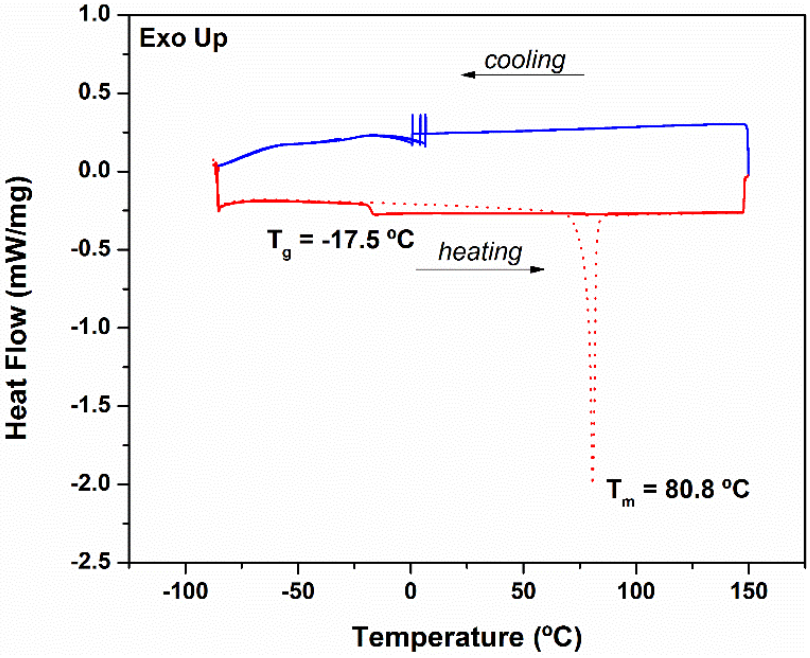

Figure A. 7.1.53 – Thermogram of $[(C_1C_3Obpy][NTf_2]_2$ was obtained with heating and cooling rate of 10 ºC/min. Glass transition temperature (T_g) was determined as midpoint on the last heating. The dot line corresponds to the first cycle, where a melting as endothermic peak is observed.

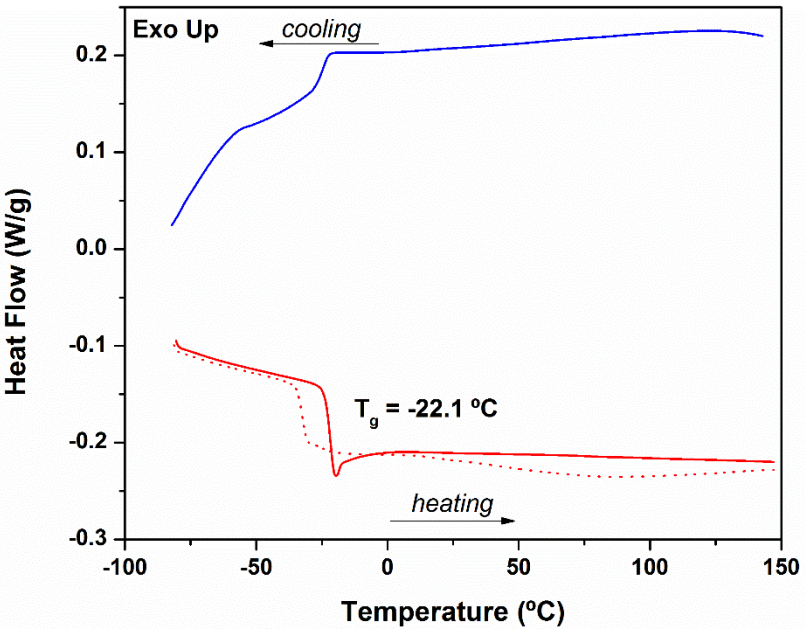

Figure A. 7.1.54 – Thermogram of $[(C_1C_5O_2bpy][NTf_2]_2$ was obtained with heating/cooling rate of 10 ºC/min. Glass transition temperature (T_g) was determined as midpoint on the last heating. The dot line corresponds to the first cycle, where a solvent evaporation process as broadly endothermic peak is observed.

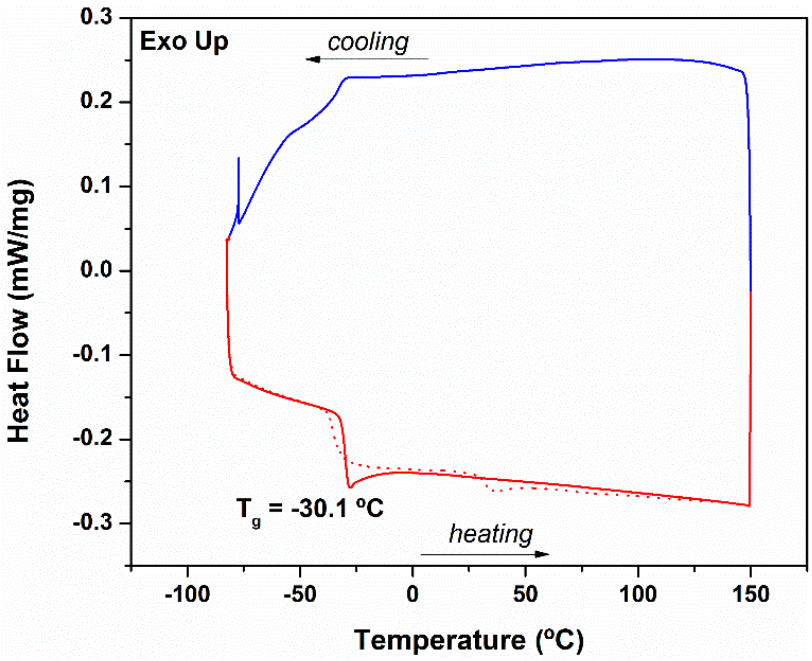

Figure A. 7.1.55 – Thermogram of $[(C_6C_5O_2bpy][NTf_2]_2$ was obtained with heating/cooling rate of 10 ºC/min. Glass transition temperature (T_g) was determined as midpoint on the last heating. The dot line corresponds to the first cycle, where a solvent evaporation process as broadly endothermic peak is observed.

7.1.3. UV-Vis spectroscopy

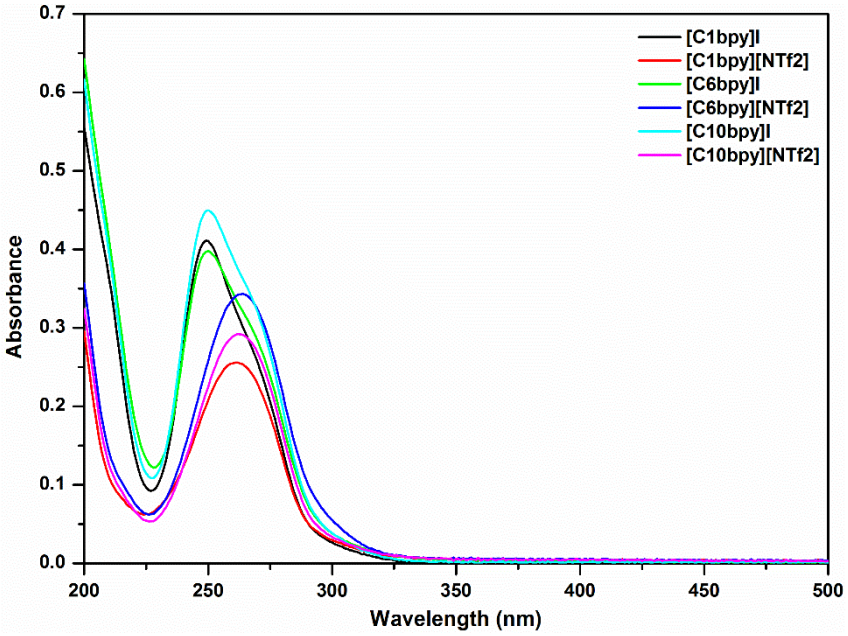

Figure A. 7.1.56 – UV-Visible spectra from mono-alkyl-4,4'-bipyridinium salts.

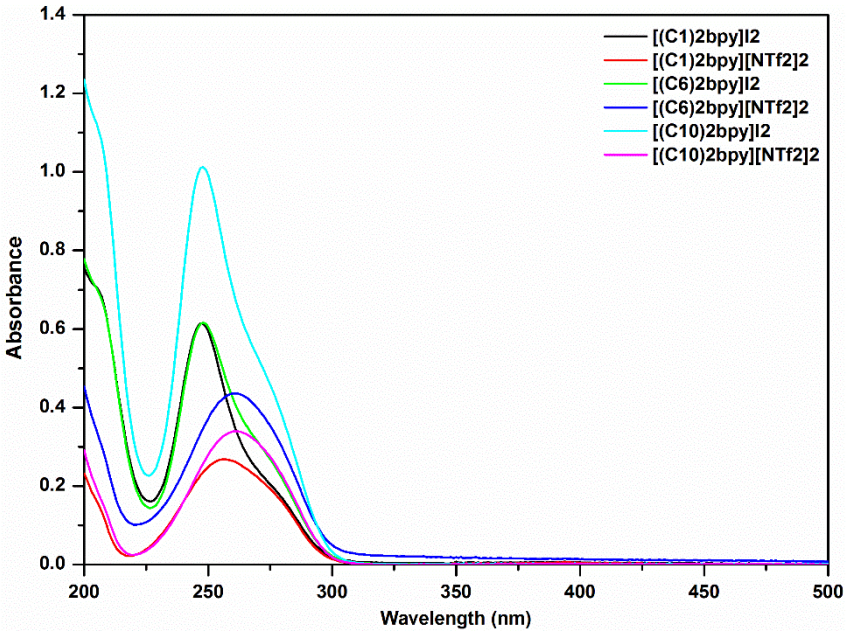

Figure A. 7.1.57 – UV-Visible spectra from symmetrical di-alkyl-4,4'-bipyridinium salts.

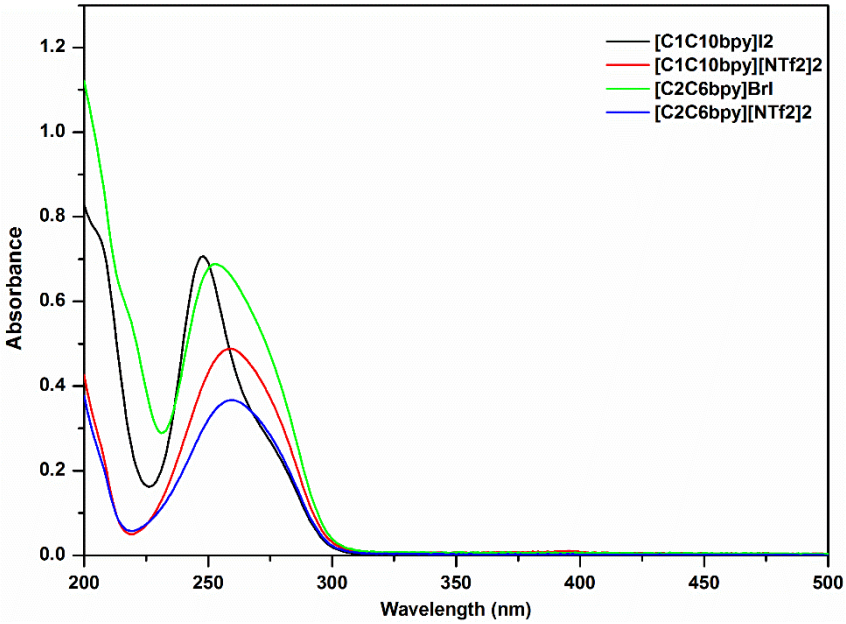

Figure A. 7.1.58 – UV-Visible spectra from asymmetrical di-alkyl-4,4'-bipyridinium salts.

7.1.4. Electrochemical Studies

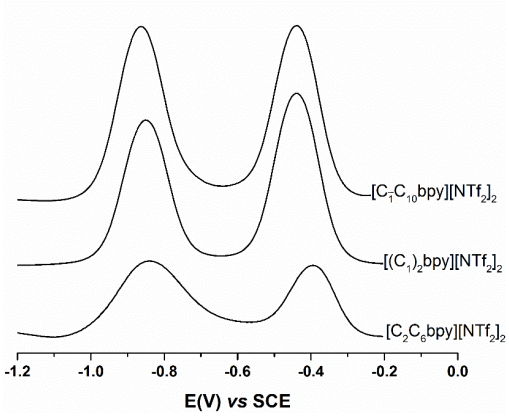

Figure A. 7.1.59 – Square Wave Voltammetry (SWV) of 1 mm solutions of 4,4'-bipyridinium based NTf_2 salts, in acetonitrile containing 0.1m TBAP, at a platinum working electrode *vs* SCE, 6 mV step potential, 60 mV pulse amplitude, 20 Hz.

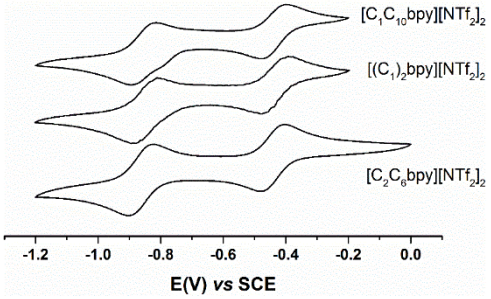

Figure A. 7.1.60 – Cyclic voltammetry (CV) of 1 mm solutions of 4,4'-bipyridinium based NTf_2 salts in acetonitrile containing 0.1m TBAP, at a platinum working electrode *vs* SCE, at 0.200 $V.s^{-1}$, showing the reversibility of first (di-cation to radical cation) and the second (radical cation to neutral compound) reduction process.

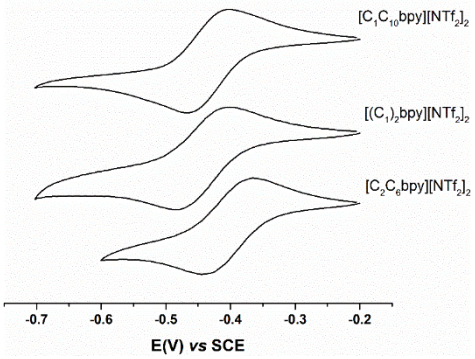

Figure A. 7.1.61 – Cyclic voltammetry (CV) of 1 mm solutions of 4,4'-bipyridinium based NTf_2 salts in acetonitrile containing 0.1m TBAP, at a platinum working electrode *vs* SCE, at 0.200 $V.s^{-1}$, showing the reversibility of first reduction process (di-cation to radical cation) in detail.

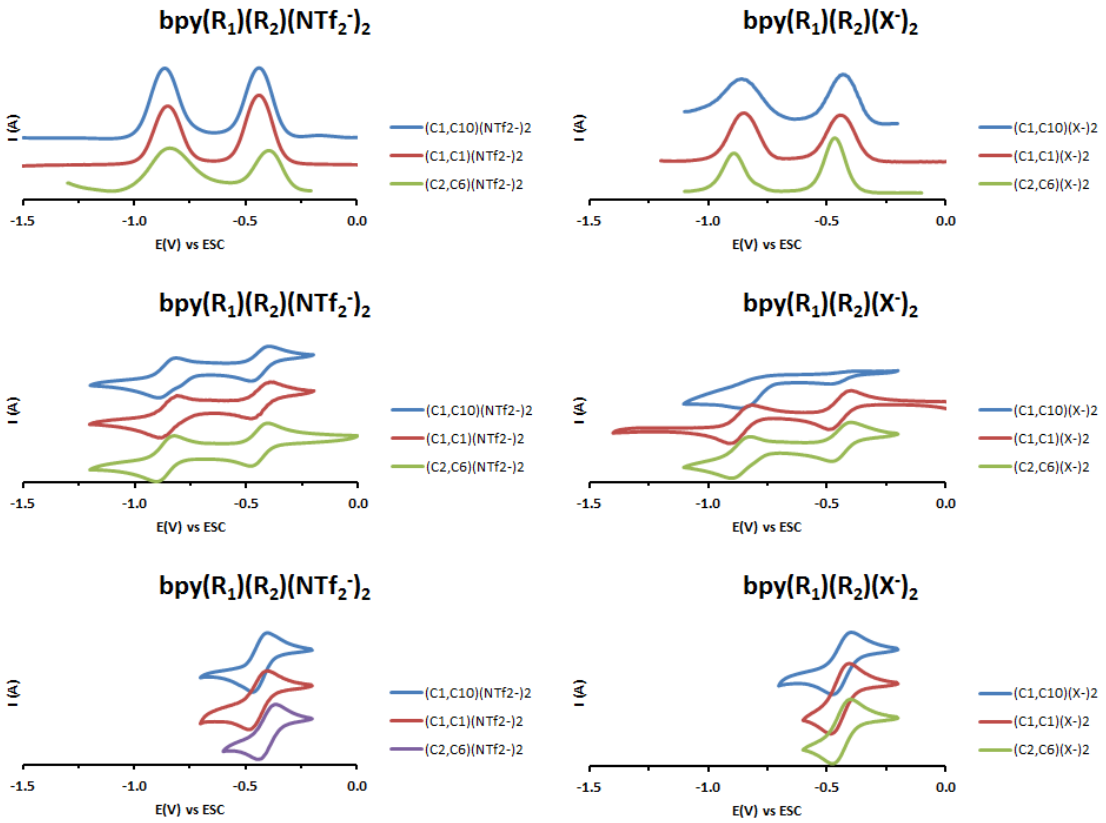

Figure A. 7.1.62 – Square Wave Voltammetry (SWV) (top) and Cyclic Voltammetry (CV) (middle) showing the two redox processes of di-alkyl-4,4'-bipyridinium combined with anions [NTf_2], [I] or [Br]; (down) detail of CV for the first reduction process; sample concentration: 1 mM; solvent and supporting electrolyte: acetonitrile with 0.1 M TBAP. Acquisition parameters: SWV at 20 Hz, CV at 0.200 V/s scan rate; working, auxilliary and reference electrodes of Pt (diameter= 1.6 mm), Pt wire and SCE, respectively; voltammograms was acquired under argon.

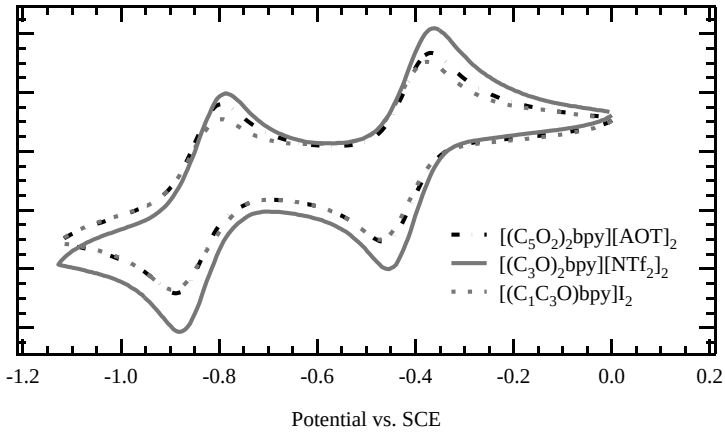

Figure A. 7.1.63 – Cyclic Voltammetry (CV) of 1 mM solutions 4,4'-bipyridinium salts combined with different anions in acetonitrile containing 0.1M TBAP, at a glassy carbon working electrode *vs* SCE, at 0.250 V/s, showing the reversibility of first and second electron-transfer process in the reduction process (dication → radical cation and radical cation → neutral specie) in detail.

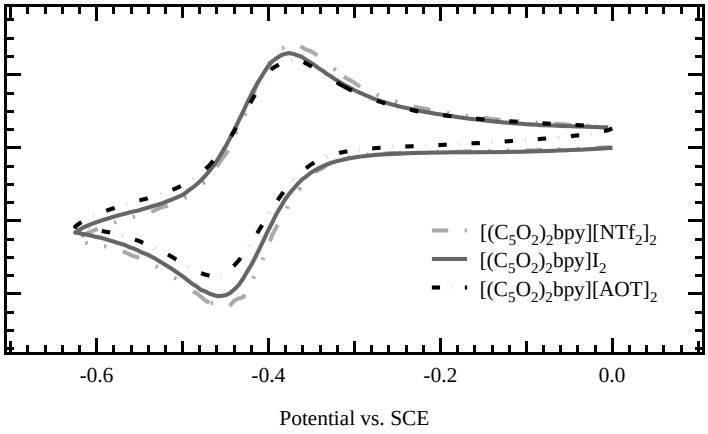

Figure A. 7.1.64 –. Cyclic Voltammetry (CV) of 1 mM solutions $[C_5O_2bpy]I_2$, $[C_5O_2bpy][NTf_2]_2$, $[C_5O_2bpy][AOT]_2$, in acetonitrile containing 0.1M TBAP, at a glassy carbon working electrode *vs* SCE, at 0.250 V/s, showing the reversibility of first electron-transfer process in the reduction process.

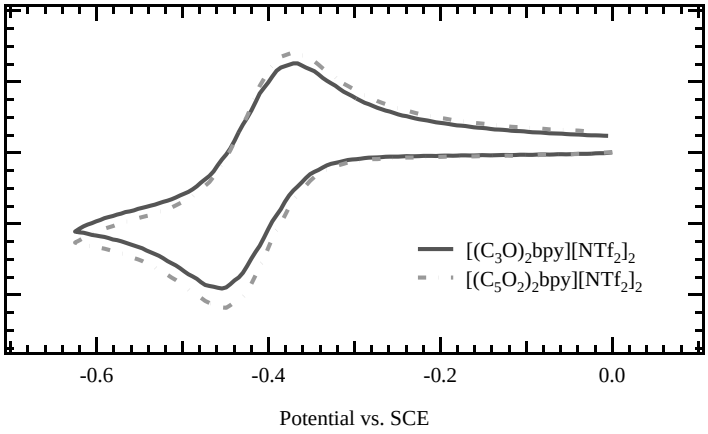

Figure A. 7.1.65 – Cyclic Voltammetry (CV) of 1 mM solutions symmetric 4,4'-bipyridinium salts combined with $[NTf_2]$ in acetonitrile containing 0.1M TBAP, at a glassy carbon working electrode *vs* SCE, at 0.250 V/s, showing the reversibility of the first electron-transfer process in the reduction process.

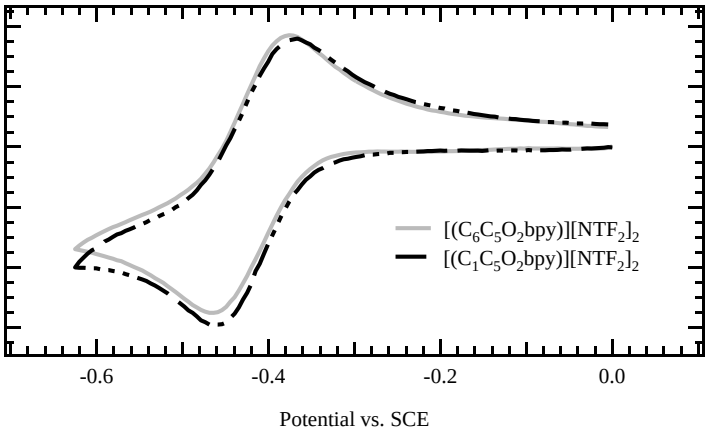

Figure A. 7.1.66 – Cyclic Voltammetry (CV) of 1 mM solutions 4,4'-bipyridinium salts combined with $[NTf_2]$ in acetonitrile containing 0.1M TBAP, at a glassy carbon working electrode *vs* SCE, at 0.250 V/s, showing the reversibility of first electron-transfer process in the reduction process.

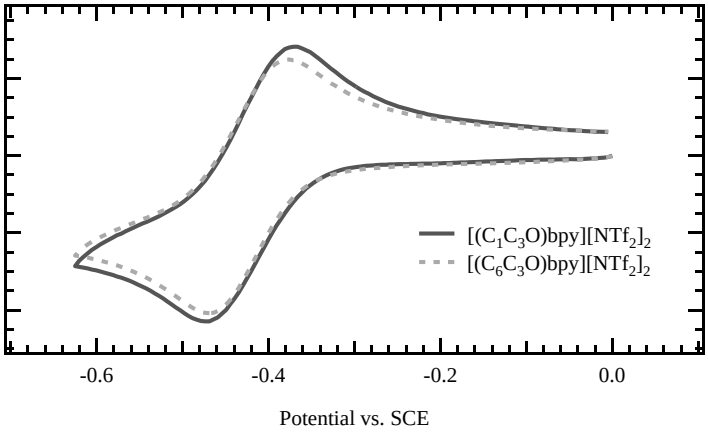

Figure A. 7.1.67 – Cyclic Voltammetry (CV) of 1 mM solutions 4,4'-bipyridinium salts combined with [NTf_2] in acetonitrile containing 0.1M TBAP, at a glassy carbon working electrode *vs* SCE, at 0.250 V/s, showing the reversibility of first electron-transfer process in the reduction process.

7.2. Electrochromic Organic Ionic Oligomers and Polymers

7.2.1. DSC and DSC/TGA

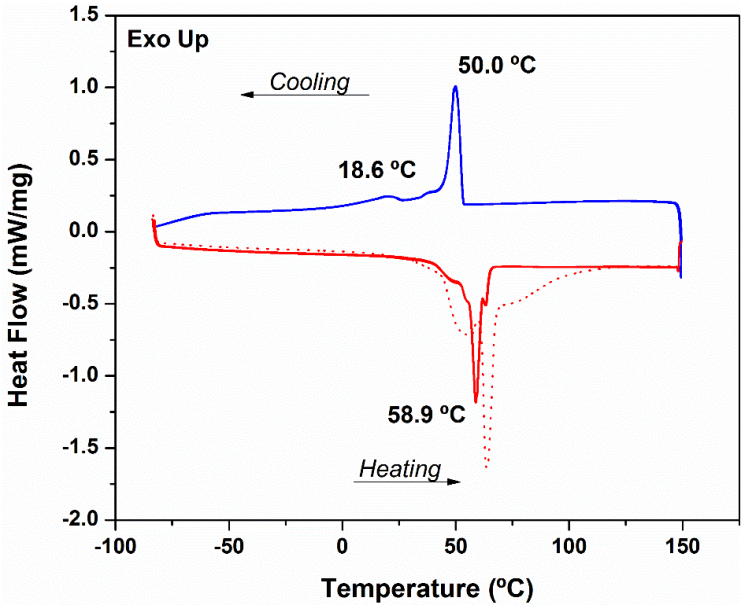

Figure A. 7.2.1 – Heat flow thermograms for $[(C_{10})bpy(C_4O)bpy(C_{10})]I_4$ obtained upon heating and cooling rate of 10 ºC/min. The dot line corresponds to the first heating run and the full line corresponds to the subsequent cooling and heating runs.

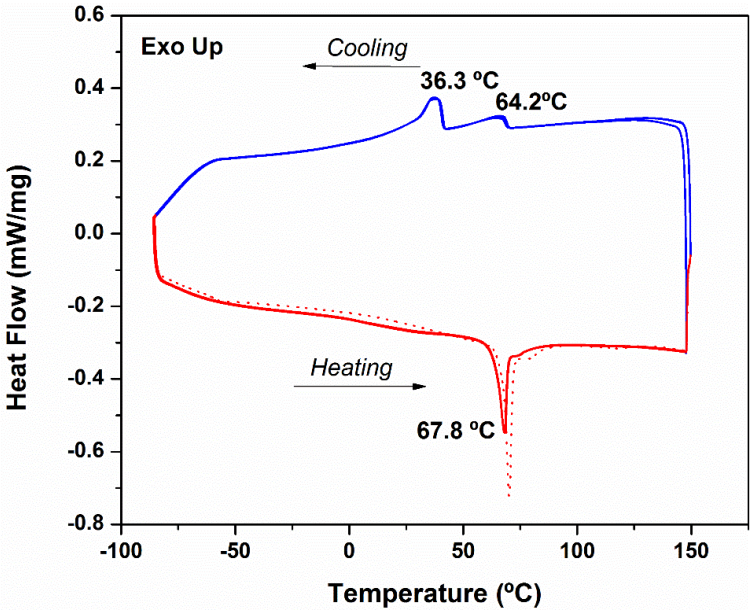

Figure A. 7.2.2 – Heat flow thermograms for $[(C_{10})bpy(C_4O)bpy(C_{10})][NTf_2]_4$ obtained upon heating and cooling rate of 10 ºC/min. The dot line corresponds to the first heating run and the full line corresponds to the subsequent cooling and heating runs.

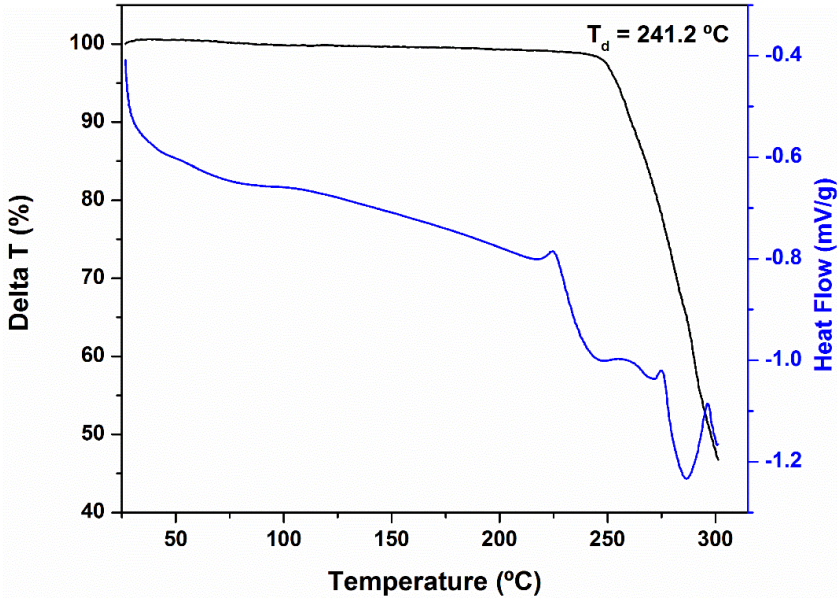

Figure A. 7.2.3 –Thermogravimetric analysis and Heat flow thermogram for [(C_3O)bpy(C_4O)bpy(C_3O)]I_4 obtained upon heating rate of 10 ºC/min. The decomposition temperature was determined as the onset temperature, which can be calculated as the intersection of the straight baseline along the temperature axis, where there is no weight loss and a horizontal tangent to the TGA curve at the inflection point, which correspond to the peak of the first derivative curve of TGA. .

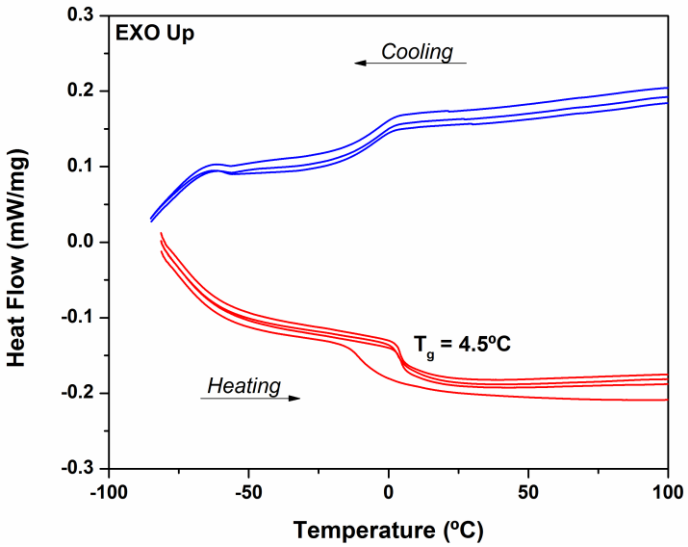

Figure A. 7.2.4 – Heat flow thermograms for [(C_{10})bpy(C_4O)bpy(C_3O)][NTf_2]$_4$ obtained upon heating and cooling rate of 10 ºC/min. Glass transition was determined as mid-point in the last heating cycle.

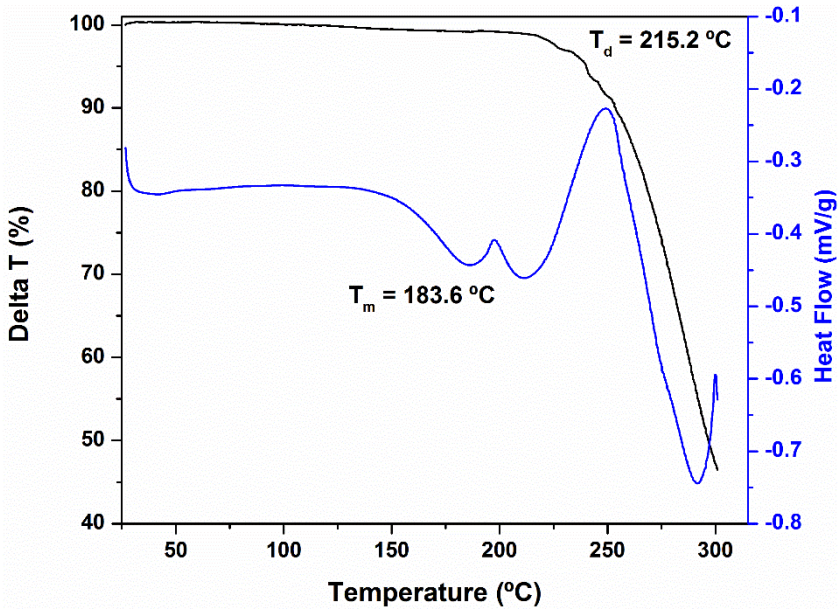

Figure A. 7.2.5 – Thermogravimetric analysis and Heat flow thermogram for [(C_3O)bpy(C_8O_3)bpy(C_3O)]I_4 obtained upon heating rate of 10 ºC/min. The decomposition temperature was determined as the onset temperature, which can be calculated as the intersection of the straight baseline along the temperature axis, where there is no weight loss and a horizontal tangent to the TGA curve at the inflection point, which correspond to the peak of the first derivative curve of TGA. The melting was detected closed to 180 ºC.

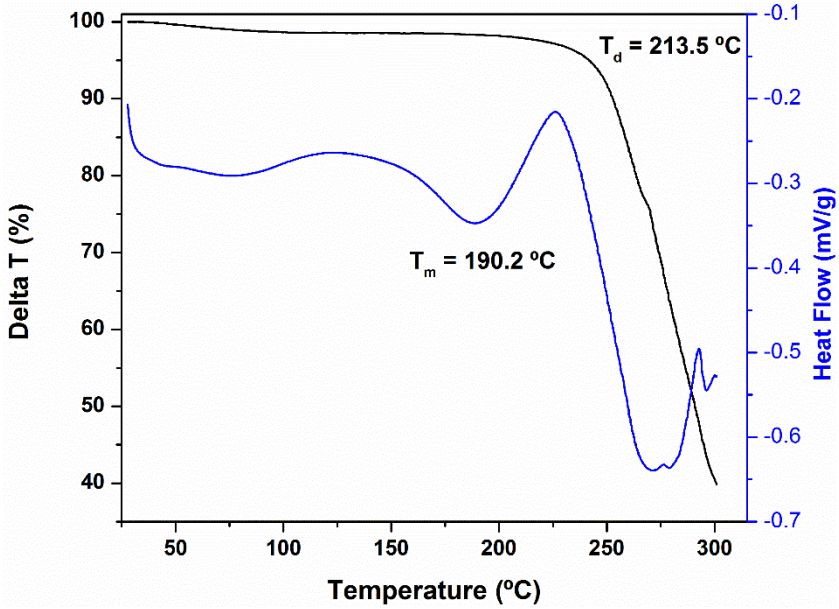

Figure A. 7.2.6 – Thermogravimetric analysis and Heat flow thermogram for [(C_{10})bpy(C_4O)bpy(C_3O)]I_4 obtained upon heating rate of 10 ºC/min. The decomposition temperature was determined as the onset temperature, which can be calculated as the intersection of the straight baseline along the temperature axis, where there is no weight loss and a horizontal tangent to the TGA curve at the inflection point, which correspond to the peak of the first derivative curve of TGA. The melting was detected closed to 190.2 ºC.

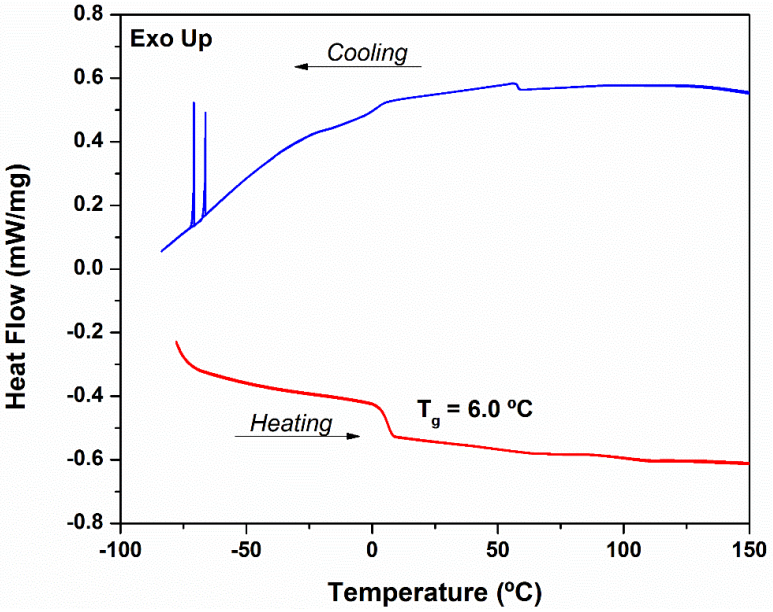

Figure A. 7.2.7 – Heat flow thermograms for $[(C_{10})bpy(C_4O)bpy(C_3O)][NTf_2]_4$ obtained upon heating and cooling rate of 20 ºC/min. Glass transition temperature was determined as mid-point in the last heating cycle.

7.3. Application of electrochromic salts in devices

7.3.1. Electrochemical Studies

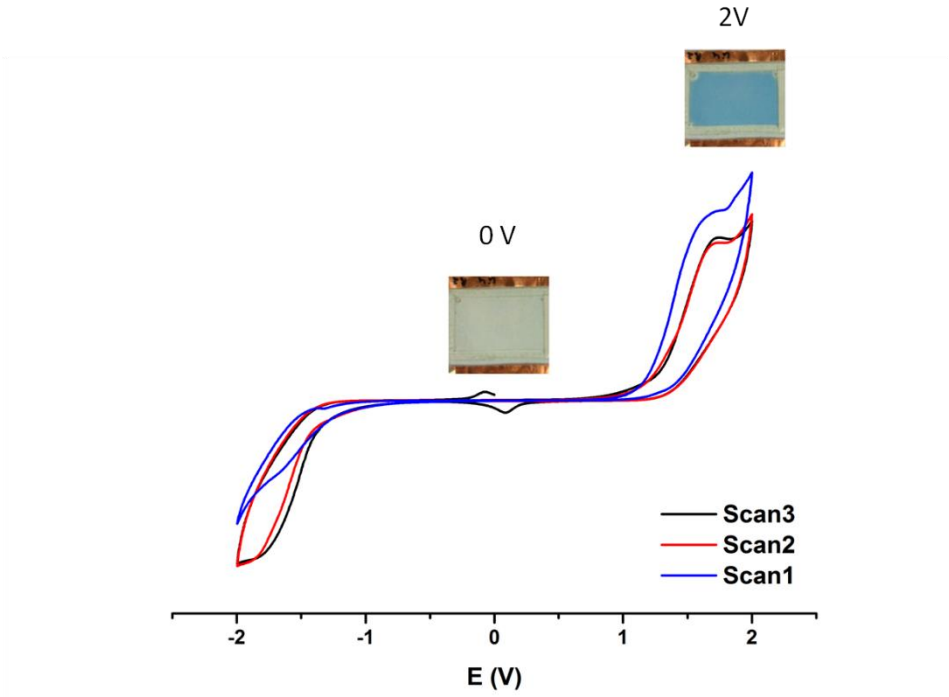

Figure A. 7.3.1 – Cyclic voltammetry of $[(C_{10})_2bpy][NTf_2]_2$ dissolved in adequate electrolyte (ca. 0.07 M) between two equal conducting PET surfaces (electrochromic device).

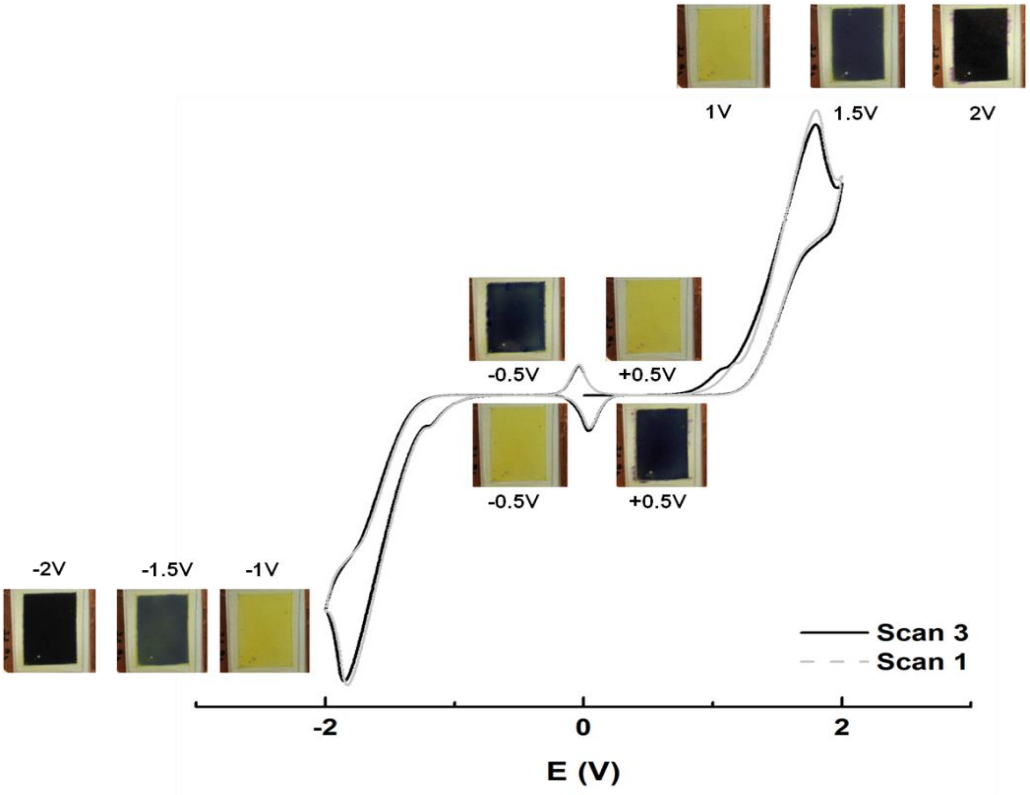

Figure A. 7.3.2 – Cyclic voltammetry of $[(C_5O_2)_2bpy]I_2$ dissolved in adequate electrolyte (ca. 0.07 M) between two equal conducting PET surfaces (electrochromic device).

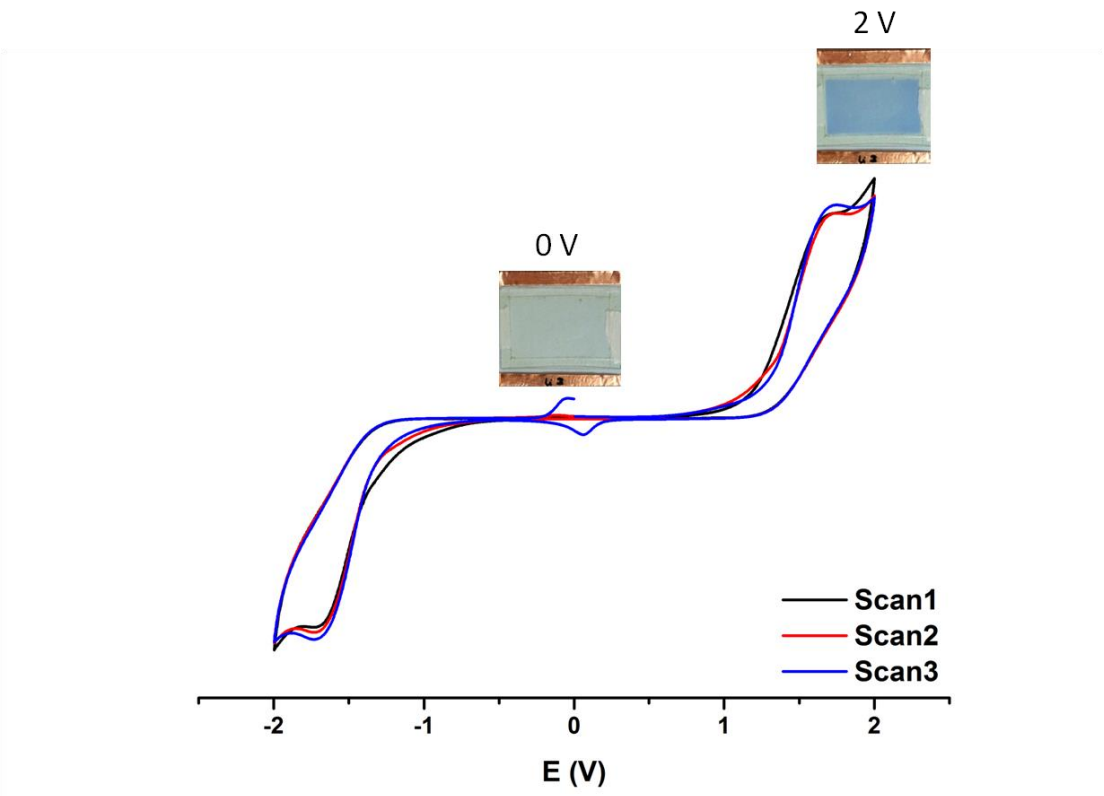

Figure A. 7.3.3 – Cyclic voltammetry of $[(C_5O_2)_2bpy][NTf_2]_2$ dissolved in adequate electrolyte (ca. 0.07 M) between two equal conducting PET surfaces (electrochromic device).

7.3.2. Spectroelectrochemistry Data

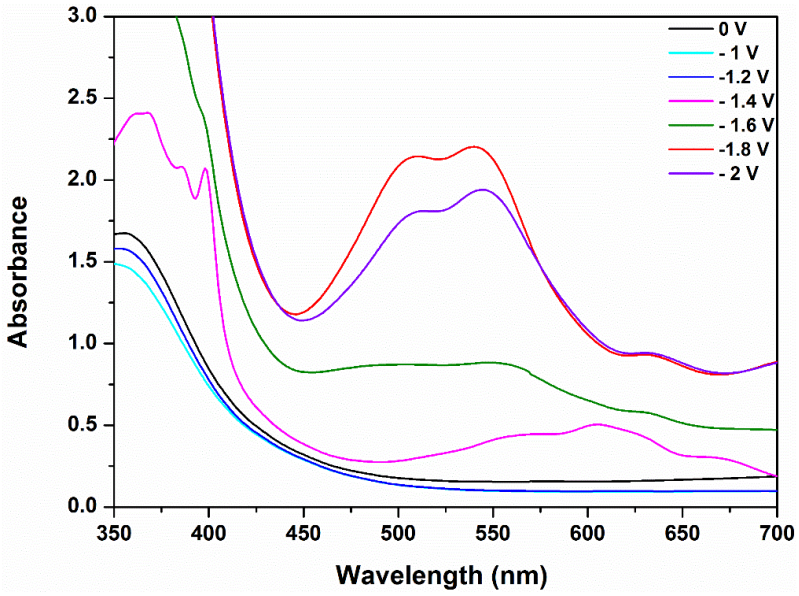

Figure A. 7.3.4 – Absorption spectra of the device containing $[(C_{10})_2bpy]I_2$ after applying a specific potential.

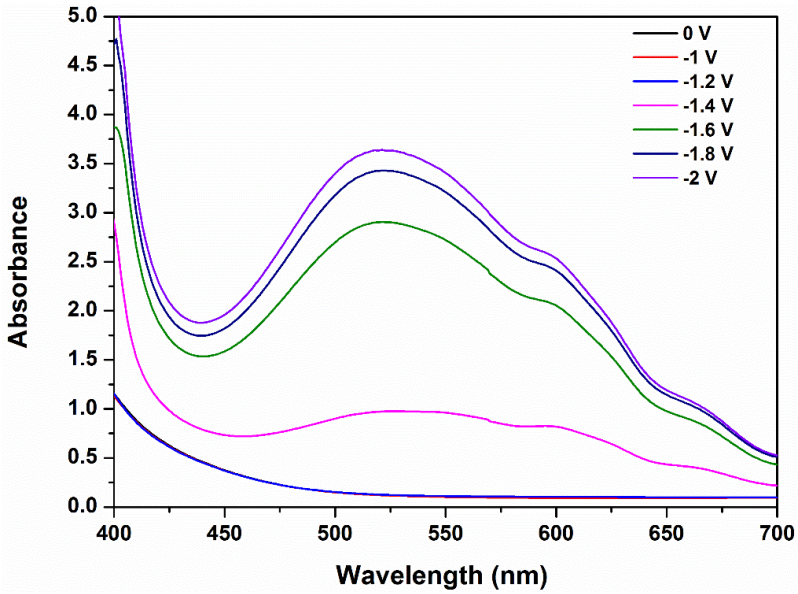

Figure A. 7.3.5 – Absorption spectra of the device containing $[(C_5O_2)_2bpy]I_2$ after applying a specific potential.

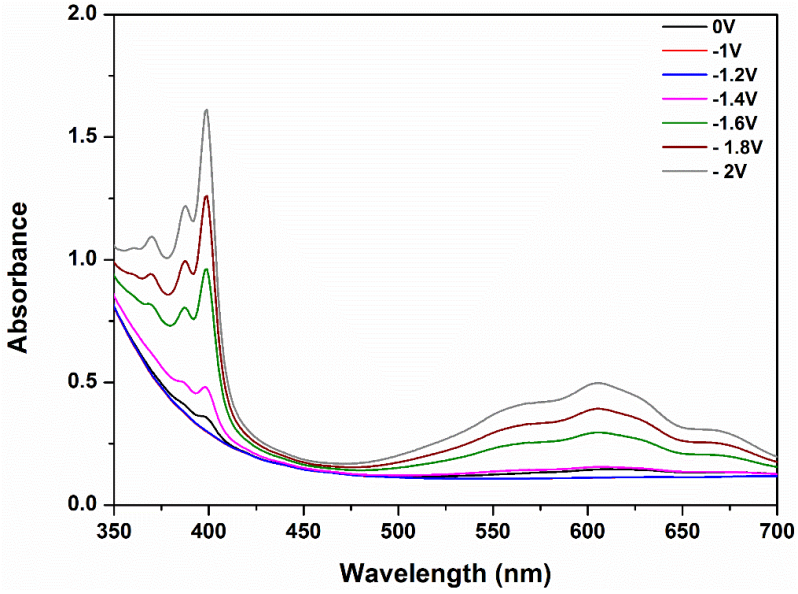

Figure A. 7.3.6 – Absorption spectra of the device containing $[(C_{10})_2bpy][NTf_2]_2$ after applying a specific potential.

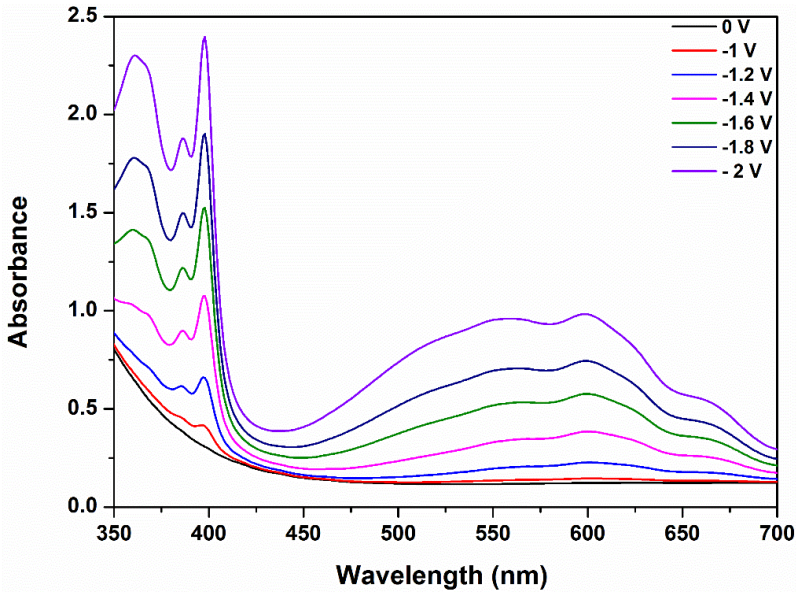

Figure A. 7.3.7 – Absorption spectra of the device containing $[(C_5O_2)_2bpy][NTf_2]_2$ after applying a specific potential.

7.4. Multi stimuli-responsive Polymer

7.4.1. DSC

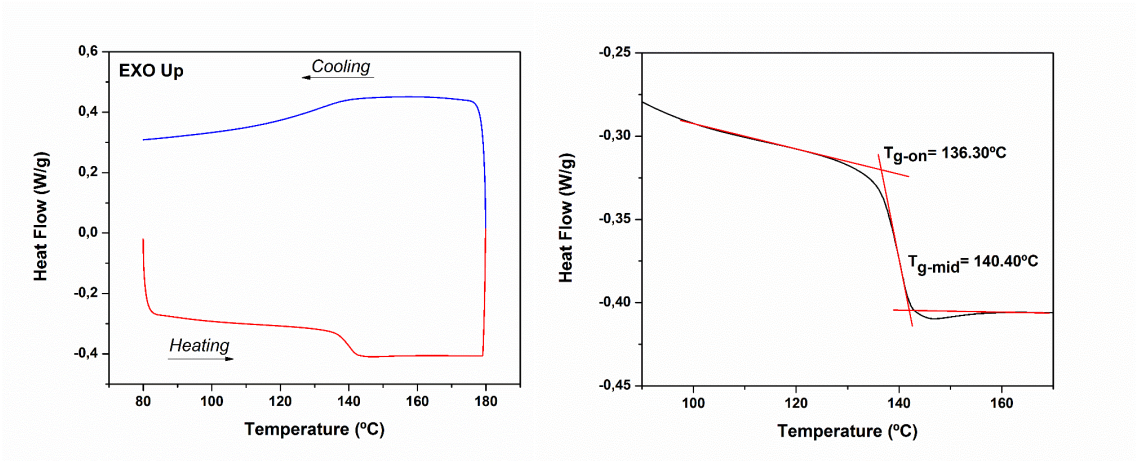

Figure A. 7.4.1 – Heat flow thermograms for dried PNIPAm (polymer control) obtained upon heating and cooling at rate of 10 ºC/min, after the sample subjected to thermal cycling treatment to remove water content (left), glass transition temperature (T_g) determination as midpoint (right).

7.4.2. FTIR

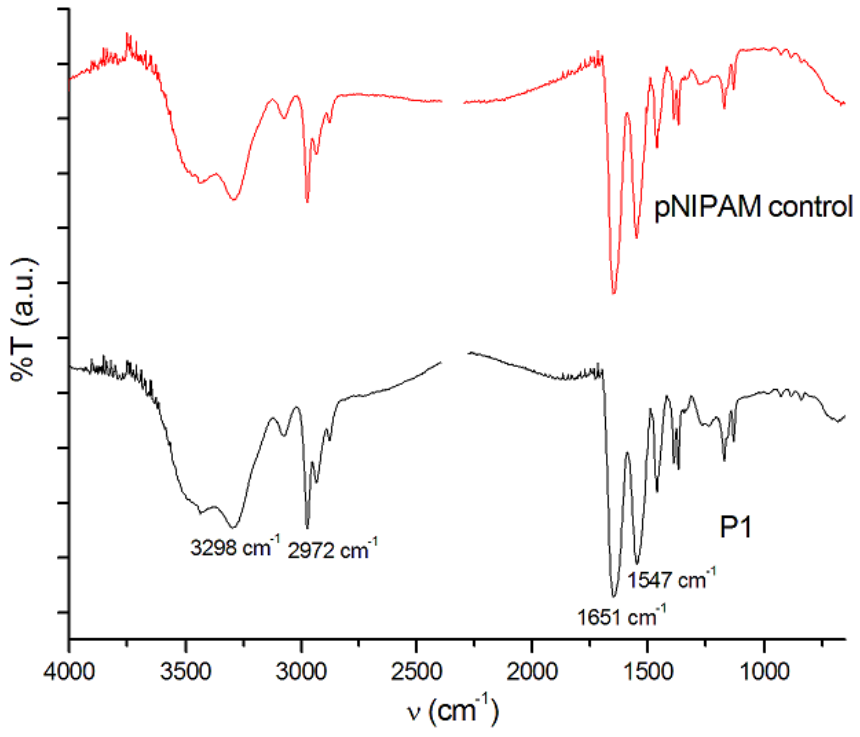

Figure A. 7.4.2 – FTIR spectra of PNIPAM control and polymer P1.

7.4.3. Maldi-TOF-MS

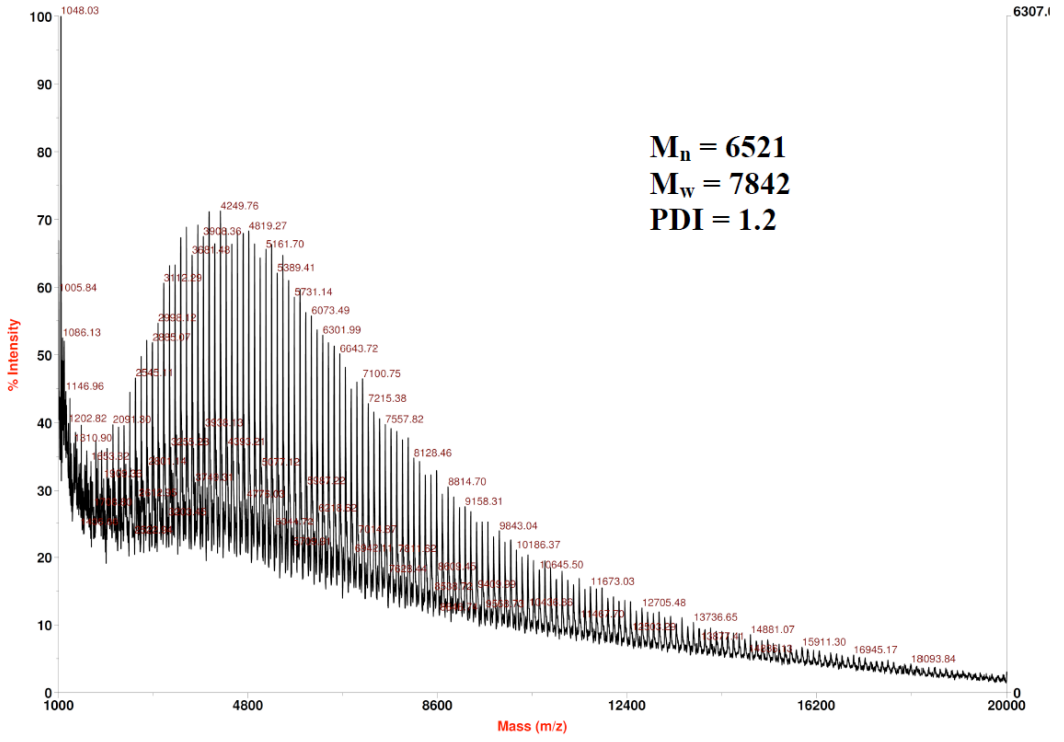

Figure A. 7.4.3 – MALDI-TOF spectrum of PNIPAM control.